

Connections in Steel Structures VI

Proceedings of the Sixth International Workshop

held at

Westin Michigan Avenue Chicago
Chicago, Illinois, USA
23-25 June, 2008

Edited by

Reidar Bjorhovde
Frans S.K. Bijlaard
Louis F. Geschwindner

American Institute of Steel Construction, Chicago, IL, USA

AISC © 2008

by

American Institute of Steel Construction

*All rights reserved. This book or any part thereof must not be reproduced in any form without the written permission of the publisher.
The AISC logo is a registered trademark of AISC.*

ISBN 1-56424-058-4

The information presented in this publication has been prepared in accordance with recognized engineering principles and is for general information only. While it is believed to be accurate, this information should not be used or relied upon for any specific application without competent professional examination and verification of its accuracy, suitability, and applicability by a licensed professional engineer, designer, or architect. The publication of the material contained herein is not intended as a representation or warranty on the part of the American Institute of Steel Construction or of any other person named herein, that this information is suitable for any general or particular use or of freedom from infringement of any patent or patents. Anyone making use of this information assumes all liability arising from such use.

Caution must be exercised when relying upon other specifications and codes developed by other bodies and incorporated by reference herein since such material may be modified or amended from time to time subsequent to the printing of this edition. The Institute bears no responsibility for such material other than to refer to it and incorporate it by reference at the time of the initial publication of this edition.

Printed in the United States of America

FOREWORD

This book presents the proceedings of the Sixth International Workshop on Connections in Steel Structures. The workshop was held at the Westin Michigan Avenue Chicago in Chicago, Illinois, USA during the period 23-25 June, 2008 under the auspices of the American Institute of Steel Construction and the European Convention for Constructional Steelwork.

The five preceding international workshops were held in Cachan, France, in 1987; Pittsburgh, Pennsylvania, USA in 1991; Trento, Italy, in 1995; Roanoke, Virginia, USA, in 2000; and in Amsterdam, The Netherlands, in 2004. Proceedings for the five preceding workshops were published by Elsevier Applied Science Publishers (1988), the American Institute of Steel Construction (1992), Pergamon/Elsevier Science (1996), the American Institute of Steel Construction (2002) and Bouwen met Staal, the Netherlands (2005).

The American Institute of Steel Construction (AISC) and the European Convention for Constructional Steel (ECCS) supported the idea of holding a sixth workshop, thus making it possible. Financial support for the workshop was provided by the American Institute of Steel Construction, Nucor-Yamato Steel, Gerdau Ameristeel, and Steel Dynamics.

The American Institute of Steel Construction was the official host of this workshop that was held in their home city. Outstanding work by the staff of AISC made the workshop possible. The contributions of Katy Preston, Elizabeth Robelet, and Ashley Melvin to the planning and on-site arrangements are particularly appreciated. Areti Carter and Janet Cummins took charge of the technical details and the preparation of these proceedings for which we are all very grateful. In addition, the participation of the individuals who served as session chairs contributed significantly to the smooth running of all three days of the workshop.

Finally, the support and technical contributions of the 71 participants from 19 countries who presented 56 technical papers must be acknowledged. Without their commitment to research, design, and construction of structural steel connections worldwide, none of this would have been possible. It is expected that the continued commitment of these participants and others to come in the future, will result in another successful workshop in Timisoara, Romania in 2012.

Louis Geschwindner
Frans Bijlaard
Reidar Bjorhovde

September 2008

**THE SIXTH INTERNATIONAL WORKSHOP
ON CONNECTIONS IN STEEL STRUCTURES**

was sponsored by

American Institute of Steel Construction, Chicago, Illinois, USA
European Convention for Constructional Steelwork, Brussels, Belgium
Nucor-Yamato Steel Co., Blytheville, Arkansas, USA
Gerdau Ameristeel, Midlothian, Texas, USA
Steel Dynamics, Columbia City, Indiana, USA

TABLE OF CONTENTS

Technical Opening of Workshop

Recent Developments in Connection Design in AISC 360-10.....1
Louis F. Geschwindner, AISC, Chicago, IL, USA

Joint Design for Economy and Verification Based on Eurocode 37
Frans S. K. Bijlaard, Delft University of Technology, Delft, the Netherlands, Jan W.P.M. Brekelmans, TNO Built Environment and Geosciences, Delft, The Netherlands

Bolts and Bolting

Evaluation of the Resistance Factors of High Strength Fasteners for Steel Building Design19
A. M. Moore, G. A. Rassati and J. A. Swanson, University of Cincinnati, Cincinnati, OH, USA

Experimental Research on Bolted Joints in High Strength Steel Members31
Dieter Ungermann and Stephan Schneider, University of Dortmund, Dortmund, Germany

Performance of the Unified Block Shear Equation for Atypical Failure Paths41
Qing Cai and Robert G. Driver, University of Alberta, Edmonton, AB, Canada

Ductility Requirements for the Design of Bolted Shear Connections51
J. Henriques, University of Coimbra, Coimbra, Portugal, J. P. Jaspart, University of Liège, Liège, Belgium and Luis Simões da Silva, University of Coimbra, Coimbra, Portugal

Tests on Bolted Shear Connections in High Strength Steel with Three or Four Bolts in Longitudinal Direction65
Primož Može and Darko Beg, University of Ljubljana, Ljubljana, Slovenia

Stiffness of Lap Joints with Preloaded Bolts75
A. M. (Nol) Gresnigt, Delft University of Technology, Delft, the Netherlands

Bracing Connections and Related Issues

Vertical Bracing Connections in the Seismic Regime93
W. A. Thornton and L. S. Muir, Cives Engineering Corporation, Roswell, GA, USA

Seismic Behavior and Performance of Buckling-Restrained Braced Frame Connections105
Larry A. Fahnestock and Victoria A. Wigle, University of Illinois at Urbana-Champaign, Urbana, IL, USA

Gusset Plate Connections for Seismic Design117
Charles W. Roeder and Dawn E. Lehman, University of Washington, Seattle, WA, USA

Minimizing the Strength of Bracing Connections127
Richard B. Vincent, Canam Group, Boucherville, PQ, Canada

Experimental Verification of the New AISC Single Plate Shear Connection Design Model143
Kirsten Baldwin-Metzger and Thomas M. Murray, Virginia Polytechnic Institute, Blacksburg, VA, USA

High-Strength Steel Connections and Other Issues

Deformation Considerations for High Strength Steel Panel Zones155
Ana M. Girão Coelho, Polytechnic Institute of Coimbra, Coimbra, Portugal, Frans S. K. Bijlaard and M. H. Kolstein, Delft University of Technology, Delft, the Netherlands

Influence of Connected Members Components on the Structural Performance of Bolted Beam-to-Column Joints of Pitched Roof Portal Frames.....165
I. M. Cristutiu, Daniel Grecea and Dan Dubina, University of Timisoara, Timisoara, Romania

Monotonic and Cyclic Tests of Steel Pretensioned Bolted End-Plate Connections of Different Types and Details175
Gang Shi, Jun Xiong, Yongjiu Shi, and Yuanqing Wang, Tsinghua University, Beijing, China

Dual-Steel T-Stub Behavior under Monotonic and Cyclic Loading185
Dan Dubina, Aurel Stratan, Nicolae Muntean and Daniel Grecea, University of Timisoara, Timisoara, Romania

Non-Linear Dynamic Behavior of Steel Portal Frames with Semi-Rigid Connections197
F. da R. de C. Lopes, J. G. S. da Silva, P. C. G. da S. Vellasco, L. R. O. de Lima and S. A. L. de Andrade, State University of Rio de Janeiro, Rio de Janeiro, Brazil

Connections with Improved Fire Resistance209
František Wald, J. Chlouba, Z. Sokol and P. Kallerová, Czech Technical University, Prague, Czech Republic

Methods of Analysis

A Generalized Modeling Approach of Steel Joints for Advanced Global Analysis and Stability of Frames.....219
Eduardo Bayo and Javier Gracia, University of Navarra, Pamplona, Spain

Application of Instantaneous Center of Rotation Concept for Cyclic Modeling of Bolted Connections in Special Bolted Moment Frames231
Atsushi Sato, Kyoto University, Kyoto, Japan and Chia-Ming Uang, University of California – San Diego, La Jolla, CA, USA

Nonlinear Analysis of Steel Frameworks with Semi-Rigid Connections243
Yuxin Liu and Lei Xu, University of Waterloo, Waterloo, ON, Canada

Design of PR Frames Using the AISC Direct Analysis Method255
Donald W. White, Georgia Institute of Technology, Atlanta, GA, USA and Arvind V. Goverdhan, Stanley D. Lindsey & Associates, Ltd., Atlanta, GA, USA

Recent Research and Development in Semi-Rigid Composite Joints with Precast Hollowcore Slabs	265
<i>Dennis Lam, University of Leeds, Leeds, England</i>	

Connections for Seismic Effects

Seismic Strength of Moment End-Plate Connections with Attached Concrete Slab	277
<i>Michael W. Seek, Walter Seek Engineering, Johnson City, TN, USA, and Thomas M. Murray, Virginia Polytechnic Institute, Blacksburg, VA, USA</i>	

Prequalification Testing of Built-Up T-Stub Components for Use in Moment Resisting Frames.....	287
<i>Elie G. Hantouche, James A. Swanson and Gian A. Rassati, University of Cincinnati, Cincinnati, OH, and Roberto T. Leon, Georgia Institute of Technology, Atlanta, GA, USA</i>	

Experimental Behavior of Link-to-Column Connections in Eccentrically Braced Frames	297
<i>Taichiro Okazaki, University of Minnesota, Minneapolis, MN, Michael D. Engelhardt, Apostolos Drolias, and Eric Schell, University of Texas, Austin, TX, USA; Jong-Kook Hong and Chia-Ming Uang, University of California, San Diego, La Jolla, CA, USA</i>	

Deformational Compatibility in Weld Groups	309
<i>Larry S. Muir, Cives Engineering Corporation, Roswell, GA, USA</i>	

Earthquake Simulations on Self-Centering Steel MRFs with Post-Tensioned Moment Connections.....	319
<i>James M. Ricles, Choung-Yeol Seo, Ying-Cheng Lin and Richard Sause, Lehigh University, Bethlehem, PA, USA</i>	

Hybrid Moment Resisting Steel Frames for Seismic Applications.....	331
<i>Finley A. Charney and Ozgur Atlayan, Virginia Polytechnic Institute, Blacksburg, VA, USA</i>	

Behavior of High Strength Steel Welded Beam-to-Column Joints with Beams of Unequal Height	343
<i>Sandra Jordão, Luis Simões da Silva, and Rui D. Simões, University of Coimbra, Coimbra, Portugal</i>	

Experimental Program for Evaluation of Moment Beam-to-Column Joints of High Strength Steel Components.....	355
<i>Dan Dubina, Aurel Stratan, Nicolae Muntean and Florea Dinu, University of Timisoara, Timisoara, Romania</i>	

Post-Tensioned Column Bases for Self-Centering Moment Resisting Frames.....	367
<i>Hoseok Chi and Judy Liu, Purdue University, West Lafayette, IN, USA</i>	

Connections with Hollow Structural Sections and Other Features

Experimental Study on Stiffening Methods for Plate-to-Circular Hollow Section Connections	377
<i>Jeffrey A. Packer and Andrew P. Voth, University of Toronto, Toronto, ON, Canada</i>	

Strain-Based Design of Structural Connections389
Peter W. Marshall and Qian Xudong, National University of Singapore, Singapore

Structural Response of K and T Tubular Joints under Static Loading401
L. R. O. de Lima, P. C. G. da S. Vellasco, L. F. da C. Neves, J. G. S. da Silva, S. A. L. de Andrade and M. C. Bittencourt, State University of Rio de Janeiro, Rio de Janeiro, Brazil

Rotation Capacity of Welded T and X Beam-Column Joints with Rectangular Hollow Sections411
Jerzy K. Szlendak, Bialystok Technical University, Bialystok, Poland

Load Bearing Capacity of Spliced Columns with Single Row Bolted Butt-Plates421
J. C. D. Hoenderkamp and H. H. Snijder, Eindhoven University of Technology, Eindhoven, the Netherlands

Robustness of Connections and Structures

Structural Integrity – What Does This Mean for Connection Design?431
Cynthia J. Duncan, Kurt Gustafson and Thomas Schlafly, AISC, Chicago, IL, USA

Performance of Seismic Moment Resisting Connections under Column Removal Scenario443
Fadim Sadek, H. S. Lew, Joseph A. Main and John L. Gross, National Institute of Standards and Technology (NIST), Gaithersburg, MD, USA

Robustness of Steel Connections.....455
J. B. Davison and A. Tyas, University of Sheffield, Sheffield, England

Robustness of Structures – Behavior of Composite Joints.....567
Jean-François Demonceau and Jean-Pierre Jaspart, University of Liège, Liège, Belgium

Fire Design of Bolted Steel Beam-to-Column Joints479
Aldina Santiago and Luis Simões da Silva, University of Coimbra, Coimbra, Portugal and Paulo Vila Real, University of Aveiro, Aveiro, Portugal

Structural Design and Design Codes

Composite Connections in EN 1994-1-1 Eurocode 4491
David Anderson, University of Warwick, Coventry, England

Application of the EC3 Design Rules to End-Plate Connections with Four Bolts in One Row.....501
Klaus Weynand and Ralf Klinkhammer, Feldmann + Weynand GmbH, Aachen, Germany; Dieter Ungermann and Stephan Schneider, University of Dortmund, Dortmund, Germany; and Otto Oberegge, Hans-Peter Hockelmann and Nicole Ritterbusch, Fachhochschule Köln, Köln, Germany

Design of Innovative SMA PR Connections Between Steel Beams and Composite Columns....513
Roberto T. Leon and Jong Wan Hu, Georgia Institute of Technology, Atlanta, GA, USA

Capacity of Welded Joints that Combine Welds in Different Directions.....525
Logan J. Callele, Gilbert Y. Grondin and Robert G. Driver, University of Alberta, Edmonton, AB, Canada

Incorporation of Full Scale Testing and Nonlinear Connection Analyses
into the Seismic Upgrade of a 15-Story Steel Moment Frame Building535
*James O. Malley, Mark Sinclair and Tim Graf, Degenkolb Engineers, San Francisco, CA, USA;
Colin Blaney and Moisey Fraynt, Crosby Group, Redwood City, CA, USA; Chia-Ming Uang,
University of California – San Diego, La Jolla, CA, USA; and Tamer Ahmed, State of California
Department of General Services, West Sacramento, CA, USA*

Special Connection Topics

Strength Reduction Factors for Storage Racks.....545
Carlos Aguirre, Technical University Federico Santa María, Valparaíso, Chile

A Reliability-Based Methodology for Evaluating
Connection Design of Self-Centering Frames.....555
*Maria E. Moreyra Garlock, Gordana Hering, and Erik VanMarckel, Princeton University,
Princeton, NJ, USA*

M-N Interaction in Connections with Thermal Separation565
*František Wald, Z. Šulcová and Z. Sokol, Czech Technical University, Prague, Czech Republic,
and Roman Rabenseifer, Slovak University of Technology, Bratislava, Slovakia*

Historic Shear Connections: Rivet and Moment Capacity Data575
*Scott Civjan, University of Massachusetts, Amherst, MA, USA, Gershon Larsen, Weidlinger
Associates, Cambridge, MA, USA, and Eric Hines, LeMessurier Consultants, Cambridge, MA,
USA*

Performance of a High Strength Friction Grip Connection with Open Slotted Hole585
Wylliam Husson and Milan Veljkovic, Luleå University of Technology, Luleå, Sweden

Workshop Summary Session

Connection Research Needs597
Reidar Bjorhovde, The Bjorhovde Group, Tucson, AZ, USA

Connection Design and Code Needs603
Charles J. Carter, AISC, Chicago, IL, USA

Participants – Connections VI Workshop611

Author Index613

RECENT DEVELOPMENTS IN CONNECTION DESIGN IN AISC 360-10

Louis F. Geschwindner

American Institute of Steel Construction, Chicago, IL, USA

Gesch@aisc.org

ABSTRACT

The last revision to the American Institute of Steel Construction *Specification for Structural Steel Buildings*, AISC 360, was completed in 2005. It was approved by the American National Standards Institute on March 9, 2005. Thus, it is known as ANSI/AISC 360-05. Immediately after completion of the 2005 standard, the AISC Committee on Specifications began discussions and deliberations on the next revision, which is expected to be completed in 2010 and would be known as AISC 360-10. While ANSI/AISC 360-05 reflected some major revisions to the previous standards, including the integration of both ASD and LRFD, the approach being pursued for the 2010 edition is one of minimal change. Thus, it is expected that connection design according to the AISC Specification will remain essentially the same for another specification cycle. This paper will highlight the few changes that are being proposed in order to provide the design community with a preliminary look at the progress being made by the AISC Committee on Specifications.

INTRODUCTION

The 2005 edition of the *Specification for Structural Steel Buildings*, ANSI/AISC 360-05, (AISC, 2005a) reflected the greatest change in the steel specification since the 1960 allowable stress design specification (ASD) and the 1986 load and resistance factor design specification (LRFD). The primary goal for the development of ANSI/AISC 360-05 was to unify the provisions for ASD and LRFD design under one specification. However, its development also provided an opportunity to introduce new provisions reflecting the knowledge gained since the previous editions of these specifications had been published, 1989 for ASD and 1999 for LRFD. For connection design, this meant several significant changes and many less significant ones. Two papers presented at the Connections in Steel Structures V workshop (Duncan 2004, and Geschwindner 2004) discussed the changes that were anticipated as the standard moved through the approval process.

Topics addressed in these two papers were;

1. New provisions for compression members with bearing joints,
2. Splices in heavy sections.
3. Beam cope and weld access hole dimensions.
4. Bolts used in combination with welds.

5. Conditions under which specific types of bolted and welded connections are required.
6. Elimination of minimum connection strength requirements.
7. Revision of effective throat dimensions for groove welds.
8. Revision of effective dimensions and terminations for fillet welds.
9. Strength increase for welds loaded at an angle.
10. Permitted material specification for high strength bolts longer than 12 inches.
11. Relaxed requirements on hole types permitted
12. Refined provisions for bolts under combined shear and tension.
13. Defined serviceability and strength limit states for high-strength bolts in slip critical connections.
14. Slightly revised provisions for shear lag in tension members.
15. Revised the provisions for block shear rupture strength.

Other changes apparent in the 2005 standard included the addition of strength provisions specifically for connected elements, a strength check for web sidesway buckling, and minimum weld sizes based on the smaller of the parts being joined. Finally, an entire chapter, Chapter K, was added to the specification in order to address the many and complex requirements for connections in hollow structural sections, HSS.

CHANGES FOR 2010

The AISC Committee on Specifications was charged by its chair to approach the development of this next standard with the idea that there would be minimal change. The structural engineering environment in the USA for the past 20 years has been one of continuous change in the standards. The structural engineer has been asked to keep abreast of rapid changes in both loading and material standards and to incorporate design for seismic events in locations where this had never before been a factor. Thus, AISC believed that approaching its next standard with a real effort to limit changes to only those topics that truly needed to be changed from a safety or economic standpoint would significantly benefit the profession. Thus, the proposed changes in the first ballot version of AISC 360-10 are quite limited.

Design Requirements

The 2005 Specification provided a section to directly address the types of connections that are permitted, simple connections and fully-restrained or partially-restrained moment connections. For 2010, the following statement is added to recognize that all connections may experience inelastic, self-limiting deformations; “Self-limiting inelastic deformations of connections are permitted.”

Additionally, in an effort to add clarity to what is expected to occur at points of support, the following sentence is added; “At points of support, beams, girders and trusses shall

be restrained against rotation about their longitudinal axis.” This emphasizes a requirement that many felt had been down played in the 2005 Specification.

Shear Lag

The shear lag provisions of the 2005 Specification were only minimally different from those of the previous two specifications. For 2010, the committee is proposing a new lower bound on the shear lag factor, U , for open cross-sections. Previously, the lower bound was given in a table as seen in Figure 1. The committee is proposing to also

7	W, M, S or HP Shapes or Tees cut from these shapes. (If U is calculated per Case 2, the larger value is permitted to be used)	with flange connected with 3 or more fasteners per line in direction of loading	$b_f \geq 2/3d \dots U = 0.90$ $b_f < 2/3d \dots U = 0.85$	—
		with web connected with 4 or more fasteners in the direction of loading	$U = 0.70$	—
8	Single angles (If U is calculated per Case 2, the larger value is permitted to be used)	with 4 or more fasteners per line in direction of loading	$U = 0.80$	—
		with 2 or 3 fasteners per line in the direction of loading	$U = 0.60$	—

Figure 1 Portion of Table D3.1 from ANSI/AISC 360-05

provide a lower bound equal to the ratio of the gross area of the connected elements to the gross area of the member. Thus, for an equal leg single angle connected through one leg, the lower bound value is approximately 0.5 while from the table the value is 0.6. For an unequal leg single angle, such as a $7 \times 4 \times 3/4$, attached in the long leg, the lower bound value would be 0.68 rather than the 0.6 in the table.

Weld Access Holes

For the 2005 specification, weld access hole dimensions were revised to be very similar to those specified in the *Structural Welding Code-Steel*, AWS D1.1 (AWS, 2004). For 2010 the dimensions of the weld access hole have been revised to be exactly the same as those found in AWS D1.1.

Permitted Bolts

While the 2005 Specification was under development, ASTM was in the process of developing materials standards for “twist-off” type high-strength tension control bolts. The timing was such that the 2005 Specification included ASTM F1852 twist-off tension control bolts which have a strength equivalent to ASTM A325 bolts. The 2010 Specification will also include ASTM F2280 twist-off bolts, the strength equivalent to ASTM A490 bolts.

Minimum Edge Distance

An arbitrary minimum edge distance for bolt holes in connected parts has been specified based on standard fabrication practices and workmanship tolerances. These minimums were set to different values at sheared edges and at rolled edges with the values being greater at sheared edges. For the 2010 Specification, minimum values are given without regard to edge type. As with the 2005 Specification, these minimums can be reduced if necessary.

High-Strength Bolts in Slip-Critical Connections

A major change incorporated into the 2005 Specification was in the provisions for high-strength bolts in slip-critical connections. Two design approaches were specified. For connections with standard holes or slots transverse to the direction of the load, the design was to be carried out for slip as a serviceability limit state. For connections with oversized holes or slots parallel to the direction of load the design was to be carried out to prevent slip at the required strength level. The same nominal strength was given for both cases but the available strength was reduced 85% for design at the strength limit state. These provisions raised some concern amongst connection designers who believed that, in many cases, they had the effect of reducing significantly the strength of slip-critical connections.

To address this issue, at least in part, the proposal for 2010 is to remove the default that required the use of the strength limit state for connections with oversized holes. The committee has determined that this requirement as a default was too conservative. Thus, the proposal is to say “Connections shall be designed for slip at a serviceability limit state except where slip would cause a reduction in the strength or stability of the structure.” Connection strength will not be changed by the 2010 Specification, only the cases where each limit state must be considered.

Design of HSS and Box Member Connections

One goal of the 2005 Specification was the integration of several separate AISC standards into one unified standard. One of the separate standards to be integrated was

the *Specification for the Design of Steel Hollow Structural Sections* which was published as part of the HSS Connections Design Manual (AISC, 1997). Incorporation of this standard in to the 2005 Specification was a major undertaking accomplished by making Chapter K Design of HSS and Box Member Connections.

For 2010, the committee has proposed a change in format to a table arrangement as indicated in Figure 2. It should be noted that, as with all of the changes discussed in this paper, this is a proposal which still must be approved by the Committee on Specifications.

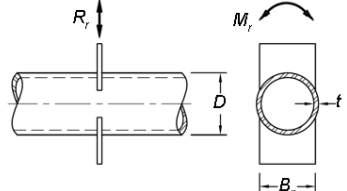
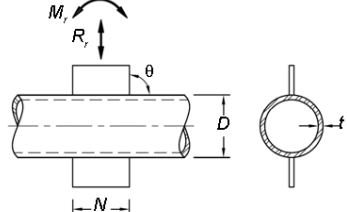
Table K1.1. Nominal Strengths of Plate-to-Round HSS Connections				
Connection Type	Connection Nominal Strength Spec. Eqn.	Branch In-Plane Bending	Branch Out-of-Plane Bending	
Transverse Plate T- and Cross-Connections 	Limit state: chord local yielding Branch Axial Load: $R_n = F_y t^2 \left[\frac{5.5}{1 - 0.81 \frac{B_p}{D}} \right] Q_t \quad (K1-1)$ $\phi = 0.90 \text{ (LRFD)} \quad \Omega = 1.67 \text{ (ASD)}$	—	$M_n = 0.5 B_p R_n$	
Longitudinal Plate T-, Y- and Cross-Connections 	Limit state: chord plastification Branch Axial Load: $R_n \sin \theta = 5.5 F_y t^2 \left[1 + 0.25 \frac{N}{D} \right] Q_t \quad (K1-8)$ $\phi = 0.90 \text{ (LRFD)} \quad \Omega = 1.67 \text{ (ASD)}$	$M_n = N R_n$	—	

Figure 2. New Format for HSS Connection Provisions

UNDER CONSIDERATION

The committee continues to consider several proposals for changes to be incorporated into the 2010 Specification. There will likely be other proposals raised and considered before the standard is fully completed.

One provision being considered is that of flexure in connected parts. The 2005 Specification includes provisions for strength of elements in tension, shear, and compression but does not address flexure. The only guidance given the designer comes from the 13th edition of the *Steel Construction Manual* (AISC, 2005b). It is expected that provisions for flexure in connected parts will be developed and proposed before the completion of the 2010 Specification.

A second area that is drawing significant attention from the committee is that of bolts in slip-critical connections. The committee has already proposed a change that would remove the perception that design for the strength limit state is the default condition, as

discussed above. They continue to assess the available data with the goal of presenting a better prediction of strength for these types of connections.

CONCLUSIONS

The goal of the Committee on Specifications for AISC 360-10 was a standard that reflected a minimal amount of change. This review of the recommendations from the connections task committee indicates that the changes in connection design will likely be quite limited. That does not mean that extensive research has been abandoned, on the contrary. AISC has funded and continues to fund significant research projects that have the potential to increase our knowledge of connection behavior. The committee continues to assess this research and the research presented at this workshop and other venues around the world. Once that research has reached an appropriate level of completion; it will be considered and appropriately implemented by the committee.

REFERENCES

AISC, (2005a). Specification from Structural Steel Buildings, ANSI/AISC 360-05, American Institute of Steel Construction, March 9, Chicago, IL.

AISC, (2005b). *Steel Construction Manual*, American Institute of Steel Construction, Chicago, IL.

AISC, (1997). *Hollow Structural Sections Connections Manual*, American Institute of Steel Construction, Chicago, IL.

AWS, (2004). *Structural Welding Code – Steel*, American Welding Society, Miami, FL.

Duncan, C. J., (2004). "Connection Design in the 2005 AISC Specification," *Proceedings of the Connections in Steel Structures V Conference*, Amsterdam, The Netherlands.

Geschwindner, L., (2004). "Evolution of Shear Lag and Block Shear Provisions in the AISC Specification," *Proceedings of the Connections in Steel Structures V Conference*, Amsterdam, The Netherlands.

JOINT DESIGN FOR ECONOMY AND VERIFICATION BASED ON EUROCODE 3

Frans S. K. Bijlaard

Delft University of Technology, Delft, The Netherlands
F.S.K.Bijlaard@tudelft.nl

Jan W.P.M. Brekelmans

TNO Built Environment and Geosciences, Delft, The Netherlands
Jan.Brekelmans@tno.nl

ABSTRACT

For countries in Western Europe, joints in steel frame structures are realised using bolts and welds. In the workshop, the components are made using welding end plates and attachments and drilling of the bolt holes. On site, these structural components are connected together using bolts and nuts. The activities on site mean a large physical effort of the steel construction workers who are not free from danger. Measures needed to ease the work and to make it safer for workers are increasingly expensive. Of the total costs of a steel structure, 50% of that amount is related to the joints whereas almost 90% of the total costs are already decided upon in the construction detailing phase. The use of semi rigid and partial strength joints could lead to cost reduction. For almost all types of joints design rules are available in Eurocode 3, Part 1.8: 'Design of joints' to make the structural safety verification of these joints possible.

INTRODUCTION

Traditionally for Western Europe countries, joints in steel frame structures are realised using bolts and welds. In the workshop the components are made using welding end plates and attachments and drilling of the bolt holes. On site these structural components are connected together using bolts and nuts. The activities on site mean a large physical effort on the part of the steel workers, and it is not free from danger. Measures that need to be taken to ease the work and to make it safer for the workers are increasingly expensive. Furthermore the availability of skilled workers who are willing to do these jobs under variable climatic conditions is decreasing. So there is a need to develop so called "plug and play" connections which can be realized using remotely controlled techniques. An extreme example is the connecting device used to dock a space shuttle to a space station. For the average steel structure we are still far away from that situation and we can do with more simple solutions but even those simple plug and play connections are so far only very limited available.

Examples of non-traditional types of joints are used in Slim Floor construction. In this type of flooring, the steel beams are integrated into a prefabricated concrete hollow core slab or a deep deck composite slab. The so called plug and play beam-to-column joints in these mixed structures are characterized by simplicity and fast erection methods. These joints could also be used in traditional steel-concrete composite flooring systems. Most often these joints are only intended to act as a hinge. However, there are some

ideas to make plug and play type joints that also can resist some bending moment even in the construction stage. For steel structures similar ideas need to be developed.

The costs of fabrication may slightly be higher than the costs of traditional joints provided that the total costs of fabrication and construction decrease. Fast and safe construction methods are required for the future.

Nowadays the pressure from society towards more environmentally friendly construction is increasing. The re-use of structures is one of the possible solutions to save energy. In that light structures need to be designed such that they are fit to be demounted and rebuilt easily. In that case components as columns and beams and consequently also joints should be able to have a second live time in another structure at an other location. With these industrial-flexible-demountable joints there is a possibility to satisfy the so-called "cradle-to-cradle approach" which means for steel structures that the path through the melting pot can be avoided.

As holds for traditional connections also plug and play joints should resist the forces and moments resulting from all types of loading related to the use of the structure and resulting from the natural circumstances such as wind and snow. For these types of joints no specific design rules are available in Eurocode 3, Part 1.8: 'Design of joints' [1] but so-called components of joints. The designer needs to use his creativity to detect the basic components in these joints that he has designed.

Some attractive joint concepts will be reviewed first.

1. Simple erection joints

New types of joints are used in so called Slim Floor construction. In this type of flooring, the steel beams are integrated into a prefabricated concrete hollow core slabs or in a deep deck composite slabs. The beam-to-column joints in these mixed structures are characterized by simplicity and fast erection methods. These joints can also be used in traditional steel-concrete composite flooring systems. These joints lead to faster construction onsite and reduce the need for construction workers to work in dangerous situations high above ground level. These joints are most often hinged connections in the erection phase as well as in the final phase. Although these joints are simple erection joints, for the final stage they should be improved with respect to the bending resistance with the aim of cost efficiency.

2. Traditional steel-concrete composite floor construction joints

In the construction stage of a traditional steel-concrete composite floor construction, the beam is often designed as a simply supported single span beam. In these cases the beam-to-column joints most often have a welded end plate or bolted web-cleats as connecting parts. In the final stage, after installing the composite slab, the beam-to-column joint can behave either as a hinge or as a partially moment resistant joint dependent on the detailing of the joint.

3. Demountable industrial joints

In temporary industrial buildings standardised demountable joints are used for all steel beam-to-column joints. The building as shown in Figure 1 is the Delftech office building in Delft in the Netherlands. This building is erected in three weeks time. A lot of joints in this building are 'pin-hole' joints. For example the prefabricated slabs are connected to the steel beams by means of pins and the pin holes can be filled with grout and as such

become the compressive flange of a composite steel-concrete beam. The steel beams are filled with concrete between the flanges (partially encased beams). One of the advantages of this way of design is the improved fire resistance and the improved resistance of the beam-to-column joint in shear and compression. The standardized beam-to-column joint is from a fabrication and erection point of view not optimal. A plug and play solution would be preferable if it could be combined with previously mentioned advantages.



Figure 1: Delftech office building in Delft, the Netherlands; built in 3 weeks time (source: [2])

COST OPTIMIZATION

Cost optimisation is one of the most important items in steel construction in order to be competitive in the market of buildings. The joints determine almost 50% of the total costs of a steel structure. As a consequence of the innovation of the fabrication process, the fabrication costs have decreased spectacularly. The costs of fabrication of plug and play joints should be the same or preferably even lower than the costs of traditional joints. The costs of fabrication of plug and play joints may only be slightly higher than the costs of traditional joints provided that the total costs of fabrication in the workshop and erection on the construction site are significantly lower.

The distribution of costs of a steel structure is indicated in Figure 2. Distinction is made in design (13%), material (38%), fabrication (27%), conservation (10%), transportation and erection (12%); so in total 100%. The costs for design can eventually be split into costs for pre-design (2%), final design (3%) and the detailing together with the preparation of the work (8%). The transportation is 2% of the total costs whereas the erection can be split into 8% for the erection and 2% for the finishing part of the erection.

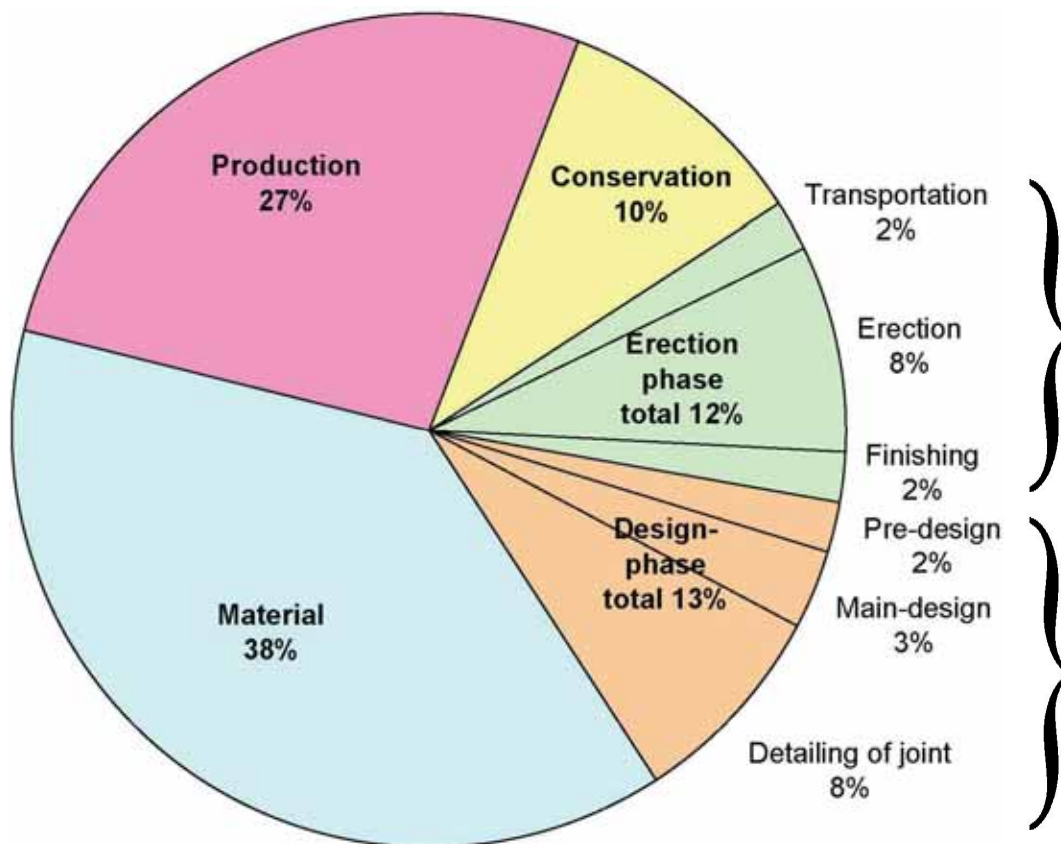


Figure 2: Cost distribution of steel structures (source: [3])

A large part of these costs are related to the joints of the structure. In Figure 3 these costs related to the joints of the structure are indicated, which are added up to 50% of the total costs. These 50% of the total costs is a result of:

Pre-design $2\% \times 33\% = 0.7\%$

Final design	$3\% \times 55\% = 1.7\%$
Detailing & preparation work	$8\% \times 77\% = 6.2\%$
Material	$38\% \times 40\% = 15.2\%$
Fabrication	$27\% \times 63\% = 17.0\%$
Conservation	$10\% \times 38\% = 3.8\%$
Erection and transportation	<u>$12\% \times 45\% = 5.4\%$</u>
Total	$100\% \times \dots = 50.0\%$

It will be clear that the choice for a type of joint and the related work for realisation of these joints have an important influence on the total costs of the steel structure.

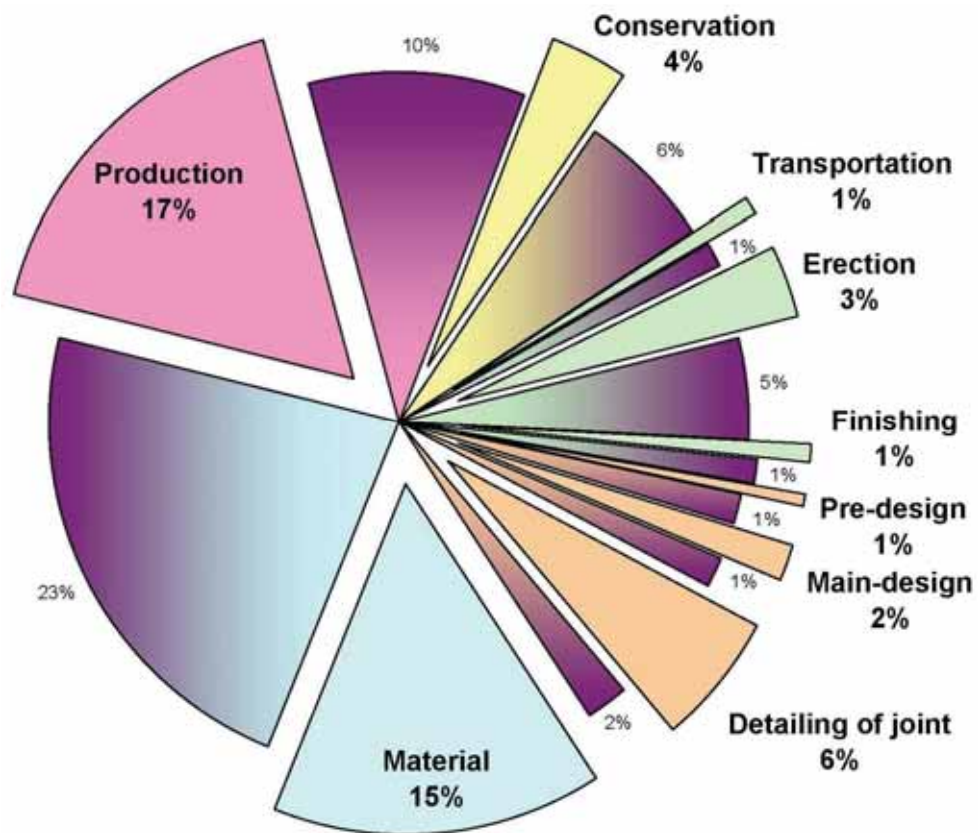


Figure 3: Costs related to the joints of the structure (source: [3])

In Figure 4 a cumulative cost overview of the workmanship and material in the several phases of the building process is illustrated. In blue the costs for workmanship is indicated; in brown the material costs. Some of the percentages are mentioned before. At the end of the design process 13 % of the total costs is spent. Then the fabrication starts and the costs increases with 27 % of the total costs for workmanship together

with 38 % of the total costs for material. That brings the costs for the fabrication stage already up to 78 % of the total costs.

The job will be finished after costs for conservation (10 %) and transportation together with erection (12 %). Now it can be seen in what stage in the building process important decisions are taken about the costs of the final structure. These are the determined costs indicated in yellow. At the design stage of the process the decisions about the material costs and the conservation are taken. During the fabrication and erection stage only a few additional decisions will affect the final total costs. So, at the end of the design phase 88 % of the total costs are already determined by the structural steel designer.

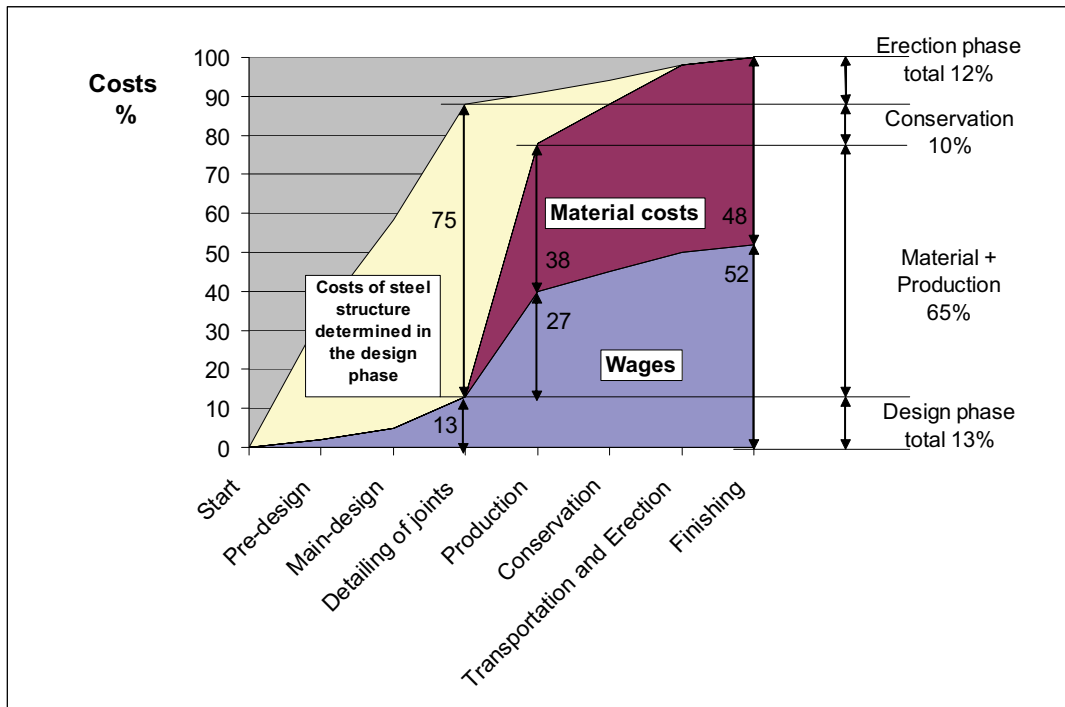


Figure 4: Phases of the building process and the related cumulative costs already determined (source: [3])

It can be concluded that the costs of the structure are mainly influenced by the decisions taken in the design phase. More attention to design considerations by the structural steel designer will result in more cost efficient structures.

Optimization in weight will in most cases not result in an optimal cost effective structure. A semi rigid joint in the final stage of the structure could result in cost reduction. At the erection stage the joints are not so much severely loaded as in the final stage. So, during the erection stage the joint could eventually act as a hinge.

VERIFICATION BASED ON EUROCODE 3

To describe possibilities for alternative joints in steel and steel-concrete construction first an analogy with a traditional steel-concrete composite floor construction is made.

1. Consequences of loading on the structure for the forces in joints

Most steel frame structures with traditional joints with connecting parts as bolts and welds are designed on the basis of forces resulting from plane frame analyses. The spatial behaviour of structure due to the loading is most times neglected because the resistance of the traditional joints against these resulting forces is normally sufficient. The wind loading on a building can produce tensile forces in the joints, while eccentric loading on the floor can produce torsional moments on the joints. Traditional joints have by themselves sufficient resistance against these tensile forces and torsional moments. Because bolts in holes, designed primarily for shear and or bending moments, are almost always capable of carrying these “secondary” forces and moments. In fact these forces are not “secondary” but primary forces and moments due to the spatial behaviour of the structures under the loading actions and most times neglected in design. In designing new concepts for plug and play joints the designer needs to be explicitly aware of these forces and moments, which can implicitly be neglected in designing traditional joints. Also loading that can appear in the onsite construction phase produces most times tension and torsion in the beams and joints. The main task of the designer is to design the joints such that robustness in order to prevent premature and progressive collapse can be demonstrated explicitly.

2. Consequences of detailing of joints for distribution of forces and moments in joints and requirements with respect to stiffness, strength and rotation capacity for joints

The distribution of forces and moments in the structure due to the loading is a result of the strength and stiffness distribution in the structure. So the structural properties of the joints such as stiffness, strength and rotation capacity, together with those of the structural components like beams and columns, produce these forces in the joints. This means that the choices made by the designer in designing the joints including the connecting parts are of direct influence on the level of forces and moments in these joints. In fact, construction is joining components such as columns and beams together while designing is making choices for components taking the structural properties such as strength and stiffness into account.

Traditional Design

In traditional design it is assumed that the joints are stiff and strong and that the forces and moments in the structure are determined using the linear-elastic theory. Because it was assumed that the joints were stiff, it needs to be checked whether the joints are really stiff. In many cases in practice this is neglected. The strength of the joints is adjusted to the level needed. As a result most joints have low deformation capacity. Last but not least, the fabrication costs are very high.

Modern Design

In modern design the joints are considered as structural components such as columns and beams with properties as stiffness, strength and deformation capacity. These structural properties of the joints are incorporated into the design on the same level as those of columns and beams. The joint layout should only be influenced by fabrication considerations and considerations for easy and safe construction on-site. The structural safety verification of all components including that of the joints is dependent on the design method used to determine the distribution of forces and moment in the structure.

a. In case that the linear elastic theory is used, the beams need to be checked for strength and for lateral torsional buckling, the columns need to be checked for strength and for beam-column stability (incl. lateral torsional buckling) and the connecting parts of the joints need to be checked to have sufficient strength to transfer bending moments, shear forces and tensile forces resulting from the linear elastic theory adjusted for the second order effects.

b. In case that the elastic-plastic-non linear theory is used, the beams and columns need to be checked for lateral torsional buckling only and the joints need to be checked to have sufficient deformation (in fact rotation) capacity.

The Eurocode 3 "Common unified rules for steel structures" contains performance based requirements to carry out these checks. The extend to which any joint can be checked using Eurocode 3 depends on the creativity of the designer to recognise components in the connecting parts of these joints that are similar to the components given in the chapters for joints in that design code. If necessary experiments have to be carried out and the results have to be evaluated statistically, in order to obtain reliable values for the stiffness, strength and rotation capacity of these joints.

Theory

A joint can be considered as a assembly of several components which individually have their own characteristic strength, stiffness and deformation capacity. Such a joint is a combination of "springs". Combining these springs will result in an overall behaviour of the whole joint. This so called "component method" is the basis of design of joints in Eurocode 3. Simplified and more sophisticated spring modeling can be assumed (see Figure 5). In scientific context the sophisticated spring model is available. However, there is an urgent need for such models in framework programmms for use in practice. The use of the simplified model leads to iterations to determine the correct distribution of moments in the structure.

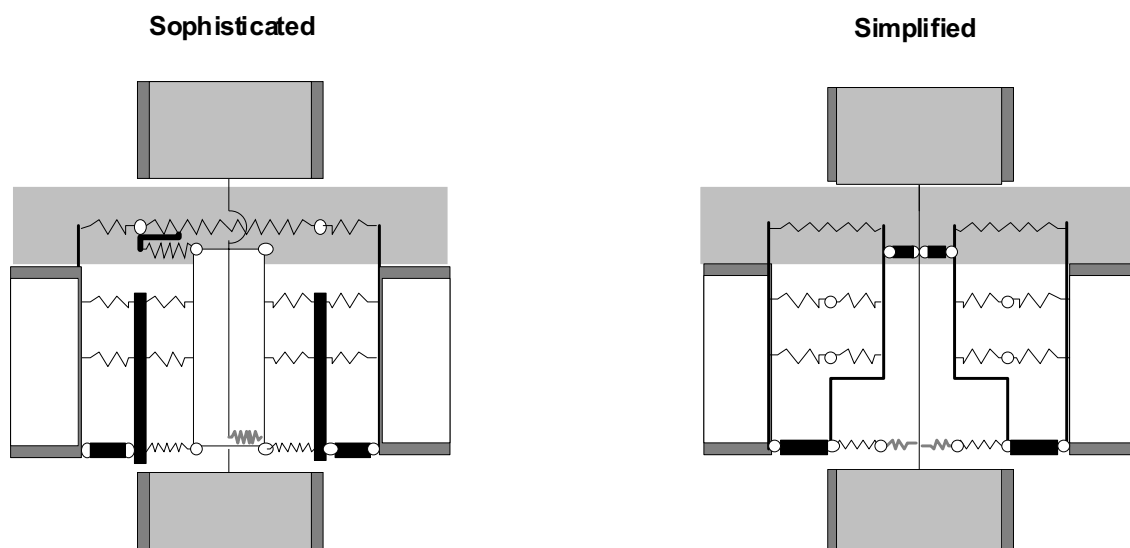


Figure 5: The component method; simplified and sophisticated modelling

Steel structures

For steel structures the development of new types of joints among these "plug and play" joints needs a boost in order to meet the goals described in the introduction. Ideas for these joints need theoretical and experimental research before these joints can be applied in practice. The philosophy for using these joints is that in the early erection phase the joints are really plug and play, resulting in joint behaviour that is sufficient for the loading conditions in the erection phase. When the access of the joints is better because of the presence of parts of the floor system, the joints can be finalised by adding bolts resulting in the final mechanical behaviour needed for the loading conditions in the final stage of the building.

Semi rigid and partial strength design consideration will also lead to substantial economic advantages in the detailing and fabrication of the joints. The flooring structure should be as light as possible before finalising the joint in the end stage of the building process, such as thin walled profiled sheetings for composite slabs or steel-board flooring systems. But, it is also possible using prefabricated thin concrete slabs on which the final concrete floor is poured without props in the end stage of the building process. The columns can be continuous or bolted at floor level, just underneath the floor finishing.

Further creativity is needed to develop "plug and play" type joints which can be considered as finalised once the beams are remotely controlled positioned and connected to the columns.

CONCLUSIONS

In order to keep a competitive position in the market, the costs of steel structures, in particular steel frames, need to be reduced as much as possible. As the costs of steel frame structures are determined for about 50% by its joints, the need to design modern "plug and play" joints is of increasing economic importance. In this way the costs of on-site construction work together with safety measures can be reduced significantly. Although design codes like Eurocode 3 "Design of Steel Structures" are still based on traditional joints with bolts and welds, in many cases the design rules can be used for the design and verification of so-called plug and play joints in which the basic components can be recognised. This is because the design rules for joints are related to the components in which almost all joints can be sub-divided and because the requirements for stiffness, strength and rotation capacity of joints are given in so-called performance based requirements and are irrespective of the type of the joint. However, where non-traditional components like clamps and hooks are used, experiments have to be carried out and the results have to be evaluated statistically, in order to obtain reliable design values for the stiffness, strength and rotation capacity of these plug and play joints to be used in the design of the structure. In near future there is a need for much further design of these "plug and play" type joints and research into the mechanical properties of these types of joints.

REFERENCES

- [1] EN 1993-1-8:2006, Eurocode 3 : Design of Steel Structures *Part 1-8 : Design of Joints*, 2006.
- [2] Frans van Herwijnen, 'Design of Structures for Functional Lifetime' *IFD-office building Delftechpark*, lecture at TU-Eindhoven, The Netherlands 2004. (in Dutch)
- [3] Brekelmans J.W.P.M., H. Evers, 'The Importance of the Design of Joints in Steel Structures', lecture for the STUMICO-meeting, 30 May 2002 at the contractor Ballast Nedam, Nieuwegein, The Netherlands. (in Dutch)

Previous publications from the same authors on this subject:

- [4] Bijlaard F.S.K. and J.W.P.M. Brekelmans, 'Plug and Play Type Joints in Steel and Steel-Concrete Composite Constructions', Proceedings of the 5th International Conference on Advances in Steel Structures (ICASS 2007), 5–7 December 2007, Singapore, Volume I: ADVANCES IN STEEL STRUCTURES – Keynote Lectures, pages 75-83, edited by J.Y. Richard Liew & Y.S. Choo (ISBN: 978-981-05-9371-1).

EVALUATION OF THE RESISTANCE FACTORS OF HIGH-STRENGTH FASTENERS FOR STEEL BUILDING DESIGN

Amy M. Moore

Bridge/Structural Engineer
LJB Inc., Dayton, OH, USA
amoore@LJBinc.com

Gian A. Rassati

University of Cincinnati, Cincinnati, OH, USA
Gian.Rassati@uc.edu

James A. Swanson

University of Cincinnati, Cincinnati, OH, USA
James.Swanson@uc.edu

ABSTRACT

The current resistance factor prescribed in ANSI/AISC 360-05 for structural bolts in tension and shear is 0.75. It is believed that the current resistance factor may be overly conservative and is based on insecurities about consistent strength, ductility, and force distribution rather than on results from statistical analyses. In order to allow for a more economical design of bolted connections, 1533 fasteners in various grades, diameters, and lengths, were tested in tension and shear with threads excluded and not excluded from the shear plane, to provide a more accurate statistical basis for the calculation of resistance factors. Resistance factors were calculated from data reported in literature and from the bolts tested. The results indicated that bolts have consistent strength and that the current resistance factor of 0.75 is overly conservative. Increased values of the resistance factor are recommended for high-strength bolts in tension and shear.

INTRODUCTION

When designing bolted connections, engineers are required to account for only 75% of the structural bolt's tension or shear strength based on Load and Resistance Factor Design (ANSI/AISC, 2005). Since only 75% of the fastener's strength is used in the design of connections, these can be more costly than welded connections, given that a large number of bolts are needed to provide the required capacity. Instead of the current resistance factor of 0.75 being based directly on statistical analyses, it is believed that a conservative value has been prescribed based on a perceived lack of ductility and on insecurities about strength consistency. This is particularly true of A490 fasteners. The main goal of this project is to provide a more accurate statistical basis for the calibration of resistance factors for high-strength fasteners. The primary objective of this research is to recalibrate the current resistance factor, based on

reliability indices and statistical reduction of the results obtained by testing a meaningful statistical population of A325/F1852 and A490/F2280 bolts in both direct tension and shear. Past data on tension and shear of structural bolts was also examined when obtaining the recommended resistance factor.

HIGH-STRENGTH BOLTS TESTED

To make a statistically sound recommendation for a resistance factor, 100 lots of high-strength bolts were obtained. Donations of roughly half of the bolts were sought from domestic manufacturers. The remaining bolts were obtained through local distributors, in order to limit the impact of possible preferential selection by the manufacturers. Based on ASTM standards, it was determined that 5 fasteners needed to be tested from each lot in tension, shear with threads excluded and not excluded, for a total of 15 fasteners per lot, or 1500 bolts total (Moore, 2007).

The bolts tested ranged from 5/8-inch to 1-1/4-inch diameter with lengths up to and including 5 inches. The 100 lots to be tested were divided among the different diameters and between A325/F1852 and A490/F2280 bolts. Since A490/F2280 bolts are perceived to have inconsistent strength and there is a limited amount of data available in literature, a higher number of lots were tested as compared to A325/F1852 bolts. The 3/4-inch to 1-inch diameter fasteners had more lots tested considering they are the most common in practice. All bolts were tested in direct tension and shear according to ASTM specifications.

CALCULATION OF RESISTANCE FACTORS

Load and Resistance Factor Design (LRFD) uses reliability indices and resistance factors and is based on the following general equation comparing a factored resistance to factored loads:

$$\phi R_n \geq \sum_{i=1}^n \gamma_i Q_{im} \quad (1)$$

Resistance factors are a function of the mean and variability of the material and geometric properties, and of the load. In addition, resistance factors take into account “the ability of the equation itself to predict capacity” (Franchuk et al., 2004). Resistance factors can be calculated based on two different equations. The first equation, identified herein as Method 1, is given by (Fisher et al., 1978; Ravindra and Galambos, 1978)

$$\phi = \Phi_{\beta} \frac{R_m}{R_n} e^{-\alpha \beta V_R} \quad (2)$$

and Method 2 is given by (Galambos, 1998)

$$\phi = \Phi_{\beta} \rho_R e^{-\alpha_R \beta V_R} \quad (3)$$

where $\Phi_{\beta} \rightarrow$ adjustment factor, $\alpha = 0.55 \rightarrow$ coefficient of separation, $\beta \rightarrow$ safety index or reliability index, $R_m \rightarrow$ average value of the resistance R of the bolts tested (kips),

$R_n \rightarrow$ nominal resistance (kips), $\rho_R \rightarrow$ bias coefficient for the resistance, $V_R \rightarrow$ coefficient of variation of R_m (Method 1) and of ρ_R (Method 2)

The first three variables defined above are identical between the two different methods. The adjustment factor accounts for the interdependence of the resistance and load factors when the reliability index, β , is not equal to 3.0 (Galambos, 1998). Five different live-to-dead load ratios were considered, from which equations to approximate the adjustment factor in terms of the reliability index were obtained (Moore, 2007). For a live-to-dead load ratio of 1.0, the adjustment factor is given by $\Phi_\beta = 0.0065\beta^2 - 0.1331\beta + 1.3404$ and is given by $\Phi_\beta = 0.0093\beta^2 - 0.1658\beta + 1.4135$ for a live-to-dead load ratio of 3.0 (Moore, 2007). The coefficient of separation, α , accounts for the interdependence of loads and resistance. The reliability index, β , “has a direct correspondence to the probability of failure of a given structural element considering both the variability of loads and resistances; a higher safety index indicates a lower probability of failure, and, hence, a higher level of safety” (Franchuk et al., 2004). For connections, a reliability index equal to 4.5 was chosen in the past (Fisher et al., 1978). However, according to the Commentary to ANSI/AISC 360 (2005), the reliability index for connections is 4.0. Both reliability index values for connections were considered.

In equation (2), R_m is the average of the maximum recorded failure load for each of the bolts tested (in kips). The nominal resistance, R_n , can be calculated in one of two ways for tension. The first model is a simplified approach, identified herein as Model A. ANSI/AISC 360 (2005) obtains the nominal tensile stress values by using 75% of the tensile strength of the bolt material. Therefore, the tensile strength is given by $R_n = F_{nt}A_b = (0.75F_u)A_b$. The ultimate stress, F_u , equals 120 ksi for A325/F1852 bolts and 150 ksi for A490/F2280 bolts. The area, A_b , is the nominal bolt area.

The second model to calculate R_n in tension, identified as Model B, is based on the effective area of a bolt given by $R_n = F_uA_{eff}$. The effective area is a better estimate of the threaded area (Kulak et al., 2001)

$$A_{eff} = \pi/4(d - (0.9743/n))^2 \quad (4)$$

where d is the nominal bolt diameter and n is the number of threads per inch.

The nominal resistance in shear, R_n , is given by the equation $R_n = F_{nv}A_b$ where F_{nv} is the nominal shear strength. The shear strength of the fasteners depends on the location of the shear plane. The strength of a single fastener with the threads excluded from the shear plane is approximately equal to 62% of the tensile strength of the bolt material regardless of the bolt grade: $F_{nv,X} = 0.62F_u$ (Kulak et al., 2001). A fastener with the threads not excluded from the shear plane has a strength approximately equal to 83% of the strength of a fastener with the threads excluded (RCSC, 2004). Thus the strength of a single fastener with the threads not excluded from the shear plane, taking 83% roughly as 80%, is $F_{nv,N} = 0.80(0.62F_u) \approx 0.50F_u$. Therefore, the nominal resistances

in shear for a single bolt with the threads not excluded and excluded from the shear plane are given by equations $R_n = 0.50F_u A_b$ and $R_n = 0.62F_u A_b$, respectively.

For Method 1, the coefficient of variation, V_R , equals the standard deviation divided by the average of the resistance of the bolts tested, R_m .

The bias coefficient, ρ_R , found in Method 2, is the average value of the ratio of the measured to the nominal resistance. The bias coefficient for the resistance is given by $\rho_R = \rho_G \rho_M \rho_P$ where ρ_G , ρ_M , and ρ_P are the bias coefficients for the geometry, material strength, and professional factor, respectively.

For Method 2, equation (3), the coefficient of variation associated with ρ_R is the square root of the sum of the squares of V_G , V_M , and V_P , which are the coefficients of variation of geometry, material strength, and professional factor, respectively.

The bias coefficient for geometry, ρ_G , is the ratio of the average applicable geometric property to the nominal value.

$$\rho_G = \frac{\text{Actual Area}}{\text{Nominal Area}} = \frac{\text{Average}\left(\frac{\pi(d_{avg})^2}{4}\right)}{\left(\frac{\pi(d_{nominal})^2}{4}\right)} = \frac{\text{Average}\left((d_{avg})^2\right)}{(d_{nominal})^2} \quad (5)$$

Before testing, the diameter of a fastener was measured using calipers at five different locations along the shank. The average of these five values is d_{avg} .

The bias coefficient for material strength, ρ_M , is the ratio of the average appropriate material property to the nominal value given in ANSI/AISC 360 (2005).

$$\rho_M = \frac{\text{Actual } F_u}{\text{Nominal } F_u} = \frac{F_{u, exp}}{F_{u, nominal}} \text{ in which } F_{u, exp} = \frac{P_{exp}}{A'_{eff}} \quad (6)$$

where P_{exp} is the experimental load at which the bolt failed in tension and A'_{eff} is given by equation (4) except it is calculated using d_{avg} instead of d . The nominal ultimate stress, $F_{u, nominal}$, equals 120 ksi and 150 ksi for A325/F1852 bolts and A490/F2280 bolts, respectively.

The bias coefficient for the professional factor, ρ_P , is the ratio of the average tested strength, determined experimentally, to the predicted strength, as calculated by a design equation using measured dimensions and material properties.

$$\rho_P = \frac{\text{Actual Strength}}{\text{Predicted Strength}} = \frac{\text{Average}(P_{exp})}{R_n \text{ based on measured values}} \quad (7)$$

The details of the bias coefficient for the professional factor are dependent on whether the bolts were tested in tension or shear. Two models are prevalent for predicting the tensile strength of bolts. The first, identified herein as Model A, is based on the approximation that the effective area is 75% of the nominal area. Using measured dimensions and material properties, the bias coefficient for the professional factor is

$$\rho_P = \frac{\text{Average}(P_{exp})}{0.75A'_b F_{u,exp}} \quad (8)$$

where A'_b is the shank area based on d_{avg} . The second model, identified as Model B, is based on the effective area calculated using the average measured shank diameters,

$$\rho_P = \frac{\text{Average}(P_{exp})}{A'_{eff} F_{u,exp}} \quad (9)$$

Two situations exist in shear, with the threads not excluded or excluded from the shear plane, respectively.

$$\rho_P = \frac{\text{Average}(P_{exp})}{0.50A'_b F_{u,exp}}, \quad \rho_P = \frac{\text{Average}(P_{exp})}{0.62A'_b F_{u,exp}} \quad (10), (11)$$

The value of $F_{u,exp}$ in equations (8) through (11) is determined as in equation (6).

Resistance factors were calculated using the equations previously described based on five different levels of detail. Resistance factors were first calculated for tension or shear based on the diameter and grade of each bolt (Level V). Secondly, resistance factors were calculated for tension or shear based on just the bolt grade (Level IV). Level III calculated resistance factors for tension or shear based on the strength of the bolts, either 120 ksi (A325 and F1852) or 150 ksi (A490 and F2280). Level II calculated one resistance factor for tension and one for shear regardless of the bolt diameter or the bolt grade whereas Level I comprised all of the data from the tension and shear tests to calculate one resistance factor valid for tension and shear.

RESULTS

Tensile Strength Compared to ASTM and RCSC

AISC and RCSC prescribe a minimum strength of 120 ksi for A325 and F1852 bolts regardless of the bolt diameter. A490 and F2280 bolts are specified to have a minimum tensile strength of 150 ksi as well as a maximum tensile strength of 173 ksi per ASTM or 170 ksi per RCSC.

The tensile strength was calculated based on the effective area and was compared to ASTM and RCSC specifications. All of the structural bolts tested in tension had strengths higher than ASTM's specified minimum. It was found that some bolts exceeded RCSC's maximum tensile strength and a few exceeded ASTM's maximum tensile strength. Table 1 summarizes the 515 bolts tested in direct tension.

After testing all A325 and F1852 bolts it was found that their tensile strength was always greater than 120 ksi, regardless of the bolt diameter. Almost 11% of the A490 and F2280 bolts tested in direct tension had a tensile strength greater than the specified RCSC maximum, whereas only about 1% had a tensile strength greater than 173 ksi. Even though some of the A490 and F2280 bolts did not meet the specifications, these

bolts were still included in the data analysis and resistance factor calculations because the manufacturers would have sold these bolts to fabricators and erectors just like they were provided for this research.

Table 1: Tensile Strength of Bolts Tested

Grade	Bolts Tested	Average (Standard Deviation) (ksi)	Minimum & Maximum (ksi)	Bolts (Percent) Greater than 150 ksi	Bolts (Percent) Greater than 170 ksi	Bolts (Percent) Greater than 173 ksi
A325	209	143.23 (6.930)	121.55 156.28	24 (11.48%)	Not Applicable	
F1852	28	148.71 (6.043)	135.46 156.09	13 (46.43%)	Not Applicable	
A325 F1852	237	143.88 (7.046)	121.55 156.28	37 (15.61%)	Not Applicable	
A490	228	163.71 (4.234)	152.06 173.06	Not Applicable	18 (7.89%)	1 (0.44%)
F2280	50	167.92 (3.150)	161.78 179.79	Not Applicable	12 (24.00%)	2 (4.00%)
A490 F2280	278	164.46 (4.367)	152.06 179.79	Not Applicable	30 (10.79%)	3 (1.08%)

Experimental to Nominal Strength

The experimental failure load for bolts tested in direct tension, shear with the threads excluded, and shear with the threads not excluded were compared to the predicted failure load given by the AISC equations. The nominal tensile strength was calculated using $R_n = 0.75F_uA_b$, as well as based on the effective area from equation (4). The nominal strength values for bolts with the threads excluded and not excluded were calculated using $R_n = 0.62F_uA_b$ and $R_n = 0.50F_uA_b$, respectively. The experimental to nominal tensile strength ratios are summarized in Table 2, whereas the experimental to nominal shear strength ratios are summarized in Table 3.

All of the 515 bolts tested in direct tension had a strength of at least 2% greater than the nominal strength specified by AISC. When the nominal strength was based on the effective area, the ratio of experimental tensile strength to nominal strength was 1.01 at a minimum. Comparing the ratio of experimental strength to nominal strength, it can be seen that, on average, the nominal strength calculated with the effective area better predicts the failure load. Since none of the 515 high-strength bolts tested in tension had a tensile strength lower than the nominal strength, it can be concluded that the AISC equation is accurately predicting the tensile strength of structural bolts.

Twenty out of the 512 shear bolts tested with the threads excluded from the shear plane had an experimental to nominal ratio less than one. Therefore, it can be observed that

the AISC equation closely predicts the shear strength with the threads excluded since only 3.9% of the bolts tested were below the AISC nominal value.

Table 2: Experimental/Nominal Ratio for Tension

Grade	Bolts Tested	Experimental/Nominal (Based on AISC)			Experimental/Nominal (Based on Effective Area)		
		Average (St. Dev.)	Minimum & Maximum	Number (Percent) Below	Average (St. Dev.)	Minimum & Maximum	Number (Percent) Below
A325	209	1.22 (0.057)	1.07 1.31	0 (0.0%)	1.19 (0.058)	1.01 1.30	0 (0.0%)
F1852	28	1.26 (0.050)	1.16 1.33	0 (0.0%)	1.24 (0.050)	1.13 1.30	0 (0.0%)
A490	228	1.11 (0.037)	1.02 1.21	0 (0.0%)	1.09 (0.028)	1.01 1.15	0 (0.0%)
F2280	50	1.14 (0.020)	1.10 1.23	0 (0.0%)	1.12 (0.021)	1.08 1.20	0 (0.0%)
All Grades	515	1.17 (0.070)	1.02 1.33	0 (0.0%)	1.14 (0.068)	1.01 1.30	0 (0.0%)

Table 3: Experimental/Nominal Ratio for Shear

Grade	Experimental/Nominal Shear Excluded				Experimental/Nominal Shear Not Excluded			
	Bolts Tested	Average (St. Dev.)	Minimum & Maximum	Number (Percent) Below	Bolts Tested	Average (St. Dev.)	Minimum & Maximum	Number (Percent) Below
A325	208	1.18 (0.058)	1.01 1.29	0 (0.0%)	203	1.12 (0.065)	0.96 1.32	7 (3.4%)
F1852	25	1.22 (0.070)	1.07 1.28	0 (0.0%)	25	1.17 (0.055)	1.06 1.26	0 (0.0%)
A490	228	1.05 (0.039)	0.92 1.15	20 (8.8%)	228	0.99 (0.050)	0.84 1.17	132 (57.9%)
F2280	51	1.07 (0.024)	1.00 1.11	0 (0.0%)	50	1.01 (0.039)	0.89 1.09	23 (46.0%)
All Grades	512	1.11 (0.079)	0.92 1.29	20 (3.9%)	506	1.05 (0.085)	0.84 1.32	162 (32.0%)

As for the bolts in shear with the threads not excluded, 162 had a shear strength below AISC's nominal value. Thus, about a third of the time AISC's equation is over predicting the shear strength of bolts with the threads not excluded.

Strength Comparison

From the bolts tested, the shear strength with the threads excluded from the shear plane was compared to the tensile strength and is shown in Figure 1. The average shear strength with the threads excluded from the shear plane was found to be approximately 60% of the average tensile strength, based on the 100 lots tested, and it is largely independent of the bolt grade. According to Kulak et al. (2001), "the average shear strength is approximately 62% of the tensile strength". It should be noted that the value from Kulak et al. (2001) was determined based on bolts tested in double shear in a tension jig.

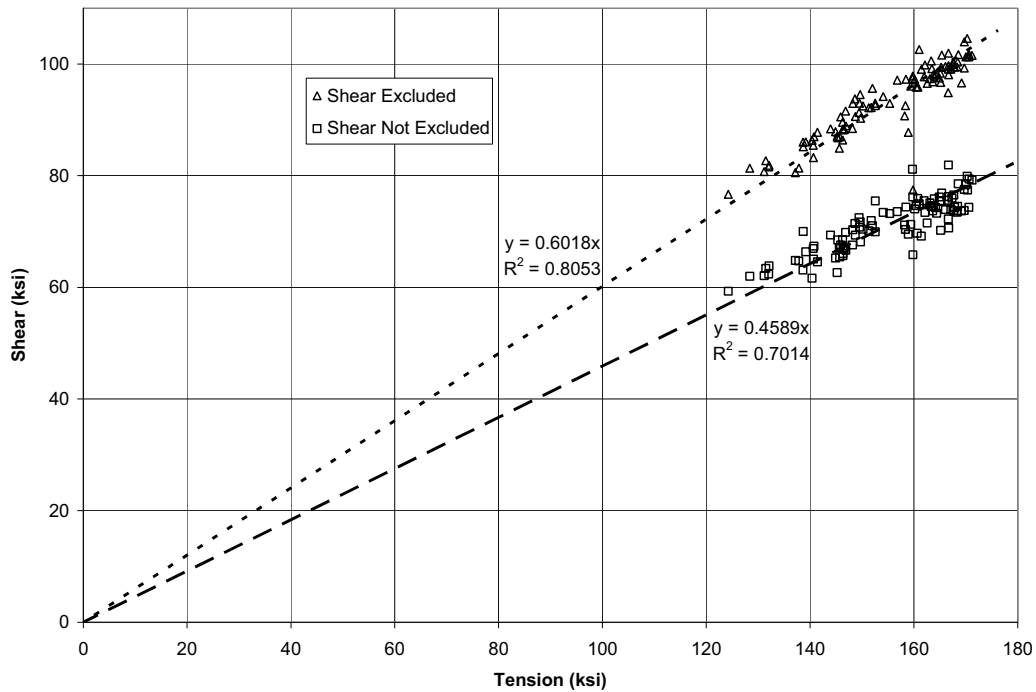


Figure 1: Shear Strength versus Tensile Strength for all Bolt Grades

Figure 1 also reports a comparison between the shear strength with the threads not excluded from the shear plane and the tensile strength for all bolt grades. The average shear strength with the threads not excluded from the shear plane was approximately 76% of the average shear strength with the threads excluded from the shear plane, independently of the bolt grade. From RCSC (2004) a fastener with the threads not excluded from the shear plane had a strength approximately equal to 83% of the strength with the threads excluded, which AISC takes as roughly 80%. It is believed that this value is based on the small amount of data that was available, which results in the difference between the AISC value and the valued obtained from the shear testing. It is worth observing that the ratio of 0.76 is close to the ratio of the area of the threaded portion to the shank area (which AISC takes as 0.75).

RESISTANCE FACTORS

Resistance Factors from Literature

Based on the tests on structural bolts reported in literature, resistance factors were calculated. Table 4 summarizes the total number of bolts which were reported in literature and used for the resistance factor calculations. Enough information was published in literature to use Method 1 for calculating resistance factors for tension and shear. Since the shank diameters were not published, some assumptions needed to be made to calculate the tension resistance factors based on Method 2. Resistance factors for shear could not be calculated based on Method 2 because the equations are

based on the bias coefficient for the material strength, which depends on experimental tensile strength values. Thus, for shear, resistance factors were calculated based on Method 1A only.

Table 4: Number of Bolts Tested and Reported in Literature

Diameter (inches)	Tension				Shear - X		Shear - N	
	A325	F1852	A490	F2280	A325	A490	A325	A490
3/4	116	60	20	-	23	2	3	2
7/8	242 +	20	93 +	14	9	-	3	-
1	38 +	12	29 +	13	10	-	-	-
1 1/8	10 +	-	1 +	-	-	-	-	-
Total	406 +	92	143 +	27	42	2	6	2

Table 5: Literature Resistance Factors - Level I

	$\beta = 4.0$		$\beta = 4.5$	
	L/D = 1.0	L/D = 3.0	L/D = 1.0	L/D = 3.0
Tension 1A	0.847	0.835	0.794	0.778
Shear 1A				
Tension 1B	0.830	0.818	0.778	0.762
Shear 1A				

Resistance factors were calculated with a reliability index equal to 4.5 and 4.0 and an adjustment factor based on a live-to-dead load ratio of 1.0 and 3.0. As shown in Table 4, there were limited shear tests so a resistance factor based on literature may not be statistically valid. There were however numerous tension results performed around the 1960s but the bolts tested were specified to ASTM's minimum strength.

Table 5 summarizes the resistance factors for Level I. Since the ANSI/AISC 360 (2005) does not use the effective area (Method B), the resistance factors calculated using Method 1A for tension should be considered. A resistance factor of 0.80 can be recommended based on the tension and shear strengths in literature, with a reliability index, β , equal to 4.0 and a live-to-dead load ratio of 3.0. A resistance factor of 0.80 for high-strength bolts in tension and shear was also recommended by Fisher et al. (1978).

Resistance Factors from Current Bolt Tests

Resistance factors were calculated based on the equations summarized previously as well as from equations modified using the data obtained after testing. It was found that the shear strength of a single high-strength bolt with the threads excluded from the shear plane is approximately 60% of its tensile strength, regardless of the bolt grade, giving the nominal shear strength for a single bolt as $R_n = 0.60F_uA_b$. The shear strength with the threads not excluded from the shear plane is approximately 76% of the average shear strength with the threads excluded from the shear plane. To reflect these two

new ratios, the nominal shear strength for a single high-strength bolt with the threads not excluded is $R_n = 0.76(0.6F_u A_b) = 0.456F_u A_b \approx 0.46F_u A_b$.

Table 6: Resistance Factors - Level II

		$\beta = 4.0$				$\beta = 4.5$			
		L/D = 1.0		L/D = 3.0		L/D = 1.0		L/D = 3.0	
		AISC	Modified	AISC	Modified	AISC	Modified	AISC	Modified
Tension	Method 1A (0.75A _g)	0.933		0.919		0.878		0.861	
	Method 1B (A _{eff})	0.915		0.902		0.862		0.845	
	Method 2A (0.75A _g)	0.923		0.910		0.868		0.851	
	Method 2B (A _{eff})	0.912		0.899		0.859		0.842	
Shear Excluded	Method 1A	0.870	0.899	0.857	0.886	0.817	0.844	0.800	0.827
	Method 2A	0.878	0.907	0.866	0.894	0.825	0.853	0.809	0.836
Shear NOT Excluded	Method 1A	0.810	0.880	0.798	0.868	0.759	0.825	0.744	0.809
	Method 2A	0.818	0.890	0.807	0.877	0.768	0.835	0.753	0.818

A summary of Level II resistance factors calculated from the 1533 bolts tested using both AISC's equations and the modified shear equations are shown in Table 6 with a reliability index of 4.0 and 4.5 as well as a live-to-dead load ratio of 1.0 and 3.0. It is recommended that a different resistance factor be used for the three types of bolt failure modes, instead of the current single resistance factor. Since AISC does not use the effective area but uses an approximation, the resistance factors based on Method 2A were considered. The Commentary to ANSI/AISC 360 (2005) recommends a reliability index of 4.0 and a live-to-dead load ratio of 3.0. Resistance factors of 0.90, 0.85, and 0.80 are recommended for bolts in tension, shear with the threads excluded and shear with the threads not excluded, respectively. Considering that the resistance factors for shear with the threads excluded and not excluded increase with the modified nominal shear equations, resistance factors of 0.90 and 0.85 are recommended for bolts in tension and shear with both the threads excluded and not excluded, respectively, using the new suggested values in the equations.

CONCLUSIONS

The current resistance factor of 0.75 (ANSI/AISC, 2005) for the tensile and shear strength of structural bolts is believed to be overly conservative. Resistance factors were calculated for the tensile and shear strength based on data obtained from testing and from results published in literature. Based on the resistance factors calculated, it was found that the current resistance factor can be increased without sacrificing safety. With a reliability index of 4.0 and a live-to-dead load ratio of 3.0, resistance factors of 0.90, 0.85, and 0.80 are recommended for bolts in tension, shear with the threads

excluded, and shear with the threads not excluded from the shear plane, respectively. The lower resistance factor for shear with the threads not excluded from the shear plane is a result of the nominal failure load by AISC over predicting the failure load compared to the experimental tests.

If the ratios of the shear strength with the threads excluded and not excluded to the tensile strength, obtained as part of this research, are incorporated into the AISC equations for the nominal shear strength, higher resistance factors are recommended. Based on a reliability index of 4.0 and a live-to-dead load ratio of 3.0, resistance factors equal to 0.90 for tension and 0.85 for shear (both with the threads excluded and not excluded from the shear plane) are recommended.

ACKNOWLEDGEMENTS

This study was sponsored by The Research Council on Structural Connections (RCSC). Thanks should also be extended to Owen Bower, Jeremy Hildebrand, Jonathan Oltman, and Aaron Taylor who offered their time to help with testing.

REFERENCES

- ANSI/AISC 360-05 (2005), Specification for Structural Steel Buildings, 13th Ed., AISC.
- Fisher, J. W., Galambos, T. V., Kulak, G. L. and Ravindra, M. K. (1978) "Load and Resistance Factor Design Criteria for Connectors," *Journal of the Structural Division, ASCE*, 104(9).
- Franchuk, C. R., Driver, R. G., and Grondin, G. Y. (2004) "Reliability Analysis of Block Shear Capacity of Coped Steel Beams," *Journal of Structural Engineering, ASCE*, 130(12).
- Galambos, T. V. (1998). Guide to Stability Design Criteria for Metal Structures, 5th Ed., John Wiley and Sons, Inc., New York.
- Kulak, G. L., Fisher, J. W., and Struik, J. H. A. (2001). Guide to Design Criteria for Bolted and Riveted Joints, 2nd Ed., American Institute of Steel Construction, Inc., Chicago.
- Moore, A. (2007) "Evaluation of the Current Resistance Factors for High-Strength Bolts," MS Thesis, Department of Civil Engineering, University of Cincinnati, Ohio.
- Ravindra, M. K. and Galambos, T. V. (1978) "Load and Resistance Factor Design for Steel," *Journal of the Structural Division, ASCE*, 104(9).
- RCSC, 2004, Specification for Structural Joints Using ASTM A325 or A490 Bolts, Research Council on Structural Connections.

EXPERIMENTAL RESEARCH ON BOLTED JOINTS IN HIGH STRENGTH STEEL MEMBERS

Dieter Ungermann and Stephan Schneider
Dortmund University of Technology, Institute of Steel Construction,
August – Schmidt – Straße 6, 44227 Dortmund, Germany
stahlbau@tu-dortmund.de

ABSTRACT

The design rules given in Eurocode 3, part 1-8 (CEN, 2005) for the shear and bearing resistance of a group of fasteners base on theoretical investigations and extensive tests with mild steels (steel grade S235 and S355). Due to the ductility of mild steels, a group of fasteners in a shear loaded connection can achieve a full plastic distribution of the internal forces. The reduced ductility of high strength steel (HSS) in comparison to mild steels raises the question about the required deformation capacity to achieve a uniformly distribution of the internal forces in a shear loaded connection in the ultimate state. In order to answer this question, an experimental program on shear loaded connections with a group of three fasteners in one row was preformed in the course of a German research project. According to Eurocode 3, part 1-12 (CEN, 2007), that includes additional application rules for steel grades up to S700, steel grade S690 have been used. The present paper gives an overview of the results of the research project.

1. INTRODUCTION

1.1 Cause and subject of the research project

There is a tendency in the modern steel industry towards the increased use of high strength steels (HSS) in civil engineering constructions. The higher yield stress of HSS allows a reduced material usage and improves the economical efficiency of steel constructions. But these economic advantages can only be utilized, if secured design rules exist, which allow the usage of HSS in building construction. With the publication of Eurocode 3, part 1-12 a specific standard is available on an international basis, which permit the use of HSS up to steel grade S700.

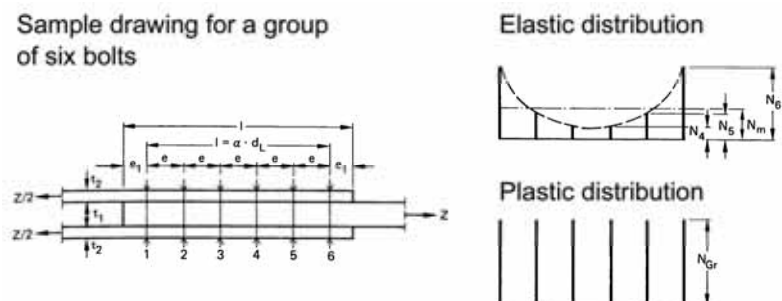


Figure 1.1: Distribution of the internal forces in a shear loaded connection

Due to the ductility of mild steels, a group of fasteners in a shear loaded connection could achieve a full plastic distribution of the internal forces, Figure 1.1. The reduced ductility of HSS raises the question whether or not a group of fasteners in HSS could achieve a uniformly distribution of the internal forces in a shear loaded connection in the ultimate state and if the design rules given in EC3, part 1-8 are adequate for bolted connections in HSS.

In order to answer this question, an experimental test program on shear loaded connections with a group of three fasteners and addition theoretical and numerical investigations was carried out at the Institute of Steel Construction, TU Dortmund.

1.2 Design resistance of fasteners according to Eurocode 3, part 1-8

According to Eurocode 3, part 1-8, Table 3.4 the shear and bearing resistance of a single bolt could be calculated as follows:

Shear resistance $F_{v,Rd}$:

$$F_{v,Rd} = \frac{\alpha_v \cdot f_{ub} \cdot A}{\gamma_{M2}} \quad (1.1)$$

Bearing resistance $F_{b,Rd}$:

$$F_{b,Rd} = \frac{k_1 \cdot \alpha_b \cdot f_u \cdot d \cdot t}{\gamma_{M2}} \cdot \beta \quad (\beta = 1,0 \text{ normal sized holes}) \quad (1.2)$$

where the coefficient k_1 and α_b are determined as:

$$k_1 = \begin{cases} \min(1,4 \cdot p_2/d_0 - 1,7; & 2,5) \\ \min(2,8 \cdot e_2/d_0 - 1,7; & 2,5) \end{cases} \quad (1.3)$$

$$\alpha_b = \min(\alpha_d; f_{ub}/f_u; 1,0) \quad \text{where: } \alpha_d = \begin{cases} p_1/(3 \cdot d_0) - 0,25 \\ e_1/(3 \cdot d_0) \end{cases} \quad (1.4)$$

Design resistance for a group of fasteners:

If the shear resistance of each individual fastener is greater or equal than its bearing resistance, the bearing resistance of the connection can be taken as the sum of the bearing resistances of the individual fasteners. Otherwise the design resistance of a group of fasteners should be calculated as the number of fasteners multiplied by the smallest design resistance of any of the individual fasteners.

Additionally for the consideration of the shear resistance of long joints:

$$F_{v,Rd}^{red} = \frac{\alpha_v \cdot f_{ub} \cdot A}{\gamma_{M2}} \cdot \beta_{LF} \quad \text{where: } \beta_{LF} = 1 - \frac{L_j - 15 \cdot d}{200 \cdot d} \begin{cases} \leq 1,00 \\ \geq 0,75 \end{cases} \quad (1.5)$$

According to Eurocode 3, part 1-12 equation (1.1) – (1.5) can be used for bolted joints in HSS. The statistical evaluation of the design rules and safety factors for mild steels were carry out on the basis of a great amount of test data.

The design resistance of a net section according to Eurocode 3, part 1-12 must not exceed:

$$N_{t,Rd} = \frac{0,9 \cdot A_{net} \cdot f_u}{\gamma_{M12}} \quad (1.6)$$

2. EXPERIMENTAL RESEARCH

2.1 Material properties and test program overview

The experimental program consisted of three different test series predicting bolt shear failure (VA – series) on the one hand and bearing failure (VL / VLI – series) on the other hand as the decisive failure mode, Table 2.1. All test specimen have three bolts M12 using bolt classes 10.9 and 12.9.

Table 2.1: Test series and predicted failure mode

Test series	No. of tests	Predicted failure mechanism	Material	
			Steel plates	Bolt class
VA – Series	4	Bolt shear failure	DILLIMAX690T	10.9 / 12.9
VL – Series	11	Bearing failure	DILLIMAX690T	10.9 / 12.9
VLI – Series	2	Bearing failure, imperfect joint	DILLIMAX690T	12.9

All steel plates used for the investigations are made of DILLIMAX 690, which is a high strength quenched and tempered, fine grained steel. The mechanical properties are achieved by water quenching followed by tempering. DILLIMAX 690 fulfils the requirements of EN 10025, part 6, Table 2.2

Table 2.2: Chemical compositions DILLIMAX 690 (material data sheet Dillinger Hütte)

	C	Si	Mn	P	S	Cr	Ni	Mo	V / Nb	B
DILLIMAX 690T	≤ 0,18	≤ 0,50	≤ 1,60	≤ 0,02	≤ 0,01	≤ 1,50	≤ 1,80	≤ 0,60	≤ 0,10	≤ 0,004

The mechanical properties of the steel plates and the bolts used in the test program where measured in coupon tests, Table 2.3.

Table 2.3: Mechanical properties

	f_u [N/mm ²]	f_y [N/mm ²]	E [N/mm ²]	A [%]
DILLIMAX690T	830	780	205.000	14
Bolt class 10.9	1.092	983	210.000	9
Bolt class 12.9	1.265	1.139	210.000	9

The end distance e_1 and the hole spacing p_1 were varied between:

$$1,00 \leq e_1 / d_0 \leq 3,00 \quad \text{and} \quad 2,20 \leq p_1 / d_0 \leq 3,75$$

Due to the results from the single bolt tests at the TU Delft (Bijlaard et. al., 2005) the smallest end distance $e_1 = 1,0d_0$ was used for the test specimen. This is below the minimum end distance $e_1 = 1,2d_0$ according to the design rules given in Eurocode 3, part 1-8. The end distance $e_1 = 3,0d_0$ and the hole spacing $p_1 = 3,75d_0$ leads to maximum bearing resistance according to equation (1.2).

To avoid net section failure the edge distance e_2 perpendicular to the force direction for all test specimen was chosen greater than $e_2 \geq 1,5d_0$, so that the coefficient determined using clause (1.3) became $k_1 = 2,5$ for all test specimen. Table 2.4 shows the nominal geometry for all test specimen.

Table 2.5: Summary of the resistance according to Eurocode 3 and test results

Test. No.	Resistance acc. to EC3-1-8 and EC3-1-12					Test results			Failure mode
	$N_{t,R}$ [kN]	$F_{b,R, end bolt}$ [kN]	$F_{b,R, inner bolt}$ [kN]	$F_{b,R}$ [kN]	$F_{v,R}$ [kN]	F_u [kN]	$F_{R,min}$ [kN]	$F_{R,min} / F_u$ [%]	
1 VA-120-220-231	517	155	188	530	445	454,7	$F_{v,R} = 445$	102,2%	bolt shear
2 VA-300-375-231	528	377	380	1138	445	445,0	$F_{v,R} = 445$	100,0%	bolt shear
3 VA-12.9-120-220-231	538	149	179	506	515	508,7	$F_{v,R} = 515$	98,8%	bolt shear
4 VA-12.9-300-375-231	528	369	370	1109	515	516,7	$F_{v,R} = 515$	100,3%	bolt shear
5 VL-100-220-385	464	57	88	234	438	297,2	$F_{b,R} = 234$	127,0%	bearing
6 VL-120-220-385	459	71	86	244	438	313,8	$F_{b,R} = 244$	128,6%	bearing
7 VL-120-270-385	453	73	116	304	438	344,6	$F_{b,R} = 304$	113,4%	bearing
8 VL-180-270-385	453	104	115	335	438	384,5	$F_{b,R} = 335$	114,8%	bearing
9 VL-240-320-385	456	140	143	426	438	431,7	$F_{b,R} = 426$	101,3%	bolt shear / bearing
10 VL-300-375-385	453	175	175	525	438	441,7	$F_{v,R} = 438$	100,8%	bolt shear
11 VL-12.9-120-220-385	466	71	87	244	515	309,4	$F_{b,R} = 244$	126,8%	bearing
12 VL-12.9-120-270-385	462	71	117	305	515	362,3	$F_{b,R} = 305$	118,8%	bearing
13 VL-12.9-180-270-385	467	107	117	342	515	408,4	$F_{b,R} = 342$	119,4%	bearing
14 VL-12.9-240-320-385	465	142	146	434	515	478,4	$F_{b,R} = 434$	110,2%	bearing
15 VL-12.9-300-375-385	462	177	177	532	515	485,1	$N_{t,R} = 462$	105,0%	net section
16 VLI-12.9-240-320-385	474	144	147	438	515	468,3	$F_{b,R} = 438$	106,9%	bearing
17 VLI-12.9-300-375-385	463	177	177	531	515	491,0	$N_{t,R} = 463$	106,0%	net section

■ $F_{R,min}$; minimal resistance acc. to EC3-1-8 / EC3-1-12

2.2.1 VA – Series, bolt shear failure

The test results of the VA – series, with bolt shear as predicted failure mode, matches the shear resistance according to Eurocode 3, part 1-8, irrespective of the end and pitch distances and the bolt class, very well, Figure 2.2.

In every test of the VA – series the shear plane passes through the unthreaded portion of the bolts. The small deviation between the design resistance and the test results show that the coefficient $\alpha_v = 0,6$ according to clause (1.1) can also be used for bolt class 12.9.

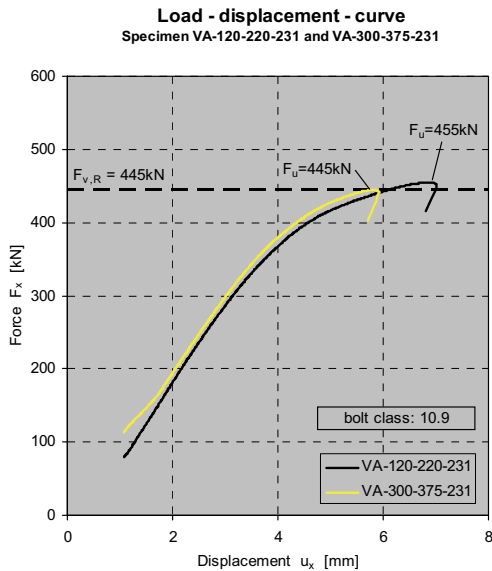


Figure 2.2: Load – displacement – curve for bolt class 10.9 and deformed bolts

The bearing deformations of the test specimen are negligible and only noticeable at the end hole. Contradictory, the shear deformation of the bolt shanks was significantly higher, Figure 2.2. These is mainly caused by the small test rate of $v = 0,008\text{mm/s}$ which was used in every test.

The effect of the length of the joint for $L_j > 15d$ according to clause (1.5) was not investigated in the test program. Additional numerical investigations on bolted joints with 5 bolts in a row, showed no negative effects.

2.2.2 VL / VLI – Series, bearing failure of the steel plates

The comparison of the design resistances, calculated on basis of a plastic distribution of the internal forces according to Eurocode 3, part 1-8, with the test results of the VL – and VLI – series, shows that all test results were on the save side, Table 2.5. The test specimen with small end and pitch distances has significant reserves up to 27% in comparison to the Eurocode 3, part 1-8 design resistance. With increasing end and pitch distances the differences between the design resistances and the test results decreases, Figure 2.3, left side.

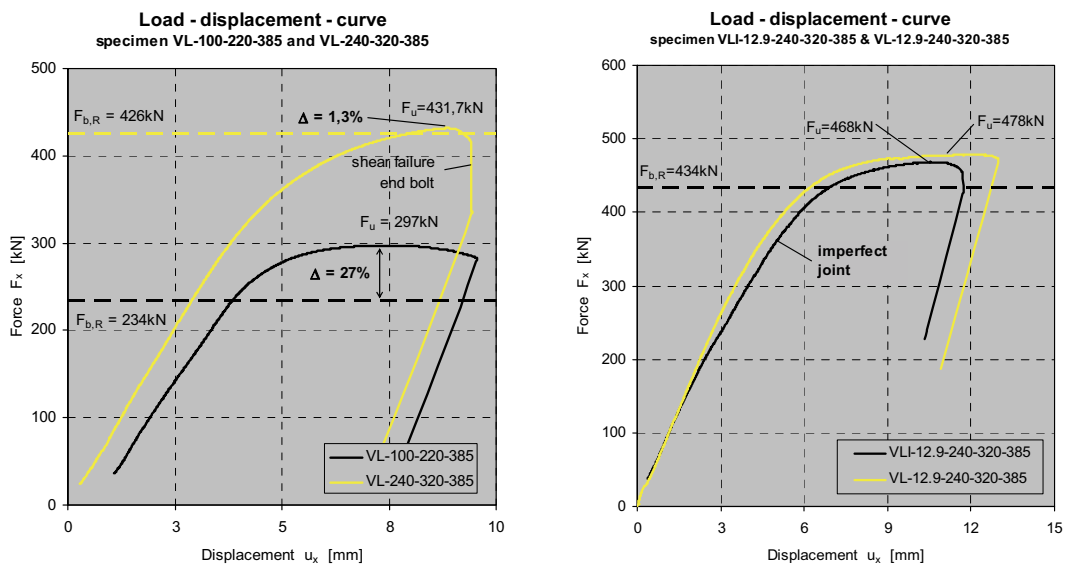


Figure 2.3: Load – displacement – curves from the VL- and VLI-Series

Therefore the deformation capacity of HSS is sufficient to achieve a full plastic distribution in bolted joints with three bolts in a row. This applies even for imperfect bolted joints with normal sized holes, as shown in the VLI - series, Figure 2.3, right side.

Imperfect bolted joints using oversized holes, which requires a significant high deformation capacity in comparison to normal sized holes, could lead to an overestimated bearing resistance, as shown in additional numerical investigations.

The reserves for small end and pitch distances are located at the inner bolts. This can be deduced from the failure modes of the test specimen. All specimen with small end distances $e_1 \leq 1,80d_0$ showed a crack in the steel plate at the end bolt and

therefore its load capacity decreases. Contradictory, the specimen with end distances $e_1 \geq 2,40d_0$ show only the beginning of a reduction in area, Figure 2.4. The numerical investigations support this assumption, Figure 3.2.



Figure 2.4: Pictures from specimen of the VL – und VLI - series

The correction of the proposal was made in the $\alpha_d = p_1 / (3 \cdot d_0) - 0,25$ -factor from clause (1.4), which takes accounts of the pitch distance in the formula for the bearing resistance according to Eurocode 3, part 1-8.

Due to the limited number of tests with small end and pitch distances there is no sufficient bases for a statistical evaluation, so that the correction factor C was calculated based on the ultimate load from the tests with $e_1/d_0 \leq 1,2d_0$ and $p_1/d_0 \leq 2,2d_0$ according to clause (2.1):

$$C = \frac{1/2 \cdot (F_u - F_{b,R,end\ bolt}^{EC3})}{F_{b,R,inner\ bolt}^{EC3}} \quad (2.1)$$

The evaluation of test – No. 5, 6 and 11 provides $C = 1,382$ and therefore:

$$k_1 = \left(\frac{p_1}{3d_0} - \frac{1}{4} \right) \cdot C = \left(\frac{0,46 \cdot p_1}{d_0} - 0,345 \right) \quad (2.2)$$

taking the coefficients k_1 and α_b as follows:

$$\underbrace{\kappa_m = \frac{k_1}{3} \cdot \left(\frac{e_1}{3d_0} + \frac{2p_1}{3d_0} - \frac{1}{2} \right)}_{\text{EC 3-1-8 standard}} \quad \underbrace{\kappa_m^* = \frac{k_1}{3} \cdot \left(\frac{e_1}{3d_0} + \left(\frac{2p_1}{3d_0} - \frac{1}{2} \right) \cdot C \right)}_{\text{EC3-1-8 modified for HSS}} \quad (2.3a) / (2.3b)$$

$$F_{b,R} = \kappa_m \cdot f_u \cdot d \cdot t \quad F_{b,R}^{HSS} = \kappa_m^* \cdot f_u \cdot d \cdot t \quad (2.4a) / (2.4b)$$

using the bearing resistance according to clauses (2.4a) and (2.4b) allows the comparison of Eurocode 3 design resistance and the proposal modification with the test results, Figure 2.5.

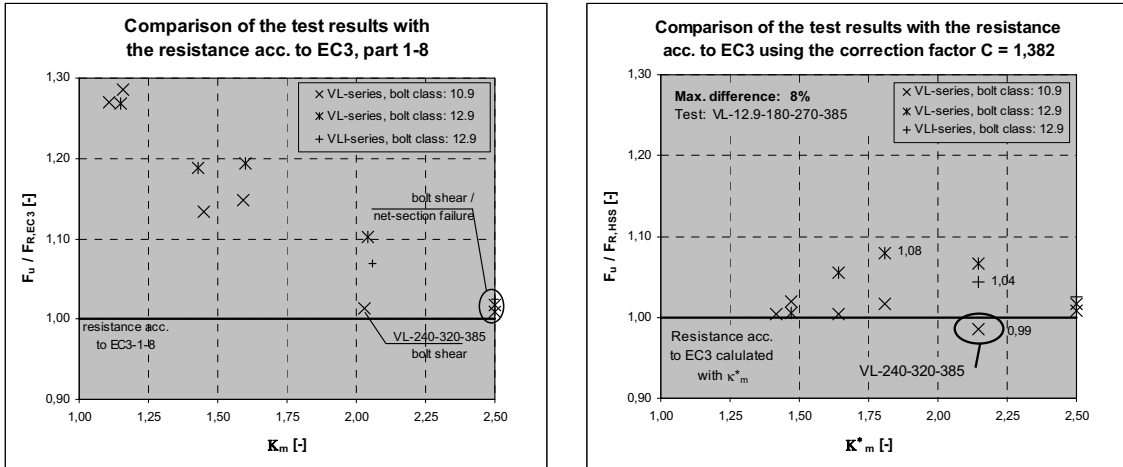


Figure 2.5: Comparison of the test results with EC3-1-8 and the proposal modification

The proposal modification shows a better accordance with the test results with deviations up to 8%. To verify the proposal modification for the α_d coefficient comparative numerical analysis were performed using the finite element method.

3. COMPARATIVE NUMERICAL INVESTIGATIONS

Comparative numerical investigations using the finite element method were performed using the FE –Software Ansys 10.0. Using symmetry – options one quarter of the bolted joint was modeled by 3D solid elements and contact elements for the interfaces between bolt shank and the steel plates. The FE – model was calibrated on the test results, Figure 3.1 and shows good agreement.

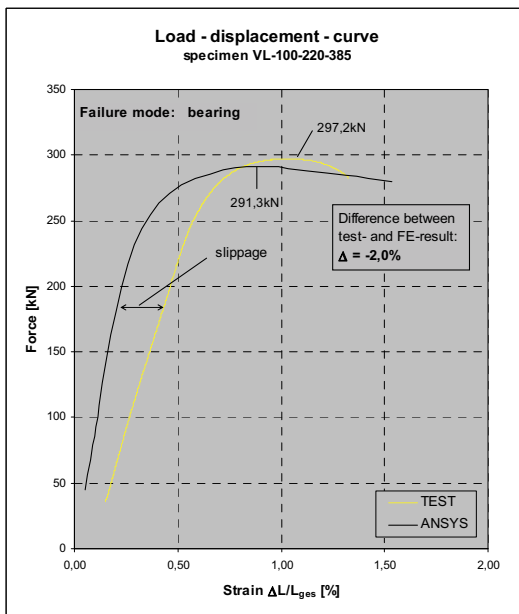


Figure 3.1: Comparison of the load – displacement – curves (FEM and test)

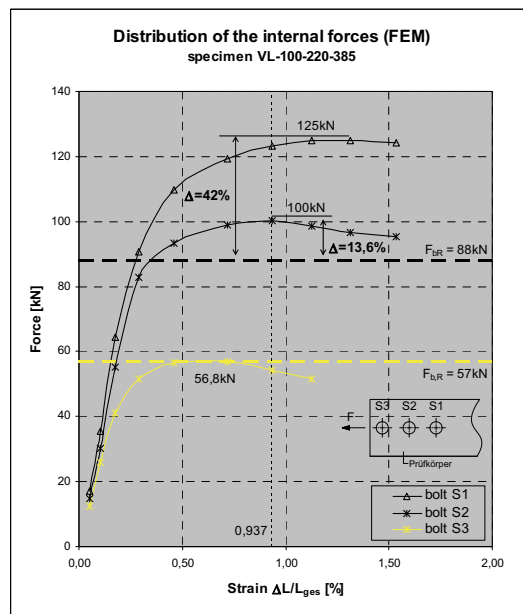


Figure 3.2: Distribution of the internal forces for test – No. VL-100-220-385

An initial parameter study (Study A) showed that the extensional stiffness has no significant effect on the distribution of the internal forces within the end and pitch distances according to the scope given in Eurocode, part 1-8.

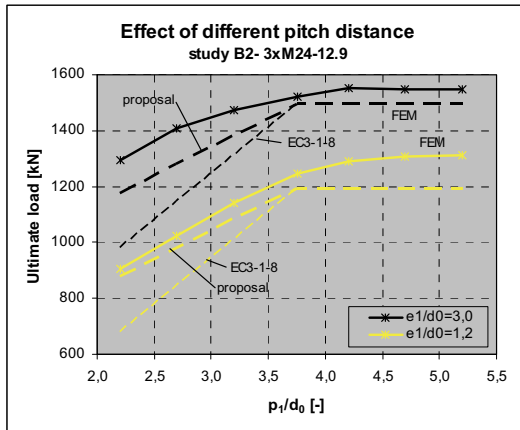


Figure 3.3: FE – results for different pitch distances

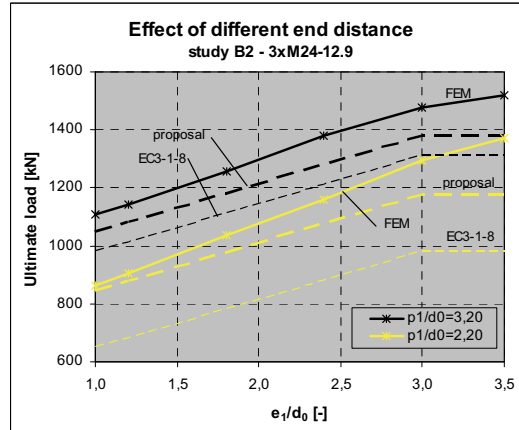


Figure 3.4: FE – results for different end distances

With Study B, where the end and pitch distance were varied between:

$$1,00 \leq e_1/d_0 \leq 3,50 \quad \text{and} \quad 2,20 \leq p_1/d_0 \leq 5,20$$

The proposal modification was verified for bolts M12-12.9 and M24-12.9. With the exception of bolted joints with small end distances and pitch distances above $p_1 > 3,75d_0$, where the design resistance according to Eurocode 3 could overestimate the ultimate load, confirm the FE – results the proposed modification, Figure 3.3. Furthermore, the FE – results shows that the design resistance according to Eurocode 3, part 1-8 is slightly conservative for end distances $e_1 > 3d_0$, Figure 3.4.

4. CONCLUSIONS

The experimental and numerical studies have shown that the HSS up to steel grade S690 has a sufficient deformation capacity to achieve a full plastic distribution of the internal forces in a bolted joint with three bolts in row.

The shear resistance according to Eurocode 3, part 1-8 matches the test results very well. The small deviation between the shear resistance and the test results show that the coefficient $\alpha_v = 0,6$ according to clause (1.1) can also be used for bolt class 12.9.

The bearing resistance according to Eurocode 3, part 1-8 is conservative for small end and pitch distances. The load reserves are located at the inner bolts and could be activated by the proposed modification for the α_d coefficient, Figure 4.1.

The minimum value for the end distance e_1 can be reduced to $e_1 = 1,0d_0$ for bolted joints in high strength steel. For end distances $e_1 > 3,0d_0$ the numerical investigation show a slightly conservative bearing resistance.

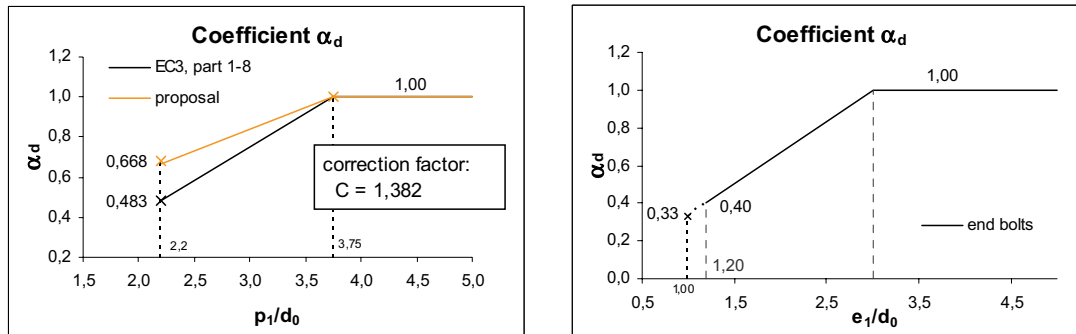


Figure 4.1: Coefficient α_d for the end bolt and the inner bolts

Bolted joints with $e_1 \leq 1,20d_0$ and $p_1 \geq 3,75 d_0$ should be avoided, because the design resistance according to Eurocode 3, part 1-8 could overestimate the ultimate load of the connection.

However, to include the results of the research project in Eurocode 3, part 1-12 further investigations on bolted joints in high strength steel are necessary, in particular bolted joints with more than three bolts in a row.

5. ACKNOWLEDGEMENTS

The research work was performed in the course of a German research project with the financial support of the FOSTA (www.fosta.de) and will be summarized in the report number P742, published by the FOSTA.

6. REFERENCES

- CEN (2005) Eurocode 3, *Design of steel structures – Part 1-8: Design of joints*; German version EN 1993-1-8:2005
- CEN (2007) Eurocode 3, , *Design of steel structures – Part 1-12: Additional rules for the extension of EN 1993 up to steel grades S700*; German version EN 1993-1-12:2007
- Aalberg, A., Larsen, P.K. (2001), Bearing strength of bolted connections in high strength steel. Nordic Steel Construction Conference 2001. Helsinki. Editors Makelainen et al.
- Bijlaard, F.S.K., de Freitas, S.T., de Vries, P. (2005), *Experimental research of single bolt connections for high strength steel S690*. V Congresso de Constructao Metálica e Mista. Lisboa 2005
- Moze, P., Beg, D., Lopatic, J. (2006): *Ductility and strength of bolted connections made of high strength steel S690*. Proceedings of the international conference in metal structures, Poiana Brasov, Romania, September 2006
- Puthli, R., Fleischer, O. (2001), *Investigations on bolted connections for high strength steel members*. Journal of Constructional Steel Research, Elsevier, 2001, pp. 313-326

PERFORMANCE OF THE UNIFIED BLOCK SHEAR EQUATION FOR ATYPICAL FAILURE PATHS

Qing Cai

University of Alberta, Edmonton, AB, T6G 2W2, Canada
qcai@ualberta.ca

Robert G. Driver

University of Alberta, Edmonton, AB, T6G 2W2, Canada
rdriver@ualberta.ca

ABSTRACT

Failure modes such as bolt tear-out and the so-called alternate block shear path observed in Tees are closely related to the classical block shear limit state, but they have not been addressed clearly in current design standards in North America. In previous work conducted at the University of Alberta, a unified block shear equation was proposed that provides accurate test-to-predicted block shear capacity ratios and results in consistent safety indices over a variety of connection types. This paper verifies that the unified equation also works well for failure modes that have atypical failure paths. A total of 104 specimens that failed in bolt tear-out and 14 Tees that failed on the alternate block shear path are considered from the literature, along with 12 new bolt tear-out tests conducted as part of this research program. It is shown that the unified block shear equation provides accurate and consistent results for these failure modes as well.

INTRODUCTION

Block shear is a well-documented failure mode that can occur in connections when a block of material in the connected region is displaced due to tension fracture on one plane of the block perimeter in combination with shear on one or more others. Bolt tear-out and alternate block shear failure can be considered block shear failures with atypical failure paths and this paper investigates the suitability of different methods of predicting block shear capacity specifically for these modes.

Bolt tear-out failure occurs by shear tearing along the two planes adjacent to the bolt hole and there is no tension fracture in the block of material due to the presence of the hole. This path is illustrated in Figure 1(a). Bearing is a closely related failure mode and is considered to constitute failure by the excessive deformation of material behind the bolt. If connection deformation is not a design consideration, the ultimate strength of a connection with relatively small end distances and pitches would generally be governed by bolt tear-out instead of bearing.

A failure mode observed by Epstein and Stamberg (2002) in Tees connected by bolts through the flange only, which was termed “alternate block shear” failure by the researchers, is depicted in Figure 1(b). This failure mode is similar to traditional block shear except that it has only one shear plane in the Tee stem and tension fracture involves the entire flange.

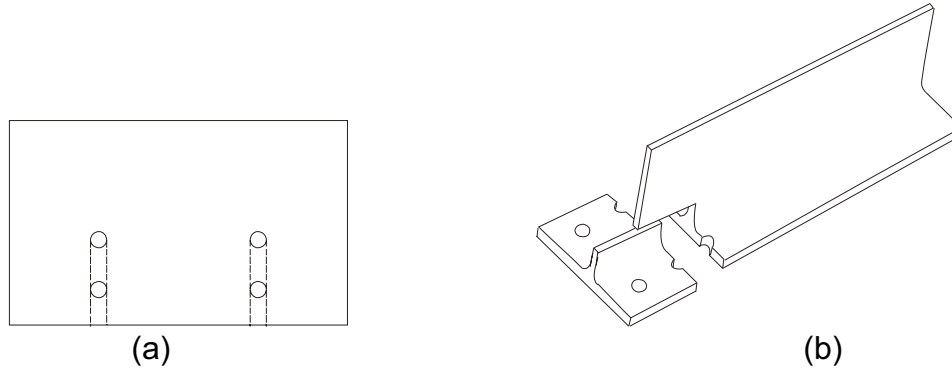


Figure 1. Failure Paths Considered: (a) Bolt Tear-out; (b) Alternate Block Shear Path in Tees

DESIGN EQUATIONS

CSA-S16-01 and AISC 2005

The provisions in the current North American design standards, CSA-S16-01 (CSA, 2001) and the AISC Specification (AISC, 2005), for predicting the block shear capacity of tension members with concentrically loaded blocks are essentially identical. The block shear capacity is taken as the lesser of:

$$P_r = \phi A_{nt} F_u + 0.60 \phi A_{gv} F_y \quad (1)$$

$$P_r = \phi A_{nt} F_u + 0.60 \phi A_{nv} F_u \quad (2)$$

Equation (1) applies when the net tension area, A_{nt} , reaches the ultimate tensile strength, F_u , and the gross shear area, A_{gv} , reaches the shear yield strength, $0.6F_y$. This phenomenon has been observed by many researchers (e.g., Franchuk. *et al.*, 2003). However, Equation (2), representing the development of the ultimate capacities of both the net tension area and net shear area, A_{nv} , is not supported by test observations. On the contrary, experimental evidence (e.g., Huns *et al.*, 2002) indicates that tension fracture occurs well before shear fracture and although the shear yield stress is exceeded, the ductility of material in tension is inadequate to allow the ultimate shear strength to be reached concurrently with the ultimate tensile strength.

There is no equation in the current design standards in North America given explicitly for bolt tear-out failure, although design equations for block shear can be used, as shown, for instance, in a design example in the CISC Handbook of Steel Construction (CISC 2006). This approach is clearly based on the assumption that bolt tear-out is a type of block shear. In this case, Equations(1) and (2) become (the lesser of):

$$P_r = 0.60\phi A_{gv} F_y \quad (3)$$

$$P_r = 0.60\phi A_{nv} F_u \quad (4)$$

Unified Equation

Based on a large number of experimental results from the literature, Kulak and Grondin (2001) observed that equations existing at that time were inconsistent in predicting the capacities of connections failing in block shear. To address this deficiency, Driver *et al.* (2006) proposed a single unified block shear equation that has been shown to provide excellent results for a variety of member and connection types failing in block shear. It represents the observation from tests that rupture on the net tension area occurs well after yielding has taken place on the gross shear plane, but prior to shear rupture. The effective shear stress in the unified equation is taken as the average of the shear yield and shear ultimate stresses to reflect this fact. For tension members with symmetrical blocks, it takes the following form (with $\sqrt{3}$ reflecting the von Mises criterion):

$$P_r = \phi A_{nt} F_u + \phi A_{gv} \left(\frac{F_y + F_u}{2\sqrt{3}} \right) \quad (5)$$

The unified block shear equation can be used for bolt tear-out simply by eliminating the tension component:

$$P_r = \phi A_{gv} \left(\frac{F_y + F_u}{2\sqrt{3}} \right) \quad (6)$$

It is postulated that the unified block shear equation can be adopted for a truly unified equation that is also suitable for predicting bolt tear-out failure. It is investigated herein for use with this mode, as well as for the alternate block shear path in Tees.

PREVIOUS RESEARCH

Although many bolt tear-out tests have been conducted on very high strength steels, due to their demonstrably different behaviour, this study focuses on common grades of steel with yield strengths no greater than 550 MPa. Considering these grades only, Udagawa and Yamada (1998) conducted 146 tests on plates, and 31 of them failed by bolt tear-out. For these 31 tests, the number of bolt lines in the direction of the applied load was one or two, while the number of bolt rows in the direction perpendicular to the applied load varied from two to four. Kim and Yura (1999) carried out 19 tests on plates with one or two bolts in a single line parallel to the applied load and all of the tests failed by bolt tear-out. Aalberg and Larsen (2001, 2002) used the connection configurations of Kim and Yura (1999) and tested eight one-bolt connections and 12 two-bolt connections, and all specimens failed by bolt tear-out. Puthli and Fleischer (2001) completed 25 tests on plates that had two bolts in a row perpendicular to the applied load, and nine of them failed in the bolt tear-out mode. Rex and Easterling (2003) conducted 46 single bolt bearing tests, and 20 plates ultimately failed by bolt tear-out.

Udagawa and Yamada (2004) carried out 42 tests on web-connected channel sections, and five of them failed by bolt tear-out. All five specimens had one bolt line in the web, and the number of bolts varied from two to four.

Epstein and Stamberg (2002) conducted 50 tests on flange-connected Tees cut from two different wide-flange shapes. Fourteen of them failed along the alternate block shear path.

There is a significant number of flat plate tests reported in the literature for which bolt tear-out is the ultimate failure mode. Conversely, only a very small number of tests were conducted on shapes. Furthermore, most connection configurations tested do not meet the minimum end distance and bolt spacing requirements specified in North American design standards, and only have either one or two bolts. Table 1 presents the number of tests from eight different research projects and the number of tests that meet each of Criteria A and B, as described in the table.

Table 1. Bolt Tear-Out Tests from Previous Research

Author (Year)	Section Type	Number of Tests			Mean T/P Ratio Criterion "A" (COV)	
		Total	Criterion A ^a	Criterion B ^b	S16-01/ AISC 2005	Unified Equation
Udagawa and Yamada (1998)	Plate	31	0	31	—	—
Kim and Yura (1999)	Plate	19	9	19	1.24 (0.14)	0.95 (0.13)
Aalberg and Larsen (2001, 2002)	Plate	20	10	20	1.17 (0.13)	0.98 (0.12)
Puthli and Fleischer (2001)	Plate	9	0	9	—	—
Rex and Easterling (2003)	Plate	20	11	20	1.21 (0.07)	0.99 (0.08)
Udagawa and Yamada (2004)	Channel	5	0	5	—	—
Epstein and Stamberg (2002)	Tee	14	14	14	1.08 (0.09)	1.05 (0.09)

a. Tests that meet the minimum end distance and bolt spacing requirements specified in North American design standards ($F_y \leq 550$ MPa).

b. Includes tests that do not meet the minimum end distance and bolt spacing requirements specified in North American design standards ($F_y \leq 550$ MPa).

EXPERIMENTAL PROGRAM

The bolt tear-out experimental program conducted as part of this research included 12 specimens that were connected through the web only, using three different wide-flange CSA-G40.21 Grade 350W steel sections. The three main variables were the gauge (G), number of bolt rows (R), and end distance (E). The connection dimensional parameters are shown in Figure 2 and the associated measured values are listed in Table 2.

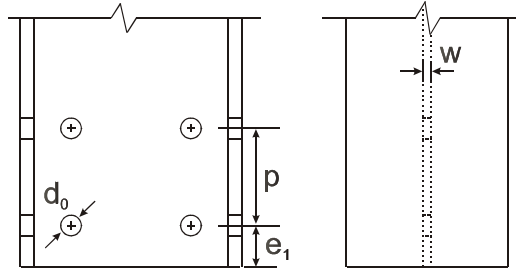


Figure 2. Connection Dimensional Parameters

Table 2. Measured Web Connection Dimensions

Specimen	Section	Hole Diameter d_0 (mm)	Web Thickness w (mm)	End Distance e_1 (mm)	Pitch p (mm)
A1G1	W310×60	20.62	7.48	28.30	54.31
A2G1	W310×60	20.57	7.52	29.27	54.20
A3R1	W310×39	20.40	6.30	28.15	53.80
A4R2	W310×39	20.56	6.22	28.30	54.08
A5E1	W250×49	20.50	7.55	31.01	54.12
A6E2	W250×49	20.53	7.51	47.74	54.14
A7G1	W310×60	20.75	7.43	28.55	53.81
A8G2	W310×60	20.75	7.44	27.05	54.11
A9R1	W310×39	20.66	6.54	27.57	53.56
A10R2	W310×39	20.79	6.55	27.07	54.27
A11E1	W250×49	20.58	7.30	28.27	53.74
A12E2	W250×49	20.73	7.34	44.02	54.34

The test set-up was designed to simulate a typical bolted connection in a tension bracing member or truss member. All specimens were 1220 mm (48") long. Specimens were connected to clevis plates at both ends, which were in turn connected to the testing machine by pin connections. All clevis plates remained elastic during loading.

Bolts used in the tests were ASTM grade A490, with a diameter, d_b , of 19.1 mm (3/4"). The pitch, as a fixed parameter, was nominally 54 mm (2-1/8") since both CSA-S16-01 and AISC 2005 specify that the pitch should not be less than $2.7d_b$. The minimum end distance for the bolts is 25 mm (1") for gas cut edges. (CSA-S16-01 also specifies that the end distance should not be less than $1.5d_b$ for connections that have either one or two bolts in a line in the direction of the applied force, but this was neglected since it does not apply to both design standards considered.) All bolt holes were drilled and of standard size, namely 20.6 mm (13/16"). Bolts had standard thread lengths that excluded the threads from the shear planes, and were tightened to the snug tight condition as defined in CSA-S16-01 (CSA, 2001).

Ancillary material tensile tests were conducted as per ASTM standard A370 (ASTM 2007). Three coupons were fabricated from the web of each section in the direction of the applied load. Mean test results for each set of coupons are listed in Table 3.

Specimens were tested in tension in a universal testing machine (MTS 6000). The load was applied quasi-statically under stroke control. One of two typical unloading points was chosen as the terminus of each test: “right after the peak load” and “drop of 5% of the peak load”. The former was selected in order to observe the load carrying mechanism at the peak load, whereas the latter was chosen to ensure that the ultimate strength of the connection had been captured.

TEST RESULTS

Test results are summarized in Table 3. All specimens failed by bolt tear-out of the web.

Table 3. Summary of Test Results

Specimen	F_y (MPa)	F_u (MPa)	Peak Load (kN)	Unloading Point
A1G1	439	519	690.7	drop of 5% of the peak load
A2G1	439	519	723.8	right after the peak load
A3R1	379	472	634.1	right after the peak load
A4R2	379	472	912.7	right after the peak load
A5E1	343	487	697.7	right after the peak load
A6E2	343	487	775.8	after a sudden load drop
A7G1	411	494	665.1	drop of 5% of the peak load
A8G2	411	494	622.1	right after the peak load
A9R1	369	478	632.8	drop of 5% of the peak load
A10R2	369	478	766.1	drop of 5% of the peak load
A11E1	376	500	691.2	drop of 5% of the peak load
A12E2	376	500	792.6	drop of 5% of the peak load

Two kinds of fractures were observed in the bolt tear-out failures: shear tears on one or both shear planes adjacent to the hole, as shown in Figure 3(a), or a single tensile splitting crack initiating at the free edge near the hole centreline, as shown in Figure 3(b). Tensile splitting cracks were caused by the development of transverse tensile stress as the material behind the bolt shank deformed into an arch shape. Most specimens eventually exhibited either shear tears or splitting cracks, although it is believed that splitting cracks did not occur until after the peak load had been reached.

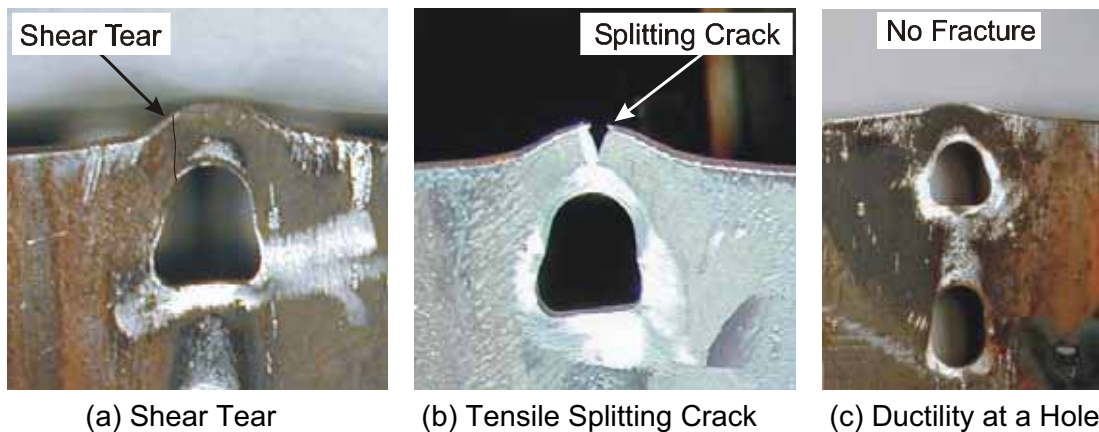


Figure 3. End Material Adjacent to Bolt Hole

From the test results, it is evident that two shear planes adjacent to each bolt participate in resisting the peak load in bolt tear-out failure despite the subsequent occurrence of tensile splitting in some specimens. In addition, the great ductility of the material behind an end bolt hole, as shown in Figure 3(c), is sufficient to allow the shear stress in the two shear planes to be developed beyond the yield stress, but not necessarily up to the ultimate stress.

Predicted capacities for each test, with the assumption that two shear planes at each bolt carry the peak load, were calculated using the CSA-S16-01/AISC 2005 block shear equations and the unified equation. The predicted capacities and the resulting test-to-predicted ratios are shown in Table 4.

Table 4. Summary of Test-to-Predicted Ratios

Specimen	Predicted Capacity		Test-to-Predicted Ratio	
	S16-01/AISC 2005 (kN)	Unified Equation (kN)	S16-01/ AISC 2005	Unified Equation
A1G1	481.2	601.4	1.44	1.01
A2G1	492.9	616.1	1.47	1.04
A7G1	451.1	563.9	1.47	1.04
A8G2	441.2	551.5	1.41	0.99
A3R1	366.5	458.1	1.73	1.25
A4R2	599.3	749.1	1.52	1.09
A9R1	376.2	470.3	1.68	1.22
A10R2	628.9	786.1	1.22	0.88
A5E1	479.7	599.6	1.45	1.13
A6E2	623.9	733.2	1.24	1.06
A11E1	448.1	560.2	1.54	1.14
A12E2	592.2	729.8	1.34	1.09
Mean (COV)	–	–	1.46 (0.10)	1.08 (0.09)

The equations in CSA-S16-01/AISC 2005 give a mean test-to-predicted ratio and coefficient of variation of 1.46 and 0.10, respectively, while the unified equation results in corresponding values of 1.08 and 0.09. A mean test-to-predicted ratio much closer to 1.0, combined with a slightly lower coefficient of variation, indicates that the unified equation better represents the behaviour of these connections than does the set of two equations used currently in the North American design standards. The mean test-to-predicted ratio considering these new tests as well as all Criterion A specimens from the literature for the unified equation is 1.02.

RELIABILITY ANALYSES

In general, an appropriate reliability index, β , which represents the probability of failure of a member or connection, can be achieved by selecting a suitable resistance factor, ϕ , for design. These two parameters are related by the bias coefficient and the coefficient of variation of resistance, which can be determined by the relevant material,

geometric, professional, and discretization parameters. Details of the procedures used in the reliability analysis presented in this paper are outlined by Cai and Driver (2008).

A total of 130 test results have been collected from the literature and this research project, including plates, channels, Tees, and wide-flange shapes with various connection configurations and conventional yield strengths (not greater than 550 MPa). The reliability study considers all 130 tests conforming to Criterion B, although only the 56 that conform to Criterion A meet the minimum end distance and pitch requirements in North American design standards.

Table 1 shows the mean test-to-predicted (T/P) ratios and the coefficients of variation (COV) of different research projects using CSA-S16-01/AISC 2005 and the unified equation. It shows that the equations in CSA-S16-01/AISC 2005 generally give high test-to-predicted ratios, while the test-to-predicted ratios for the unified equation are much closer to 1.0. The coefficients of variation for the two methods are similar.

Table 5 presents the reliability indices for the design equations considered, with the values associated with connections that would be permitted by the design standards shown in bold. Widely accepted target values for the reliability index range from 4.0 to 4.5 for connections. The resistance factor specified in CSA-S16-01 for block shear failure is 0.9, resulting in reliability indices that vary from 3.2 to 5.3. In AISC 2005, the resistance factor is 0.75 for block shear, resulting in reliability indices that vary from 4.3 to 6.6. The unified equation, with a resistance factor of 0.75 (as in the current 2009 draft of CSA-S16), provides a desired level of safety, with reliability indices ranging from 4.2 to 4.7. The greatly improved consistency over the various connection types indicates that the unified equation provides a better representation of the bolt tear-out failure behaviour than the current block shear equations. Moreover, even if the specimens that violate the North American minimum end distance and pitch requirements are included, the unified equation still gives acceptable levels of safety, as shown in Table 5.

Table 5. Reliability Indices Provided by Design Equations

Section	Number of Tests	Reliability Index β		
		S16-01 ($\phi = 0.9$)	AISC 2005 ($\phi = 0.75$)	Unified Equation ($\phi = 0.75$)
Plates	30 ^a	4.4	5.5	4.3
Plates	99 ^b	4.3	5.3	4.1
Channels (Web Failure)	5 ^b	4.9	6.3	4.3
W-Shapes (Web Failure)	12 ^{a,b}	5.3	6.6	4.7
Tees (Web and Flanges)	14 ^{a,b}	3.2	4.3	4.2

a. Criterion A

b. Criterion B

SUMMARY AND CONCLUSIONS

A total of 12 full-scale tests designed specifically to investigate bolt tear-out failure have been completed on wide-flange tension members. Along with tests conducted by other researchers, a total of 130 test results were analyzed. It was found that the block shear equations in CSA-S16-01/AISC 2005 generally provide highly conservative capacity predictions for bolt tear-out, while the unified equation gives accurate strength predictions. With the resistance factor of 0.9, CSA-S16-01 provides inconsistent reliability indices, and an unacceptably low reliability index was revealed in the case of failure of Tees along the alternate block shear path. With the resistance factor of 0.75, AISC 2005 generally provides very high and inconsistent reliability indices. On the other hand, with a resistance factor of 0.75 the unified equation achieves desired and consistent levels of safety for the atypical block shear paths considered.

The following conclusions can be drawn from the test results of this research project, along with the test results from the literature:

1. The unified equation gives much more accurate connection strength predictions and consistent reliability indices compared to the design equations in North American standards for block shear failure with atypical failure paths, and the unified equation is recommended for all block shear failures, regardless of whether the failure paths are classical or atypical.
2. In spite of the occurrence of tensile splitting cracks at the end bolts of some specimens that failed by bolt tear-out, the laboratory tests and strength calculations indicate that two shear planes adjacent to each bolt line carry the load until the peak stress implied by the unified equation is reached.
3. For the bolt tear-out failure mode, the average stress on the shear planes at failure exceeds the shear yield stress but may not reach the ultimate shear stress.

The unified equation has been adopted into the current 2009 draft edition of CSA-S16.

ACKNOWLEDGEMENTS

This research program was funded by the Steel Structures Education Foundation and the Natural Sciences and Engineering Research Council of Canada.

REFERENCES

- Aalberg, A and Larsen, P. K. (2001), "Bearing strength of bolted connections in high strength steel", *9th Nordic Steel Construction Conference*, Helsinki (pp. 859-866).
- Aalberg, A and Larsen, P. K. (2002), "The effect of steel strength and ductility on bearing failure of bolted connections", *3rd European Conference Steel Structures*, Coimbra, Portugal (pp. 869-878).
- AISC (2005), "Specification for structural steel buildings", American Institute of Steel Construction, Chicago, IL.

- ASTM (2007), "A370-07 Standard test methods and definitions for mechanical testing of steel products", ASTM International, Philadelphia, PA.
- Cai, Q. and Driver, R. G., (2008), "End tear-out failures of bolted tension members", *Structural Engineering Report No. 278*, Department of Civil and Environmental Engineering, University of Alberta, Edmonton, AB.
- CISC (2006), "Handbook of steel construction", Canadian Institute of Steel Construction, Willowdale, ON.
- CSA (2001), "Limit states design of steel structures", CSA-S16-01, Canadian Standards Association, Toronto, ON.
- Driver, R. G., Grondin, G. Y., and Kulak, G. L. (2006), "Unified block shear equation for achieving consistent reliability", *Journal of Constructional Steel Research*, Vol. 62 (pp. 210-222).
- Epstein, H. I., and Stamberg, H. (2002), "Block shear and net section capacities of structural Tees in tension: test results and code implications", *AISC Engineering Journal*, Vol. 39, Fourth quarter (pp. 228-239).
- Franchuk, C. R., Driver, R. G., and Grondin, G. Y. (2003), "Experimental investigation of block shear failure in coped steel beams", *Canadian Journal of Civil Engineering*, Vol. 30 (pp. 871-881).
- Huns, B. B. S., Grondin, G. Y., and Driver, R. G. (2002), "Block shear behaviour of bolted gusset plates", *Structural Engineering Report No. 248*, Department of Civil and Environmental Engineering, University of Alberta, Edmonton, AB.
- Kim, H. J. and Yura, J. A. (1999), "The effect of ultimate-to-yield ratio on the bearing strength of bolted connections", *Journal of Constructional Steel Research*, Vol. 49, No. 3, (pp. 255-269).
- Kulak, G. L. and Grondin, G. Y. (2001), "Block shear failure in steel members – a review of design practice", *AISC Engineering Journal*, Vol. 38, No. 4 (pp. 199-203).
- Puthli, R. and Fleischer, O. (2001), "Investigations on bolted connections for high strength steel members", *Journal of Constructional Steel Research*, Vol. 57, No. 3 (pp. 313-326).
- Rex, C. O. and Easterling, W. S. (2003), "Behavior and modeling of a bolt bearing on a single plate", *ASCE Journal of Structural Engineering*, Vol. 129, No. 6 (pp. 792-800).
- Udagawa, K. and Yamada, T. (1998), "Failure modes and ultimate tensile strength of steel plates jointed with high-strength bolts", *Journal of Structural and Construction Engineering*, Architectural Institute of Japan, Vol. 505 (pp. 115-122). (in Japanese)
- Udagawa, K. and Yamada, T. (2004), "Ultimate strength and failure modes of tension channels jointed with high strength bolts", *13th World Conference on Earthquake Engineering Conference*, Vancouver, BC.

DUCTILITY REQUIREMENTS FOR THE DESIGN OF BOLTED SHEAR CONNECTIONS

J. Henriques, University of Coimbra, Coimbra, Portugal
J. P. Jaspart, University of Liège, Liège, Belgium
L. Simões da Silva, University of Coimbra, Coimbra, Portugal

ABSTRACT

The resistance of shear bolted connections is traditionally evaluated by considering an equal distribution of internal forces amongst the bolts. In fact, such an assumption may only be seen as the result of a plastic redistribution of the internal forces, what requires shear ductility in the vicinity of the bolts. In the present paper, ductility requirements are proposed. They have been derived by the first author during a two-year stay at Liège University. For more details about this work, the interested reader is requested to refer to the Henriques thesis [5].

SHEAR BOLTED CONNECTIONS

A connection can be classified as Shear Bolted Connection when the forces transferred between the elements induce pure shear in the bolts. Two types of shear connections, also called lap connections, may be found: single and double overlap connections. The difference consists in the number of shear planes that cross the bolt shanks.

In Shear Bolted Connections, two different elements may be distinguished: connectors (bolts) and connected elements (plates). The term plate is used to refer to column flanges, beam flanges, beam webs, splice plates, etc.

When a bolted connection is submitted to shear, forces are transferred from one plate to the other (others) by plate-to-bolt contact. Neglecting the small friction developed between plates and negligible bending of the bolt, four different resistance and deformation modes should be considered:

- Bearing of the plate and/or bolt;
- Shear in the plates;
- Tension in the plates;
- Shear in the bolt shanks.

From these, the behaviour of a shear bolted connection can be defined by the response of two different parts: bolt zone, where bearing and shear forces develop; and the plate between holes where direct forces develop in the plate. The work presented in this article focuses on the bolt zone; so the failure of the connection by excess of tension in the connected plates is here not considered.

In these types of connections, the load to be transferred between the plates is distributed non-uniformly amongst the bolt-rows (Figure 1-a), Ju et al. [8]. If sufficient deformation is provided around each connector, a full plastic redistribution of forces may be noticed, otherwise failure is reached by lack of ductility and the maximum external force to be transferred is lower than the full plastic distribution. Schematically, the different stages of forces distribution in a shear bolted connection may be represented as in Figure 1.

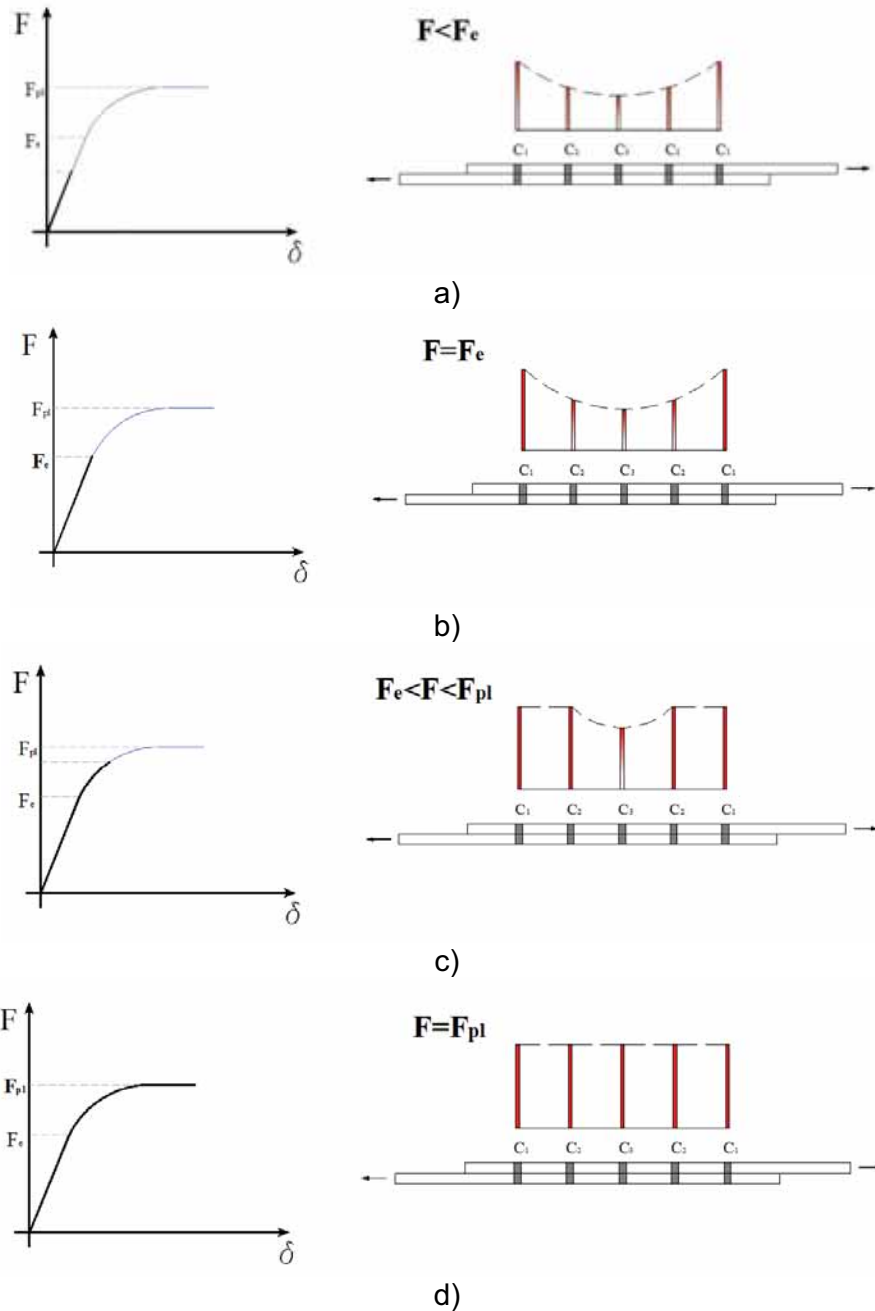


Figure 1 – a) None of the bolt rows yield; b) outsider bolt rows yield (elastic resistance of the connection); c) the following bolt rows yield; d) the remaining bolt row yield (full plastic resistance of the connection).

In the same study, Ju et al. [8] showed that in the nonlinear range the maximum load achieved by the connection is almost linearly proportional to the bolt number arranged in the connection. In part 1-8 of Eurocode 3 [1], a full plastic distribution of forces can be assumed as long as the connection length is limited.

Pietrapetrosa et al. [13] approached the subject by only considering fitted bolts. Their study showed that, inside the limits given by the code and by practical guidance, sufficient ductility to achieve a full plastic distribution of internal forces is available. However, the common practice is the use of non fitted bolts and the presence of imperfections is also a reality. Consequently, the lack-of-fit will increase the demands of ductility as some bolts bear before the others, as verified by Wald et al. [14]. They showed that for certain values of gap in some bolt rows, failure was first attained in the extreme bolts and therefore a full plastic resistance was not reached.

EUROCODE 3 DESIGN PROCEDURE FOR BOLTED CONNECTIONS IN SHEAR

According to the classification system for joints in Eurocode 3 part 1.8 [1], the connections considered here belong to category A: Shear Bolted Connections – Bearing Type. These ones resist by transferring forces through plate/bolt contact and bolt shearing. Non preloaded bolts are used and the small friction resistance between the contact surfaces is neglected.

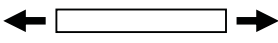
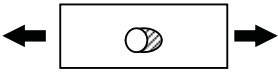
Part 1.8 of Eurocode 3 [1] is dedicated to the design of joints in steel structures; it prescribes the so-called component approach for the evaluation of the mechanical properties of the joints. The analysis of shear bolted connections is not specifically treated. But the code gives recommendations for the evaluation of the stiffness and resistance properties of several individual components; the engineer has then to identify the involved components and to assemble them so as to finally predict the response of the whole connection.

Amongst the individual components presented in Table 6.1 of EC 3 part 1.8 [1], the following ones should be here considered: bolt in shear, plate/bolt in bearing and plate in tension. Furthermore it is then assumed that the failure mode of a bolt zone (i.e. a zone where a shear force is locally transferred from one plate to another) is associated to that of the weakest component. Through this procedure, the resistance and stiffness properties of the bolt zone may so be evaluated; however, no information is given for the deformation capacity. Table 1 summarises this procedure.

The application of the component method to evaluate the response of the whole shear bolted connection (Figure 2-a) requires now to consider the mechanical model shown in Figure 2-b. Here, each individual component is modelled through extensional springs. In the bolt zone, one observes that three springs act in series and therefore their behaviour may be assembled into an equivalent one (describing the bolt zone response). Thus, a simplified model is obtained

where the components at the bolt zone are represented by a so-called equivalent bolt zone component, Figure 2-c.

Table 1 – Eurocode 3 expressions to evaluate the characteristic resistance (R_c) and the stiffness (S_c) of the basic components.

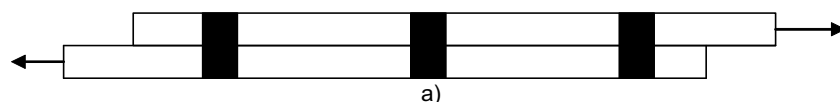
		S_c	R_c
Plate in tension		$S_{pl} = EA/p_b$	$R_{pl} = \min(A f_y; 0,9 A_{net} f_u)$
Bolt in shear		$S_b = 8 d^2 f_{ub}/d_{M16}$	$R_b = \alpha_s f_{ub} A_b$
Plate in bearing		$S_p = 12 k_b k_t d f_u$	$R_p = k_1 \alpha_b f_u d t$
Equivalent component		$S_{eq} = (S_b^{-1} + S_{p1}^{-1} + S_{p2}^{-1})^{-1}$	$R_{eq} = \min(R_b, R_{p1}, R_{p2})$
E	Young Modulus	d	diameter of the bolt
A	gross area of the plate	d_0	diameter of the bolt hole
A_{net}	net area of the plate	d_{M16}	nominal diameter of a M16 bolt
p_b	pitch distance (// to load transfer)	e_2	edge distance (\perp to load transfer)
e_b	end distance (// to load transfer)	p_2	pitch distance (\perp to load transfer)
f_y	yield strength of the plate	k_b	$= \min(k_{b1}; k_{b2})$
f_u	ultimate strength of the plate	k_{b1}	$= 0,25 e_b/d + 0,5$ but $k_{b1} \leq 1,25$
t	thickness of the plate	k_{b2}	$= 0,25 p_b/d + 0,375$ but $k_{b2} \leq 1,25$
A_b	shear area of the bolt (nominal or area)	k_t	$= 1,5 t / d_{M16}$ but $k_t < 2,5$
f_{ub}	ultimate strength of the bolt	α_s	$= 0,5$ or $0,6$
		α_b	$= \min(e_b/3d_0; p_b/3d_0 - 0,25; f_{ub}/f_u; 1,0)$
		k_1	$= \min(2,8 e_2/d_0 - 1,7; 1,4 p_2/d_0 - 1,7; 2,5)$

For shear connections with more than one bolt zone “in length”, two recommendations given by the code are relevant. One is related to the resistance of connections with a limited number of bolt zones “in length”; this one is obtained as follows:

$$\left\{ \begin{array}{l} \text{if } F_{v,Rd,i} \geq F_{b,Rd,i} \quad \forall i \Rightarrow F_{Rd} = \sum F_{b,Rd,i} \\ \text{if not } F_{Rd} = n \min \{ F_{Rd,i} \} \quad \text{with } F_{Rd,i} = \min(F_{v,Rd,i}; F_{b,Rd,i}) \end{array} \right. \quad (1)$$

Where:

- F_{Rd} is the resistance of the whole connection;
- n is the number of bolt zones “in length”;
- i indicates the bolt zone number;
- $F_{b,Rd,i}$ and $F_{v,Rd,i}$ are respectively the bearing and shear resistances of bolt zone i .



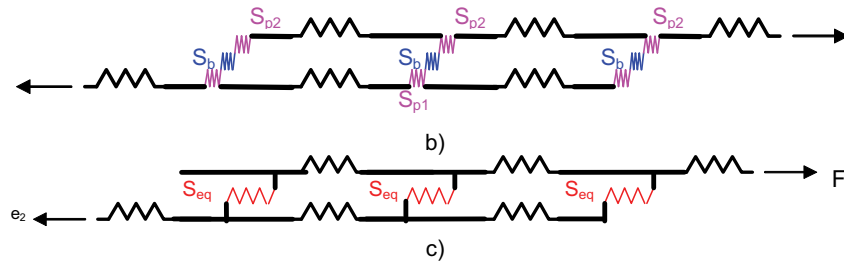


Figure 2 –a) Shear connection with three bolts; b) Real mechanical model; c) Simplified mechanical model.

The second rule is related to long joints where the shear resistance should be reduced if the connection length (L_j) exceeds $15d$. In this case the following reduction factor should be applied to the connection resistance initially evaluated through Formula (1):

$$\beta_{L_f} = 1 - \frac{L_j - 15d}{200d} \text{ but } 0.75 \leq \beta_{L_f} \leq 1.0 \quad (2)$$

EVALUATION OF IMPERFECTIONS/LACK OF FIT

As in every construction type, imperfections related to fabrication have to be considered in steel structures. As far as the response of shear connections is concerned, the discrepancy between the nominal and the real values of bolt diameters, hole diameters and positions (itches and end distances) may affect the behaviour of the connections as the imperfections will lead to a non simultaneous transfer of forces between the bolts, as it would be the case for “perfect” connections (for instance, connections with fitted bolts).

Values of tolerances are given in European Standard for the Execution of Steel Structures and Aluminium Structures, pre-EN 1090-2 [2], in ISO/DIS 4759-1 [6] and in ISO286-2 [7]. Based on these values the lack of fit in bolted connection may be quantified. However, due to the multiple parameters involved, this task is complex. In order to simplify, and have in consideration the evaluation of the maximum required deformation in a bolt zone, some assumptions are established in order to get the “worst situation” (i.e. the one for which the highest demand in terms of ductility is required from a bolt zone):

- Possibility to have different values of real hole diameters in every plate;
- Possibility to have different hole deviations in every plate, and consequently different values of pitch and end distances in every plate;
- The bolt initially in contact with the plates is one of the outer bolts (henceforth this bolt will be designated as FBW [First Bolt Working], while the notation RB [Rest of the Bolts] will be used for all the others), this allows to maximise the requested deformation capacity for the FBW bolts;

- The “worst situation” results from the combination of all these possibilities. Even if this is not the more realistic pattern, it could anyway happen; and for sure it is the one leading to the highest request in terms of ductility.

Using the standards values for tolerances and the previous assumptions, several connection layouts may be drawn to identify the “worst case”, as illustrated in Figure 3.

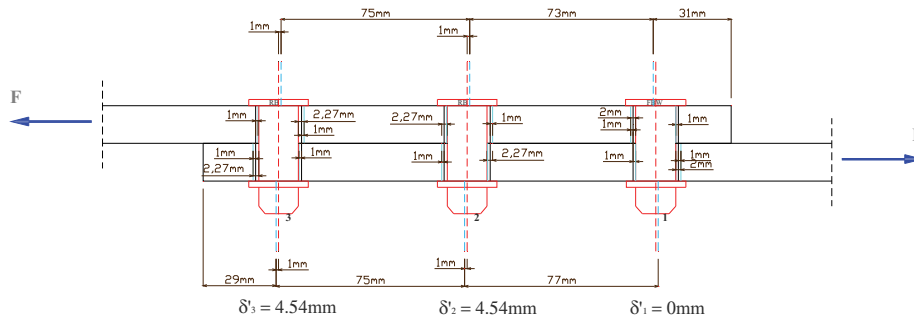


Figure 3 – Connection layout considering the presence of imperfections.

Analysing several situations, as different bolt diameters, one obtains the gaps to be considered in a bolted connection which follows the previous assumptions. Table 2 presents maximum gaps that may be observed in a connection layout according to the bolt diameter used.

Table 2 – Gaps in bolted connections

Bolts	2, 3 or more Bolts		
	FBW gap	RB gap	Max. Gap
M12-M14	0.00	3.08	3.08
M16	0.00	4.54	4.54
M18-M24	0.00	4.66	4.66
M27	1.00	5.66	4.66
over	1.00	5.78	4.78

The main factors which distinguish the different values obtained are the hole clearance and the tolerances allowed by standards.

RESPONSE OF THE INDIVIDUAL COMPONENTS

As mentioned before, two different individual components interact in the bolt zone: the bolt in shear and the plate/bolt in bearing. And in order to analyze shear bolted connections, the behaviour of these components has first to be predicted. Hereafter, code recommendations and results of former investigations are used to achieve it.

Bolt in Shear

In Moscow, Karmalin et al. [10] have performed numerous experimental tests on bolts in shear. Resistance, stiffness and deformation capacity of bolts subjected to shear have been measured for M16, M20 and M24 with grades 5.8, 8.8 and also for bolts with a minimum tensile strength equal to 1100MPa (high strength). The tested specimens consisted of single bolted connections with two-shear planes.

In Table 3 are presented the test results.

Table 3 – Moscow test results

Bolts Grade	$R_{u,b}$ [kN]			$\delta_{u,b}$ [mm]		
	M16	M20	M24	M16	M20	M24
5.8	63 – 72	97 – 110	137 – 150	2.9 – 3.4	3.4 – 3.8	4.1 – 4.4
8.8	81 – 93	124 – 141	175 – 193	2.2 – 2.5	2.6 – 3.0	3.1 – 3.5
High-strength	126 – 150	195 – 220	275 – 308	1.6 – 2.0	1.8 – 2.2	2.1 – 2.7

Based on the EC3 part 1.8 [1] expressions (see Table 1) and on these experimental results, expressions to determine the ultimate deformation capacity, ultimate resistance and strain-hardening stiffness of bolts in shear have been derived. With the aim to refer explicitly to Eurocodes, the here-above listed parameters are expressed as a function of the initial stiffness (S_b) and of the nominal resistance (R_b), the values of which are given in Eurocode 3 (see Table 1). Table 4 presents these expressions.

Table 4 – Ultimate resistance, ultimate deformation capacity and strain-hardening stiffness for the “bolt in shear” component.

Bolts Grade	$\delta_{u,b}$			$S_{st,b}$	$R_{u,b}$
	M16	M20	M24		
5.8	4.7 R_b/S_b	5.5 R_b/S_b	6.7 R_b/S_b	$S_b/2.5$	1.58 R_b
8.8	3.0 R_b/S_b	3.5 R_b/S_b	4.2 R_b/S_b	$S_b/7.0$	1.05 R_b
High-strength	2.6 R_b/S_b	2.9 R_b/S_b	3.4 R_b/S_b	$S_b/1.5$	1.44 R_b

Plate and bolt in bearing

During the research period, numerical works have been achieved. The main goal was to develop a numerical model for the simulation of bearing phenomena. Bearing problems are complex as they deal with contact between two bodies consequently the number of tools available to reproduce the contact problems is reduced. In the present investigations, the Lagamine code [11], software developed at the University of Liège, has been used.

As it had not been planned to carry out experimental tests in Liège, available tests made in others universities are used to calibrate the numerical model. Tests made on shear bolted connections at the University of Ljubljana [12] and at the Technical University of Delft are used [4].

One of the main objectives was to be able to model bearing failure; this goal was not completely achieved at the end of the research period. Further related investigations are therefore still needed.

As a consequence, the characterization of the plate/bolt in bearing behaviour is based hereafter on the existent knowledge: the elastic stiffness and the nominal resistance re determined using code recommendations, see Table 1, while, for the other parameters (strain-hardening stiffness, ultimate resistance and ultimate deformation), expressions from previous works ([5], [9] and [13]) are used.

$$S_{sb,p,b} = \frac{S_{p,b}}{40} \quad (3)$$

$$R_{u,p,b} = 1.25R_{p,b} \quad (4)$$

$$\delta_{u,p,b} = 11 \frac{R_{p,b}}{S_{p,b}} \quad (5)$$

Plate in tension

Although present research work focuses on the bolt zone and on its capability to redistribute forces, the deformability of a plate in tension has an important influence on the distribution of forces amongst the bolts. The stiffness of the plate in tension has therefore to be predicted too; an expression is provided in Table 1.

Assembly of the basic components

In this part, the individual basic components are assembled with the objective to derive the available ductility of the equivalent bolt zone components and the ductility required to allow a full redistribution of internal forces in shear bolted connections.

Available deformation capacity of the equivalent bolt zone component

The deformation available in the equivalent bolt zone component is obtained through the “association” of the two basic components: the bolt in shear and the plate/bolt in bearing. Each basic component is characterized and the deformation capacity evaluated according to the knowledge presented in the previous sections. Subsequently an assembly is done according to their resistance and deformability. The complete behaviour of the equivalent bolt zone component is then obtained.

The derivation of formulae to determine the available deformation capacity of the equivalent component depends on several factors such as: single or double overlap connections, plates with equal or different behaviour (different thickness, different steel properties), and the relation between the resistances of the individual components. So, many cases may be obtained. In Figure 4 is exemplified one of these cases and in Table 5 are presented a list of expressions for several common cases.

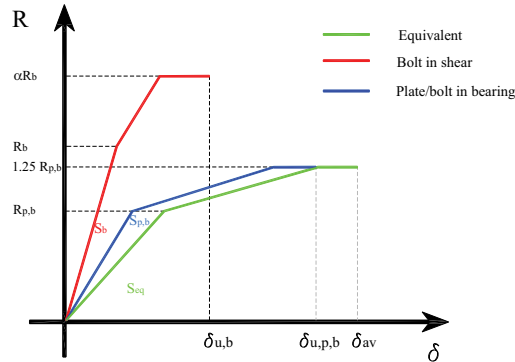


Figure 4 – Assemblage of the individual components behaviour.

Table 5 – Derived expressions to determine the available deformation capacity.

Plates with equal mechanical and geometrical properties	
Single Overlap Connections	Double Overlap Connections
Case: $R_b > 1.25R_{p,b}$	
$\delta_{av} = \frac{R_{eq}}{S_{eq}} + 2 * \left(\delta_{u,p,b} - \frac{R_{eq}}{S_{p,b}} \right) + \frac{0.25R_{eq}}{S_b}$	$\delta_{av} = \frac{R_{eq}}{S_{eq}} + \left(\delta_{u,p,b} - \frac{R_{eq}}{S_{p,b}} \right) + \frac{0.125R_{eq}}{S_b} + \frac{0.125R_{eq}}{S_{p,b}}$
Case: $R_{p,b} > \alpha R_b$	
$\delta_{av} = \frac{R_{eq}}{S_{eq}} + \left(\delta_{u,b} - \frac{R_{eq}}{S_b} \right) + 2 * \frac{(\alpha - 1)R_{eq}}{S_{p,b}}$	$\delta_{av} = \frac{R_{eq}}{S_{eq}} + \left(\delta_{u,b} - \frac{R_{eq}}{S_b} \right) + \frac{(\alpha - 1)R_{eq}}{S_{p,b}} + \frac{(\alpha - 1)R_{eq}}{S_{p,b}}$
Case: $1 \leq R_b / R_{p,b} \leq 1.25$	
$\delta_{av} = \frac{R_{eq}}{S_{eq}} + 2 * \left(\delta_{u,p,b} - \frac{R_{eq}}{S_{p,b}} \right) + \frac{R_{e,b} - R_{eq}}{S_b} + \frac{(1.25R_{eq} - R_{e,b})}{S_b / \beta}$	$\delta_{av} = \frac{R_{eq}}{S_{eq}} + \left(\delta_{u,p,b} - \frac{R_{eq}}{S_{p,b}} \right) + \frac{0.125R_{eq}}{S_{p,b}} + \frac{R_{e,b} - 0.5R_{eq}}{S_b} + \frac{(0.625R_{eq} - R_{e,b})}{S_b / \beta}$
Case: $1 \leq R_{p,b} / R_b \leq \alpha$	
$\delta_{av} = \frac{R_{eq}}{S_{eq}} + \left(\delta_{u,b} - \frac{R_{eq}}{S_b} \right) + 2 * \frac{R_{p,b} - R_{eq}}{S_{p,b}} + 2 * \frac{(1.25R_{eq} - R_{p,b})}{S_{p,b} / 40}$	$\delta_{av} = \frac{R_{eq}}{S_{eq}} + \left(\delta_{u,b} - \frac{R_{eq}}{S_b} \right) + \frac{R_{p,b} - 2R_{eq}}{S_{p,b}} + \frac{(2\alpha R_{eq} - R_{p,b})}{S_{p,b} / 40} + \frac{\alpha * R_{eq}}{S_{p,b}}$

Required deformation capacity in actual shear bolted connections

The required deformation capacity is the deformation which should be reached in the most loaded bolt zone in order to reach a full plastic redistribution of efforts in the connection.

In the work done by Pietrapertosa et al. [13] expressions to determine the required deformation of the equivalent bolt zone component for fitted bolts have been proposed. Based in this study, similar expressions for actual connections, taken into account the presence of imperfections, are proposed.

The derived expressions should consider the most demanding situation that has been assumed before; i.e. the case where one of the extreme bolts is in contact while the others are not. Several cases have been analysed and it has been concluded that the most demanding case is obtained when the middle bolt zone (or middle bolt zones in the case of even number of bolt rows) is (are) the last one(s) to reach its (their) maximum resistance. Figure 5 shows the deformed shape and the distribution of internal forces for a connection with 5 bolt rows.

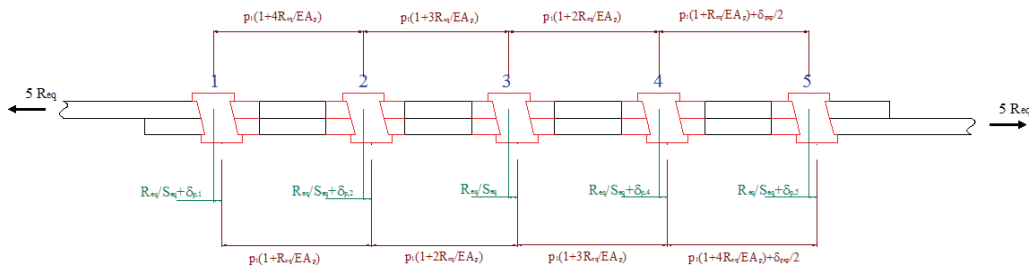


Figure 5 – Connection with 5 bolt rows.

This analysis has been extended to other cases (different number of bolt rows) and the following general expression has been obtained:

$$\delta_{req} = R_{eq} \left(\frac{1}{S_{eq}} + \rho \frac{p_1}{EA_p} \right) + \delta_{gap}$$

with

$$\rho = \sum_{i=1}^{n_1/2} (n_1 - 2i) \text{ for an even value of } n$$

$$\rho = \sum_{i=1}^{(n_1-1)/2} (n_1 - 2i) \text{ for an odd value of } n$$

(6)

Additionally, a numerical model based on the use of the Liège home-made nonlinear FEM software FINELG [3] allowed validating all the analytical results.

Ductility requirements for shear bolted connections

In order to determine ductility requirements that a connection should satisfy so as to ensure a full plastic redistribution of the internal forces amongst the bolt

zones, reference will obviously be made to the expressions derived before for the available and required ductility in bolt zone components; hence, such ductility requirements are for sure dependent on all the geometrical and mechanical parameters that influence the two previously mentioned values of ductility:

- Steel grade of the plate;
- Bolt grade;
- Geometrical properties of the connection [t , b , e_1 , e_2 , p_1 , p_2 , d , d_0];
- Number of bolt rows (n_1 – in the direction of loading) and number of bolt lines (n_2 – in the perpendicular direction of loading).

The ductility criterion which is expressed below and which constitutes the main outcome of the study is based on an intensive parametrical study where all the above-listed geometrical and mechanical parameters have been considered, but for single overlap connections only (what is not really restrictive). As mentioned before, situations where tension plate failure is relevant have been omitted.

In order to define this criterion, two fundamental parameters defined below have been identified. Figure 6 illustrates the basis of the criterion.

The parameter on the vertical axis represents the ratio between the available and the required deformation capacities. This ratio reflects the sufficient or insufficient ductility exhibited by the equivalent bolt zone component. The second fundamental parameter represents the ratio between the nominal resistance of the plate/bolt in bearing component and the ultimate resistance of the bolt in shear component. These two parameters embody all the important mechanical and geometrical parameters listed before.

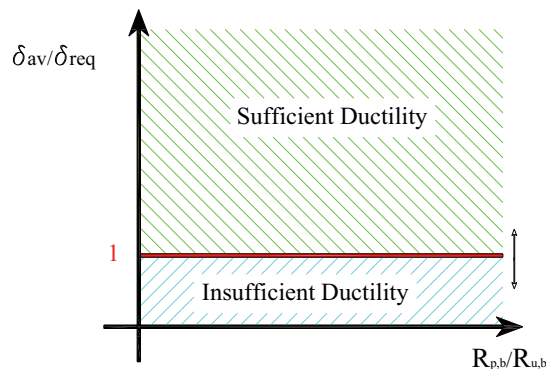


Figure 6 – Two fundamental parameters

Figure 7 presents the results of the parametrical analysis in which the following variation of the basic parameters have been considered:

- Steel grade: S235 and S355;
- Bolt diameters: M16, M20 and M24;
- Spacing, end and edge distances: max and min of e_1 , e_2 , p_1 and p_2 ;

- Width of the plates: max and min values e_2 and p_2 as well as max and min values of b taken into account;
- Thickness of the plate: the variation of t is made in order to cover the whole ranges of $R_{p,b}/R_{u,b}$;
- Finally, the number of bolt rows and lines varies: n_1 , from 2 to 10, and n_2 , from 1 to 5.

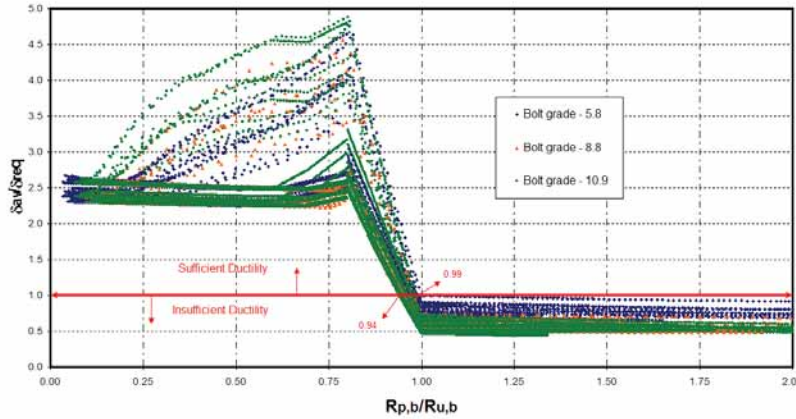


Figure 7 – Parametric analysis results.

One can observe that the variation of the fundamental parameter $R_{p,b}/R_{u,b}$, close to the boundary between sufficient and insufficient ductility ($\delta_{av}/\delta_{req}=1$) is small, from 0.94 to 0.99. So, a safe and simplified ductility criterion may be suggested as follows:

$$\left\{ \begin{array}{l} \text{If } \frac{R_{p,b}}{R_{u,b}} \leq 0.94 \Rightarrow F_{r,c} = n_1 n_2 R_{eq} \text{ (plastic distribution of internal forces allowed)} \\ \text{If } \frac{R_{p,b}}{R_{u,b}} > 0.94 \Rightarrow F_{r,c} < n_1 n_2 R_{eq} \text{ (plastic distribution of internal forces not allowed)} \end{array} \right. \quad (7)$$

In order to apply the criterion, some practical cases have been considered and the results have been compared with the present Eurocode 3 rules. This comparison considered two situations, one where the criterion is verified and another where it is not, as shown in Figure 8.

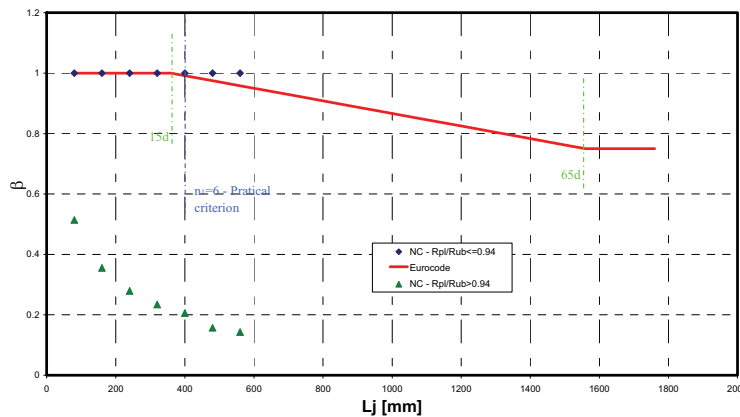


Figure 8 – Comparison with the Eurocode 3 criterion.

CONCLUSIONS

The present work proposes a criterion to check whether sufficient ductility for a full plastic redistribution of internal forces may be contemplated in actual shear connections with non preloaded bolts. It is based on the presence of imperfections in the connection layout which can lead to situations where some bolts bear before the others.

All the aspects inherent to shear bolted connections have been approached: the evaluation of imperfections according to the standards for tolerances; the characterization of the individual component response; the derivation of expressions to determine the available deformation capacity in the bolt zone component; the required deformation in the bolt zone component for a full plastic redistribution of forces.

The application of the proposed criterion showed considerable differences between the code criterion and the proposed one. This fact shows that imperfections may have a relevant effect in the connection behaviour if the bolt in shear component is the “weakest”. Actually, in these cases the transferred force is considerably smaller than the one determined according to the code provisions, as observed in Figure 8. This situation should then be further investigated in future works. At the same time the evaluation of the imperfections in the connection layout should be better analysed. The values here obtained (based on the “worst” layout of imperfections) seem to be too severe for the case of “weak” bolts, as seen in Figure 8.

REFERENCES

- [1] CEN, European Committee for Standardization (2005) – “*Eurocode 3: Design of steel structures – Part 1-8: Design of joints*”, Final Draft prEN 1993-1-8, December 2003, Brussels, Belgium.
- [2] CEN, European Committee for Standardization (2005) – “*Execution of steel structures and aluminium structures – Part 2: Technical requirements for the execution of steel structures – Stage 34*”, Draft prEN 1090-2, April 2005, Brussels, Belgium.
- [3] FineLg User’s manual, V9.0 (2004) – University of Liège (M&S) / Design office Greisch, Belgium.
- [4] Freitas, S. T. (2005) – “*Experimental research project on bolted connections in bearing for high strength steel*”, Final report of the framework of the Socrates-Erasmus program, June 2005.

- [5] Henriques, J. (2008) – “Ductility requirements in shear bolted connections”, Master Thesis, Coimbra, Portugal, January 21.
- [6] ISO (1999) – “*Tolérances des éléments de fixation – Partie 1: Vis, goujons et écrous – Grades A, B et C*”, Projet de Norme Internationale, ISO/DIS 4759-1.2.
- [7] ISO (2006) – “*Système ISO de tolérance et d’ajustements – Partie 2: Tables des degrés de tolérance normalisés et écarts limites des alésages et des arbres*” – Norme Base”, ISO 286/DIN 267 – 2.
- [8] Ju, S.-H.; Fan, C.-Y.; Wu, G. H. (2003) – “*Three-dimensional finite elements of steel bolted connections*”, Engineering Structures 26, 2004, 403-413.
- [9] Jaspert, J. P. (1991) – “*Etude de la semi-rigidité des nœuds poutre-colonne et son influence sur la résistance et la stabilité des ossatures en acier*”, Ph. D. Thesis, M&S Département, Liège University, Belgium.
- [10] Karmalin, V. V. and Pavlov A. B. (1989) – “*Load capacity and deformability of bearing and friction-bearing connections*”, Proceedings of the International Colloquium on Bolted and Special Structural Connections, USSR, Moscow, May 15-20, pp. 52-60.
- [11] LAGAMINE code, Finite Element Software, ArGENCO Department, Liège University, Belgium.
- [12] Moze, P.; Beg, D.; Lopatic, J. (2006) – “*Ductility and Strength of bolted connections made of high strength steel*”, International conference in metal structures “*Steel – A new and traditional material for buildings*”, Poiana Brasov, Romania, September 20-22, pp. 323-330.
- [13] Pietrapertosa C.; Piraprez E.; Jaspert J.P. (2004) – “*Ductility requirements in shear bolted connections*”, ECCS/AISC Workshop: Connections in steel structures V: Behaviour, Strength and Design, Amsterdam, The Netherlands, June 3-4, pp. 335-345.
- [14] Wald, F.; Sokol, Z.; Moal, M.; Mazura, V.; Muzeau, J. P. (2002) – “*Stiffness of cover plate connections with slotted holes*”, Eurosteel: Third European conference on Steel Structures, Coimbra, Portugal, pp. 1007-1016.

TESTS ON BOLTED SHEAR CONNECTION IN HIGH-STRENGTH STEEL WITH THREE OR FOUR BOLTS IN LONGITUDINAL DIRECTION

Primož Može

University of Ljubljana, Ljubljana, Slovenia
primoz.moze@fgg.uni-lj.si

Darko Beg

University of Ljubljana, Ljubljana, Slovenia
darko.beg@fgg.uni-lj.si

ABSTRACT

The paper presents the results of 26 experiments on tension splices with three or four bolts in double shear. The connections were made of high-strength steel of grade S690. Due to low f_u/f_y ratio of high-strength steels, the unfavorable effect of fabrication tolerances was accounted for in the experimental work. The experiments were numerically simulated. The results of numerical simulations are used for the description of stress state in the connection plates. The experimental results of similar connections were gathered from literature. These experiments were also numerically simulated. The distribution of bearing forces between bolts as a result of numerical simulations is compared to Eurocode bearing.

INTRODUCTION

This paper focuses on tension splice connections made of high strength steel (HSS) with bolts in double shear (see Fig. 1). In the sequel these connections are also referred to as bearing type bolted shear connections. The problem is that HSSs (steels with yield strength $f_y \geq 420$ MPa) are considered to be less ductile than conventional (steels up to grade S355) steels. Very typical steel S690 has relative fracture elongation ε_{fr} more than 14%, uniform strain ε_u that corresponds to tensile strength f_u around 5% and ultimate-to-yield ratio around $f_u/f_y = 1.05$ (Može et al. 2007). The local ductility is extremely important at bearing type connections where loading from one steel plate to another is transferred by the contact between the bolt and the plates. The contact is characterized by high stresses that enforce transverse shear in the bolts and high local compression stress to the plate. Concentrations of stresses are therefore unavoidable. Another characteristic of bearing type connections is initial slip due to bolt-hole clearance. In general, contacts between bolts and plates are not established simultaneously. A contact at one bolt may be established first. In such case the whole loading is transferred through single bolt. For that reason, the local ductility of the connection in terms of plastic deformations has to be sufficient in order to assure bolt-hole elongation, so that the remaining contacts will be established and the loading will be transferred through all bolts. If local ductility was not sufficient, the stress concentration would cause rupture of the steel plate or shear fracture of the bolt. In either case the maximum connection resistance would be equal to the resistance of a single bolt connection. The

strength ratio in connections made of HSS is in favor of the steel plate. Therefore bolts should be at least of grade 8.8 or higher.

The research reported in this paper is part of larger experimental and numerical investigation on tension splices (Može 2008). Herein only the experimental research on 26 bearing type connections with very thick cover plates is presented. The connections, where the stiffness of the cover plates and inner plate is equal is presented in Može (2008). The stiffness of cover plates affects the distribution of bearing forces. The research was performed in order to investigate local ductility of HSS. The negative influence of the fabrication tolerances in relation to bolt-hole clearance was studied, as well. Additionally, the experiments were numerically simulated in order to obtain the distribution of bearing forces between bolts.

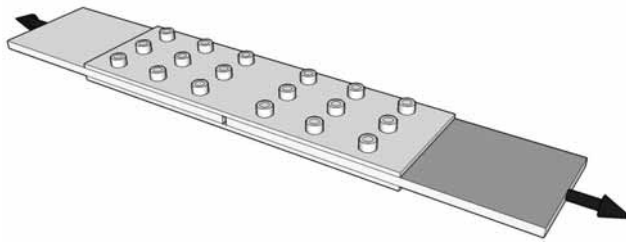


Fig. 1: Simple tension splice with bolts in double shear

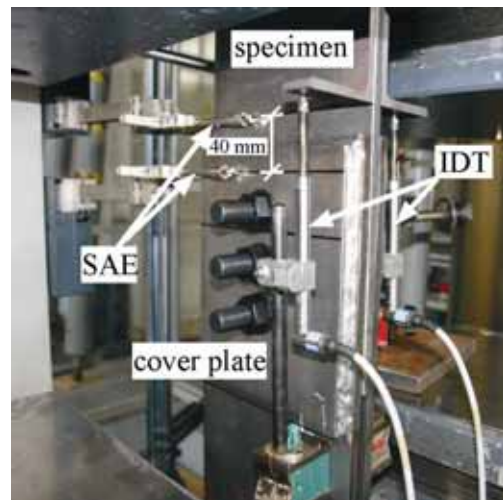


Fig. 2: Specimen type L equipped with measuring devices

TESTING PROGRAMME

The testing programme included bolted shear connections with three or four bolts positioned in the loading direction. A total of 26 specimens type L were tested. The specimen was fastened between two thick cover plates with three or four bolts M20 12.9 in standard holes ($d_0 = 22$ mm) to form tension splice with bolts in double shear. The cover plates were welded together to form forks. Together with the bolts, they were not the subject of the investigation, thus they were designed accordingly. The bolts were snug tightened. The forks and the specimens were fabricated from 10 mm thick steel plate, grade S690. The functional fabrication tolerances were simulated at specimens coded by s (see Table 1), where the first or the last hole was shifted by 2 mm. In this way, only one bolt was carrying the bearing load for the first 2 mm of hole elongation and after that the remaining bolts were activated. The geometry of the specimens was designed to cover different types of failures. The ranges of pitches p_1 and end distances e_1 were selected from minimum allowed distances by EN 1993-1-8 (CEN 2005) to the most common ones. The edge distance e_2 was constant for all specimens and was equal to $4.5d_0$ to prevent premature net cross-section failure. The nominal geometries of specimen type L are listed in Table 1.

Testing machine with capacity of 2500 kN was used for the tests. They were carried out at a prescribed displacement rate 1.5 mm/min. A relative displacement between the specimen and the cover plates was measured by two inductive displacement transducers (IDT) and alternatively by sensor arm extensometers (SAE). The positions of measuring instruments are illustrated in Fig. 2. The SAEs were also used to control test speed. The tests were carried out until fracture of plate in bearing or the bolt (except at L18 and L20s where the test was stopped significantly before failure).

Material characteristics of steel plate S690 were measured on three specimens fabricated and tested according to the procedures given in relevant standards. The following average material characteristics were obtained: yield strength $f_y = 796$ MPa, tensile strength $f_u = 844$ MPa, ultimate elongation $\varepsilon_u = 6.4\%$, strain at fracture $\varepsilon_U = 17.1\%$ and measured percentage reduction area equaling 59.4%.

Table 1: Geometry and test results

Specimen name	e_1/d_0	p_1/d_0	e_2/d_0	d_0 [mm]	b [mm]	t [mm]	d [mm]	No. of bolts	Failure mode ^a	F_{max} [kN]
L01	1.5	2.0	4.5	22	198	10	20	3	1	778
L02	2.0	2.0	4.5	22	198	10	20	3	1	908
L03	3.0	2.0	4.5	22	198	10	20	3	2	1088
L04	1.5	2.0	4.5	22	198	10	20	4	1	1066
L04s	1.5	2.0	4.5	22	198	10	20	4	1	1057
L05	2.0	2.0	4.5	22	198	10	20	4	1	1185
L06	3.0	2.0	4.5	22	198	10	20	4	2	1386
L06s	3.0	2.0	4.5	22	198	10	20	4	2	1374
L07	1.5	2.5	4.5	22	198	10	20	3	1	945
L08	1.5	2.5	4.5	22	198	10	20	4	1	1294
L09	2.5	2.5	4.5	22	198	10	20	4	3	1521
L10	3.0	2.5	4.5	22	198	10	20	4	3	1522
L11	2.0	3.0	4.5	22	198	10	20	3	1	1155
L12	2.5	3.0	4.5	22	198	10	20	3	1	1268
L13	3.0	3.0	4.5	22	198	10	20	3	4	1329
L14	1.23	3.0	4.5	22	198	10	20	4	1	1425
L15	1.5	3.0	4.5	22	198	10	20	4	1	1501
L16	2.0	3.0	4.5	22	198	10	20	4	3	1537
L17	2.5	3.0	4.5	22	198	10	20	4	3	1539
L18	3.0	3.0	4.5	22	198	10	20	4	3	1537
L18s ^b	3.0	3.0	4.5	22	198	10	20	4	3	1533
L19	5.0	3.0	4.5	22	198	10	20	4	3	1507
L20	2.0	3.50	4.5	22	198	10	20	4	3	1527
L20s ^b	2.0	3.50	4.5	22	198	10	20	4	3	1480
L21	2.0	3.50	4.5	22	198	10	20	3	1, 4	1271
L22	2.0	3.77	4.5	22	198	10	20	3	1, 4	1250

s – hole shifted by 2 mm

(L04s, L06s, L18s – bolt B1 activates first, L20s – bolt B3 activates first)

- ^a
- 1 fracture in the specimen between hole and free edge perpendicular to the direction of load
 - 2 fracture in the specimen between bolt holes
 - 3 net cross-section failure
 - 4 shear failure of the bolt

^b test stopped before failure

NUMERICAL SIMULATIONS

Numerical simulations in finite element environment ABAQUS v6.7 (SIMULIA 2007) were performed in order to obtain stress-strain state of the connections and to

determine the bearing forces on bolts. The numerical model was assembled of three deformable, solid parts: inner plate (specimen), two cover plates and three or four bolts. An elastic material was prescribed to the bolts and to the cover plates, while elastic-plastic material model was prescribed to the inner plate. The individual contact interactions were prescribed between the parts. The “hard” contact in normal direction was defined between the bolt shank and the bolt-hole. The frictional contact in tangential direction was prescribed between the cover and the inner plate. The coefficient of friction equaling 0.25 was applied as a contact parameter. Its value was obtained through an iterative process for one connection, so that numerical resistance matched the experimental one. The same friction coefficient was then applied to the whole series of connections.

Due to the bearing pressure the inner plate deformed in thickness direction, generating pressure to the cover plates. The displacement of cover plates was restrained by bolts, although snug tight. The bolts acted like elastic springs, controlling the amount of friction.

TEST RESULTS

Test results are described herein by means of numerical simulations. The validation of numerical results is shown in Figs. 3-4. In Fig. 3 Mises stresses on a deformed mesh are plotted over actual specimens that failed in different ways. The fit of the deformed state (Fig. 4) as well as load-displacement curves (Fig. 3) is remarkable. The only exceptions are the connections where bolt shear failure was observed (see Table 1 – L13, L21, L22) or where the test was stopped before reaching the maximum resistance (L20s).

The bolts within the connection are denoted as B1, B2, B3 and B4, where bolt B1 is the closest to specimen’s free edge (see Fig. 4c). Similar notification is considered for holes. Hole H1 on the specimen is paired with bolt B1 and is considered as the first hole.

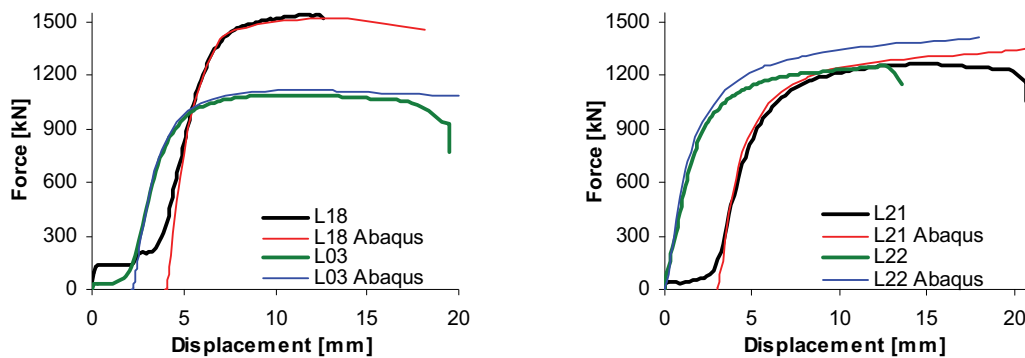
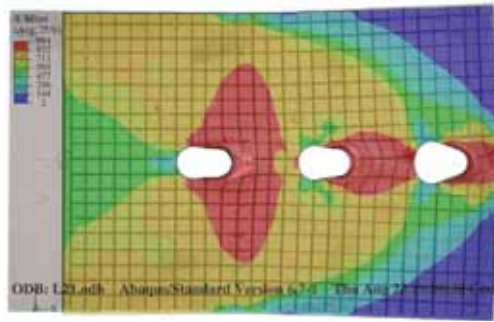
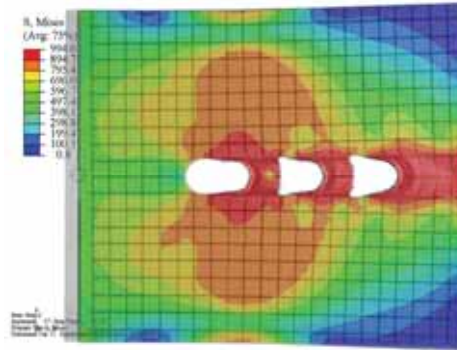


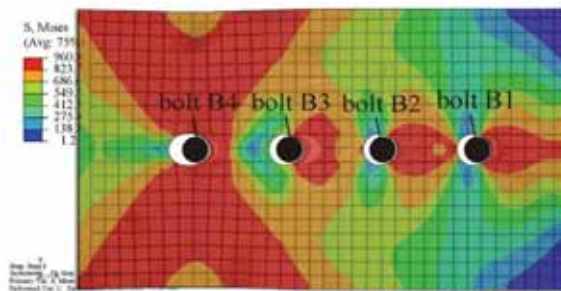
Fig. 3: Experimental and numerical load-displacement curves for specimens L03, L18, L21, L22



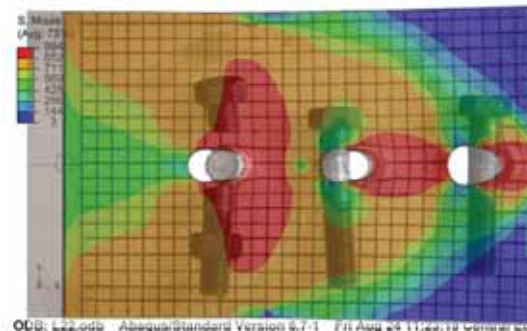
a) splitting failure of the material in front of hole H1; L21



b) shear failure between bolts; L03



c) net cross-section failure; L18



d) bolt shear failure; L22

Fig. 4: Mises stress on deformed mesh plotted over the actual specimens that failed in different modes

In general four types of failures were observed. The first type was the splitting failure (Fig. 4a). Due to transverse tension (see Fig. 5a) on the free edge perpendicular to the direction of loading, the crack was initiated. This kind of failure was observed in several cases (L04, L04s, L07, L08, L14, L15, L21), where the end distance was small ($e_1 \leq 2d_0$) and smaller than the pitch p_1 ($e_1 < p_1$). Unequal distribution of bearing forces (Fig. 6) is typical for this failure mode. It is important to understand stiffness of the cover plates changes the distribution of bearing forces on bolts (Može 2008). The second type was the shear failure. The fractures formed between bolts symmetrically to the bolt line (see Fig. 4b). The direction of the fractures coincided with maximum shear stresses in the plate in the direction of loading. The shear failures are distinctive of the connections with large end distance e_1 ($e_1 \geq 3d_0$) and small pitches p_1 ($p_1 \approx 2d_0$). High ductility (Fig. 3) and equal distribution of bearing forces (Fig. 6) characterized this failure mode. The third type of failure was a typical net cross-section failure (Fig. 4c) with two types of tensile flow instabilities, distinctive of a sheet tensile specimen. The diffuse necking as the first unstable flow was followed by localized necking, where the neck was a narrow band about equal to the plate thickness inclined at an angle to the specimen axis, across the width of the specimen. Net cross-section failure developed in case of narrow connection plates, large number of bolts or large pitches p_1 . The failure was ductile due to bolt-hole elongations and necking (Fig. 4c). The experimental load-displacement curve for specimen L18 (see Fig. 3) was characterized by initial sliding and several plateaus before reaching its true stiffness. This was due to bolt-hole clearance and geometrical tolerances of the forks to which specimen L18 was attached. The distribution of bearing forces between bolts was balanced equally, although bearing force on bolts B4 decreased when net cross-section yielded (Fig. 6). The shear failure

of the bolt was observed at specimens L13, L21, L22. In all three cases the last bolt B3 failed. Shear deformation of the bolt (Fig. 4d) was small due to high steel grade of bolts 12.9. In these cases the numerical load-displacement curves deviated from the experimental ones, because the bolts were modeled elastically (see Fig. 3).

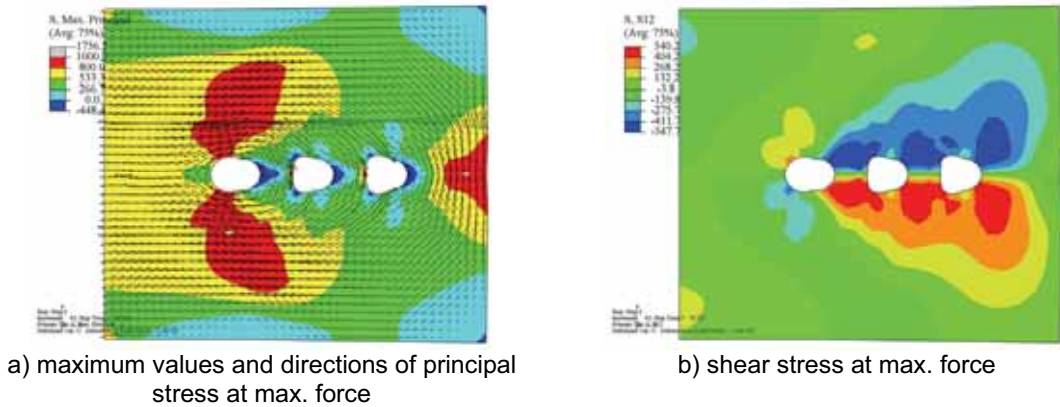


Fig. 5: Stress state of specimen L03

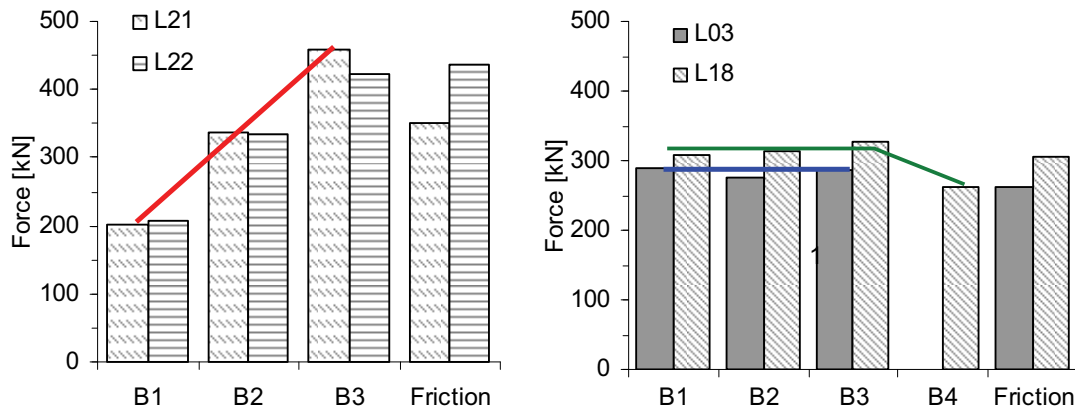


Fig. 6: Distribution of bearing forces at maximum resistance

Surprisingly, friction had significant impact on resistance and also on failure mode. Its magnitude at maximum resistance was equal to bearing force of one bolt (Fig. 6). Although the bolts were only snug tightened, the friction developed due to high bearing pressure. The stress peaks were eliminated by yielding of the material. Therefore, the plate deformed plastically in thickness, creating pressure on the cover plates. The deformation was restricted by bolts that acted as elastic springs. The contact area generating the friction was actually quite small, located in the bearing (stressed) edge of bolt-holes, as can be seen in Fig. 4 as the shiny surface before the bolt-holes. Due to large friction force, net cross-section failure could develop instead of some other failure mode. Moreover, this friction force is hard to estimate and should therefore be interpreted with caution.

The bolt-hole clearance had almost no effect on the connection resistance. As expected, the distribution of bearing forces between bolts was affected. Load displacement curves for connections with perfect (L04, L06) and shifted (L04s, L06s) geometry are plotted in Fig. 7. In both connections with shifted holes (L04s, L06s) the hole closest to the free edge was shifted by 2 mm (equal to bolt-hole clearance), thus

bolt B1 was activated before all the remaining bolts. The connections behaved as single bolt shear connections for the first 2 mm of deformation (bolt-hole clearance). After that the remaining bolts were activated and the distribution of bearing forces tended to become equal to the connection with perfect geometry (Figs. 7-10). In the previous tests of single bolt shear connections it was shown that the maximum resistance of the connection was developed at a displacement much larger than 2 mm (Može et al. 2006a; b). Therefore, the significant decrease of bearing force on bolt B1 (Fig. 7) was merely load redistribution and not connection component failure. At L06 and L06s the bearing force reached local maximum on bolt B1 at 285 and 320 kN (see Fig. 9), respectively. Bearing forces on the remaining bolts were always lower than 285 kN (see Figs. 9-10). In case of specimen L06s, the maximum bearing force on the bolt increased by 12% due to fabrication tolerances.

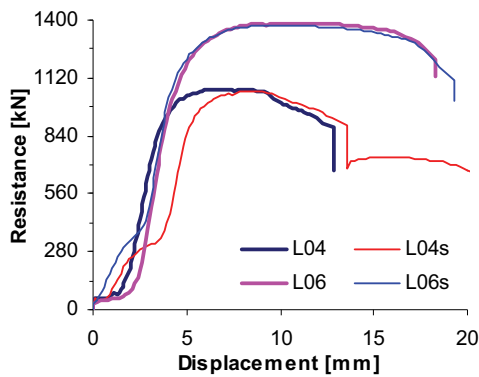


Fig. 7: Experimental and numerical load-displacement curves for specimens L04, L04s, L06, L06s

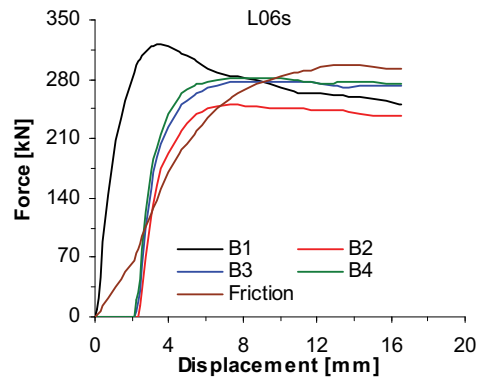


Fig. 8: Load-displacement curves of forces on bolts for specimen L06s

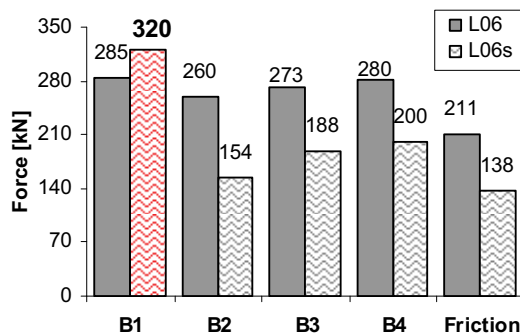


Fig. 9: Distribution of bearing forces for specimens L06, L06s at maximum force on bolt B1 (see Fig. 8)

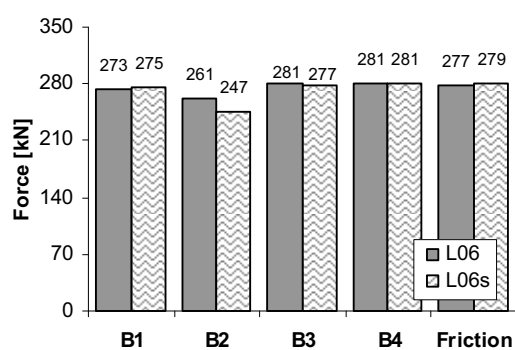


Fig. 10: Distribution of bearing forces for specimens L06, L06s at maximum resistance

ANALYSIS OF BEARING RESISTANCES IN RELATION TO EN 1993-1-8

Eurocode defines bearing resistance by mean bearing stress. The mean bearing stress is limited to control hole elongations (Snijder et al. 1988). Therefore, this control is not an ultimate limit state. Hence, Eurocode bearing resistance formula should always give lower values of bearing force than maximum actual bearing force.

In EN 1993-1-8 (CEN 2005) the design bearing resistance per bolt is defined as:

$$F_{b,Rd} = \frac{k_1 \alpha_b f_u d t}{\gamma_{M2}}, \quad (1)$$

where f_u is nominal ultimate tensile strength of the plate, d is bolt diameter, t is plate thickness and partial factor γ_{M2} with the recommended value of 1.25. Parameters α_b and k_1 are defined as given below and take into account mainly geometrical parameters:

- in the direction of load transfer

$$\alpha_b = \min\left(\alpha_d; \frac{f_{ub}}{f_u}; 1\right) \quad (2)$$

$$\alpha_d = \frac{e_1}{3d_0} \quad \text{for end bolts} \quad (3)$$

$$\alpha_d = \frac{p_1}{3d_0} - \frac{1}{4} \quad \text{for inner bolts} \quad (4)$$

- perpendicular to the direction of load transfer

$$k_1 = \min\left(2.8 \frac{e_2}{d_0} - 1.7; 2.5\right) \quad \text{for edge bolts} \quad (5)$$

$$k_1 = \min\left(1.4 \frac{p_2}{d_0} - 1.7; 2.5\right) \quad \text{for inner bolts} \quad (6)$$

According to Eurocode standard for HSS, the design net cross-section resistance is defined as:

$$N_{u,Rd} = \frac{0.9 f_u A_{net}}{\gamma_{M2}}. \quad (7)$$

In equation (7) the recommended value of partial factor γ_{M2} equals to $\gamma_{M2} = 1.25$ and A_{net} is the net cross section.

To compare Eurocode bearing resistance to actual bearing force on bolt, equations (1) and (7) are used without partial factors (γ_{M2} , γ_{M12}) and with actual geometry and material parameters.

In Fig. 11 the bearing force on the edge bolt calculated according to Eurocode is compared to the bearing force on the edge bolt as a result of the numerical analysis. The experimental results on tension splices in HSS with several bolts positioned in the direction of loading were gathered from literature (Kouhi and Kortessmaa 1990; Kim and Yura 1999; Aalberg and Larsen 2001; 2002). In order to obtain the bearing force on the individual bolts, we replicated the experiments by numerical simulations. These results are also presented together in Figs. 11-12. Eurocode formula estimates the bearing force on the edge bolt too bravely, since almost all points in Fig. 11 are positioned below the dotted diagonal. Considering the bearing force on the inner bolts (Fig. 12), the situation is the opposite. The bearing force was underestimated only for connections that failed in the net area that had large end and pitch distances. The resistance of the inner bolt was taken as the maximum bearing resistances on all except the edge bolt.

At the absence of bolt shear failure, the resistance of group of bolts is the sum of bearing resistances on the individual bolt. The minimum of this sum and net cross

section resistance (equation (7)) is considered as the connection maximum resistance. If this minimum is compared to the numerically obtained maximum connection resistance (including friction – see Fig. 13), all points move significantly above the dotted diagonal. The scatter of points is lower and the design function (1) is together with design net cross-section resistance (CEN 2007) reliable, since the required partial factor equals to 1.133. The reliability analysis was done according to Annex D of EN 1990 (CEN 2004).

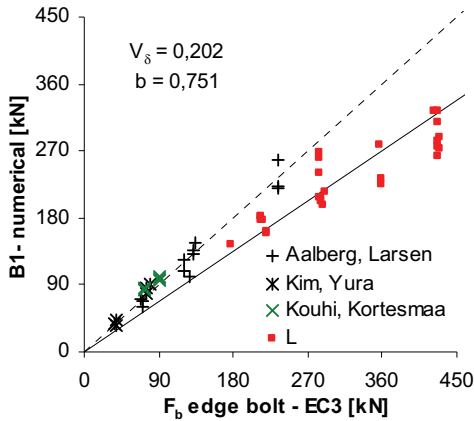


Fig. 11: Bearing force on the *edge* bolt as a result of numerical simulation versus Eurocode bearing resistance

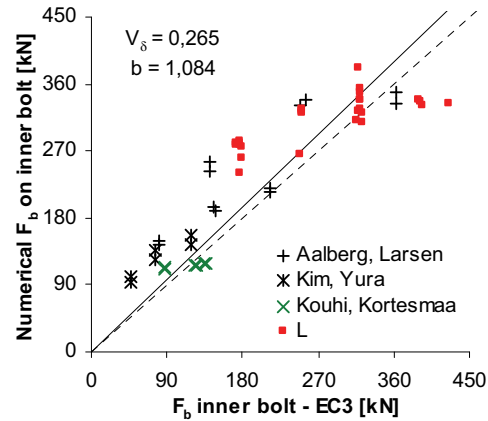


Fig. 12: Bearing force on the *inner* bolt as a result of numerical simulation versus Eurocode bearing resistance

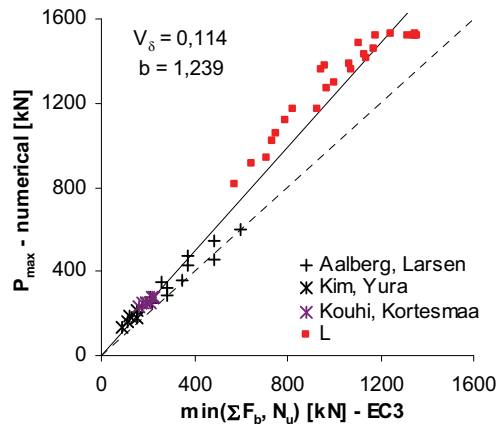


Fig. 13: Minimum of sum of bearing resistance and net area resistance according to Eurocode compared to maximum resistance of the connection

CONCLUSIONS

The distribution of bearing forces on bolts was obtained by the numerical simulations of the experiments on tension splices made of high strength steel with 3 or 4 bolts in double shear. It had been shown that certain geometries result in very unequal distribution of bearing forces. Although high strengths steels are considered to be less ductile, the local ductility in multi-bolt connections is sufficient for reducing stress concentrations and for the redistribution of bearing forces between all bolts. The current

Eurocode design rule for bearing resistance on individual bolt estimates the bearing force on the edge bolt too optimistically.

REFERENCES

Aalberg, A., and Larsen, P. K. (2001). "Bearing strength of bolted connections in high strength steel." *Nordic Steel Construction Conference 2001 - NSCC 2001 : proceedings*, Helsinki, 859-866.

Aalberg, A., and Larsen, P. K. (2002). "The effect of steel strength and ductility on bearing failure of bolted connections." *The Third European Conference on Steel Structures: Proceedings of the 3rd European conference on steel structures*, Coimbra, 869-878.

CEN. (2004). "Eurocode - Basis of structural design." EN 1990, European Committee for Standardisation, Brussels.

CEN. (2005). "Eurocode 3: Design of steel structures - Part 1-8: Design of joints." EN 1993-1-8, European Committee for Standardisation, Brussels.

CEN. (2007). "Eurocode 3: Design of steel structures - Part 1-12: Additional rules for the extension of EN 1993 up to steel grades S 700." EN 1993-1-12, European Committee for Standardisation, Brussels.

Kim, H. J., and Yura, J. A. (1999). "The effect of ultimate-to-yield ratio on the bearing strength of bolted connections." *Journal of Constructional Steel Research*, 49(3), 255-270.

Kouhi, J., and Korteesmaa, M. (1990). "Strength tests on bolted connections using high-strength steels (HSS steels) as a base material." *Research notes 1185*, Technical Research Centre of Finland, Espoo.

Može, P. (2008). "Ductility and resistance of bolted connections in structures made of high strength steels," Doctoral thesis, University of Ljubljana, Faculty of Civil and Geodetic Engineering, Ljubljana.

Može, P., Beg, D., and Lopatič, J. (2006a). "Ductility and strength of bolted connections made of high strength steel." *Steel - a new and traditional material for building: proceedings of the International Conference in Metal Structures*, Poiana Brasov, Romania, 323-330.

Može, P., Beg, D., and Lopatič, J. (2006b). "Local ductility of structures made of high strength steel." *STESSA 2006: proceedings of the fifth International conference on behaviour of steel structures in seismic areas*, Yokohama, Japan, 169-174.

Može, P., Beg, D., and Lopatič, J. (2007). "Net cross-section design resistance and local ductility of elements made of high strength steel." *Journal of Constructional Steel Research*, 63(11), 1431-1441.

SIMULIA. (2007). "Abaqus Online Documentation: Version 6.7." Dassault Systèmes.

Snijder, H. H., Ungermann, D., Stark, J. W. B., Sedlacek, G., Bijlaard, F. S. K., and Hemmert-Halswick, A. (1988). "Evaluation of test results on bolted connections in order to obtain strength functions and suitable model factors - Part A: Results." *Document 6.01*, Eurocode 3 Editorial Group.

STIFFNESS OF LAP JOINTS WITH PRELOADED BOLTS

A.M. (NoI) Gresnigt
Delft University of Technology, The Netherlands
a.m.gresnigt@tudelft.nl

ABSTRACT

A model for the determination of the load deformation behaviour of lap joints with preloaded bolts is presented. The influence of the plate conditions grit blasted and as rolled with mill scale is taken into account, based on recent test results at the Stevin Laboratory in Delft. Also the effect of repeated slip on the load deformation behaviour is reported. The stiffness of the lap joints is compared with the stiffness of welded joints. This is important where bolted and welded connections act together in fatigue loading. The application of the model in the design of partly welded and partly bolted connections in the main girders of the movable part of the Van Brienenoord Bridge in Rotterdam is demonstrated.

INTRODUCTION

In 1997, fatigue cracks were found in the deck of the movable part of one of the two Van Brienenoord Bridges near Rotterdam (Figure 1). Figure 2 gives an impression of the cross-section and the layout of the bridge deck where the cracks were found.

Several methods of repair and strengthening of the bridge deck were considered. An important factor in the decision process was the demand to limit the time of closure as much as possible. The work was to be started and completed within one week in a "low traffic" period of the year (beginning of August 1998). Repair and strengthening of the deck in situ would take too much time.

It was decided to replace the damaged part just before the main hinges (pivots). This meant the cutting of the two main girders, the removal of the old deck, the positioning of the new deck and the connection of its main girders to the remaining part (the joint in Figure 2). Figure 3 gives an impression of the installation of the new bridge deck.

At the joint, the main girders are about 8100 mm high, the web has a thickness of 40 mm and the bottom flanges have a cross-section of 1000 x 70 mm. Welding would take far too much time. The other possibility was bolting. But bolting at the bridge deck level, the top flange, was not considered a real option because of the demands on flatness of the bridge deck. It was decided to investigate the possibility of a partly welded, partly bolted joint.

For the fatigue resistance it is important to carefully consider the point where the weld in the web stops and the bolted joint begins. In order to avoid stress concentrations, the

stiffness of the welded part and the bolted part should be about equal, with a preference for a slightly stiffer bolted joint, to be discussed later.

Therefore, a study was carried out into the stiffness of bolted lap joints, to be compared with the stiffness of welded joints. Figure 4 shows the design of the joint where the top flange and a part of the web below (500 mm) is welded and the remainder of the web and the bottom flange are bolted with high strength friction grip (HSFG) bolts M36-10.9.



Figure 1. The Van Brienenoord bridges in the main North-South highway in Rotterdam. The words *wegens vermoeiing* mean *because of fatigue*.

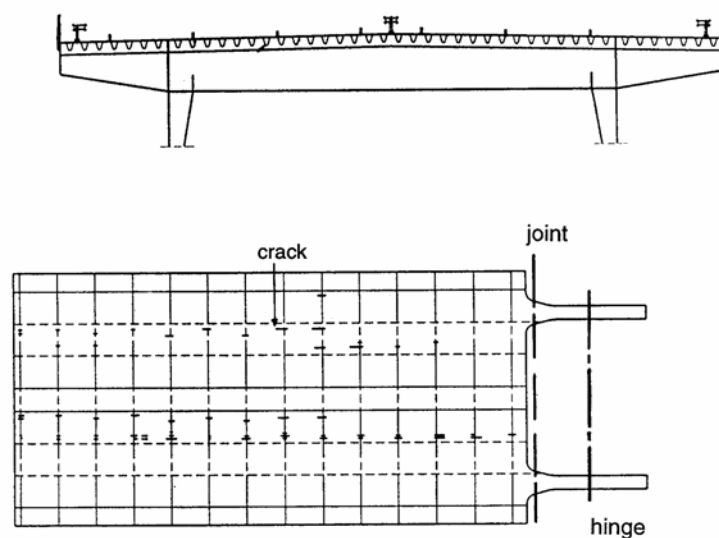


Figure 2. Cross-section and layout of the movable bridge. The length of the deck is 54 meter. The bridge has 2 x 3 lanes.

In the study a model for the determination of the load distribution in the bolts and the stiffness of the lap joint was developed. The model was presented in 2000 in a workshop in Greece on "The Paramount Role of Joints into the Reliable Response of Structures", (Gresnigt, Steenhuis, 2000). At the 2004 ECCS – AISC Connections V Workshop in Amsterdam, Pietrapertosa (2004) presented a paper on the ductility requirements in shear bolted connections. To determine the distribution of forces in the bolted lap joints a similar model was applied.

In this paper, a model for the determination of the load distribution in the HSFG bolts and the stiffness of lap joints is given. The model is validated with several tests that were available at the time of the study in 1999 and with test results that were obtained in a test programme carried out in 2004 in the TU-Delft Stevin Laboratory.

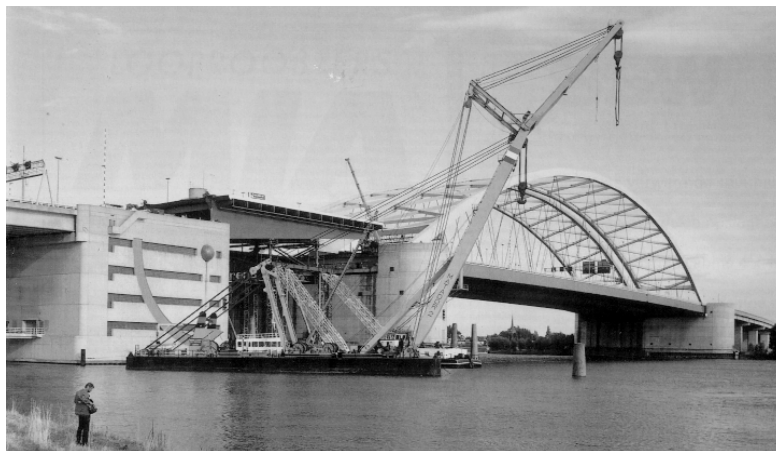


Figure 3. Installation of the new bridge deck.

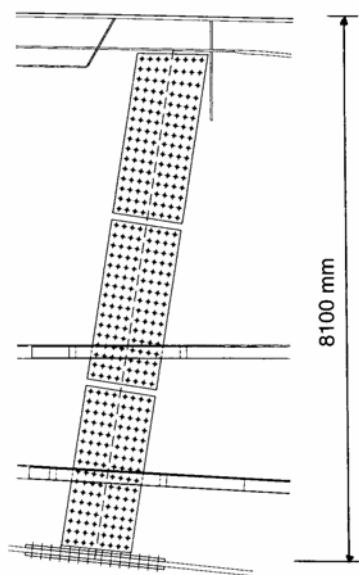


Figure 4. The partly welded and partly bolted joint in the main girders. For the bolted part of the web, lap joints were proposed with 1040 x 25 mm plates and for the bottom flange lap joints with 1200 x 40 mm plates.

DESIGN MODEL

Figure 5 gives the geometry of a bolt row in the web of the Van Brienoord Bridge. Also the geometry of a welded joint with the same "measuring length" is given. The web thickness is 40 mm. The thickness of the cover plates is 25 mm. The standard distance between the bolt rows is 150 mm. At the top end of the bolted part, the bolt rows are not parallel (distance between bolt rows about 150 and 190 mm). For the calculations a distance of 175 mm is adopted. HSFG bolts M36 – 10.9 were applied.

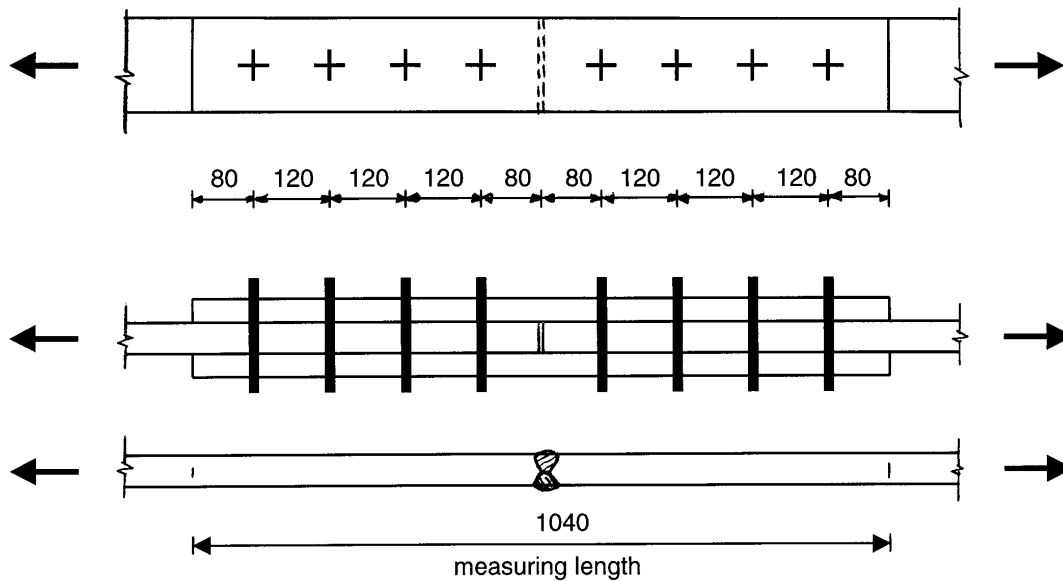


Figure 5. Bolted lap joint and welded joint in the Van Brienoord Bridge.

The joint can be conceived as a system of springs, each spring having its own characteristic stiffness, see Figure 6. For the bolts the most important factor is the deformation caused by the load transfer by friction. Because of symmetry, half of the bolted lap joint is taken into account. In the model, the following notations are used.

- A_h : Cross-sectional area of the main plate: $A_h = t_h * b$
- A_s : Cross-sectional area of the cover plate: $A_s = t_s * b$
- b : Width of the plate (distance between bolt rows)
- p : Pitch (distance between bolts)
- l_{begin} : Edge distance cover plates
- l_{end} : Edge distance main plate
- $B_1 B_2 B_3 B_4$: Forces transmitted by HSFG bolts
- $H_0 H_1 H_2 H_3$: Parts in the main plate
- $S_1 S_2 S_3 S_4$: Parts in the cover plates
- $\sigma_{h0} \sigma_{h1} \sigma_{h2} \sigma_{h3}$: Stresses in the main plate
- $\sigma_{s1} \sigma_{s2} \sigma_{s3} \sigma_{s4}$: Stresses in the cover plates
- $d_{b1} d_{b2} d_{b3} d_{b4}$: Displacements in the bolts B_1, B_2, B_3, B_4
- $d_{h0} d_{h1} d_{h2} d_{h3}$: Displacements in the parts H_0, H_1, H_2, H_3 of the main plate.

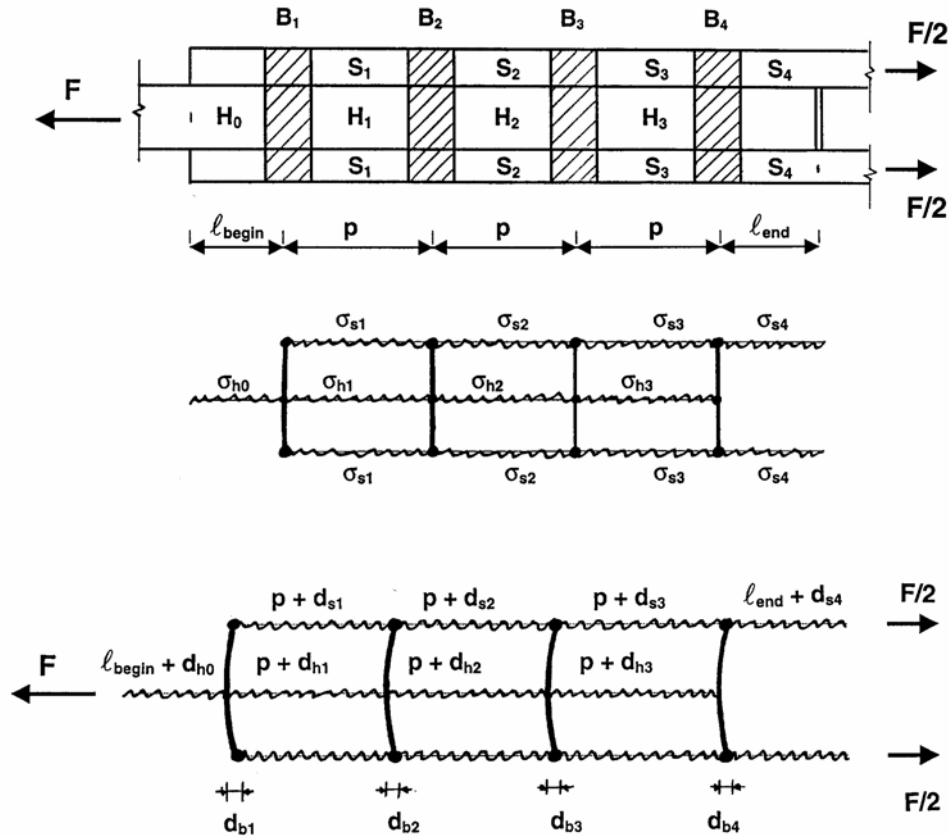


Figure 6. Spring model for a lap joint with four high strength friction grip bolts.

The displacements in the bolts are a function of the load to be transmitted by the bolt and the properties (condition) of the plate surfaces at the friction plane. Also the geometry of the bolt-plate assembly will have some influence. The relation between the bolt forces B_1, B_2, B_3, B_4 and the displacements $d_{b1}, d_{b2}, d_{b3}, d_{b4}$ will be discussed in the next section on the load deformation behaviour of a single bolt. The stresses in the main plates and cover plates are:

$$\sigma_{h1} = \frac{F - B_1}{A_h} \quad (1a) \quad \sigma_{s1} = \frac{B_1}{2 \cdot A_s} \quad (2a)$$

$$\sigma_{h2} = \frac{F - B_1 - B_2}{A_h} \quad (1b) \quad \sigma_{s2} = \frac{B_1 + B_2}{2 \cdot A_s} \quad (2b)$$

$$\sigma_{h3} = \frac{F - B_1 - B_2 - B_3}{A_h} \quad (1c) \quad \sigma_{s3} = \frac{B_1 + B_2 + B_3}{2 \cdot A_s} \quad (2c)$$

$$\sigma_{h0} = \frac{F}{A_h} \quad (1d) \quad \sigma_{s4} = \frac{B_1 + B_2 + B_3 + B_4}{2 \cdot A_s} \quad (2d)$$

The elongations in the main plates and cover plates can be calculated as follows:

$$d_{h1} = \frac{\sigma_{h1}}{E} \cdot p \quad (3a) \quad d_{s1} = \frac{\sigma_{s1}}{E} \cdot p \quad (4a)$$

$$d_{h2} = \frac{\sigma_{h2}}{E} \cdot p \quad (3b)$$

$$d_{s2} = \frac{\sigma_{s2}}{E} \cdot p \quad (4b)$$

$$d_{h3} = \frac{\sigma_{h3}}{E} \cdot p \quad (3c)$$

$$d_{s3} = \frac{\sigma_{s3}}{E} \cdot p \quad (4c)$$

$$d_{h0} = \frac{\sigma_{h0}}{E} \cdot \ell_{begin} \quad (3d)$$

$$d_{s4} = \frac{\sigma_{s4}}{E} \cdot \ell_{end} \quad (4d)$$

The compatibility conditions are:

$$\begin{aligned} d_{b1} + p + d_{s1} &= p + d_{h1} + d_{b2} \\ d_{b2} + p + d_{s2} &= p + d_{h2} + d_{b3} \\ d_{b3} + p + d_{s3} &= p + d_{h3} + d_{b4} \end{aligned} \quad (5)$$

The total elongation is:

$$\delta_{tot} = d_{h0} + d_{h1} + d_{h2} + d_{h3} + d_{b4} + d_{s4} \quad (6a)$$

Also:

$$\delta_{tot} = d_{h0} + d_{b1} + d_{s1} + d_{s2} + d_{s3} + d_{s4} \quad (6b)$$

The total load F is:

$$F = B_1 + B_2 + B_3 + B_4 \quad (7)$$

With these equations, the unknowns can be determined and the elongation can be calculated for different values of F, if also the load-deformation behaviour of single bolts is known, see next section.

THE LOAD-DEFORMATION BEHAVIOUR OF A SINGLE BOLT

As indicated before, it is necessary to know the load-deformation behaviour of a single bolt as an input parameter in the spring model. A literature study has been carried out to collect relevant test data. Only a rather small number of test data were found where the elongation of lap joints was measured over the measuring length as defined in Figure 5.

In 1966-1967, the Otto-Graf-Institute carried out many tests on HSFG bolted lap joints for the "Office for Research and Experiments of the International Union of Railways" (ORE, 1966). Several tests were lap joints with two bolts at each side of the lap joint. Figure 7 and Figure 8 give the test specimen and the test set-up. It is noted that in this test set-up, there was a direct measurement of the deformation at the bolts. Figure 9 gives, as an example, the measured load-deformation diagrams of one of the tests.

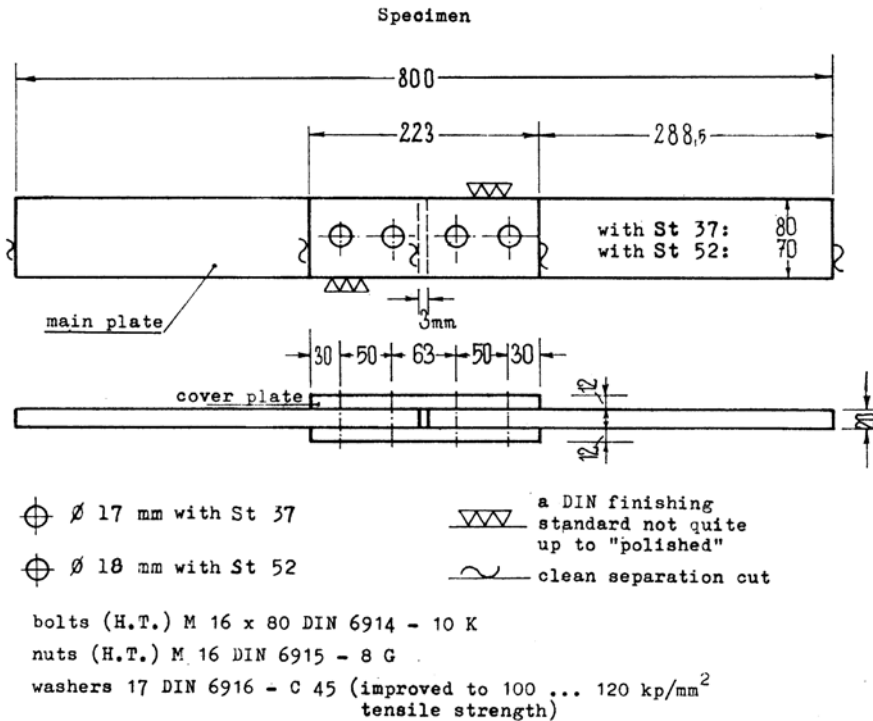


Figure 7. Test specimen ORE-tests with 2 * 2 bolts.

Further to Figure 7, the ORE-report gives the following details:

- The surfaces were blasted with chilled iron grit grain size 34, sharp edged, hardness HVI = 700-800 kg/mm², grain size mixture: 75% of grain size 0,3 to 0,5 mm, 25% of oversized grain and/or undersized grain.
- Steel grade St 52-3 (DIN 17100) and St 37-2. The steel grade had a minor influence on the results (less than the scatter in the tests with the same steel grade).
- Because of the fact that the thickness of the main plate was 20 mm, while the total thickness of the cover plates was 24 mm, the load transfer of the inner bolts was slightly lower than of the outer bolts. With the model, the bolt forces ($B_1 + B_2 = F$) were calculated. The following values serve as an example: $60,0 + 56,8 = 116,8$ kN and $120,0 + 118,2 = 238,2$ kN.

From Figure 8 it can be seen that the displacements between both plates were measured at the bolt level. In some other test series the deformations were measured over the measuring length as defined in Figure 5, but in most test series found, the displacements were measured between the end of the cover plate and the adjacent main plate. These measurements are not very useful for the present model, because they only contain the deformation of the outer bolt (B_1) and the elongation of a part of the main plate (d_{h0}).

Figure 9 gives the measured load-deformation diagrams of one of the ORE tests. The pre-load in the M16 bolts was 100,0 and 100,0 kN (upper bolts) and 99,4 and 110,5 kN

(lower bolts). The friction coefficient for the upper bolts was 0,667 and for the lower bolts 0,683.

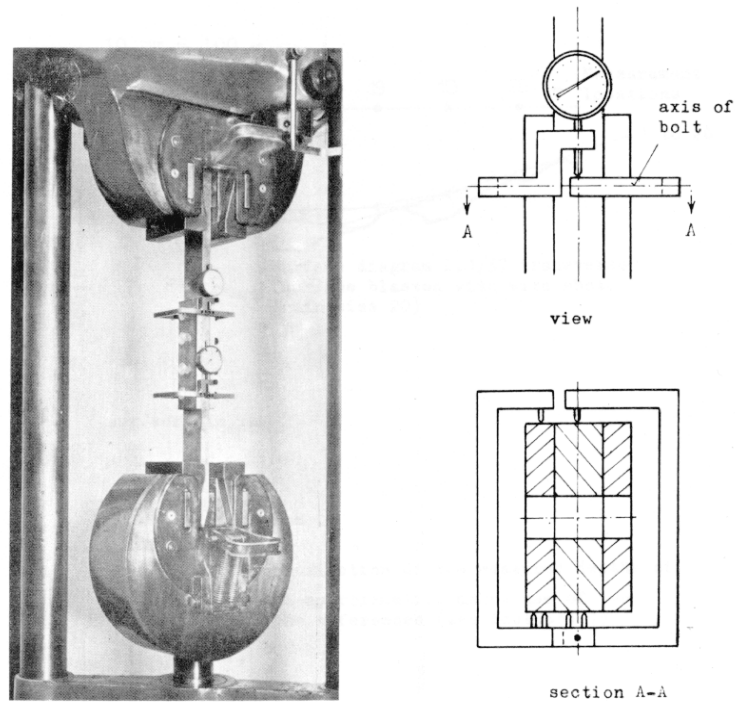


Figure 8. Test set-up of the ORE-tests with 2 * 2 bolts.

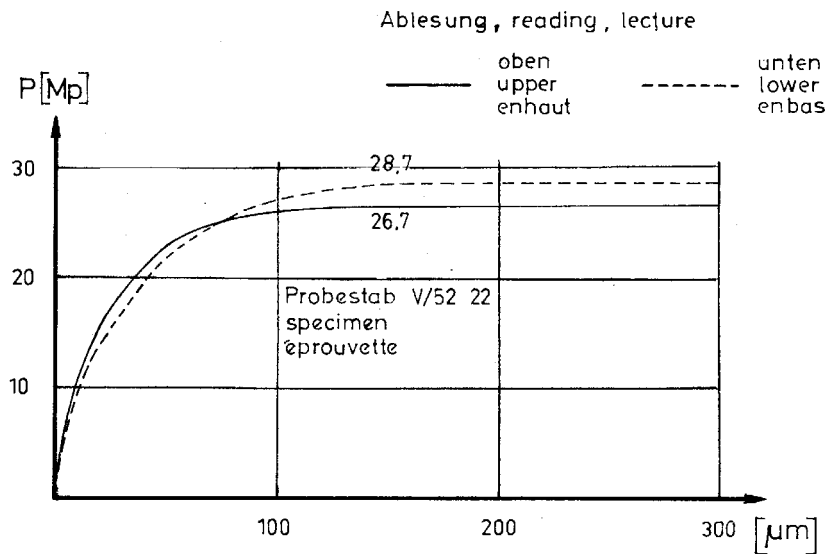


Figure 9. Measured load-deformation diagrams of test V/52-22.

In Figure 10 the results of four tests are compared with the model (equation 8). The vertical axis is made non-dimensional by dividing the load by the slip-load. It can be seen that quite some scatter occurs, despite the careful way of preparing the test specimens and execution of the tests.

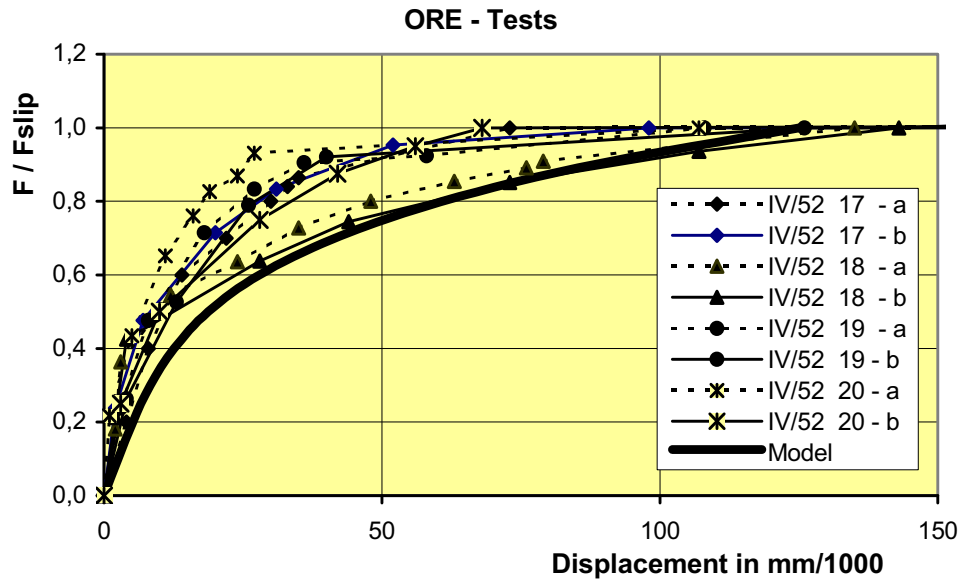


Figure 10. Dimensionless load-deformation diagrams of bolts in tests IV/52-17, IV/52-18, IV/52-19 and IV/52-20, compared with the model.

From the ORE tests and also from other tests it appears that the load-deformation characteristic is non-linear. For the spring model we developed the following equation:

$$\delta = 100 \left(\frac{F}{F_{slip}} \right)^{\alpha} + 25 \frac{F}{F_{slip}} \quad (8)$$

where:

- δ : displacement (mm/1000)
- α : coefficient ($\alpha = 4$)
- F : force transferred by the HSFG bolt (kN)
- F_{slip} : slip force (kN).

This equation gives a reasonable fit with the ORE test results, see Figure 10.

VALIDATION OF THE MODEL WITH OTHER TESTS

In the literature, a number of test series is found where the load-deformation behaviour for test specimens with more bolts was measured. The tests by Foreman-Rumpf (1961) and Klöppel-Seeger (1965) are most suited for this comparison. Figure 11 gives one of the test specimens and test results according to Foreman-Rumpf (1961). Figure 12 gives the comparison of these test results with the model.

Foreman-Rumpf have compared riveted and HSFGB bolted joints. In Figure 11, A_g is the load-deformation behaviour of a plate, while A_n is the load-deformation behaviour of the main plate in a bolted or riveted joint, taking into account the influence of the bolt holes.

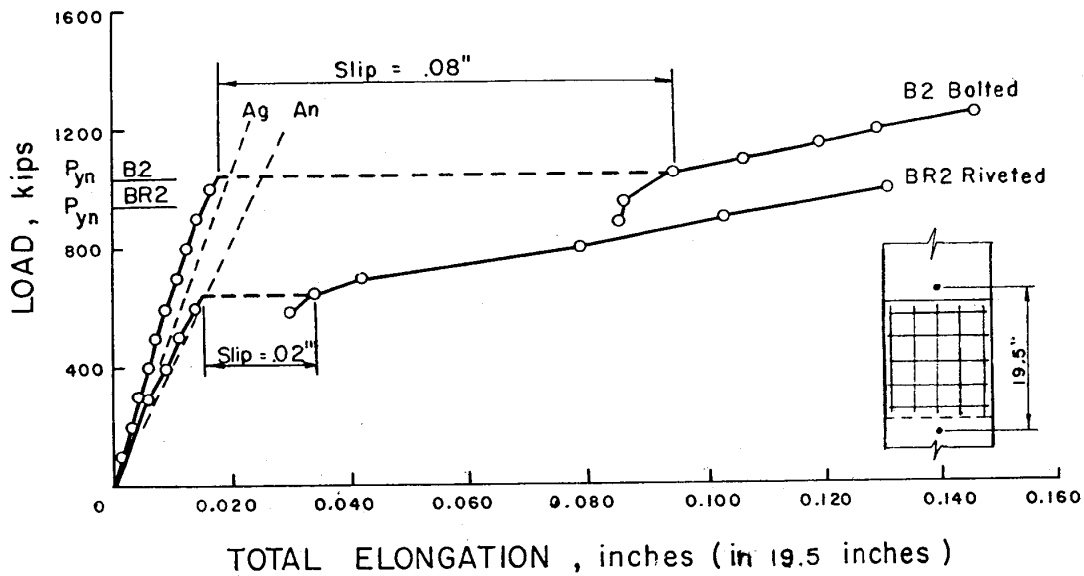


Figure 11. One of the test specimens and test results according to figure 7 according to Foreman-Rumpf (1961).

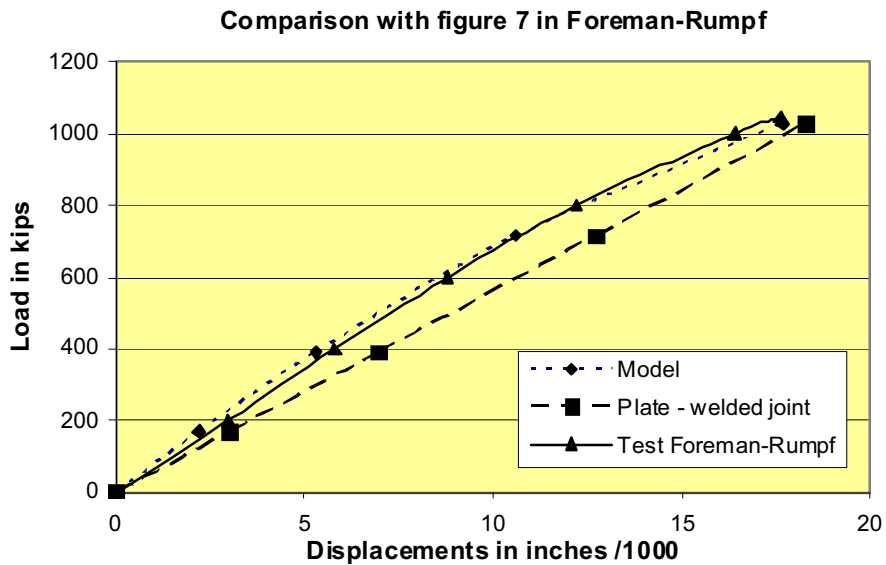


Figure 12. Load-deformation behaviour of the HSFGB bolted joint and welded joint (= plate only), compared with the model.

Figure 13 gives one of the test specimens and two test results according to Klöppel-Seeger (1965). In these two tests the surfaces were sandblasted, then during 6 weeks,

the plates were subjected to corrosion in a wet condition and finally brushed before assembling the test specimens. Figure 14 gives the comparison of these test results with the model.

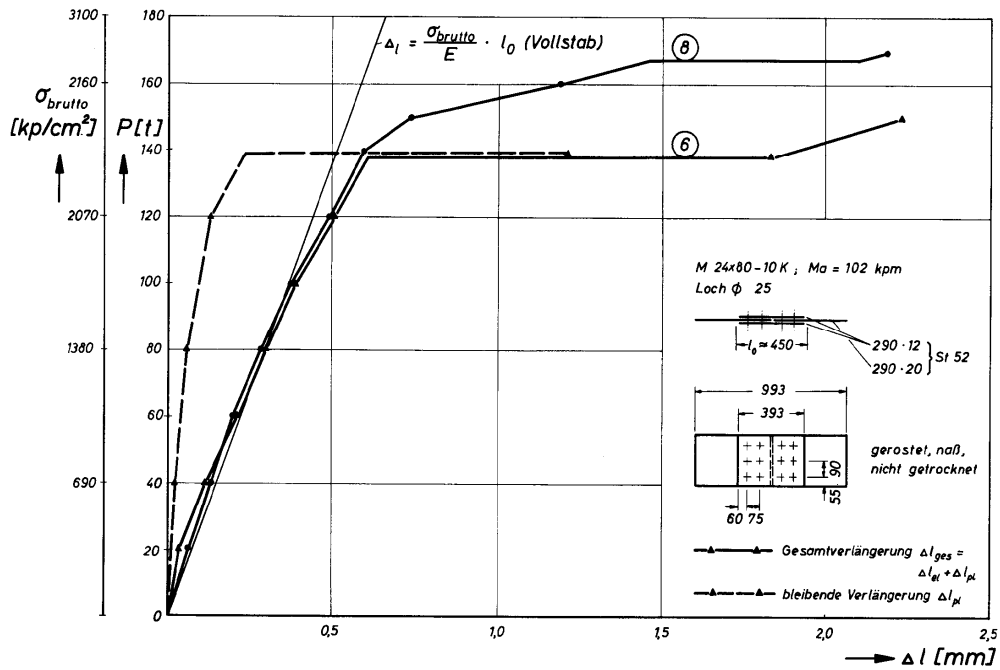


Figure 13. Test specimens and two test results according to "Bild23" on page 65 of Klöppel-Seeger (1965).

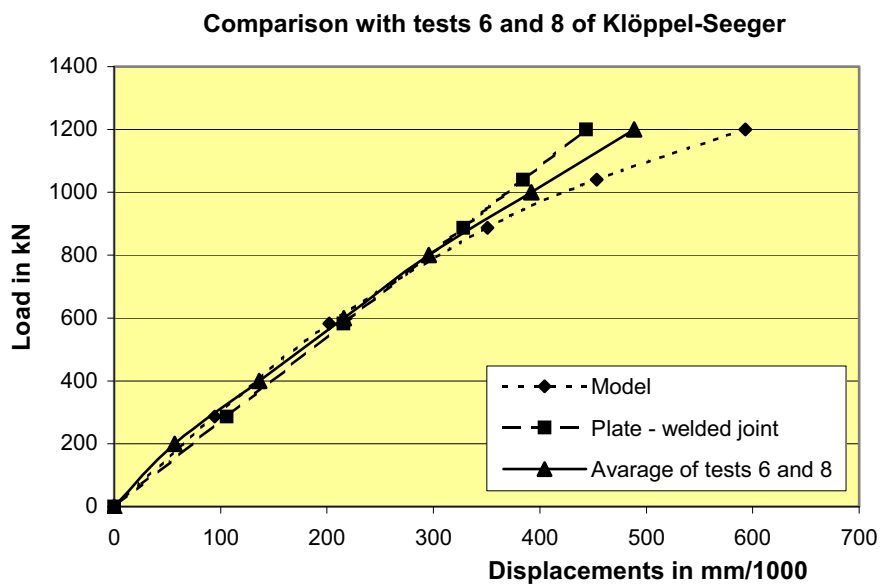


Figure 14. Load-deformation behaviour of the HSFGB bolted joint and a welded joint according to Figure 13, compared with the model.

TESTS AT THE STEVIN LABORATORY TU-DELFT

In 2004 tests were carried out for further validation of equation (8). The tests were performed in a students education programme. The test set-up is shown in Figure 15.



Measurement of the displacement between the main plate and the cover plate at bolt level (LVDT bolt).

- Steel S355
- Bolts M36 grade 10.9
- Holes 39 mm
- Main plate 150 x 15 mm²
- Cover plates: 150 x 10 x 400 mm
- End distance 80 mm

Figure 15. Test set up to measure load-deformation behaviour of preloaded connection.

In order to prevent slip at the upper bolt, the preload of the upper bolt was about 20 % higher than the preload of the lower bolt. The preload of the lower bolt was measured with a hollow load cell. The tests were carried out in a standard tensile machine. The following measurements were carried out:

- The force in the tensile machine.
- The change of the preload in the bolt.
- The displacement "LVDT bolt" between main plate and cover plate at the bolt level.
- The displacement "LVDT a" between the main plate and the cover plate at the end of the cover plate. The distance between the end of the cover plate and the centre of the glued block with "LVDT a" was 65 mm.
- The overall displacement "LVDT b". The measuring length was 440 mm.

Tests were carried out with plates as rolled (with mill scale) and grit blasted. Several plates were used two times and two plates even three times. In doing this, the effect of slip of previous test(s) could be studied. Table 1 gives an overview of the tests that were carried out. Test 2 was not performed and in test 5 and 17 the measuring equipment failed.

Table 1. Overview of tests carried out at TU-Delft. The values of the LVDT's are the values measured at maximum load (F-slip).

Test	Date	Surface	F-slip [kN]	F-preload [kN]	Friction μ	LVDT bolt [mm]	LVDT a [mm]	LVDT b [mm]
1	10-11-04	Mill scale	143	309	0,23	0,023	0,070	
3	12-11-04	Mill scale	149	302	0,25	0,038	0,075	
4	12-11-04	Mill scale	218	308	0,35	0,071	0,125	
6	18-11-04	Grit 1st	304	337	0,45	0,043	0,148	
7	19-11-04	Grit 1st	314	246	0,64	0,097	0,156	
8	19-11-04	Grit 2nd	260	326	0,40	0,052	0,087	
9	24-11-04	Grit 2nd	288	306	0,47	0,055	0,117	0,290
10	25-11-04	Grit 1st	356	288	0,62	0,086	0,176	0,454
11	26-11-04	Mill scale	156	335	0,23	0,038	0,073	0,168
12	26-11-04	Grit 2nd	264	277	0,48	0,051	0,131	0,270
13	1-12-04	Mill scale	176	316	0,28	0,048	0,054	0,111
14	2-12-04	Grit 1st	363	315	0,58	0,082	0,163	0,481
15	3-12-04	Mill scale	136	320	0,21	0,033	0,053	0,136
16	8-12-04	Grit 3rd	248	327	0,38	0,045	0,102	0,262
18	10-12-04	Grit 3rd	263	305	0,43	0,054	0,108	0,271

The main test results for the test specimens with grit blasted surfaces are given in Figure 16 and Figure 17. Also the load-deformation diagrams according to the model are given.

- From Figure 16 (left figure) it appears that there is practically no difference between the stiffness of the test specimens with surfaces that were used for the first time, second time or third time, especially at low loads.
- Reference is made to the research carried out by Van der Vegte and Makino (2007) on the effect of the friction coefficient on the cyclic behaviour of bolted beam-to-RHS column connections. They found that for contact between untreated (i.e. rusted) surfaces, the friction coefficient slightly reduces as the cumulative slip length increases. For reversed loading between shot brushed surfaces, the friction coefficient may vary sharply i.e. may initially decline and increase later as cycling continues due to severe damage of the contact surfaces.
- In the dimensionless load deformation behaviour, there is a clear difference between the specimens with surfaces that were used for the first time or second or third time,

see Figure 16 (right figure). The reason is slip at relatively low loads (low coefficient of friction μ). In the model a low coefficient of friction reduces the stiffness. Probably the best solution is to introduce a minimum value of μ in the model, e.g. $\mu = 0,4$.

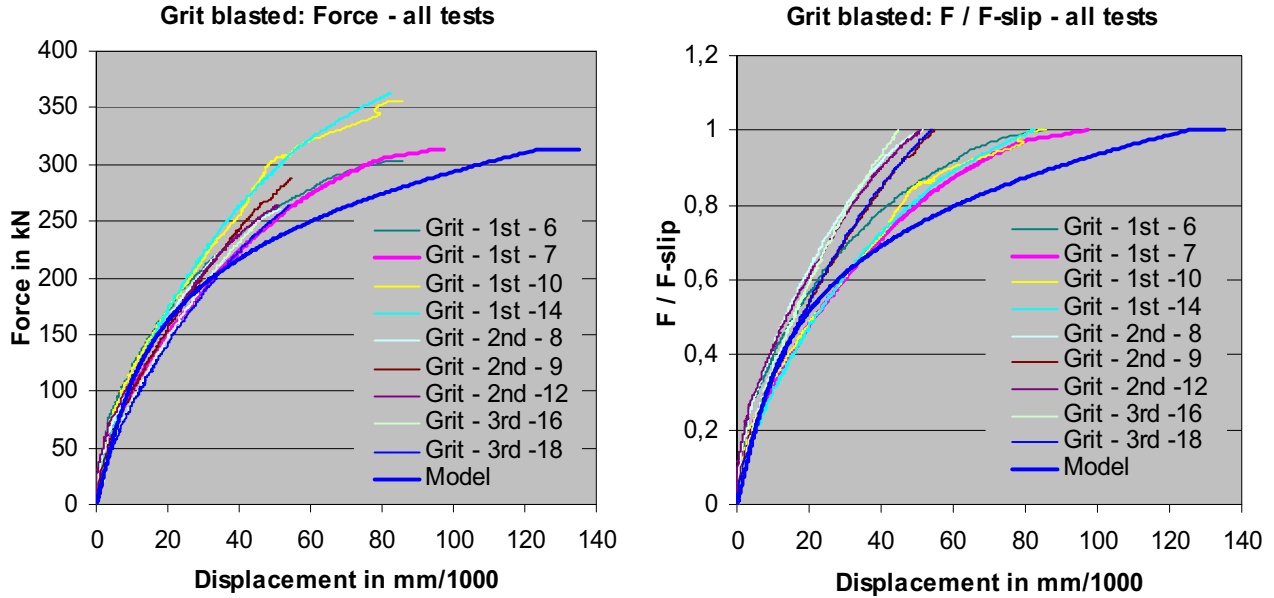


Figure 16. Load-deformation diagrams of all tests with grit blasted surface. The model in the left figure is given for test 7 with a coefficient of friction $\mu = 0,64$.

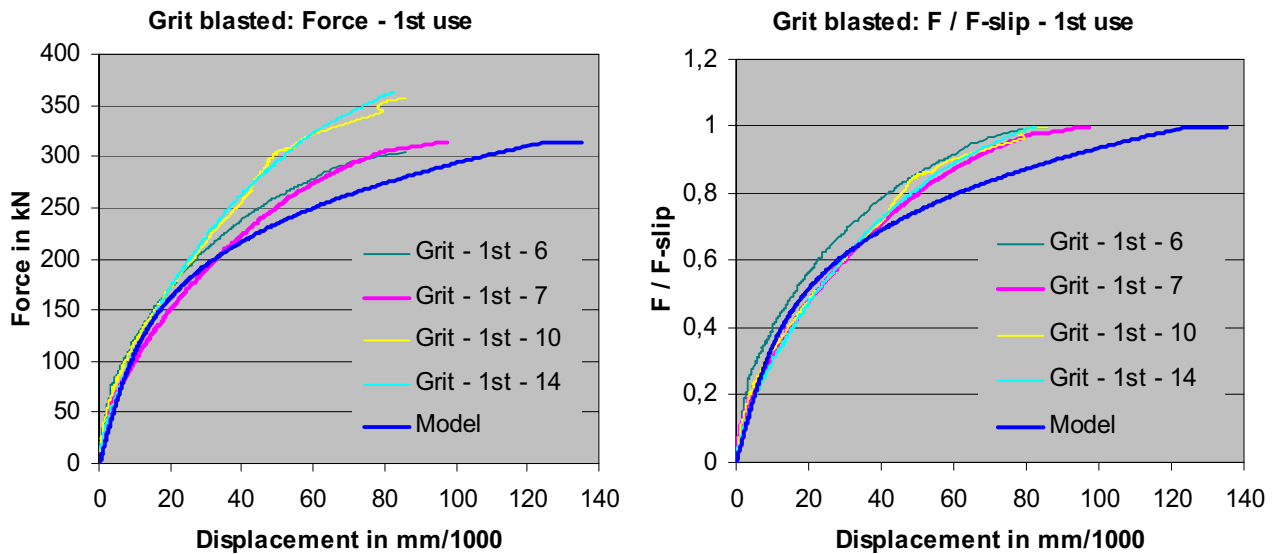


Figure 17. Load-deformation diagrams of the tests with grit blasted surface, first use. The model in the left figure is given for test 7 with $\mu = 0,64$.

The test results for the test specimens with mill scale are given in Figure 18. Also the load-deformation diagrams according to the model are given.

- From the left figure in Figure 18 it appears that also the stiffness of the test specimens with mill scale give good agreement with the model. The model is given for a preload in the bolt of 320 kN and a coefficient of friction $\mu = 0,35$. This gives a slip load of 224 kN.
- In the dimensionless load deformation behaviour, the agreement is less good. As in the tests with grit blasted surfaces, the reason is slip at relatively loads (low coefficient of friction). Probably the best solution is to introduce a minimum coefficient of friction μ in the model of e.g. 0,3 or 0,4.

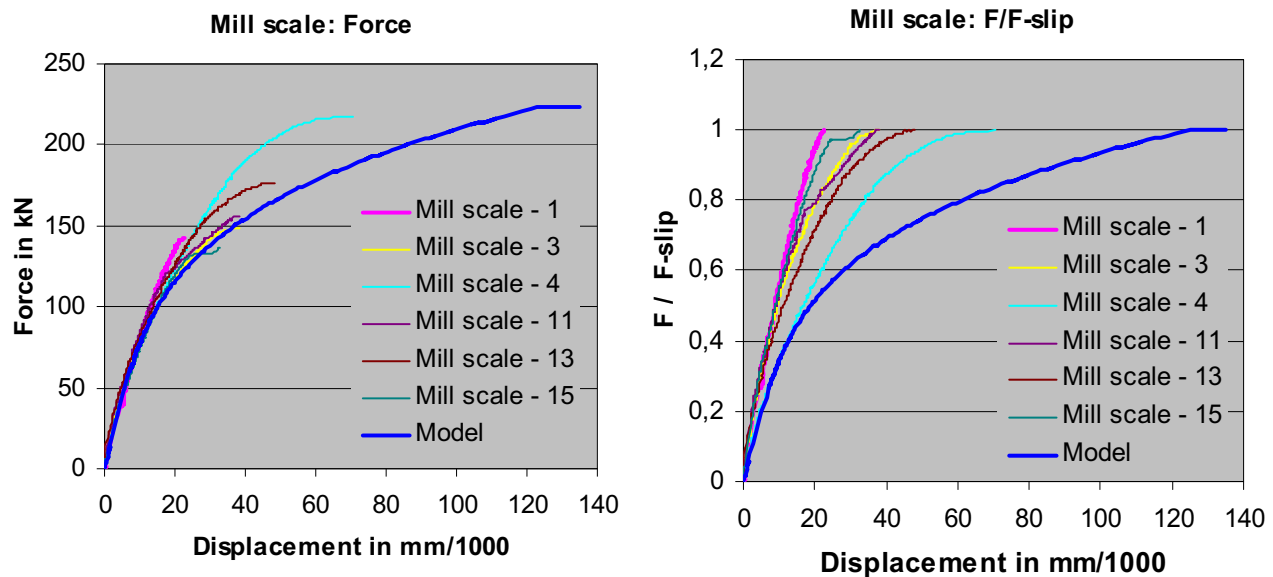


Figure 18. Load-deformation diagrams of the tests with mill scale.

Displacements between the main plate and the cover plate

Also the displacements between the main plate and the cover plate at the end of the cover plate (measured with the "LVDT's a") were checked with the model. The predicted displacements were somewhat higher than the measured values. This is on the safe side as will be explained later.

Till about 70 % of the slip load, these differences were less than 10 to 20 %. At larger loads the differences increase as can be expected from the measurements at the bolt level (Figure 16 - Figure 18).

APPLICATION TO THE VAN BRIENENOORD BRIDGE

Figure 19 gives the load-deformation behaviour of the proposed bolted joint in the web of the main girders compared to the load-deformation behaviour of a welded joint with the same length. The figure contains two lines for the calculated stiffness of the bolted joint.

The model with constants 25 and 100 gives the results for the load-deformation behaviour of the bolts according to equation (9). The model with constants 50 and 150 gives the results for less stiff load-deformation behaviour of the bolt where in equation (9) the constants 25 and 100 are replaced by 50 and 150. In both cases the bolted joint is stiffer than the welded one.

The fact that the bolted joint is stiffer than the welded joint is on the safe side, since the fatigue strength of HSFG bolted joints is better than of butt welded joints, especially at the ends of welded joints. The results also show that in case the rather heavy bolts give somewhat larger displacements, there is not much danger that the bolted joint is less stiff than the welded one.

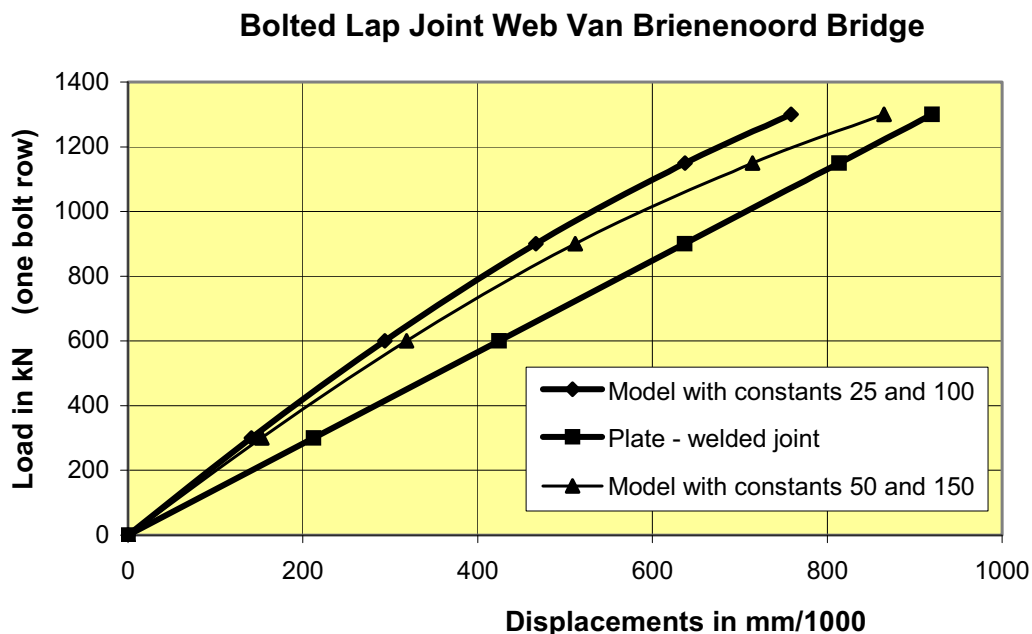


Figure 19. Calculated load-deformation behaviour of the HSFG bolted web joint and the welded joint in the Van Brienoord Bridge (top bolt rows near the weld, where the distance between the rows is taken as 175 mm).

Table 2 gives the calculated bolt forces stresses and displacements for the various parts of the joint for a total load of 900 kN per bolt row. With a width over the bolt rows of 175 mm, the cross-section is 7000 mm² for the main plate per bolt row and 8750 mm²

for the two cover plates per bolt row. The measuring length was 1040 mm. It is noted that at low loads, the bolt forces are more uneven than at high loads. The reason is the relatively less stiff behaviour of the bolts at higher loads.

Table 2. Calculated bolt forces stresses and displacements for $F = 900$ kN for the model with constants 25 and 100 and a distance between the bolt rows of 175 mm.

Number	F_{bolt} (B_i) (kN)	δ_{bolt} (d_{bi}) (mm/1000)	σ_{main} (σ_{hi}) (N/mm ²)	σ_{cover} (σ_{si}) (N/mm ²)	δ_{main} (d_{hi}) (mm/1000)	δ_{cover} (d_{si}) (mm/1000)
0	-	-	129	-	49,0	-
1	280	53,4	89	32	50,6	18,3
2	194	21,1	61	54	34,8	30,9
3	175	17,3	36	74	20,5	42,4
4	251	39,2	-	103	-	39,2

CONCLUSIONS

- a. In joints where both welds and bolts are applied, it is important to take carefully into consideration not only the strength of the fasteners, but also the differences in stiffness and deformation capacity. The stiffness properties are especially important in fatigue loaded structures.
- b. A spring model has been developed for the determination of the load-deformation behaviour of HSFG bolted lap joints. The model can be used as a design tool for lap joints where the stiffness is important, e.g. because of fatigue loading in joints that are partly welded and partly bolted.
- c. The model has been validated with several tests from the literature and a test series carried out at the Stevin Laboratory of the Delft University of Technology.
- d. The spring model enables a good insight in the uneven distribution of bolt forces as a function of the joint geometry (length, width, thickness of main plate and cover plates and number, placing, size and preload of the HSFG bolts).
- e. Bolt forces may be very uneven. Knowledge of the bolt force distribution is important for the analysis of the fatigue resistance and of possible partial slip in long joints.
- f. The above insight may be very useful when estimating the fatigue resistance of long bolted lap joints. For example, the model has been used for the evaluation of long bolted joints in some other movable bridges where fatigue fractures had occurred.
- g. The extra flexibility due to load transfer by friction can be compensated by the lower stresses and strains in the cross-section because of the greater total thickness of main plate plus cover plate.

REFERENCES

- Foreman, R.T. and Rumpf, I.L. (1961), *Static Tension Tests of Compact Bolted Joints*. Transactions ASCE, Vol. 126, Part II, 228-254.
- Gresnigt A.M., Steenhuis C.M., (2000), *Stiffness of Lap Joints with Preloaded Bolts*. The Paramount Role of Joints into the Reliable Response of Structures, edited by C.C. Baniotopoulos and F. Wald, Kluwer Academic Publishers, published in cooperation with NATO Scientific Affairs Division (pp. 435-448).
- Klöppel, K. and Seeger, T. (1965), *Sicherheit und Bemessung von HV-Verbindungen aus St 37 und St 52 nach Versuchen unter Dauerbelastung und ruhender Belastung*, Veröffentlichungen des Instituts für Statistik und Stahlbau der Technischen Hochschule Darmstadt, Heft 1 (Selbstverlag).
- ORE (1966), *Problems of high strength bolted connections in steel construction*. Report D 90/RP 1/E, Office for Research and Experiments of the International Union of Railways, Utrecht.
- Pietrapertosa, C., Piraprez, E., Jaspert, J.P., (2004), *Ductility Requirements in Shear Bolted Connections*, Proceedings of the Fifth International Workshop Connections in Steel Structures, Behaviour, Strength & Design, Amsterdam. Edited by F.S.K. Bijlaard, A.M. Gresnigt, G.J. van der Vegte. Bouwen met Staal, Zoetermeer, The Netherlands. (pp. 335-345).
- Steinhardt, O., Möhler, K. and Valtinat, G. (1969), *Versuche zur Anwendung vorgespannter Schrauben im Stahlbau*. Berichte des Deutschen Ausschusses für Stahlbau, Heft 25.
- Van der Weijde, H. (1999), *Val vervangen wegens vermoeiing (Van Brienenoord Bridge deck replaced because of fatigue)*. Bouwen met Staal 146, January/Februari 1999, pp 40-44.
- Vegte, G.J., van der, Makino, Y., (2007), *The effect of friction coefficient on the cyclic behaviour of bolted beam-to-RHS column connections*. In YC Wang & CK Choi (Eds.), Steel and composite structures, London, Taylor & Francis Group (pp. 767-772).

VERTICAL BRACING CONNECTIONS IN THE SEISMIC REGIME

William A. Thornton

Cives Engineering Corporation, Roswell, GA, USA
bthornton@cives.com

Larry S. Muir

Cives Engineering Corporation, Roswell, GA, USA
lmuir@cives.com

ABSTRACT

The effect of frame distortions have been routinely neglected in the design of bracing connections. It is coming to be realized that, because of the large story drifts that occur during seismic events, that this practice may not be adequate to provide a structure that can survive an earthquake without collapse. This paper is abstracted from a forthcoming AISC design guide on vertical bracing connections.

INTRODUCTION

It is coming to be realized for high seismic applications where story drifts of 2-2½% must be accommodated, frame distortion cannot be ignored. These story drifts of 2-2½ % are on the order of ten times the drifts that are expected for wind and low seismic ($R \leq 3$) design. They occur in part because the actual maximum considered earthquake ("MCE") forces are reduced to about $1/9$ of the forces the MCE could produce. This is done by first using $2/3$ of the MCE forces and then dividing them by an "R" factor on the order of 6, so the MCE load reduction factor is $6 \times 2/3 = 4$.

The rationale for this reduction factor is twofold: (1) the forces are of short duration and are reversing, so the response to them does not necessarily achieve the maximum values, and (2) to allow economical designs to be achieved. The price paid for this MCE force reduction is the high drift, and the requirement for ductile response that allows large distortions without fracture and resulting building collapse. If one used an R of 1, or even $2/3$, the drift under even the MCE forces would be no greater (and probably less because of the duration factor) than traditional wind design. Some designers of hospitals (Walters et al, 2004) and nuclear power plants do just this.

The current AISC Seismic Provisions (2005) have no requirement to consider frame distortions and the resulting distortional forces.

DISTORTIONAL FORCES

These forces exist because a braced frame, although considered a pinned structure, is in reality a braced rigid frame. They would be reduced to essentially zero by the use of an actual pin as shown in Fig. 1, or they can be controlled by the use of a designed hinge in the beam as shown in Fig. 2. If no pin or hinge is used, the maximum distortional forces can be derived from the maximum distortional moment,

$$M_D = \min\{2M_{P_{column}}, M_{P_{beam}}\}$$

In this formula, the column is considered continuous above and below the location being considered. Fig. 3 shows a statically admissible distortional forces distribution. These forces are to be added algebraically to those resulting from the Uniform Force Method (AISC 2005) of bracing connection analysis.

Note that, when the brace force is tension, the distortional forces F_D are compression. These forces tend to “pinch” the gusset and can cause the gusset to buckle even when the brace is in tension. This gusset pinching has been observed in physical tests (Lopez et al, 2004).

AN EXAMPLE

Figure 4 shows a connection designed to satisfy the current Seismic Provisions (AISC, 2005). This design, which does not consider distortional forces, is given in the Design Guide (AISC, 2008). The statically admissible interface forces for the connection of Fig. 4 are given in Fig. 5. These forces would be correct if a beam hinge such as shown in Figs. 1 or 2, were used. However, with no hinge as shown in Fig. 4, the maximum possible (demand) distortional moment is

$$\begin{aligned} M_D &= \min\{R_y M_{P_{beam}}, 2R_y M_{P_{column}}\} \\ &= \min\{1.1(826), 2(1.1)2260\} \\ &= 909 \text{kip-ft} \end{aligned}$$

From the geometry of Figs. 3 and 4,

$$F_D = \frac{M_D}{\beta + e_b} \left(\frac{\beta}{\alpha} \right)^2 = \frac{909}{14.5 + 8.5} \left(\frac{14.5}{18} \right)^2 = 609 \text{kips}$$

where e_b is the half depth of the beam.

The horizontal component of F_D is

$$H_D = \frac{\bar{\alpha}}{\sqrt{\bar{\alpha}^2 + \bar{\beta}^2}} \times 609 = 474 \text{ kips}$$

This value, which is compression when the brace force is tension, can be compared to the 176 kip horizontal force of Fig. 5 between the gusset and the column, which is tension when the brace force is tension. It can be seen that it is not reasonable to neglect the distortional forces.

Note that the large distortional forces may not be able to be achieved because of column and beam web yielding and crippling, and gusset pinching (buckling when the brace is in tension). The Design Guide (AISC, 2008) proposes using the plate buckling theory given in the Manual pages 9-8 and 9-9 (AISC, 2005) to control gusset pinching. The Manual formulations can be written as

$$F_{cr} = QF_y$$

$$Q = 1.0 \text{ for } \lambda \leq 0.7 \text{ (yielding)}$$

$$Q = 1.34 - 0.486\lambda \text{ for } 0.7 < \lambda \leq 1.41 \text{ (inelastic buckling)}$$

$$Q = \frac{1.30}{\lambda^2} \text{ for } \lambda > 1.41 \text{ (elastic buckling)}$$

$$\lambda = \frac{\left(\frac{b}{t}\right)\sqrt{F_y}}{5\sqrt{475 + \frac{1120}{\left(\frac{a}{b}\right)^2}}}$$

where

a = length of “free” edge—distance between points A and B of Fig. 4.

b = the perpendicular distance from the “free” edge to the gusset junction point at the beam and column, point C of Fig. 4.

From the geometry of Fig. 4,

$$a = 44.3 \text{ in. } b = 21.2 \text{ in.}, t = \frac{3}{4} \text{ in.}$$

$$\frac{a}{b} = 2.09, \frac{b}{t} = 28.3$$

$$\lambda = \frac{28.3\sqrt{50}}{5\sqrt{475 + \frac{1120}{2.09^2}}} = 1.48$$

$$Q = \frac{1.30}{1.48^2} = 0.594$$

$$\phi F_{cr} = 0.9 \times 0.594 \times 50 = 26.7 \text{ ksi}$$

The actual stress is

$$f_a = \frac{609}{0.75 \times 21.2} = 38.3 \text{ ksi}$$

Since $38.3 \text{ ksi} > 26.5 \text{ ksi}$, the gusset will buckle in the pinching mode when the brace is in tension. This buckling will prevent the distortional moment $M_b = 909 \text{ k-ft}$ from being achieved, but this out-of-plane buckling is undesirable because it could cause low cycle fatigue cracks to form in the gusset and its connections.

CONTROL OF DISTORTIONAL FORCES WITH A BEAM HINGE

The idea is shown in Figs. 1 and 2, and has been tested in the context of buckling restrained braced frames (Fahnestock et al, 2006). A completely designed example with a beam hinge is shown in Fig. 6. The loads and geometry are the same as the example of Fig. 4. The Design Guide (AISC, 2008) gives complete calculations for this example. Because of the beam hinge, the distortional force F_D is reduced to 204 kips. The design shown in Fig. 6 satisfies all the usual limit states, plus gusset pinching, with the original $\frac{3}{4}$ in. gusset plate.

SUMMARY

A forthcoming AISC Design Guide (AISC, 2008) on Vertical Bracing Connections treats many types of bracing connections and loadings. This paper, which is abstracted from the Design Guide, presents a rational state of the art treatment of the distortional forces induced by large seismic drifts.

REFERENCES

AISC (2008), *Design Guide for Vertical Bracing Connections*, W.A. Thornton and L.S. Muir, to appear.

AISC (2005), *Manual of Steel Construction*, 13th Edition, AISC, Chicago, IL.

AISC (2005), *Seismic Provisions for Structural Steel Buildings*, AISC, Chicago, IL.

Fahnestock, Larry A., Ricles, James M., and Sause, Richard, (2006) "Design, Analysis, and Testing of an Earthquake-Resistance Buckling-Restrained Braced Frame," *SEAOC 75th Annual Proceedings*.

Lopez, Walterio A., Gwie, David S., Lauck, Thomas W., and Saunders, Mark (2004), "Structural Design and Experimental Verification of a Buckling-Restrained Braced Frame System," *AISC Engineering Journal*, Fourth Quarter, p. 177-186.

Walters, Mason T., Maxwell, Benjamin H., and Berkowitz, Russell H. (2004), "Design for Improved Performance of Buckling-Restrained Braced Frames," *SEAOC Annual Convention Proceedings*.

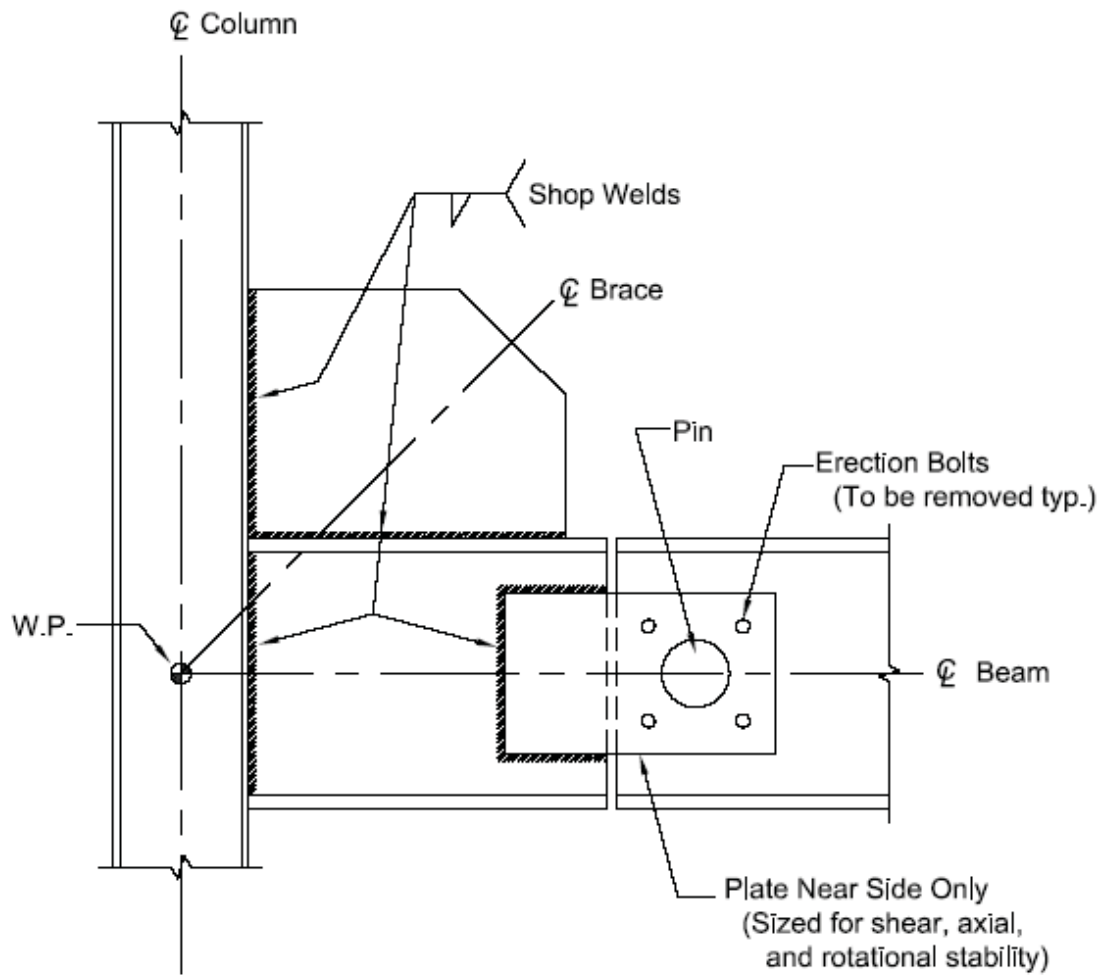


Figure 1. Connection to Minimize Distortional Forces

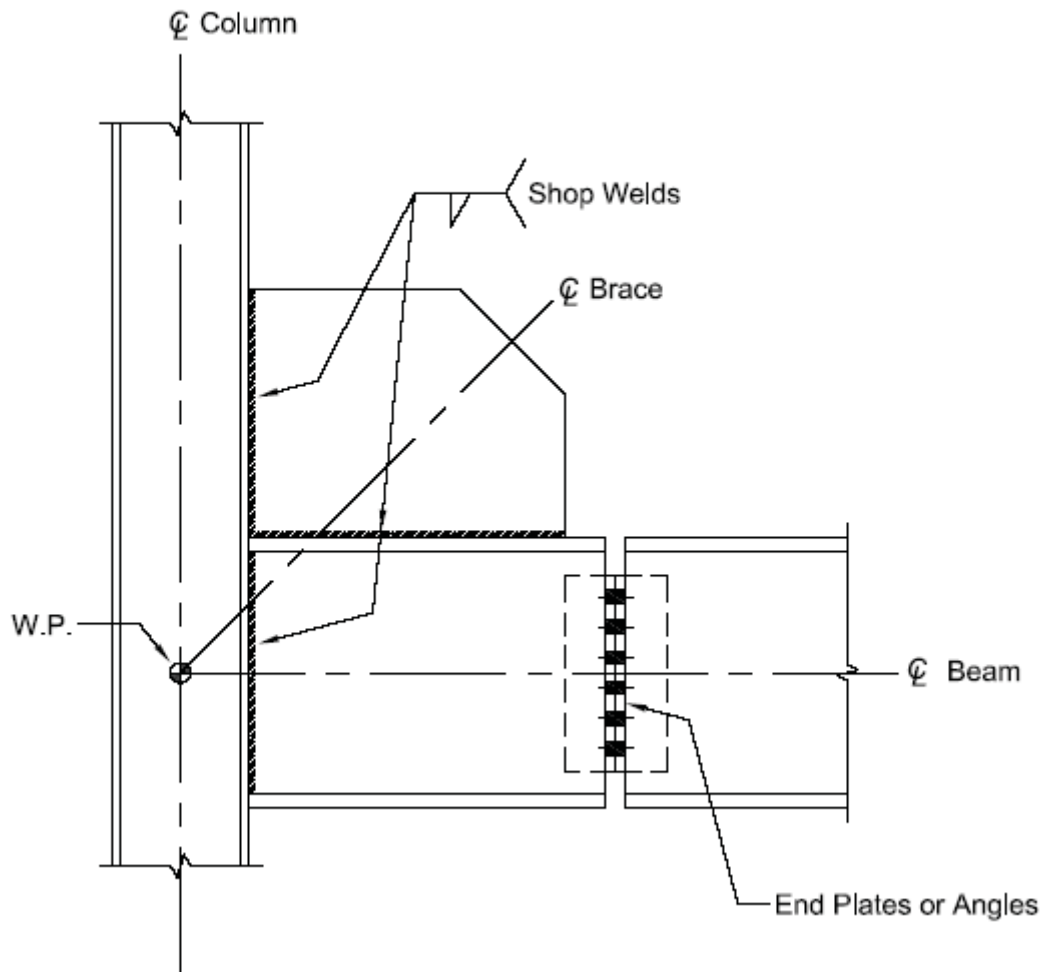


Figure 2. Shear Splice to Control Distortional Forces

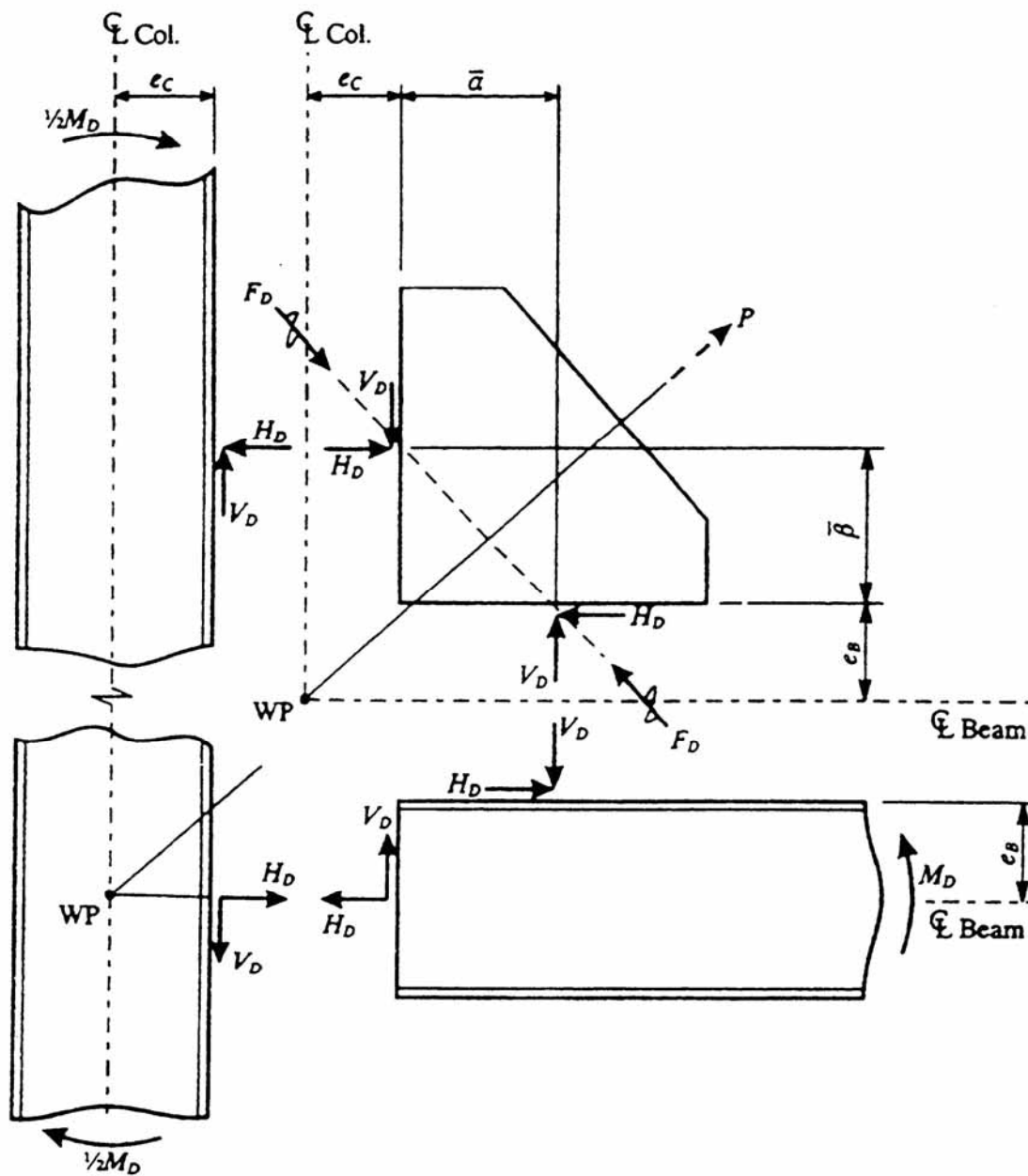


Figure 3. Admissible Distribution of Distortional Forces

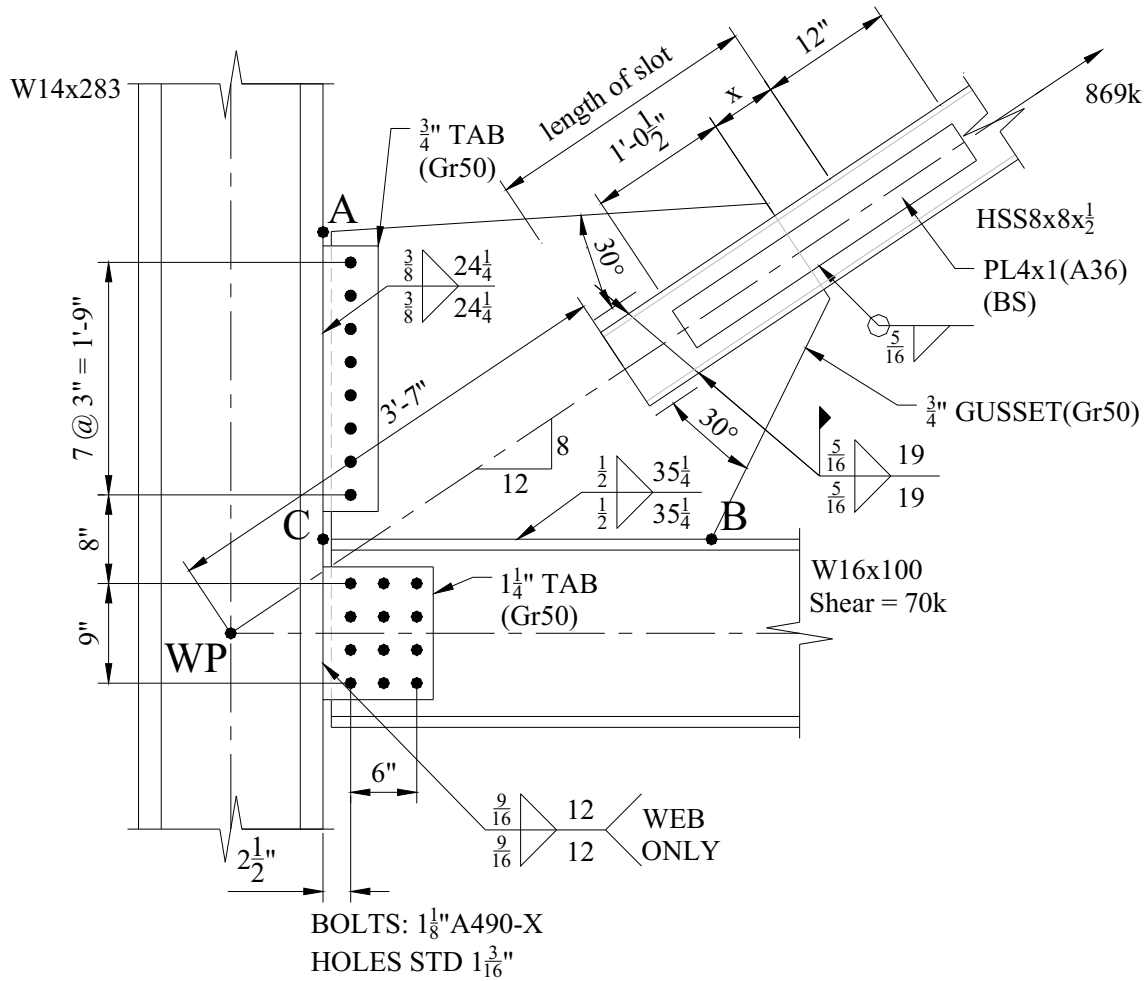


Figure 4. SCBF Connection

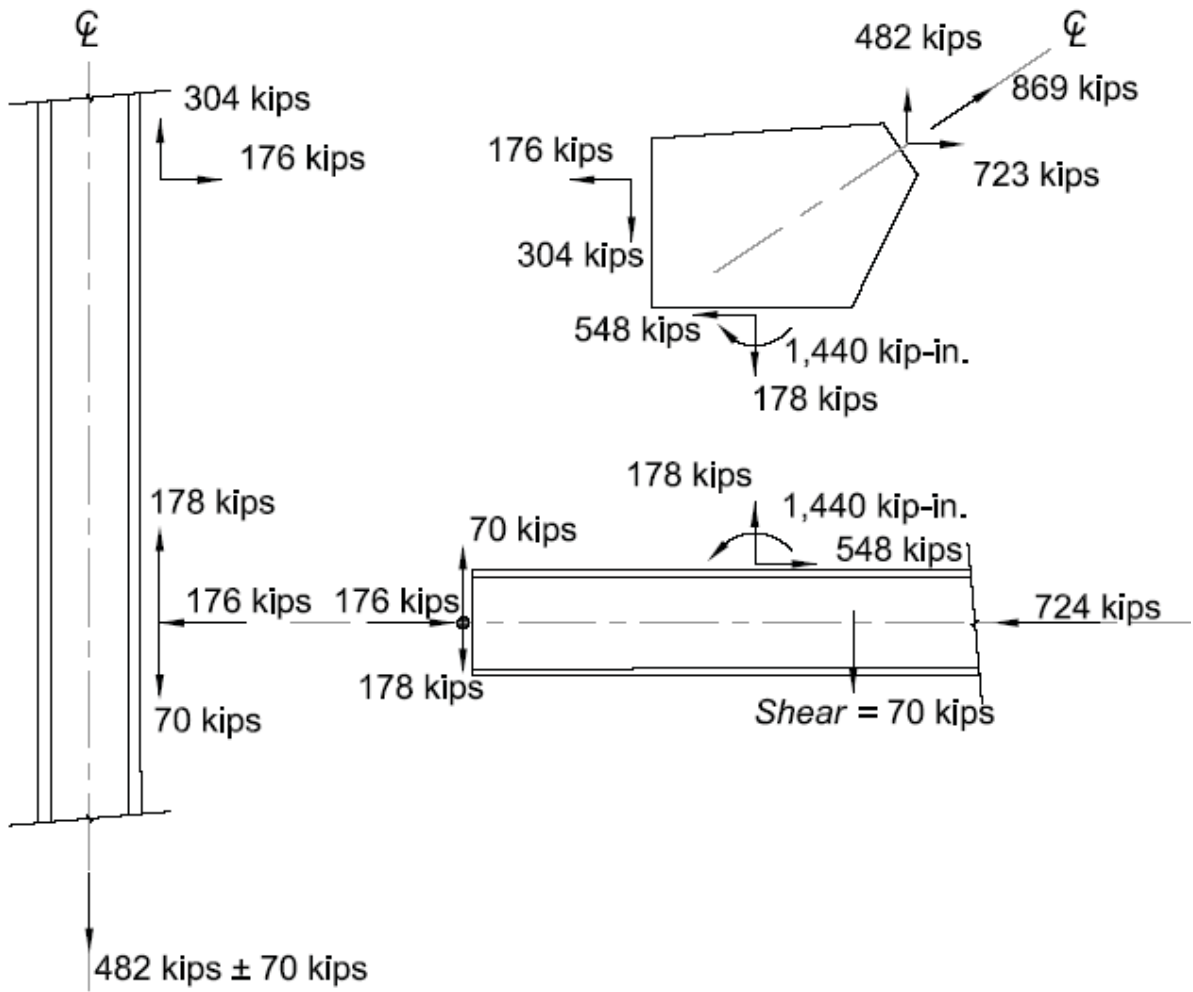


Figure 5. Admissible Force Field for Connection of Figure 4

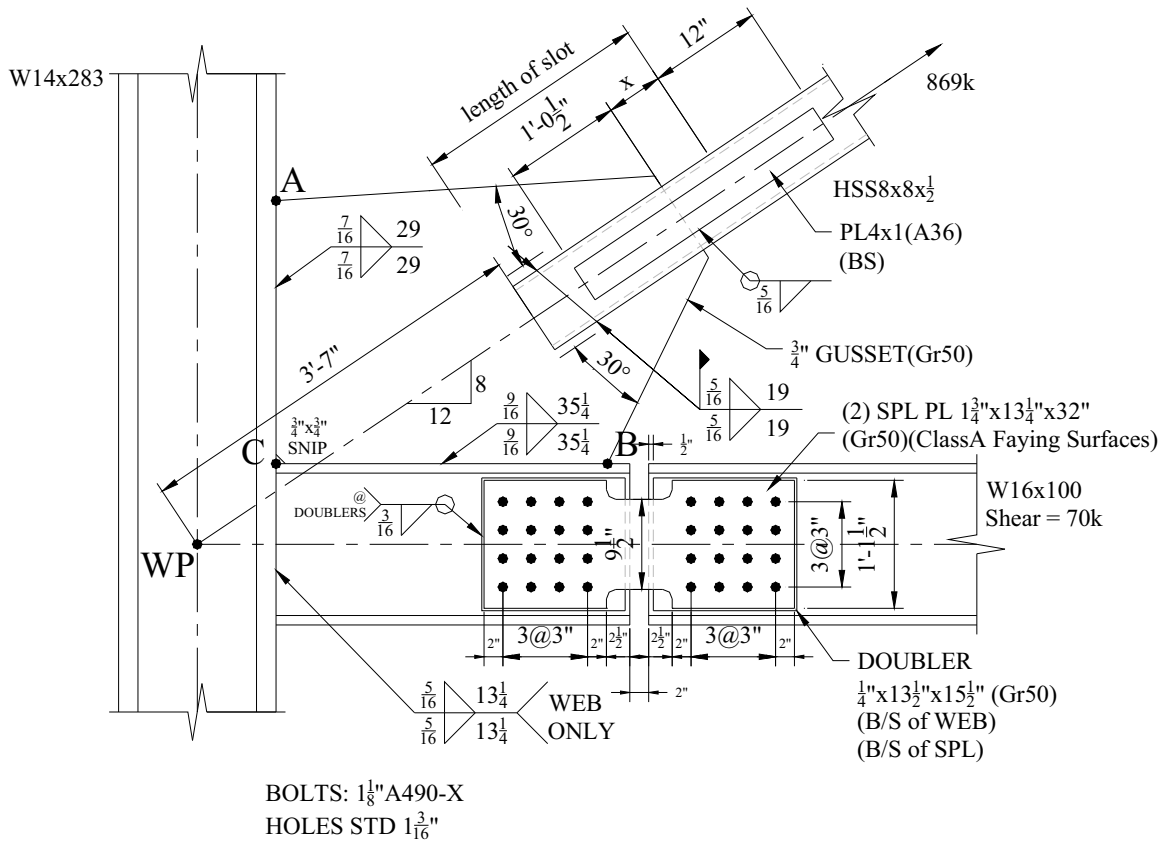


Figure 6. High Seismic Design Including Distortional Forces

SEISMIC BEHAVIOR AND PERFORMANCE OF BUCKLING-RESTRAINED BRACED FRAME CONNECTIONS

Larry A. Fahnestock

University of Illinois at Urbana-Champaign, Urbana, IL 61801

fhnstck@uiuc.edu

Victoria R. Wigle

University of Illinois at Urbana-Champaign, Urbana, IL 61801

vwigle2@uiuc.edu

ABSTRACT

Large-scale experimental studies of buckling-restrained braced frames (BRBFs) have shown that although they display good overall performance, they may have limitations due to undesirable failure modes in the connection regions. These experimental results motivate further investigation of BRBF connection behavior and performance. In this study, three-dimensional nonlinear finite element models were used to study behavior and performance of BRBF connections with emphasis placed on the beam-column-brace connection regions. The models focused on a one-story subassembly that is part of a four-story BRBF, which was tested previously. After the baseline finite element analysis results were verified with experimental data, a parametric study was conducted exploring variations in connection configuration. Results are discussed on global and local levels. The effects of the parametric connection variations are assessed, key issues that influence performance are identified and future work is outlined.

INTRODUCTION AND BACKGROUND

Buckling-restrained braced frames (BRBFs), which are concentrically braced frames (CBFs) with buckling-restrained braces (BRBs), provide significantly better seismic performance than conventional steel CBFs. The superior performance of BRBFs is a result of the robust cyclic performance exhibited by BRBs. Whereas conventional steel braces yield in tension but buckle in compression, leading to sudden strength and stiffness degradation, BRBs yield in tension and compression and develop significant energy dissipation capacity and ductility. These favorable attributes have prompted rapid implementation of BRBFs in the western United States in regions of high seismicity. Figure 1 illustrates a typical BRB configuration (Fahnestock et al., 2007a). Numerous isolated tests of BRBs have demonstrated the favorable cyclic characteristics described above and have supported the quick adoption of BRBFs into U.S. design provisions (AISC, 2005a; ASCE, 2005). Table 1 shows a sample of ductility demands, where μ_{\max} = maximum ductility demand and μ_c = cumulative plastic ductility demand, imposed on BRB test specimens and Table 2 shows a summary of story drift, θ_{story} , and

BRB ductility demands that were obtained from nonlinear dynamic analyses of prototype BRBFs subjected to suites of earthquake ground motions scaled to the maximum considered earthquake (MCE) hazard level. These results suggest that BRBs are capable of sustaining the demands that are expected under major seismic events. However, this conclusion is based on the assumption that BRBs in frame systems will perform in the same way as the isolated BRBs.

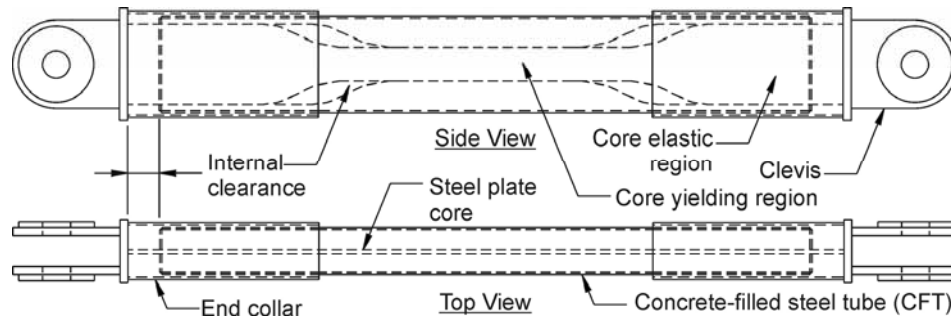


Figure 1 – Typical BRB Configuration

Several recent large-scale experimental studies of BRBFs have shown that although they display good overall performance, they may have limitations due to undesirable failure modes in the connection regions. The standardized BRB qualification testing protocol (AISC, 2005a) attempts to replicate the demands that would be imposed on a BRB in a frame system, but it has become evident that realistic frame conditions lead to BRB demands that have not been fully represented in qualification tests. Results from large-scale experimental studies of BRBFs provide the best insight into system performance since interaction between the various frame elements (e.g., BRBs, beams, columns and connections) is more realistically represented. Four research programs studying BRBF system performance are summarized below. These experimental results motivate further investigation of BRBF connection behavior and performance.

Table 1 – Experimental BRB Ductility Demands

Reference	BRB	μ_{max}	μ_c
Black et al. (2002)	99-1	20	324
	99-2	10	879
	99-3	10	279
	00-11	15	1045
	00-12	15	538
Merritt et al. (2003)	1	15	900
	2	15	600
	3	10	1600
	4	15	1100
	5	15	1300
	6	15	800
	7	10	1000
	8	10	1000

Table 2 – Demands from BRBF Nonlinear Dynamic Analyses (MCE Hazard Level)

Reference	Response	θ_{story}	μ_{max}	μ_c
Sabelli (2001)	mean	0.045	17.4	139
	mean + one standard deviation	0.066	25.1	185
Fahnestock et al. (2007a)	mean	0.033	18.4	179
	mean + one standard deviation	0.041	22.7	391

RELEVANT PREVIOUS RESEARCH

Aiken et al. (2002) conducted cyclic tests on a 0.7-scale one-bay one-story BRBF with full-penetration welded beam-column connections and bolted brace-gusset connections, similar to the detail shown in Figure 2(a). In Test 1, the columns yielded in flexure and shear and the gusset plates and beams yielded at the beam-column-brace connections. In Test 2, similar response was observed and cracks formed in a column-gusset weld in a beam-column-brace connection at a story drift less than 0.02 radians. The cracks propagated at story drifts greater than 0.02 radians and gusset plate distortion was observed. Before Test 3, new gusset plates were installed and stiffener plates were welded at the free edges of the gusset plates adjacent to the columns. During Test 3 at a story drift less than 0.02 radians, a crack initiated at a beam-column-brace connection in the weld between the beam bottom flange and the column. In the first excursion to a story drift of 0.026 radians, a crack developed in the beam bottom flange at the end of the gusset plate in a beam-column-brace connection and propagated through the flange and into the web. This fracture led to beam torsional rotations and BRB out-of-plane displacement and subsequently the strength degraded severely.

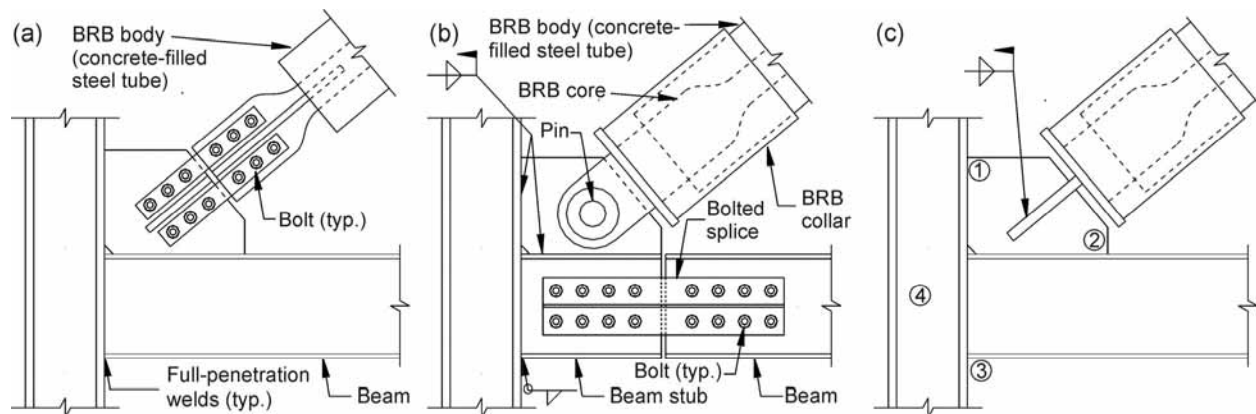


Figure 2 – BRBF Connection Details

Tsai et al. (2003) tested a full-scale 3-story 3-bay dual MRF-BRBF using hybrid pseudo-dynamic earthquake simulations. In the BRBF portion of the system, the brace-gusset connections were bolted and bolted web splices were used to connect the beams to beam stubs that were welded to the columns. In Phase 1, out-of-plane gusset plate distortion was observed at various locations in the frame during several tests. Gusset plate stiffeners and lateral braces were added in an attempt to prevent this behavior. Phase 1 ended when BRBs failed due to out-of-plane buckling at a story drift of 0.025 radians. After Phase 1, gusset plates were repaired, new BRBs were installed and stiffeners were added at the gusset plate free edges. The Phase 2 tests demonstrated acceptable BRB and connection performance up to a story drift of 0.025 radians. In a later experimental program, a full-scale one-bay two-story BRBF with improved connection details demonstrated reasonable performance with a maximum story drift of 0.022 radians although cracks developed in column-gusset welds (Tsai et al., 2006).

Christopoulos (2005) tested five full-scale one-bay one-story BRBFs under cyclic displacement histories. The brace-gusset connections were bolted and the beams were connected to the columns with single-plate shear tabs. The tests investigated the effects of gusset plate geometry, type of bolted brace-gusset connection and orientation of the BRB core plate. Variations between test specimens had minimal influence on performance and four of the five BRBFs failed by out-of-plane deformation of the BRB at story drifts between 0.022 and 0.024 radians. BRB failure was typically preceded by yielding and buckling of the beams and columns adjacent to the gusset plates.

Fahnestock et al. (2007b) tested a 0.6-scale four-story BRBF using hybrid pseudo-dynamic earthquake simulations and quasi-static cyclic loading. The brace-gusset connections were pinned and bolted web splices were used to connect the beams to beam stubs, as shown in Figure 2(b). The test frame was subjected to four earthquake simulations and extensive quasi-static cyclic loading. During the earthquake simulations, the test frame sustained story drifts up to 0.048 radians with minimal damage and no stiffness or strength degradation. Following the earthquake simulations, one level of the test frame was modified to remove the bolted web splices and make the beam continuous between the columns. The modified test frame was then subjected to quasi-static cyclic displacement histories that imposed story drifts up to 0.05 radians. The connections and BRBs performed as expected and did not exhibit undesirable failure modes. After undergoing appreciable ductility demands, the core yielding regions of five BRBs fractured and the testing program was concluded. In contrast to the tests summarized above, where undesirable connection and BRB failure modes were typically observed at story drifts between 0.02 and 0.025 radians, this testing program demonstrated that a properly detailed BRBF can withstand severe seismic input and maintain its load-carrying capacity.

RESEARCH MOTIVATION AND PLAN

The first three experimental programs described above (Aiken et al., 2002; Tsai et al., 2003; Christopoulos, 2005) exhibited similar behavior and performance but contrast starkly with the behavior and performance exhibited in the final experimental program described above (Fahnestock et al., 2007b). The large difference in story drift capacity, 0.025 radians compared to 0.05 radians, indicates that connection details have a major impact on global system performance. Further research is necessary to explore the critical connection parameters that affect system performance and to determine reliable approaches for designing connections that do not lead to undesirable failure modes but that allow the significant energy dissipation capacity and ductility of BRBs to be fully exploited.

In view of this need, the present research aims to explore seismic behavior and performance of BRBF connections through finite element analysis parametric studies. The four-story BRBF that was tested by Fahnestock et al. (2007b) was chosen as the prototype structure. A three-dimensional nonlinear finite element model was created using the ABAQUS computer program (ABAQUS, 2006), test results were used to verify

the model and the model was modified to study variations in connection configuration. The current status and future direction of this research are described below.

FINITE ELEMENT MODEL

The third story of the four-story BRBF from Fahnstock et al. (2007b) was chosen for detailed study. As shown in Figure 3, a subassembly was modeled with three- and four-node shell elements with standard integration and the remainder of the BRBF was modeled using frame elements with lumped plastic hinges for beams and columns and nonlinear springs for the BRBs and bolted beam splices. In the detailed region of the model, the BRB casing was not modeled explicitly, but the BRB core was restrained from buckling to replicate the effect of the restraining mechanism.

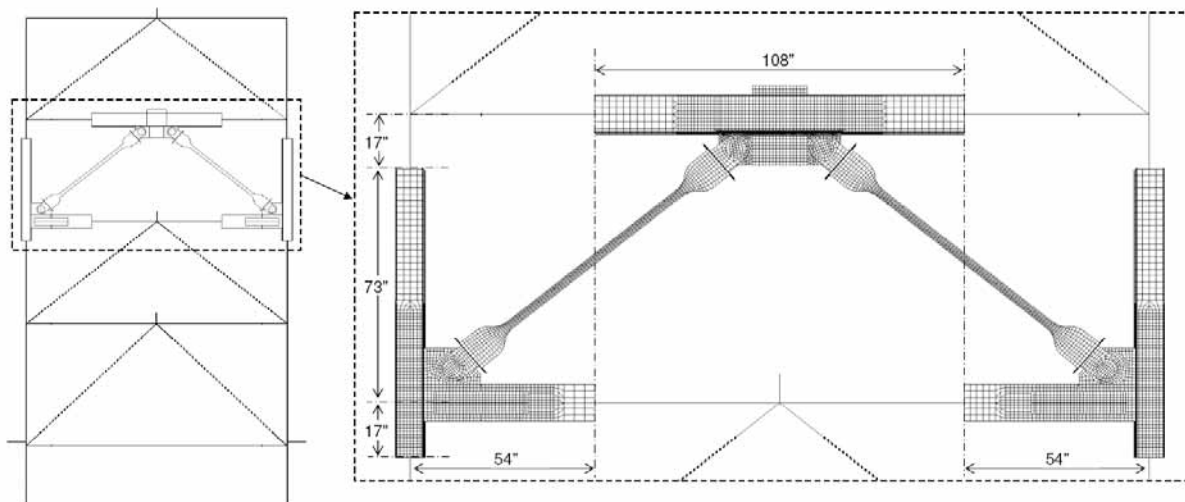


Figure 3 – BRBF Finite Element Model

Geometric nonlinearities were included in the model through a finite strain large displacement formulation. Material nonlinearities were incorporated through a metal plasticity model, which is based on the von Mises yield criterion, with combined isotropic and kinematic strain hardening. Steel stress-strain properties were based on measured material properties (Fahnstock et al., 2007b) and hardening parameters were calibrated to match representative cyclic steel stress-strain data (Kaufmann and Pense, 1999). For the BRBs in the detailed subassembly region, a yield stress of 38 ksi with the calibrated hardening parameters was used instead of the actual yield stress of 46 ksi in order to better match stress-strain behavior at larger strains, as shown in Figure 4.

In the connection regions, several simplifications were employed. At all welded interfaces, full attachment was modeled. Thus, fillet welds were not explicitly represented. For the bolted beam splices, bolts and bolt holes were not modeled, but the corresponding nodes in the connected parts were slaved to represent force transfer through bolt bearing. Geometric imperfections were introduced into the subassembly model in order to realistically represent typical as-built conditions. Local imperfection patterns in the beams and gusset plates were determined using eigenvalue buckling

analysis with amplitudes based on allowable production and fabrication tolerances (AISC, 2005b). In addition, to produce eccentricity in the BRB loading, the upper gusset plate in the detailed subassembly was offset from the beam centerline by $\frac{3}{16}$ inch, which was based on the permissible out-of-plumbness for a typical story (AISC, 2005c).

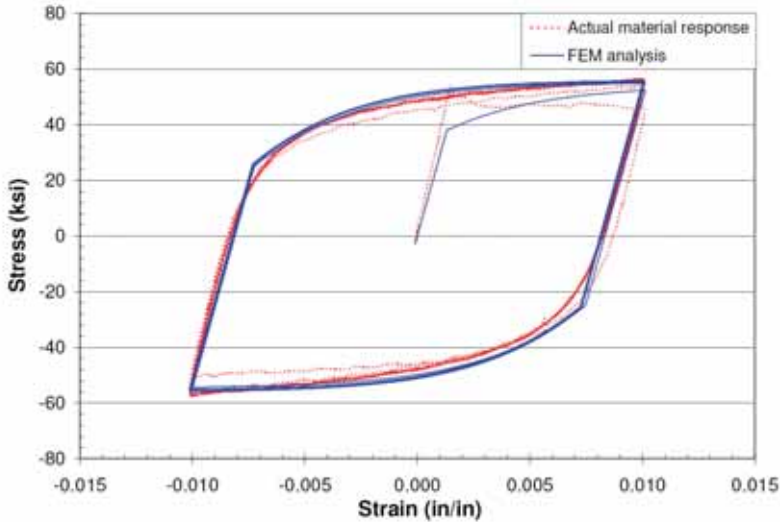


Figure 4 – Steel Stress-Strain Properties

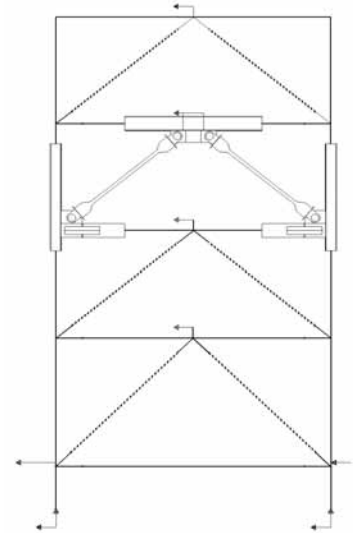


Figure 5 – Model Loading

To verify the accuracy of the BRBF model, it was subjected to load and displacement boundary conditions that were recorded during the experimental earthquake simulations (Fahnestock et al., 2007b). First, a vertical load was applied at the midspan of each beam to account for gravity effects and to introduce appropriate initial BRB forces. Second, measured displacements from the earthquake simulations were imposed at the locations shown in Figure 5. Comparisons between the finite element analysis and the experimental results for story shear-drift and BRB axial force-deformation are shown in Figures 6(a) and 6(b), respectively. Brace behavior matches reasonably well although the compressive response is underestimated by the finite element model at larger deformations. This is due to confinement of the core and the frictional forces that develop between the core and the restraining concrete when the brace is in compression, which are not captured in the material model of the BRB core. As a result of this effect, negative story shear is also under-predicted by the model. Apart from this difference, story behavior agrees sufficiently between the model and the experiment.

PARAMETRIC STUDIES

The baseline model described above was used to study behavior and performance for variations in the beam-column-brace connection configuration. Bolted, pinned and welded BRB connections, which are shown schematically in Figures 2(a), 2(b) and 2(c), respectively, were considered and spliced or continuous beams were considered for a total of six cases. Figures 2(a) and 2(c) show the continuous beam case whereas Figure 2(b) shows the spliced beam case. For the bolted BRBs, stiffeners were added

to the gusset plates to accommodate the typical cruciform connection configuration. Since the bolts were assumed to be slip critical, the plates connecting the BRB core to the stiffened gusset were tied directly. For a BRB with welded connections, shown in Figure 2(c), the brace core is welded to an end plate like the BRB with pinned connections, but instead of knife plates and a pin, two plates oriented perpendicular to the brace core are welded to the end plate and fillet welded to the gusset plate. Like other welded interfaces in the model, full attachment was modeled between the connection and gusset plates.

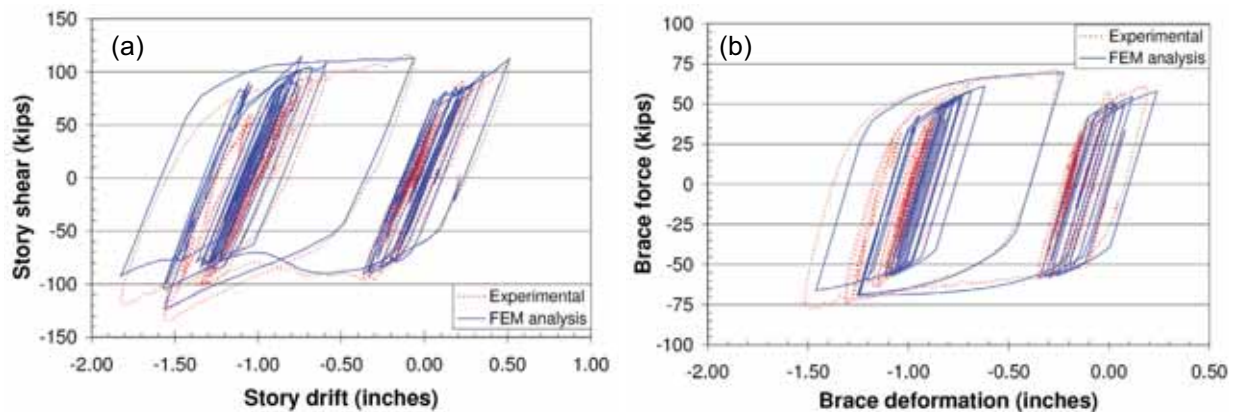


Figure 6 – BRBF Detailed Subassembly (Story 3) Model Verification

Each frame model was loaded monotonically to a story drift of 0.04 radians, based on the typical story drift expected for the MCE hazard level. These analyses are intended to make relative comparisons between the different connection configurations with the assumption that conclusions about cyclic behavior and performance can be inferred. Global force and deformation quantities as well as local measures of stress and equivalent plastic strain are explored with emphasis on the beam-column-gusset connection at the compression BRB in story 3. Since loading reversal is not considered and out-of-plane movement of the BRB core is not permitted in the current model, some of the undesirable failure modes observed in previous research do not occur in the analyses presented below. However, ongoing research is considering these issues.

Figures 7(a) and 7(b) present story shear-drift and BRB axial force-deformation, respectively, for the different connection configurations. As shown, the BRB behavior changes little between cases. However, story shear is much larger for the continuous beam cases when compared to the spliced beam cases at the same story drift. This additional story shear results from increased column shear, which arises as a result of the rigid frame behavior created by the transfer of moment at the beam-column joints.

In the spliced beam cases, the bolted splices significantly limit the moment that can be transferred and reduce the demands on the connection region. The moment transferred by the bolted splice is approximately 15% of the moment transferred when the beam is continuous. In both cases, plastic hinges are formed adjacent to the connection region in the beam or the splice elements. Contour plots of the von Mises stresses for the

continuous and spliced beam cases are shown in Figures 8(a) and 8(b), respectively. These plots qualitatively illustrate the role that the splices play in limiting the connection region demands. For the continuous beam case, a diagonal region of higher stress is observed in the gusset plate due to the frame action that causes the joint to open. When the brace is in tension and the joint is closing, this effect may lead to out-of-plane deformation of the gusset plate.

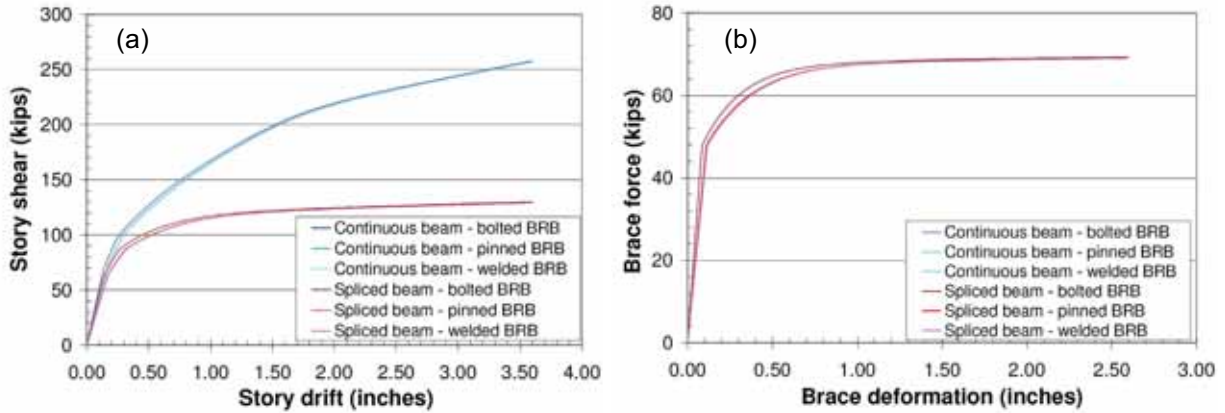


Figure 7 – BRBF Detailed Subassembly (Story 3) Parametric Studies

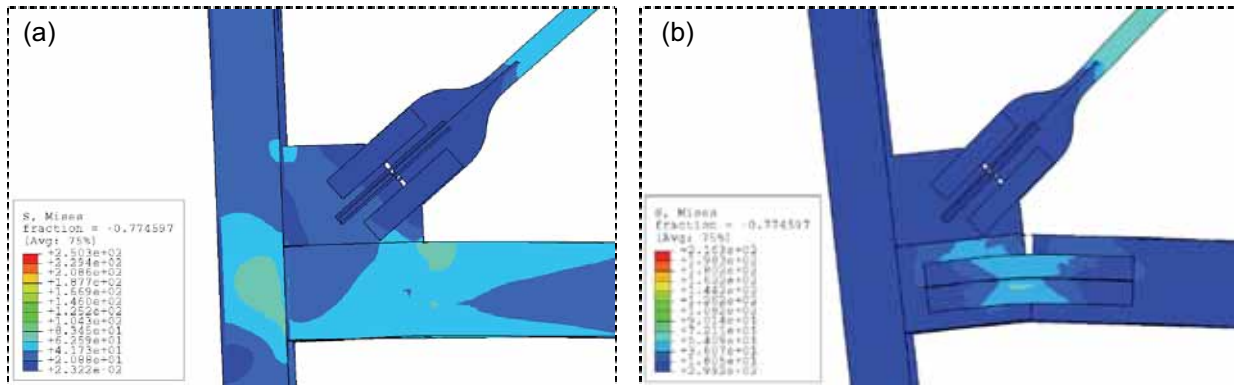


Figure 8 – von Mises Stress Contours (Bolted BRB)

Figures 9(a) and 9(b) plot equivalent plastic strain and von Mises stress, respectively, for four critical regions in the connection detail. These regions are labeled 1, 2, 3 and 4 in Figure 2(c). Figure 9 is for the bolted BRB connections with continuous and spliced beams, but similar trends were observed for pinned and welded BRB connections. As illustrated graphically in Figure 8, the stresses for the spliced beam are significantly lower than for the continuous beam for all regions due to the relief provided by the splice. In addition, equivalent plastic strain is essentially zero for all critical regions in the spliced beam.

For the continuous beam case, Region 2, at the free edge of the beam-gusset junction, is most critical in terms of both equivalent plastic strain and von Mises stress. The

stress is approximately 25% greater in Region 2 than in the other three regions while the equivalent plastic strain is approximately an order of magnitude larger. The equivalent plastic strain is used as an indicator of regions that are expected to have greater fracture potential. Regions 1, 2 and 3 are of particular interest since they represent welded interfaces. Based on the magnitude of equivalent plastic strain, Region 1, at the free edge of the column-gusset junction, appears to be more critical than Region 3, at the junction between the column and the beam bottom flange. Region 4, in the column panel zone, also exhibits high stress as well as equivalent plastic strain with magnitude between that observed in Regions 1 and 3. It should be noted that the results discussed here do not include effects due to out-of-plane BRB response, which is expected to have significant impact on behavior and performance.

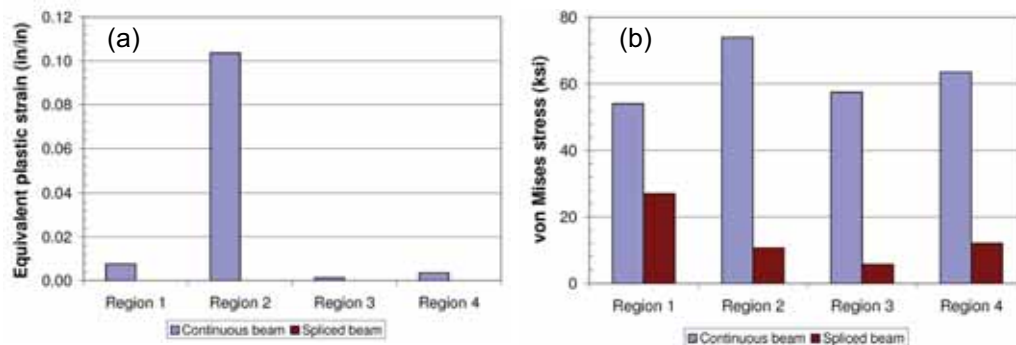


Figure 9 – Equivalent Plastic Strain and von Mises Stress (Bolted BRB)

CONCLUSIONS AND FUTURE WORK

As noted above, the results presented in this paper provide general insight into parameters that influence behavior and performance of beam-column-brace connections in BRBFs. Work is ongoing to extend these preliminary studies. From the analysis results presented, the following conclusions can be drawn:

- BRB axial force-deformation behavior showed minimal variation for different BRB end connections and between continuous and spliced beams. Thus, if undesirable connection-related failure modes are precluded, it is expected that the BRBs are capable of achieving performance similar to that observed in isolated BRB tests.
- Story shear-drift behavior showed minimal variation for different BRB end connections but showed significant variation between the continuous and spliced beams. Thus, for the continuous beam configuration, there are essentially two lateral systems acting in parallel, the BRBF and a de facto moment frame.
- BRB connection type had little effect on the stress and plastic strain demands in the connection region, but stress and plastic strain magnitudes and patterns were appreciably different for the continuous and spliced beam cases. The bolted beam web splice was found to significantly reduce demands on the connection region.
- For the continuous beam, the free edge of the beam-gusset junction appears to be most critical in terms of stress and plastic strain. For the spliced beam, large stress

and plastic strain demands were limited to the splice elements and the remainder of the connection appears to be free of potentially detrimental localizations of stress and plastic strain.

To extend the work presented above, several model refinements are in progress. First, to allow for potentially critical connection failure modes, the BRB core must be restrained from buckling yet permitted to move out-of-plane as a unit. Second, to capture the most critical BRB condition with regard to stability (i.e., when a BRB has been extended and the unrestrained core region is longest), loading reversal must be considered so that the elongated BRB is then loaded in compression. Third, to incorporate the additional BRB post-yield compressive stiffness that arises due to confinement and friction, the BRB core material definition must be modified. These refinements will produce a detailed model for evaluating critical BRB connection failure modes and developing design recommendations that lead to reliable performance.

REFERENCES

ABAQUS (2006), "ABAQUS Version 6.6 Documentation," Simulia.

Aiken, I.D., Mahin, S.A., Uriz, P. (2002), "Large-Scale Testing of BRBFs", *Proceedings, Japan Passive Control Symposium*, Tokyo Institute of Technology, Yokohama, Japan.

AISC (2005a), *Seismic Provisions for Structural Steel Buildings*.

AISC (2005b), *Steel Construction Manual, 13th Edition*.

AISC (2005c), *Code of Standard Practice for Steel Buildings and Bridges*.

ASCE (2005), *ASCE 7-05 – Minimum Design Loads for Buildings and Other Structures*.

Black, C.J., Makris, N. and Aiken, I.D. (2002), "Component Testing, Seismic Evaluation and Characterization of BRBs," *Journal of Structural Engineering*, 130 (6): 880-894.

Christopoulos, A.S. (2005), "Improved Seismic Performance of BRBFs," M.S. Thesis, University of Washington, Seattle.

Fahnestock, L.A., Sause, R. and Ricles, J.M. (2007a), "Seismic Response and Performance of BRBFs," *Journal of Structural Engineering*, 133 (9): 1195-1204.

Fahnestock, L.A., Ricles, J.M. and Sause, R. (2007b) "Experimental Evaluation of a Large-Scale BRBF," *Journal of Structural Engineering*, 133 (9): 1205-1214.

Kaufmann, E.J. and Pense, A.W. (1999), "Characterization of Cyclic Inelastic Strain Behavior on Properties of A572 Gr. 50 and A913 Rolled Sections," *AISC-PITA Project Progress Report*, ATLSS Research Center, Lehigh University.

Merritt, S., Uang, C.M. and Benzoni, G. (2003), "Subassemblage Testing of Star Seismic BRBs," *Structural Systems Research Project Report No. TR-2003/04*, University of California, San Diego.

Sabelli R. (2001), "Research on Improving the Design and Analysis of Earthquake-Resistant Steel Braced Frames," *NEHRP Professional Fellowship Report*, EERI.

Tsai, K.C., Hsiao, B.C., Lai, J.W., Chen, C.H., Lin, M.L. and Weng, Y.T. (2003), "Pseudo Dynamic Experimental Response of a Full Scale CFT/BRB Composite Frame," *Proceedings, Joint NCREE/JRC Workshop*, Tapei, Taiwan.

Tsai, K. C., Weng, Y. T., Wang, K. J., Tsai, C. Y. and Lai, J. W. (2006), "Bi-directional Sub-structural Pseudo-dynamic Tests of a Full-scale 2-story BRBF, Part 1: Seismic Design, Analytical and Experimental Performance Assessments," *Proceedings, 8th U.S. National Conference on Earthquake Engineering*, EERI.

GUSSET PLATE CONNECTIONS FOR SEISMIC DESIGN

Charles W. Roeder

University of Washington, Seattle, WA, USA
croeder@u.washington.edu

Dawn E. Lehman

University of Washington, Seattle, WA, USA
delehman@u.washington.edu

ABSTRACT

Concentrically braced frames (CBFs) are commonly used for seismic design, and gusset plate connections join the brace to other frame members. Inelastic response is a critical part of economical seismic design, and Special Concentrically Braced Frames (SCBFs) dissipate energy through tensile yield and post-buckling inelastic deformation of the brace. This inelastic deformation places severe force and deformation demands on the connection. An extensive experimental and analytical research study is in progress to develop improved seismic design methods for these connections. The work shows that gusset plate connections must be designed to have sufficient strength and stiffness to develop the full plastic capacity of the brace, but additional stiffness and resistance adversely affects the seismic performance of the system. CBFs are initially designed as trusses, but the connections do not create pinned joints, and hence the gusset plate causes significant inelastic deformation in beams and columns adjacent to the gusset. An elliptical clearance model was developed to produce thin, compact gusset plates to reduce the inelastic deformation in framing members and to improve the seismic performance of the system.

INTRODUCTION

Large, infrequent earthquakes induce large internal forces in structures, and seismic design employs a multi-level design approach to economically address this seismic design. To assure serviceability during small, frequent events, structures are designed to remain elastic for these conditions. Cyclic, inelastic deformation is used to assure structural integrity and prevent collapse during large seismic events. This design concept is simple and results in economical design, but it is difficult to reliably and accurately apply in practice. Special concentrically braced frames (SCBFs) are stiff, strong structures, which economically meet serviceability limits states. The inelastic lateral response of the SCBF is dominated by post-buckling and tensile yield behavior of the braces, but post-buckling behavior is not well understood by structural engineers. The brace provides great lateral stiffness to the frame, and it attracts large axial forces during earthquake loading. Therefore, the brace buckles in compression and yields in tension as illustrated in Fig. 1. Zones 0-A, A-B, B-C, C-D and D-E in Figs. 1a and 1b

illustrate the sequence of buckling, post-buckling and tensile yield behaviors. Buckling initiates as Zone 0-A, and plastic hinges form within the brace after buckling, because of the $P-\delta$ moments as illustrated in Zone A-B. The hinges cause permanent plastic rotations in the middle of the brace, and stiffness and compressive resistance of the brace deteriorate in subsequent cycles because of the plastic hinge in the brace as shown in Fig. 1b. During load reversals, the brace is subjected to a tensile force as shown in Zones B-C, C-D and D-E, and significant axial deformation is required to straighten the brace and achieve the full tensile stiffness and resistance. This leads to the one-sided axial force-deflection behavior of the braced shown in Fig. 1b. Braces are placed in opposing pairs and produce the inelastic hysteretic behavior shown in Fig. 1c, because of this one-sided behavior.

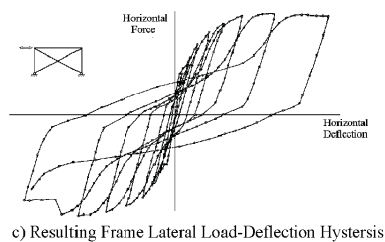
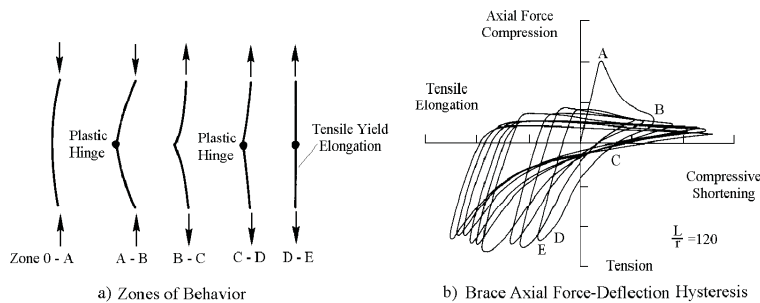


Figure 1. Behavior of Special Concentrically Braced Frames

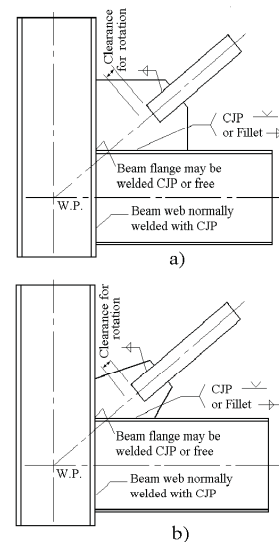


Figure 2. Schematic of Gusset Plate Connections; a) Rectangular, b) Tapered

Braces are joined to the beams and columns of the frame through gusset plate connections as depicted in Fig. 2, and the complex inelastic behavior of the brace places significant cyclic load and deformation demands on these connections. End rotations of the brace after buckling (see Zone A-B in Fig. 1) places significant rotation demands on the gusset plate. The axial resistance of the brace in compression decreases with increasing post-buckling deformation of the brace as shown in Fig. 1b, but the connection must retain its integrity and deformation, while continuing to develop the tensile and compressive resistance of the brace during this cyclic deformation.

CURRENT CONNECTION DESIGN METHOD

Gusset plate connections are designed by variations of the AISC Uniform Force Method (UFM) (Thornton, 1991; AISC, 2005b), and the method is adapted to seismic design through the application of the AISC Seismic Design Provisions (AISC, 2005a). Initially, the brace, beam and column members are designed to resist the factored seismic design forces, P_u . Gusset plate connections then are designed to assure that the

factored resistance, ϕR_n , for each connection design failure mode within the connection exceeds the expected compressive ($P_u = R_y A_g F_{cr}$) and tensile yield ($P_u = R_y A_g F_y$) capacities of the brace. R_y is the ratio of the mean or expected yield stress to the minimum specified yield stress, F_y , and A_g is the gross area of the brace. In addition, the geometry of the gusset plate is selected to provide a $2t_p$ linear clearance to permit brace end rotation as depicted in Fig. 2.

Figure 3 illustrates specific design checks or failure modes considered during seismic design of gusset plate connections. High strength steel tubes are frequently used for the brace. The tube is slotted to slip over the gusset plate and is welded as shown in Fig. 3a. The welds or bolts joining the brace to the gusset are sized to develop the expected tensile capacity of the brace. Net section (tensile) fracture of the brace may occur at the end of the slot, and local reinforcement of the brace is required at this location, because of:

- the low resistance factor used for net section design,
- the high yield stress to tensile strength ratio of the steel tube, and
- the shear lag factor, U , employed in net section design.

For bolted brace connections, net section fracture of the brace may occur at the last row of bolts away from the beam-column connection (see Fig. 3c). Next, block shear of the gusset is checked for both bolted or welded braces. Then the Whitmore width (Whitmore, 1950) of the gusset plate is defined at the end of the brace-to-gusset weld (see Fig. 3a) or at the first row of bolts (see Fig 3c) by projecting a 30° angle from the start to the end of the bolted or welded joint. Once the Whitmore width is established, the defined width and gusset plate area are used to assure that:

- buckling capacity of the gusset exceeds the expected compressive resistance of the brace,
- tensile yield capacity of the gusset exceeds the expected tensile resistance of the brace, and
- tensile fracture capacity of the net section of the gusset exceeds the expected tensile resistance of the brace, for bolted braces.

In some cases, the buckling capacity of the gusset is computed from the average length based upon key points across the Whitmore width as depicted in Fig. 3c, and in others a centroidal length is used (see Fig. 3a). Edge buckling (Brown 1988, Astenah 1998) is often checked based on the free edge length as depicted in Fig. 3b. Edge stiffeners to the gusset may be used to control this buckling, but recent research suggests that this edge buckling criteria has great scatter and is of limited value in controlling gusset plate buckling for corner gussets (Roeder et al., 2005). These checks define the gusset plate geometry and thickness. The fillet welds joining the gusset plate to the beam and column are then sized. The weld design forces are determined by equilibrium with the expected tensile force in the brace as depicted in Fig. 3b. Bolted gusset-to-column joints are used for nonseismic applications, but bolted joints between the gusset plate and the other framing members currently are uncommon for seismic design. However,

bolted joints are being investigated as part of this research. Complete joint penetration welds may also be used to join the gusset to the beams and columns.

The beam-column connection is also affected by the gusset plate design. Forces transferred by the gusset to adjacent members must often be transferred through this beam-column connection to assure equilibrium for the system. In addition, drag struts collect large seismic forces throughout the structure, and transfer these forces to the braced bay through these beam-column connections. As a result, some engineers use CJP welds to join the beam and column flanges to assure full force transfer. These CJP flange welds are costly, and other engineers use a single plate beam-column connection.

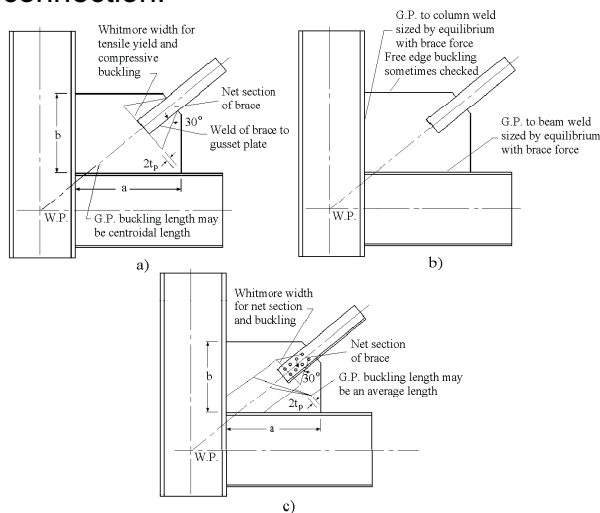


Figure 3. Gusset Plate Design Checks;
a) Welded Tube, b) Free Edge Buckling and Gusset Plate Welds, c) Bolted Brace

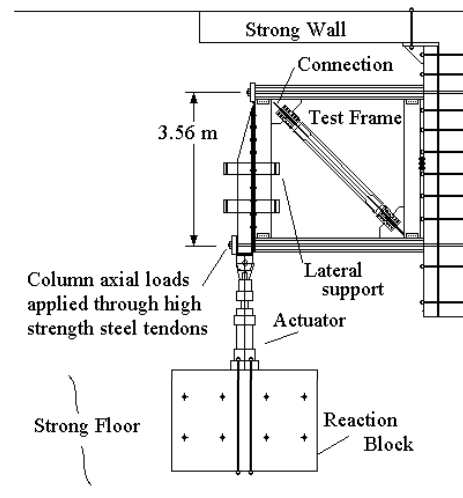


Figure 4. Test Setup

EXPERIMENTAL PROGRAM

An experimental program has evaluated the seismic performance of gusset plate connections, and Fig. 4 illustrates the test specimens and test setup. The frames are full-scale simulations of a single braced bay, which may occur in the bottom story of a 3- or 4-story building or in upper stories of a taller building. The specimens include the brace, beams above and below the brace, gusset plate connections at each end of the brace, and columns of each side of the brace to complete the single bay frame assembly. The complete bay is tested because connection performance is affected by and interrelated with the framing members, member size, and frame geometry. The braces are usually HSS $5 \times 5 \times \frac{3}{8}$ tubes, and the columns are W12x72 sections of A992 steel. Most beams are W16x45 sections of A992 steel, but heavier sections were used for some specimens. The gusset plate connections were varied from specimen to specimen to evaluate:

- current AISC and UFM design procedures,

- weld requirements between the gusset plate and framing members,
- $2t_p$ clearance requirements and an alternate elliptical clearance model for brace end rotation,
- thickness of the gusset and relative stiffness of the brace, gusset and framing members,
- tapered and rectangular gusset plates, and
- bolted connection options.

The specimens were subjected to a cyclic inelastic deformation history based upon the ATC-24 testing protocol (ATC, 1992).

Twentythree SCBF frames have been tested, and Table 1 summarizes the specimens and experimental results. The complete results are lengthy and are discussed in greater detail elsewhere (Lehman et al., 2008), but a few specific comparisons are made in Figs. 5 and 6. Figures 5a and 6a show the connection details and behavior for the baseline specimen, Specimen 1. This specimen was designed using the current AISC UFM method with the $2t_p$ clearance requirement, and gusset plate welds were sized to achieve the expected resistance of the brace. The ductility of this specimen was limited as a result of weld fracture of the fillet welds joining the gusset plate to the beam and column as shown in the photo of Fig. 7a. This weld fracture initiated as ductile weld tearing, but abrupt fracture occurred as the weld cracks grew to significant length. The welds for these specimens qualify as AISC demand critical welds. These results show that it is essential to design the gusset plate welds to develop the plastic capacity of the gusset plate rather than the expected capacity of the brace.

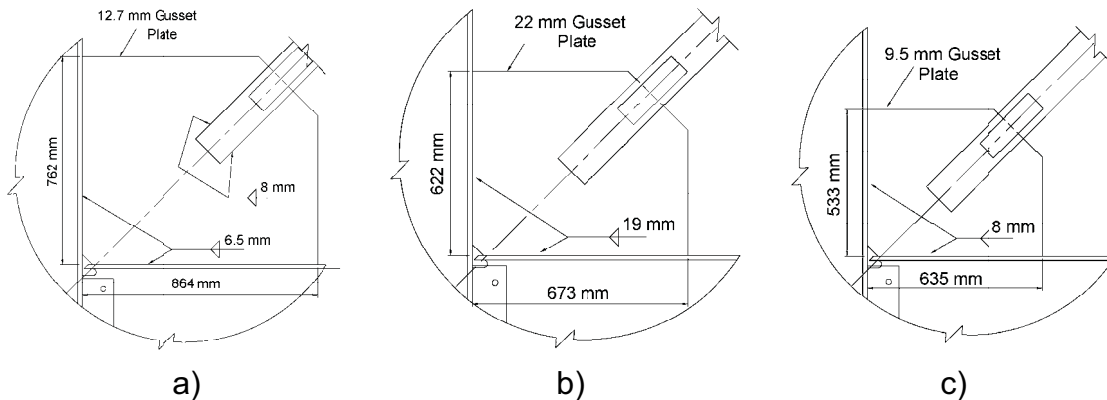


Figure 5. Gusset plate design; a) Spec. 1, b) Spec. 7, and c) Spec. 5

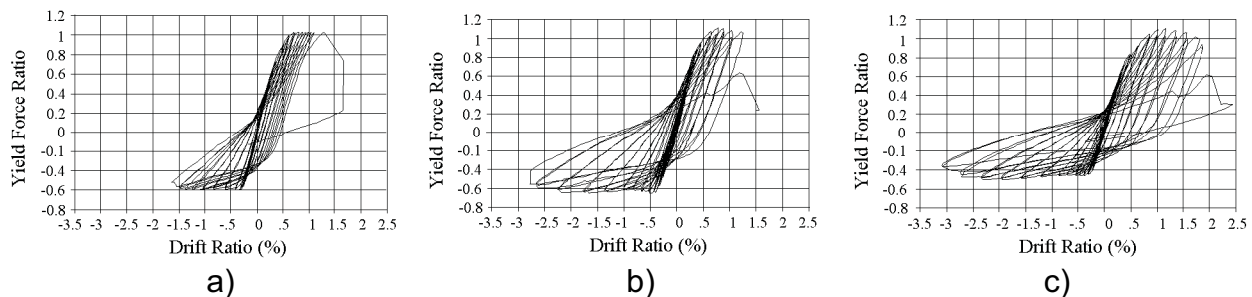


Figure 6. Cyclic force-deflection behaviors; a) Spec. 1, b) Spec. 7, and c) Spec. 5



a) b) c)

Figure 7. Photographs of test results; a) Weld fracture of 1, b) Large out-of-plane buckling deformation of HSS5, c) Brace fracture

Table 1. Summary of Test Program

Spec.	Specimen Description	Failure Mode	Drift Range
1	Baseline - UFM w/ $2 t_p$ linear clearance.	Weld fracture	2.6%
2	#1 except weld sized to plastic capacity of plate & $5.8 t_p$ elliptical clearance	Brace fracture	4.0%
3	#2 except thinner, more flexible gusset	Brace fracture	4.6%
4	#3 except $9.4 t_p$ elliptical clearance	Brace fracture	4.6%
5	# 2 or 3 except $7.7 t_p$ elliptical clearance	Brace fracture	4.8%
6	#5 except ends of fillet welds reinforced	Brace fracture	4.7%
7	Thick gusset with fillet & $6.4 t_p$ elliptical	Brace fracture	3.9%
8	#3 except $3.3 t_p$ elliptical clearance	Brace fracture	4.6%
9	Slightly thicker gusset w/ CJP weld & $5.7 t_p$ elliptical	Brace fracture	3.6%
10	Tapered gusset plate with $7 t_p$ elliptical	Brace fracture w/ weld cracking	4.4%
11	Thick gusset w/ heavy beam & $6.4 t_p$ elliptical	Brace fracture	2.4%
12	#1 ($2 t_p$ linear clearance) except CJP weld	Brace fracture	3.6%
13	#10 except CJP weld & $7 t_p$ elliptical	Brace fracture	3.5%
14	#5 but $6 t_p$ elliptical w/o net section reinforcement	Brace Fracture	4.0%
15	#14 but $6 t_p$ elliptical & minimum for block shear	Brace fracture.	4.1%
16	One sided slip critical bolted brace connection with $2 t_p$ linear clearance in extension plate	Net section fract below brace cap	5.8%
17	#10 but thinner gusset & $9.3 t_p$ elliptical	Brace fracture	4.8%
18	#5 w/ $8 t_p$ elliptical & bolted shear tab beam conn	Brace fracture	3.8%
19	Double-T bolted brace connection	Conn fracture	1.5%
20	Bolted end plate gusset connection	Brace fracture	4.5%
21	Bolted end plate gusset connection	Bolt fracture	3.5%
22	Tapered gusset, Unwelded beam flanges as #18	Gusset tearing	3.9%
23	Wide flange brace, $8 t_p$ elliptical	Gusset weld fracture	5.6%

The $2t_p$ linear clearance model shown in Fig. 2 results in large gusset plates, which forces significant local yield deformation in the beam and column adjacent to the gusset as shown in Fig. 7c. An elliptical clearance model as shown in Fig 8a results in thinner, more compact gusset plates. This can be seen by comparing Specimens 1 and 5 in Figs. 5a and 5c. The elliptical clearance with thin, compact gussets reduces the inelastic deformation in the beams and columns and increases the inelastic deformation capacity of the system as seen in the resulting force-deflection behavior in Fig. 6c and Table 1. This elliptical yield pattern is consistent with the yielding observed during the experiments (see Fig. 8b) and the yield pattern predicted in nonlinear FE analysis for a wide range of connection geometries (Yoo, 2006) (see Fig 8c). With this elliptical clearance model and clearance limits in the order of $6t_p$ to $8t_p$ (see Fig. 8a), the gusset plate had adequate resistance to develop the brace force with little excess resistance. The specimen attained much larger ductility and inelastic deformation capacity than Specimen 1. The brace of Specimen 5 experienced large out-of-plane deformation seen in the photo of Fig. 7b and ultimately fractured at the center of the buckled region.

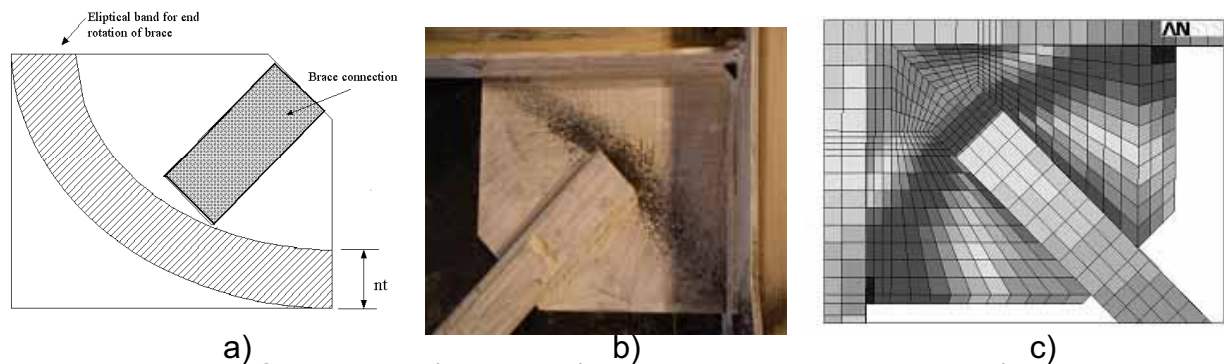


Figure 8. Elliptical Clearance, a) Model, b) Experimental Yield Pattern, c) FEM Prediction

The current seismic design procedure for gusset plate connections often leads to the erroneous hypothesis that a stiff, strong gusset plate is the ideal, and Specimen 7 was designed to test this concept. Figures 5b and 6b illustrate this connection and the resulting behavior. The gusset was thicker, stiffer, and stronger for Specimen 7 than for Specimen 5, but otherwise the designs were the same. Comparison shows that the stiffer, stronger gusset plate had inferior system performance with reduced inelastic deformation capacity. Specimen 11 further tested this concept, since this specimen had a stiffer, stronger gusset plate, but it also had a stiffer, stronger beam member. The results of this test are not plotted, but Table 1 shows that it dramatically reduced the inelastic deformation capacity and seismic performance of the system.

Numerous other specimens were tested and summarized in Table 1, but are not discussed here. A number of important design recommendations have been derived from this experimental research including:

- Welds joining the gusset plate to the beam and column must be designed to achieve the plastic capacity of the gusset plate rather than the expected brace resistance.
- The elliptical clearance model performs equal or better than the $2t_p$ linear clearance model if the elliptical clearance shown in Fig. 8a is in the range of $6t_p$ to $8t_p$.

- Yielding in the Whitmore width of the gusset plate is desirable yield mechanism after initial yielding and buckling of the brace, since it minimizes damage to the welds, and reduces local buckling and deformation in adjacent members.
- The strength and stiffness of the gusset plate should not be excessively large, because stiff, strong connections concentrate inelastic deformation in the center of the brace and cause early brace fracture.
- Tapered gusset plates may provide good end rotational capacity for the brace, but result in thicker gussets and greater inelastic demands on the gusset plate welds.
- The effective length of the brace may be taken as 1.0 based upon the true brace length.

ANALYTICAL STUDY

Nonlinear finite element (FE) analyses were performed with the ANSYS computer program to further investigate the full range of design parameters influencing the frame performance (Yoo et al., 2008). The FE model was constructed from quadrilateral shell elements. Large-deflection models including geometric stiffness with bilinear kinematic plastic hardening material behavior were employed. The cyclic inelastic behavior for the full load history of all test specimens was computed and compared to the test results. The comparison between experiments and analyses were very good at both the global performance and local deformation levels as described elsewhere (Yoo et al, 2008). Figure 9 illustrates a typical comparison of the global force deflection response for one test specimen, and Figs. 8b and 8c provide comparison of observed and computed results at a more local level. The analytical results are not described in this paper to control the paper length. However, there was strong correlation between the predicted inelastic analysis results and the experimental results. Further, the analysis suggested models for predicting initiation of cracking and fracture in the brace and connections. It also suggested that net section fracture of the brace may be rationally controlled without net section reinforcement in some cases.

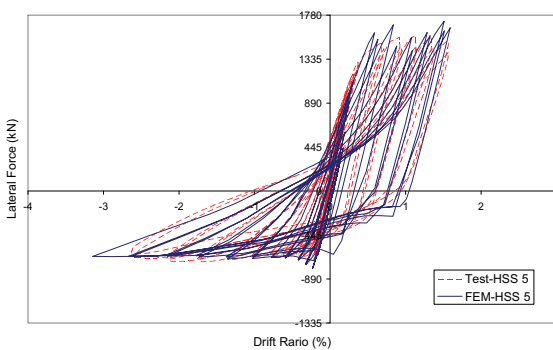


Figure 9. Measured and Computed Force-Deflection Behavior Specimen 5

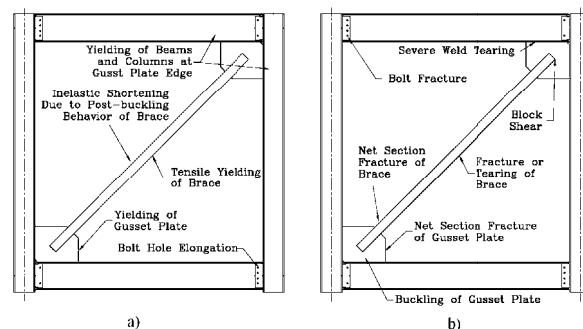


Figure 10. Typical behaviors for SCBFs; a) Yield mechanisms, b) Failure modes

PROPOSED DESIGN METHOD

A seismic design methodology based on balancing yield mechanisms and preventing undesirable failure modes is proposed to incorporate these experimental and analytical

concepts and to improve the seismic performance of gusset plate connections. As before, framing elements are designed to develop required factored loads, and connections are designed to develop the expected tensile yield and compressive buckling resistances of the brace. However, greater ductility is achieved with the proposed method by assuring that multiple, desirable yield mechanisms are developed prior to fracture or failure of the brace with the proposed capacity design balance procedure defined in Equations 1 and 2. The balance procedure assures a sequence of yielding mechanisms and increased inelastic deformation before undesirable failure modes are permitted by providing multiple sources of yield deformation.

Figure 10 illustrates the possible yield mechanisms and failure modes for CBFs, and Eq. 1 expresses the proposed yield mechanism balance procedure.

$$P_u = R_y A_g F_{cr} \text{ or } P_u = R_y A_g F_y \text{ as appropriate } \leq \beta_{yield,1} R_y R_{yield,1} \leq \beta_{yield,2} R_y R_{yield,2} \dots \dots \dots \leq \beta_{yield,i} R_y R_{yield,i} \quad (1)$$

The nominal yield resistances, R_{yield} , for the various yield mechanisms are separated by balance factors, β_{yield} , to assure development of the preferred yield mechanism and provide a sequence of yielding through the inequalities and balance conditions. The β values are based on the ductility and experimental performance of the various yield mechanisms and the separation required to achieve the performance goals rather than the minimum resistance as achieved with resistance factors, ϕ , in LRFD design. Failure modes cause fracture, tearing, reduction of resistance, or deterioration of performance. A single failure mode typically will not result in collapse or total failure of the system, but it will cause significant, irrecoverable damage. As a result, the balancing procedure shown in Eq. 2 is used to separate and balance critical failure mode resistances relative to the controlling yield resistance.

$$R_y R_{yield,1} \leq \beta_{fail,1} R_{fail,1} \leq \beta_{fail,2} R_{fail,2} \dots \dots \dots \leq \beta_{fail,i} R_y R_{fail,i} \quad (2)$$

This balanced design approach assures that the resistance of all failure modes, R_{fail} , exceed the strength of the primary yield mechanism, and it assures that less favorable failure modes have greater separation than more favorable failure behaviors, and the least favorable failure modes have smaller probability of occurrence. The relative magnitude of the β_{yield} and β_{fail} values assure the number of secondary yield mechanisms to be expected and the separation between braced frame yielding and initial failure of the SCBF system. An earlier paper (Roeder, Lehman and Yoo 2005) describes this balance procedure and the rationale for establishing the β factors.

ACKNOWLEDGEMENTS

This research work is funded by the National Science Foundation through Grant CMS-0301792, Performance-Based Seismic Design of Centrally Braced Frames. Supplemental funding was provided by the American Institute of Steel Construction with Mr. Tom Schlafly providing technical contact. The structural steel shapes for the test

specimens were provided by Nucor-Yamato steel, and the HSS tubes were donated by Columbia Structural Tubing. This support is gratefully acknowledged. Tom Schlafly of AISC, Tim Fraser of CANRON, John Hooper and Cheryl Burwell of Magnusson and Klemencic, Walterio Lopez of Rutherford and Chekene, and Rafael Sabelli of DASSE Design provided advice and guidance on this research. Their assistance is greatly appreciated.

REFERENCES

AISC, (2005a). "Seismic Provisions for Structural Steel Buildings," American Institute of Steel Construction, Chicago, IL.

AISC, (2005b) "Manual of Steel Construction," 13th Edition, American Institute of Steel Construction, Chicago, IL.

Astaneh-Asl, A., (1989) "Simple Methods for Design of Steel Gusset Plates," Proceedings ASCE Structures Conference, San Francisco, CA.

Brown, V.L.S., (1988) " Stability of Gusseted Connections in Steel Structures," A thesis submitted in partial fulfillment of Doctor of Philosophy in Civil Engineering, University of Delaware.

Lehman, D.E., Roeder, C.W., Herman, D., Johnson, S., and Kotulka, B., (2008) "Improved Seismic Performance of Gusset Plate Connections," ASCE, *Journal of Structural Engineering*, Vol. 134, No.6, Reston, VA.

Roeder, C.W., Lehman, D.E., and Yoo, J.H., (2005) "Improved Seismic Design of Steel Frame Connections," *International Journal of Steel Structures*, Korean Society of Steel Construction, Seoul, Korea, Vol. 5, No. 2, pgs 141-53

Thornton, W.A., (1991) "On the Analysis and Design of Bracing Connections," AISC, *Proceedings of National Steel Construction Conference*, Section 26, pgs 1-33.

Yoo, J.H., Roeder, C.W., and Lehman, D.E., (2008) "FEM Simulation and Failure Analysis of Special Concentrically Braced Frame Tests," approved and awaiting publication, ASCE, *Journal of Structural Engineering*.

Whitmore, R.E., (1950) "Experimental Investigation of Stresses in Gusset Plates," a thesis submitted in partial fulfillment of the Master of Science Degree at the University of Tennessee, Knoxville, Tennessee.

MINIMIZING THE STRENGTH OF BRACING CONNECTIONS

Richard B. Vincent

Canam Group Inc., Boucherville, Quebec J4B 5X9, Canada

richard.vincent@canam.ws

ABSTRACT

Steel bracing members and connections of Seismic Force Resisting Systems designed to meet North American codes are based on capacity design principles requiring that the connection be designed to allow the tensile brace member to achieve yield. Brace member selection is based on the compressive resistance of the element making the probable tensile resistance of the brace member significantly larger, necessitating excessively strong joints and increasing the cost of the structure. Capacity design principles also require that the columns supporting the braced members be designed to resist the probable tensile resistance of the brace, dictating increases in column size, especially for multiple storey structures, and further increasing the cost of the SFRS. This paper will describe a typical WF brace connection from a recent project and propose a method of limiting the tensile resistance for braced members in bolted connections while not reducing their compressive resistance.

INTRODUCTION

Steel structures must be designed to resist lateral forces due to wind, seismic and crane lateral forces. The lateral force resisting systems employed to resist these forces include rigid frames, steel plate shear walls and by far the most prevalent, vertical bracing systems. Conventional bracing systems are simple to design and provide effective and economical lateral force resisting systems. Bracing systems can be constructed in many different configurations, often established by specific clearance constraints or to behave in predetermined fashion. Bracing configurations include tension only and tension compression cross braces, single tension compression diagonal braces and chevron or inverted chevron tension compression braces. These systems may be designed and detailed as concentrically or eccentrically braced frames. Sizing of the brace member is normally a simple task as the section is designed only to resist an axial tension or a compressive force. Braced members may be oversized in order to limit its axial deformation in order to control interstory drift.

The selection of the actual brace member is driven by economy and for smaller forces a single angle member is usually selected or possibly even a bar shape, either a rod or flat for a tension only system. As the design force increases, the member of choice becomes interconnected double angles for their ease of connection, fabrication and installation. As lateral forces continue to get larger, it becomes more effective to use hollow structural sections due to their high ratio of compressive resistance to mass.

Once the range and capacity of hollow sections is exceeded, wide flange sections are utilized. Forces beyond the capacity of wide flange shapes require custom built up sections. High rise buildings and heavy industrial plants typically fall into the category of structures where wide flange members are the common member choice to use as bracing members.

The Canadian design standard CAN/CSA-S16-05, "Limit States Design of Steel Structures", provides the requirements for the design of members and their connections in the seismic-force-resisting system (SFRS) for steel buildings. The code provisions are based on capacity design principles whereby specific elements or mechanisms are designed to dissipate energy and all other elements must be sufficiently strong for this energy dissipation to be achieved. In vertical bracing systems, the braces are the energy dissipating elements and the beams, columns and connections in the SFRS must be proportioned such that energy dissipation can occur. Steel used in the energy dissipating elements is limited to a maximum specified yield strength of 350 MPa (50 ksi). The United States design specification, ANSI/AISC 360-05 "Specification For Structural Steel Buildings", has very similar provisions for the design of members and their connections in the SFRS for steel buildings. The paper will concentrate on the technical problems associated with connection design for wide flange bracing in seismic areas in meeting the SFRS requirements and present a method to reduce the connection demand by introducing a fuse limiting the tension resistance of the brace, somewhat similar to the reduced beam section connection developed and tested for moment frames.

CONNECTION TYPES

Connection design can truly be considered an art. Fabricators consider good connection designers to be worth their weight in gold. The cost related to shop fabrication is totally dependant on the man hours required to produce the connections linking individual members. No shop fabrication man hours are spent on the shaft portion of the member between connection points.

A good connection must of course resist the design forces but must also be economical and erectable in the field. The total cost of a connection includes the shop cost for the shop man hours required to manufacture the connection, the cost for the man hours to assemble and complete the connection in the field plus the cost of the connection materials. In many locations, the cost of a man hour, whether in the shop or in the field, is relatively the same and the least total number of man hours necessary to complete the connection, produces the best result. This however, is not the case in many of the large cities in the Northern cities of North America such as New York, Boston, Philadelphia, Chicago, etc. where field workers are unionized and the cost of a field man hour may easily be double than that of a shop man hour. The availability of skilled field workmen such as welders also influences the choice for the optimum connection. The time required to complete a connection in the field is also an important factor. Field welded connections increase the overall field time duration when compared to the time

required to complete the equivalent field bolted connection. In the large cities cited above, field costs and labor shortages demand that bracing connections be bolted rather than welded.

One method of evaluating connection performance is to determine the “level” of the connection. This is a method that is used internally at Canam to assess relative connection cost. Lower “level” ratings indicate more efficient connections. The connection “level” is established by counting the number of times the design force needs to be transferred. One can presume that the cost to make one full connection of the design force is relatively the same whether it is bolted or welded or made in the plant or in the field. Thus a “level” one connection only requires the member force to be transferred one single time. An example of a “level” one connection is a field welded moment connection of a beam to a column. The connection force is only transferred once, directly by welding of the beam flanges to the column flange. If the column flange requires stiffeners in order to locally reinforce the flange, then this becomes a “level” two connection as the design force must be transferred through to the stiffeners. An example of a simple “level” two connection is a field bolted double angle tension brace connected to a gusset plate that is welded to a column base plate. This connection requires the force to be transferred twice, first by field bolting of the angles to the gusset plate and then by welding of the gusset plate to the column base. The “level” method is a fairly good predictor for assessing the relative costs when comparing connections.

Wide flange brace sections pose a problem in attaining simple efficient connections. Typically, column sections are used for the brace members. For all hot rolled North American wide flange column sections in the W10 (W250), W12 (W310) and W14 (W360) series of shapes, the area of each flange is relatively constant in proportion to the total area of the section, between 38% and 41%. This means the area of the web is between 18% and 24% of the total area of the section. Thus significant forces need to be connected occurring from both orthogonal planes. There are two possible orientations for a wide flange brace section, either with the web in a vertical plane or with the flanges in the vertical plane. The design of the connection of course depends on the orientation of the supporting column and strut girder. The floor beam/strut always has its web orientated in the vertical plane while the column may be turned along either axis. We shall now look at the two different brace orientations and the possible connections geometries.

Bolted WF Brace Connection With Web Vertical

When the brace web is aligned with the floor beam/strut web, the logical choice is to have a vertical gusset plate aligned with both the strut and brace member webs. The horizontal portion of the gusset plate can be welded directly to the floor beam/strut flange while the vertical segment of the gusset plate can be welded to the beam end plate that is in turn bolted to the column flange or web. Figure 1 shows a perspective of a braced bay and Figure 2 shows an enlarged detail of this connection arrangement. The bolts have been omitted for the sake of clarity. The brace web force is connected using two splice plates placed on each side of the brace web enabling the bolts to act in

double shear. The flanges are connected to splice plates slotted to fit through the vertical gusset plate and attached to it by welding on both sides. The brace flanges can either be bolted or welded to the splice plates. This a “level” 3.5 connection for the brace web force, “level” 3 for the horizontal connection component and “level” 4 for the vertical component. This is also a “level” 3.5 connection for the flange force, “level” 3 for the horizontal connection component and “level” 4 for the vertical component. The bolted web splice plates allow the brace to be erected from one side between the flange splice plates. This arrangement allows the option of connecting the flange force by either field welding or field bolting.

Bolted WF Brace Connection With Web Horizontal

When the brace web is horizontal, no simple connection arrangements become self evident. Connection geometry has to be based on the main member sizes selected and the corresponding widths of the elements. Most arrangements produce connection “levels” of 4 or more.

In order to make this configuration economical, planning of the connection geometry must be performed by the designer prior to member selection. When the vertical braced bay is only along one grid line axis, column orientation should be such that the column flanges line up with the brace flanges. Should vertical bracing be required along both perpendicular grid axes, box columns should be used and the depth of the box chosen so that the bracing gusset plates can be directly welded to the individual column flanges coordinating the depth so that the bracing member will fit with erection clearance inside the space between the pair of gusset plates. Figure 3 shows the basic concept of this connection.

Careful consideration should also be given to the design of the strut member. Two different choices can be made to facilitate connection design. The first is to have a boxed floor beam/strut that would be made the same width as the brace member, as shown in Figure 3. Both webs would be connected to the gusset plate that would serve to connect the vertical beam reaction and to transfer the horizontal component of the brace reaction. A hand hole is required at the top flange of the beam/strut to accommodate field bolting. A second option is to use a hot rolled wide flange section built up with two Tee sections on either side, as shown in Figure 4. The web of the beam is connected for vertical shear while the Tee flanges are designed to take horizontal brace force component. The Tee extends sufficiently to develop this force taking account shear lag effects. For clarity, bracing is only shown on only one axis in Figures 3 and 4, and the column illustrated is a box section. A wide flange section could be used with the web oriented perpendicular to the braced grid line for bracing in one axis only.

The first option described utilizing the box section is the less costly of the two even though it requires the fabrication of a built up section. Both joint configurations require additional fabrication cost being invested into the fabrication of the main members but the overall simplicity and effectiveness of the connection more than makes up for this

cost with savings in the weight of connection elements and shop hours required for brace fabrication. Additionally, both these connections can be erected quickly and minimize overall field time. The connection using a boxed floor beam/strut is a “level 2” connection while the use of a wide flange shape with Tee’s is a “level” 2.5 connection.

EXAMPLE CONNECTION - NEW YORK STADIUM PROJECT

Canam is presently constructing four outdoor stadium projects in the greater New York City area. All four stadiums are designed as braced structures and some are mandated to be designed to meet the seismic provisions of the AISC Specification. Figure 1 is a perspective elevation of a typical bent created from the 3 Dimensional detailing model. Figure 2 is a close up of the connection at the column-beam joint. The diagonal brace is a W14x233 (W360x347), the beam/strut is a W30x108 (WF760x161), the column at the upper connection level is a W14x257 (W360x382) while the column receiving the brace at its base plate is a W30x326 (W760x484). Both 3D figures are drawn to scale. The gusset plates are detailed to provide for out of plane buckling for the brace with a fold line equal to $2t$. The center to center distance between columns is 30.0 ft. (9.144 m) and the distance from under side of base plate to the centerline of the strut/floor beam is 26.33 ft. (8.026 m), resulting in a work point (WP) to work point brace length of 39.62 ft. (12.167 m).

The W14x233 brace has been designed with a $k=1$ and based on its WP to WP unsupported length has an axial resistance of 1,130 kips (5,030 kN). The tension resistance of this brace is 3,080 kips (13,700 kN) and the expected yield strength of the brace in tension, defined as $R_y F_y A_g$ is 3,780 kips (16,800 kN). The actual buckling length from gusset plate fold line to gusset plate fold line is actually 28.70 ft. (8.75 m). This actual unsupported length makes the true design axial resistance equal to 1,840 kips (8180 kN), indicating that the section has been significantly oversized. Having such large design over strengths is often the case in the design of compression braces.

Several engineers of large consulting firms were surveyed to discuss their current practice for the design of compression braces and all agreed that they design tension compression bracing using the WP to WP as the unsupported length of the brace and furthermore take an effective length factor k equal to 1.0.

The vertical component of the expected yield strength of the brace in this example is 64.9% of the brace force. Thus, according to capacity design principles, the column has to be designed to support an additional vertical load equal to 64.9% x (3,780-1,130) kips or 1,720 kips (7,640 kN). This extra force requires an additional 38.2 in² (24,600 mm²) of area or 130 plf (193 kg/m) of steel for the column. In fact, this additional area may be somewhat smaller as it is possible that the column may have been originally sized for a different load combination case.

In order to reduce the significant additional costs required by capacity design of the bracing system, it is proposed to introduce a fuse that would limit the tension resistance

of the brace while not affecting the compressive resistance of the brace, thereby greatly reducing the over strength required in both the connection and column.

In the New York City area, field labor costs dictate that the connection is field bolted. The bolt holes reduce the net section through the connection and the wide flange shape must be locally reinforced to preclude this failure mode and allow gross section yielding to occur at the brace midspan. The cover plates that replace the removed area must of course be developed beyond the extent of the bolted connection again adding further cost. These cover plates can be seen in Figure 4.

PROPOSED WIDE FLANGE BRACE FUSE

The purpose of a fuse in tension compression braces is to predetermine the location and the load level at which tension yielding of the brace will occur. The fuse must of course allow the brace to yield in compression and therefore should be designed to remain elastic during the compressive load cycle. This requires that the fuse not buckle locally in compression while the brace goes through its inelastic cyclic deformation. The fuse proposed is shown in Figure 5 (a) & (b). The figure only shows a fuse located at the top flange but a similar cutout would be located at both the top and bottom flanges, symmetrically about the neutral axis of the beam. The fuse is created by removing a portion of the brace area. One method of achieving the desired result is to drill six holes at the corner points of the slotted area, four in the flanges and two in the web. The web is then cut horizontally between the lower horizontal tangents of the holes and vertically from the outer vertical tangents of the holes into the start of the k distance of the flange. Horizontal cuts are then performed from the top of the flange again joining the tangents of the holes. Finally, two transverse cuts are made from the tangents of the holes directly above the cuts previously made into the web. The result is a neat hole cut out of the wide flange section. Grinding may be necessary at the junction of the flange and web if the vertical web cut and the transverse flange cut are not perfectly aligned. The size of the fuse may be adjusted to achieve the desired load. Shop tests have been conducted for making this cut and the described procedure gives satisfactory results.

In tension compression bracing, inelastic buckling occurs at interstory drifts between 0.3 and 0.5 percent. In order to achieve sufficient ductility in the fuse, the brace should be designed to resist an interstory drift of 2%. The strain at initial strain hardening occurs at a strain rate of 0.015 in./in. for high-strength low-alloy steels such as the standard steel grade ASTM A992 utilized in building construction today. Limiting the strain in the fuse to this level would require a much too long fuse length. It is therefore proposed to increase the strain in the fuse section to 0.10 in./in.

In order to assess the expected yield stress of the fuse area, a factor $R_y = 1.1$ has to be applied to the specified yield stress to obtain the expected yield stress. At a strain rate of 10%, an additional R_{SH} factor needs to be applied on top of the R_y factor to take into account the effect of strain hardening. For A992 grade 50 steel, the minimum specified yield stress F_y is 50 ksi, the minimum tensile strength F_u is 65 ksi and the maximum

ratio of F_y/F_u is 0.85. A conservative value for a typical ratio of F_y/F_u is 0.75. Thus the ultimate strength can be expected to be around 73.3 ksi. At 10% strain, the stress is very nearly half way between the yield strength and the ultimate strength indicating the stress would be in the range of 64.5 ksi. This would indicate that the expected stress due to hardening at a 10% strain should be approximately $(73.3 \text{ ksi} - 55 \text{ ksi})/2 + 55 \text{ ksi} = 64.2 \text{ ksi}$. This result gives a value of 1.17 for R_{SH} and conservatively this value may be taken as 1.18, giving a combined effect of $R_y \cdot R_{SH} = 1.3$.

We will now look at the requirements for a fuse in the example of the New York stadium brace. The bay spacing is 30 ft. and the vertical height from base plate to neutral axis of the floor beam/strut is 26.33 ft. resulting in a brace length of 39.93 ft. At a 2% drift, the brace has an elongation of 0.453 ft. Thus, the design for a fuse length at a strain rate of 10% results in a minimum fuse length of 4.53 feet. This fuse length is quite long and to avoid the possibility of local buckling of a fuse component, it is proposed to use two fuses, one at each end of the brace, each having a length of 28 inches for a total overall length of 4.67 ft.

The proposed fuse will have a width of 5 inches (127.0 mm) across the top flange and a depth of 3.75 inches (95.25 mm) measured from the top of the flange to the horizontal cut along the web. This fuse removes 30.9% of the gross area of the brace, leaving a net area of 46.7 in² (30,100 mm²). The expected tensile yield strength of the brace is given by the expression $R_y \cdot R_{SH} \cdot F_y \cdot A_{fuse}$ or $1.3 \times 50 \text{ ksi} \times 46.7 \text{ in}^2 = 3,040 \text{ kips}$, well above the design load of 1,130 kips and the estimated compressive resistance of the brace of $R_y \times 1,840 \text{ kips} / 0.9 = 2,250 \text{ kips}$.

The advantage of this fuse is that the section properties through the fuse in the axis of buckling are greater than the properties of the original section. For instance, r_{yy} increases from 4.09" to 4.80" while r_{xx} remains about the same from 6.61" to 6.52". The 4 remaining flange sections through the fuse are steel blocks having a width of 5.01" with a thickness of 1.72". The radii of gyration for these blocks are $r_{xx} = 0.50"$ and $r_{yy} = 1.46"$. The restraint conditions for the fuse blocks are fixed for local buckling about both principal axes, so that a k value of 0.5 can be assumed. The fuse length is 28" resulting in kL/r values of 28 and 9.6 for the fuse block. As the fuse is located within proximity of the end connection, both overall buckling and local buckling of the fuse are eliminated. This needs to be confirmed by a testing program. For smaller wide flange sections having thinner flanges, local buckling can be prevented by welding a small flat to the underside of the flange block creating a stronger Tee section that will prevent local buckling. The cost associated with the placement of the flats would still result in significant overall economies. This is illustrated in the subsequent example.

The introduction of the fuse results in designing the connection for 3,040 kips versus 3,780 kips, a reduce connection force of 19.6%. This is sufficient to allow the net section through the bolt holes to remain unreinforced.

Economy for a Tension Brace with Fuse

The cost saving that can be achieved with an adequately designed tension brace fuse can be enormous. The actual shop fabrication drawings for the connections shown in Figures 1 and 2 are presented as Figures 6 through 9. Figure 6 shows the shop detail drawing for the floor beam/strut. Figure 7 is the shop drawing for the column that receives the brace at its base plate. Figure 8 is the shop detail drawing for the wide flange brace while Figure 9 is an enlarged detail of the brace connection.

The connection was redesigned for the reduced forces created by the introduction of the fuse. As a comparison, the connection components for the original design are listed and immediately followed in parenthesis by the components resulting from a fuse design.

- 1: 2 flange cover plates PL18" x 1" x 67.5" in length to restore the net section through the bolt holes, each attached by 70" of 1/2" fillet welds and 104.5" of 5/16" fillet welds. (Cover plates are completely eliminated)
- 2: 2 flange splice plates PL21" x 2 3/8" x 75.1" attached to the gusset plate with 8 - 11/16" fillet welds each 31.75" in length and requiring 44 - 1 1/8" diameter A490 bolts Slip Critical Class B bolts per plate. (Splice plates PL21" x 1 3/4" x 54.5" with 8 - 5/8" welds x 22" in length and 32 same type bolts per plate)
- 3: 2 web plates PL9" x 1" x 31.25" field bolted with 16 - 1 1/8" diameter A490 bolts Slip Critical Class B bolts. (No change)
- 4: 1 gusset plate PL 69" x 1 3/4" x 77" connected with 15/16" fillet weld for a total length of 260". (Gusset PL52" x 1 1/2" x 60" with 7/8" fillets for length of 210")
- 5: 1 base plate extension PL54" x 1" x 57" welded to the base plate with a full penetration weld. (No change)

Total savings per brace end are as follows:

- 1: The number of bolts goes from 104 to 80 for a saving of 24 - 1 1/8" diameter A490 bolts Slip Critical Class B bolts. The estimated cost of an installed bolt in New York City is in excess of \$20 per bolt that gives a saving in excess of \$480.
- 2: The connection material weight goes from 6,479 pounds to 3,495 pounds resulting in a savings of 2,984 pounds. The estimated cost of plate material is approximately \$1,200 per ton resulting in a saving of \$1,790.
- 3: The weld volume is reduced by about 77 in³ resulting in a reduction of 7 man hours of weld time or a cost of \$420.

The total estimated savings per brace end are in the vicinity of \$2,700 or a total of about \$5,400 per brace. This particular project has more than 200 braces but not all of this size. A preliminary estimate would indicate that the fuse concept could save in the order of \$500,000 for this project. This estimate excludes any weight savings in the columns due to lesser capacity design demand.

CONCLUSIONS

Vertical bracing is by far the most economical method of providing a Seismic Force Resisting System to a building. Recent code requirements for capacity design in SFRS have greatly increased the cost for braced structures by significantly increasing the demand on the connection and the related cost of the connection in material weight, fabrication man hour content and the number of field hours necessary to complete the connection. Additionally, column and strut members at connection joints need to be increased in size to resist the greater connection force and to meet capacity design obligations.

The introduction of a fuse in the brace member can significantly reduce the connection demand while at the same time moderate the capacity demand on the column and struts. The proposed fuse meets these objectives while adding little additional cost to the manufacturing of the brace. Testing of the fuse will of course be necessary but the preliminary analysis conducted to date indicates that the fuse will allow the brace to yield cyclically in compression without affecting the overall brace resistance.

REFERENCES

American Institute of Steel Construction (2005), *Seismic Provisions for Structural Steel Buildings*, ANSI/AISC Standard 341-05, AISC, Chicago, IL, USA.

American Institute of Steel Construction (2005), *Specification for Structural Steel Buildings*, ANSI/AISC Standard 360-05, AISC, Chicago, IL, USA.

Canadian Institute of Steel Construction (2006), *Handbook of Steel Construction*, 9th Ed., CISC, Willowdale, ON, Canada.

Canadian Standards Association (2006), *Limit States Design of Steel Structures*, CSA Standard S16-01, Update No. 3, CSA, Toronto, ON, Canada.

Kassis, D. and Tremblay, R. (2008), "Brace Fuse System for Cost-Effective Design of Low-Rise Steel Buildings", *Proceedings*, 2008 Annual Conference, Canadian Society of Civil Engineering, Montreal, PQ, Canada.

National Research Council of Canada (2005), *National Building Code of Canada, Part 4*, NRC, Ottawa, ON, Canada.

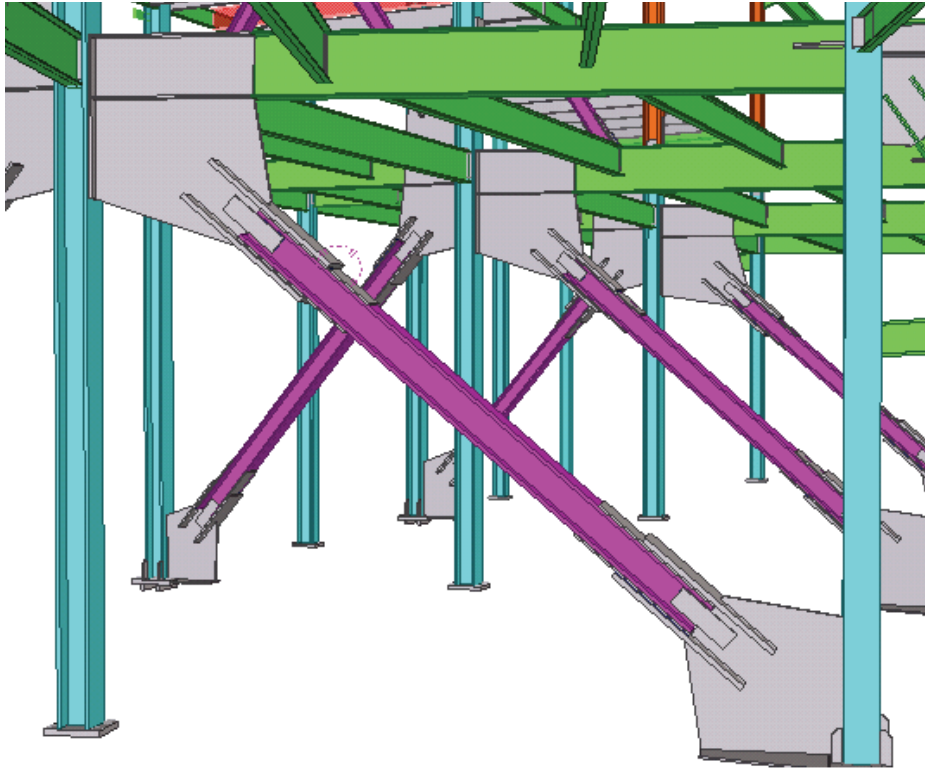


Figure 1: Perspective View of Braced Bay

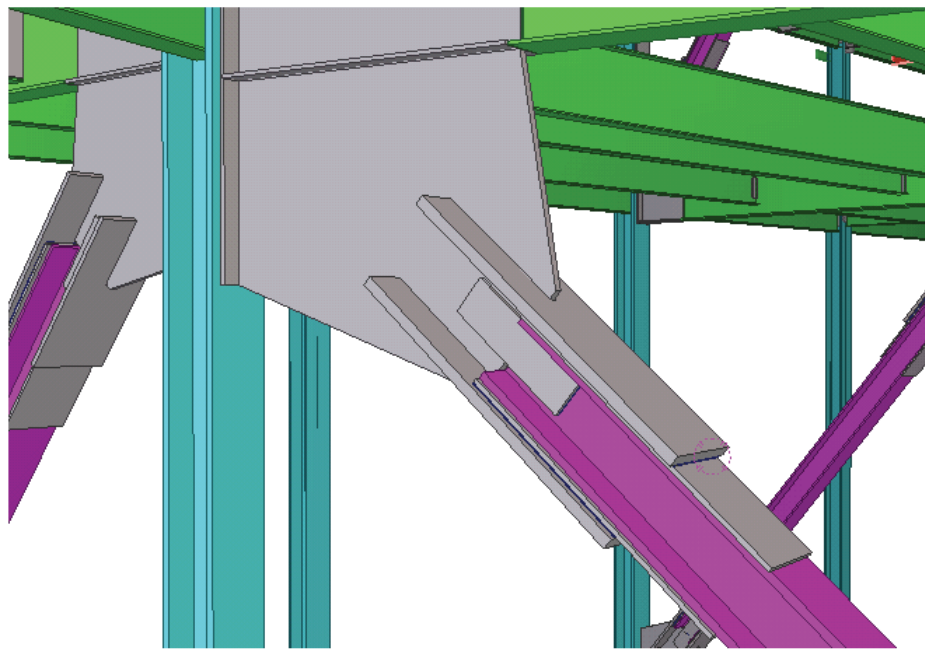


Figure 2: Enlarged Detail of Wide Flange Brace Connection

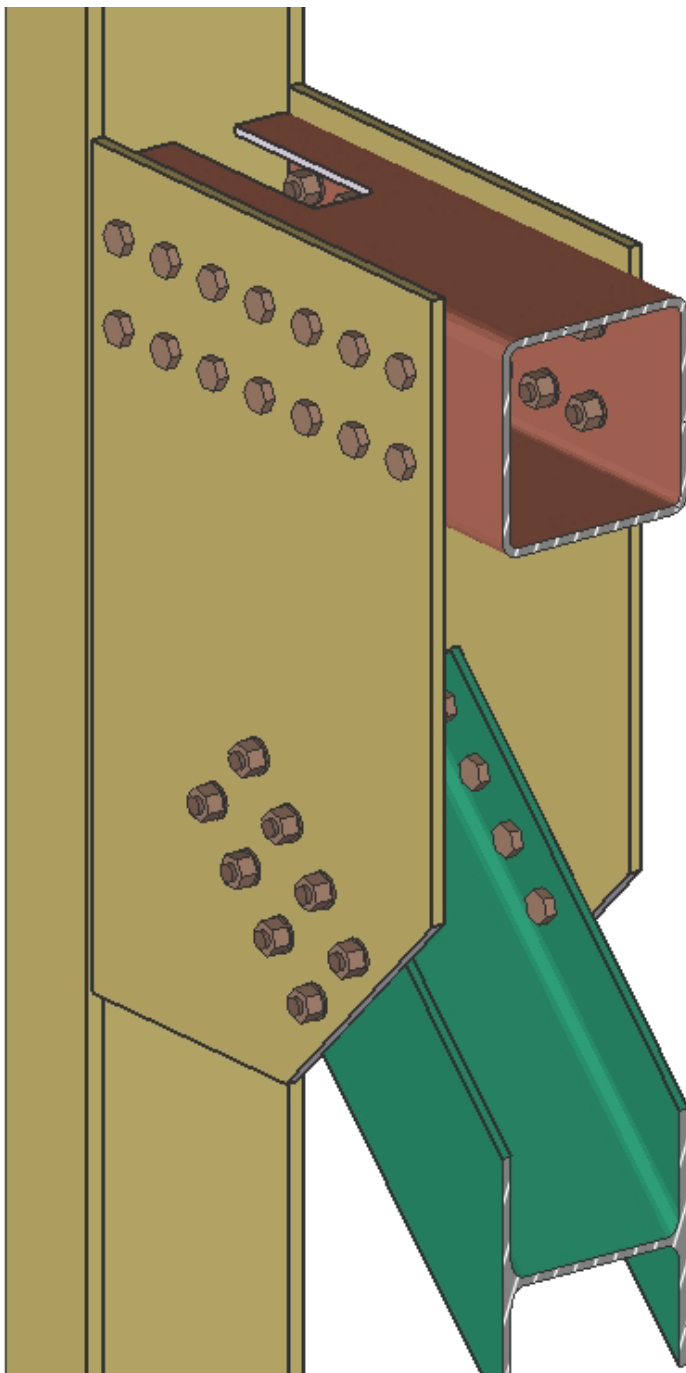


Figure 3: Detail of Wide Flange Brace Connection with Vertical Flanges & Box Section Floor Strut

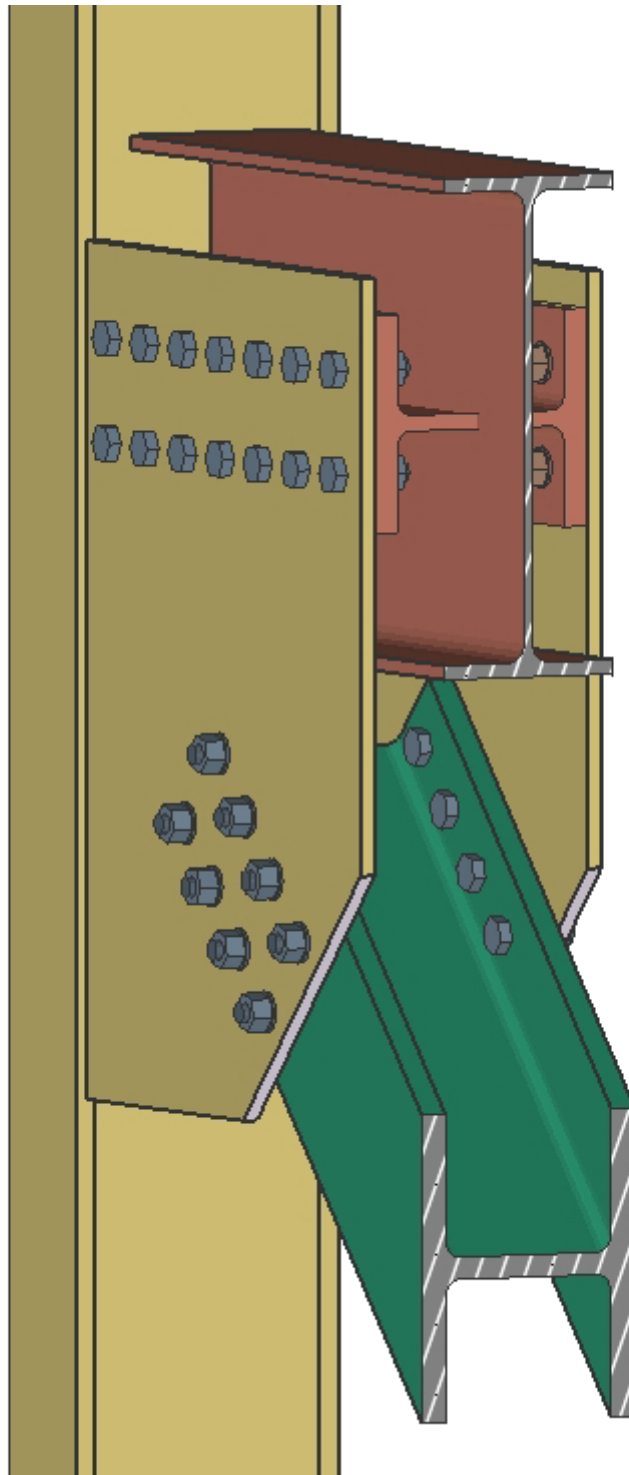


Figure 4: Detail of Wide Flange Brace Connection with Vertical Flanges & Wide Flange Floor Strut

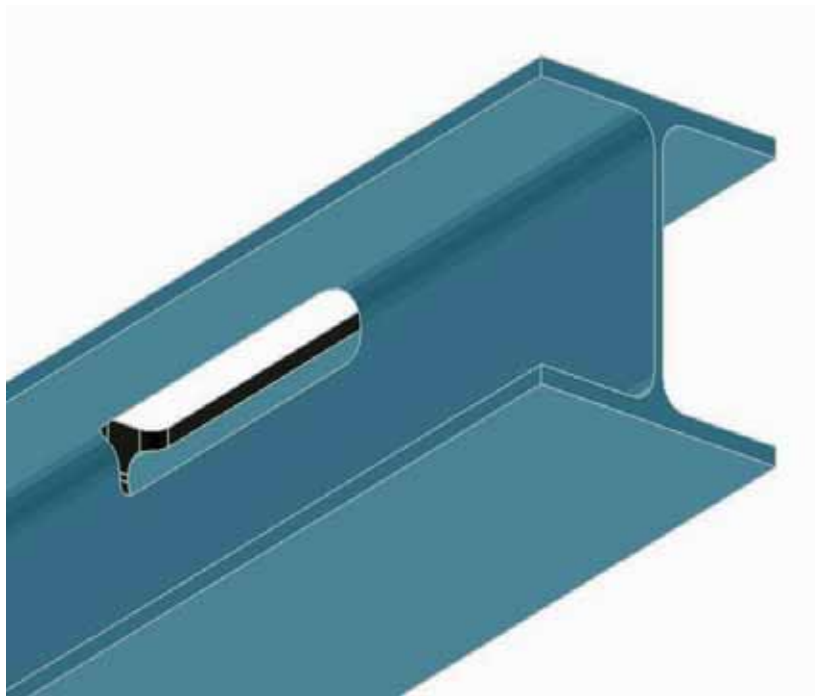


Figure 5 (a): Perspective View of Fuse From Below



Figure 5 (b): Perspective View of Fuse From Above

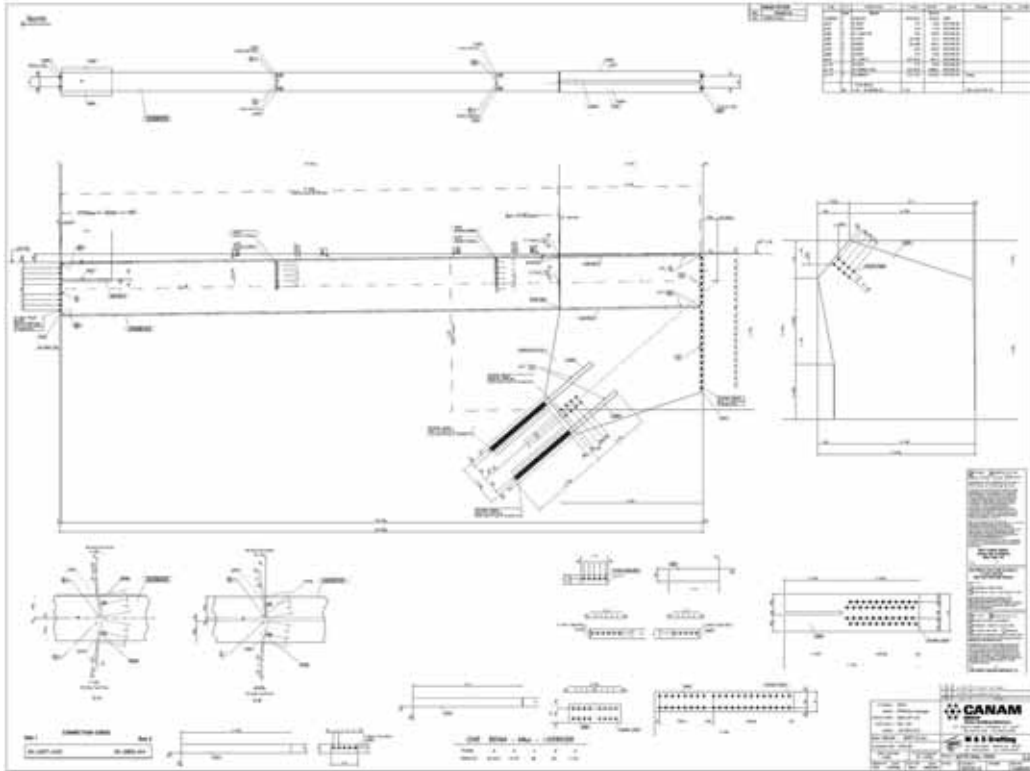


Figure 6: Shop Detail Drawing for Floor Beam/Strut

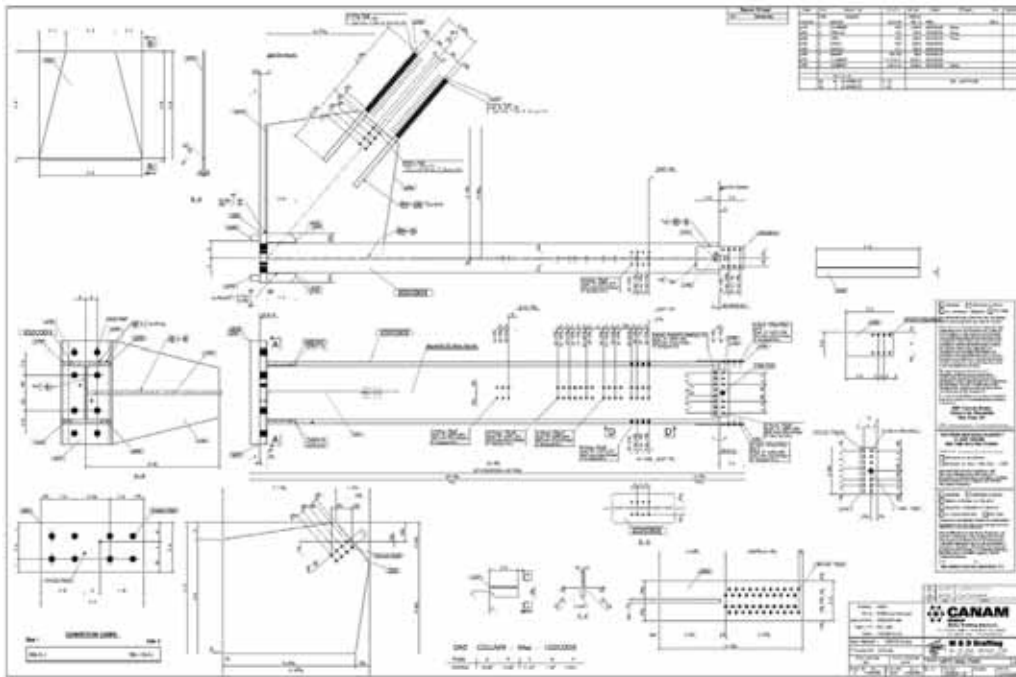


Figure 7: Shop Detail Drawing for Column With Base Plate Brace Connection

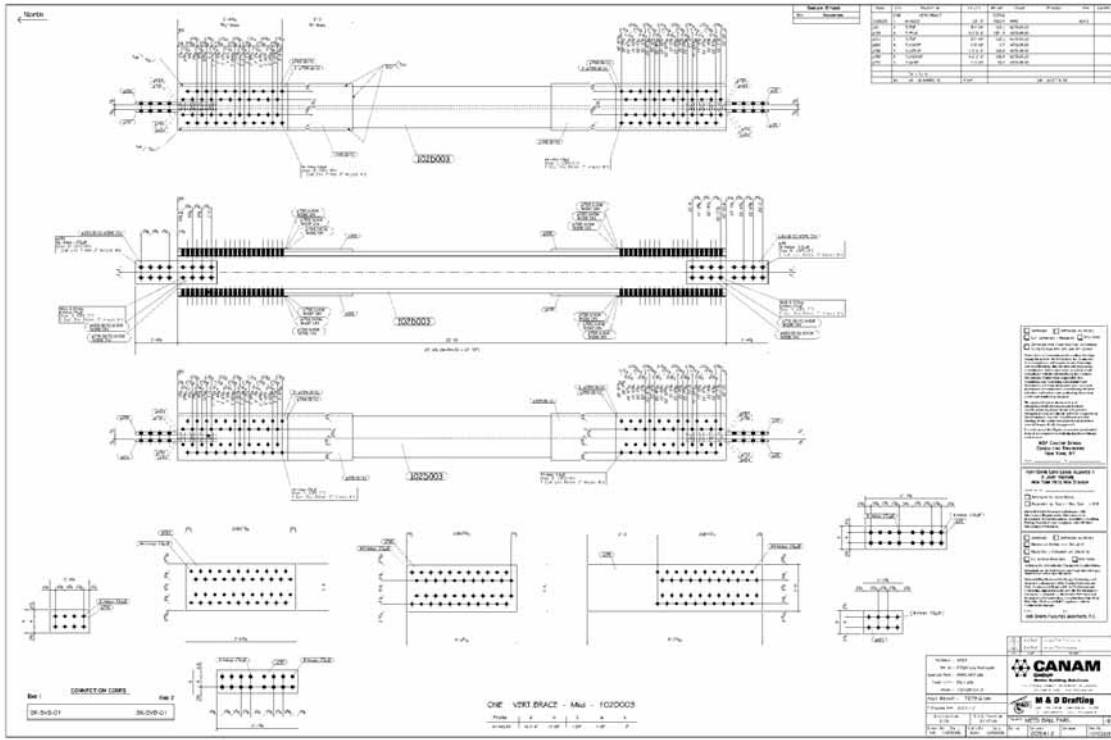


Figure 8: Shop Detail Drawing for Wide Flange Brace

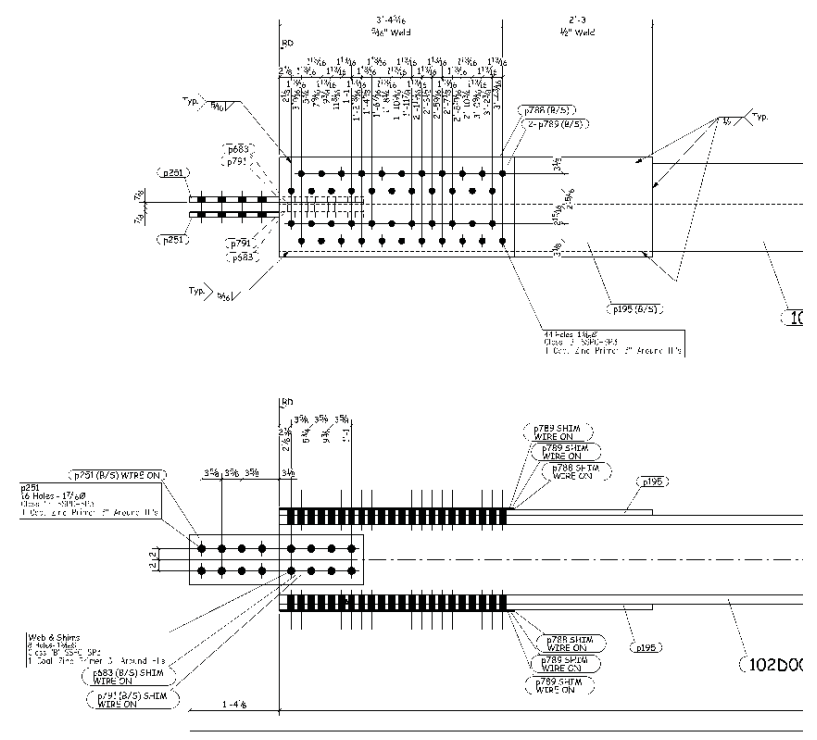


Figure 9: Enlarged Shop Detail Drawing for Wide Flange Brace Connection

EXPERIMENTAL VERIFICATION OF THE NEW AISC SINGLE-PLATE SHEAR CONNECTION DESIGN MODEL

Kirsten A. Baldwin Metzger

Former Graduate Research Assistant

Thomas M. Murray

Montague-Betts Professor of Structural Steel Design

thmurray@vt.edu

Via Department of Civil & Environmental Engineering

Virginia Tech, Blacksburg, Virginia, USA

ABSTRACT

The results of eight single-plate shear connection tests designed using the 2005 AISC procedure are presented. Four conventional and four extended tests were conducted using simply supported beams. Strengths and rotation capacities are reported and compared to the design procedure predictions.

INTRODUCTION

The procedure for the design of single-plate shear connections in the American Institute of Steel Construction 13th Ed. Steel Construction Manual (AISC 2005) is a significant deviation from the methods presented in previous editions of the AISC Manual, particularly with regard to dimensional flexibility and eccentricity calculations. In the new procedure, which will be referred to as the 2005 AISC Procedure hereafter, single-plate connections are divided into two categories as shown in Figure 1: (a) those meeting several dimensional limitations, which are classified as “conventional configuration”, and (b) all others, which are classified as “extended configuration”. To verify this procedure, a set of eight tests was conducted. Four of the tests met the conventional configuration requirements, and four were in the extended configuration category.

In the 2005 AISC procedure when standard holes are used, eccentricity is not directly considered for connections with less than ten bolts in the conventional configuration category. This change is based upon the recognition that the bolt shear strengths have been reduced by a “bolt group action factor” of 20 percent (Kulak 2002). The inclusion of this factor in the AISC Specifications is based on research done with tension splice plate connections. In these connections, it was found that bolts toward the end of the connection had higher levels of strain than those towards the center, and that the average bolt stress determined from the ultimate strength of the connections was approximately 20 percent less than the average bolt stress found from individual bolt shear tests for connections up to 50 in. in length. Eurocode 3(1992) excludes a similar

reduction for framing connections. Kulak (2002) in the AISC Design Guide 17 states that “it is reasonable to think that the same phenomenon at least does not take place to the same degree,” in framing type connections.

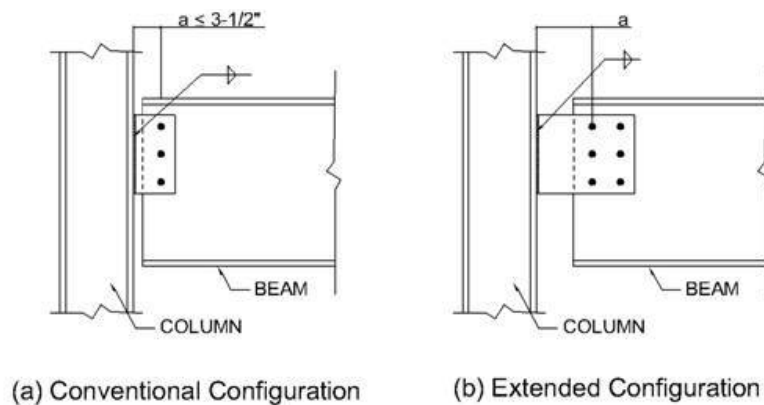


Figure 1. Conventional and Extended Single-Plate Connections

For 10, 11, and 12 bolt conventional connections, eccentricity causes a strength reduction of greater than 20 percent; therefore, eccentricity is taken into account. However, the calculated eccentricity coefficient, C , in Table 7-7 of the 13th Ed. AISC Manual is then multiplied by 1.25. Eccentricity is not considered when short slotted holes are used, and no distinction is made between flexible and rigid supports.

Single plate connections designed using the extended configuration procedure are to include an eccentricity equal to the “ a -distance”, measured from the face of the supporting element (girder web, column web, or column flange) to the first column of the bolt group. An exception is provided for the connection designer to use alternate methods when justified by rational analysis.

In the new procedure, the weld size required to develop the plate strength has been reduced from $3/4$ times the plate thickness to $5/8$ times the plate thickness. This change is based on work by Dr. William Thornton as reported by Muir (2006). The previous weld thickness limitation was determined by ensuring that the single plate would yield prior to the weld yielding, where the weld yield strength is estimated as one half of the tensile strength for E70 electrodes. Thornton determined that the single-plate connection weld size should be such that the plate will yield before weld fracture, as opposed to weld yield. He found that a weld thickness equal to $5/8$ times the plate thickness guarantees that the plate will yield in pure moment, pure shear, or a combination of shear and moment prior to weld fracture.

Both the conventional and extended configuration procedures require edge distances to be consistent with Chapter J of the AISC Specification (AISC 2005a). Several design steps were added to create dimensional flexibility in the extended configuration including ensuring that the moment strength of the plate is less than the moment strength of the bolt group, checking plate flexure using Von-Mises shear reduction, and checking for plate buckling using the double coped beam procedure found in the AISC Manual (AISC 2005).

excluding eccentricity and bearing on the test beam were evaluated.

Test Number	Test Specimen	a-Distance (Eccentricity) (in.)	Single Plate Dimensions	Weld Size (in.)	Beam Section	Beam Length
1	3B1C-3 -3/8	3 (3)	3/8" x 4-1/2" x 8-1/2"	3/16	W18x55	21'-7"
2	4B1C-3-3/8	3 (3)	3/8" x 4-1/2" x 11-1/2"	3/16	W24x76	27'-7"
3	5B1C-3-3/8	3 (3)	3/8" x 4-1/2" x 14-1/2"	3/16	W24x76	23'-1"
4	7B1C-3-3/8	3 (3)	3/8" x 4-1/2" x 20-1/2"	3/16	W30x108	27'-7"
5	6B2C-4.5-1/2	3 (4-1/2)	1/2" x 7-1/2" x 8-1/2"	1/4	W18x55	18'-7"
6	10B2C-4.5-1/2	3 (4-1 1/2)	1/2" x 7-1/2" x 14-1/2"	1/4	W30x108	24'-7"
7	7B1C-9-3/8	9 (9)	3/8" x 10-1/2" x 20-1/2"	1/4	W24X62	22'-10-1/2"
8	10B2C-10.5-1/2	9 (10-1/2)	1/2" x 13-1/2" x 14-1/2"	5/16	W24X62	22'-10-1/2"

Table 1. Test Matrix

Extended Configuration Connections

The first two extended configuration tests had two vertical columns of bolts in standard holes with an a-distance of 3 in. and an eccentricity of 4-1/2 in. The third test had a single vertical column of bolts with an a-distance of 9 in., and the final test had two vertical columns of bolts with an a-distance of 9 in. and an eccentricity of 10-1/2 in. Similar to the conventional configuration connections, the connections were off-axis. A reduced weld size equal to one-half times the thickness of the plate was specified for the first two tests; the second two tests had weld sizes of 5/8 times the plate thickness. To provide connection ductility, the single plates were designed to have a moment strength less than the moment strength of the bolt group in eccentric shear as required by the 2005 AISC Procedure. To determine the design strength of the connection, bolt shear rupture including eccentricity, plate flexure including the Von-Mises shear reduction, and plate buckling were checked in addition to the limit states checked for the conventional configuration configurations.

The test beam sections and lengths are listed in Table 1. The beam length was chosen so that an end rotation of approximately 0.03 radians would occur at the connection nominal strength. Two W21x62 test columns were used for the tests. Each column had four shear tabs welded to the flanges with two on each side. The test columns were designed to be flipped vertically and rotated to create four tests from one column. The single plates were welded off-center so that the centerlines of the beam web and the column web were in line when the connection was in place.

The test beam and column steel was specified as ASTM A992 with nominal yield strength of 50 ksi. ASTM A572 Grade 50 steel was specified for the single plates. All bolts were ASTM A325-N with ASTM A563 nuts and ASTM F436 structural washers.

One washer was placed under the nut and additional washers were used under the bolt head to ensure that bolt threads were in the connection shear plane as required for an N-type connection. The single plates were welded to the column flanges using E70 or equivalent electrodes.

A variety of instrumentation was used to monitor the specimens during testing. Data from three load cells was used to determine the applied connection force. Displacement potentiometers were used to measure the beam end rotation relative to the test column.

In several of the tests, lateral torsional buckling occurred before the desired rotation was obtained. Several test beams had yield strengths considerably above the nominal yield strength and did not yield within the capacity of the test setup. To cause flexural yielding, the test beam sections were reduced as described below.

Weld rupture did not occur in the conventional configuration tests where 3/16 in. fillet welds were used. The 3/16 in. fillet welds of the extended configuration Tests 5 (6B2C-4.5-1/2) and 6 (10B2C-4.5-1/2) failed prematurely. The steel fabricator used a lower amperage than usual because these welds were smaller than those typically made in their shop practice, which is believed to have resulted in the lower strength. The Test 6 connection was re-welded by Laboratory personnel using stick electrodes and the connection was successfully retested with 3/16 in. welds. The original one-half plate thickness welds in Test 7 (7B1C-9-3/8) and Test 8 (10B2C-10.5-1/2) were removed prior to testing and re-welded by Laboratory personnel with 5/8 times the plate thickness welds, 1/4 in. and 5/16 in. fillet welds, respectively.

ASTM 370-05 tensile coupon test results for the single plate and beam flange material are listed in Table 2. The average yield stress of the single plate material is 68.5 ksi or 37% greater than the nominal stress, 50 ksi. The average flange material yield stress is 58.6 ksi or 17% greater than the nominal stress, 50 ksi. Bolt shear tests were performed on a sampling of the test connection bolts to determine the individual bolt shear strengths. Results are summarized in Table 3.

Table 2. Tensile Coupon Test Results

	Material Tested	Corresponding Connection Test	Yield Stress, F_y (ksi)	Ultimate Stress, F_u (ksi)	Elongation 8 in. (%)
Plates			69.3	96.3	20
	3/8 in.	3B1C-3-3/8, B1C-3-3/8 5B1C-3-3/8, 7B1C-3-3/8	68.1	97.5	28
	1/2 in.	6B2C-4.5-1/2, 10B2C-4.5-1/2	68.2	97.7	22
	1/2 in.	10B2C-10.5-1/2	68.5	97.0	27
Flanges	W18x55	3BIC-3-3/8	55.0	72.0	36
	W24x76	4BIC-3-3/8	56.5	74.9	29
	W24x76	5BIC-3-3/8	57.6	75.3	28
	W30x108	7BIC-3-3/8	62.6	80.1	25

Shank Length (in.)	Corresponding Single Plate Test	Plate t (in)	Bolts	Maximum Shear Force (kips)	Bolt Shear Stress (ksi)	Average Shear Stress (ksi)	Average Experimental Stress/Nominal Stress (48 ksi)
2-1/4	3B1C-3-3/8	3/8	3	81.0	61.1	61.4	1.28
2-1/4	4B1C-3-3/8	3/8	4	109	61.7		
2-1/4	7B1C-3-3/8	3/8	4	109	61.7		
2-1/2	5B1C-3-3/8	1/2	2	61.2	69.3	70.2	1.46
2-1/2	6B1C-4.5-1/2	1/2	2	61.9	70.1		
2-1/2	10B2C-4.5-1/2	1/2	2	61.9	70.1		
2-1/2	10B2C-10.5-1/2	1/2	2	61.9	70.1		
2-1/2	7B1C-9-3/8	3/8	2	63.1	71.4	79.3	31
	W30x108	10B2C-4.5-1/2		61.5	79.3		
	W24x62	7B1C-10-3/8		58.0	77.1		
	W24x62	10B2C-11.5-1/2		58.4	77.6		

Table 3. Bolt Shear Test Results

CONNECTION TEST RESULTS

Table 4 provides a summary of the test results; complete results are found in Baldwin Metzger (2006).

Conventional Configuration Connections

Tests 1 (3B1C-3-3/8) and 2 (4B1C-3-3/8) were terminated prior to connection failure due to lateral torsional buckling of the test beam. The maximum connection forces in Tests 1 and 2 were 81 kips and 110 kips with beam end rotations of 0.032 and 0.027 radians, respectively. The failure mode for Test 3 (5B1C-3-3/8) was bolt shear rupture at a connection force of 146 kips. In Test 4 (7B1C-3-3/8), the test beam was loaded to a connection force of 200 kips, which was the capacity of the test setup, at a beam end rotation of 0.013 radians. The load was removed from the beam, and the beam section at mid-span was reduced by cutting 1-1/2 in. from each side of the beam bottom flange for a 2 ft length at mid-span. Upon retesting, the top bolt of the connection ruptured at a connection force of 173 kips and a rotation of 0.018 radians.

Extended Configuration Connections

Tests 5 and 6 consisted of two vertical columns of bolts with conventional 3 in. a-distances and eccentricities of 4-1/2 in. A connection force of 89.7 kips and a beam end rotation of 0.030 radians was achieved. The test was stopped prior to the beam reaching its full plastic moment. In Test 6, load was applied to a connection force of 200 kips and a beam end rotation of 0.010 radians. The load was removed from the test beam, and the beam section at mid-span was reduced by cutting 2-1/4 in. from each side of the beam bottom flange for a 2 ft length at mid-span. The beam was then

reloaded until failure occurred when the plate-to-column flange weld ruptured at a connection force of approximately 200 kips and a beam end rotation of 0.025 radians. No deformation was observed in the connection bolts, at the bolt holes, or in the single plate.

Test 7 (7B1C-9-3/8) was a single column connection with an extended a-distance of 9 in. The connection was loaded to a force of 97 kips and a beam end rotation of 0.034 radians. Failure occurred when the test beam laterally buckled at mid-span and no additional force could be applied to the connection. Minor yielding was observed in the beam around the top two bolt holes and the bottom bolt hole. Yielding was also evident in the single plate at the bottom near the beam side.

In Test 8 (10B2C-10.5-1/2), a double column connection with an extended a-distance of 9 in. and an eccentricity of 10-1/2 in., the connection was loaded in four cycles to demonstrate the inelastic behavior of the connection and test beam. Failure occurred in the test beam by local buckling of the web at mid-span at a connection force of 97 kips and a beam end rotation of 0.035 radians. Yielding at the bottom of the single plate was observed.

Table 4. Experimental Results

		Test ID	Columns of Bolts	Bolt Rows	Maximum Connection Force (kips)	Maximum Connection Rotation (Radians)	Connection Failure Mode
Convention Configurations	1	3B1C-3-3/8	1	3	81.0	0.032	-- ¹
	2	4B1C-3-3/8	1	4	110	0.027	-- ¹
	3	5B1C-3-3/8	1	5	146	0.030	Bolt Shear
	4	7B1C-3-3/8	1	7	200	0.018	Bolt Shear
Extended Configurations	5	6B2C-4.5-1/2	2	6	89.0	0.030	-- ²
	6	10B2C-4.5-1/2	2	10	200	0.026	Weld Rupture
	7	7B1C-9-3/8	1	7	97.0	0.034	-- ¹
	8	10B2C-10.5-1/2	2	10	97.0	0.035	-- ¹

¹Connection failure did not occur. ²Connection failure did not occur, see text for details.

ANALYSES OF EXPERIMENTAL RESULTS

Tables 5 and 6 show comparisons of experimental values to predicted values for the limit states in the 2005 AISC procedure, as well as bearing on the beam web. The bolt group strength calculated using the AISC procedure, but excluding the bolt group action factor (BGAF), 0.8, is included for comparison. The predicted values are based on the

measured material properties listed in Tables 3 and 4. Strength reduction (Φ -) and safety (Ω -) factors were not included in the calculations.

The predicted controlling limit state for all connections was bolt shear. All connections reached experimental shear values which exceeded the predicted strengths by an average of 23 percent with a standard deviation of 0.06. Since not all connections failed, the reported connection force values are actually lower bound connection strengths.

The lack of deformation at the bolt holes in the connection tests is supported by the supplemental bolt shear tests, whose results were described previously. No evidence of bolt hole deformation was evident prior to bolt rupture under direct shear loading for the 3/8 in. or the 1/2 in. plate material. This was as expected since the single plate bearing strength is greater than the connection bolt strength as shown in Tables 5 and 6.

Table 5. Summary of Connection Limit State Values for the Conventional Connections

		Test 1 (3B1C-3-3/8)	Test 2 (4B1C-3-3/8)	Test 3 (5B1C-3-3/8)	Test 4 (7B1C-3-3/8)
		Predicted ¹	Predicted ¹	Predicted ¹	Predicted ¹
Connection Limit States (kips)	Bolt Shear Rupture (including BGAF)	65.1	86.8	124	152
	Bolt Eccentricity	Neglected	Neglected	Neglected	Neglected
	Bolt Shear Rupture (excluding BGAF) ²	81.4	109	155	190
	Plate Shear Yielding	130	176	222	314
	Plate Shear Rupture	129	176	222	315
	Plate Block Shear	154	196	242	334
	Plate: Bearing	169	234	300	432
	Beam: Bearing	152	237	298	550
Experimental Values	Failure Mode	Beam Failure	Beam Failure	Bolt Shear	Bolt Shear
	Maximum Rotation (radians)	0.032	0.027	0.030	0.018
	Maximum Connection Force (kips)	81.0	110	146	200
	Experimental/ Predicted Strength	1.24	1.27	1.18	1.32

¹ Material strength values are taken from tensile tests and bolt shear tests performed at Virginia Tech.

² Not a permitted limit state in the 2005 AISC procedure.

Table 6. Summary of Connection Limit State Values for the Extended Connections

		Test 5 (6B2C-4.5-1/2)	Test 6 (10B2C-4.5-1/2)	Test 7 (7B1C-10-3/8)	Test 8 (10B2C-11.5-1/2)
		Predicted ¹	Predicted ¹	Predicted ¹	Predicted ¹
Connection Limit States (kips)	Beam Steel	77.6	79.3	77.1	77.6
	Bolt Shear Rupture (including BGAF)	70.0	159	84.6	84.1
	Bolt Eccentricity	4.5	4.5	9.0	10.5
	Bolt Shear Rupture (excluding BGAF) ²	87.5	199	106	105
	Plate Shear Yielding	174	297	319	298
	Plate Shear Rupture	172	297	311	295
	Plate Block Shear	304	427	332	426
	Plate: Bearing	451	802	426	797
Experimental Values	Beam: Bearing	327	778	417	601
	Failure Mode	Weld Rupture	Weld Rupture	Beam Failure	Beam Failure
	Maximum Rotation (radians)	0.030	0.025	0.034	0.035
	Maximum Connection Force (kips)	89.0	200	97.0	97.0
	Experimental/ Predicted Strength	1.27	1.26	1.15	1.15

¹ Material strength values are taken from tensile tests and bolt shear tests performed at Virginia Tech.

² Not a permitted limit state in the 2005 AISC procedure.

SUMMARY AND RECOMMENDATIONS

Connection Strength

The experimental results indicate that the AISC 2005 procedure conservatively predicts the ultimate strength of both the conventional configuration and the extended configuration single plate shear connections. Connection failure was not achieved in all tests; however, all of the maximum connection forces reported here exceed the predicted strengths using measured material properties and therefore reflect a lower bound strength prediction.

Connection Bolt Strength

The bolt group shear strengths were conservatively predicted by the AISC 2005 procedure. A more accurate method for bolt shear strength prediction determined in this study was found by excluding the bolt group action factor (0.8) and including the connection eccentricity in the calculations. However, this method would violate the nominal bolt shear strengths in the AISC Specification (2005a). It is recommended that future editions of the Specification address this problem.

Weld Strength

A weld size of 1/2 times the plate thickness was used in Tests 1 through 6 in an attempt to reduce the current 2005 AISC recommendation of 5/8 times the plate thickness. The recommended weld size was determined by ensuring that the plate would yield prior to

weld rupture. Tests 1 through 4 showed no evidence of plate yielding, and no weld rupture occurred. However, weld rupture occurred in Tests 5 and 6, but no plate yielding was observed. Due to the atypical welding procedures used to fabricate the welds, it was not possible to confirm if the weld rupture was due to fabrication issues or the weld size itself. Until further testing is completed on connections with a reduced weld size, it is recommended that the current 2005 AISC requirement be used for both conventional and extended configuration connections.

Rotational Ductility

Rotational ductility in single plate shear connections is typically assumed to be obtained by elongation of the bolt holes (bolt plowing) in the single plate or beam and/or yielding of the single plate. However, the dimensional requirements to ensure that the ductility is provided are experimentally based on testing with A36 plates. No elongation of the bolt holes was found in this series of tests, where plate yield stresses were over 68 ksi. Plate yielding was observed in only two of the eight tests. It is recommended that a series of tests be performed where the bolt diameter-to-plate thickness ratio is varied to determine a maximum allowable plate thickness for nominal 50 ksi plate material.

Connection Bracing

The connections tested with extended a-distances required additional bracing at the beam end near the connection due to twisting of the single plate. It is recommended that bracing be required at the connection if the a-distance is large. This bracing requirement may be satisfied by the presence of a composite slab.

CONCLUSION

In conclusion, the testing presented here showed that the design procedures for conventional and extended single plate connection in the 13th Ed. of the AISC *Steel Construction Manual* adequately predict the strength of such connection even when the single plate yield stress exceeds 60 ksi.

ACKNOWLEDGEMENTS

The research presented here was supported by Cives Steel Company and The Charles E. Via, Jr. Department of Civil and Environmental Engineering. The authors thank Mr. Larry Muir and Dr. William Thornton of Cives Engineering for sharing their advice and experience throughout the project, and Mr. Robert Kerr and John Goode of the Mid-Atlanta Division of Cives for providing the steel specimens and their expert welding advice.

REFERENCES

AISC (2005), *Steel Construction Manual*, American Institute of Steel Construction, 13th Ed., Chicago, IL.

AISC (2005a), *Specification for Structural Steel Buildings*, American Institute of Steel Construction, March 9, Chicago, IL.

Baldwin Metzger, K. (2006), "Experimental Verification of a New Single Plate Shear Connection Design Model," *Master of Science Thesis*, Virginia Polytechnic Institute and State University, Blacksburg, Virginia.

European Committee for Standardization (1992), *Eurocode3: Design of Steel Structures*, ENV 1993-1-1, Brussels.

Kulak, G. I., (2002) *Steel Design Guide 17: High Strength Bolts: A Primer for Structural Engineers*, American Institute of Steel Construction, Chicago, IL.

Muir, Larry, (2006) E-mail to authors. 22 March.

DEFORMATION CONSIDERATIONS FOR HIGH STRENGTH STEEL PANEL ZONES

Ana M. Girão Coelho
Polytechnic Institute of Coimbra, Portugal
Delft University of Technology, The Netherlands
a.m.girao@clix.pt

Frans S. K. Bijlaard and Henk Kolstein
Delft University of Technology, The Netherlands
f.s.k.bijlaard@tudelft.nl and m.h.kolstein@tudelft.nl

ABSTRACT

The paper summarizes research on high strength steel (specified yield stress of 690 MPa – grade S690, and 960 MPa – grade S960) panel zones with the following objectives: (i) to characterize the nonlinear behaviour from a deformation and strength standpoints, (ii) to investigate the governing failure mechanisms and (iii) to evaluate the effect of key geometric and loading parameters on the deformation capacity and ductility characteristics. The relevant results are summarized and discussed.

INTRODUCTION

Current European standard EN 1993 allows the design of beam-column joints within the semi-continuous/partially-restrained concept, provided that those joints accommodate large plastic rotations. In the framework of the component method, the rotational response of the joint is generated from the deformation behaviour of the individual components (e.g. panel zone, column flange in bending, welds, etc.). Joints should be designed such that inelastic actions are concentrated in those components which provide high ductility and satisfy high deformation demands.

The panel zone of the column is often the critical joint-component, especially in frames that are subjected to significant lateral loads, such as seismic events. This imposes ductility and deformation requirements to the panel that strongly depend on the geometry (web slenderness and aspect ratio), loading conditions (effect of column axial loads) and, more particularly, on the material characteristics. Conventional steels (yield stress ≤ 460 MPa) are characterized by good or satisfactory deformability and ductility properties. High strength structural steels (yield stress > 460 MPa) are generally less ductile and less deformable. This explains the restrictions adopted in EN 1993 for inelastic panel zone design procedures to steel grades with a yield stress > 460 MPa.

Recent breakthroughs in steel making technologies have produced high strength steels (HSS) with enhanced tensile mechanical properties, particularly in terms of deformability and ductility. Whether or not HSS can be used in plastic design will depend on the outcome of intensive research work that demonstrates that panel zones made from

HSS provide adequate deformation behaviour. For this purposes, a comprehensive re- search programme is being conducted at the Delft University of Technology. The complete documentation of the programme can be found in Girão Coelho et al. (2007, 2008a, 2008b). This research includes an experimental work that is supplemented with finite element (FE) modelling. All the pertinent research results of this study are presented and discussed below to provide answers to the following questions:

1. How does the steel grade influence the failure mechanism of web shear panels?
2. What are the main characteristics of the shear-deformation response of such panels?
3. Do HSS panel zones satisfy high deformation demands?

TESTING PROGRAMME

Two-span I-beams loaded transversely as shown in Fig. 1 are proposed to study the behaviour of HSS web shear panels. The force transfer mechanism that exists in the I-beam is identical to that of beam-column joints, which carry the shear force from beam moment by coupling tension with compression at the beam flanges.

The experimental programme comprises 19 I-beam specimens that were tested to failure under four-point bending in a 10000 kN test machine. The specimens were designed to EN 1993, part 1.8 (EN 1993-1-8, 2005), neglecting current restrictions to the use of HSS, and fabricated from two beam sets (Fig. 2). Section 1 web slenderness satisfies the condition given in clause 6.2.6.1(1) in EN 1993-1-8:

$$\frac{d_w}{t_w} \leq 69\varepsilon \quad \text{and} \quad \varepsilon = \sqrt{\frac{235}{f_{y,w}}} \quad (1)$$

whereby d_w : clear depth, t_w : thickness and $f_{y,w}$: yield stress of the web. Section 2 was

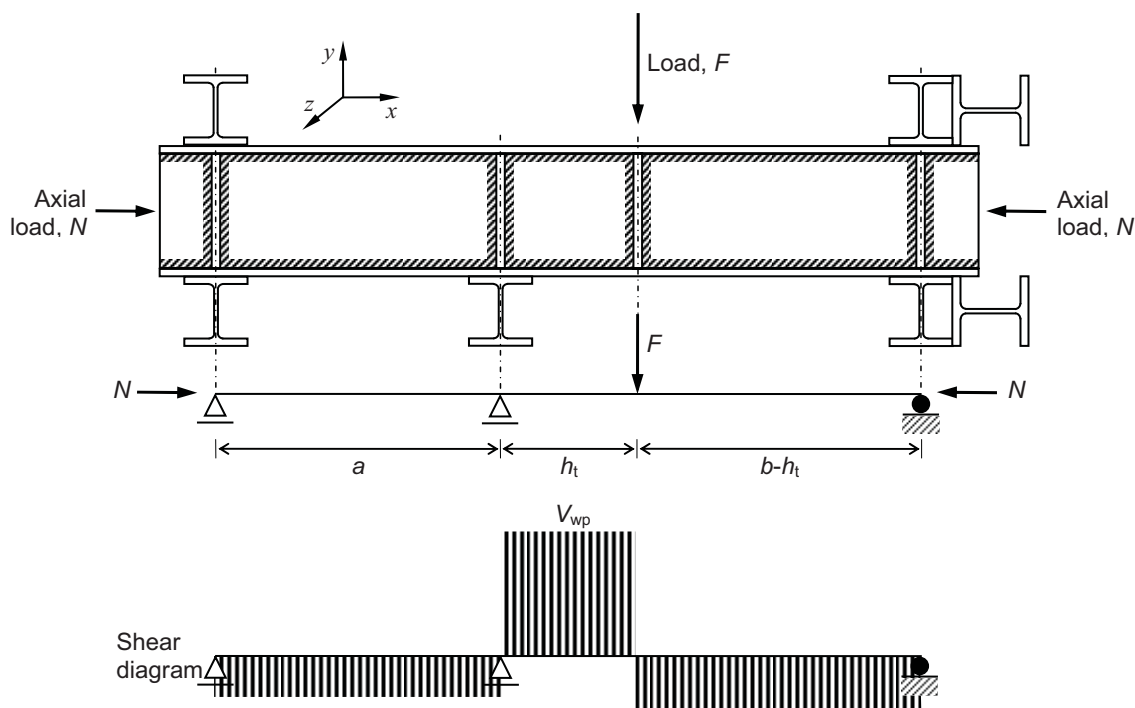


Fig. 1: Geometry of the test I-beams

deliberately designed to violate such criterion. Details of the I-beams are given in Table 1 (a , b and h_t are defined in Fig. 1; $\epsilon_{f,w}$: strain at rupture from uniaxial tension tests on the web; N_{pl} : squash load of the I-beam). Another important geometric parameter is varied over the practical range of interest, the aspect ratio h_t/h_w of the panel, in order to evaluate the effect on the panel inelastic behaviour. For all test configurations, the level of axial (compression) load N is also varied to analyse this effect on the overall behaviour.

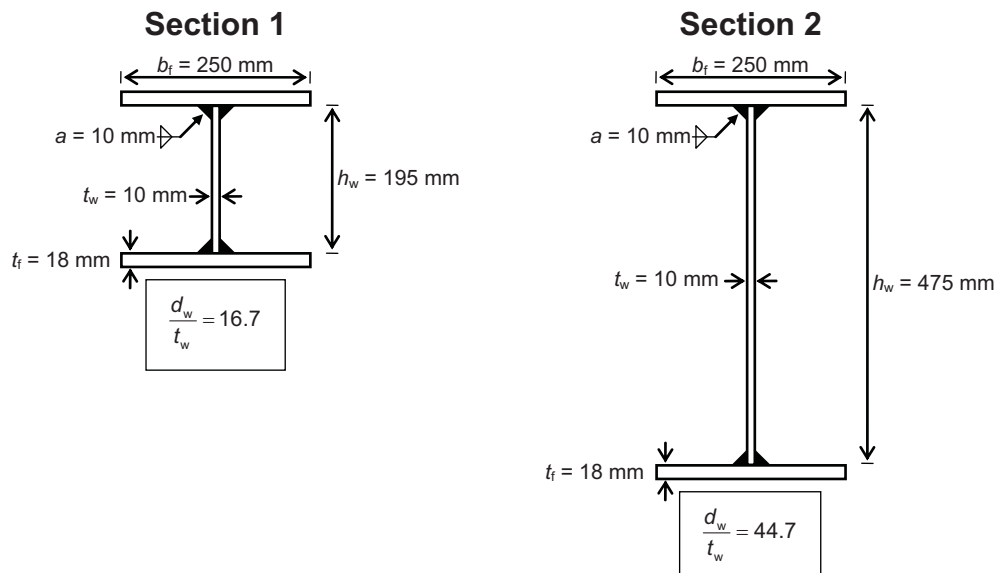


Fig. 2: I-beams cross-sections

Table 1: Details of the test specimens (actual geometric and mechanical characteristics)

Test	Section (Fig. 2)	a (mm)	b (mm)	h_t (mm)	h_t/h_w	$f_{y,w}$ (MPa)	$\epsilon_{f,w}$	N/N_{pl}
1	1	600	792	193.1	0.98	756	0.159	0.00
2	1	600	792	192.4	0.99	756	0.159	0.10
3	1	600	792	191.0	0.98	756	0.159	0.20
4	1	600	987	366.4	1.88	756	0.159	0.00
5	1	600	987	386.1	1.98	756	0.159	0.10
6	1	600	895	277.2	1.42	756	0.159	0.00
7	1	600	895	295.0	1.51	756	0.159	0.10
8	2	600	987	411.5	0.87	756	0.159	0.00
9	2	600	987	412.8	0.87	756	0.159	0.10
11	1	600	792	190.8	0.97	958	0.138	0.00
12	1	600	792	215.0	1.10	958	0.138	0.10
13	1	600	792	231.3	1.18	958	0.138	0.15
14	1	600	987	392.5	2.01	958	0.138	0.00
15	1	600	987	393.0	2.01	958	0.138	0.10
16	1	600	895	322.8	1.65	958	0.138	0.00
17	1	600	895	317.1	1.62	958	0.138	0.10
18	2	600	987	430.4	0.91	958	0.138	0.00
19	2	600	987	422.6	0.89	958	0.138	0.10
20	2	600	987	426.9	0.90	958	0.138	0.12

A numerical model complements the experiments. A three-dimensional FE model that encompasses all the geometrical and material nonlinearities is presented and discussed in Girão Coelho et al. (2008b). Comparison between the numerical analysis and experimental results conclusively establishes the accuracy of the FE model. This model has the advantage of allowing a large number of geometric configurations to be analysed fairly quickly. The implementation of this parametric study is currently being carried by the authors.

EVALUATION OF THE PANEL ZONE BEHAVIOUR

The main results of the testing programme are evaluated and discussed below to shed light on the load-carrying and deformation behaviour of panel zones made from HSS. Special emphasis is placed on the characterization of (i) the modes of failure and (ii) the main features of the shear-deformation response.

Modes of Failure

Failure of the panel zone can develop due to two potential mechanisms (or a combination of both). The first mode is that of shear yielding of the web, which is a stable and ductile failure mode, in nature. Beyond yielding, the panel is able to carry additional load with decreasing stiffness but with no instability, until shear deformation becomes excessive. This post-yield stiffness is mainly attributed to strain hardening in the material. A second failure mode can occur if the web is slender, that is web buckling due to shear. This is essentially a local buckling phenomenon. Depending on the panel zone geometry, the web plate can carry additional load and behave ductile after buckling due to the diagonal tension field that develops within the web panel.

The occurrence of a given panel failure mode depends on geometrical and material parameters, that is, the slenderness of the column web d_w/t_w , the aspect ratio of the panel h_t/h_w , the presence of axial loads and the material yield stress. Geometrically identical panels made from lower steel grades, i.e. classes of steel with lower yield stress, achieve larger inelastic deformations and, consequently, behave more ductile. Vayas et al. (1995) proposed the following boundaries:

1. $\bar{\lambda} \leq 0.8$, shear yielding and large inelastic deformations govern failure.
2. $0.8 < \bar{\lambda} < 1.25$, inelastic buckling occurs and therefore the reduced yield shear stress is given by:

$$\overline{\tau_{y,w-red}} = \left[1 - 0.8(\bar{\lambda} - 0.8) \right] \overline{\tau_{y,w}} \quad (2)$$

3. $\bar{\lambda} \geq 1.25$, elastic shear buckling precedes shear yielding.

$\bar{\lambda} = \sqrt{\overline{\tau_{y,w}}/\tau_{cr}}$ is the relative slenderness of a web panel for shear buckling, whereby $\overline{\tau_{y,w}}$: the yield shear stress allowing for interaction with axial load (Krawinkler et al. 1975):

$$\overline{\tau_{y,w}} = \frac{f_{y,w}}{\sqrt{3}} \sqrt{1 - \left(\frac{N}{N_{pl}} \right)^2} \quad (3)$$

and τ_{cr} : elastic shear buckling strength of web panels under the assumption that the web panel is simply supported along its edges (Timoshenko and Gere 1961):

$$\tau_{cr} = k_s \frac{\pi^2 E}{12(1-\nu^2)} \left(\frac{t_w}{d_w} \right)^2 \quad \text{and} \quad k_s = \begin{cases} 4 + 5.34 \left(\frac{h_t}{h_w} \right)^{-2} & \leftarrow \frac{h_t}{h_w} < 1 \\ 5.34 + 4 \left(\frac{h_t}{h_w} \right)^{-2} & \leftarrow \frac{h_t}{h_w} \geq 1 \end{cases} \quad (4)$$

where E : Young modulus and ν : Poisson's ratio.

Table 2 sets out the predictions for the potential failure mode of each specimen based on actual panel geometry and mechanical properties. Fig. 3 illustrates typical web failure modes observed in the experiments (see also Table 2; HAZ: heat affected zone due to welding of the plates). All specimens underwent large inelastic distortions before rupture. The following are general observations regarding the modes of failure of the tested HSS panels:

1. Shear yielding was the dominant failure mode and rupture was mostly governed by fracture of material. Figs. 3a through 3c show photographs of specimens 1, 14 and 4 that completely plastified in shear. Fig. 3cii) illustrates the Von Mises stress contours obtained from a FE analysis of specimen 4 and highlights the large stresses within the web panel at rupture (Girão Coelho et al. 2008b). For those specimens, the tension diagonal of the panels extended about the same

Table 2: Summary of the modes of failure

Test	τ_{cr} (MPa)	$\overline{\tau_{y,w}}$ (MPa)	$\overline{\lambda}$	Predicted failure mode	Observed failure mode	
1	4843	436.5	0.3	Shear yielding	Shear yielding and plastification	
2	4947	434.3	0.3			
3	4929	427.7	0.3			
4	3567	436.5	0.4		Shear yielding and plastification; web buckling at very large deformations	
5	3413	434.3	0.4			
6	4074	436.5	0.3			
7	3640	434.3	0.3			
8	1023	436.5	0.7			Combined failure mechanism (material cracking at large deformations)
9	989	434.3	0.7			
11	5024	553.1	0.3	Shear yielding	Shear yielding; fracture of the material at the lower flange in the HAZ and web	
12	5183	550.3	0.3			
13	4041	546.8	0.4		Shear yielding; cracks at the weld connecting the web and the lower flange	
14	3071	553.1	0.4			
15	3728	550.3	0.4			Shear yielding and fracture of the material at the upper flange in the HAZ
16	3634	553.1	0.4			
17	4032	550.3	0.4		Shear yielding; fracture of the material at the lower flange in the HAZ and web	
18	875	553.1	0.8		Inelastic shear buckling	Inelastic shear buckling (material cracking at large deformations)
19	902	550.3	0.8			
20	892	549.1	0.8			

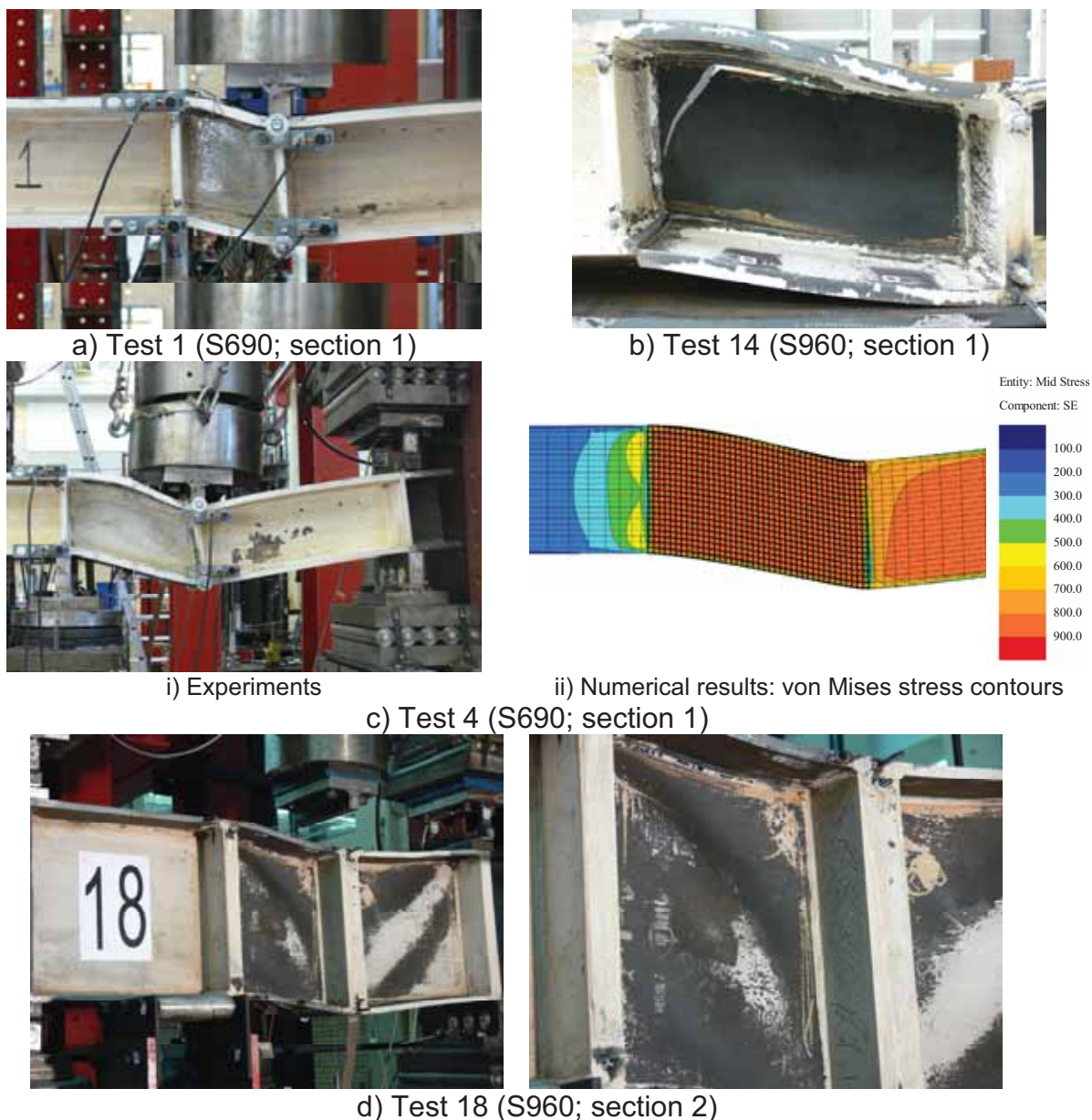


Fig. 3: Illustration of the various panel failure modes

- amount as the compression diagonal shortened.
2. Panels made from S960 were subjected to high strain concentrations at the regions close to the welds. This led to fracture of the material at high shear distortions of the panel, as shown in Fig. 3b, and was accompanied by a drop in strength in most cases. Nevertheless, the fracture mechanism involving the flanges, as depicted in this photograph, is not expected in an actual beam-column joint. This mechanism is highly influenced by the support conditions in these tests.
 3. Slender panels made from S690 buckled in shear late in the course of loading. The web distortion did not begin until the plastic resistance of the panel had been reached.
 4. The shear buckling mode was predominant in slender panels made from S960 (tests 18 through 20). Fig. 3d shows photographs of specimen 18 that exhibited inelastic shear buckling. A detail of the buckles in the web after the ultimate load was reached is also shown.

An examination of Table 2 and Fig. 3 shows that the above limits are reasonable for the prediction of the potential failure mode of HSS web panels. However, the 0.8 limit of the relative slenderness for shear buckling should be further considered in parametric FE analysis. The experimental observations suggest that this value can be quite large in the case of HSS web panels.

Shear-Deformation Response

The most significant characteristic describing the overall panel nonlinear behaviour is the shear-deformation response ($V_{wp}-\gamma$). Typical curves show two distinct regions. The first, the elastic region, is characterized by a quasi-linear behaviour (stiffness $K_{wp,el}$). A second range with decreasing stiffness follows on. The transition between these two ranges defines the pseudo-plastic shear resistance of the panel $V_{wp,Rp}$ that naturally depends on the failure mode. The term “pseudo-plastic” is adopted from literature (Jaspart 1997). The quantitative evaluation of these curves is made in Table 3. The maximum shear force $V_{wp,max}$ and maximum distortion γ_{max} are also indicated. Fig. 4 plots illustrative $V_{wp}-\gamma$ curves of the tests that were carried out. This plot shows a significant growth in inelastic deformation after the ultimate load is reached, particularly in those specimens that fail in plastic shear mode (e.g. T4, T14).

The following observations can be made from this study:

1. The behaviour of nonslender web panels (section 1) is stable and the decrease in stiffening after yielding is small and gradual. The drop in strength is only noticeable at very large inelastic distortions. The behaviour of slender web panels

Table 3: Evaluation of the principal characteristics of the shear-deformation response

Test	$K_{wp,el}$ (kN/mrad)	$V_{wp,Rp}$ (kN)	$V_{wp,max}$ (kN)	γ_{max} (mrad)
1	382	1390	1666 ($\gamma = 91$ mrad)	91 ($V_{wp} = 1.0V_{wp,max}$)
2	285	1380	1499 ($\gamma = 71$ mrad)	95 ($V_{wp} = 0.94V_{wp,max}$)
3	446	1290	1390 ($\gamma = 35$ mrad)	94 ($V_{wp} = 0.83V_{wp,max}$)
4	188	970	1295 ($\gamma = 131$ mrad)	186 ($V_{wp} = 0.92V_{wp,max}$)
5	220	960	1081 ($\gamma = 85$ mrad)	160 ($V_{wp} = 0.90V_{wp,max}$)
6	235	1160	1394 ($\gamma = 117$ mrad)	145 ($V_{wp} = 0.91V_{wp,max}$)
7	255	1040	1125 ($\gamma = 108$ mrad)	158 ($V_{wp} = 0.89V_{wp,max}$)
8	1111	2320	2570 ($\gamma = 19$ mrad)	42 ($V_{wp} = 0.93V_{wp,max}$)
9	1231	2250	2419 ($\gamma = 18$ mrad)	43 ($V_{wp} = 0.88V_{wp,max}$)
11	350	1690	2016 ($\gamma = 50$ mrad)	55 ($V_{wp} = 0.94V_{wp,max}$)
12	307	1610	1720 ($\gamma = 38$ mrad)	52 ($V_{wp} = 0.99V_{wp,max}$)
13	400	1485	1689 ($\gamma = 26$ mrad)	57 ($V_{wp} = 0.95V_{wp,max}$)
14	270	1330	1600 ($\gamma = 82$ mrad)	110 ($V_{wp} = 0.77V_{wp,max}$)
15	184	1270	1339 ($\gamma = 60$ mrad)	92 ($V_{wp} = 0.69V_{wp,max}$)
16	202	1500	1691 ($\gamma = 82$ mrad)	101 ($V_{wp} = 0.99V_{wp,max}$)
17	331	1355	1397 ($\gamma = 50$ mrad)	100 ($V_{wp} = 0.91V_{wp,max}$)
18	1470	2765	2977 ($\gamma = 10$ mrad)	38 ($V_{wp} = 0.92V_{wp,max}$)
19	1233	2850	3005 ($\gamma = 17$ mrad)	53 ($V_{wp} = 0.88V_{wp,max}$)
20	1015	2850	2987 ($\gamma = 9$ mrad)	53 ($V_{wp} = 0.89V_{wp,max}$)

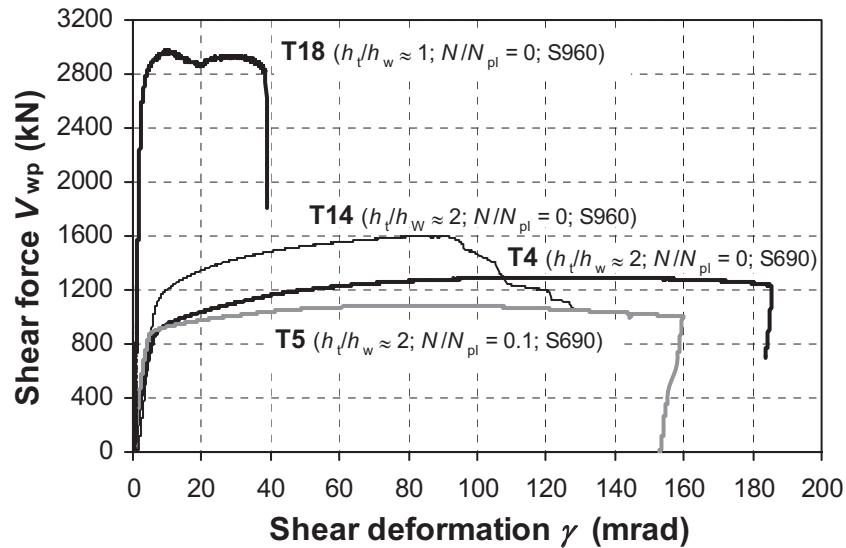


Fig. 4: Shear force vs. panel zone distortion for different configurations

is quite different: the panel can carry additional load after buckling and have some post-buckling deformation reserve. The drop in strength however occurs at relatively small deformations.

2. Nonslender panels exhibit a remarkable ductility and undergo very large deformations before failure. It is possible to have deformation capacities above 100 mrad for HSS. This characteristic is particularly relevant for the S960 panels. The ductile response results from the progressive shear yielding of the panel.
3. Larger panels accommodate significantly higher inelastic shear deformations than the shorter panels (e.g. tests 1, 4 and 6).
4. The presence of I-beam axial load leads to a drop in strength and ductility of the panels (e.g. tests 4 and 5) and accelerates the onset of yielding. The interaction between compressive normal stresses and shear stresses has a negative influence on the panel behaviour.

PARAMETERS AFFECTING THE DEFORMATION CAPACITY AND DUCTILITY

The deformation capacity and ductility of web panels mostly depends on the geometry and mechanical characteristics, as already pointed out. Plastic deformation capacity of the web panel can be used as a measure of ductility. Additionally, the two following indices are defined as a means of expressing ductility:

1. resistance index R_{wp} , defined as the maximum shear force divided by the pseudo-plastic shear level ($R_{wp} = V_{wp,max}/V_{wp,Rp}$);
2. ductility index μ_{wp} , that relates the deformation to the deformation value corresponding to first yielding γ_y ($\mu_{wp} = \gamma/\gamma_y$), whereby γ_y is evaluated according to Faella et al. (2000):

$$\gamma_y = \frac{2/3 V_{wp,Rp}}{K_{wp,el}} \quad (5)$$

Eq. (5) implies that excessive shear yielding governs failure of the panel. For consistency the authors propose the same expression even if shear buckling is the determinant failure mode.

Table 4: Evaluation of performance indicators of ductility characteristics

Test	Resistance index, R_{wp}	Ductility index, μ_{wp}		$\gamma_{pl,max V}$ (mrad)
		$\mu_{wp,max V}$	$\mu_{wp,u}$	
1	1.20	37.5	37.5	87
2	1.09	22.0	29.4	66
3	1.08	18.2	48.7	32
4	1.34	38.1	54.1	124
5	1.13	29.2	55.0	80
6	1.20	35.6	44.1	111
7	1.08	39.7	58.1	104
8	1.11	13.6	30.2	17
9	1.08	14.8	35.3	16
11	1.19	15.5	17.1	44
12	1.07	10.9	14.9	32
13	1.14	10.5	23.0	22
14	1.20	25.0	33.5	76
15	1.05	13.0	20.0	53
16	1.13	16.6	20.4	74
17	1.03	18.3	36.6	46
18	1.08	8.0	30.3	8
19	1.05	11.0	34.4	15
20	1.05	4.8	28.3	6

The resistance index indicates the margin of post-yield or post-buckling resistance (depending on the mode of failure) of the web panel. The ductility index reflects the length of the post-limit plateau that corresponds to the deformations past γ_y . The latter quantity is sampled at deformation levels corresponding to the maximum shear resistance $\mu_{wp,max V}$ and at failure $\mu_{wp,u}$.

To compare the behaviour of the different HSS shear panels configurations analysed above and to assess the effect of the key parameters that influence the deformation supply and the ductility, the two above indices are computed in Table 4. For identical geometric configurations, both indices decrease with the material yield stress. Larger aspect ratios of the panels improve both of these performance indicators. Again, it is quite clear from the data in the table the unfavourable effect of the axial load on the panel ductility.

It is usually recommended a minimum joint plastic rotation of 30 mrad in seismically designed steel-framed structures (El-Tawil et al. 1999). This value represents the contributions of all joint-components, namely the panel zone plastic deformation. To gain insight into the available plastic deformation of the tested specimens, the shear deformation at maximum load $\gamma_{pl,max V}$ is also computed in Table 4. Slender panels do not supply plastic deformations above 30 mrad. The remaining tested panels satisfy these limits.

CONCLUSIONS

The following conclusions are briefly summarized:

1. For section 1 (Fig. 2) the web slenderness complies with the limits of EN 1993-

- 1-8 – Eq. (1). All configurations utilizing this section developed the full plastic shear resistance and underwent very large plastic deformations.
2. The modes of failure limit the panel resistance and ductility. HSS web panels in shear can exhibit ductile behaviour and satisfy very high deformation demands, depending on the web slenderness, that ultimately determines the failure mode.
3. The ductile behaviour can be assured by setting requirements to the resistance and ductility indices defined above, as well as the plastic deformation supply.
4. The need for the inelastic design restrictions on HSS web panels adopted in EN 1993-1-8 should be revisited.

REFERENCES

El-Tawil S., Vidarsson E., Mikesell T. and Kunnath S.K. (1999), “Inelastic behavior and design of steel panel zones”, *Journal of Structural Engineering ASCE*, Vol. 125, No. 2 (pp. 183-193).

EN 1993-1-8 (2005), Eurocode 3: Design of Steel Structures – Part 1-8: Design of Joints, *European Committee for Standardization (CEN)*.

Faella C., Piluso V. and Rizzano G. (2000), *Structural Semi-Rigid Connections – Theory, Design and Software*. CRC Press, USA.

Girão Coelho A.M., Bijlaard F.S.K. and Kolstein M.H. (2007), “Behaviour of high strength steel web shear panels”, *Stevin Report 6-07-2 – Delft University of Technology* (to be published).

Girão Coelho A.M., Bijlaard F.S.K. and Kolstein M.H. (2008a), “Experimental behaviour of high strength steel web shear panels”, *Engineering Structures* (submitted for publication).

Girão Coelho A.M., Bijlaard F.S.K. and Kolstein M.H. (2008b), “Numerical modelling of high strength steel column web shear panel behaviour”, *Proc. Eurosteel 2008* (accepted for publication).

Jaspart J.P. (1997), “Contributions to recent advances in the field of steel joints – column bases and further configurations for beam-to-column joints and beam splices”, *Aggregation Thesis, University of Liège, Belgium*.

Krawinkler H., Bertero V.V. and Popov E.P. (1975), “Shear behaviour of steel frame joints”, *Journal of the Structural Division ASCE*, Vol. 101, No. 11 (pp. 2317-2336).

Vayas I., Ermopoulos J. and Pasternak H. (1995), “Design of steel frames with slender joint-panels”, *Journal of Constructional Steel Research*, Vol. 35 (pp. 165-187).

Timoshenko S.P. and Gere J.W. (1961), *Theory of Elastic Stability*. McGraw-Hill, New York (2nd edition).

INFLUENCE OF CONNECTED MEMBERS COMPONENTS ON THE STRUCTURAL PERFORMANCE OF BOLTED BEAM-TO- COLUMN JOINTS OF PITCHED ROOF PORTAL FRAMES

Ionel-Mircea Cristutiu

“Politehnica” University of Timisoara 300224 (RO)
mircea.cristutiu@arh.upt.ro

Daniel Grecea

“Politehnica” University of Timisoara 300224 (RO)
daniel.grecea@arh.upt.ro

Dan Dubina

“Politehnica” University of Timisoara 300224 (RO)
dan.dubina@ct.upt.ro

ABSTRACT

Pitched roof portal frames, largely used for industrial steel buildings are usually made of slender welded sections, characterized as low dissipative. Frame members are of variable cross-section in accordance with stress and stiffness demand and Class 3 and/or Class 4 web section may be obtained (see figure). A large parametrical investigation on a significant number of pitched roof portal frames with tapered column and hunched rafter is presented in order to establish their sensitivity due to the variation of different components of the joint. The sensitivity is analysed through the joint main characteristics and the rotation capacity point of view. The parametric study is performed by FEM non-linear elastic-plastic analysis. The models are calibrated with experimental results.

INTRODUCTION

The modern industrial halls are made of steel pitched roof portal frames with slender sections of Class 3 and 4. The structural elements have variable sections (e.g. tapered column and hunched rafters) in accordance with the stress and stiffness demand in component elements.

Because important axial compressive stresses develop in the rafter, an increased sensitivity to lateral-torsional instability characterizes the behavior of these members. If there are no lateral restrains, their lateral-torsional buckling strength is generally poor. However, the lateral restraining provided by the secondary structure and diaphragm effect of the envelope, significantly improve their response against buckling.

Due to non-rectangular shape of the web of connected members, the knee joint detail is very particular. Usually bolted connection with extended end plate on the top or at the face of the column are used. Hereafter the case of the top connection will be examined. A large parametrical investigation on a significant number of beam-to-column joints for pitched roof portal frames with tapered column and hunched rafter is presented in order to establish their sensitivity due to the variation of different components of the joint. Different steel grades and thickness are used for flange and in order to obtain sections of Class 3 and/or Class 4.

Moment capacity and stiffness of the joints are monitored by parametric study and advanced FEM non-linear elastic-plastic analysis is applied. The models are calibrated with experimental results. Final results concerning the joint characteristics are compared with results obtained through the component method of EN 1993-1-8.

TESTING PROGRAM-CALIBRATION OF THE MODELS

Specimens for the testing program

In order to define realistic specimen configurations, a simple pitched-roof portal frame, as the one in Figure 1, was firstly designed: span 18 m, bay 6 m, height 5 m and roof angle $\alpha=8^\circ$. Common load cases in the Romanian design practice were considered i.e: dead load of roof cladding 0.25 kN/m^2 ($\gamma_{ULS}=1.35$); technological load 0.20 kN/m^2 ($\gamma_{ULS}=1.35$); snow load 2.0 kN/m^2 ($\gamma_{ULS}=1.5$). S355 steel frames were analyzed and designed according to the current EN 1993-1-1 rules. Finally a number of 3 frames were obtained with different cross-section classes. The thickness, width and height of cross-section elements were changed to obtain approximately similar stiffness and stress distribution in the frame.

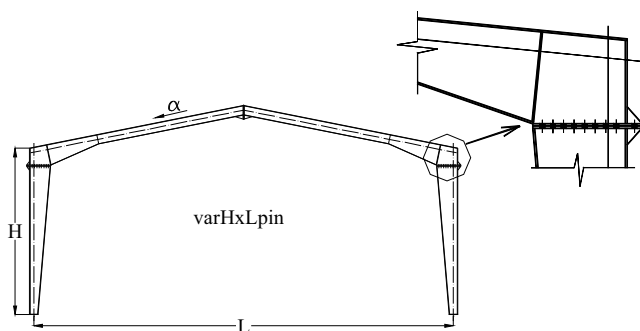


Fig. 1. Reference frame

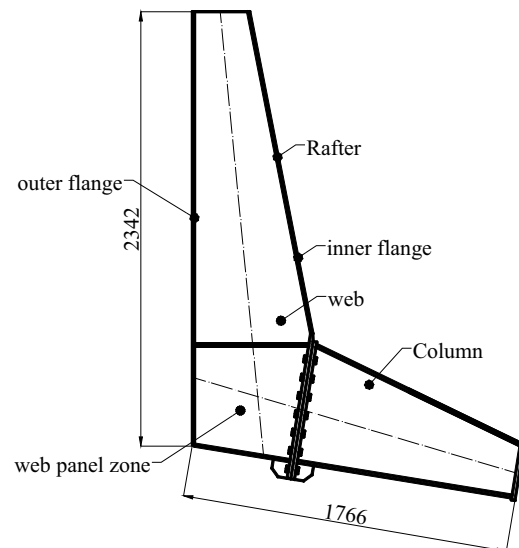


Fig. 2. Top rafter-to column joint

The three different joint configurations are: J2-3 (rafter and column of class 2 flanges and class 3 webs); J2-4 (rafter and column of class 2 flanges and class 4 webs); J3-4 (rafter and column of class 3 flanges and class 4 webs).

From design, the following joint dimensions and configurations were obtained (Table 1):

Table 1. Joint dimensions and characteristics

Joint	Column (H*B*t _f *t _w)	Rafter (H*B*t _f *t _w)
J2-3	650*240*15*8	650*200*12*8
J2-4	700*240*15*6	700*200*12*6
J3-4	700*280*12*6	700*230*10*6

where H = depth of the section; B = width of the rafter; t_f = thickness of the flange; and t_w = thickness of the web.

Design of joints was made using the component method in EN1993-1-8, adopted to account for significant axial force in the rafter (Cerfontaine, 2003). M20-10.9 bolts and 20 mm end plates were used in all specimens. A particular aspect of this type of joint is location of the zone of the web panel, working in shear at the end of the rafter that is bolted on the top of the column (Fig. 2).

Test setup

Two specimens of each configuration were tested, one under monotonic and the other under cyclic loading. Figure 3 shows the loading scheme and specimen instrumentation. The tests have been conducted in displacement control procedure. Lateral restraints were applied at the points indicated in Figure 3, to avoid out of plane displacement due to inherent imperfection. Load was applied quasi-statically with a displacement velocity of 3.33 mm/min.

For cyclic tests, two alternative loading procedures were used, i.e: (1) the standard ECCS loading procedure, and (2) a modified cyclic procedure, suggested by the authors, which is based on ECCS procedure. An important observation during the cyclic testing was that the recommended ECCS procedure (Fig. 5a) for cyclic testing proved to be unsuitable due to limited ductility of specimens. The increase of displacement from 1e_y directly to 2e_y is too large, in this case the second step being beyond the failure of specimen, making impossible to assess the characteristics of the cyclic behaviour. For this reason, a modified ECCS loading procedure was used (Fig. 5b). In this procedure the increment of 0.2e_y (instead of 2e_y) was used after reaching the yield point.

In order to identify the material behaviour tensile test have been performed on the specimens, extracted from the tested joints. The results of the tensile tests lead to the conclusion that S275 steel grade was used by fabricator instead of S355. Therefore, further on, S275 steel grade was considered.

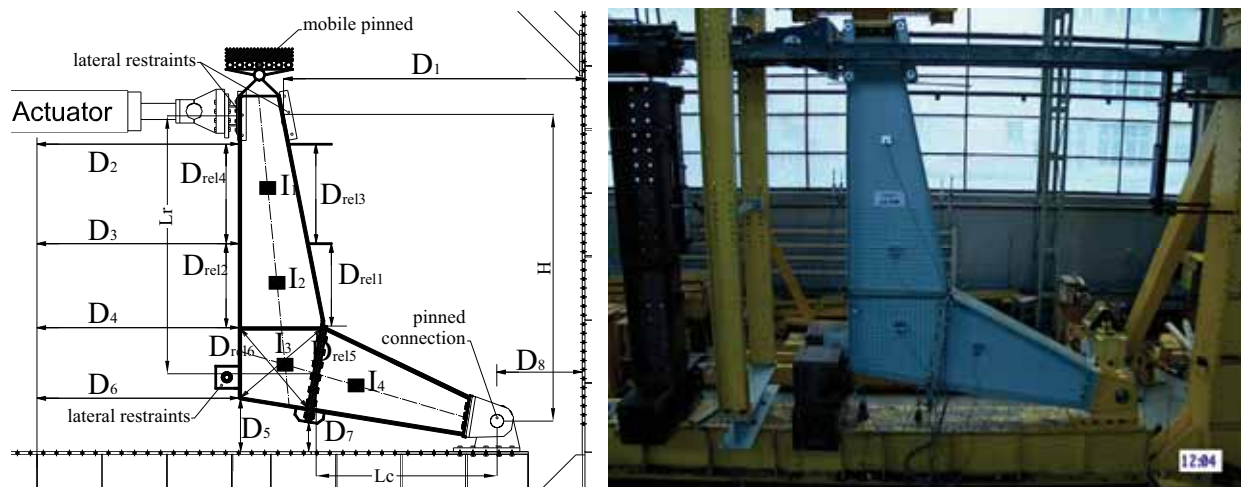


Figure 3. Loading scheme and instrumentation, where D_1 = measured displacement; D_{reli} = measured relative displacement; I_i = inclinometers.

The yield displacement was determined according to the ECCS (1985) procedure (Fig. 4).

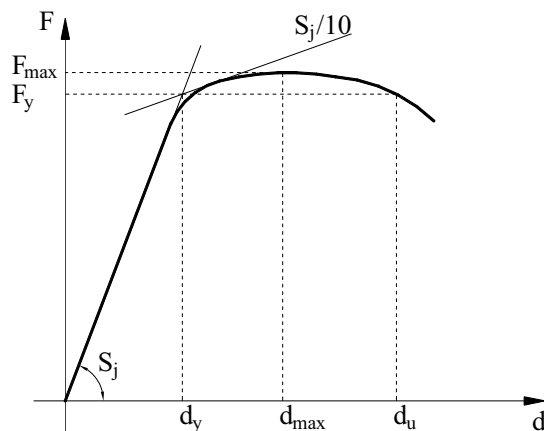


Figure 4. ECCS procedure for determining the yield displacement

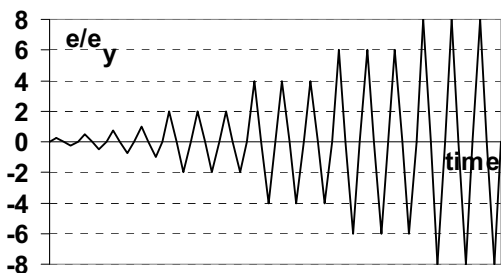


Figure 5a. Standard ECCS loading procedure

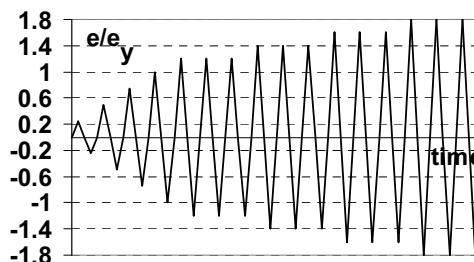


Figure 5b. Modified ECCS loading procedure

Results of testing program

Comparative moment-rotation experimental curves for the tested specimens, under monotonic loading, are presented in Figure 4. As it can be seen, in all cases, the values of initial stiffness of the joints are very close. The failure mode characterized by distortion of the compressed flange coupled with local buckling of the rafter web, are presented in Figure 5 for the 3 (three) different joint configuration (Cristutiu et al, 2006).

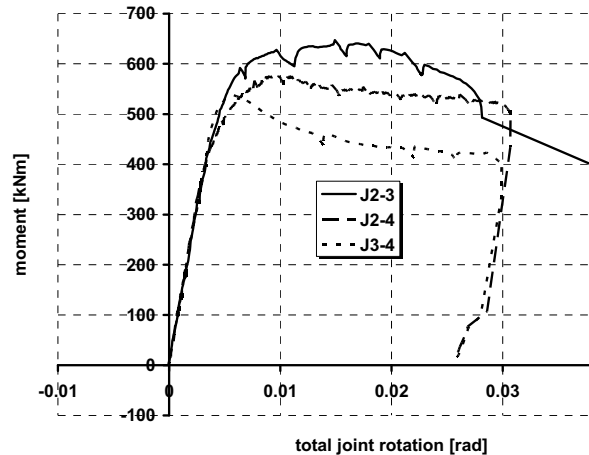


Figure 4. Comparative results from monotonic tests



Figure 5a. Failure mode of specimen J2-3m – monotonic loading

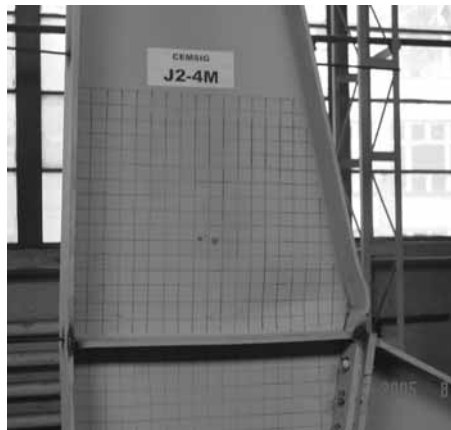


Figure 5b. Failure mode of specimen J2-4m – monotonic loading



Figure 5c. Failure mode of specimen J3-4m – monotonic loading

Comparative moment-rotation experimental curves for the tested specimens, under cyclic loading, are presented in Figure 6, for different joint configurations. Failure of the joints occurred, in all cases, under positive cycles, when the ultimate moment capacity is reached. The behaviour of the joints is presented in Figures 6 and failure modes are presented Figures 7. Comparable values of moment capacity of tested joints have been observed in case of monotonic and cyclic tests.

The initial stiffness of the joints is not influenced by the class of the cross section and direction of loading.

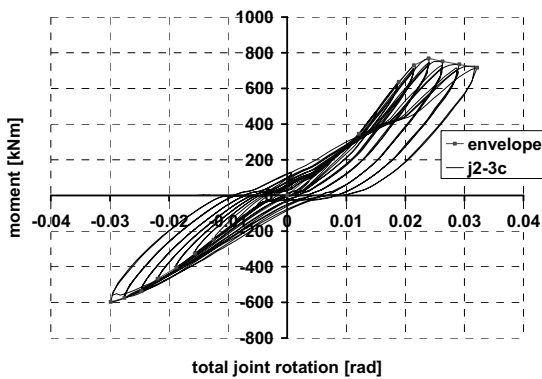


Figure 6a. Behaviour of joint J2-3c – cyclic loading

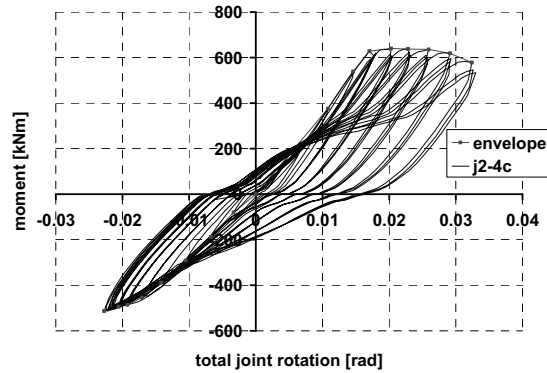


Figure 6b. Behaviour of joint J2-4c – cyclic loading

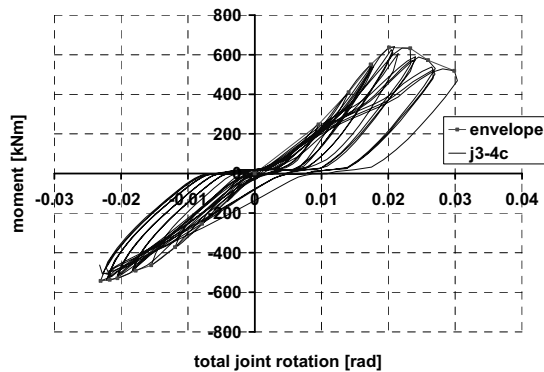


Figure 6c. Behaviour of joint J3-4c – cyclic loading

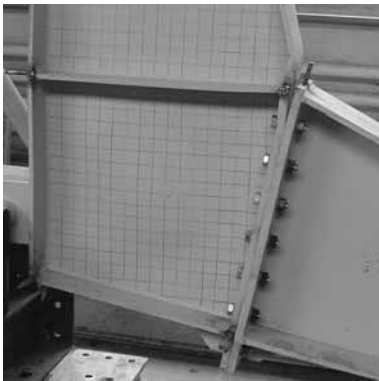


Figure 7a. Failure mode of specimen J2-3m – cyclic loading



Figure 7b. Failure mode of specimen J2-4m – cyclic loading

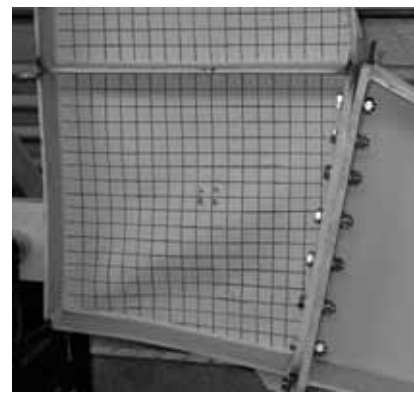


Figure 7c. Failure mode of specimen J3-4m – cyclic loading

In case of cyclic loading, the failure of specimens occurs by distortion of the inner flange of rafter coupled with the local buckling and shear buckling of web in the panel zone without causing degradation of positive cycles (Fig. 7). In case of negative loads, the local buckling of the web in panel zone and bending of the end plate was observed.

Under repeated cycles, in case of J2-4c specimen, cracks in web panel zone occurred (e.g. low cycle fatigue failure mode). In case of specimens J2-3c and J2-4c the hysteretic loops are stable and characterized by a reduced degradation of joint moment capacity under positive loads. Obviously, is significantly larger in case of J3-4c specimen. In all cases due to unsymmetry of the joint, the ultimate moment capacity was not reached under negative loads (e.g. negative cycles).

NUMERICAL SIMULATION PROGRAM

Modelling

An advanced non-linear elastic plastic FEM model has been calibrated using test results. On this purpose Ansys computer program, using Shell 43 elements enabling for large strain plastic analysis was applied. The material behavior was introduced by a bilinear elastic-perfectly plastic model, with a yielding limit of 275 N/mm^2 . Between the end plates of the column and rafter, contact elements were used (Fig. 8a).

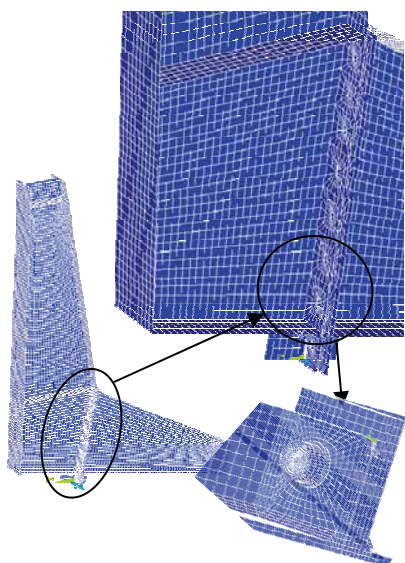


Figure 8a. FEM model

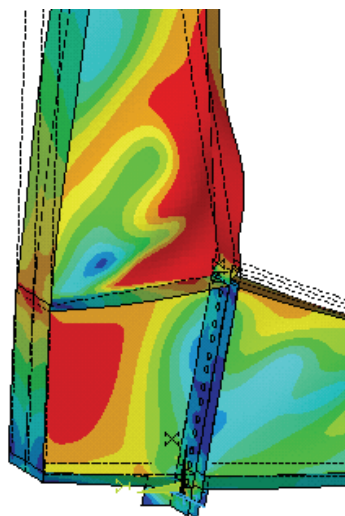


Figure 8b. Failure mode of the joint according to FEM simulation



Figure 8c. Failure mode of the joint – experimental test

The FEM analysis qualitatively shows the location of the stress concentration and the failure modes characterizing the different joint configurations. The same failure mode of the joint was identified with FEM simulation and in case of experimental tests (Fig. 5) i.e.: distortion of the compressed flange coupled with local buckling of the rafter web. Comparison between moment rotation curves of experimental tests, component method (Cerfontaine, 2003) and FEM is presented in Figure 9. From Figure 9, it can be observed a good similitude between experimental curves and FEM simulation, in what concerns, capacity of the joint and stiffness.

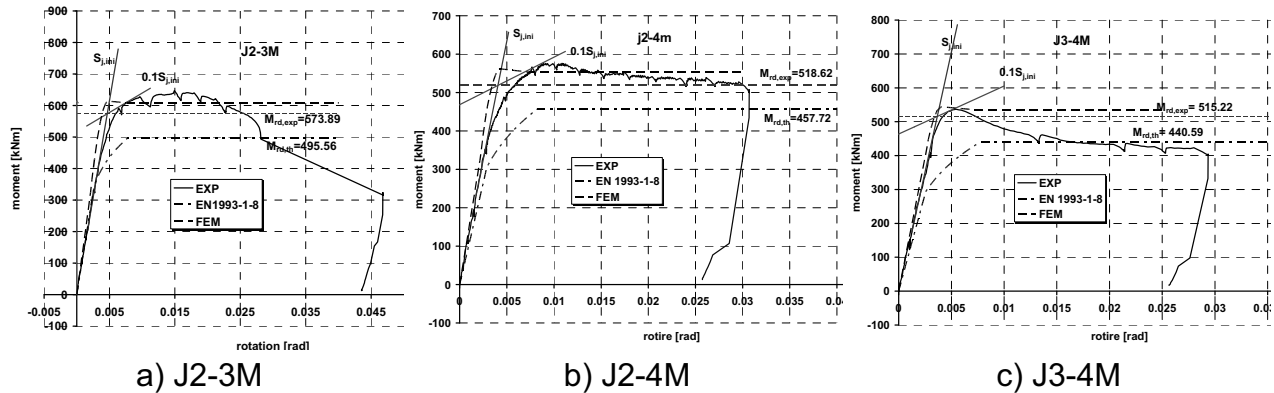


Figure 9. Comparison between experimental curves, EN 1993-1-8 and FEM curves

Parametric study

It is very well known that experimental test, mainly when dealing with big specimens, are time and labour consuming. An alternative to experimental test is represented by numerical simulations, where it should be taken into account all the effects that might appear during test.

Further on numerical simulation were made in order to determine the joint characteristic (moment and rotation capacity) and its behaviour. The numerical simulations were made through nonlinear-elastic-plastic analysis, using the same joint configurations as for experimental test (see Fig. 2, 8a), but different steel grade and different web thicknesses (6 or 8 mm) were used. The steel grades were S235, S355 and S460. The dimensions of joint components used in the numerical simulation are presented in Table 3.

Table 3. Main dimensions of the analysed joints

Steel grade	Joint name	Column			Rafter		
		Dimension H*b*tf*tw [mm]	Section class		Dimension H*b*tf*tw [mm]	Section class	
			flange	web		flange	web
S235	S235_650-1	650*240*15*8	2	3	650*200*12*8	2	3
	S235_650-2	650*240*15*6	2	3	650*240*15*6	2	3
	S235_700-1	700*240*15*8	2	3	700*200*12*8	2	3
	S235_700-2	700*240*15*6	2	4	700*200*12*6	2	4
S355	S355_650-1	650*240*15*8	2	3	650*200*12*8	2	3
	S355_650-2	650*240*15*6	2	3	650*240*15*6	2	3
	S355_700-1	700*240*15*8	2	3	700*200*12*8	2	3
	S355_700-2	700*240*15*6	2	4	700*200*12*6	2	4
S460	S460_650-1	650*240*15*8	2	3	650*200*12*8	2	3
	S460_650-2	650*240*15*6	2	3	650*240*15*6	2	3
	S460_700-1	700*240*15*8	2	3	700*200*12*8	2	3
	S460_700-2	700*240*15*6	2	4	700*200*12*6	2	4

In the numerical analysis, the same static scheme as for experimental test was used (see Fig. 3).

Comparative analysis

The obtained results via numerical analysis, expressed in terms of, moment capacity ($M_{Rk,FEM}$), yield rotation ($\Phi_{el,FEM}$) and initial stiffness ($S_{j,ini,FEM}$) are plotted in Table 4. The moment capacity ($M_{Rk,th}$) of the joint was evaluated by means of component method, too, and results are presented in Table 4. If the values of moment capacity obtained by FEM simulation, $M_{Rk,FEM}$, are taken as reference, one concludes that in all cases the results obtained with the component method are on the safe side. Comparative results between moment capacity evaluated with FEM ($M_{Rk,FEM}$) and the theoretical one ($M_{Rd,th}$) are presented in Figure 10.

Table 4. Results of numerical simulation vs Component Method of EN1993-1.8

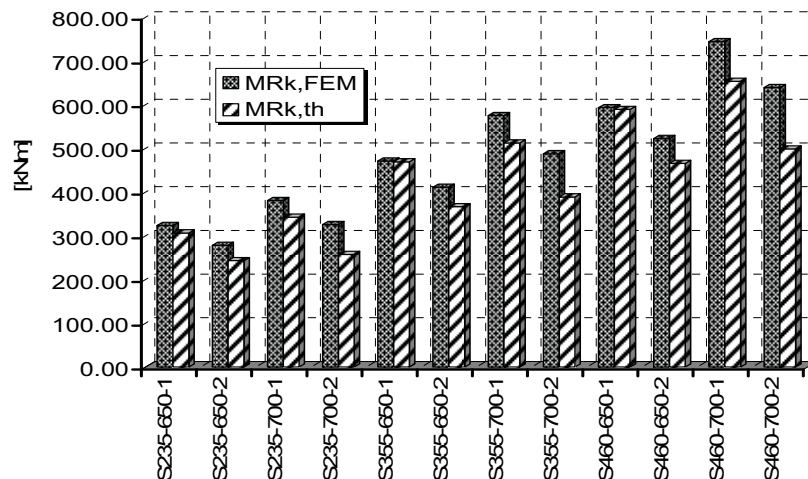
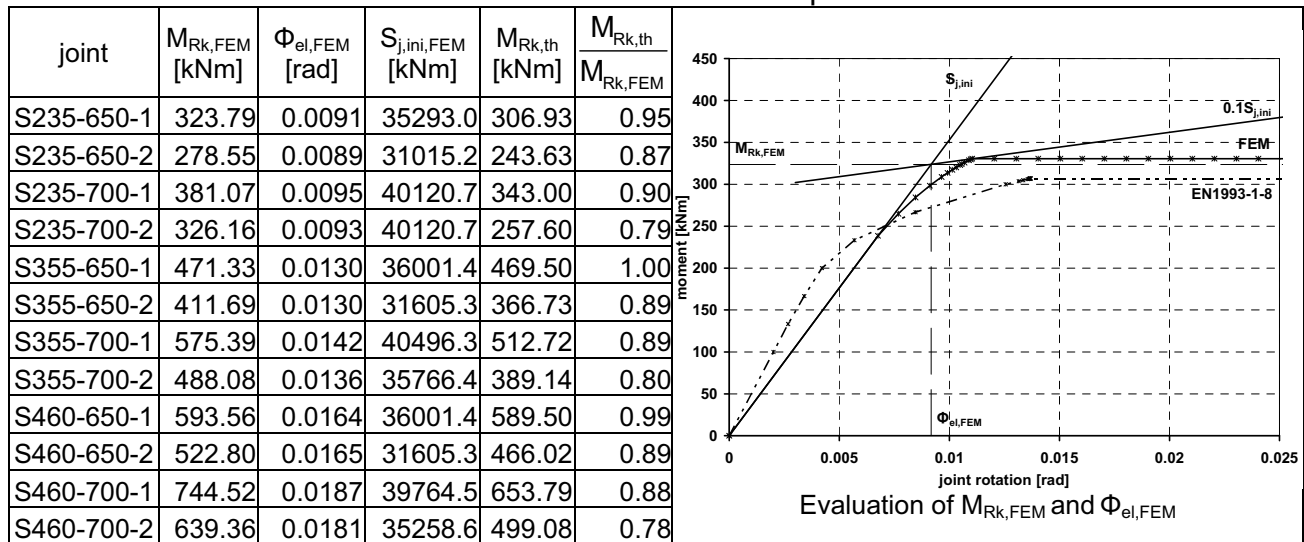


Figure 10. Comparative results $M_{Rk,FEM}$ and $M_{Rk,th}$

CONCLUSIONS

A large number of rafter-to-column joints were analysed in order to determine the influence of the changing of one of the following parameters: steel grade, web thickness and height of the cross section, all joints are full strength and rigid. Finite element models were calibrated with experimental test carried out at the CEMSIG (<http://cemsig.ct.upt.ro>) research centre of the Politehnica University of Timisoara. The results obtained analytically were compared, thereafter, with the ones obtained via General Method of EN1993-1-8.

The same failure mode was obtained in all cases, i. e. distortion of the compressed flange coupled with local buckling of the rafter web (see Fig. 5), even changes in height of the cross section and thickness of the web was performed. In case of component method, the component that governs the capacity of the joint is the rafter flange and web in compression.

For the same steel grade, the most significant influence in the moment capacity of the joint has the height of the cross sections.

The initial stiffness of the joint is not significantly influenced by the chosen parameters (steel grade, cross section height or web thickness).

The difference in the moment capacity of the joint, between elements of class 3 and class 4, increases by increasing the steel grade.

REFERENCES

- EN 1993-1.1: Eurocode 3: Design of Steel Structures. Part 1.1: General rules and rules for buildings, may 2005, CEN, Brussels, Belgium;
- EN 1993-1.8: Eurocode 3: Design of Steel Structures. Part 1.8: Design of joints, may 2005, CEN, Brussels, Belgium;
- ECCS 1985 Recommended testing procedures for assessing the behaviour of structural elements under cyclic loads. European Convention for Constructional Steelwork (ECCS) 1985, Tchn. Comm. 1, TWG 13-Seismic design, No. 45;
- Cristuțiu I.M. , Dubină D., Stratan A. și Grecea D., - Moment-rotation characteristics of bolted beam-to-column connections of pitched-roof portal frames with class 3 and 4 sections. Steel Structures in Seismic Area STESSA-2006, Yokohama Japan. aug. 2006
- Cerfontaine F. (2003), "Etude de l'interaction entre moment de flexion et effort normal dans les assemblages boulonnées" PHd Thesis. Universite de Liege, Faculte des Science Appliquees 2003.
- ECCS 1985 Recommended testing procedures for assessing the behaviour of structural elements under cyclic loads. European Convention for Constructional Steelwork (ECCS) 1985, Tchn. Comm. 1, TWG 13-Seismic design, No. 45;

Monotonic and Cyclic Tests of Steel Pretensioned Bolted End-Plate Connections of Different Types and Details

Gang Shi*, Jun Xiong, Yongjiu Shi, Yuanqing Wang
Tsinghua University, Beijing 100084, China
shigang@tsinghua.edu.cn

Abstract: In this paper, the same two groups of steel beam-to-column pretensioned bolted end-plate connections are tested under monotonic and cyclic loads respectively to investigate its static and seismic behavior comprehensively. Each group includes 8 connections of various types and details, in which all the bolts are high strength pretensioned. The experimental results are presented in terms of moment capacity, rotational stiffness, rotation capacity, monotonic and hysteretic moment-rotation ($M-\phi$) curves. The influences of flush and extended type, column stiffener, end-plate rib stiffener, bolt size and end-plate thickness etc on the joint behavior have been analyzed. Based on the comparison and analysis of the monotonic and cyclic loading test results, types and details of end-plate moment connections for seismic steel frames have been suggested, and the connection failure mode requirements have been recommended to assure that the end-plate connection can provide enough joint rotation capacity and energy dissipation capacity under earthquake loading and its ultimate failure mode is ductile.

Key Words: end-plate connection; semi-rigid; moment-rotation, joint stiffness

INTRODUCTION

Bolted end-plate connections are widely used in steel structures as moment-resistant connections including column base joints (Ádány et al. 2001). Because the bolted beam-to-column connection is less rigid than beam-to-column welded connections, end-plate connections offer enhanced ductility at the beam-to-column connection. They also have the advantages of easy fabrication and fast erection compared to directly welded connections. The typical end-plate connections are: flush end-plate connections and extended end-plate connections.

Many relevant researches suggest that experimental testing is the most reliable method to investigate the behavior of the connection, especially its seismic behavior. And the experiment is also the benchmark to verify other methods. Therefore many tests of end-plate connections have been performed.

In this paper, the same 2 groups of specimens are tested under monotonic and cyclic loading respectively in order to compare the joint behavior under different

loading, in which each group includes 8 specimens of beam-to-column bolted end-plate connections with various details including the flush and extended type, column stiffener, end-plate rib stiffener, bolt size and end-plate thickness etc. The contribution of the panel zone and the gap between the end-plate and column flange to the joint rotation has been investigated. With a special method to measure the bolt strain, the bolt tension force distribution and the development of bolt tension forces have been measured.

TEST SPECIMENS AND PROCEDURE

All the 16 specimens of these 2 groups are beam-to-side-column connections. The first group specimens are named with a prefix 'SC' and tested under monotonic loading. And the second group specimens are named with a prefix 'JD' and tested under cyclic loading. The details of these 16 specimens are shown in Table 1 and Fig. 1. All the specimen beams and columns have the same dimensions respectively listed in Table 2. The thickness of the column flange is the same as the end-plate within the range of 100mm above and below the extension edge of the end-plate. The thickness of column stiffener and end-plate rib stiffener is 12mm and 10mm respectively. The test configuration is shown in Fig. 2, in which, No. 1 was used to monitor the displacement at the loading point, Nos. 2~10 measure the relative deformation between the end-plate and column flange, Nos. 11 and 12 measure the inner shearing deformation of the panel zone, Nos. 13 and 14 were arranged next to the column stiffeners to measure the shearing deformation of the panel zone, and No. 15 measures the slippage between the end-plate and column flange.

Table 1. Types and details of specimens

Specimen number	Connection type	End-plate thickness (mm)	Bolt diameter (mm)	Number of bolts	Column stiffener	End-plate stiffener
SC1/JD1	flush	20	20	6	Yes	—
SC2/JD2	extended	20	20	8	Yes	Yes
SC3/JD3	extended	20	20	8	Yes	No
SC4/JD4	extended	20	20	8	No	Yes
SC5/JD5	extended	25	20	8	Yes	Yes
SC6/JD6	extended	20	24	8	Yes	Yes
SC7/JD7	extended	25	24	8	Yes	Yes
SC8/JD8	extended	16	20	8	Yes	Yes

Table 2. Sectional dimensions of beams and columns (unit: mm)

	Section Depth	Web thickness	Flange width	Flange thickness
Beam	300	8	200	12
Column	300	8	250	12

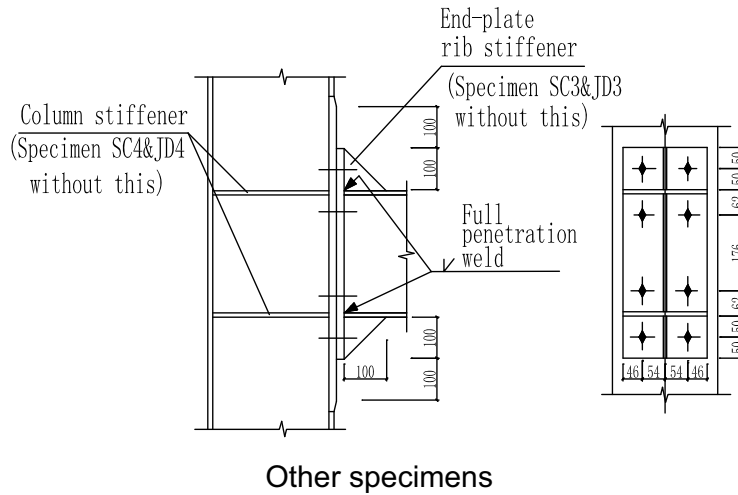
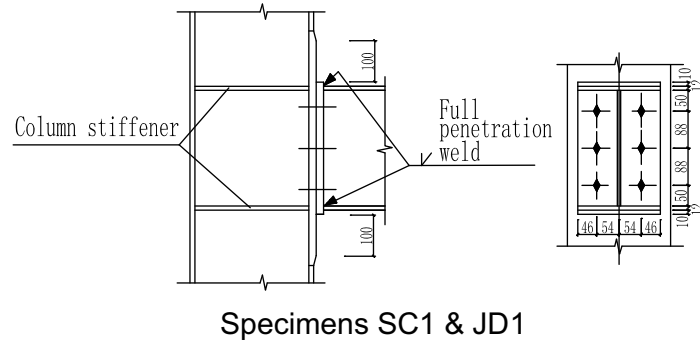


FIG. 1. Details of connections

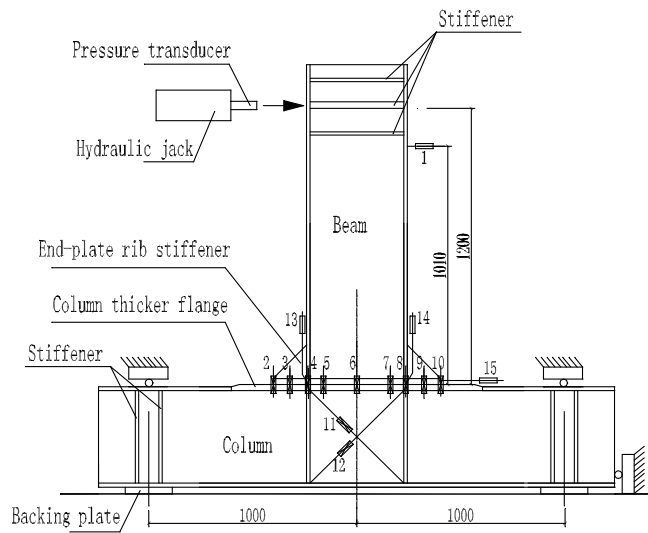


FIG. 2. Test specimen and loading arrangement

Q345 steel (nominal yielding stress $f_y=345\text{MPa}$) is applied for all the specimens, and the bolts are high strength friction-grip bolts (grade 10.9). The material properties of the steel and bolts are obtained from tensile tests on coupons and from the bolts certificate of quality, as shown in Table 3. The proof elastic modulus of the bolts is

206000MPa. Except that the welds between the end-plate and beam flanges as well as the column flange splices are full penetration welds, all the other welds, including the welds between flanges and webs of beams and columns, end-plates and beam webs, are fillet welds with an 8mm leg size. The applied bolt pretension force are listed in Table 3. The contact surface between the end-plate and column flange was prepared by blast and the slip coefficient is 0.44.

Table 3. Material properties

Material	Measured yield strength (MPa) (SC/JD)	Measured tensile strength (MPa) (SC/JD)	Measured elastic modulus (MPa) (SC/JD)	Measured bolt average pretension force (kN) (SC/JD)
Steel (thickness≤16mm)	391/409	559/537	190707/ 195452	—
Steel (thickness>16mm)	363/373	537/537	204228/ 188671	—
Bolts (M20)	995	1160	—	185/199
Bolts (M24)	975	1188	—	251/283

Specimens SC1~SC8 were tested under monotonic loads which were applied by the hydraulic jack at the end of the beam until failure. Specimens JD1~JD8 were applied cyclic loads, for which the column axial force is 485kN which was applied by the pressure jack at one end of the column and kept constant during the cyclic loading process. After the column axial force was applied, cyclic loads were applied by the hydraulic jack at the end of the beam. The cyclic loading procedure was load/displacement control method according to the current specification for seismic testing method (JGJ 101-96). Before the specimen yields, the load control is adopted and the yielding load is applied by three incremental steps, and for each incremental load step the number of cycles is only one. After yielding appears, the load is applied by controlling the displacement at the end of the beam (i.e. the displacement measured by No. 1 displacement transducer in Figure 2). Each displacement incremental step is 10mm, and for each displacement incremental step the number of cycles is two. The load values of the initial three load steps are listed in Table 4.

TEST RESULTS AND DISCUSSION

(1) Monotonic loading tests

The test results of specimens SC1~SC8 are summarized in Table 5, in which, P_u is the loading capacity, i.e., the maximum pushing force during the tests; M_u is the maximum moment resistance of specimen connections which is calculated by multiplying P_u with the arm of the loading, 1.2m; ΔM_u is the specimen connection maximum moment resistance change compared with specimen SC2; K_i is the specimen connection initial rotational stiffness, which is the secant stiffness for the

connection moment 60kN-m; ΔK_i is the specimen connection initial rotational stiffness change compared with specimen SC2; and ϕ is the connection rotation capacity.

Table 4. The load values of the initial three load steps of cyclic tests (kN)

Specimen number	First load step	Second load step	Third load step
JD1	40	80	120
JD2	60	120	180
JD3	56	112	168
JD4	60	120	180
JD5	56	112	168
JD6	70	140	210
JD7	70	140	210
JD8	60	120	180

Table 5. Monotonic loading test results

Specimen number	P_u (kN)	M_u (kN-m)	ΔM_u (%)	K_i (kN.m/rad)	ΔK_i (%)	ϕ (rad)	Failure mode ^a
SC1	155.3	186.4	-45.8	23544	-55.0	0.043	BF
SC2	286.4	343.7	—	52276	—	0.070	BF
SC3	256.9	308.3	-10.3	49093	-6.1	0.067	BF
SC4	256.6	307.9	-10.4	51535	-1.4	0.050	BC
SC5	268.4	322.1	-6.3	46094	-11.8	0.043	BF
SC6	325.3	390.3	13.6	46066	-11.9	0.108	BB
SC7	342.3	410.8	19.5	47469	-9.2	0.073	BB
SC8	296.1	355.4	3.4	41634	-20.4	0.101	BF & BEC

^a BF: Bolt fracture; BC: Buckling of column web in compression; BB: Buckling of beam flange and web in compression; BEC: Buckling of the end-plate rib stiffener in compression.

In this paper, the joint rotation ϕ of the beam-to-column end-plate connection is defined as the relative rotation of the center lines of the beam top and bottom flanges at the beam end, and it usually includes two parts: the shearing rotation ϕ_s , contributed by the panel zone of the column, and the gap rotation ϕ_{ep} , caused by the relative deformation between the end-plate and the column flange including the bending deformation of the end-plate and column flange as well as the elongation of the bolts (Fig. 3). M- ϕ curves of all the specimens are shown in Fig. 4.

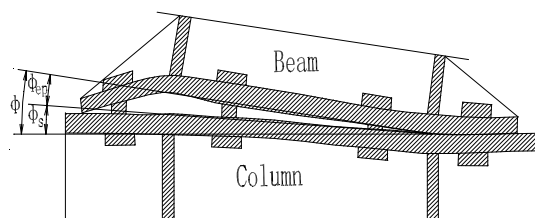


FIG. 3. Definition of joint rotation

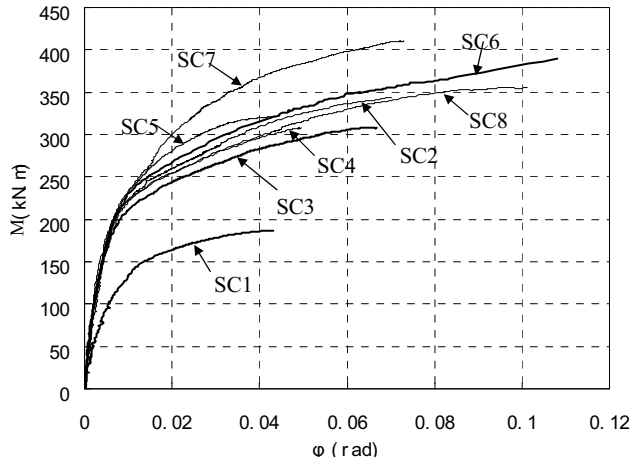
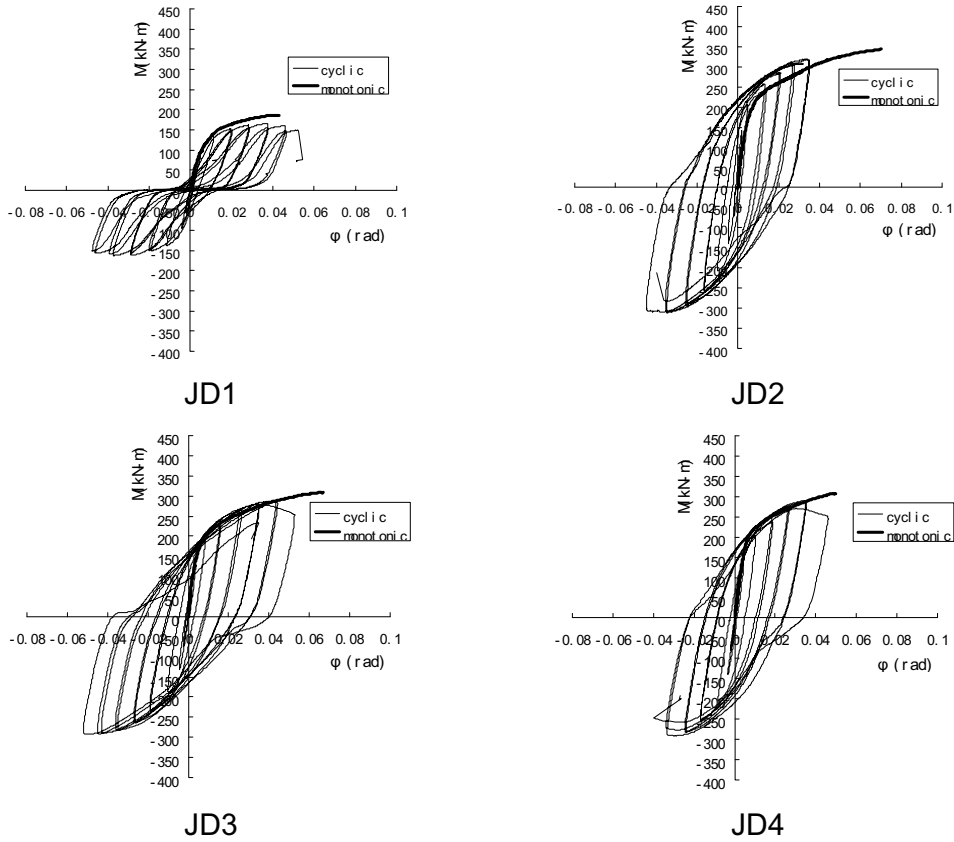


FIG. 4. M-φ curves of the monotonic loading tests

(2). Cyclic loading tests

The moment-rotation(M-φ) hysteretic curves of specimens JD1~JD8 are shown in Figure 5. The corresponding curves of specimens SC1~SC8 under monotonic loads are also shown in these figures for comparison.



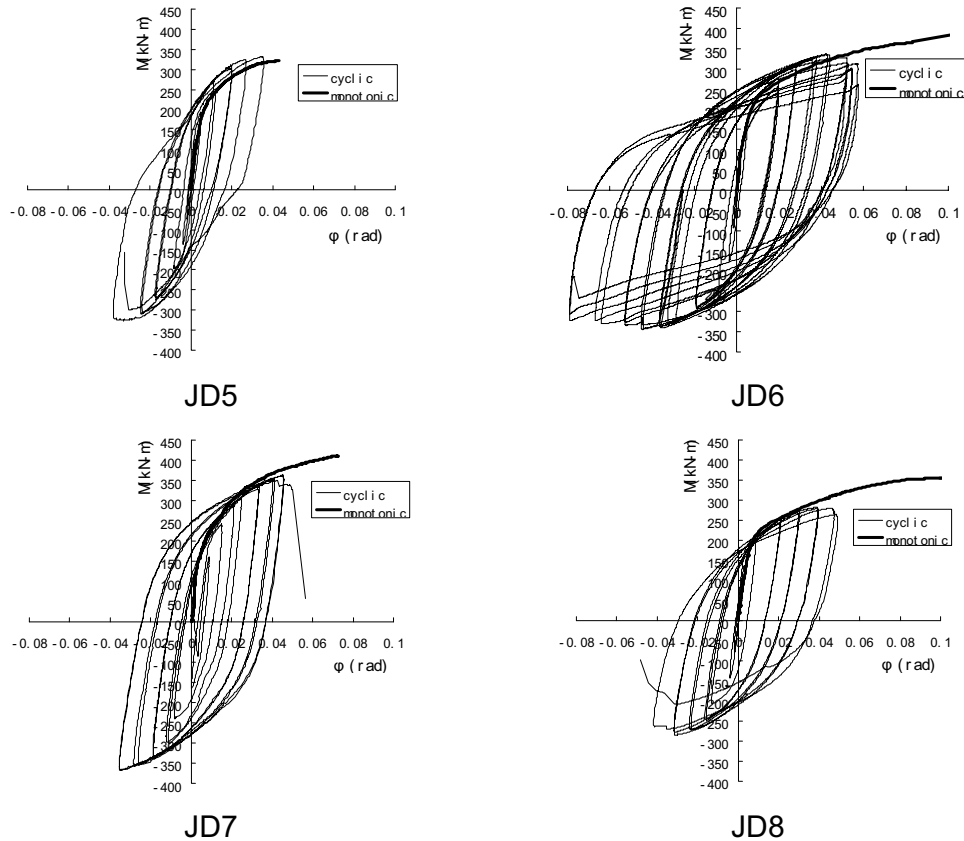


FIG. 5. M- ϕ curves of the cyclic loading tests

Test results are summarized in Table 6, where the definitions of M_u , ΔM_u , K_i and ΔK_i are the same as in Table 5. And M_u is the maximum value of the joint moment during the whole cyclic loading procedure, not the maximum moment of the last load cycle. K_i is the secant rotational stiffness corresponding to the load of the first load cycle listed in Table 4. ϕ_u^+ and ϕ_u^- are the positive and negative rotation capacity of the specimen connections respectively, and when the force applied at the end of the beam is push force, it is positive, and when pull force, it is negative; ϕ_u is the average rotation capacity, equal to $(\phi_u^+ + \phi_u^-)/2$, and $\Delta\phi_u$ is the specimen connection average rotation capacity change compared with specimen JD2.

It can be summarized as following by the test results comparison in Tables 5 and 6 and some other researches:

(1). From the view point of joint rotation capacity and ductility, generally extended end-plate connections are better than flush end-plate connections, especially when the end-plate extended on both sides (Bernuzzi et al., 1996; Girão Coelho et al., 2006).

(2). Column stiffeners (i.e. continuity plate) can avoid the premature buckling of the column web in compression so to increase the connection rotational stiffness, moment capacity and rotation capacity. End-plate connections with unstiffened columns showed very poor behavior compared with those stiffened (Ghobarah et al.,

1990, 1992; Korol et al., 1990, Shi et al., 2007b).

Table 6. Cyclic loading test results

Specimen number	M_u (kN-m)	ΔM_u (%)	K_i (kN-m/rad)	ΔK_i (%)	φ_u^+ (rad)	φ_u^- (rad)	φ_u (rad)	$\Delta \varphi_u$ (%)	Failure mode ^b
JD1	164.5	-48.6	28011	-59.1	0.047	0.048	0.047	17.8	BF, EY
JD2	320.1	—	68407	—	0.035	0.045	0.040	—	BF
JD3	288.4	-9.9	32547	-52.4	0.053	0.052	0.052	30.8	BF, EY
JD4	289.4	-9.6	35810	-47.7	0.046	0.034	0.040	0.1	BF, BCWC
JD5	331.4	3.5	57248	-16.3	0.036	0.038	0.037	-7.8	BF
JD6	336.2	5.0	41310	-39.6	0.057	0.079	0.068	70.9	ESF, SBP, LBCF, WF
JD7	364.0	13.7	52502	-23.3	0.046	0.035	0.041	1.4	ESF, WF
JD8	283.5	-11.4	44776	-34.5	0.049	0.042	0.045	13.7	BF, ESF, EF

^b BF: Bolt fracture; EY: End-plate yielding; ESF: End-plate stiffener fracture; BCWC: Buckling of the column web panel in compression; SBP: Shearing buckling of the panel zone; LBCF: Local buckling of the column flange; WF: Weld between the beam flange and the end-plate fracture; EF: End-plate fracture.

(3). The use of extended stiffeners can increase the connection moment resistance (Shi et al., 2004), rotation capacity and energy dissipation capacity, as the stiffeners can prevent that inelasticity and deformation are concentrated in the roots of the end-plate extension too much, and can transform the deformation mode of the end-plate extension from uniaxial bending to biaxial bending which would improve the end plate deformation ability and energy dissipation capacity. This would improve the connection seismic behaviour (Adey et al., 2000; Tsai and Popov 1990).

(4). The end-plate should not be too thick so as to be much stronger than the bolts, which will lead that the bolt is the critical component in the connection and this deems to decrease the connection rotation capacity and ductility very much. The end-plate connection with a moderate-thickness end-plate and large bolts will exhibit better rotation capacity and ductility (Girão Coelho et al., 2004).

According to the above test results and other relevant research results, standard details of end-plate moment connections for seismic steel frames can be proposed as following.

- (a). The end-plate extends on both sides.
- (b). The column flange is stiffened and the stiffener (i.e. continuity plate) thickness is

not less than the beam flange.

(c). The extended end-plate is stiffened and the stiffener thickness is not less than the beam web.

(d). The end-plate with moderate thickness and large bolts are adopted.

Except for these, in order to assure that the end-plate connection can provide enough joint rotation capacity and energy dissipation capacity under earthquake loading and its ultimate failure mode is ductile, three failure mode requirements have been proposed as following:

(i). The failure mode of the end-plate and column flange should be bending failure and not punching shear failure under earthquake loading.

(ii). The panel zone yields preceding the end-plate and bolts

(iii). The end-plate fails prior to the bolts.

All these three failure mode requirements can be achieved by comparing the loading capacities of these components (Shi et al., 2007a).

CONCLUSIONS

In this paper, 16 full-scale steel beam-to-column end-plate moment connections were tested under monotonic and cyclic loading to investigate the influences on the connection moment resistance, rotational stiffness, rotation capacity and ductility. Based on the test results and analysis, several conclusions can be made:

(1). End-plate connection details, including flush and extended types, column stiffener, end-plate rib stiffener, bolt size, end-plate thickness etc, influence the joint moment resistance, initial rotational stiffness, rotation capacity and failure mode significantly. Especially there are 5 extended end-plate connection specimens with the end-plate and column flange both stiffened in these specimens, and because there is very little experimental research for this type of end-plate connections until now, the tests results of this paper have offered a solid foundation for the future research about this end-plate connection type.

(2). The end-plate connection extended on both sides can provide the strength, joint rotational stiffness, ductility and energy dissipation capacity required for use in seismic moment frames. The hysteretic loop of the flush end-plate connection pinches significantly and its stiffness degrades seriously which indicates its energy dissipation capacity is not adequate, and it is not recommended to be used as moment resistant connections in seismic steel frames.

(3). Standard details and three failure mode requirements for end-plate moment connections in seismic steel frames have been proposed, which can ensure that the end-plate connection can provide enough joint rotation capacity and energy dissipation capacity under earthquake loading and its ultimate failure mode is ductile.

ACKNOWLEDGEMENTS

This work was jointly supported by the National Natural Science Foundation of China (No. 50578083) and Program for Changjiang Scholars and Innovative

Research Team in University (IRT00736).

REFERENCES

- Ádány, S., Calado, L. and Dunai, L. (2001), "Experimental study on the cyclic behaviour of bolted end-plate joints", *Steel and Composite Structures*, Vol. 1, No. 1 (pp.33-50).
- Adey, B. T., Grondin, G. Y. and Cheng, J. J. R. (2000), "Cyclic loading of end plate moment connections". *Canadian Journal of Civil Engineering*, Vol. 27, No. 4 (pp.683-701).
- Bernuzzi, C., Zandonini, R., and Zanon, P. (1996). "Experimental analysis and modelling of semi-rigid steel joints under cyclic reversal loading", *Journal of Constructional Steel Research*, Vol. 38, No. 2 (pp.95-123).
- Ghobarah, A., Osman, A. and Korol R. M. (1990), "Behaviour of extended end-plate connections under cyclic loading", *Engineering Structures*,; Vol. 12, No. 1 (pp.15-27).
- Ghobarah, A., Korol, R. M. and Osman, A. (1992), "Cyclic behaviour of extended end-plate joints", *Journal of Structural Engineering*, Vol. 118, No. 5 (pp.1333-1353).
- Girão Coelho, A.M., Bijlaard, F., and Simões da Silva, L. (2004), "Experimental assessment of the ductility of extended end plate connections", *Engineering Structures*, Vol. 26 (pp.1185-1206).
- Girão Coelho, A.M., Simões da Silva, L. and Bijlaard, F. (2006), "Ductility analysis of bolted extended end plate beam-to-column connections in the framework of the component method", *Steel and Composite Structures*, Vol. 6, No. 1 (pp.33-53).
- JGJ 101-96. Specification for building seismic testing method. 1996 (in Chinese)
- Korol, R. M., Ghobarah, A. and Osman, A. (1990), "Extended end-plate connections under cyclic loading: behaviour and design", *Journal of Constructional Steel Research*, Vol. 16 (pp.253-280).
- Shi, G., Shi, Y. J., and Chen H. (2004). "Finite Element Analysis of Beam-Column Bolted End-Plate Connections in Steel Frames". Seventh Pacific Structural Steel Conference. Long Beach, California, U S A, March 24-27.
- Shi, G., Shi, Y. J. and Wang, Y. Q. (2007a), "Behaviour of End-Plate Moment Connections under Earthquake Loading". *Engineering Structures*, Vol. 29, No. 5 (pp.703-716).
- Shi, Y. J., Shi, G. and Wang, Y. Q. (2007b), "Experimental and theoretical analysis of the moment-rotation behaviour of stiffened extended end-plate connections". *Journal of Constructional Steel Research*, Vol. 63, No. 9 (pp.1279-1293).
- Tsai, K. C., and Popov, E. P. (1990). "Cyclic Behavior of End-Plate Moment Connections". *Journal of Structural Engineering*, ASCE, Vol. 116, No. 11 (pp.2917-2930).

DUAL-STEEL T-STUB BEHAVIOR UNDER MONOTONIC AND CYCLIC LOADING

Dan Dubina

"Politehnica" University of Timisoara, Timisoara 300224, Romania
dan.dubina@ct.upt.ro

Aurel Stratan

"Politehnica" University of Timisoara, Timisoara 300224, Romania
aurel.stratan@ct.upt.ro

Nicolae Muntean

"Politehnica" University of Timisoara, Timisoara 300224, Romania
nicolae.muntean@ct.upt.ro

Daniel Grecea

"Politehnica" University of Timisoara, Timisoara 300224, Romania
daniel.grecea@arh.upt.ro

ABSTRACT

The paper summarizes the first part of an extensive experimental program aiming to evaluate the performance of moment resisting beam-to-column joints in dual-steel building frames. Joint components, both bolted and welded, are of High Strength Steel (HSS) and Mild Carbon Steel (MCS). In this paper, test results on different weld details, used to connect HSS with MCS components and bolted T-stub specimens are presented and analyzed.

INTRODUCTION

Previous studies realized by authors (Dubina and Dinu, 2007, Dubina et al., in print) showed the advantages of using High Strength Steel (HSS) in combination with Mild Carbon Steel (MCS) in so called Dual-Steel Structures (DSS), to enhance robustness and better control of the response of seismic resistant building frames.

To get a rational design of a seismic resistant structure – i.e. both safe and economic – the dissipative elements have to approach the plastic capacity under design forces, in order to reduce the demand on non-dissipative members. The best way to accomplish this is not by changing size of sections in dissipative and non-dissipative members because it also changes their stiffness, but to realize them of MCS and HSS, correspondingly. Such a DSS system, if properly designed to obtain a good balance between stiffness, strength and ductility of members and connections, enables to achieve the three critical tasks of a seismically robust structure i.e.: (1) secure plastic deformations in structural members targeted as dissipative; (2) prepare multiple routes for transfer of forces and ensure their redistribution through

yielding of other members; (3) provide sufficient overstrength to structural members that are not allowed to yield.

In a DSS system, MCS members have to behave like fuses, dissipating the seismic energy through plastic deformation, while HSS members have to remain predominantly elastic, or with limited damage, being responsible for robustness of the structure. This principle applies both, for members and joint components. In case of moment resisting frames designed according to the strong column - weak beam philosophy, the columns are usually designed to remain predominantly elastic during earthquakes, while the beams have to be ductile. For welded beam-to-column joints, the main contributors for ductility are column web in shear and the beam end, while for extended end-plate bolted connection, beside the beam end and the column web, the end-plate in bending becomes very important.

Starting from the above considerations, a large experimental research program was carried out at the "Politehnica" University of Timisoara, CEMSIG Research Centre (<http://cemsig.ct.upt.ro>) in order to study the performance of dual-steel configuration for beam-to-column joints under monotonic and cyclic loading. When HSS is used in members designed to remain predominantly elastic, as columns, for instance, or in end-plates of bolted joints, T-stub components made of two steel grades are obtained. The aim of the testing program which is summarized hereafter was to investigate experimentally the performance of welded connections and bolted T-stub components realized from two different steel grades. Similar tests on T-stubs were realized by (Girao Coelho et al., 2004), but without cyclic loading and stiffener on the end-plate, and by (Piluso and Rizzano, 2007), which applied cyclic loading but no HSS components and stiffener on end-plate.

DESCRIPTION OF THE TESTING PROGRAM

The objective of the experimental program was to study the performance of welded and bolted end-plate beam to column joints realized from two different steel grades. The experimental program consisted in tests on materials, welded components, T-stub components, and beam to column joints. This paper describes only the investigations performed on materials, welded components and T-stub components. Tests on beam-column joints are presented in a companion paper (Dubina et al., 2008).

Standard tensile and Charpy V-notch toughness tests were performed in order to determine mechanical characteristics of base materials and welded material. Welded details (see Table 1) were considered in order to reproduce the welded connection between beam flange and column flange, as well as the one between the beam flange and end-plate. The web was always S235, while the end-plate was realized from S235, S460 and S690 steel grades. Both fillet welds and three types of full-penetration welds were used. Tests were performed under monotonic and pulsating cyclic loading. Tests on welded details were performed in order to validate the welding technology and to investigate performance of welded connections when realized from steel of different grades.

T-stubs are basic components of the design method used in EN 1993-1.8 (2003) for evaluation of strength and stiffness of bolted end-plate beam to column joints. Both

monotonic and alternating cyclic tests were performed on T-stub components obtained by welding S235 web plates to S235, S460 and S690 end-plates, using K beveled full-penetration welds (see Table 1). MAG welding was used, with G3Si1 (EN 440) electrodes for S235 to S235 welds, and ER 100S-G/AWS A5.28 (LNM Moniva) for S235 to S460 and S690 welds. Loading was applied in displacement control under tension and force control under compression. Compressive force was chosen so as to prevent buckling of the specimen. T-stubs were connected using M20 gr. 8.8 bolts. EN 1993-1.8 was used to obtain the design strength of T-stubs and failure modes. Thickness of end-plates was determined so that the unstiffened T-stub (type C) would fail in mode 1 (end-plate) and mode 2 (combined failure through end-plate bending and bolt fracture). The same end-plate thickness was then used for the stiffened T-stubs (type B and A), see Table 1 and Table 2. The testing program is summarized in Table 1.

Table 1. Summary of testing program

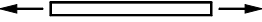
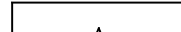
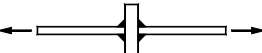
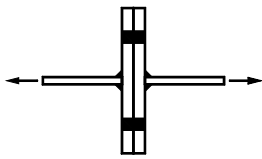
Test type	Scheme and steel grades	Test characteristics	No. of specimens	
			Per type	Total
Materials (MAT): Base and weld	 S235 S460 S690	monotonic quasi-static tensile tests	3	42
	 S235 S460 S690	Charpy V-notch toughness tests (-20°C)	3	42
Welded connections (SUD)	 web and stiffeners: S235, t = 15 mm end-plate: S235, t = 20 mm S460, t = 15 mm S690, t = 12 mm	weld type: - fillet weld - 1/2V bevel weld without root rewelding - 1/2V bevel weld with root rewelding - K bevel weld type of loading: - monotonic quasi-static - cyclic quasi-static	3	72
T-stub specimens (STUB)	 web and stiffeners: S235, t = 15 mm end-plate: S235, t = 12, 20 mm S460, t = 10, 15 mm S690, t = 8, 12 mm	type of T-stubs: from welded plates with K bevel weld type of loading: - monotonic quasi-static - cyclic quasi-static thickness of end plate corresponding to: - end-plate failure - mixed failure mode T-stub stiffening: - no stiffeners - T-stub with one stiffener - T-stub with two stiffeners	3	108

Table 2. T-stub characteristics

T-stub type	Label	Web	End-plate	Design failure mode
	TST-12A-S235	S235 t=15 mm	S235 t = 12 mm	2
	TST-20A-S235		S235 t = 20 mm	2 → 3
	TST-10A-S460		S460 t = 10 mm	2
	TST-16A-S460		S460 t = 16 mm	2 → 3
	TST-8A-S690		S690 t = 8 mm	2
	TST-12A-S690		S690 t = 12 mm	2 → 3
	TST-12B-S235	S235 t=15 mm	S235 t = 12 mm	2
	TST-20B-S235		S235 t = 20 mm	2 → 3
	TST-10B-S460		S460 t = 10 mm	2
	TST-16B-S460		S460 t = 16 mm	2 → 3
	TST-8B-S690		S690 t = 8 mm	2
	TST-12B-S690		S690 t = 12 mm	2 → 3
	TST-12C-S235	S235 t=15 mm	S235 t = 12 mm	1
	TST-20C-S235		S235 t = 20 mm	2
	TST-10C-S460		S460 t = 10 mm	1
	TST-16C-S460		S460 t = 16 mm	2
	TST-8C-S690		S690 t = 8 mm	1
	TST-12C-S690		S690 t = 12 mm	2

Note: failure mode 1 – end plate; mode 2 – end-plate and bolts; mode 3 – bolts.
→ denotes "close to"

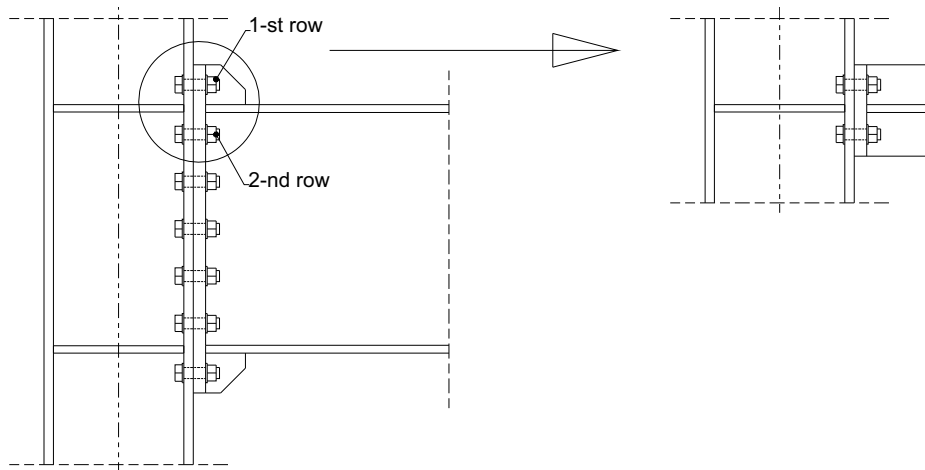


Figure 1. Assumption for A-type T-stub

A very important objective of T-stub tests was to confirm the assumption that the T-stub type A (see Table 2), corresponding to stiffened extended end-plate, which contains the first bolt row, can be calculated considering the contribution of stiffener as the one of "beam-web", and use the EN 1993-1.8 formula for second bolt row (see Figure 1).

TEST RESULTS

Materials

Flat materials used for T-stub and welds details were supplied by UNIONOCEL, Czech Republic. Table 3 shows the measured average values of yield stress f_y , tensile strength f_u and elongation at rupture A . It has to be recognized that the value of elongation for S460 is surprisingly large. Bolts were tested in tension as well, showing an average ultimate strength of 862.6 N/mm^2 .

Table 3. Material properties

Nominal steel grade	f_y , N/mm ²	f_u , N/mm ²	A , %	Actual steel grade
S235	266	414	38	S235
S460	458	545	25	S460
S690	831	859	13	S690

Weld details

Tests on weld details were performed in order to assess the performance of welds connecting different steel grades and to validate the welding technology. Weld preparation and the technology for $\frac{1}{2}$ V bevel weld, for instance, is shown in Figure 2. Sample of some weld experimental force-displacement are shown in Figure 3, while Figure 4 shows the state of strain in the area of the weld and the Heat Affected Zone (HAZ). In fact, since the weaker material was S235 in the "web", there are no significant differences in terms of steel grades of "end-plate". It has to be noticed that all the welds proved a very good behavior with failure at the end of HAZ or in vicinity, as expected. So, both the choice of welding materials and technology were confirmed. Pulsating cyclic loading did not affect much the response in comparison with monotonic loading.

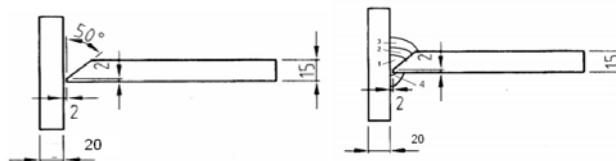
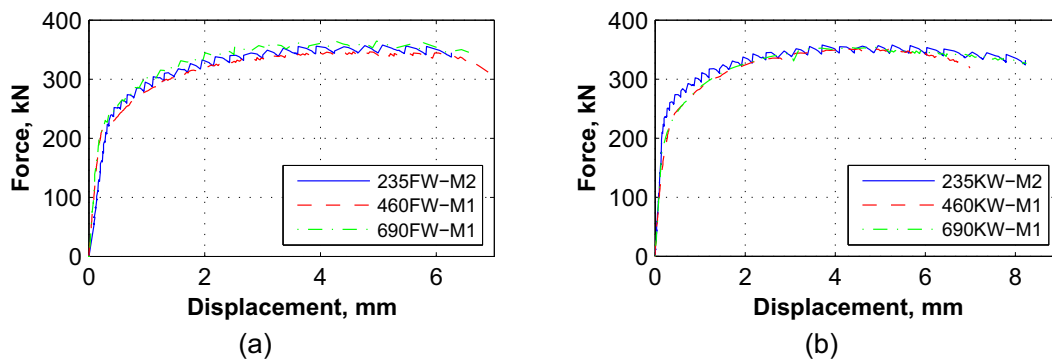


Figure 2. Welding technology



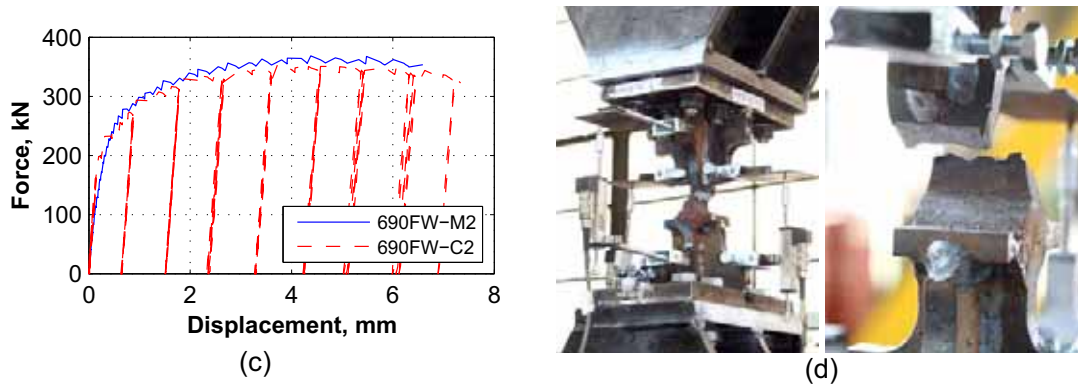


Figure 3. Test results on welded specimens: fillet welds (a); double bevel welds (b); monotonic vs. cyclic loading (c) and failure mode (d)

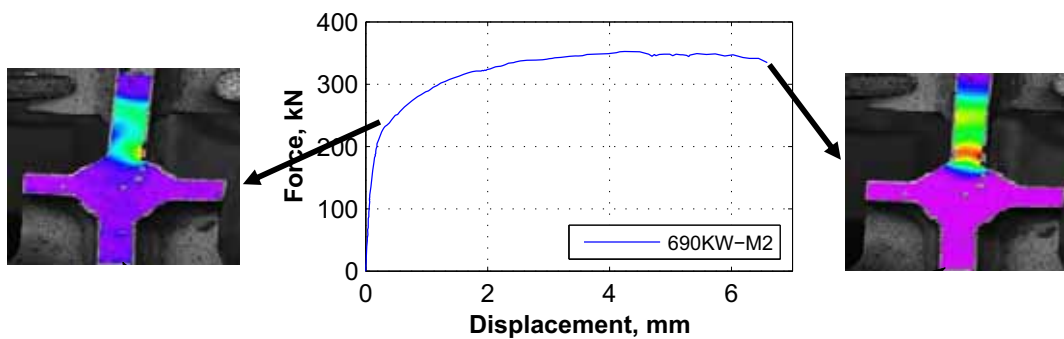


Figure 4. State of strain in welded specimens at yield and failure using digital image correlation technique

T-stubs

An overview of force-displacement relationships of T-stub specimens is presented in Table 4, while Figure 5 shows examples with observed failure modes. There were no significant differences between failure modes of monotonic and cyclic specimens, both generally agreeing with analytical predictions by EN 1993-1.8.



Figure 5. Examples of failure modes of T-stub specimens

For the T-stub specimens, the following parameters were determined for each experimental test: initial stiffness K_{ini} , maximum force F_{max} , yield force F_y , and ultimate deformation, D_y . The initial stiffness was obtained by fitting a linear polynomial to the force-displacement curve between 0 and 25% of the maximum force. The yield force was determined at the intersection of the initial stiffness and tangent stiffness line, where the tangent stiffness was obtained by fitting a linear polynomial to force-displacement curve between 75% and 100% of the maximum force. The ultimate deformation was determined as the displacement corresponding to a 10% drop of the maximum force (see Figure 6).

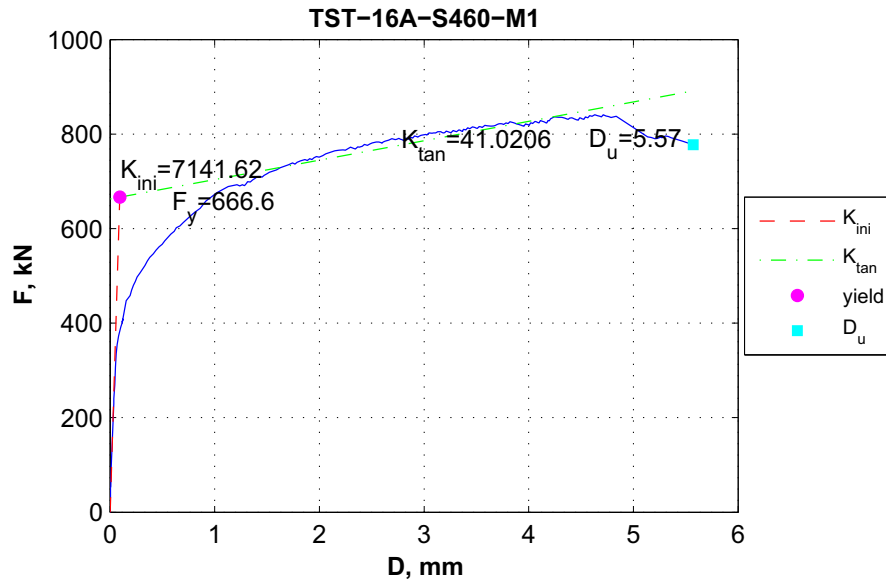


Figure 6. Experimental characteristics of T-stub specimens

Cyclic loading reduced the maximum force of the T-stub specimens, though the reduction was not significant. The ductility of the T-stub specimens was quantified through the ultimate displacement D_u . Under monotonic loading, ultimate displacement was smaller for specimens with thicker end-plates that failed in modes 2 and 3 involving bolt failure (see Figure 7a). Cyclic loading reduced significantly ultimate displacement of specimens with thinner end-plates that failed in mode 1. This behavior is attributed to low-cycle fatigue that generated cracks in the HAZ near the welds, along yield lines. On the other hand, cyclic loading did not affect much ultimate displacement for specimens with thicker end-plates that failed in modes 2 and 3, governed by bolt response. It is interesting to note that specimens realized from high-strength end plates (S460 and s690, with lower elongation at rupture), had a ductility comparable with the one of specimens realized from mild carbon steel (S235). The parameters governing the ductility of T-stubs were type of loading (monotonic / cyclic) and failure mode (end-plate or bolts).

A comparison between experimental and analytical results was made (Table 5 and Figure 7). Theoretical characteristics were evaluated by component method from EN1993-1.8. It may be remarked that, with some exceptions, the procedure from EN1993-1.8, including specimens of type A is confirmed; the exceptions can be covered by safety coefficients.

Table 4. Sample of results for T-stub specimens

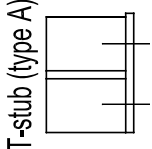
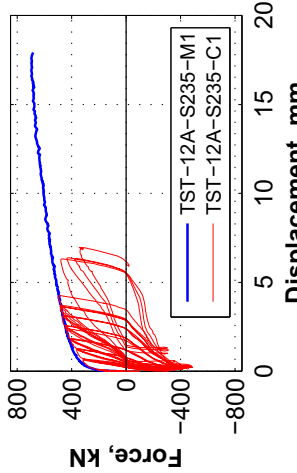
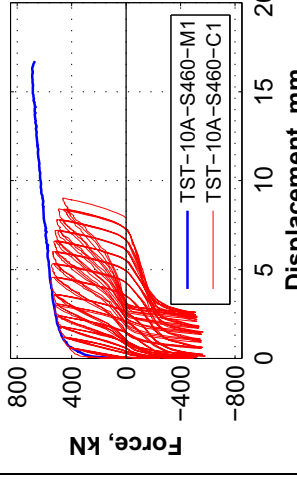
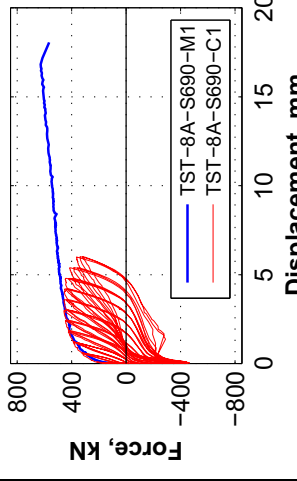
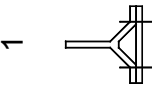
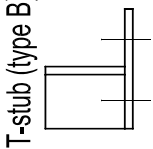
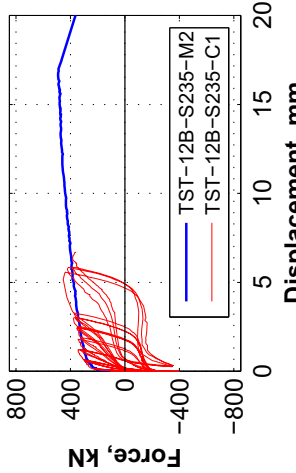
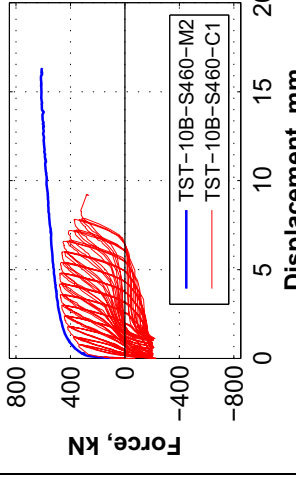
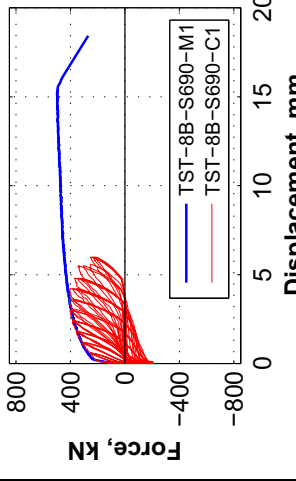
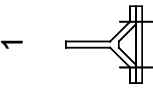
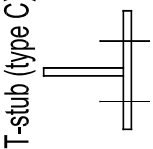
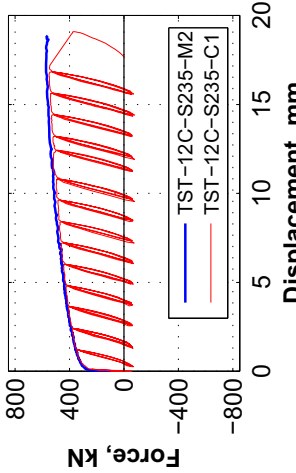
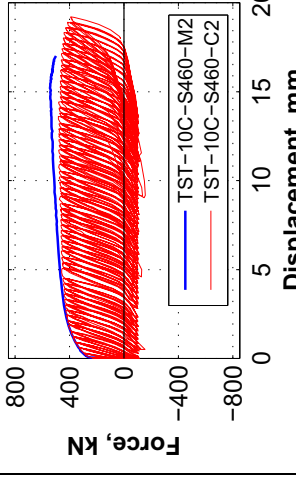
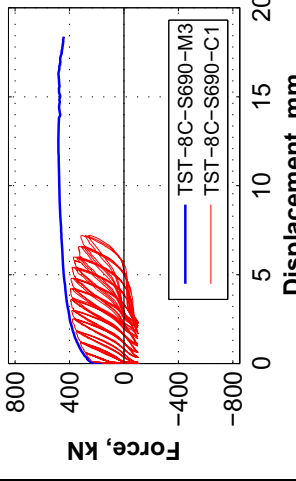
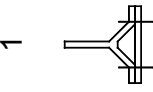
T-stub type	Force-displacement relationship for T-stubs with "thin" end-plates			Failure mode
 <p>T-stub (type A)</p>				 <p>1</p>
 <p>T-stub (type B)</p>				 <p>1</p>
 <p>T-stub (type C)</p>				 <p>1</p>

Table 4. (continued)

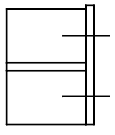
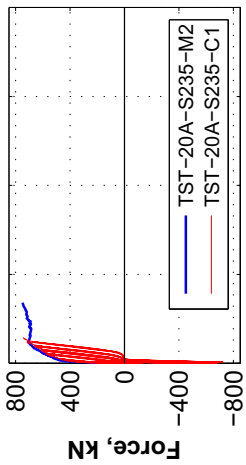
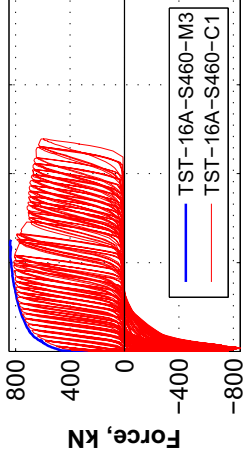
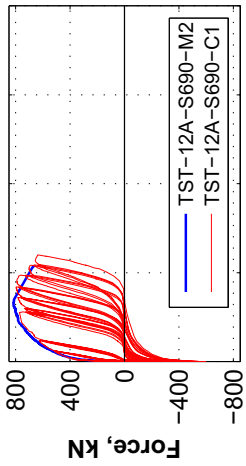
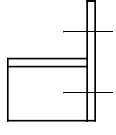
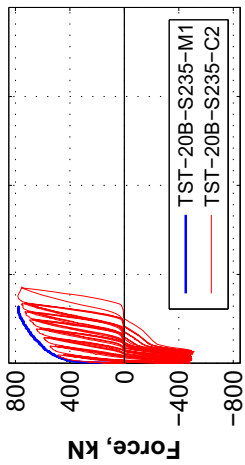
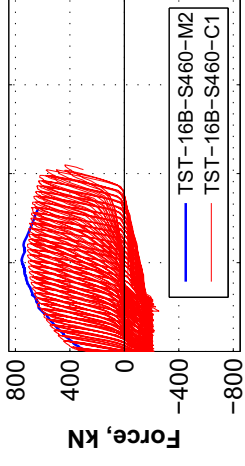
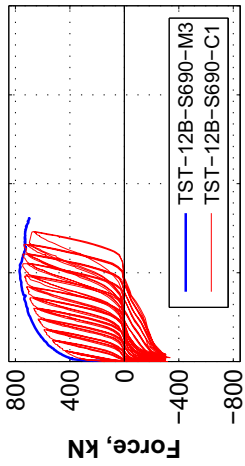
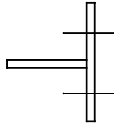
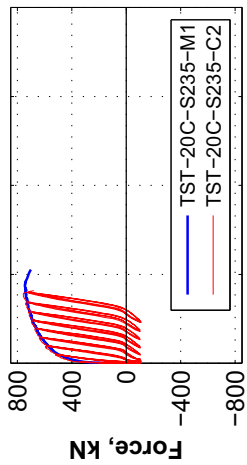
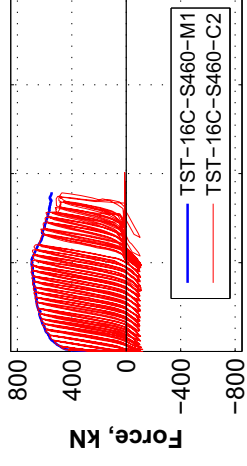
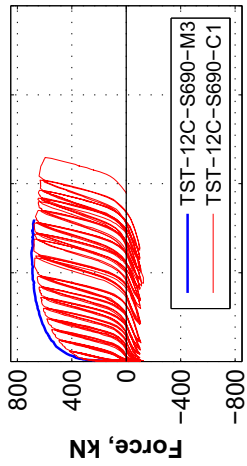
T-stub type	Force-displacement relationship for T-stubs with "thick" end-plates			Failure mode
T-stub (type A) 				3 
T-stub (type B) 				2 & 2→3 
T-stub (type C) 				2 

Table 5. Experimental (monotonic) and analytical T-stub characteristics

Specimen	$F_{y,exp,average}$ [kN]	$F_{y,EC3-1.8}$ [kN]	$F_{y,EC3}/F_{y,exp}$	$F_{max,exp}$ [kN]	$D_{u,exp}$ [mm]	$K_{ini,exp}$ [kN/mm ²]
TST-12A-S235	463.9	449.0	0.97	705.6	20.6	4709.4
TST-12B-S235	395.0	369.6	0.94	559.0	18.3	4097.9
TST-12C-S235	397.8	290.3	0.73	582.6	20.2	4352.2
TST-20A-S235	576.4	669.2	1.16	760.8	4.2	5312.4
TST-20B-S235	509.0	616.2	1.21	744.2	4.4	5561.8
TST-20C-S235	559.5	563.2	1.01	758.3	5.4	6737.8
TST-10A-S460	508.3	473.5	0.93	688.7	16.2	3703.6
TST-10B-S460	451.7	410.6	0.91	606.4	15.3	3063.3
TST-10C-S460	423.8	347.7	0.82	550.2	17.6	5916.5
TST-16A-S460	656.8	705.0	1.07	832.8	5.5	6242.1
TST-16B-S460	541.2	641.4	1.19	745.9	7.5	5114.8
TST-16C-S460	538.6	577.9	1.07	687.5	8.8	5436.1
TST-8A-S690	432.0	497.3	1.15	618.4	17.7	2756.1
TST-8B-S690	380.5	450.4	1.18	511.3	13.6	2392.7
TST-8C-S690	379.6	403.5	1.06	474.2	17.9	5262.6
TST-12A-S690	560.7	712.6	1.27	799.5	4.0	3005.0
TST-12B-S690	561.8	646.8	1.15	771.0	6.7	4431.4
TST-12C-S690	522.4	581.0	1.11	693.5	6.9	4756.2

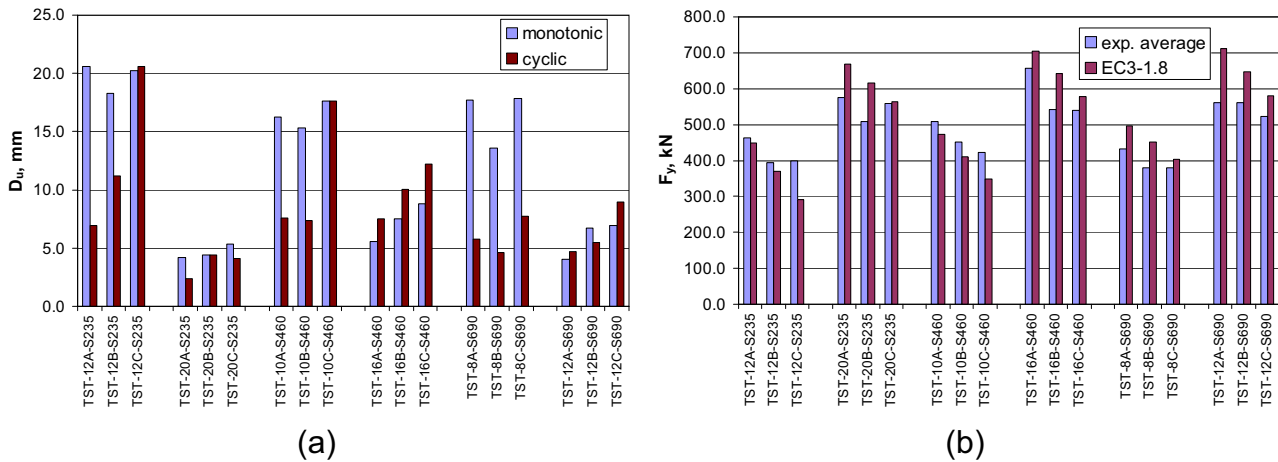


Figure 7. Ultimate displacement of T-stub specimens: monotonic vs. cyclic loading (a); and comparison of experimental (monotonic) and analytical values of yield force (b)

CONCLUSIONS

The objective of the experimental study on welded details and T-stubs described in this paper was to investigate performance of components in beam to column joints realized from mild and high strength steel grades.

Tests on welded details indicated that welds between components of different steel grades performed adequately under both monotonic and cyclic loading, for all types of welds (fillet, single bevel and double bevel).

The most important factor affecting the ductility of T-stub components under monotonic loading was the failure mode. Most ductile response was observed for components failing by end-plate bending (mode 1), while failure modes involving bolts (mode 2 and 3) were less ductile. The degree in which cyclic loading affected the ductility of T-stubs was, again, very much dependent on the failure mode. Specimens failing by end-plate bending (mode 1) were characterized by an important decrease of ductility with respect to monotonic loading, due to low-cycle fatigue. On the other hand, ductility of specimens involving bolt failure (modes 2 and 3) was not much affected by cyclic loading. Stiffening of Y-stubs increased their strength, but reduced slightly the ductility.

T-stubs with end-plates realized from high strength steel showed comparable strength with those realized from mild carbon steel. However, one remarks that thinner end plates realized from high strength steel, at the same strength, are provide equal or even larger ductility (due to failure in mode 1 or 2) than thicker mild carbon steel, even if elongation at rupture of high strength steel was lower than the one of mild carbon steel.

The EN1993-1.8 calculation procedure for T-stub components was in general confirmed by test results, even if the definition of experimental values for yield force still remains a matter of study. Moreover, the use for T-stub of type A, corresponding to the stiffened end-plate, of the same approach as for second bolt row was confirmed, consequently, it can be used to predict the strength and stiffness of bolted beam-to-column joints with stiffened extended end-plates. This confirmation is an important achievement of this research, because the connection of this type has been used for joint specimens, see companion paper (Dubina et al., 2008).

ACKNOWLEDGMENT

This research was supported by the contract no. 29/2005 "STOPRISC", funded by Romanian Ministry of Education and Research, within the frame of "Excellence Research" Program, CEEX – Matnatech.

REFERENCES

EN 1993-1.8. (2003), Design of steel structures. Part 1-8: Design of joints, *European standard*.

Dubina, D., Stratan, A. and Ciutina, A. (2005), "Components and Macro-Components of Rotation Capacity of Moment Connections" *20th CTA Congress Advances in Steel Constructions*, ACS ACAI, Milano, (pp. 417-426).

Dubina, D. and Dinu, F. (2007), "High strength steel for seismic resistant building frames", *6th Int. Conf. Steel and Aluminium Structures – ICSAS'07* (Ed. R. G. Beale), *Oxford Brooks Univ.* (pp. 133-140).

Dubina, D., Stratan, A. Dinu, F. (in print). "Dual high-strength steel eccentrically braced frames with removable links". *Earthquake Engineering & Structural Dynamics*, Published Online: 10 Jul 2008.

Dubina, D., Stratan, A. Muntean, N. and Dinu, F. (2008), "Experimental program for evaluation of Moment Beam-to-Column Joints of High Strength Steel Components", *ECCS/AISC Workshop: Connections in Steel Structures VI*, Chicago, Illinois, USA, June 23-25, 2008.

Girao Coelho, A.M. and Bijlaard, F.S.K. (2007), "Ductility of High performance Steel Moment Connections", *Advanced Steel Construction*, Vol.3, No.4, (pp.765-783).

Girao Coelho, A.M., Bijlaard, F.S.K., Gresnigt, N. and Simoes da Silva, L. (2004), "Experimental assessment of the behaviour of bolted T-stub connections made up of welded plates", *Journal of Constructional Steel Research* 60, (pp. 269-311).

Lu, L.W., Ricles, J.M., Mao, C. and Fisher, J.W. (2000), "Critical issues in achieving ductile behaviour of welded moment connections", *Journal of Constructional Steel Research*: 55, (pp. 325-341).

Piluso, V. and Rizzano, G. (2007), "Experimental analysis and modelling of bolted T-stubs under cyclic loads", *Journal of Constructional Steel Research*, doi:10.1016/j.jcsr.2007.12.009

NON-LINEAR DYNAMICAL BEHAVIOUR OF STEEL PORTAL FRAMES WITH SEMI-RIGID CONNECTIONS

Fernanda da R. de C. Lopes

State University of Rio de Janeiro, Rio de Janeiro, Brazil
fernanda.rcl@gmail.com

José Guilherme S. da Silva

State University of Rio de Janeiro, Rio de Janeiro, Brazil
jgss@uerj.br

Pedro C. G. da S. Vellasco

State University of Rio de Janeiro, Rio de Janeiro, Brazil
vellasco@uerj.br

Luciano R. O. de Lima

State University of Rio de Janeiro, Rio de Janeiro, Brazil
lucianolima@uerj.br

Sebastião A. L. de Andrade

State University of Rio de Janeiro, Rio de Janeiro, Brazil
seb.andrade@uol.com.br

ABSTRACT

This paper presents a semi-rigid low-rise portal frame non-linear dynamic analysis. One of the main objectives of this work is to propose a modelling strategy to properly represent the semi-rigid joint response under dynamic loads implemented on the ANSYS finite element software. The developed finite element model included the geometrical non-linearity and considered the influence of non-linear and hysteretic connections. The updated Lagrangean formulation was used to model the geometrical non-linearity. Another important investigated issue concerned the assessment of the structure dynamical behaviour due to the presence of symmetrical and non-symmetrical beam-to-column semi-rigid joints and, especially, the column base plates. The results indicated that the resonance physical phenomenon was not reached in the non-linear semi-rigid frames dynamic response. This fact was due to the hysteretic damping induced by the energy dissipation of the non-linear hysteretic loops associate to the modelled non-linear joints.

INTRODUCTION

Traditionally, the steel portal frame design assumes that beam-to-column connections are rigid or pinned. Rigid connections, where no relative rotations occur between the connected members, transfer not only a significant amount of bending moments, but also shear and axial forces. On the other extreme, pinned connections are characterized by almost free rotation movement between the connected elements that prevents the bending moment transmission. Despite these facts, it is largely recognized

that the great majority of joints does not exhibit such idealized behaviour. These connections are called semi-rigid, and their design should be performed according to their actual structural behaviour.

Extensive research has been performed over the past twenty-five years to estimate the actual behaviour of such joints. Numerous studies were made on composite and steel semi-rigid connections including: state of the art reports (Chen, et al., 1993), (Jaspar, 2000), numerical studies (Bursi and Jarpart, 1997), and experiments (Carvalho, et al., 1998), (Lima et al., 2002). The fundamental results of these investigations led to code specifications that provided structural designers with adequate procedures to evaluate the semi-rigid connections structural capacity. A good example of this new design trend is found in Eurocode 3 (Eurocode 3, 1997).

One of the main objectives of the present study is to propose a modelling strategy to properly represent the semi-rigid joint response under dynamic loads. Another important investigated issue concerned the assessment of the structure dynamical behaviour due to the presence of beam-to-column semi-rigid joints. The structural analysis was made with the aid of the Ansys (Ansys, 2005) finite element software. The adopted finite element model included the geometrical non-linearity and considered the semi-rigid connection dynamical response (Castro et al., 2006), (Silva et al., 2008).

Another issue that required an accurate dynamic analysis was related to the steel and composite structures design under dynamic actions. The safety factor concept for a static analysis may not be strictly applicable to dynamic situations since the resonance phenomenon may occur when the excitation frequency is equal or even close to the structure fundamental frequency. Since most of the structural steel connections are semi-rigid, the consideration of the non-linear and hysteretic joint stiffness proves to be significant for an accurate and balanced evaluation of steel and composite structures, (Silva et al., 2008).

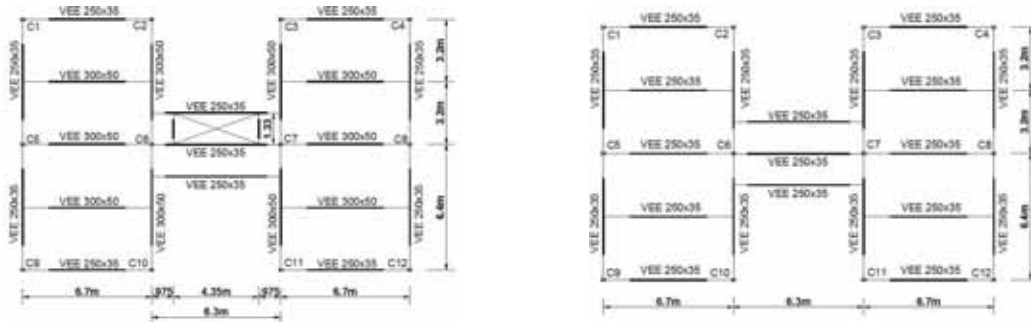
This paper presents the dynamical response of steel portal frames with semi-rigid connections simulated and analysed with plane frame models. The mathematical model calibration was made through comparisons with tests and other numerical models found in literature (Chui and Chen, 1996), (Nader and Astaneh, 1992). A detailed analysis of the investigated numerical simulation and experimental tests indicated that the hysteretic loops under repeated and reversed loading were very stable and repetitive. This fact indicated the use of static moment versus rotation curves in dynamic analysis producing accurate results.

However, it must be emphasized that cautions must be taken on the direct use of these results in structural design. This is due to the fact that when semi-rigid joints geometrical non-linearity effects are considered in the steel frames dynamical response some significant discrepancies in the frame dynamical behaviour could be observed.

STRUCTURAL MODEL

The steel building investigated in the present paper is based on low-cost residential buildings developed by Usiminas, a Brazilian Steel Mill (Usiminas, 2000), Fig. 1) The

building has a total of sixteen individual residential units. The building possesses three typical floors, a ground floor and a roof floor containing a water reservoir.



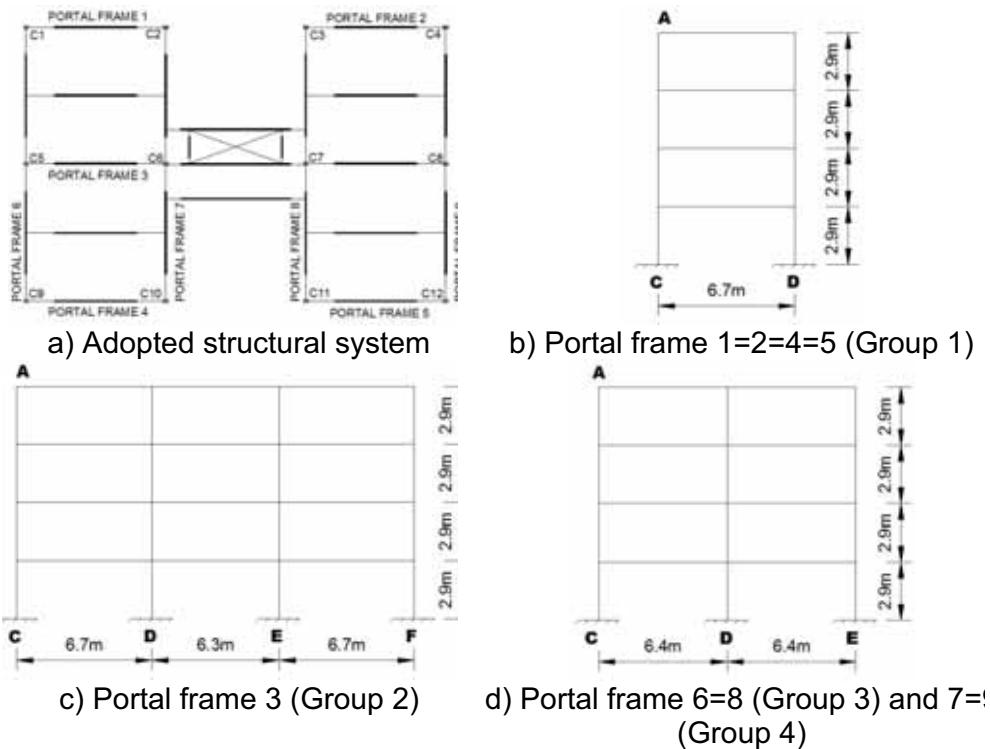
a) Typical framing plan.

b) Roof building floor plan.

Figure 1: Investigated structure.

The beams, spanning between 6.3m to 6.7m, are connected to columns or primary beams. The beam-to-column joints considered three possibilities: rigid, pinned and semi-rigid behaviour according to the adopted structural system. The beam-to-beam connections were considered pinned.

The wind loading is resisted by rigid, semi-continuous or braced portal frames. The column section disposition was adopted aiming to optimise the sway portal frame lateral resistance. Using this philosophy the adopted portal frame structures can have two, three or four columns, Fig. 2.



a) Adopted structural system

b) Portal frame 1=2=4=5 (Group 1)

c) Portal frame 3 (Group 2)

d) Portal frame 6=8 (Group 3) and 7=9 (Group 4)

Figure 2: Portal frame layout

A detailed description of the adopted beam and column steel sections is depicted in Table 1, , where h and b_f represent the section height and flange width while t_w and t_f are, respectively, the web and flange thicknesses.

Adopted Beam and Column Sections	h (mm)	t_w (mm)	t_f (mm)	b_f (mm)
VEE 250×35	250	4.75	9.50	175
VEE 300×50	300	4.75	12.5	200
C1=C2=C3=C4=C9=C10=C11=C12: CVS 300×57	300	8.0	12.5	200
C5=C6=C7=C8: CVS 350×136 (1 ⁰ and 2 ⁰ pavement)	350	16	25	250
C5=C6=C7=C8: CVS 350×73 (3 ⁰ and 4 ⁰ pavement)	350	9.5	12.5	250

Table 1: Detailed description of the adopted beams and columns steel sections.

FINITE ELEMENT MODEL

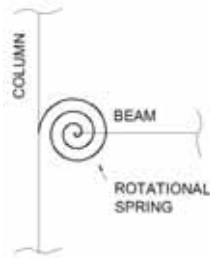
Finite element models were developed to simulate the structural behaviour of steel portal frames with semi-rigid connections. Geometrical non-linearities were incorporated in the finite element model aiming to simulate, as accurately as possible, the dynamical behaviour. In the present investigation the following basic assumptions were considered:

- The cross sections remain plane after deformation (Bernoulli's hypothesis).
- Warping and cross section distortion were not considered.
- Small strains but arbitrarily large displacements and rotations were considered.
- The material was assumed to remain elastic throughout the analysis.
- The connection stiffness can be approximated by mathematical function.
- The connection element length is equal to zero.

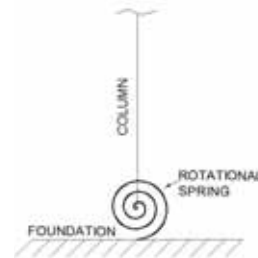
The beam-to-column and base plates joints models

A non-linear rotational spring, Fig. 3, was used to accurately simulate the dynamical response of the steel frames with semi-rigid connections. This element incorporated second order effects (geometrical non-linearities), associated to the beam-to-column and to the base plate joints moment *versus* rotation curve, and also included the non-linear and hysteretic connection stiffness. The updated Lagrangean formulation was used to model the geometrical non-linearity.

The adopted moment versus rotation curve for the symmetric and non-symmetric beam-to-column connections were experimentally obtained by Carvalho et al. (Carvalho et al., 1998). The moment versus rotation curve used in base plate connections was proposed by Kontoleon et al. (Kontoleon et al., 1999), obtained through parametric analysis of semi-rigid steel base plate connection, Fig. 4. The base plate model response depends on the steel column axial load (N) magnitude, Fig. 4.

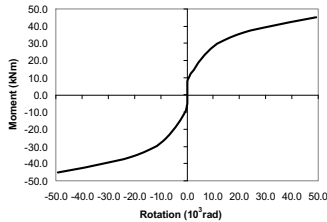


a) Beam-to-column joint connection

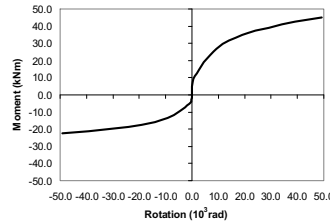


b) Base plate joint connection

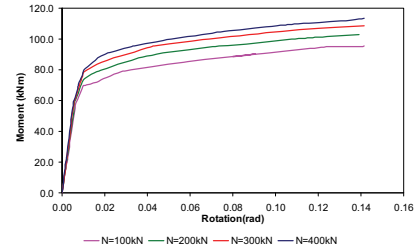
Figure 3: Rotational spring element adopted in the computational model.



(a) Symmetric beam-to-column connection



(b) Non-symmetric beam-to-column connection



(c) Base plate connection

Figure 4: Moment versus rotation curves for the joints connections

The Chan & Chui (Chan and Chui, 1996) algorithm was used to simulate the joints hysteretic behaviour where the moment transmitted by the joints can be determined from their associate moment versus rotation curve. If at any time the structure is unloaded, the adopted compressive moment versus rotation curve is a straight line parallel to the tension curve initial stiffness. If in subsequent steps further loads are applied to the structure the joint moments can also be determined by their associated moment versus rotation curve, see Fig. 5..

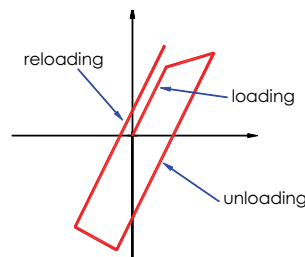


Figure 5: Adopted hysteretic model.

NATURAL FREQUENCIES AND MODE VIBRATIONS

The investigated frames were divided into four groups, Fig. 2. The steel frames natural frequencies and associated mode shapes were obtained based on an eigenvalue analysis. Table 2 presents the structure natural frequencies based on the beam to column and base plate curves presented in Fig. 4. Figure 6 illustrates the modes shapes related to the three natural frequencies of the first portal frame group, Fig. 2. that adopted semi-rigid base plate connections.

It is important to observe that since the eigenvalue analysis does not consider any nonlinearity, the natural frequencies obtained for the models with symmetrical connections are identical to those obtained using non-symmetrical connections. Therefore, Table 2 only presents the natural frequencies obtained for the models with symmetrical connections.

Frequencies	Frame Groups with Semi-Rigid Base Plates				Frame Groups with Rigid Base Plates			
	1	2	3	4	1	2	3	4
f_{01} (Hz)	3.18	2.62	2.93	2.97	3.81	2.97	3.72	3.77
f_{02} (Hz)	12.72	8.27	10.34	10.58	14.21	9.74	13.09	14.48
f_{03} (Hz)	27.86	16.73	24.21	25.82	30.16	18.82	25.60	26.43

Table 2: Investigated frame groups natural frequencies.

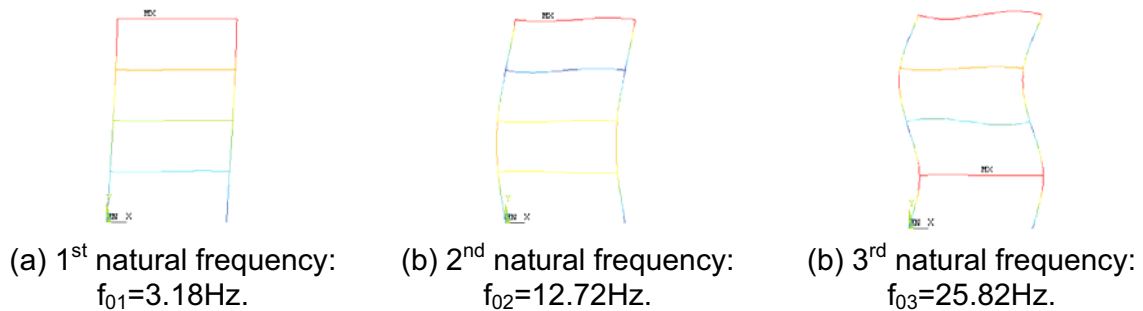


Figure 6: Modes shapes. First portal frame group with semi-rigid base plate.

It could also be observed that the sway frames with semi-rigid plate bases presented lower natural frequencies when compared to their equivalent sway frames with rigid supports, as presented in Table 2. This affirmative demonstrates the coherence of the computational model since the adopted rigid supports increase the global structural stiffness.

The results illustrated in Table 2 indicate that a variation of the natural frequency values, especially in terms of the fundamental frequency, f_{01} , occurred when the sway frames with semi-rigid plate bases and rigid support cases were considered. This frequency variation ranged from 10% up to 30%, when the sway frames fundamental frequency was considered.

NON-LINEAR DYNAMIC ANALYSIS

The sway frames structural response was obtained based on a non-linear dynamic analysis where second order effects (geometric non-linearity) were considered. The modifications on the steel frame dynamical response were investigated to access the influence of the joint non-linearities. The steel frame groups, see Fig. 2, were submitted to the loads indicated in Fig. 7 to Fig. 10 and in Table 3 and Table 4.

Group 1	Group 2
---------	---------

Permanent load	G1	G2	G3	G4	G5	G6
	7.00	12.28	11.40	3.63	22.96	7.05
Live load	Q1	Q2	Q3	Q4	Q5	Q6
	0.80	2.40	1.60	0.70	4.80	4.60
Wind load	W1		W2		W3	
	2,78		5,67		11,34	
G and Q in kN/m and P and W in kN.						

Table 3: Portal frames loads related to the first and second groups.

Permanent load	Group 3				Group 4					
	G7	G8	P _{G1}	P _{G2}	G9	G10	P _{G3}	P _{G4}	P _{G5}	P _{G6}
	2.50	3.75	38.19	48.24	2.50	3.75	38.19	13.61	48.24	20.48
Live load	Q7	Q8	P _{Q1}	P _{Q2}	Q9	Q10	P _{Q3}	P _{Q4}	P _{Q5}	P _{Q6}
	0.00	0.00	5.36	16.08	0.00	0.00	5.36	1.10	16.08	12.60
Wind load	W5	W6	W7	W8	W9	W10	W11	W12		
	2.33	0.63	4.66	1.26	4.52	1.23	9.05	2.45		
G and Q in kN/m and P and W in kN.										

Table 4: Portal frames loads related to the third and fourth groups.

The permanent and variable vertical loads were considered static. The wind effects (horizontal effects) were simulated as a deterministic sinusoidal function represented by: $F(t) = F_0 \sin(\omega t)$. The harmonic amplitude, F_0 , was associated to the wind effects and assumed the following values (Lopes, 2008): W1 and W2 (first group frames); W3 and W4 (second group frames); W5, W6, W7 and W8 (third group frames), W9, W10, W11 and W12 (fourth group frames), Fig. 7 to Fig. 10.

The excitation frequency, ω , was made equal to each frame group fundamental frequency, respectively, simulating a resonance situation (Silva et al., 2008). The current investigation, adopted a 10^{-5} s ($\Delta t=10^{-5}$ s) time step. The joint non-linearity (symmetric and non-symmetric connections) and the hysteretic effect present in the beam-to-column and base plate non-linear joint were considered throughout the analysis. The Newmark algorithm (Newmark, 1959) was used to evaluate the sway frames dynamic response.

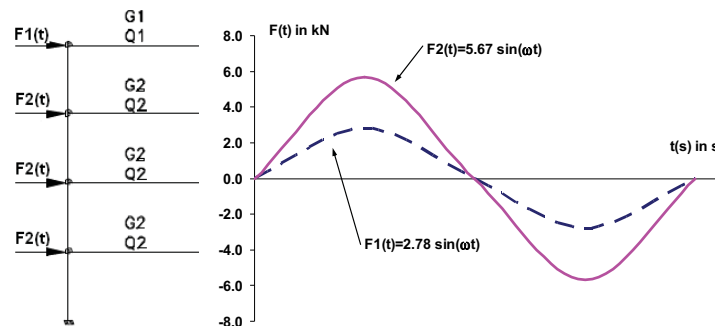


Figure 7: First frame group acting loads.

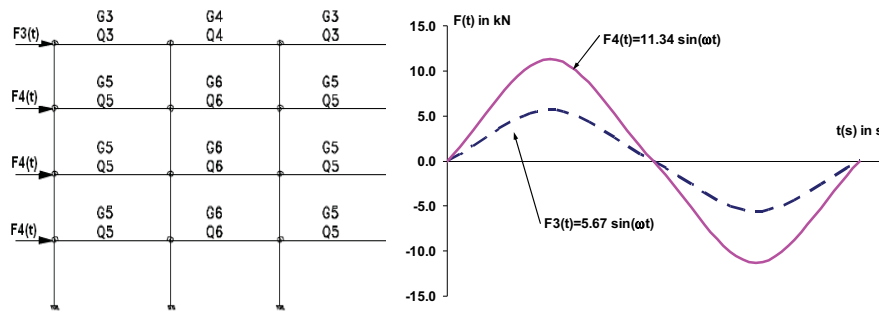


Figure 8: Second frame group acting loads.

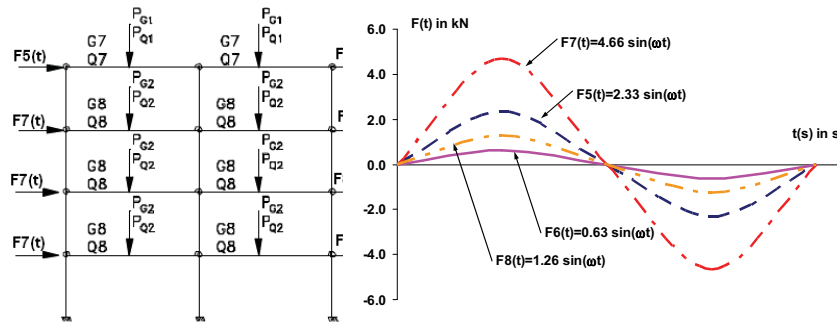


Figure 9: Third frame group acting loads.

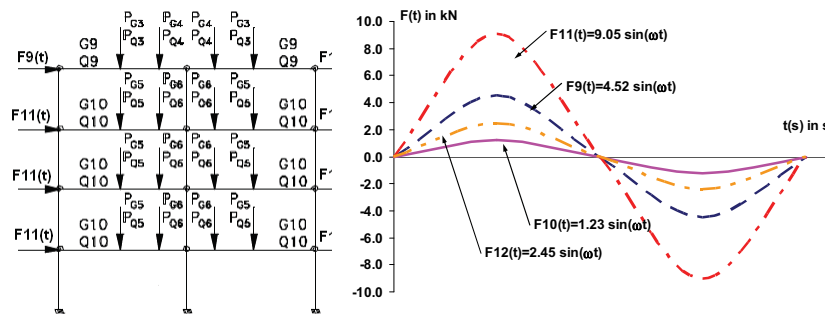


Figure 10: fourth frame group acting loads.

Figure 11 presents the first frame group (portal frame 1=2=4=5) dynamic response based on the horizontal displacements amplification factor at point A, see Fig. 2. Two cases were considered: symmetric and non-symmetric beam-to-column connections. Semi-rigid and rigid base plates were considered on the analysed sway frames. The first frame group (portal frame 1=2=4=5) was chosen to illustrate the structural models dynamic response because it typically represents the whole set of the investigated structural solutions.

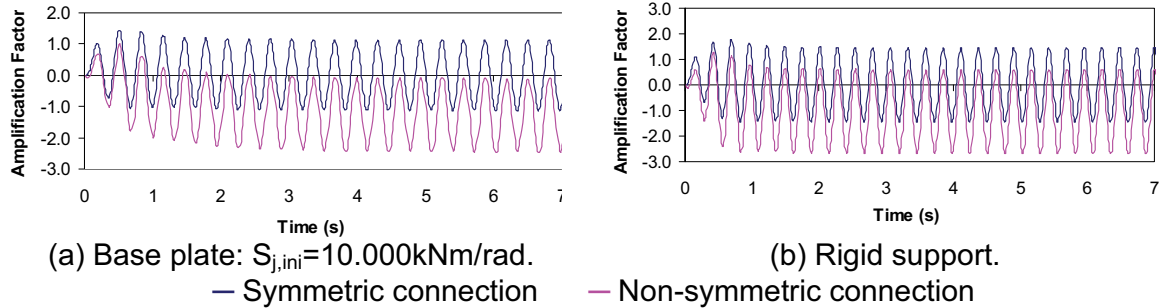


Figure 11: Horizontal displacements amplification factor at point A. Portal frame 1=2=4=5 (First group). Non-linear dynamic analysis.

The resonance physical phenomenon occurs when the excitation frequency was equal (or near) the structure fundamental frequency. This investigation indicated that, for the non-linear semi-rigid joints, the resonance phenomenon did not occurred when the geometrical non-linearity (second order effects), joint non-linearity (non-linear rotational spring element) and the joints hysteretic behaviour were considered, as illustrated in Fig. 11. However, this behaviour is completely different when a first order linear elastic analysis is adopted, as it can be observed in Fig. 12.

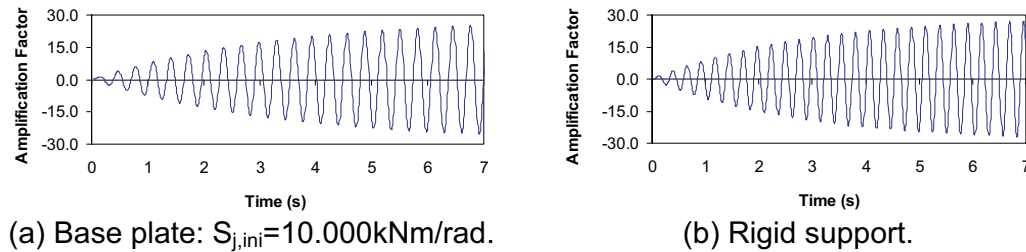


Figure 12: Horizontal displacements amplification factor at point A. Portal frame 1=2=4=5 (First group). Linear dynamic analysis.

It was also noted that the connection behaviour had significant influence on the sway frames dynamic response. It could be observed that the portal frames dynamic response with symmetric connections were very different from those when non-symmetric connections were considered. This difference occurred because the non-symmetric connections have a very different moment versus rotation curve (compression behaviour), as presented in Fig. 4.

Due to this issue the damping induced by the energy dissipation of the non-linear hysteretic loops at the non-linear joints, caused by the hysteretic effects, was completely different at each investigated situation (symmetric and non-symmetric connections), modifying the structural model dynamic response, see Fig. 11.

Considering that the column base plates and beam-to-column joints plays a fundamental role in the steel frames design, the presented results emphasise the importance of considering the geometrical non-linearity and the joints hysteretic behaviour in structural design of this particular type of structure.

FINAL REMARKS

This investigation indicated that dynamic response (linear and non-linear) of the analysed steel portal frames was significantly affected by the structural behaviour of their structural element joints. Base plates and beam-to-column joints play a major role in internal force distribution, as well as in lateral displacement magnitude of these particular structural systems.

This paper was focused on the evaluation of steel portal frames dynamic response. This task was performed by a developed numerical model capable to adequately simulate the column base plates and beam-to-column joint (pinned, semi-rigid and rigid) effects.

This computational model was centred on the use of a rotational spring non-linear element to properly represent the column base plates and semi-rigid connections behaviour. The proposed analysis methodology, for the structural system dynamic analysis, considered the non-linearity effects associated to the frame geometry (second order effects), column base plates and beam-to-column joints (non-linear rotational spring element), as well as the joint hysteretic response.

The results indicated that the resonance physical phenomenon was not reached in the non-linear semi-rigid frames dynamic response. The resonance does not occur in these systems due to the hysteretic damping induced by the energy dissipation of the non-linear hysteretic loops at the non-linear joints. It was also concluded that the hysteretic damping could not be observed in simple linear stiffness joint models emphasizing the important damping character developed in non-linear hysteretic joints.

REFERENCES

- ANSYS (2005), Swanson Analysis Systems, Inc., P.O. Box 65, Johnson Road, Houston, PA, 15342-0065, Version 10.0, Basic analysis procedures, 2nd edition.
- Bursi O. S., Jaspart J. P. (1997), "Benchmarks for finite element modelling of bolted steel connections", *Journal of Constructional Steel Research*; Vol. 43 (pp. 17–42).
- Carvalho, L. C. V. de, Andrade, S. A. L. de, Vellasco, P. C. G. da S. (1998), "Experimental analysis of bolted semi-rigid connections", *Journal of Constructional Steel Research*; Vol. 46 (pp. 1-3).
- Castro, R. A. de, Silva, J. G. S. da; Vellasco, P. C. G. da S., Andrade, S. A. L. de, Lima, L. R. O. de, Neves, L. F. da C. (2006), "Non-Linear Dynamical Response of Steel Portal Frames with Semi-Rigid Connections", 3rd European Conference on Computation Solid and Structural Mechanics - ECOMAS, Lisbon.
- Chen, W. F., Lorens, R. F. and Kato, B. (1993), *Semi-Rigid. Connections in Steel Frames*. McGraw-Hill, Inc., Tokyo.

Chui, P. P. T., Chan S. L. (1996), "Transient Response of Moment-Resistant Steel Frames with Flexible and Hysteretic Joints". *Journal of Constructional Steel Research*, Vol. 39 (pp. 221-243).

European Committee for Standardisation, Eurocode 3, ENV-1993-1-1, Revised Annex J (1997), "Design of Steel Structures", Doc. CEN/TC250/SC3-N419E.

Jaspart, J. P. (2000), "General Report: Session on Connections". *Journal of Constructional Steel Research*, Vol. 55 (pp. 69-89).

Kontoleon, M. J., Mistakidis, E. S., Baniotopoulos, C. C., Panagiotopoulos, P. D. (1999), "Parametric analysis of the structural response of steel base plate connections", *Computers and Structures*, Vol. 71(pp. 87-103).

Lima, L. R. O. de, Vellasco, P. C. G. da S., Andrade, S. A. L. de, Silva, L. A. P. S. da (2002), "Experimental and mechanical model for predicting the behaviour of minor axis beam-to-column semi-rigid joints", *International Journal of Mechanical Sciences*; Vol. 44 (pp. 1047-1065).

Lopes, F. da R. de C. (2008), "Influência do Comportamento Semi-Rígido de Placas de Base e de Ligações Viga-Coluna na Resposta Dinâmica de Pórticos de Aço", MSc Dissertation (In Portuguese), Post-graduate Programme in Civil Engineering, State University of Rio de Janeiro, UERJ, Rio de Janeiro, Brazil.

Nader, M. N., Astaneh, A. (1991), "Dynamic behaviour of flexible, semi-rigid and rigid steel frames", *Journal of Constructional Steel Research*; Vol. 18 (pp. 179-192).

Newmark, N. M., "A Method of Computation for Structural Dynamics", ASCE, *Journal of Mechanical Division*, Vol. 85, 1959.

Silva, J. G. S. da, Lima, L. R. O. de, Vellasco, P. C. G. da S., Andrade, S. A. L. de, Castro, R. A. de (2008), "Nonlinear Dynamic Analysis of Steel Portal Frames with Semi-Rigid Connections". *Engineering Structures*, Vol. 30 (Paper accepted for publication in 20 February 2008).

USIMINAS, "Usiteto - Solução Usiminas Para Habitação Popular", 2000, (In Portuguese).

CONNECTIONS WITH IMPROVED FIRE RESISTANCE

František Wald, Jiří Chlouba, Zdeněk Sokol, Petra Kallerová
Czech Technical University, Praha, Czech Republic
wald@fsv.cvut.cz

ABSTRACT

To study global structural and thermal behaviour, a research project was conducted on a three storey steel frame building at Mittal Steel Ostrava before demolition. The main goal of the experiment was to verify the prediction method of the joint temperature and to improve it during the cooling phase. The fire compartment of floor area of 24 m² was built at the second floor. The fire load was 140 kg/m² of wood and the ventilation was delimited by an opening of 1400 x 1970 mm. This paper summarises the experimental programme and presents the time-temperature curves of the development of fire in the fire compartment and in the primary and secondary beams and its header plate connections. Comparisons are also made between the test results and the temperatures predicted by the structural Eurocodes.

INTRODUCTION

The tests of separate structural elements, e.g. beams, columns and joints in furnaces helped to prepare the prediction design models of elements, see (Buchanan, 2003). The behaviour of the whole structure under a natural fire may be evaluated during the natural fire only. The knowledge related to the structural integrity depends on element stiffness, resistance and deformation capacity of elements and connections. The main aim of the fire test in Mittal Steel Ostrava was to learn more about the connection temperatures and the internal forces into structure. The behaviour of restrained beams during compartment fire at elevated temperatures, the heating of external element as well as column during local fire and the temperature of sandwich panels, light timber based panels and timber concrete element was studied under the heating by natural fire as well.

Simplified design of structure in fire is based on the design of structure at ambient temperature. The advanced design takes into account the structure loaded by a temperature fire curve and the joints are exposed to forces caused by the elongation during the warming and by the contraction during the cooling phase as well. In this field is the knowledge limited to a few experiments on real structures, e.g. Cardington experiment (Moore and Lennon, 1997). During the fire situation, the temperature development in the joint is different from the temperature development in the adjacent members. The temperature in the joint increases slower than the temperature in the attached members and during the cooling phase is the temperature higher than in the adjacent members. The highest temperature reached in the joint is lower than the highest temperature of the gas. This is caused by the mass concentration in the joint, see (Wald et al., 2006).

The standard for fire safety of steel structures EN 1993-1-2:2005 for joints recommends usage of the same fire protection for joints as for the adjacent structure. Alternatively it provides the prediction of the temperature distribution within the connection, the reduction of the material properties of connectors by elevated temperature, and the analysis of the structure using the component method (Spyrou et al., 2002).

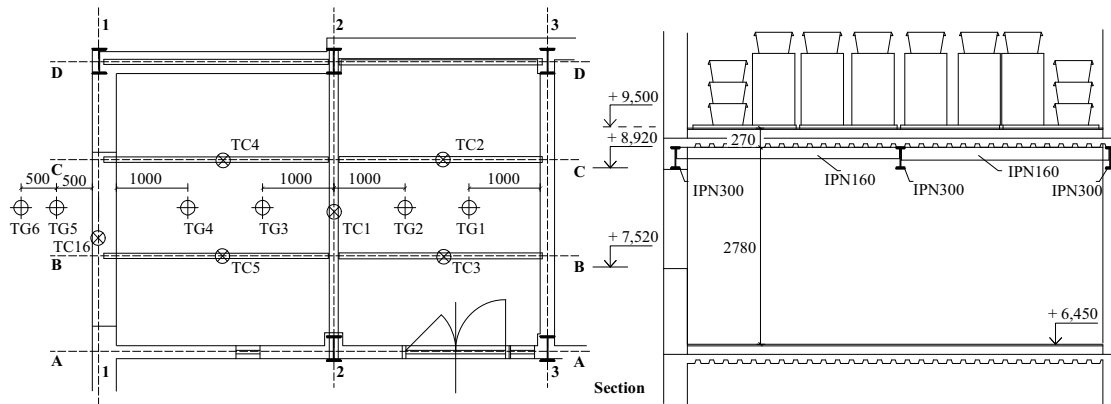


Fig. 1 - The position of the thermocouples for recording of gas and beams temperatures.

A local fire test was performed on June 15, 2006 and a compartment fire test on June 16 on structure of Ammoniac Separator II in company Mittal Steel Ostrava, see (Kallerová and Wald, 2006). The structure was composed of three storey steel structure with the composite slabs, steel beams of hot rolled sections IPN160, IPN180 and IPN300, the beam-to-beam and beam-to-column header plate connections, and the diagonal wind bracings. Internal size of fire compartment was designed 3.80 x 5.95 m with height of 2.78 m, see Fig. 1. The structure of enclosure was made from the light silicate and ceramic bricks. Opening of 2400 x 1400 mm ventilated the room during the fire. The doors of fire compartment 1400 x 1970 mm and columns were equipped by the fire isolation by boards. The mechanical load on the floor above the fire compartment was composed of the dead and life load. The life load was simulated by about 1 m of water, which was placed into 26 steel barrels and 50 plastic boxes equally distributed on the floor. One box was stored on each barrel and the rest of boxes placed at the ends of floor. The barrels and boxes were thermo-isolated from the floor by 50 mm of a miner wall and placed on the pallets.

Fire load was represented by the unwrought timber bars 50 x 50 mm of length 1 m from softwood with moisture till 13%. For the compartment fire were the bars placed into eight piles. A pile consists of 13 rows with ten bars each plus two bars on the top, which means 132 bars per pile. The simultaneous ignition of piles was reached by its connection by the steel thin walled channels filled by a mineral wall and penetrated by paraffin. The channels located in the second layer of bars connected by four piles.

The gas temperature in the fire compartment was measured by four thermocouples 300 mm below ceiling, marked at Fig. 1 as TG_i. Two thermocouples were placed in front of the fire compartment 0.5 m and 1 m from front wall. On steel were located

sixth thermocouples, and on joints next seven, in Fig. 2 marked as TCi. The position of thermocouples on the lower flange of beams at their mid span is documented on Fig. 1. Two thermo imagine cameras and seven video cameras scanned the experiment. Two video cameras were installed behind thermo resistant glass in the additionally prepared windows into the compartment internal wall.

The comparison of the development of the gas temperatures show, that at the beginning of the fire, till 30 min about, was warmer the gas in the front part of the compartment of about 200 °C, TG3 and TG4. During the full developed fire, after 30 min, were the highest temperatures recorded in the back of the fire compartment, max 1050 °C, TG1 and TG2. In the front part was measured only 920 °C. The beam lower flange temperatures correspond to the beam positions in the fire compartment. The front beam, TC16, reached maximum temperature of its lower flange of 775 °C compared to the secondary beam in the back of the fire compartment with the measured maximal 970 °C, TC2.

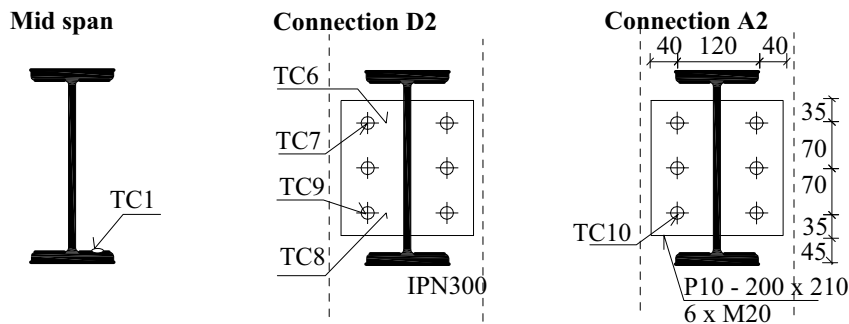


Fig. 2 - Position of the thermocouples on the header plate connections.

CONNECTION TEMPERATURES

For the temperature development in the connection, there are predicted two analytical methods, see (EN 1993-1-2:2005). In the step by step method is the temperature calculated as element, where the heat is brought in/brought out by the member surface and the member volume is heated/cooled.

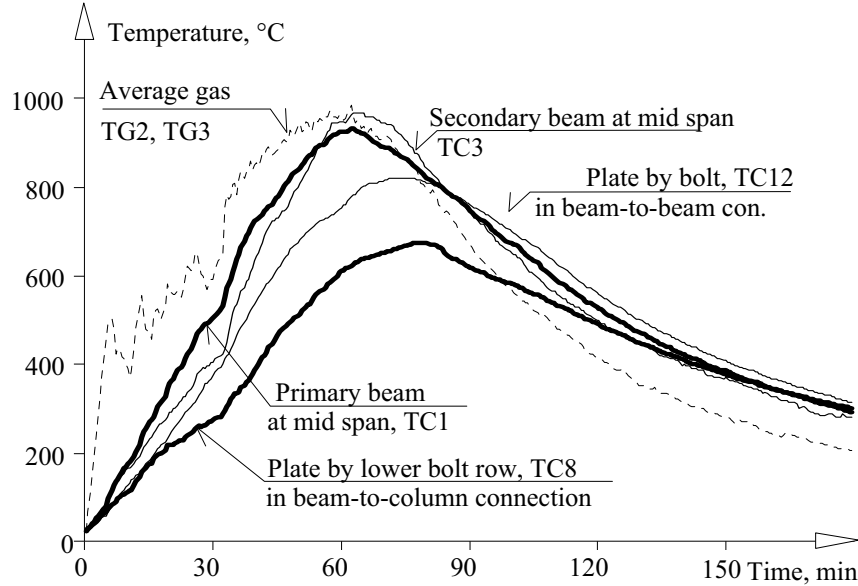


Fig. 3 - Comparison of the measured temperatures on the header plate connection to the gas and beam mid span temperatures.

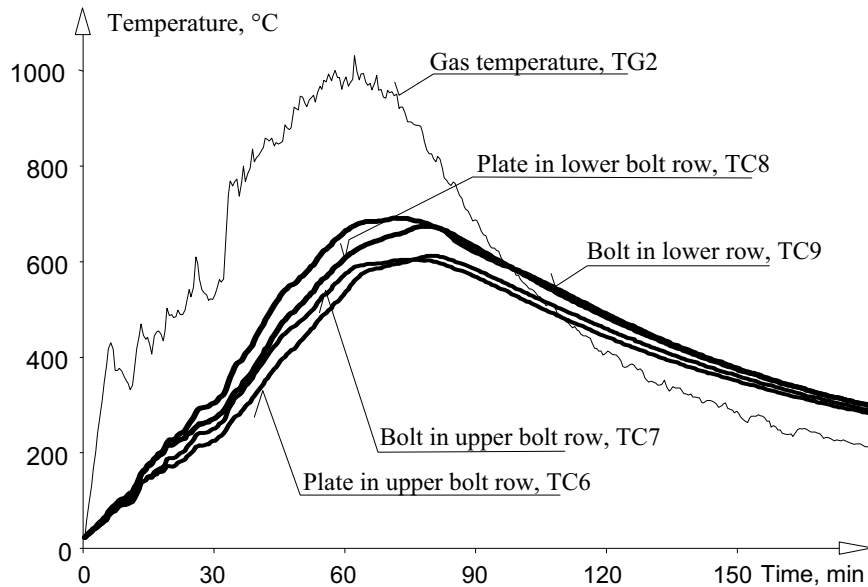


Fig. 4 - Measured temperatures over the height of beam-to-column header plate connection.

Geometrical characteristic of the section is the section factor A_m/V of the steel parts of which the joint is composed. The section factor indicates the relation between the surface area of the connection A_m per unit of length exposed to the fire and the

volume of the connection V per unit length which is being heated. The temperature of the unprotected inner steel structure is given by

$$\Delta\theta_{a,t} = k_{sh} \frac{A_m/V}{c_a \rho_a} \dot{h}_{net} \Delta t \quad (1)$$

where A_m/V is the section factor in m^{-1} , c_a the specific heat depending on the temperature in $J\ kg^{-1}K^{-1}$, ρ_a the volume weight of steel in $kg\ m^{-3}$, \dot{h}_{net} the design value of the net heat flux per unit area in $W\ m^{-2}$, Δt the time increment in s, and k_{sh} the correction factor for the shadow effect which is used by the heating using the nominal fire curve. The temperature of a joint may be assessed using the local section factor A_m/V , the value of the parts forming the joint. As simplification, it is possible to consider uniform temperature distribution within the section and to take into account the biggest A_m/V value of the steel parts connected into the joint.

The temperature of either beam-to-beam or beam-to-column connection covered with a concrete slab can be determined from the temperature of the beam flange in the middle of the span. It is assumed, that the temperature of the particular parts of the connection depends directly only on the distance Δ from the lower edge of the connected beam and indirectly on the prediction of the temperature of the lower flange calculated usually by the step by step procedure. If the height of the beam is smaller or equal to 400 mm ($h_k \leq 400\ mm$), the temperature is given by

$$\theta_h = 0,88 \theta_0 [1 - 0,3 (h_k / h)] \quad (2)$$

where θ_h is the temperature in the height h_k of the beam, θ_0 is the lower flange temperature in the mid span and h is the overall beam height.

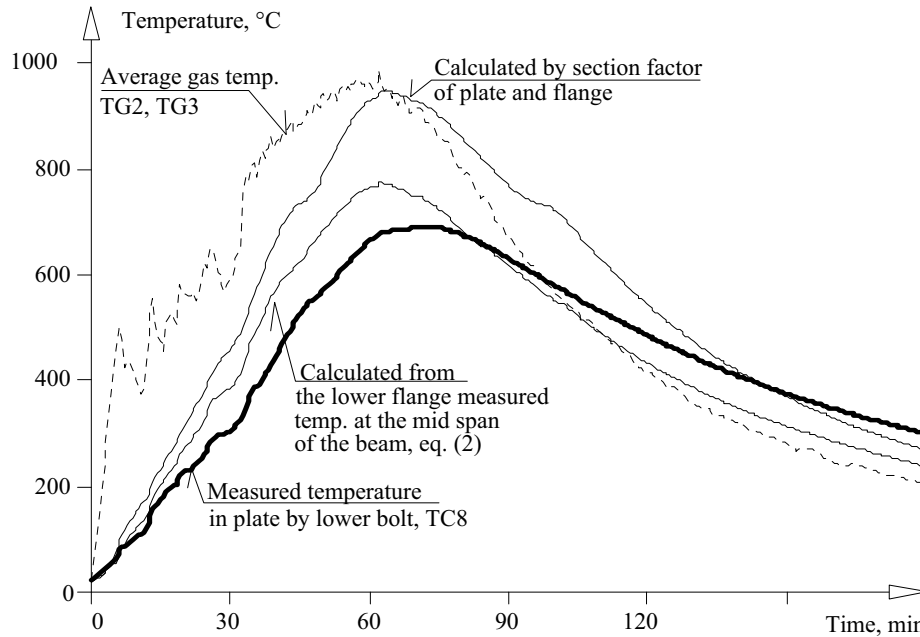


Fig. 5 - Comparison of the predicted temperatures from gas temperature to measured temperatures at the beam to column connection.

The temperature of the beam-to-column connection was calculated from the measured temperature of the beam's lower flange in the mid span, see Fig. 5 according to eq. (2). The highest temperature is conservative but in the cooling phase is the predicted temperature lower than the actually measured. By applying the section factor, the highest value of section factors of the connected members may be taken into account, e.g. $A_m/V = 138 \text{ m}^{-1}$, and the results are conservative for the maximum temperature. If the section factor of the head plate is considered, e.g. $A_m/V = 105 \text{ m}^{-1}$ only, the results are less conservative. The difference between these two considerations is 20°C .

CONNECTION RESISTANCE

At elevated temperature the material properties reduced. The reduction may be introduced by factor expressing the ratio between the property under elevated temperature to property at ambient temperature, see Tables 3.1 and D1 in (EN 1993-1-2:2005).

The reduction of the plate in connection A2 close to lower bolt row according to thermocouple TC9, of the plate according to thermocouple TC8, and of the weld according to thermocouple TC8 are shown on Fig. 6. E.g. in 45 min the resistance decrease based on the measured values in plate to 71 %, in the welds to 57 % and in the bolts to 48 %. The sensitivity of the prediction may be expressed by the reduction of the resistance of bolts, see Fig. 7. The bolt resistance decrease in 45 min of fire to 19 % in case of prediction by lower flange temperature and to 6 % by prediction from section factor of connected beam, but the reduction to 48 % only was evaluated based on the measured temperature.

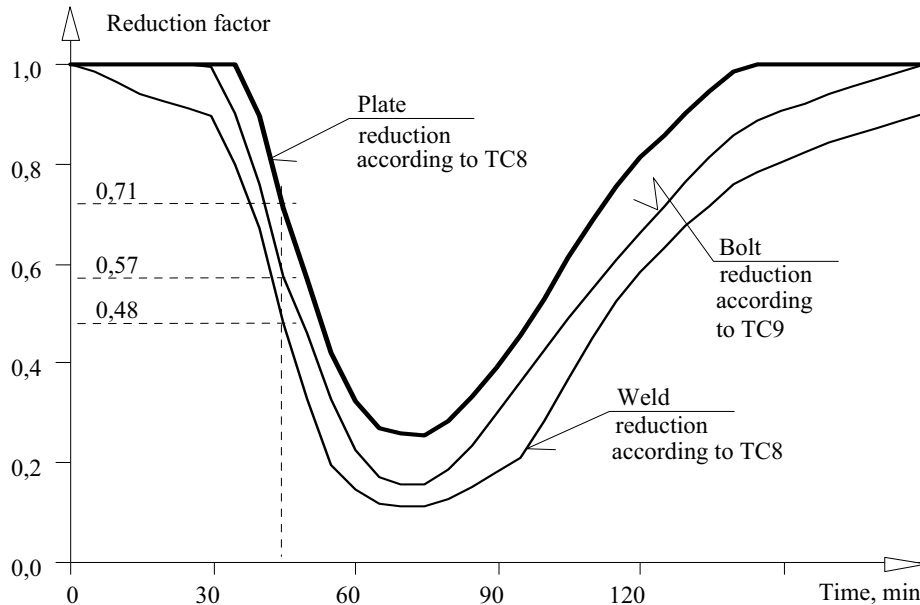


Fig. 6 - Reduction of the resistance of components in connection A2 according to the measured temperatures.

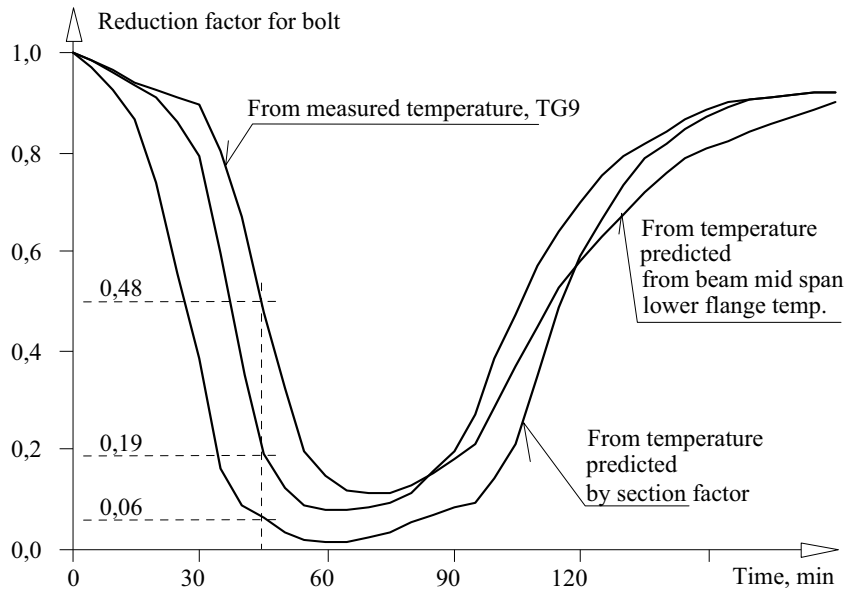


Fig. 7 - Reduction of the resistance of bolts in the lower row of the connection A2 according to the different models compared to the reduction obtained from the measured temperature.

PARTIALLY ENCASED CONNECTION

On the figures above, there is quite obvious that the connection resistance very much depends on the temperatures of the particular parts of the connection. Therefore, it seems reasonable to protect the connection - or at least some part of it - from the direct contact with the fire and by that to secure the connection from the reduction of resistance.

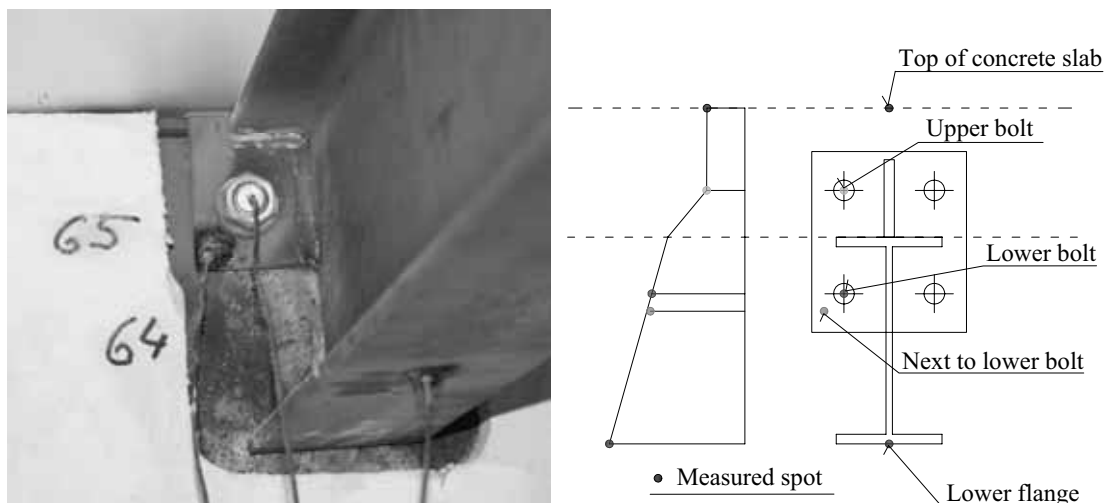


Fig. 8 - Connection with improved fire resistance, temperature profile

On Fig. 8 there is an example of a partially encased connection. It is a header plate connection with 4 grade 8.8 bolts, where the upper row of bolts is above the upper

flange of the connected member and the lower row is between the flanges, as usual. This should ensure some heat protection to the upper bolts and by that the resistance degradation should be smaller.

This connection was subjected to similar fire conditions as in the case of connections on Fig. 2. A steel concrete beam with partially encased connections on both sides was attached to a thermally insulated frame representing the neighbouring structure and placed in a gas furnace. Then it was heated with approximately same heating regime as in the case of natural fire.

On Fig. 9 there are viewed the measured temperatures over the connection, according to the marking on Fig. 8. There are larger differences in temperatures in particular parts of the connection. This is due to the partial encasement of the connection in the concrete. When compared to the results on Fig. 4 it is visible, that the encased connection has reached lower temperatures than the commonly used connection.

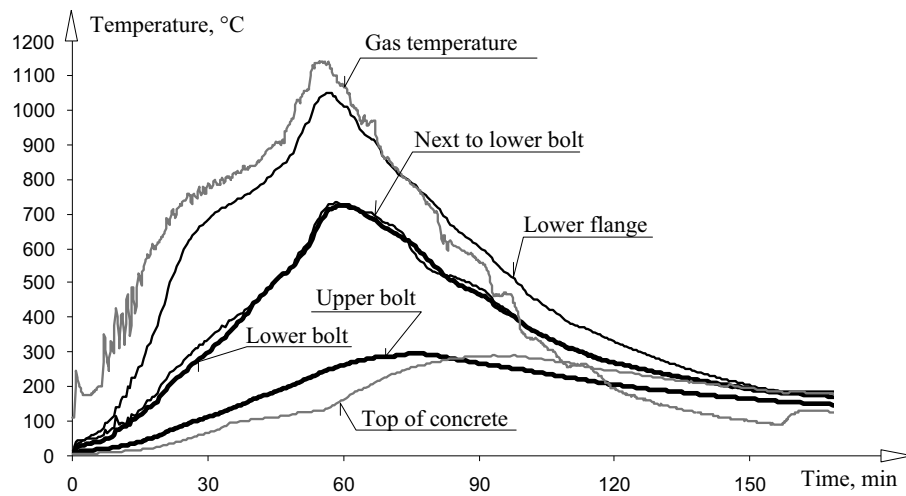


Fig. 9 - Temperatures measured over the height of the encased connection

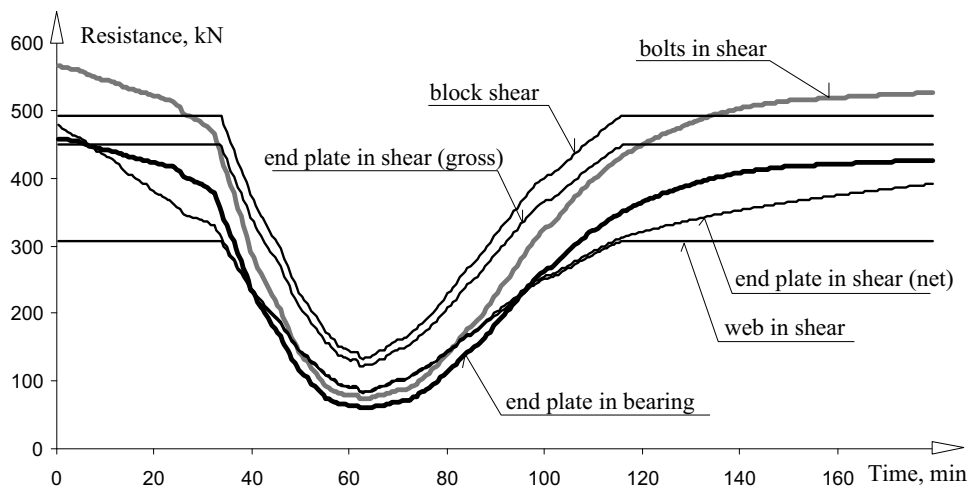


Fig. 10 - Resistance of individual components of common header plate connection

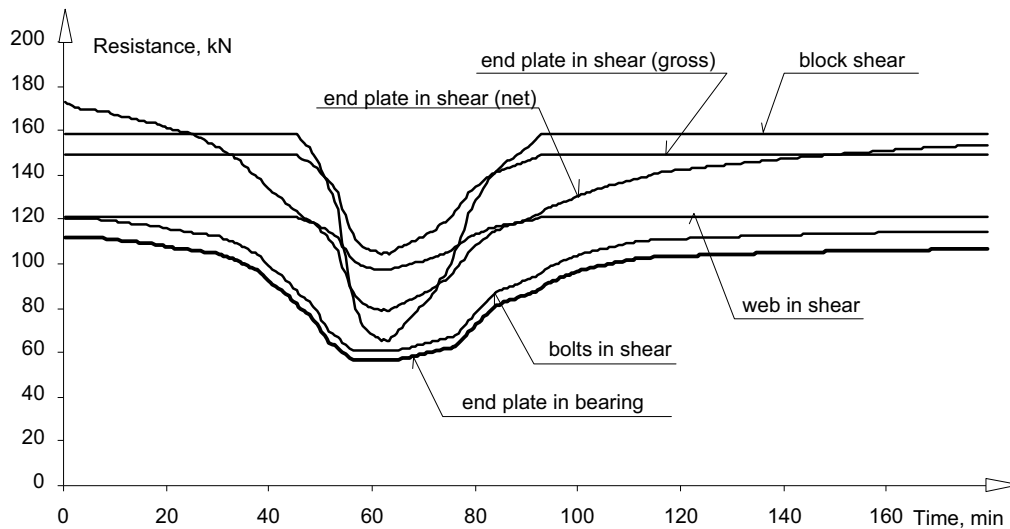


Fig. 11 - Resistance of individual components of the encased connection

This temperature difference can be expressed also by strength of individual components of the connection. On Fig. 10 there are displayed these values for the commonly used connection (typical header plate connection) as a function of time by the use of the reduction factors introduced in EN 1993-1-2:2005.

For comparison, Fig. 11 shows similar diagram for the connection with improved fire resistance. This connection reached relatively higher resistance than the common connection. For the common connection the reduction due to the temperature increase is more significant.

CONCLUSIONS

On the June 15, 2006 a full-scale fire test was carried out at the Ammoniac Separator II in company Mittal Steel Ostrava. One of the main aims of this fire test was to collect data on the distribution of temperatures within the connections. In this paper a comparison is also made with the analytical methods given in EN 1993-1-2:2005 for calculating the temperature and temperature distributions in the structural steel members. From these comparisons it can be concluded that:

The methods for calculating the compartment temperature given in EN 1991-1-2:2003 for parametric fire curve in Annex A agreed well with the measured data. The incremental analytical models allow presuming temperatures of the unprotected beams with a good accuracy.

Calculating the temperature of the beam-to-column connection from the measured gas temperature in the fire compartment based on the mass of the connection parts is too conservative during the heating phase, see Fig. 5. A calculation based on the bottom flange temperature of the supported beam is less conservative.

The relatively high sensitivity of the temperature prediction was shown on the reduction of the resistance of bolts for different temperature prediction models, which

was compared to the measured values. The next generation of analytical prediction models brings more economical design into highest temperatures and closer prediction into the cooling phase of the fire.

ACKNOWLEDGEMENTS

The work was prepared with support of Czech Grant Agency GAČR 103/07/1142. The paper describes contributions of the Czech partner to the Action Cost C26 Urban Habitat Constructions under Catastrophic Events, which is focused into the connection behaviour prediction and the structural integrity under fire conditions.

REFERENCES

Buchanan A. H. (2003), *Structural design for fire safety*, John Wiley & Sons, ISBN 0-471-89060-X.

EN 1991-1-2:2002. Eurocode 1: *Basis of design and actions on structures* – Part 2-2: Actions on structures – Actions on structures exposed to fire, CEN, Brussels.

EN 1993-1-2:2005. Eurocode 3: *Design of steel structures* – Part 1-2: General Rules – Structural fire design, CEN, Brussels.

Kallerová P. and Wald F. (2006), *Ostrava fire test*, Czech Technical University, Praha, CIDEAS report No. 3-2-2-4/2, p.18.

Moore D.B. and Lennon T. (1997), Fire engineering design of steel structures, *Progress in Structural Engineering and Materials*, 1 (1), 1997, pp. 4-9.

Spyrou S., Davison B., Burgess I. and Plank R. (2002), Component-based studies on the behaviour of steel joints at elevated temperatures, in *Proceedings of Eurosteel 2002 – 3rd European Conference on Steel Structures*, pp. 1469-1478, Coimbra, ISBN 972-98376-3-5.

Wald, F., Simões da Silva, L., Moore, D.B., Lennon, T., Chladná, M., Santiago, A., Beneš, M. and Borges, L. (2006), Experimental behaviour of a steel structure under natural fire, *Fire Safety Journal*, Volume 41, Issue 7, October 2006, pp. 509-522.

A GENERALIZED MODELING APPROACH OF STEEL JOINTS FOR ADVANCED GLOBAL ANALYSIS AND STABILITY OF FRAMES

Eduardo Bayo and Javier Gracia
University of Navarra, 31080 Pamplona, Spain
ebayo@unav.es

ABSTRACT

This paper deals with a generalized component based approach to model internal and external connections (rigid, semi-rigid or simple) for global analysis and stability of steel and composite frames. The method is based on a finite sized elastic-plastic joint element that takes into consideration its deformation characteristics including those of the panel zone as well as the left and right connections. In addition, all the internal forces that concur at the joint coming from the beams and columns and their eccentricities are also considered.

In the context of advanced global analysis allowed by modern codes, the use of the proposed model could be particularly useful since the joint has its own identity and is modeled independently like any other element of the structure. Therefore, its properties may be used to obtain an initial imperfection of the frame based on the first buckling mode, such as in EC3, or a reduced elastic stiffness, such as in 2005 AISC Direct Analysis Method.

INTRODUCTION

Substantial effort has been carried out to characterise the behaviour of connections. Modern structural steel codes (Eurocode 3, 2003; AISC, 2005), include guidelines and formula to define both the stiffness and resistance of the connections so that they may be used for the global analysis and design of the structure. The most common approach to model the connections for global structural analyses is by means of zero-length springs attached to the end of the beams at both sides of the joint (see Fig. 1). Joint spring models proposed in the USA include the Frye-Morris polynomial model (Frye and Morris, 1975), the modified exponential model (Kishi and Chen, 1986) or the three-parameter power model (Kishi et al, 1988), among others. These models accurately represent the characteristics of the connections at both sides of the joint, but do not take into account the finite size of the joint, and the panel deformations due to shear, and compressive forces. EC3 also defines the behavior of the right and left connections, and when it comes to the panel it introduces an approximation by means of a transformation parameter, β , which depends on the internal moments and shear forces acting on the panel that come from the adjacent beams and columns. The parameter β affects both the stiffness and the resistance of the zero-length springs.

The early experimental work of Krawinkler (1978) showed the importance of panel shear deformations for stable energy dissipation under cyclic loading. More recent research (Ivanyi and Baniotopoulos, 2000; Charney and Downs, 2004; Castro et al, 2005) has stressed the need for a correct definition of the panel zone deformations under static conditions due to its influence on the overall sway behavior of the frame. An increase in frame drift due to panel-zone shear deformation may render the frame unserviceable. This may even happen for commonly considered rigid joints. Modeling of the panel is also important for the avoidance of local failure of the columns under ultimate limit state conditions. An added complexity appears in the panel zone of interior joints with beams of different heights (Silva, 2008).

Other mechanical models of the joints with actual dimensions have also been presented (SSEDTA (2001)). These models consist of rigid and flexible bar elements as well as springs that are subsequently attached to the ends of the beams for global analysis. Although they take into account the panel deformation modes and the finite size of the joint, they require from the user the definition of the physical properties, inertias and areas of the mechanical elements that comprise the model. What is more, they add a sizable number of elements to the model, and the rigid bars may add numerical instability during the solution process.

Finite element models have also been proposed to introduce the web panel deformations (Chen et al. 1996) in the global analysis of frames. These finite element models take into account in an accurate manner the material properties, shear deformation, extension and bending in the panel. However, they do not model important local phenomena such as local buckling. Moreover, additional springs have to be attached to take into account the remaining parts of the connections: bolts, end plate, stiffeners, angles, etc.

This paper deals with a generalized *component* based approach to model internal and external connections (rigid, semi-rigid or simple) for global analysis and stability of steel and composite frames. The element is an extension of that proposed by Bayo et al. (2006a), and is based on a finite sized elastic-plastic joint element that takes into consideration its deformation characteristics (*components*), including those of the panel zone; and all the internal forces that concur at the joint. As a consequence, this new element avoids the use of the transformation parameter β , and the inherent iterative process that it requires. In addition, the eccentricities of the internal forces coming from the beams and columns that meet at the joint are automatically considered.

FORMULATION OF THE GENERALIZED JOINT ELEMENT

Interior Joints

Fig. 2 shows a mechanical model of an interior connection with rigid links and springs. The springs K_1 and K_2 represent the connection stiffness at each side of the joint coming from the components such as: column web in tension, column right flange in

bending, end-plate in bending, angles, bolts in tension and reinforcement in the case of composite structures. The springs K_{cws} and K_{cwc} represent the overall stiffness of the panel zone under shear and compression, respectively. These are usually the most critical components of the joint.

This model may be introduced as is in a global analysis as mentioned before, however, this adds complexity to the designer and possible numerical round off errors in the global structural analysis.

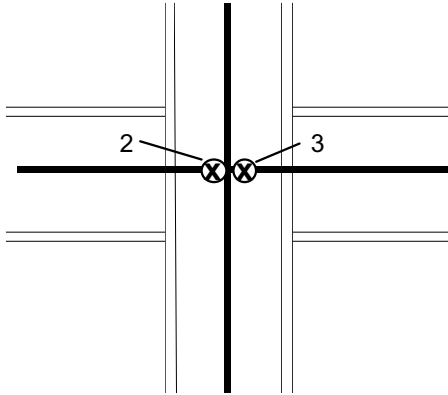


Fig. 1. Zero-length two-spring joint model

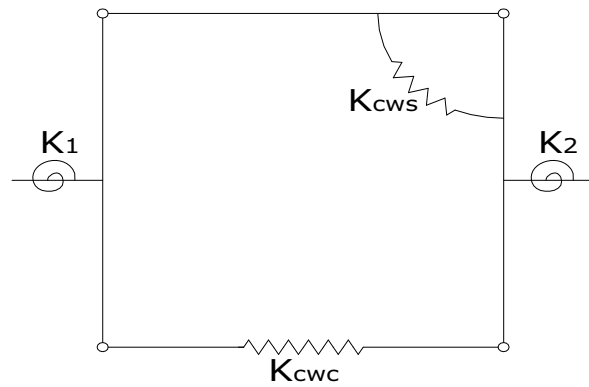


Fig. 2. Mechanical model of a joint

As an alternative a generalized element is proposed (see Fig. 3) with 4 nodes and 12 degrees of freedom (d.o.f.) for the planar case. The base element shown in Fig. 4 will be used to obtain the basic flexibility and stiffness matrices. The dimension d is equal to the width of the column, and the height h corresponds to the lever arm. Afterwards, the contribution of the rigid body modes can be added to obtain the complete stiffness matrix in terms of the 12 d.o.f. as shown in Fig. 3.

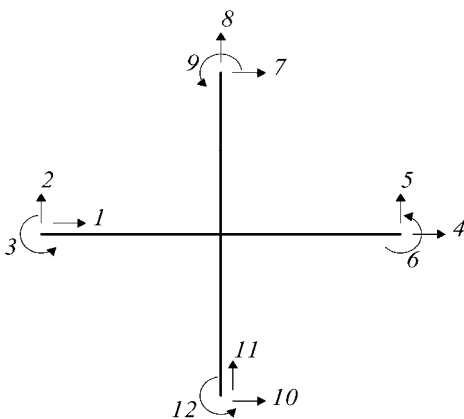


Fig. 3. Proposed joint model (12 d.o.f)

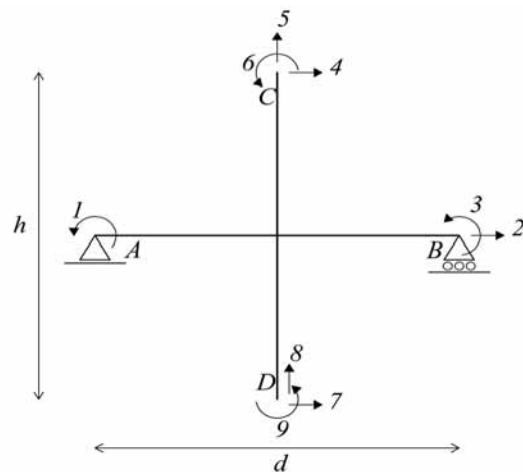


Fig. 4. Base joint element (9 d.o.f)

It should be noticed that all the forces and moments coming from the adjacent beams

and columns concur at the joint at points A, B, C and D. Therefore the complete force field in the panel zone is known with no need of a transformation parameter (β). Also, since the real dimensions of the joint are being considered, the eccentric moments are automatically taken into account.

We follow a flexibility approach, and in order to develop the element stiffness matrix the following steps are carried out:

1. Consider the panel by itself and its deformations modes such as shear and compression, which are characterized by the springs K_{cws} and K_{cwc} , respectively (Fig. 5). In principle, other modes such as compression (longitudinal and transversal), bending or those arising from beams of different height could also be included. The terms of the 9 d.o.f. (see Fig. 4) flexibility matrix, \mathbf{F} , corresponding to the panel zone including the effects of the shear, compression, bending, and longitudinal and transversal axial deformation modes are derived in Appendix A.

2.

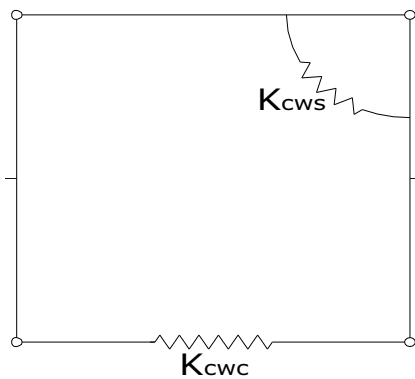


Fig. 5. Panel zone only

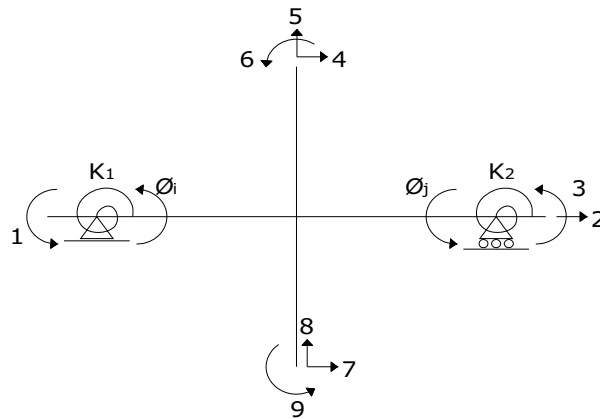


Fig. 6. Base element with connection springs

3. Once the flexibility matrix of the panel has been obtained the basic stiffness matrix may be calculated through matrix inversion:

$$\mathbf{K}_b = \mathbf{F}^{-1} \quad (1)$$

This inversion may be carried analytically by means of a symbolic computational tool, thus avoiding the numerical overhead.

4. The springs K_1 and K_2 (coming from EC3 or any other model) that represent the left and right connections can now be added to the basic stiffness. The internal rotations ϕ_i and ϕ_j (see Fig. 6) corresponding to the panel zone may be eliminated by means of static condensation.
5. Following standard procedures in matrix structural analysis (McGuire et al, 2000) the rigid body modes may be added by means of a transformation matrix \mathbf{T} . Thus, the basic stiffness \mathbf{K}_b may be transformed to obtain the general stiffness matrix in terms

of the 12 d.o.f (see Fig. 3) as follows:

$$\mathbf{K} = \mathbf{T} \mathbf{K}_b \mathbf{T}^T \quad (2)$$

External Joints

The external and corner joints will only have 9 and 6 degrees of freedom, respectively, as shown in Figs. 7 and 8. Their stiffness matrices may be obtained from the 12 d.o.f. stiffness matrix of the interior joint, \mathbf{K} , by means of the static condensation algorithm that helps eliminating those degrees of freedom that are not necessary.

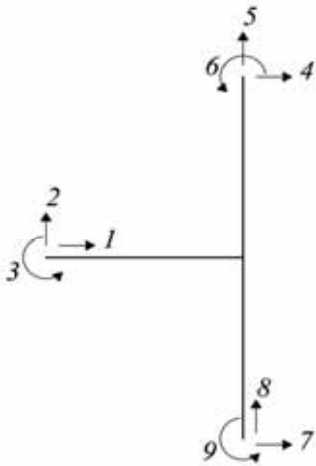


Fig. 7. Exterior element

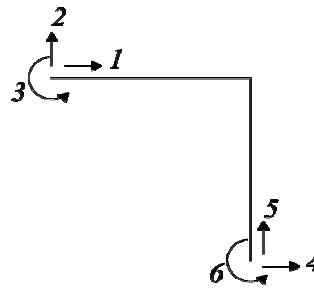


Fig. 8. Corner element

3-D Joints

Although research has already been carried out to characterize the behavior of 3-D joints (Cabrero and Bayo, 2007a and 2007b; Silva, 2008) still further work is needed to fully characterize the three dimensional behavior of key components (Silva, 2008). Once this is accomplished, the method presented above for the planar case can be extended in a straightforward manner to model 3-D joints.

NUMERICAL EXAMPLES

Example 1

The simple frame shown in Fig. 9 has been proposed as a benchmark problem to check the behavior of semi-rigid connections (Faella et al., 2000). This example is solved using the generalized element just described and the mechanical model (Fig. 2). Two beam elements are used to model each girder. The structural model with the proposed joint has 6 elements and 19 d.o.f. The mechanical model leads to 12 elements and 31 d.o.f. All the simulations are performed using the program Matlab.

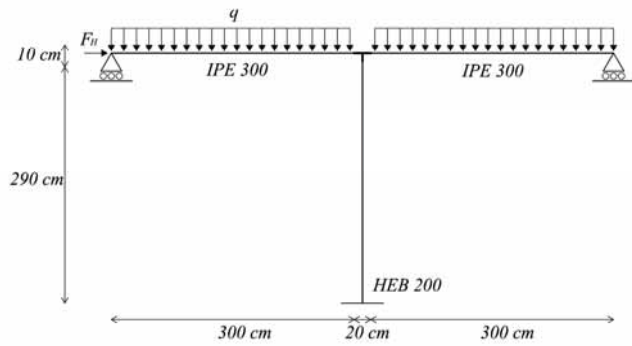


Fig. 9. Frame for Example 1

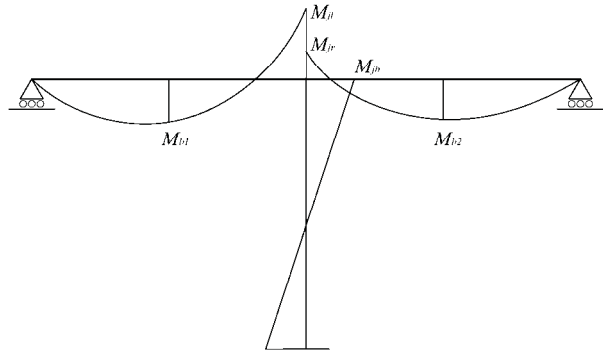


Fig. 10. Moment diagram for Example 1

The frame is loaded by a uniform distributed load q in the girder, and a horizontal load, F_H , that accounts for the lateral loading. The overall configuration of the bending moment diagram resulting from the analysis is depicted in Fig. 10. The moments M_{jl} and M_{jr} drift away from each other as the value of the horizontal load F_H increases, and both moments may reach different signs after F_H goes beyond a particular value. The characteristics of the connection according to the model of Fig.2 are given in Table 1.

K_{cws} (kN.cm)	K_{cwc} (kN/cm)	K_1 (kN.cm)	K_2 (kN.cm)	h (cm)	d (cm)
6.164E6	21426	12.742E6	12.742E6	29.85	20

Table 1. Characteristics of the connection for Example 1.

Table 2 illustrates the four loading conditions and types of analysis that are carried out. For the first three the analysis is elastic, and for the last one the analysis is plastic.

Load Case	Type of Analysis	q [kN/m]	F_H [kN]
A	Elastic	100	0
B	Elastic	80	33
C	Elastic	53	80
D	Plastic	80	120

Table 2. Load cases and types of analyses for Example 1

The values chosen for the different loading conditions are such that for the load case A, the moments at both sides of the joints M_{jl} and M_{jr} are the same. For the load case B the moments drift away maintaining their sign, reaching a situation similar to that illustrated in Fig. 10. In case C the moment on the right of the joint M_{jr} continues drifting and reverses to positive. Finally in the case of loading D the joint becomes plastic due to shear yielding of the panel zone.

The bending moments at the joint and at the middle of the beams resulting from the

analysis are shown in Table 3. It may be observed that the values obtained by both methods are very similar.

Loading	Proposed Element				Mechanism Model			
	M_{b1}	M_{b2}	M_{jl}	M_{jr}	M_{b1}	M_{b2}	M_{jl}	M_{jr}
A	6828	6828	8843	8843	6828	6828	8844	8844
B	4415	6509	9169	4980	4410	6495	9176	5022
C	1128	6155	9744	311	1064	6176	9864	359
D	1859	9066	14281	132	1878	9075	14444	149

Table 3. Comparison of moments (kN.cm) at the joint and at the beam mid-spans

Example 2

The frame subassembly shown in Fig. 11 consists of a column attached to beams by means of semi-rigid connections. Two different sections are considered for the column, namely, HEB220 and HEB240. All the beams are IPE400. The external loads for the ultimate limit state are also specified in Fig. 11. The frame out-of-plumbness imperfection described in EC3 is also introduced. The characteristics of the semi-rigid connections according to the model of Fig.2 are given in Table 4.

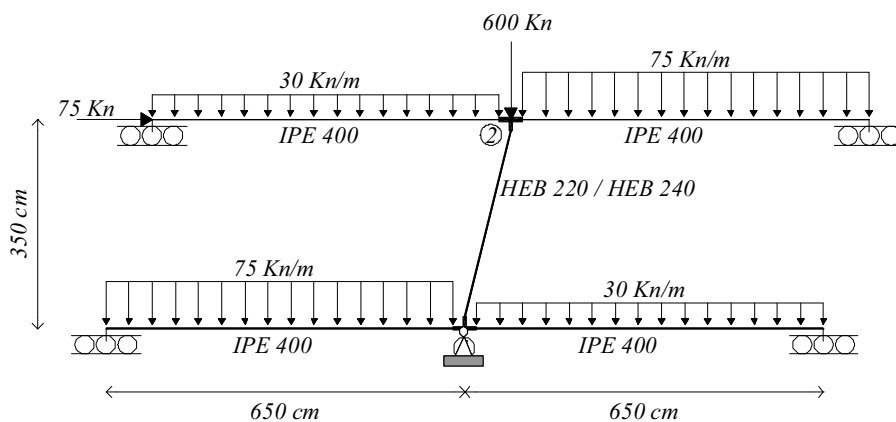


Figure 11. Subassembly of a sway frame with semi-rigid connections.

Connection	K_{cws} (kN.cm)	K_{cwc} (kN/cm)	K_1 and K_2 (kN.cm)	$M_{j,Rd}$ (kN.cm)	h (cm)	d (cm)
HEB 240	10.701E6	22070	17.278E6	18783	39.51	24
HEB 220	8.995E6	20785	16.997E6	15884	39.49	22

Table 4. Characteristics of the semi-rigid connections.

The example is solved using the 4-node element described above. Only in-plane buckling is taken into account. The following cases are contemplated:

- Case A: 2nd order analysis of the frame followed by member stability check with non-sway buckling length.
- Case B: 2nd order analysis of the frame followed by member stability check with system buckling length.
- Case C: 2nd order analysis of the frame starting from a global deformation coming from the out-of-plumbness shape to which the critical non-sway buckling mode is added. The critical buckling mode is scaled according to an energy procedure explained in Bayo and Lourerio, (2001) and Bayo et al (2006b).

Table 5 illustrates the utilization factors obtained from the application of these three methods. It may be seen from those results that the proposed method compares well with those obtained by the member-by-member stability checks based on design formulae.

	HEB-240	HEB-220
A: 2nd order & member check with non-sway buckling length	0.77	0.94
B: 2nd order & member check with system buckling length	0.78	0.97
D: Energy scaled non-sway global buckling mode + 2 nd order	0.71	0.98

Table 4: Utilization factors of the columns for Example 2.

CONCLUSIONS

In this paper a generalized joint element has been proposed for the global analysis of steel and composite frames. The element takes into consideration the deformation characteristics (components) of both the panel zone as well as the left and right connections. All the internal forces that concur at the joint and their eccentricities due to the joint finite size are also considered; therefore no transformation parameters are needed. The proposed joint model encompasses the behavior of rigid, simple and semi-rigid connections.

A key aspect of the proposed approach is that the joint is treated independently of the rest of the elements in a structure. In this way, the behavior of a connection is not added, as traditionally done, to the end of a beam but rather the connections, left and right, and the web panel are all treated jointly and seamlessly in a single joint element.

Simulations have been performed with cases that include elastic and plastic analyses in steel structures. The proposed element is capable of solving all the cases considered with accuracy and numerical efficiency.

Further research is needed to address the behaviour of key components in 3-D connections. Once this is accomplished, the method presented in this paper can be extended to the global analysis of 3-D frames.

In the context of advanced global analysis (that is, second order analyses that avoid element stability checks) allowed by modern codes, the use of the proposed general model could be particularly useful since the joint has its own identity and is modeled like any other element of the structure. Therefore, its properties may be used to obtain an initial imperfection of the frame based on the first buckling mode, such as in EC3, or a reduced elastic stiffness, such as in LRFD.

After all the effort that the scientific community has dedicated to the characterization of the properties and behavior of joints in both steel and composite structures, attention should be given to further improving the global analysis by taking advantage of formulations such as those presented in this paper. It is recommended to perform global analyses with procedures that will incorporate all the joint properties with precision and accuracy, particularly in the context of advanced global analyses.

ACKNOWLEDGEMENTS

The financial support provided by the Arcelor-Mittal Chair of the University of Navarra is greatly appreciated.

REFERENCES

AISC (2005). Specification for Structural Steel Buildings. American Institute of Steel Construction, Chicago, USA.

Bayo E., Loureiro A. (2001). "An Efficient and Direct Method for Buckling Analysis of Steel Frame Structures". *Journal of Constructional Steel Research*. Vol. 57, No. 12, pp. 1321-1336.

Bayo E., Cabrero J.M., Gil B. (2006a). "An effective component based method to model semi-rigid connections for the global analysis of steel and composite structures". *Journal of Engineering Structures*. Vol. 28, No. 1, pp. 97-108.

Bayo E., Gracia J., Cabrero J.M, Gil B. (2006b) "Advanced global-member stability analysis of semi-rigid frames". International Colloquium on Stability and Ductility of Steel Structures. Lisbon. Portugal (Sep. 2006).

Cabrero J.M., Bayo E. (2007a). "The semi-rigid behaviour of three-dimensional steel beam to-column joints subjected to proportional loading. Part I. Experimental evaluation". *Journal of Constructional Steel Research*, Vol. 63, No. 9, pp 1241-1253.

Cabrero J.M., Bayo E. (2007b). "The semi-rigid behaviour of three-dimensional steel beam to-column joints subjected to proportional loading. Part II. Theoretical model and validation". *Journal of Constructional Steel Research*, Vol. 63, No. 9, pp 1254-1267.

- Castro JM, Elghazouli AY, Izzuddin, BA. (2005). "Modeling of the panel zone in steel and composite frames". *Engineering Structures*, Vol. 27, pp. 129-144.
- CEN. Eurocode 3 (2003). Design of Steel Structures. Part 1.8: Design of Joints (prEN 1993-1-8). Stage 49 draft (ed.).
- Charney, F.A., Downs, WM. (2004). "Modeling procedures for panel zone deformations in moment resisting frames". *Connections in Steel Structures V*.
- Chen WF., Goto Y., and Liew JYR. (1996). *Stability Design of Semi-Rigid Frames*. John Wiley & Sons.
- Faella C. Piluso V, Rizzano G. (2000). *Structural Steel Semirigid Connections: Theory, Design and Software*. CRC Publishers.
- Frye MJ., Morris GA. (1975). "Analysis of flexible connected steel frames". *Canadian Journal of Civil Engineers*, Vol. 2, pp. 119-136.
- Ivanyi M, Baniotopoulos C (Editors) (2000). *Semi-rigid connections in structural steel work*. Springer-Verlag Wien New York.
- Kishi N, Chen WF. (1986). "Data base of steel column connections". Structural Engineering Report CE-STR-86-26. Purdue University, West Lafayette IN, 1986.
- Kishi N., Chen WF., Matsuoka KG., Nomachi, SG. (1988). "Moment rotation relation of single/double web angle connections". Proceedings of the state of the art workshop on connections and the behavior, strength and design of steel structures, pp- 135-149. Elsevier, London.
- Krawinkler H. (1978). "Shear in beam-column joints in seismic design of steel frames". *Engineering Journal, AISC*, Vol. 5, pp. 82-90.
- McGuire W., Gallagher R., Ziemian R. (2000). *Matrix Structural Analysis*. John Wiley.
- Silva L. S., Santiago A., Vila Real P. (2002). "Post-Limit stiffness and ductility of end-plate beam-to-column steel joints". *Computers & Structures*, Vol. 80, pp. 515-531, 2002.
- Silva L.S. (2008). "Towards a consistent design approach for steel joints under generalized loading". *Journal of Constructional Steel Research*. Special issue: Imperial College Centenary. To appear.
- SSEDTA. Eurocodes for Composite Structures (2001). Structural Steelwork Eurocodes Development of a trans-national approach. Module 4: joints.

APPENDIX A

This Appendix contains the terms of the 9 d.o.f. (see Fig. 4) flexibility matrix corresponding to the panel zone. The effects of the shear, compression, bending, and longitudinal and transversal axial deformation modes are included in these terms. In principle other modes such as those arising from beams of different height could also be included. Due to the stiffening effect of the column flanges the segment AB (see Fig. 4) is supposed to be rigid under the shear forces coming from the beams. Thus, the resulting non-zero elements of the upper triangular part of the 9x9 flexibility matrix are

the following:

$$\begin{aligned}
 F_{11} &= \left(\frac{1}{K_{cws}} + \frac{1}{h^2 K_{cwc}} \right) ; F_{13} = \frac{1}{K_{cws}} ; F_{14} = -\frac{h}{2K_{cws}} - \frac{d}{2EA_{cc}} ; F_{17} = -F_{14} \\
 F_{22} &= \frac{d}{EA_{cc}} ; F_{24} = \frac{F_{22}}{2} ; F_{27} = F_{24} \\
 F_{33} &= \left(\frac{1}{K_{cws}} + \frac{1}{h^2 K_{cwc}} \right) ; F_{34} = F_{14} ; F_{37} = F_{17} \\
 F_{44} &= \frac{h^2}{4K_{cws}} + \frac{h^3}{24EI_c} + \frac{d}{2EA_{cc}} ; F_{46} = -\frac{h^2}{8EI_c} ; F_{47} = -\frac{h^2}{4K_{cws}} + \frac{h^3}{24EI_c} + \frac{d}{2EA_{cc}} \\
 F_{55} &= \frac{h}{2EA_c} ; F_{66} = \frac{h}{2EI_c} ; F_{77} = F_{44} ; F_{88} = F_{55} ; F_{99} = F_{66}
 \end{aligned}$$

where A_c and I_c represent the area and inertia of the column under bending, respectively; and A_{cc} represents the effective area of the column under transversal axial force. The bilinear behavior of the springs has been defined according to the values given in EC3 along with the post limit stiffness provided by Silva et al. (2002).

APPLICATION OF INSTANTANEOUS CENTER OF ROTATION CONCEPT FOR CYCLIC MODELING OF BOLTED CONNECTIONS IN SPECIAL BOLTED MOMENT FRAMES

Atsushi Sato

Kyoto University, Kyoto, Japan
asato@archi.kyoto-u.ac.jp

Chia-Ming Uang

University of California, San Diego, La Jolla, CA, USA
cmu@ucsd.edu

ABSTRACT

Seismic design of Cold-Formed Steel – Special Bolted Moment Frames (CFS – SBMF) relies on high ductility through bolt friction and bearing in the bolted moment connection region. For modeling purposes and for establishing the required beam and column design seismic forces for capacity design, a procedure based on the instantaneous center of rotation concept was proposed. Based on available cyclic test data of beam-column assemblies, both the slip coefficient and bolt tension force for snug-tight high-strength bolts were established to model the slip characteristics of the bolt. The same data set was also used to modify an existing model for bolt bearing. With the proposed procedure, results from monotonic load analysis are shown to envelope the cyclic response reliably. Including the effect of bearing deformation, the proposed procedure can also simulate the hardening behavior and the growth of slip range under cyclic loading.

INTRODUCTION

American Iron and Steel Institute (AISI) is in the process of developing a seismic design standard (AISI S110: *Standard for Seismic Design of Cold-Formed Steel Structural Systems—Special Bolted Moment Frames*) for cold-formed steel structures (AISI 2007a). The first seismic force-resisting system introduced in this seismic standard is termed Cold-Formed Steel—Special Bolted Moment Frames (CFS—SBMF). This type of moment frames, usually one story in height, is typically composed of cold-formed Hollow Structural Section (HSS) columns and double-channel beams. Beams are connected to the column by snug-tight high-strength bolts; see Fig.1 for a typical moment connection detail.

Full-scale cyclic testing of beam-column subassemblies (Hong and Uang, 2004) showed that the bolted moment connection can provide high ductility capacity through bolt slippage and bearing (Fig. 2). The test results also showed that buckling of the beams and columns should be avoided because it could result in significant strength degradation. Therefore, the seismic design philosophy for this type of system is to

confine the energy dissipation through inelastic action in the bolted moment connection only. Beams and columns are then designed to remain elastic during a significant seismic event. This capacity design concept requires that a reliable mathematical model for the bolted moment connection be established such that, given a design story drift, the maximum force in the connection, and hence the beam and column connecting to it, can be calculated.

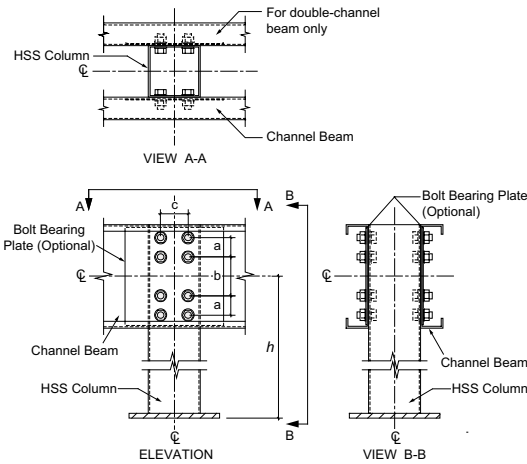


Fig. 1 Typical Bolted Moment Connection Detail

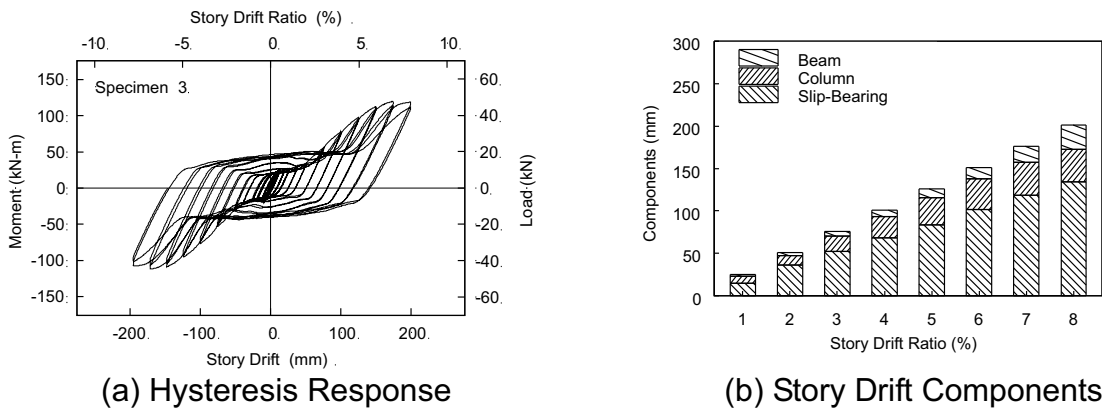


Fig. 2 Typical Cyclic Response of CFS-SBMF Beam-Column Subassembly

Table 1 Member Sizes and Bolted Connection Configurations

Specimen No.	Beam, mm	Column, mm	Bolted Connection**			Bolt Bearing Plate, mm
			a,mm	b,mm	c,mm	
1, 2	2C305×89×2.7 (2C12×3½×0.105)*	HSS203×203×6.4 (HSS8×8×¼)	64 (2½)	76 (3)	108 (4¼)	3.4 (0.135)
3	2C406×89×2.7 (2C16×3½×0.105)	HSS203×203×6.4 (HSS8×8×¼)	76 (3)	152 (6)	108 (4¼)	N/A
4	2C406×89×2.7 (2C16×3½×0.105)	HSS203×203×6.4 (HSS8×8×¼)	76 (3)	152 (6)	108 (4¼)	3.4 (0.135)
5, 6, 7	2C406×89×3.4 (2C16×3½×0.135)	HSS203×203×6.4 (HSS8×8×¼)	76 (3)	152 (6)	108 (4¼)	N/A
8, 9	2C508×89×3.4 (2C20×3½×0.135)	HSS254×254×6.4 (HSS10×10×¼)	76 (3)	254 (10)	159 (6¼)	N/A

* Dimensions in inch.

** Bolt: 25.4-mm (1-in.) dia. SAE J429 Grade 5, Bearing Type High-Strength Bolt., see Fig. 1.

EXPERIMENTAL TEST DATABASE

A total of nine full-scale specimens were tested; see Table 1 and Fig. 1 for the member sizes and bolt configurations (Hong and Uang, 2004). Cyclic test results of these specimens form the basis for the correlation of the proposed model.

The typical response in Fig. 2(a) shows that the story drift was mainly contributed by the deformation in the bolted moment connection region. The individual contributions from the beam, column and bolted connection are shown in Fig. 3. Fig. 3(c) shows that the bolted moment connection behavior is characterized by four regions: rigid loading, slip, significant hardening, and rigid unloading; the slip range also increases with the imposed story drift level from previous cycles. The column remained elastic for this specimen; the beam also remained elastic until local buckling occurred at a story drift beyond 6% of the story height. Therefore, the global response in the practical drift range of interest was dominated by the inelastic action in the bolted moment connection.

MOMENT CONNECTION FORCE-RESISTING MECHANISMS

Fig. 4(b) shows the freebody of a column with beams connected to it. With the pin-based column resisting a shear force at the support, the bolt group in the connection

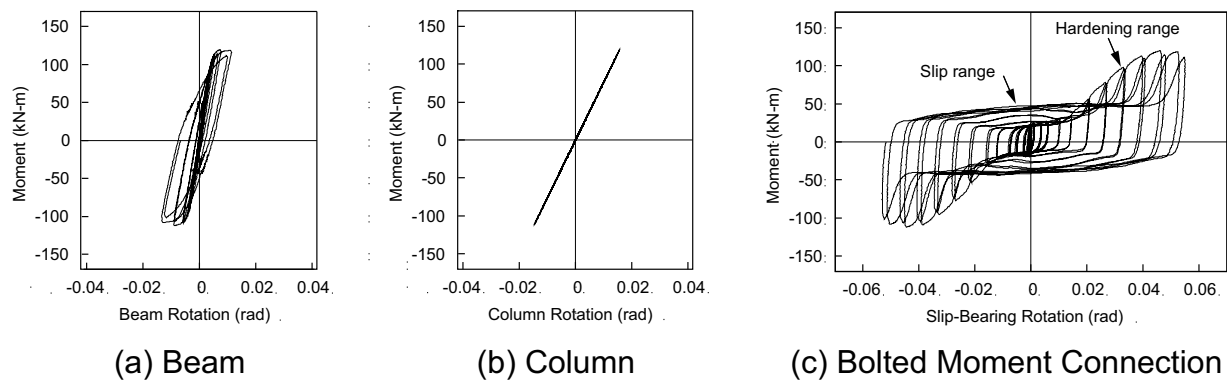


Fig. 3 Components of Story Drift

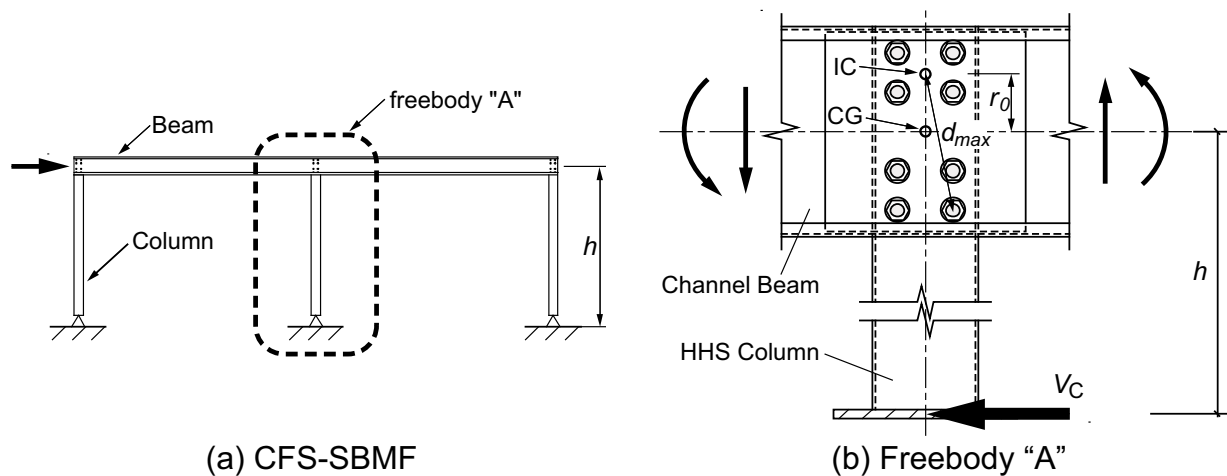


Fig. 4 Bolt Group in Eccentric Shear

region is subjected to a load V_C with a large eccentricity, h , which is the story height measured to the center of gravity (CG) of the bolt group. Such eccentric shear produces both horizontal translation and rotation of the bolt group. The response can be analyzed by the concept of instantaneous center (IC) of rotation, in which both translation and rotation of the bolt group can be reduced to pure rotation about IC (Crawford and Kulak, 1971; Salmon and Johnson, 1996). This analysis procedure is based on the assumptions made by Kulak et al. (2001).

Bolt Friction Characteristics

The friction resistance, R_s , of a single bolt can be expressed by the following (AISC, 2005):

$$R_s = kT \quad (1)$$

where k = slip coefficient, T = bolt tension force. Snug-tight A325 or SAE J429 Grade 5 high-strength bolts are commonly used for the construction of CFS-SBMF. For clean mill condition of structural steels, an average slip coefficient of 0.33 with a standard

deviation of 0.07 can be assumed for k (Kulak et al., 2001). Minimum pretension is specified in the AISC Specification (AISC, 2005) for pretensioned bolts. Nevertheless, bolt tension in snug-tight condition, which is defined as the tightness that is attained with a few impacts of an impact wrench or the full effort of an ironworker using an ordinary spud wrench to bring the connected plies into firm contact (AISC, 2005), is highly variable (Fisher et al., 1963). Lacking data for snug-tight bolt tension force, a trial-and-error procedure was used based on the cyclic test data of nine beam-column subassemblies (Table 1). With $k = 0.33$, the values of T listed in Table 2 provide a good correlation with the cyclic test data; see the following sections for the results.

The slip range observed in Fig. 3(c) depends on the size of the bolt hole. With standard holes commonly used for CFS–SBMF construction, the typical hole oversize, h_{OS} , is 1.6 mm (1/16 in.) initially. Once the slip resistance of the bolt group is overcome, the most critical bolt will start bearing against the connected members. Bearing deformation will occur, which results in a larger hole size. The effect of such hole ovalization, which is responsible for the larger slip range at higher drift cycles shown in Fig. 3(c), will be considered in the cyclic modeling of the bolted moment connection.

Bolt Bearing Characteristics

A bolt transfers shear through bearing in addition to friction once slip overcomes the hole oversize. The bearing resistance, R_B , of a single bolt can be expressed by the following (Fisher, 1965; AISC, 2005):

Table 2 Assumed Coefficients and Snug-Tight Bolt Tension Force

Specimen No.	k	T , kN	μ	λ
1 to 7	0.33	44.5 (10) ^a	5	0.55
8, 9		91.0 (21)		

^a Snug-Tight Bolt Tension Force in kips

$$R_B = R_{ult} \left[1 - e^{-\mu(\delta_{br}/25.4)} \right]^\lambda \quad (2)$$

where δ_{br} = bearing deformation (mm), R_{ult} = ultimate bearing strength, $e = 2.718$, and μ , λ = regression coefficients. Based on the study of Crawford and Kulak (1971), the following values were adopted by AISC (2005) for establishing the design strength of eccentrically loaded bolt groups: $\mu = 10$ and $\lambda = 0.55$. However, a direct adoption of these values for application in CFS–SBMF is questionable because the regression was conducted on test data with thicker plates connected by high-strength bolts, implying that the bearing deformation (δ_{br}) was contributed by both the connected plates and bolts. Since the thicknesses of the connected beam and column webs in CFS–SBMF are much smaller, the deformation is contributed mainly by the connected webs, not the bolts. Lacking component test data similar to that used by Crawford and Kulak, a trial-and-error procedure was used to determine these two coefficients and R_{ult} . It will be shown in the following presentation that μ and λ values listed in Table 2 and $R_{ult} = 2.1dtF_u$ provide a

good correlation with cyclic test data of nine beam-column subassemblies, where t and F_u are, respectively, the web thickness and tensile strength of the connected member (i.e., either beam or column), and d is the bolt diameter.

MONOTONIC LOAD ANALYSIS

Based on the bolt friction and bearing characteristics presented above, an iterative procedure based on the concept of instantaneous center of rotation is shown in Fig. 5. Part A in Fig. 5(a) is for calculating the response in the slip range, and Part B is for calculating the response in the hardening range. For a given column shear, V_C , the location of IC, expressed in terms of r_0 , is determined by iteration such that force equilibrium, shown in Fig. 5(b), is satisfied. The bolt resistance in the hardening region includes both friction and bearing. The analysis is repeated by increasing the load magnitude until the maximum bearing deformation ($\delta_{br,u}$) of the most critical bolt reaches 8.6 mm (0.34 in.) (AISC, 2005). The calculated column shear, when multiplied by the eccentricity, h , is the moment at the center of the bolt group.

The rotation of the bolt group is contributed by the deformations from both the beam and column. In the slip range, the amount of rotation is computed as

$$\theta_{slip} = \frac{\sum h_{OS}}{d_{max}} \quad (3)$$

where d_{max} = distance from IC to the outermost bolt [see Fig. 5(c)], and $\sum h_{OS}$ = summation of the hole oversizes in the beam and column. With the same initial hole oversize in the beam and column, Eq. (3) can be simplified as

$$\theta_{slip} = \frac{2h_{OS}}{d_{max}} \quad (4)$$

For monotonic analysis, $h_{OS} = 1.6$ mm (1/16 in.) for standard hole.

In the hardening range, the rotation of the bolt group is

$$\theta = \theta_{slip} + \theta_{bearing} \quad (5)$$

where θ_{slip} is from Eq. (4), and $\theta_{bearing}$ is due to the bearing deformation in both the beam and column. To compute $\theta_{bearing}$, it is necessary to distinguish which one of the beam and column is weaker in terms of bearing strength; the relative bearing strength between these two members can be measured by tF_u .

It should be noted that Part B in Fig. 5(a) considers only the bearing deformation in the weaker member (either beam or column), and the stronger member is assumed to be rigid. Define the bearing deformation at the outermost bolt of the weaker member as

$\delta_{br,W}$; this corresponds to point “a” in the first quadrant of the bearing force versus bearing deformation plot in Fig. 6. Since the same bolt bearing force acts on both the weaker and stronger members (point “b” in the second quadrant of the plot in Fig. 6), the corresponding bearing deformation (unit in mm) in the stronger member can be derived as follows:

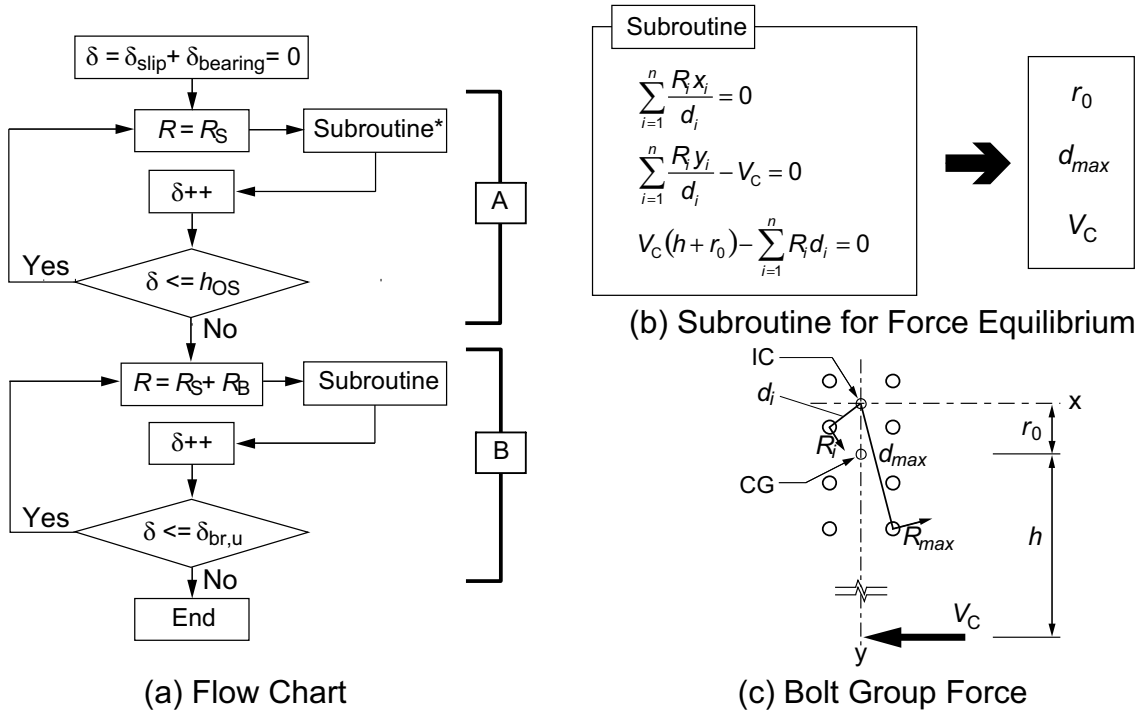


Fig. 5 Numerical Algorithm of Resisting Mechanism

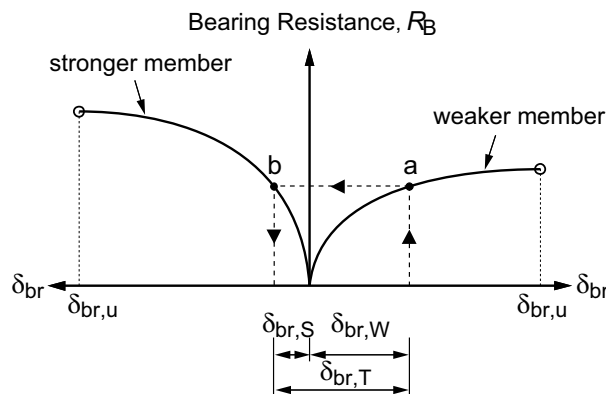


Fig. 6 Bolt Bearing Deformation in Weaker and Stronger Members

$$\delta_{br,S} = -\frac{25.4}{\mu} \ln \left[1 - \left(1 - e^{-\mu(\delta_{br,W}/25.4)} \right) \left(\frac{(tF_u)_W}{(tF_u)_S} \right)^{1/\lambda} \right] \quad (6)$$

where W and S stand for weaker and stronger members, respectively. The bearing component of the bolt group rotation is, therefore, computed as

$$\theta_{bearing} = \frac{\delta_{br,W} + \delta_{br,S}}{d_{max}} \quad (7)$$

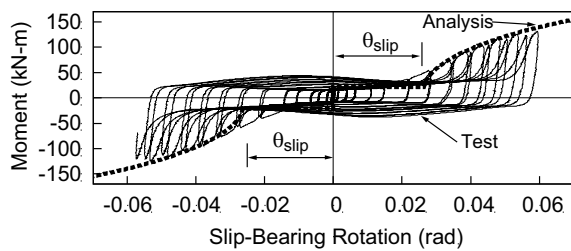
The predicted monotonic responses of representative specimens are compared with the cyclic test data in Fig. 7. The predicted response envelopes very well the cyclic response of the test specimens with varying member sizes and bolt configurations.

The satisfactory correlation of the response envelope shown in Fig. 7 was based on a bolt bearing strength of $R_{ult} = 2.1dtF_u$. According to AISI (2007b), the bearing strength is $3.0dtF_u$ when the bolt hole deformation is not a design concern. With this value, Fig. 8 shows that the response envelope is over-predicted in the hardening region. When the bolt hole deformation is a design concern, AISI gives the following expression for the bearing strength:

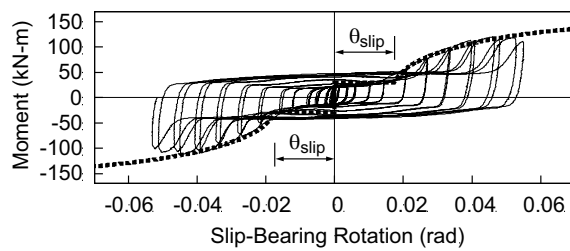
$$R_{ult} = (4.64\alpha t + 1.53)dtF_u \quad (8)$$

where $\alpha = 0.0394$ for SI units (with t in mm). Fig. 9 shows that this bearing strength increases linearly with the plate thickness; beyond 4.76 mm (3/16 in.) the bearing strength equals $2.4dtF_u$ (AISC, 2005). But Fig. 8 shows that a bearing strength of $2.4dtF_u$ still over-predicts the response envelope. To simplify the bearing strength calculation for seismic applications, it is suggested that a value of $2.1dtF_u$ be used.

It is also of interest to examine the movement of IC (i.e., r_0 in Fig. 5) as the load is increased. A sample result is shown in Fig. 10. The location of IC is stationary in the friction range due to the constant slip resistance (i.e., $R = R_s$) of each bolt. IC moves rapidly toward the CG of the bolt group as soon as bearing starts to occur.



(a) Specimen 2



(b) Specimen 3

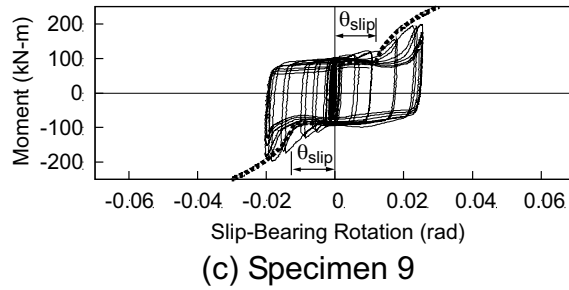


Fig. 7 Correlation of Response Envelope

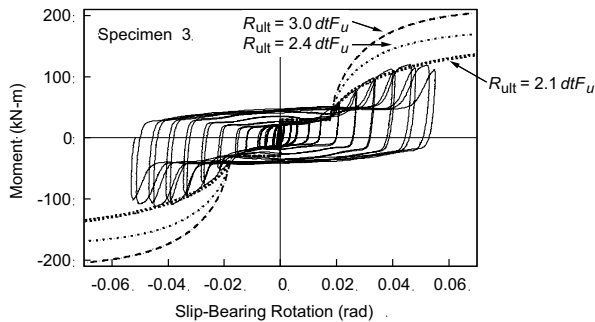


Fig. 8 Effect of Bolt Bearing Strength

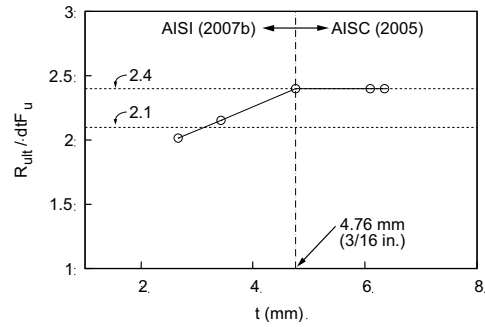


Fig. 9 Bolt Bearing Strength

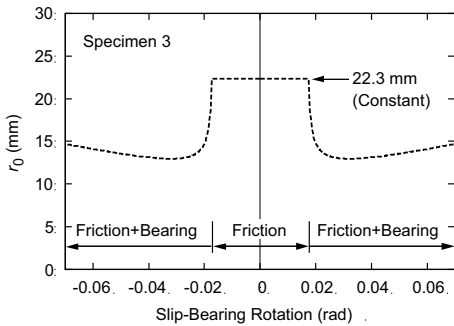


Fig. 10 Variation of IC Location

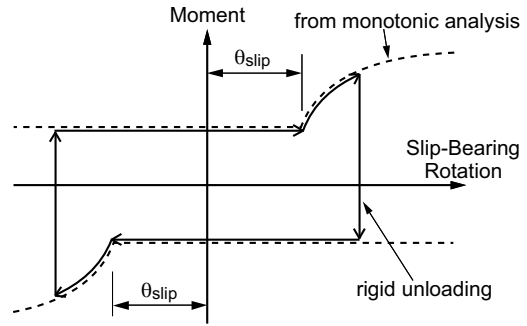


Fig. 11 Proposed Hysteresis Rule

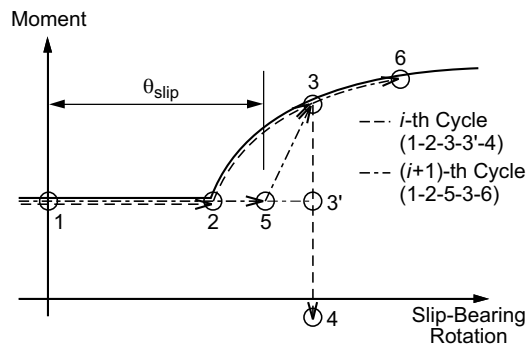


Fig. 12 Growth of Slip Range under Cyclic Loading

CYCLIC LOAD ANALYSIS

The instantaneous center of rotation analysis procedure can be generalized for cyclic loading. The proposed hysteresis rule is shown in Fig. 11. Test results also showed that the slip range will grow due to the development of bearing deformation in prior cycles. Such effect is simulated as shown in Fig. 12. For cyclic analysis, Eq. (3) needs to be modified for calculating the elongated slip range:

$$\theta_{\text{slip}} = \frac{\sum h_{\text{OS}} + \sum \delta_{\text{br}}}{d_{\text{max}}} = \frac{2h_{\text{OS}} + \delta_{\text{br,W}} + \delta_{\text{br,S}}}{d_{\text{max}}} \quad (9)$$

The simulated cyclic responses of representative specimens are compared with the test results in Fig. 13. It is observed that the proposed modeling procedure can simulate the actual response, including the hardening behavior and the growth of the slip range, reasonably well.

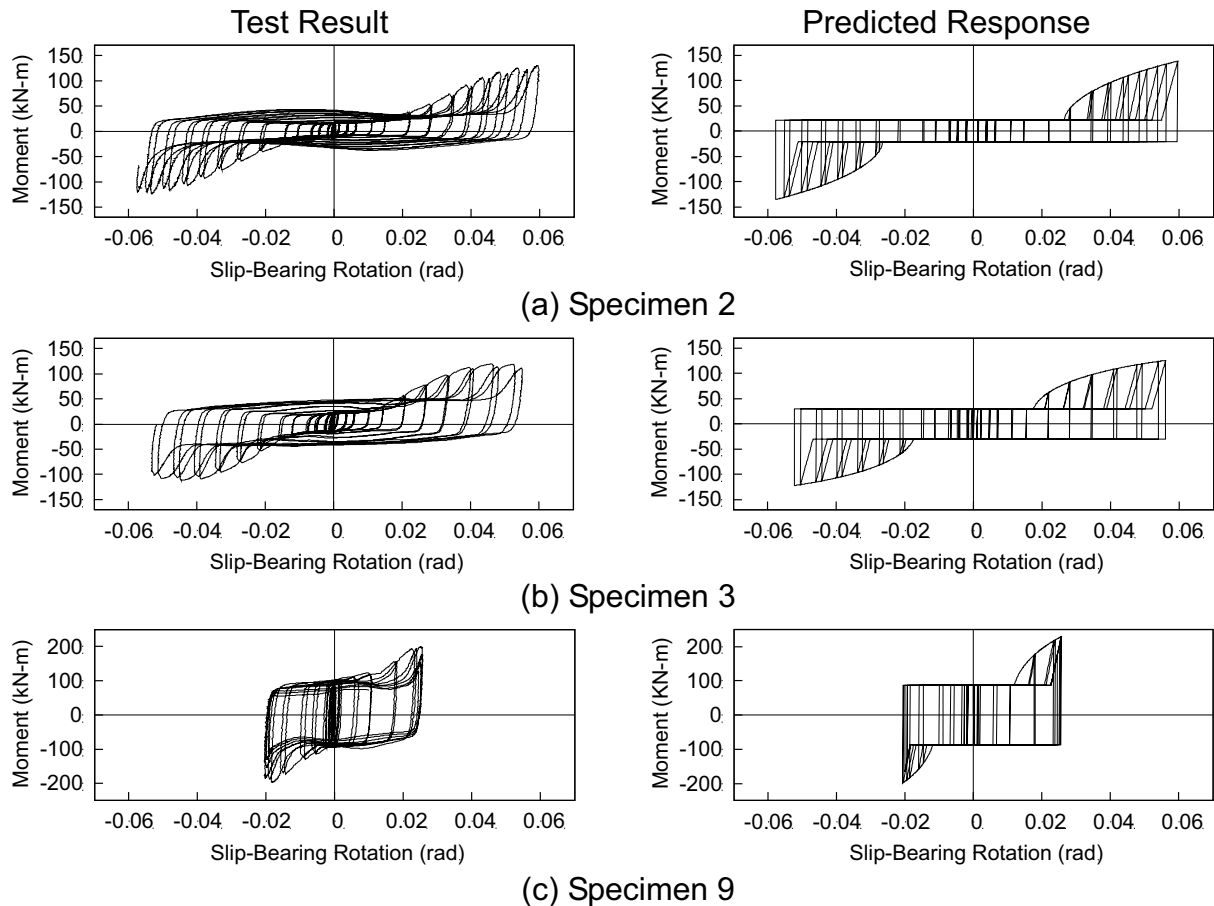


Fig. 13 Correlation of Cyclic Response

SUMMARY AND CONCLUSIONS

Cyclic testing of full-scale beam-column subassemblies showed that Cold-Formed Steel—Special Bolted Moment Frames can provide a high ductility capacity through bolt slippage and bearing. For seismic design of this type of framing system, it is recommended that inelastic action be confined in the bolted moment connections, and that beams and columns remain elastic. The development of a seismic design procedure, therefore, requires that the cyclic behavior of the bolted moment connection be modeled reliably. Test results showed that the cyclic response of a bolted moment connection is characterized by rigid loading followed by a slip region, a hardening region, and rigid unloading. Motivated by the fact that the bolt group in a moment connection is subjected to an eccentric shear, the concept of instantaneous center (IC) of rotation was adopted for modeling purposes.

To model the slip resistance of a snug-tight bolted moment connection, the values of slip coefficient and bolt tension force were established from the test data (see Table 2). The slip range is a function of the bolt hole oversize. Once the hole oversize is overcome, bolt resistance is contributed by both friction and bearing. As soon as bearing starts, the location of IC shifts rapidly toward the center of gravity of the bolt group (see Fig. 10). In determining the rotation in the hardening region, a procedure to account for the bearing deformation from not only the weaker member (either beam or column) but also the stronger member was presented. With the iterative procedure presented in Fig. 5, monotonic analysis results are shown to envelope the cyclic test data very well (see Fig. 7).

The concept of instantaneous center of rotation was also extended for cyclic loading analysis. Including the effect of bearing deformation from prior cycles, the proposed analysis procedure can simulate reliably the growth of slip range at higher drift cycles (Fig. 13). An explanation based on the shift of IC location in the slip and hardening regions was provided for the level of rotation at which the beginning of bearing action was observed from cyclic test data.

ACKNOWLEDGMENTS

This research was sponsored by American Iron and Steel Institute. Additional funding was provided by the Japan Iron and Steel Federation to the first author.

REFERENCES

AISC. (2005), *Steel Construction Manual, 13th Edition*, AISC, Chicago, IL.

AISI. (2007a), *Standard for Seismic Design of Cold-Formed Steel Structural Systems—Special Bolted Moment Frames*, AISI S110-07, AISI, Washington, DC.

AISI. (2007b), *North American Specification for the Design of Cold-Formed Steel Structural Members*, AISI S100-07, AISI, Washington, DC.

Crawford, S. F. and Kulak, G. L. (1971), "Eccentrically Loaded Bolted Connections", *Journal of the Structural Division*, 97(ST3), (pp. 765-783).

Hong, J.K. and Uang, C.M. (2004), "Cyclic Testing of A Type of Cold-Formed Steel Moment Connections for Pre-Fabricated Mezzanines" *Report No. TR-04/03*, Department of Structural Engineering, University of California, San Diego, CA.

Fisher, J.W. (1965), "Behavior of Fasteners and Plates with Holes", *Journal of the Structural Division*, 91(ST6), (pp. 265-286).

Fisher, J.W., Ramseier, P.O. and Beedle, L.S. (1963), "Strength of A440 Steel Joints Fastened with A325 Bolts", Publication, IABSE, 23.

Kulak, G. L., Fisher, J. W., and Struik, J. H. A. (1987), *Guide to Design Criteria for Bolted and Riveted Joints*, 2nd Edition, AISC, Chicago, IL.

Salmon, C. G., and Johnson, J. E. (1996), "Steel Structures Design and Behavior", 4th Edition, HarperCollins College Publishers, New York, NY.

NONLINEAR ANALYSIS OF STEEL FRAMEWORKS WITH SEMI-RIGID CONNECTIONS

Yuxin Liu

Atomic Energy of Canada Limited, Ontario, Canada
liuyu@aecl.ca

Lei Xu

University of Waterloo, Ontario, Canada
lxu@uwaterloo.ca

ABSTRACT

Presented in this paper is an analysis procedure for steel frameworks accounting for inelasticity, geometric nonlinearity of members, and semi-rigid behaviour of connections. Member inelasticity is represented by a spring that simulates a cross section from initial yield to full plasticity by an elliptic function, while the geometric nonlinearity is accounted for by means of stability function. The nonlinear behaviour of semi-rigid connections is simulated by the Richard-Abbott four-parameter function. Nondimensional factors are used to characterize stiffness degradation associated with nonlinear behaviour of connections and inelastic members. A compound element model is introduced to establish member stiffness matrix for the nonlinear analysis of frameworks. A two-bay and two-storey steel framework example in the context of the progressive-failure analysis is presented to demonstrate the analysis procedure.

INTRODUCTION

Although semi-rigid steel framing construction has been adopted in design specifications for a long period of time, it has not gained much popularity in recent years. In current practice, beam-to-column connections of steel frameworks are commonly assumed as either rigid or pinned, in which the semi-rigid behaviour between bending moment and rotation at a joint is generally neglected. Although the adoption of such idealized joint behaviour simplifies the analysis and design process, it by no means represents the actual behaviour of the structure. Most connections used in current practice actually exhibit semi-rigid deformation behaviour that can contribute substantially to overall stability, displacements, and the distribution of internal forces for both the structure and its members. Therefore, the predicted response of an idealized structure may be quite unrealistic compared to that of the corresponding actual structure. The importance of effects of semi-rigid connections must not be underestimated. This is especially true in the case of progressive-failure analysis, in which the modeling of connection behaviour, failure, and nonlinear behaviour of the member are essential for accurately predicting the stability, strength demand, ductility, and deformation capacity of steel frameworks in both intact and damaged forms. To

address this issue, a compound element model which combines the member with its end connections is proposed by Liu et al. (2007) for nonlinear analysis of semi-rigid frameworks. The compound element model includes the effects of member geometric nonlinearity, member inelasticity, member shear deformation, and connection nonlinearity. This paper extends the application of the compound element method to progressive-failure analysis with accounting for the effect of damage degree of joints.

MODEL OF COMPOUND ELEMENT

Through the use of an assembly of springs, connected in series as shown in Fig.1, a compound element representing the combined stiffness behaviour of a semi-rigid connection and a member-end inelastic hinge is presented in this section. The models for member inelasticity and connection flexibility are discussed to establish the general compound element model for structural analysis.

Member Inelasticity

The inelastic force-deformation (F - D) relationship (bending, shearing, or axial) of a member cross section can be generally characterized by the following elliptic curves (Grierson et al., 2005; Xu et al., 2005):

$$F = F_y + (F_p - F_y) \left[1 - \left(1 - \frac{D}{D_p} \right)^{e_0} \right]^{1/e_0} \quad 0 \leq \frac{D}{D_p} < 1, \quad \frac{F_y}{F_p} \leq \frac{F}{F_p} \leq 1 \quad (1)$$

where F_y represents the initial-yield bending, shear, and axial capacity (M_y , V_y or P_y) of the cross section, F_p is the corresponding full-yield capacity (M_p , V_p or P_p), and D_p is the plastic deformation (rotation, transverse deflection or axial deformation) associated with F_p . The value of the exponent e_0 (>1) associated with the force $F = M$, V or P may be determined by means of the experimentation for the cross section profiles (Liu, 2007).

The inelastic bending, shearing, or axial stiffness of the section, $S_p = dF/dD = R_p$, T_p or N_p , can be obtained by differentiating Eq. (1) with respect to the deformation D as,

$$S_p = \frac{dF}{dD} = \frac{(F_p - F_y)}{D_p} \left(1 - \frac{D}{D_p} \right)^{e_0 - 1} \left[1 - \left(1 - \frac{D}{D_p} \right)^{e_0} \right]^{\frac{1 - e_0}{e_0}} \quad 0 \leq \frac{D}{D_p} \leq 1, \quad \frac{F_y}{F_p} \leq \frac{F}{F_p} \leq 1 \quad (2)$$

where, $S_p = \infty$ if the inelastic deformation $D = 0$ and $dF/dD = 0$ if $D \geq D_p$.

Semi-rigid Connection model

The four-parameter power model, originally proposed for inelastic stress-strain behaviour (Richard and Abbott, 1975), has been adopted to characterize the moment-rotation behaviour of beam-to-column connections in steel frameworks. Experimental data for extended-end-plate and flush-end-plate connections confirm that this model is

effective and accurate for predicting the connection behaviour (Kishi et al., 2004). Thus, the model is employed herein to simulate the nonlinearity of semi-rigid connections,

$$M = \frac{(R_{ce} - R_{cp})\theta_c}{\{1 + [(R_{ce} - R_{cp})\theta_c / M_0]^\gamma\}^{1/\gamma}} + R_{cp}\theta_c \quad (3)$$

where θ_c denotes the connection rotation, and the four parameters R_{ce} , R_{cp} , M_0 , and γ are the initial elastic stiffness, plastic stiffness, reference moment, and shape parameter for the connection, respectively. The shape of the moment-rotation curve is influenced by the parameter γ , whose magnitude is related to the strain hardening behaviour of the connection. Reference moment M_0 , plastic stiffness R_{cp} , and nominal rotation θ_{cn} determine the nominal moment capacity of the connection to be,

$$M_n = M_0 + \theta_{cn}R_{cp} \quad (4)$$

where θ_{cn} depends on the connection type and is determined from published research results. For example, when the moment-rotation response does not have a humped point, the nominal moment capacity is determined by the moment at which $\theta_{cn} = 0.02$, as suggested in the AISC design specifications (2005).

By differentiating Eq. (3) with respect to rotation θ , the tangent stiffness R_c of the connection is given by,

$$R_c = \frac{dM}{d\theta_c} = R_{cp} + \frac{R_{ce} - R_{cp}}{\{1 + [(R_{ce} - R_{cp})\theta_c / M_0]^\gamma\}^{1+1/\gamma}} \quad (5)$$

It can be seen from Eq. (5) that R_{ce} is the stiffness at the initial condition $\theta_c = 0$, and R_{cp} is the plastic stiffness as rotation θ_c tends to infinity. For practical analysis of steel frameworks, the rotation θ_c is upwardly limited by the rotation value at which the connection fracture occurs.

It is observed from Eqs. (3) and (5) that the four-parameter model reduces to a linear model with $R_c = R_{ce}$ when R_{cp} tends to R_{ce} . A bi-linear model is realized when the shape parameter γ approaches infinity; i.e., when $\theta_c < M_0 / (R_{ce} - R_{cp})$, the term $[(R_{ce} - R_{cp})\theta_c / M_0]^\gamma$ tends to zero and Eq. (5) reduces to $R_c = R_{ce}$. When $\theta_c > M_0 / (R_{ce} - R_{cp})$, the term $[(R_{ce} - R_{cp})\theta_c / M_0]^\gamma$ tends to infinity and Eq. (5) reduces to $R_c = R_{cp}$.

Stiffness Degradation Factors

To characterize the stiffness degradation as the result of member inelasticity and connection flexibility, non-dimensional factors are introduced to facilitate analysis. A rotational stiffness degradation factor associated with the member inelastic stiffness R_p obtained from Eq. (2) is given by (Grierson et al., 2005, Xu et al., 2005),

$$r_p = 1/(1 + 3EI/LR_p) \quad (6)$$

where factor r_p is interpreted as the ratio of the elastic rotation $ML/3EI$ to the total elastic and inelastic rotation $ML/3EI + M/R_p$ due to bending moment M applied at the end connected to the compound element, where the far end of the elastic member is simply supported (Xu et al., 2005). Similarly, for the member inelastic transverse shear and axial stiffnesses, T_p and N_p , defined in Eq. (2), the corresponding stiffness degradation factors t_p and n_p for the member section are given by,

$$t_p = 1/(1 + 3EI/L^3T_p); n_p = 1/(1 + EA/LN_p) \quad (7a, b)$$

The flexural stiffness degradation factor associated with the rotational stiffness of the semi-rigid connection R_c , defined in Eq. (5), is similarly given by,

$$r_c = 1/(1 + 3EI/LR_c) \quad (8)$$

which is interpreted as the ratio of the end rotation of an elastic member to the combined rotation of the member; and the semi-rigid connection due to an unit end-moment, where the far end of the member is simply supported.

Similar to that of Eqs. (7), the following two factors may be introduced to simulate the degradation of the transverse shear and normal axial stiffness of the connection,

$$t_c = 1/(1 + 3EI/L^3T_c); n_c = 1/(1 + EA/LN_c) \quad (9a, b)$$

The transverse shear and normal axial stiffnesses of the connection, T_c and N_c , in Eqs. (9) may be determined from experimental tests or other reasonable analytical means (e.g., from finite element analysis). Since little information exists in literature in this regard, it is assumed henceforth for simplicity that the stiffness degradation factor t_c and n_c defined in Eqs. (9) are to be either unity or zero, which corresponds the elastic or plastic state.

With the degradation factors defined to characterize the member inelasticity and connection flexibility, an inelastic member with semi-rigid connections at ends 1 and 2 is modeled by an assembly of end springs with an elastic member as shown in Fig. 1. Note that L = member length, E = material Young's modulus, G = material shear modulus, I = cross-section moment of inertia, A = cross-section area, and A_s = equivalent shear area.

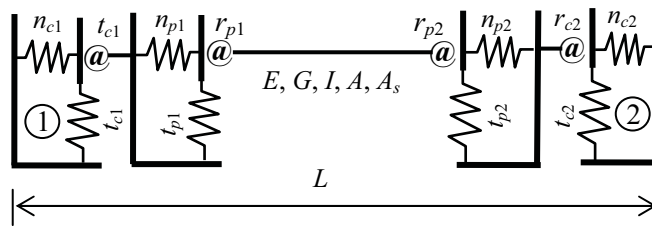


Fig. 1. Modeling of an Inelastic Member with Semi-rigid Connections

Compound Element Model

To incorporate the member inelasticity and connection flexibility into the conventional frame analysis program, a compound element model is adopted for simplicity, instead of that in Fig. 1. Given the inelastic rotational stiffness R_c and R_p determined from Eq. (5) and (2) respectively, for an applied incremental moment ΔM , the corresponding incremental rotations $\Delta\theta_c$ and $\Delta\theta_p$ can be respectively expressed as,

$$\Delta\theta_c = \Delta M / R_c; \quad \Delta\theta_p = \Delta M / R_p \quad (10a, b)$$

The total incremental rotation $\Delta\theta$ between the joint and the elastic member end is,

$$\Delta\theta = \Delta\theta_c + \Delta\theta_p = \Delta M / R_c + \Delta M / R_p = \Delta M / R \quad (11)$$

from which it is observed that a compound rotational stiffness accounting for the connection and member inelasticity is defined in the following,

$$R = \frac{1}{1/R_c + 1/R_p} = \frac{R_c R_p}{R_c + R_p} \quad (12)$$

To evaluate the combined stiffness effect, a stiffness degradation factor for the compound stiffness R defined by Eq. (12) is introduced and expressed as,

$$r = 1 / (1 + 3EI / LR) \quad (13)$$

which is the ratio of the elastic element's rotation to the sum total rotation of the compound element, and the rotation of the elastic member, when it is simply supported at the far end. From Eqs. (6), (8), (12), and (13), the compound stiffness degradation factor is expressed as,

$$r = \frac{1}{1 + 3EI / LR_c + 3EI / LR_p} = \frac{r_c r_p}{r_c + r_p - r_c r_p} \quad (14)$$

which maps $R \in [0, \infty]$ to $r \in [0, 1]$. From Eq. (14), the stiffness degradation factor for the compound element is a function of the degradation factors of the connection and member inelasticity. If any of these factors degrades to zero, the stiffness of the compound element degrades to zero as well.

In a similar manner, the compound transverse shear and normal axial stiffnesses, accounting for semi-rigid connection and member inelasticity, can be defined in the following,

$$T = \frac{T_c T_p}{T_c + T_p}; N = \frac{N_c N_p}{N_c + N_p} \quad (15a, b)$$

Thus, the corresponding compound shearing and axial stiffness degradation factors t and n are similarly given by,

$$t = \frac{t_c t_p}{t_c + t_p - t_c t_p}; n = \frac{n_c n_p}{n_c + n_p - n_c n_p} \quad (16a, b)$$

Once the compound degradation factors are defined, the compound element with six degrees of freedom shown in Fig. 2 can be adopted for the analysis of planar semi-rigid steel frameworks. The member-end displacements and forces are denoted by d_i and f_i ($i = 1, 2, \dots, 6$), respectively.

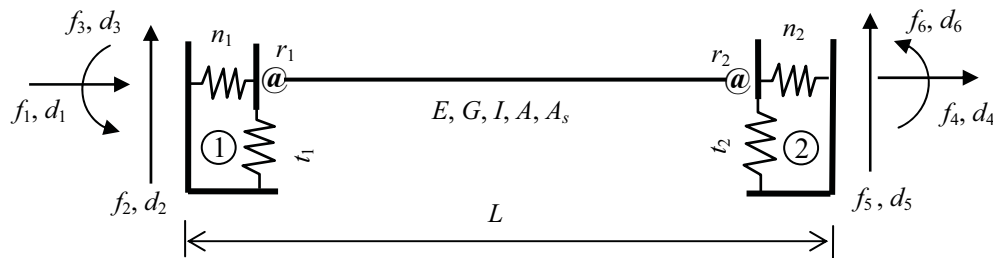


Fig. 2. Modeling of Compound Element

JOINT DAMAGE

Often, connection failures have been observed to trigger the progressive collapse of building structures. However, current analysis guidelines for conducting alternate-load path analysis (GSA, 2003; DoD, 2005) assume that structural members fail without any damage to their end-joint connections. A more likely scenario is that a connection is also damaged when a member disengages from it, and that the connection damage influences the ensuing behaviour of the remaining structure. That being the case, a

progressive-failure analysis should take connection damage into account if it is to reasonably predict the behaviour of structures subjected to abnormal loading.

As a member is removed due to local collapse, the two joints connected to the failed member are likely to undergo some damage caused by the removal. In fact, all member-ends connected to the two joints of the remaining structure are likely to undergo local damage to some degree. To take such local damage into account, two cases of stiffness deduction are considered in this study. For a joint that connects to multiple members, the damage for individual member-ends connected to the joint is characterised by modifying the corresponding stiffness degradation factor as,

$$r_{ph} = hr_p = h/(1 + 3EI/R_pL) \quad (17)$$

where r_p is the member inelastic stiffness degradation factor defined in Eq. (6). The parameter h in Eq. (17) is a joint health index that characterizes the degree of local damage. When the joint health index $h = 1$, the member-end connected to the joint is perfectly healthy, while $h = 0$ indicates the member-end is completely damaged.

In a similar manner, if a semi-rigid connection is located at the joint associated with the member removal, the joint health index h is assumed to modify the connection stiffness degradation factor as,

$$r_{ch} = hr_c = h/(1 + 3EI/R_cL) \quad (18)$$

where r_c is the member-connection degradation factor defined in Eq. (8). When $h = 1$ the connection is perfectly healthy, while $h = 0$ indicates the connection is completely damaged.

This study only considers the damage that diminishes the rotational stiffness capacity of the connections and members. However, by following similar reason as discussed in the foregoing, it is possible to account for diminished shear and axial stiffness connection capacity in the progressive-failure analysis.

NONLINEAR STRUCTURAL ANALYSIS

Once the stiffness degradation factors for the compound element shown in Fig. 2 are determined, the member stiffness matrix can be derived for the analysis of semi-rigid steel frameworks based on an incremental-load analysis procedure.

Consider a planar semi-rigid steel framework that is discretized as an assembly of members with compact or non-compact sections, for which inelastic deformation is not precluded by local buckling (AISC, 2005). The effect of the out-of-plane torsion and buckling of a member is not accounted for in the planar frame analysis. Thus, the end force-displacement relationship for the compound element in Fig. 2 is symbolically expressed as in compact matrix form as,

$$\mathbf{f} = \mathbf{k}\mathbf{d} \quad (19)$$

where $\mathbf{d} = [d_1 \ d_2 \ d_3 \ d_4 \ d_5 \ d_6]^T$ is the nodal displacement vector corresponding to end-force vector $\mathbf{f} = [f_1 \ f_2 \ f_3 \ f_4 \ f_5 \ f_6]^T$ as shown in Fig. 2. The coefficients of member stiffness matrix \mathbf{k} are summarized in the previous work (Liu et al., 2007).

After forming each local stiffness matrix \mathbf{k} for the framework based on Eq. (19), the local-axis stiffness matrices for all elements are transformed into the global coordinate system, and then assembled as the structure stiffness matrix \mathbf{K}_i , where subscript i refers to the i^{th} incremental-load analysis procedure. If \mathbf{K}_i is non-singular at the end of the i^{th} load step, the corresponding incremental nodal displacements $\Delta\mathbf{u}_i$ are solved for, and incremental member-end forces $\Delta\mathbf{f}_i$ and deformations $\Delta\mathbf{d}_i$ are found. As well, total nodal displacement at j^{th} stage $\mathbf{u}_j = \Sigma\Delta\mathbf{u}_i$, member-end forces $\mathbf{f}_j = \Sigma\Delta\mathbf{f}_i$ and deformations $\mathbf{d}_j = \Sigma\Delta\mathbf{d}_i$ accumulated over the loading history are found when local collapse occurs. The initial-yield and full-yield conditions for each member-end section are checked to detect inelastic behaviour. Degraded stiffnesses R_c , T_c and/or N_c are determined based on the moment, shear and axial forces found by the analysis at the current loading level. Stiffness degradation factors (r_p , t_p , n_p , r_c , t_c , and n_c) are applied to modify each element stiffness matrix \mathbf{k} and the structure stiffness matrix \mathbf{K} before commencing the next load step. The incremental-load analysis procedure continues until either a specified load level \mathbf{F} is reached or the structure stiffness matrix \mathbf{K} becomes singular at a lower load level, as a consequence of the failure of part or all of the structure.

The previous procedure is for conventional nonlinear analysis of steel frameworks. As progressive-collapse behaviour is taken into account for the local collapse of a frame, the above nonlinear analysis is extended to a stage-by-stage procedure. An analysis stage refers to an increment process up to a loading level at which the structure stiffness matrix \mathbf{K} become singular, or the loads are completely applied to the structure. At the end of an analysis stage, if the loads are not completely applied to the structure, and the singularity of \mathbf{K} leads to a local collapse mechanism, then the local failed member(s) is/are removed and the appropriate value of joint health index h is applied to the relevant member-ends or connections. The next stage analysis is conducted for the remainder structure under the actions of the unloading due to the removed member(s), debris loading, and the remainder loads from the previous stage. Such a stage-by-stage procedure terminates when all the external loads are completely applied to the remainder structure, or when the loading reaches a level at which the structure progressively collapses to the ground. Detailed procedure is illustrated in the following example study.

EXAMPLE STUDY

The semi-rigid steel framework shown in Fig. 3, found in the study of Liu et al. (2007), is selected to illustrate the described progressive-failure analysis procedure. The analysis investigates the collapse behaviour of the semi-rigid frame due to the removal of column C₆₉ under blast loading. Young's modulus and shear modulus of steel are $E = 200000$

MPa and $G = 77000$ MPa, respectively. The residual stress σ_r is taken $0.3\sigma_y$ for bending and axial behaviour, while for shearing behaviour it is $\tau_r = 0.05\tau_y$, where σ_y and τ_y are the normal yield stress and shearing yield stress of the steel material. The nonlinear analysis is carried out for the framework, shown in Fig. 3, in which column C₆₉ is removed due to internal blast loading.

Parameters M_n , R_{ce} , R_{ce} , and γ for the four connections are adopted from Kishi et al. (2004), and are shown in Table 1. The nonlinear moment-rotation relationships of the connections are demonstrated in Fig. 4. It is observed that the initial stiffness of all the connections satisfy the criterion being fully-rigid (Bjorhovede,1990; AISC, 2005). The related degradation factors are determined from Eq. (8) for the connections with using the tangent stiffness of the moment-rotation curves in Fig. 4. In this example, all the degradation factors defined in Eqs. (9) for shear and axial connections are set to unity; i.e., the effects of shear and axial stiffness degradations on structural response are neglected.

As the load increases in accordance with the load-incremental procedure of nonlinear analysis, the stiffness degradations due to the evolution of member inelasticity are determined, using Eqs. (6) and (7), by following the tangent stiffness defined in Eq. (2). Also, when the effect of joint damage degree is taken into account, the corresponding degradation factors r_p and r_c are modified using Eqs. (17) and (18), respectively.

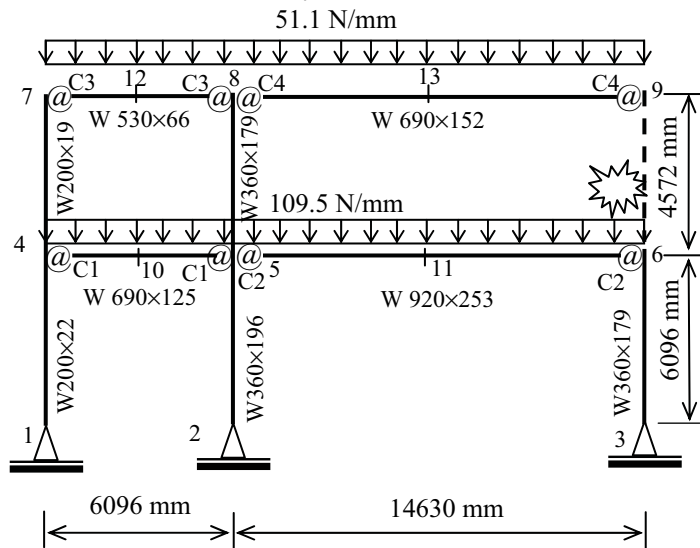


Fig. 3. Framework and Loading

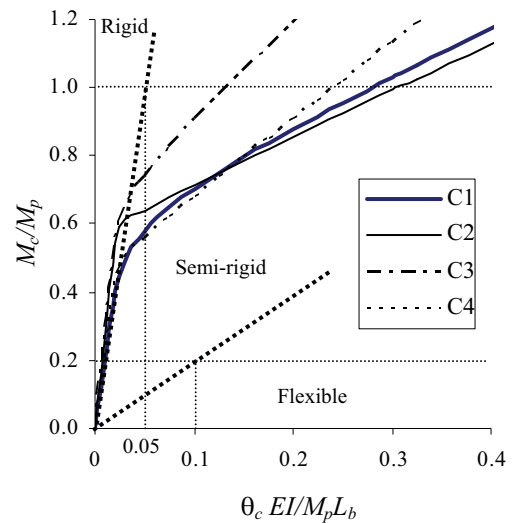


Fig. 4. Connection Curves

Table1. Connection Parameters (Kishi et al., 2004)

Connection	M_p (kN-m)	M_n (kN-m)	R_{ce} (kN-m/rad)	R_{cp} (kN-m/rad)	γ
C1 (CF6-U12x96)	995	1736	1240000	56900	1.39
C2 (EP8 with shim)	2773	3252	15300000	81600	1.20
C3 (CF5-U10x49)	387	867	893000	30300	1.18
C4 (CF5-U10x68)	1240	1494	1020000	46100	1.69

At the initial loading state of the first-stage analysis, all the values of member inelastic stiffness degradation factors r_{p0} , t_{p0} , and n_{p0} are set to unity. The initial values of the connection stiffness degradation factor r_{c0} , as shown in Table 2, are computed based on the corresponding elastic stiffnesses, R_{ce} , in Table 1. At the same time, the joint health indices are set to unity for all joints except for joint 6, where h_6 is set to 0.5 to account for the removal of column C_{69} . There is no debris load to be applied on the structure associated with the removal of column C_{69} at this stage. The vertical loads shown in Fig. 3 are incrementally applied to the frame until the occurrence of a plastic hinge at end E8 of beam B_{89} , at loading level $\lambda_{f1} = 0.226$. At this point the first stage analysis is completed because of the local collapse of beam B_{89} . The obtained degradation factors r_c , r_p , r , and member end moment M at the end of the first stage analysis are given in Table 2.

Prior to the second stage analysis, unloading occurs from disengagement of end E8 of beam B_{89} . In doing so, the applied bending moment, shear force, and axial force at end E8 are inversely applied at joint 8, and the elastic structural analysis is performed for the frame with the values of stiffness degradation factors corresponding to their elastic stiffnesses. The obtained internal forces and joint displacements are superimposed to those from stage 1. At the same time, all the loads on beam B_{89} are multiplied by an impact factor of 2, to form debris loads being applied on beam B_{56} .

At the beginning of the second stage, all degradation factors retain the values obtained at the end of the first stage analysis prior to the unloading, and the health index h_8 is set to 0.5 to account for the removal of beam B_{89} . The debris loads are applied by using the same incremental load-step size as that for the 77.4% reminder loads form the first stage analysis. The second stage analysis is ended at loading level $\lambda_{f2} = 0.859$ because of the occurrence of global instability of the frame. The stiffness degradation factors r_c , r_p , r and member end moments M at the state of $\lambda_{f2} = 0.859$ are also presented in Table 2.

Table 2. Accounting for Connection Damage and Semi-rigid Behaviour

Beam	End	r_{c0}	First stage ($\lambda_{f1} = 0.226$)				Second stage ($\lambda_f = 0.859$)			
			r_c	r_p	r	M	r_c	r_p	r	M
C ₁₄	E4	1.000	1.000	1.000	1.000	2.166	1.000	1.000	1.000	8.185
C ₂₅	E5	1.000	1.000	1.000	1.000	-188.1	1.000	0.680	0.680	-628.5
C ₃₆	E6	1.000	1.000	0.500	0.500	150.9	1.000	0.000	0.000	744.8
C ₄₇	E4	1.000	1.000	0.000	0.000	45.53	1.000	0.000	0.000	45.53

C ₄₇	E7	1.000	1.000	0.000	0.000	45.78	1.000	0.000	0.000	45.78
C ₅₈	E5	1.000	1.000	0.802	0.802	746.1	1.000	0.802	0.802	231.3
C ₅₈	E8	1.000	1.000	0.000	0.000	-853.4	1.000	0.000	0.000	-309.0
B ₄₅	E4	0.792	0.152	1.000	0.152	-47.69	0.152	1.000	0.152	-53.70
B ₄₅	E5	0.792	0.131	1.000	0.131	-339.9	0.115	0.846	0.113	-677.8
B ₅₆	E5	0.776	0.686	1.000	0.686	-218.0	0.140	0.979	0.139	1075
B ₅₆	E6	0.776	0.366	1.000	0.366	-150.9	0.083	1.000	0.083	-744.9
B ₇₈	E7	0.901	0.799	1.000	0.799	-45.78	0.799	1.000	0.799	-45.75
B ₇₈	E8	0.901	0.046	0.000	0.000	-385.6	0.023	0.000	0.000	309.0
B ₈₉	E8	0.878	0.197	0.000	0.000	1239	-	-	-	-

Note: $h_6 = h_8 = 0.5$, and M stands for member end moment (kN-m)

The effect of joint damage on the results of the progressive-failure analysis is studied in this example. It is found that the differences in the load carrying capacities of the frame are insignificant; with or without accounting for joint damages. For instance, the value of λ_{f1} associated with the first stage analysis without accounting for joint damages is nearly the same, while the value of λ_{f2} with accounting for joint damages only 0.46% less than that without accounting for the damages. However, considerable differences of inelastic stiffness degradation factors and bending moments of members adjacent to the removed member are observed in the cases with and without accounting for joint damages for both of the first and second-stage analysis.

CONCLUSIONS

Characterized by the member and connection inelastic stiffness degradation factors, the compound element method which accounts for the effects of member geometric nonlinearity, inelasticity, shear deformation, and connection nonlinearity has been extended to progressive-failure analysis by accounting for the effect of the degree of damage on joints. Preliminary analysis results show that the severity of damaged joints significantly influences the internal loading redistribution, but not the loading carrying capacity of the whole structure. Further study is needed to model and quantify the effect of joint damages.

REFERENCES

- AISC. (2005). Specification for Structural Steel buildings. ANSI/AISC 360-05, *American Institute of Steel Construction*, Chicago, IL.
- Bjorhovde, R., Brozzeti, J., and Colson, A. (1990), "A Classification System for Beam to Column Connections", *J. Struc. Engrg.*, ASCE, Vol. 116, No. 11 (pp. 3059-3076).
- DoD. (2005), *Design of Buildings to Resist Progressive Collapse*. Unified Facilities Criteria UFC 4-023-03, Department of Defense, USA.

- Grierson, D.E., Xu, L., and Liu, Y. (2005), "Progressive-failure Analysis of Buildings Subjected to Abnormal Loading", *Journal of Computer-Aided Civil and Infrastructure Engineering*, Vol. 20, No. 3 (pp. 155-171).
- GSA. (2003), Progressive collapse analysis and design guidelines for new federal office buildings and major modernization projects. Office of Chief Architect, General Services Administration, Washington, D. C.
- Kishi, N., Komuro, M., and Chen W.F. (2004), "Four-parameter Power Model for M- θ Curves of End-plate Connections", ECCS/AISC Workshop Connections in Steel Structures V: Innovative Steel Connections, Amsterdam, The Netherlands.
- Liu, Y. (2007), Progressive-failure Analysis of Steel Building Structures under Abnormal Loads, PhD Thesis, University of Waterloo, Waterloo, ON, Canada.
- Liu, Y., Xu, L., and Grierson D.E. (2007), "Compound-element Modeling Accounting for Semi-rigid Connections and Member plasticity", *Engineering Structures*, in press.
- Richard, R.M., and Abbott, B.J. (1975), "Versatile Elastic-plastic Stress-strain Formula", *J. Engrg. Mech. Div.*, ASCE, Vol. 101, No. 4 (pp. 511-515).
- Xu, L., Liu, Y., and Grierson, D.E. (2005), "Nonlinear Analysis of Steel Frameworks through Direct Modification of Member Stiffness Properties", *Advances in Engineering Software*, Vol. 36, No. 5 (pp. 312-324).

DESIGN OF PR FRAMES USING THE AISC DIRECT ANALYSIS METHOD

Donald W. White
Georgia Institute of Technology, Atlanta, GA 30332-0355, USA
dwhite@ce.gatech.edu

Arvind V. Goverdhan
Stanley D. Lindsey and Associates, Ltd., Atlanta, GA 30339, USA
agoverdhan@stl-atl.com

This paper discusses the application of the 2005 AISC Direct Analysis Method (DM) to the practical design of PR framing systems. The relative simplicity and efficacy of the DM for the design of these types of structures is emphasized. Key considerations essential to the performance of PR frames, regardless of the method of design, are listed.

INTRODUCTION

The 2005 AISC Direct Analysis Method (DM) provides a simple and intuitive approach for the stability design of all types of framing systems by incorporating nominal stiffness reductions and geometric imperfection effects into the structural analysis. This approach provides a more rational representation of the demand on the beams and beam-to-column connections. This demand is largely associated with the progressive loss of connection stiffness due to moments from combined gravity and lateral loads along with the progressive increase in $P\Delta$ effects on the imperfect structure under the application of the design loadings. Traditional approaches have emphasized the column effective length associated with a bifurcation from the initial perfect geometry, a focus that is somewhat indirect to the stability behavior of these structures. The DM utilizes the actual unsupported lengths for the member checks.

The second-order sidesway stability effects can be significant in PR frames as these structures approach their strength limit. The influence of sidesway deflections on the forces in the structure must be considered. Equilibrium must be evaluated on the deflected structure geometry. The DM accomplishes this with an accounting for overall geometric imperfections, member and connection distributed yielding effects, and uncertainty in the component stiffnesses and strengths.

With the DM, the engineer models the nonlinear connection moment-rotation responses directly/explicitly. More and more commercial programs are becoming available that allow explicit modeling of connection nonlinear moment-rotation characteristics. The DM highly streamlines the calculations while also providing a more rigorous characterization of the structural response.

OVERVIEW OF THE DM

The Direct Analysis Method (DM) uses 80 % of the elastic stiffness for all of the stiffness contributions except for heavily loaded columns with $P_u/P_y > 0.5$, where the flexural rigidity is reduced by $0.8\tau_b$. For any components that exhibit a gradual yielding response, only the component elastic stiffnesses are reduced. This requires the separation of the component deformations into elastic and plastic parts. A resistance factor of 0.9 is applied to all the member and connection resistances. The explicit nonlinear connection $M-\theta$ curve is used in the DM analysis. Also, a nominal out-of-plumbness (or imperfection effect) of $0.002L$ is assumed. The geometric imperfection effect may be modeled using a notional lateral load of $0.002Y_i$ if desired, where Y_i is the total gravity load at a given floor level. If the sidesway amplification is less than 1.5 based on the nominal stiffness (1.71 based on the reduced stiffness), the geometric imperfection effect need be included only for gravity-only load combinations). These attributes account nominally for the influence of distributed yielding and geometric imperfections at strength load levels. For purposes of simplicity, the above initial out-of-plumbness may be included for all the load combinations. The out-of-plumbness facilitates the nonlinear solution for gravity loads, since it perturbs the system into elastic unloading of the "windward" connections when connection plastic hinges start to form. All of above stiffness and strength reductions and imperfections are related to the ultimate strength assessment and need not be applied for service load analysis.

Use of a pushover analysis is recommended with the DM for consideration of lateral load combinations. The gravity loads are applied first, followed by the lateral loads. A proportional load analysis typically gives a more conservative estimate of the resistance. However a proportional load analysis is less apt to encounter nonlinear solution difficulty in lateral load combinations where hinges form at both ends of the girders under gravity load (followed by the frame swaying to the side, causing the connections on the side opposite from the sway to elastically unload).

There are important implications with respect to the application of the lower-bound theorem of plastic design when second-order effects are important. For instance, one practice employed in traditional "Type 2" PR frame designs is to analyze for gravity loads assuming perfectly pinned conditions at the beam ends but then to analyze for lateral loads assuming perfectly rigid beam-to-column connections. For structures in which the members and connections are sufficiently ductile and in which second-order effects are negligible, this practice is justified since it in effect produces a set of forces in the structure that satisfy equilibrium. However, any connections that provide substantial resistance to sidesway moments will also attract gravity moments. These additional moments, which are missed in traditional "Type 2" designs as well as in the more recent flexible moment connection method proposed by Geschwindner and Disque (2005), can cause additional yielding. This in turn affects the stiffness of the structure and influences the magnitude of the second-order effects. Indiscriminate application of the lower-bound theorem of limit analysis to problems where the resistance of the components is governed by rupture or other non-ductile limits, or application of the lower-bound theorem without consideration of significant second-order effects is generally unwise.

ANALYSIS AND DESIGN OF PR FRAMES /S INELASTIC ANALYSIS AND DESIGN

It is important to note that the design of PR frames is truly inelastic analysis and design. Appendix 1 of the 2005 AISC Specification gives the requirements for inelastic design of steel frame structures in the context of non-seismic loading. Section 1.9 of Appendix 1 calls for sufficient connection “strength and ductility to sustain the *forces* and deformations imposed under the required loads.” However, Appendix 1 focuses predominantly on requirements aimed at ensuring member ductility.

It should be noted that in PR frames, the predominant inelastic deformations often occur in the beam-to-column connections. However, in some situations, one can encounter plastic hinging in the beams, e.g., hinging within positive moment region of some of the beams in lateral load combinations. In this case, Appendix 1 applies to ensure that the beams have sufficient inelastic deformation capacity to allow beam plastic hinge rotations and inelastic redistribution. Appendix 1 requires that these beams must have:

- Compact flanges and webs in flexure, and
- “Compact” spacing of lateral braces (or continuous lateral bracing) at beam plastic hinge locations.

The slab may be designed to provide continuous lateral bracing in the positive moment regions. For beams satisfying the Appendix 1 ductility requirements, the LRFD design strength is always $\phi_b M_n = 0.9M_p$.

In addition, Appendix 1 requires that “For beam-columns, connections and connected members, the required strengths shall be determined from a second-order inelastic analysis, where equilibrium is satisfied on the deformed geometry, taking into account the change in stiffness due to yielding.” The DM satisfies this requirement directly and naturally, simply by progressively inserting member plastic hinges into the analysis in the same way that PR connection plastic hinges may be modeled. Many of the members in PR frames are not loaded to levels that involve plastic hinging at any of their cross-sections. The only change in the design of these members from conventional elastic design is that their strength requirements include forces redistributed from other regions of the structure due to the progressive yielding plus stability effects.

In cases where the design economy of PR frames leads to stiffer and stronger connections that may approach FR classification, some designs may allow inelastic limit states to be reached also in the column members (where strong-beam weak-column designs are considered adequate). For instance, traditional AISC Type 2 designs typically result in “overstressing” of the exterior building columns (Gerstle and Ackroyd 1989). The DM may be applied as a more rigorous tool than the Effective Length Method for assessing the strengths of these structures, including inelastic redistribution from the beam-column members that reach their strength limits.

White et al. (2006) explain how the DM may be applied to satisfy the provisions of AISC Appendix 1. Four example frame designs are investigated in their paper to illustrate the usefulness of the procedures. Basically, for doubly-symmetric I-section members that:

- 1) Satisfy the member ductility requirements of Appendix 1,
- 2) Are bent predominantly about their major-axis,

- 3) Have dimensions such that their out-of-plane lateral torsional buckling resistance given by Eq. (H1-2) does not govern over the in-plane resistance equations, and
- 4) If the member is subjected to large axial force, an out-of-straightness is included in the analysis ($\delta_o = L/1000$ is recommended when $P_u/P_y > 0.1$),

the beam-column failure mode always involves the member IN-PLANE inelastic strength, and the beam-column response is captured quite accurately by the DM model using Eqs. H1-1 with $P_n = P_y$ and $M_n = M_p$ as the plastic hinge yield surface. This is because, in this case, Eqs. H1-1 provide an accurate representation of the reduced beam-column plastic moment resistance accounting for the effects of the axial force. Figure 1 shows an example comparison of Eqs. H1-1 to rigorous cross-section fully plastic strengths for both a column-type and a beam-type wide-flange section.

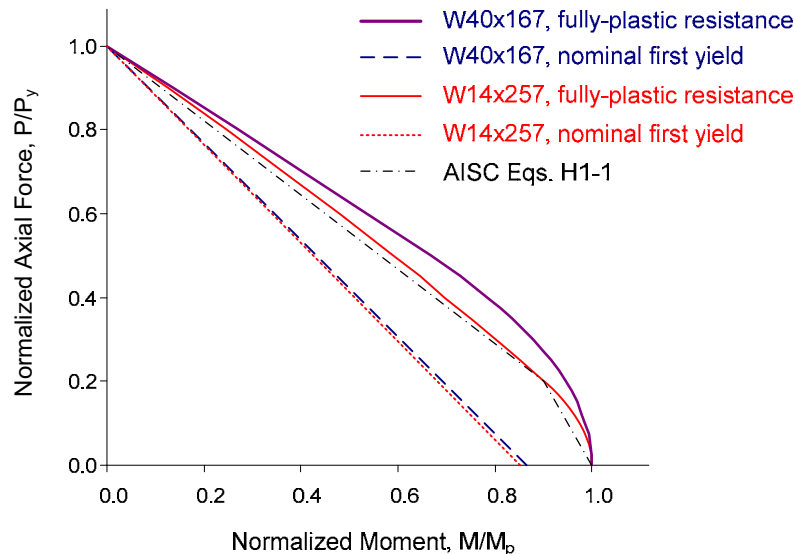


Fig. 1. Representative nominal first-yield and fully-plastic axial force-moment strength envelopes compact doubly-symmetric wide-flange sections.

In lieu of including member out-of-straightness in the frame analysis, Eqs. H1-1 may be applied using P_n based on the actual unsupported length in the plane of bending. This is precisely the approach used in the DM as it is outlined in Appendix 7 of the AISC Specification. The use of P_n based on the actual unsupported length in Eqs. H1-1 captures any potential beam-column non-sway buckling limit states in an accurate to somewhat conservative fashion. When the beam-column also satisfies requirements (1) through (4) listed above, inelastic redistribution may be allowed from the corresponding member plastic hinges. White et al. (2006) provide further details of this *inelastic* DM approach, including the handling of beam-columns subjected predominantly to minor-axis bending and axial compression. This type of approach was first suggested by Liew et al. (1994).

KEY CONSIDERATIONS

Generally speaking, any components of a structure designed such that they encounter yielding at an early load level must be proportioned carefully such that their ductility is ensured, and such that this yielding does not reduce the ultimate strength and service

stiffness of the structure below acceptable levels. For practical design of PR Frames, the following steps may be taken to help ensure good performance simplify the design:

- 1) Use a large number of PR connections throughout the structure. In contrast with FR frames, where one may limit the total number of FR connections in the structure and use simple gravity framing as much as possible, PR frames achieve their economy via the use of a large number of relatively inexpensive connections throughout the structure to develop the total required sidesway stiffness and strength.
- 2) Design the PR connections such that they fall within the intermediate range of PR behavior to close to the FR range using a classification system such as in Bjorhovde et al. (1991) The designer must be cognizant of the fact that, when elements that yield early are made weaker, the concentration of inelastic deformations in these components is certain to grow, the elastic stiffness of the components is reduced, the design against service deflection limits becomes more difficult, the likelihood that the connections will be subjected to alternating plasticity under static loadings is increased, and the likelihood that incremental collapse (including the influence of residual $P-\Delta$ moments) becomes more of a factor. Blodgett (1966) suggests that even simple connections should be designed for 0.2 times the fixed-end elastic beam moment. Tin-Loi and Vimonsatit (1993) conclude that for connection plastic resistances less than about $0.3M_p$ of the beams, alternating plasticity may be critical and can dramatically reduce the shakedown limit of the structure. In the view of the authors, PR connection strengths larger than $0.5M_p$ of the beams are advisable.
- 3) "Protect" the potentially non-ductile elements of the connections against the adverse effects of over-strength from other elements. For example, in top and seat angle connections, many designers may naively use $M-\theta$ curves from references such as Kim and Chen (1998) without ensuring against a non-ductile failure associated with the shear rupture of the fasteners attaching the angles to the beam or the tension rupture of the fasteners attaching the angles to the column.
- 4) Ensure the ductility of elements that are intended to yield. It is essential to always follow through in developing the assumed load paths and to ensure the ductile behavior of elements that respond inelastically. Engineers must be particularly mindful of the ductility of components that respond inelastically at service load levels.
- 5) Restrict the frame permanent lateral and vertical displacements to negligible values at load levels associated with a selected acceptable MRI on service gravity and lateral loads. Satisfy service drift and vertical deflection limits at load levels associated with a selected acceptable MRI on the service gravity and lateral loads. Even FR sidesway moment frames are often governed by service drift considerations. When PR connections are used, it is prudent to size the connections early in the design process to ensure that service drift limits are satisfied. Nevertheless, one cannot generally ensure a safe PR design just by providing sufficient elastic connection stiffnesses and eliminating connection yielding under the service loads.
- 6) Limit the extent of the connection elastic unloading responses. For structures designed based on the above considerations, the extent of the connection elastic unloading can be estimated reliably by subjecting the frame to a fairly simple sequential applications of the design loads. If sufficient data documenting the connection response upon moment reversal is unavailable, the connection unloading should be restricted to a portion of the theoretical elastic unloading response. The

reversed loading response of certain types of connections is relatively unknown. If a selected limit on the unloading is violated, e.g., if one does not allow moment reversal, one must select a connection configuration with a larger moment capacity. It is not appropriate to assume that connections unload in an infinitely elastic fashion for the strength design, and it is not appropriate to assume that they are either infinitely elastic or rigid for checking serviceability. The connection elastic stiffnesses and strengths are key contributors to the service deflections in PR frames. A number of methods have been suggested in the literature that over-optimistically assume rigid or fully-elastic connection response when checking service load deflections.

- 7) Consider the complete $M-\theta$ response of the PR connections. One must note that the tangent stiffness of many types of PR connections drops significantly relative to the initial tangent stiffness even at relatively small load levels. The elastic unloading response may also be nonlinear, showing a reduction in the tangent stiffness prior to the moment returning to zero and the reversal of the direction of the moment.
- 8) Carefully assess the base conditions of the structure. It is highly advantageous for PR frame designs to count upon any dependable base restraint. Griffis and White (2008) provide specific recommendations for estimating base fixity, including the incidental restraint from simple base details using $G=10$ ($K_{\text{base}} = 0.6EI_c/L_c$), or using component-based estimates including the foundation stiffness when a more accurate assessment is important. PR frames can be strongly influenced by base fixity assumptions. They can behave almost as inverted pendulums cantilevering off of the base, when the connections are weak, or after plastic hinging of a number of the connections. In some cases, the moments in the infinitely elastic $G=10$ model will approach the base capacity. The designer must recognize this so that the assumptions in the structural analysis are consistent with the behavior. The above considerations (2) through (4) should be applied for column bases that attract substantial moment.
- 9) Most building structures need to withstand the strength load combinations only a very limited number of times at most. Variable repeated application of the strength loads is not required. The recurrence interval associated with the strength load combinations is well beyond any level that need be considered as a significant repeated event. Therefore, the ability of the structure to shakedown under strength load combinations need not be explicitly evaluated. This philosophy is evident in traditional load factor design and is discussed in various books on plastic design including Horne (1979) and ASCE (1971). In a specific study of the shakedown response of traditional Type 2 steel frames, Cook and Gerstle (1987) state, "Wind- and live-load combinations that may be expected to recur several times during the lifetime of a building structure will be at levels below specified code values." Horne and Morris (1981) suggest that if checking of shakedown is thought to be necessary, "...then the incremental collapse shakedown limit must not be less than the load level at which between 20 and 50 load cycles have the same probability as a single application of the static collapse load level." They also state, "For alternating yield, the shakedown limit must not be less than the load level at which 1000 load cycles have the same probability as static collapse." Assuming a 100 year building life, the load levels associated with these actions are substantially smaller than the load levels associated with the strength load combinations.

SIMPLE ILLUSTRATIVE EXAMPLE

The geometry and loadings for a basic example frame are illustrated in Fig. 2. This layout has been studied previously by a number of authors including Geschwindner and Disque (2005). The frame is considered for non-seismic loadings including dead, roof live, floor live and wind load. The behavior under seismic loading is beyond the scope of the present discussion. The yield strength is taken as $F_y = 50$ ksi. The beams are assumed to be noncomposite but with continuously-braced top flanges. Flange-plate connections are selected in this example to simplify the connection design considerations and to allow the reader to easily follow, duplicate and scrutinize the design using basic second-order frame analysis software such as Mastan2 (Ziemian and McGuire 2006).

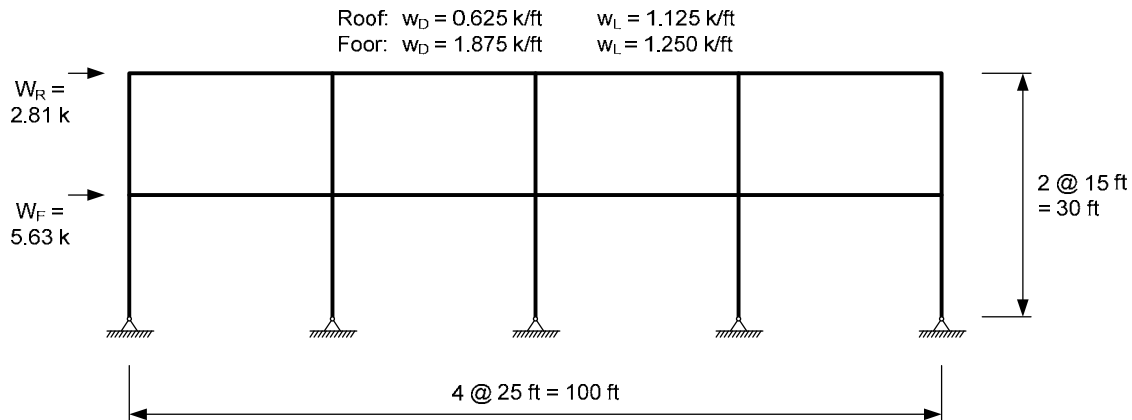


Fig. 2. Example PR frame.

One preliminary design procedure is as follows, recognizing that a wide range of procedures can be appropriate depending on the specifics of any given frame design:

- (1) Determine preliminary beam sizes using gravity load combinations and assuming moments between $w_u L_b^2/8$ and $w_u L_b^2/16$. Typically a value of $w_u L_b^2/12$ is sufficient.
- (2) Estimate the second-order sidesway amplification based on a selected service wind load and a selected drift limit for this loading (typically $L/400$ is an appropriate limit to guard against damage to typical exterior curtain or window walls or interior gypsum drywall, although larger values may be accommodated if suitable architectural details are provided (Griffis 1993)). Use the nominal (unreduced) stiffnesses in conducting these checks. Given a limit on the actual service *second-order* drift, the necessary corresponding *first-order* drift limit may be determined using a simple conversion equation discussed by White et al. (2007).
- (3) Size the columns such that the above second- and first-order drift limits are satisfied assuming ideally rigid beam-to-column connections and ideally pinned base conditions (unless explicit base fixity is to be considered in the design). If the beam flexibilities contribute substantially to the sidesway deflections, increase the beam sizes as necessary to satisfy the required drift limits.
- (4) Check the columns for strength under the anticipated critical strength load combinations. Determine the column gravity load axial forces by a simple load take-down based on tributary area. Estimate the column gravity moment using a representative unbalanced loading on the beam members framing in at the column ends. Estimate

the first-order column lateral load moments and axial forces using an approximate solution such as the portal method. Apply a second-order amplifier similar to the one used in Step (2), but considering the strength loads and the appropriate stiffness reduction at the strength load level in the DM, to these sidesway moments.

- (5) Size the beam-to-column connections such that their ultimate moment capacities are larger than a selected fraction of the connection moments determined from the above analyses, which are based on the assumption of rigid connection response. The assumed fraction here is intended to account for the fact that the connection moments will actually tend to be smaller due to the finite connection stiffnesses.
- (6) Check the PR frame with all the above preliminary connection and member sizes for the expected most critical sidesway service load combination using a second-order analysis. Modify the connections and members to satisfy the required drift limits.
- (7) In many situations, frames that are “optimally” proportioned to satisfy the above requirements will easily satisfy the various LRFD strength load combination requirements. Analyze and check the frame by the DM for the various LRFD strength load requirements considering the explicit connection $M-\theta$ responses.

Based on the above process, the following design is obtained for the example frame:

- W16x26 roof beams
- W18x35 floor beams
- W10x39 columns
- Flange-plate roof beam-to-column connections using a 5/16 x 2-3/4 inch section within the reduced-width portion of the flange plate.
- Flange-plate floor beam-to-column connections using a 7/16 x 4 inch section within the reduced-width portion of the flange plate.

The following simplified set of load combinations are considered in this example design:

- Strength Load Case 1: $1.2D + 1.6L + 0.5L_r$
- Strength Load Case 2: $1.2D + 1.6L_r + 0.5L$
- Strength Load Case 3: $1.2D + 1.6L_r + 0.8W$
- Strength Load Case 4: $1.2D + 1.3W + 0.5L + 0.5L_r$ (1.3W is used rather than the ASCE 7-05 value of 1.6W to be consistent with Geschwindner and Disque (2005))
- Service Wind plus Gravity Load Combination: $1.0D + 0.5L + 0.5L_r + 0.7W$
- Maximum Gravity Load for Consideration of Shakedown: $1.0D + 1.0L + 1.0L_r$
- Combined Gravity and Wind Load for Simplified Evaluation of Shakedown:
 $1.0D + 0.5L + 0.5L_r \pm 1.0W$

As would be expected based on the above discussions, one of the critical load combinations for this frame is the service wind plus gravity load combination. Figure 3 shows the deflected shape, connection plastic hinge locations, fractions of the applied load at the formation of the plastic hinges, and the moment diagrams for this load combination, determined under a proportional application of this loading.

Some plastic hinging of the connections occurs, but the second-order drift of the first story is limited to 0.476 in, a drift ratio of 1/378. This is close to 1/400, and thus is considered acceptable. Upon removal of the wind load, a residual drift of 0.077 in remains (a permanent story drift ratio of 1/2340). The frame has some marginal yielding

of the connections at the service load level of $1.0D + 0.5L + 0.5L_r + 0.7W$. However, all but one of the connections stays elastic up to 95 % of this load combination. A comparable design using the flexible moment connection method is grossly inadequate relative to the requirements of minor plastic deformations, service total drift, and permanent (inelastic) drift based on these loadings.

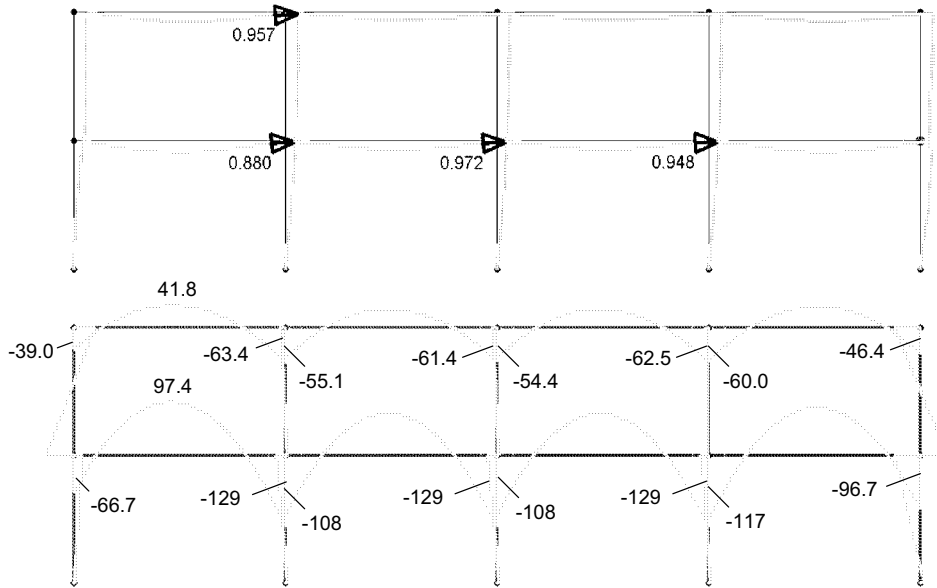


Fig. 3. Deflected geometry, connection plastic hinge locations and moment diagrams (ft-kips) under a proportional application of $1.0D + 0.5L + 0.5L_r + 0.7W$.

The deflected geometry and the sequence of plastic hinge formation for Load Case 1 are shown in Fig. 4. Plastic hinges start to form at the ends of the floor beams at 0.499 of this strength load combination. At full application of the design load, all the connections have reached their plastic capacities on the leeward (right-hand) side of both the floor beams and the roof beams. The maximum plastic rotation in the floor beam connections is 0.021 radians and the maximum plastic rotation in the roof beam connections is 0.0066 radians. These rotations occur at the interior end of the left-most beams.

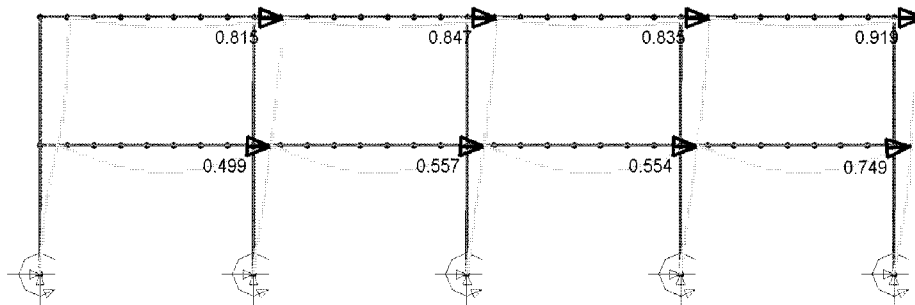


Fig. 4. Deflected geometry and sequence of connection plastic hinge formation for Strength Load Case 1 ($1.2D + 1.6L + 0.5L_r$).

An important attribute regarding the shakedown behavior is that the connection moments tend to return to their fully-plastic values upon repeated application of a selected maximum loading causing prior plastification. Therefore, the beam mid-span moments

under the maximum loads are not increased. This general tendency can be expected for all PR frames in which the connections are sufficiently stiff and strong to satisfy both strength and service drift criteria. An individual strength condition on the beams cannot be reached without the formation of a three-hinge mechanism, short of having a dramatic reduction in the loading capacity due to incremental collapse. However, the frame will never see the strength load combination levels for a sufficient number of times to induce this type of failure. Hence, there is no need to design the beams conservatively for the simple span moments as required by some PR frame design methods.

REFERENCES

- Gerstle, K. and Ackroyd, M. (1989). "Behavior and Design of Flexibly Connected Frames," Proceedings of 1989 National Steel Construction Conference, pp. 1-1 to 1-28.
- ASCE (1971). *Plastic Design in Steel, A Guide and Commentary*, American Society of Civil Engineers, 2nd Ed.
- Bjorhovde, R., Colson, A. and Brozzetti, J. (1990). "Classification System for Beam-to-Column Connections," ASCE, *Journal of Structural Engineering*, 116(11), 3059-3076.
- Blodgett, O. (1966). *Design of Welded Structures*, James F. Lincoln Arc Welding Foundation, Cleveland, OH.
- Cook, N. Jr. and Gerstle, K. (1987b). "Safety of Type 2 Steel Frames under Load Cycles," *Journal of Structural Engineering*, ASCE, 113(7), 1456-1467.
- Geschwindner, L. and Disque, R. (2005). "Flexible Moment Connections for Unbraced Frames Subject to Lateral Forces," *Engineering Journal*, AISC, 42(2), 99-112.
- Griffis, L. (1993). "Serviceability Limit States Under Wind Loading," *Engineering Journal*, AISC, 1st Quarter, 1-16.
- Griffis, L. and White, D. (2008). *Stability Design of Steel Buildings*, Design Guide, AISC.
- Horne, M. (1979). *Plastic Theory of Structures*, Pergamon Press, 2nd Ed.
- Horne, M. and Morris, L. (1981). *Plastic Design of Low-Rise Frames*, MIT Press, Cambridge, MA.
- Kim, Y. and Chen, W. (1998). "Design Tables for Top- and Seat-Angle with Double Web-Angle Connections," *Engineering Journal*, AISC, 35(2), 50-75 (Errata: *Engineering Journal*, 39(3), 2002, p. 166).
- Liew, J., White, D., and Chen, W. (1994). "Notional Load Plastic Hinge Method for Frame Design." *Journal of Structural Engineering*, ASCE, 120(5), 1434-1454.
- Tin-Loi, F. and Vimonsatit, V. (1993). "Shakedown of Frames with Semirigid Connections," *Journal of Structural Engineering*, ASCE, 119(6), 1694-1711.
- White, D., Surovek, A., Alemdar, B. and Chang, C., Kim, Y., and Kuchenbecker, G. (2006). "Stability Analysis and Design of Steel Building Frames Using the 2005 AISC Specification," *International Journal of Steel Structures*, 6(2), 71-91.
- White, D., Surovek, A. and Chang, C. (2007). "Direct Analysis and Design Using Amplified First-Order Analysis, Part 2 – Moment Frames and General Rectangular Framing Systems," *Engineering Journal*, AISC, 44(4), 323-340.

RECENT RESEARCH AND DEVELOPMENT IN SEMI-RIGID COMPOSITE JOINTS WITH PRECAST HOLLOWCORE SLABS

Dennis Lam

School of Civil Engineering, University of Leeds, Leeds, LS2 9JT, UK

d.lam@leeds.ac.uk

ABSTRACT

Composite structure incorporating steel beams and precast hollowcore slabs is a recently developed composite floor system for building structures. This form of composite construction is so far limited to simple beam-column connections. Although the concept of semi-rigid composite joints has been widely researched in the past, most of the research has been carried out on composite joints with metal deck flooring and solid concrete slabs. Research on composite joints with precast hollowcore slabs is rather limited. As the construction industry demands for rapid construction with reduction in cost and environmental impacts, this form of composite floor system, which does not require major onsite concreting, has become very popular among the designers and engineers in the UK. In this paper, full-scale tests of beam-to-column semi-rigid composite joints with steel beam and precast hollowcore slabs are reported. Based on the tests data, the structural behaviour of these semi-rigid composite joints is discussed together with numerical and finite element modelling. Through parametric studies, an analytical model for the semi-rigid composite joints is proposed and is verified by both the experimental data and finite element model; and good agreement is obtained.

INTRODUCTION

Composite floor incorporating steel beams and precast hollowcore slabs is a recently developed system for building structures. This form of composite construction is so far limited to simple beam-column connections. Compared with the traditional composite floor systems like solid R.C. slab or metal profiled decking floor system, precast floors can save construction time, reduce cost of concrete casting, etc., therefore, it is becoming more and more popular in the current construction market in the UK. In the past decades, a large number of studies have been conducted on the behaviour of composite joints, but the majority of these researches has been conducted on composite joint between steel column and composite beam with metal deck flooring system, little research has been conducted on this type of composite connection so far. As this form of composite design becoming more and more popular by the engineers and designers in the UK, a calculation method to determine the moment and rotational capacity for semi-rigid composite joint is badly needed.

Moment rotation characteristics of semi-rigid connection with metal decking slabs were first investigated by Johnson and Hope-Gill (1972). Ren et al (1995) and Anderson et al (2000) used different springs to represent the different components of the composite connections in order to calculate the joint stiffness, which is the basis of the component method which has been widely used today. Work by

Tschemmemegg (1988), Madas (1993) and Rassati et al (2004) are all based on this method.

In order to study the moment and rotation characteristic of the composite connections with precast hollowcore slabs, the best way is by carrying out full-scale tests. However, due to the expenses and limitation of the full-scale tests, non-linear finite elements method is an attractive tool for investigating this form of connection. The use of finite element could explore large number of variables and potential failure modes, which could complement the experimental studies. Lam et al (2000) were the first to simulate the behaviour of composite girders with precast hollowcore slabs; a 2-D finite element model was built using ABAQUS (2005). A 3-D FE model of the steel-precast composite beams was built by El-Lobody and Lam (2003) using ABAQUS to model the behaviour of the composite beams with precast hollowcore slabs; elastic-plastic material was used for the simulation. The model was validated against the test results and good agreement is obtained. Although there were some researches towards modelling this form of composite construction, most of the work is towards the simulation of the composite beams and little work has been done on the composite connections. Bayo et al (2006) used a new component-based approach to model internal and external semi-rigid connections for the global analysis of steel and composite frames. The method is based on a finite dimensional elastic-plastic four-node joint element that takes into consideration the joint deformation characteristics including those of the panel zone and all the internal forces that concur at the joint. Braconi et al (2007) proposed a refined component model to predict the inelastic monotonic response of exterior and interior beam-to-column joints for partial-strength composite steel-concrete moment-resisting frames. The joint typology is designed to exhibit ductile seismic response through plastic deformation developing simultaneously in the column web panel, the bolted end-plate, the column flanges and the steel reinforcement. The model can handle large inelastic deformations consistent and high ductility moment-resisting frames. Recently, attempt has been made by Fu et al (2007) to model the composite joint with precast hollowcore slabs using 3-D finite element method, however, the use of FE modelling is still far too complex and impractical for designers and a simple but accurate analytical method to calculate the moment and rotation capacities for this form of composite joint is badly needed. In this paper, an analytical method for calculating the moment and rotation capacity is presented and comparison with the full-scale tests result is made to validate its accuracy.

FULL SCALE TESTS

Full-scale joint tests with flush endplate composite connection and precast hollowcore slabs were conducted by Fu and Lam (2006). The main variables investigated were stud spacing, degree of the shear connections and the amount of longitudinal reinforcement. All specimens were of cruciform arrangement as shown in Figure 1 to replicate the internal beam-column joints in a semi-rigid composite frame. The specimen was assembled from two 3300 mm long 457×191×89UB grade S275 universal beams and one 254×254×167UC grade S275 universal column to form the cruciform arrangement. The beams were connected to the column flanges using 10mm thick flush end plates with two rows of M20 Grade 8.8 bolts. A single row of

19mm diameter headed shear studs were pre-welded to the top flange of the steel beams. The steel connection used is a typical connection used in UK practice for simple joint. Results of all the composite joint tests are shown in Table 1 and Figure 2.

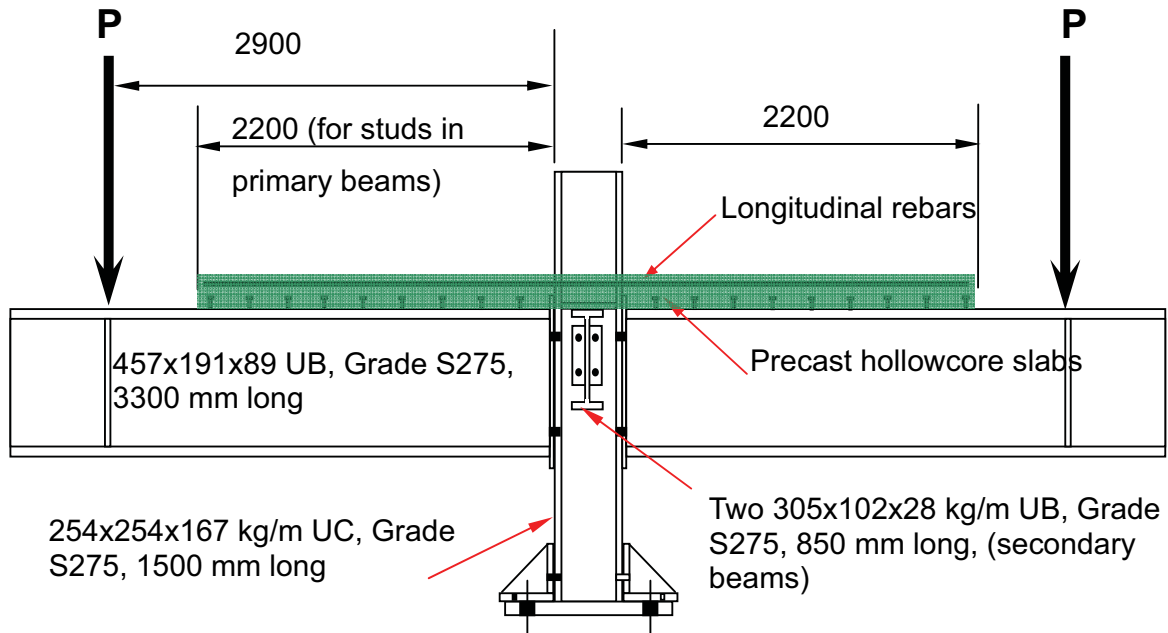


Figure 1: General arrangement of test set-up

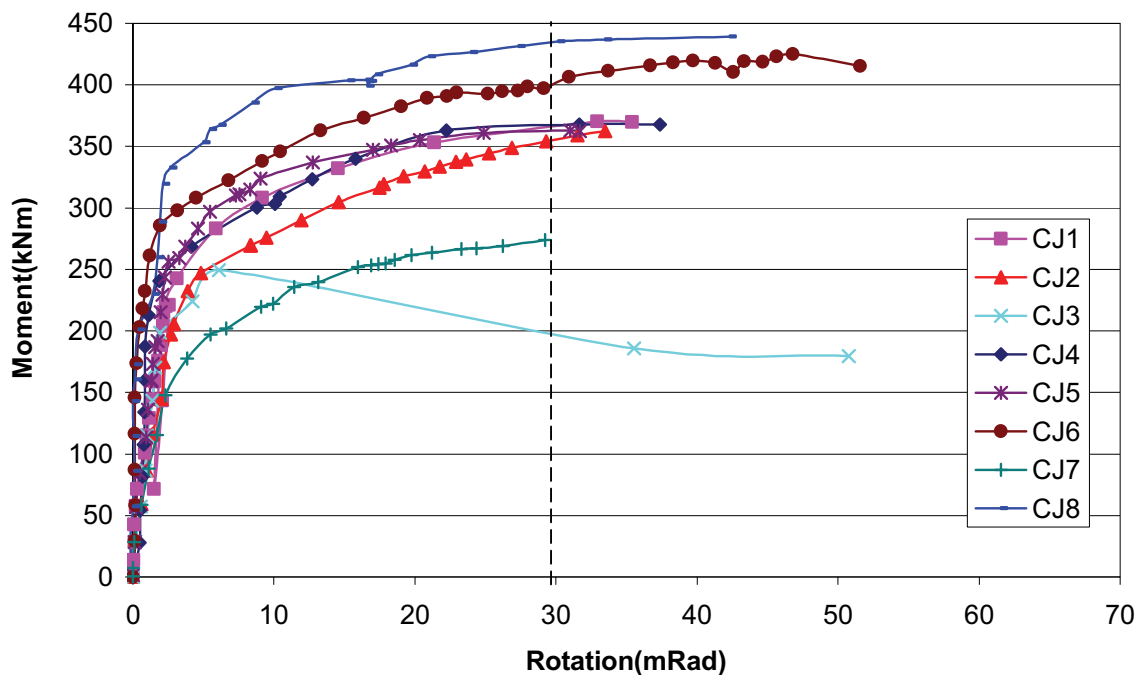


Figure 2: Moment vs. rotation curves

TABLE 1: TESTS RESULT

Reference	CJ1	CJ2	CJ3	CJ4	CJ5	CJ6	CJ7	CJ8
Moment capacity (kNm)	370	363	250	368	363	425	274	439
Rotation capacity (mRad)	35.4	33.5	6.1	37.4	31.7	46.8	30	42.3
Long. reinf. – yield (kN)	326	326	326	326	326	424	212	424
Long. reinf. – Ultimate (kN)	387	387	387	387	387	486	243	486
Shear connector capacity (kN)	896	512	256	384	384	512	256	512
Max. strain in long. reinf. ($\mu\epsilon$)	26,000	23,000	2,031	16,000	13,706	26,000	23,000	23,000
Maximum end slip (mm)	0.34	0.8	5.8	3.5	3.5	0.84	0.4	1.6
Failure mode	RF	RF	CF & SF	CF	CF	RF	RF	RF

RF – reinforcement fracture; CF – connector fracture; SF – slab shear failure

All tests except Test CJ3 failed in a ductile manner with beam rotation well in excess of 30 mRad with the moment capacity above 0.3 Mp of the composite beams, it can be concluded that these types of joints can provide sufficient moment and rotation capacity for plastic design. Tests CJ1, CJ2, CJ6, CJ7, and CJ8 were failed due to the fracture of longitudinal reinforcement while Tests CJ3, CJ4 and CJ5 failed by fracture of the shear connectors. No yielding or buckling to the column was observed. For all the tests conducted, no bond failure between the in-situ and the precast concrete was observed, therefore it can be concluded that the in-situ and the precast hollowcore slabs were acting compositely throughout.

FINITE ELEMENT MODEL

The moment and the rotation capacity of the joints were studied using the 3-D finite element method. Using the general-purpose finite element package ABAQUS, a 3-D finite element model was built to simulate the behaviour of semi-rigid composite connection with precast hollowcore slabs. As shown in Figure 3, the model use three-dimensional solid elements to replicates the composite joint of the actual full scale test. The boundary condition and method of loading adopted in the finite element analysis followed closely to those used in the tests. The load was applied at the end of the beam as shown in Figure 3. Material nonlinearity was included in the finite element model by specifying the stress-strain curves of the material taken from the test specimens. Comparisons of the FE model with the test results are shown in Table 2 and 3 and typical moment rotation curve is shown in Figure 4. It can be seen that the model results has good agreement with the experiment data.

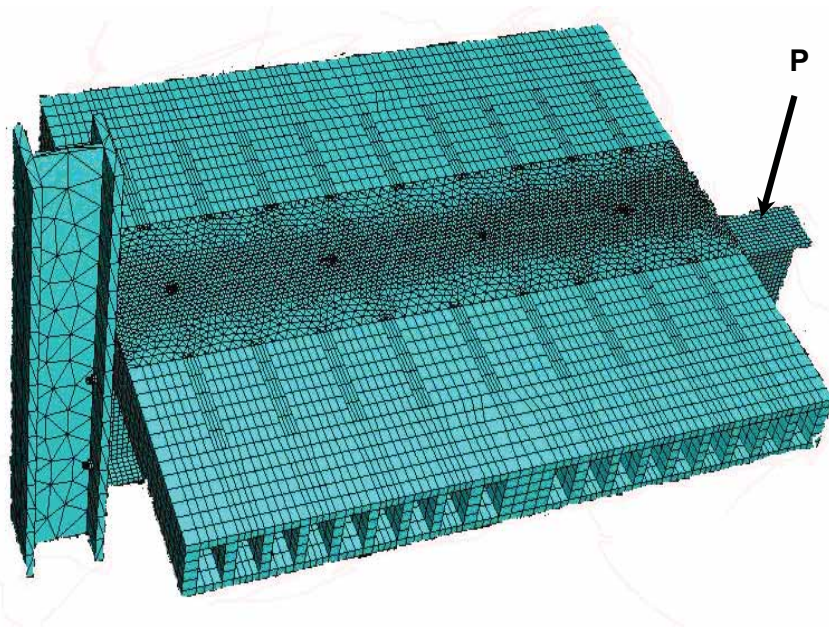


Figure 3: Finite Element Model of the Semi-Rigid Composite Joint

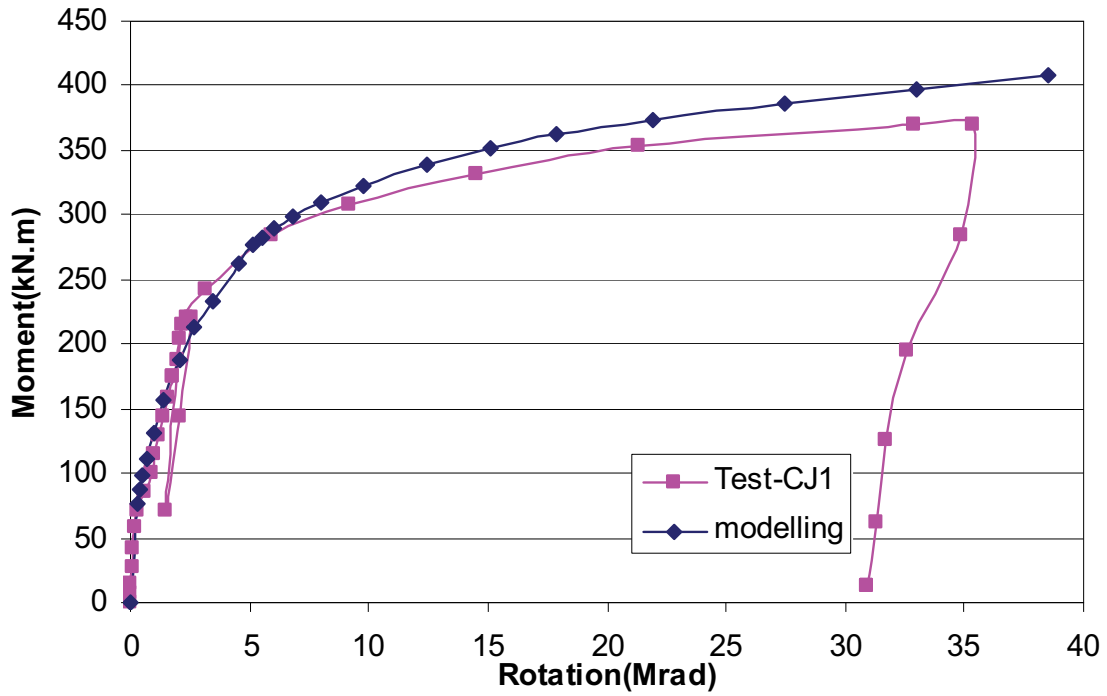


Figure 4: Comparison of Test CJ1 and the FE model

TABLE 2: COMPARISON OF MOMENT CAPACITY

Reference	CJ1	CJ2	CJ3	CJ4	CJ5	CJ6	CJ7	CJ8
Test result (kNm)	370	363	250	368	363	425	274	439
FE Model (kNm)	407	402.9	253.7	383	398	437.6	292	475

TABLE 3: COMPARISON OF ROTATION CAPACITY

Reference	CJ1	CJ2	CJ3	CJ4	CJ5	CJ6	CJ7	CJ8
Test result (mRad)	35.4	33.5	6.1	37.4	31.7	46.8	30	42.3
FE Model (mRad)	38.5	33.9	11.5	36	36.1	51.4	31.5	49.7

ANALYTICAL MODEL

Base on the full scale tests and parametric studies by Fu et al. (2007), an analytical model to calculate the moment and rotation capacity for this type of connection is derived. Figure 5 describes the force transfer mechanism for the composite joint with flush end-plates composite connection.

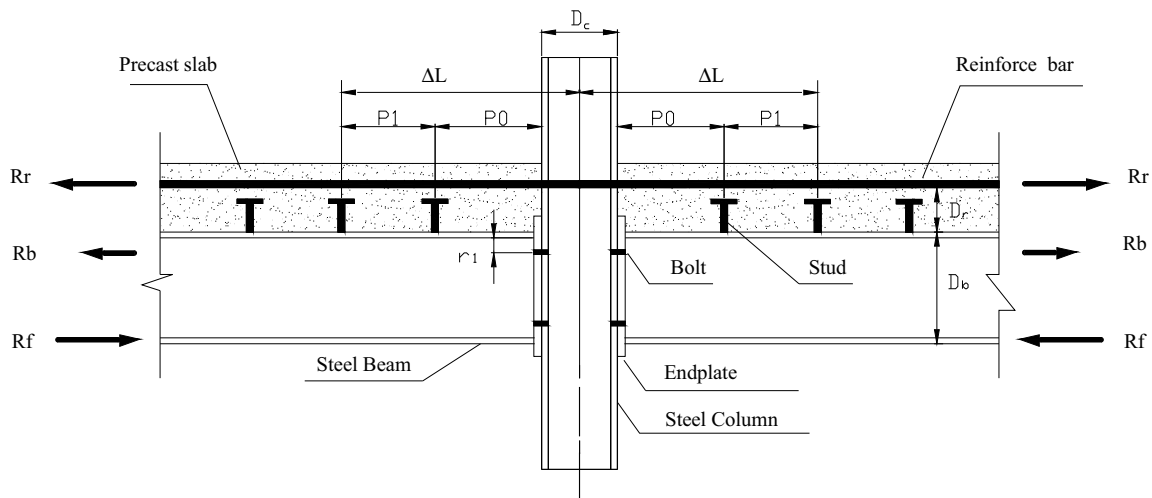


Figure 5: Load Transfer Mechanism for the Composite Joint

Tests result showed that the compression force transfer through direct bearing of the bottom flange of the beam. Due to strain hardening, it is possible for the bottom flange to resist compressive stresses of up to 1.2 times the yield strength. The tensile strength of the concrete is ignored as the tensile force of the slabs is relatively small, only the tensile strength of the longitudinal reinforcing bars was considered. A method to predict the moment capacity for this type of semi-rigid connection is proposed.

The proposed method assumes that:

$$\text{For } R_f \geq R_b + R_r,$$

R_f = compressive resistance of the bottom flange of the steel beam,

R_r = tensile strength of the longitudinal reinforcement,

R_b = effective tensile resistance of the bolt group.

The moment resistance of the composite connection, $M_{c,Rd}$

$$M_{c,Rd} = R_r(D_b + D_r - 0.5t_f) + R_b(D_b - r_1 - 0.5t_f) \quad (1)$$

D_b = the depth of the beam;

r_1 = the distance of the first row of bolts below the top of the beam;

D_r = the distance of the reinforcement above the top of the beam;

t_f = the flange thickness of the steel beam.

For $R_f < R_b + R_r$,

The neutral axis, $y_c = \frac{(R_r + R_b - R_f)}{t_w p_y}$

t_w = the web thickness;

p_y = the design strength of steel section.

The moment resistance of the composite connection, $M_{c,Rd}$

$$M_{c,Rd} = R_r(D_b + D_r - 0.5t_f) + R_b(D_b - r_1 - 0.5t_f) - R_w \frac{y_c}{2} \quad (2)$$

$$R_w = y_c t_w p_y$$

The comparison of the test results and the results from the proposed method above is shown in Table 4. The results showed that the moment capacity of the semi-rigid composite connections is dependent to the strength and the ability to mobilize the longitudinal reinforcing bars. The influential factor for their mobilization is depending on the degree of the shear connection, which is determined by the number and the capacity of the shear studs in the hogging moment region.

TABLE 4: COMPARISON OF MOMENT CAPACITY

Reference	CJ1	CJ2	CJ3	CJ4	CJ5	CJ6	CJ7	CJ8
Test result (kNm)	370	363	250	368	363	425	274	439
Analytical model (kNm)	365.8	365.8	284.5	365.0	366.6	422.3	274.0	446.7

The available rotation capacity is dependent on the mode of failure for this form of construction. For the composite joints, the deformation is provided by yielding and inelastic elongation of the slab reinforcement and slip of the shear connectors. An analytical method is proposed for predicting the rotation capacity for this form of composite joints:

$$\phi_j = \frac{\Delta_r}{D_b + D_r} + \frac{S}{D_b} \quad (3)$$

In order to determine the elongation of the longitudinal steel bar, the effective deformation length of the longitudinal rebar, ΔL need to be determined first. From the tests result, it showed that the yielding of the longitudinal reinforcement only occurred at the distance between the centre line of the column and the second stud if the distance between the first stud and the column flange is less than 900 mm. The strain in the other part of the rebar is relatively small. Hence, the effective

deformation length is assumed to be $P_0 + P_1 + D_c/2$ as shown in Figure 5 until the ultimate stress is reached. This demonstrates that position of the headed studs played an important role in the rotation capacity of the composite connections.

The deformation capacity is influenced not only by the effective deformation length and ductility of the reinforcing bars in the region near the joint but also by tension stiffening. When the concrete is cracked and yielding of the reinforcement occurred, the effect of tension stiffening increases significantly. This is because the bond between concrete and reinforcement lowers the strain away from the cracks as shown in Figure 6.

The stress-strain relationship for embedded reinforcement provides a higher stiffness and rupture at a lower ductility than the reinforcement alone. The ultimate mean strain, ϵ_{smu} in embedded reinforcement, with the tension stiffening effect taken into account, which will arise from the crack over the transmission length, L_t which the bond has broken down.

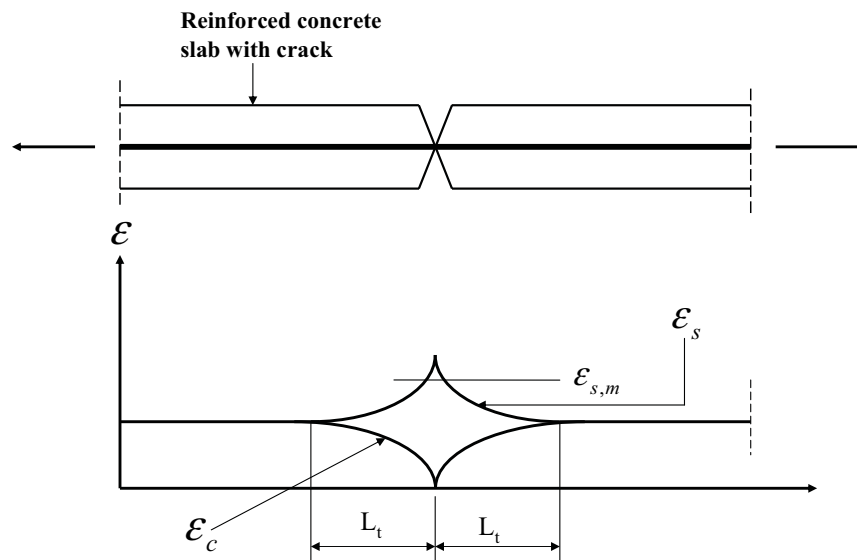


Figure 6: Strain in Cracked Reinforced Concrete

The ultimate mean strain, ϵ_{smu}

$$\epsilon_{smu} = \frac{1}{2}(\epsilon_{su} + \epsilon_{sy}) \quad (4)$$

ϵ_{su} is the ultimate strain of the reinforcement
 ϵ_{sy} is the yield strain of the reinforcement

The transmission length, L_t

$$L_t = \frac{k_c f_{ctm} \phi}{4\tau_{sm}\rho} \quad (5)$$

f_{ctm} is the tensile strength of concrete

ρ is the longitudinal reinforcement ratio where $\rho = \frac{A_s}{A_c}$

- A_s is the area of the longitudinal bar
 A_c is the area of the effective concrete slab, for composite precast hollowcore slabs, the region of the in-situ concrete infill is used.
 k_c is a coefficient that allows for the self-equilibrating stresses and the stress distribution in the slab prior to cracking where $k_c = \frac{1}{1 + \frac{h_{cs}}{2z_0}}$
 h_{cs} is the thickness of the precast slab
 z_0 is the vertical distance from the centroid of the uncracked unreinforced concrete flange to the neutral axis of uncracked unreinforced composite section, which is calculated ignoring the reinforcement and using the modular ratio for short-term effects, E_s/E_{cm} .
 ϕ is the diameter of the rebars
 τ_{sm} is the average bond stress along the transmission length and is taken as $1.8 f_{ctm}$

For full shear connection, the formula for calculating the elongation of the longitudinal rebar, Δ_r is defined as follows:

For $\rho \leq 1.0\%$,

$$\Delta_r = \left(\frac{D_c}{2} + 2L_t \right) \times \varepsilon_{smu} \quad (6)$$

For $\rho > 1.0\%$ and $P_0 \leq L_t$

$$\Delta_r = \left(\frac{D_c}{2} + 2L_t \right) \times \varepsilon_{smu} + (P_1 - L_t) \times \varepsilon_y \quad (7)$$

For $\rho > 1.0\%$ and $P_0 > L_t$

$$\Delta_r = \left(\frac{D_c}{2} + P_0 + L_t \right) \times \varepsilon_{smu} + (P_1 - L_t) \times \varepsilon_y \quad (8)$$

For partial shear connection, the ultimate mean strain, ε_{smu} is taken at the on set of strain hardening if yielding of the longitudinal reinforcement can be achieved. Otherwise, ε_{smu} is taken as the yield strain, ε_y . The stress strain curve of the longitudinal rebar is shown in Figure 7.

The slip of the shear connectors can be taken directly from the standard push test. Figure 8 shows the load vs. slip curve of the 19mm headed shear stud. The correspondence shear force of the stud is taken as

$$F_s = \frac{A_s f_y}{n} \quad (9)$$

- $A_s f_y$ is the maximum yield strength of the longitudinal reinforcement;
 n is the total numbers of shear connector.

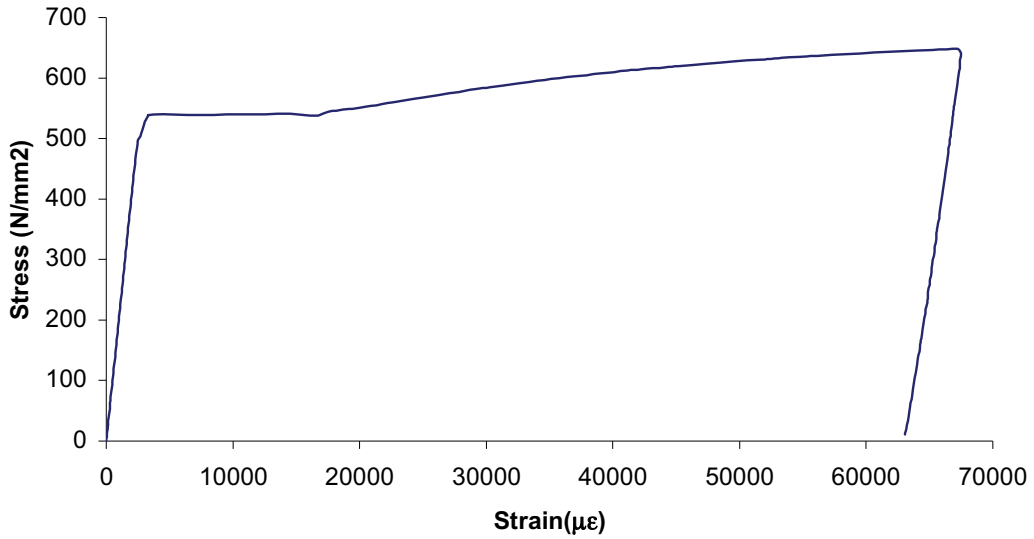


Figure 7: Stress vs. Strain Curve of the Reinforcing Bar

The comparison of the test results and the results from the analytical method for rotation capacity above is shown in Table 5. Results showed a reasonable agreement between the test results and the analytical method with the exception of CJ3 which is due to premature failure of the slabs.

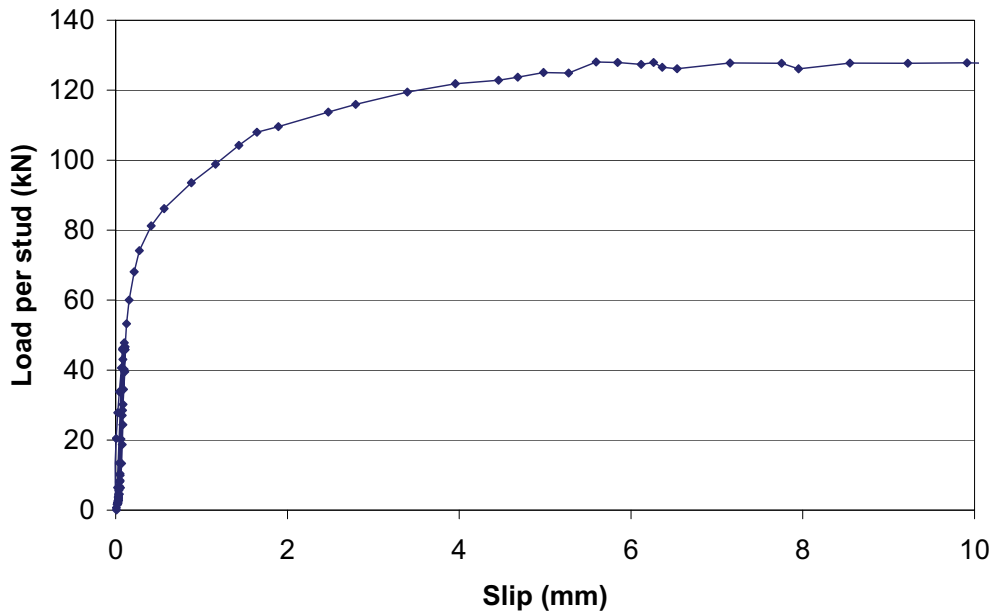


Figure 8: Load vs. Slip of 19mm Headed Shear Stud

TABLE 5: COMPARISON OF ROTATION CAPACITY

Reference	CJ1	CJ2	CJ3	CJ4	CJ5	CJ6	CJ7	CJ8
Test result (mRad)	35.4	33.5	6.1	37.4	31.7	46.8	30	42.3
Analytical method (mRad)	29.1	31.3	18.7	30.0	28.7	43.4	27.9	53.6

CONCLUSIONS

Tests program designed to study the moment and rotation capacity of the composite joints with precast hollowcore slabs has been described as well as the FE model built to investigate the structural behaviour of the composite joints. The comparison with the test results showed that the proposed model can accurately represent the overall behaviour of the composite joints. Based on the parametric studies and experimental results, an analytical method to calculate the moment and rotation capacity of the composite joints with precast hollowcore slabs were derived and good agreement has been obtained when compare with the tests results. The results show that the proposed analytical method is adequate to use for designing this form of composite joints.

REFERENCES

- ABAQUS, (2005), Hibbitt, Karlson and Sorensen, Inc., Version 6.4.
- Anderson, D., Aribert, J.M., Bode, H., and Kronenburger, H.J. (2000), 'Design rotation capacity of composite joints', *The Structural Engineering*, Vol.78, No.6, pp.25-29.
- Bayo E., Cabrero J.M. and Gil B. (2006), 'An effective component-based method to model semi-rigid connections for the global analysis of steel and composite structures', *Engineering Structures*, Volume 28, Issue 1, pp 97-108.
- Braconi A., Salvatore W., Tremblay R. and Bursi O. S. (2007), 'Behaviour and modelling of partial-strength beam-to-column composite joints for seismic applications', *Earthquake, Engineering and Structural Dynamics*, Vol.36, pp142–161.
- Ei-Lobody, E. and Lam, D. (2003), 'Finite Element Analysis of Steel– Concrete Composite Girders', *Advances in Structural Engineering*, Vol.6, No.4, pp. 267 – 281.
- Fu, F. and Lam, D., (2006) 'Experimental study on semi-rigid composite joints with steel beams and precast hollowcore slabs', *Journal of Constructional Steel Research*, Vol.62, No. 8, pp 771-782.
- Fu, F., Lam, D. and Ye, J.Q. (2007), 'Parametric study of semi-rigid composite connections with 3-D Finite element approach', *Engineering structures*, Vol. 29, Issue 6, ,pp. 888-898.
- Johnson, R.P., and Hope-Gill, M.C. (1972), 'Semi-rigid joints in composite frames', *International Association for Bridge and Structural Engineering*, Ninth Congress, Amsterdam, pp.133-44.

Lam, D., Elliott, K. S. and Nethercot, D. A. (2000), 'Parametric study on composite steel beams with precast concrete hollow core floor slabs', *Journal of Constructional Steel Research*, Vol. 54 (2), pp. 283-304.

Madas, P.J. (1993), 'Advanced modelling of composite frames subject to earthquake loading', Ph.D. Thesis, University of London.

Rassati, G.A., Leon, R.T., and Noe, S. (2004), 'Component modeling of partially restrained composite joints under cyclic and dynamic loading', *Journal of Structural Engineering*, ASCE, Vol. 130(2), pp. 343 - 351.

Ren, P., and Crisinel, M. (1995), 'Prediction method for moment-rotation behaviour of composite beam to steel column connections', *Third international workshop on connections in steel structures*, Trento University, Italy.

Tschemmernegg, F. (1998), 'On the nonlinear behaviour of joints in steel frames, *Connections in steel structures: Behaviour, strength and design*', Elsevier Applied Science Publishers, London, pp.158-165.

SEISMIC STRENGTH OF MOMENT END-PLATE CONNECTIONS WITH ATTACHED CONCRETE SLAB

Michael W. Seek

Walter Seek Engineering, Johnson City, TN 37601, USA
mseek@vt.edu

Thomas M. Murray

Virginia Tech, Blacksburg, VA 24061, USA
thmurray@vt.edu

ABSTRACT

This paper presents the results of a test of an eight-bolt stiffened moment end-plate connection with a concrete slab attached. During a previous test of a moment end-plate connection with a concrete slab, premature tension bolt rupture occurred because the concrete slab was placed directly against the supporting column flanges. This successful test was conducted with a gap between the concrete and the column flanges. It is shown that with proper detailing, moment end-plate connections with floor slabs can be used in special moment frames. Recommendations for detailing concrete slabs at moment end-plate and similar bolted connections are made.

INTRODUCTION

A test was conducted to verify that a moment end-plate connection used in conjunction with a concrete structural slab could perform satisfactorily to pre-qualify the connection for use in Special Moment Frames provided that the concrete structural slab is properly detailed. A test reported by Sumner, et. al. (2000) of an end-plate connection with a concrete structural slab showed that the bolts at the flange opposite the structural slab could fail prematurely when compressive forces are developed in the structural slab at the connection. To prevent engagement of the structural slab near the connection, for this test, the slab was detailed to provide a gap between the structural slab and the column face at the connection and shear studs were eliminated for a distance of 1.5 times the beam depth from the expected plastic hinge location as recommended in Sumner and Murray (2002).

DESCRIPTION OF TEST SPECIMEN

The test specimen consisted of two W27x84 (A992) beams attached to each flange of a W14x311, A36 steel column in an interior configuration. (Because of funding constraints an available A36 section was used for the column.) The beam-column connections were made with eight-bolt, extended, stiffened end-plate connections. The

connections were designed using the procedures in the AISC Steel Design Guide 4, 2nd Ed, (Murray and Sumner 2004). The connection was designed such that the no-prying moment strengths (M_{PR}) of the bolts and the end-plate were as close as possible to the probable maximum beam moment (M_f). Because the measured yield strength of the beam was larger than anticipated, the probable maximum moment exceeded the no-prying moment capacity of the connection by 8.8%.

Each connection consisted of two rows of two bolts on the outside of each flange and two rows of two bolts on the inside of each flange. All bolts were 1-1/8 in. diameter, Grade A325. The bolts were on a 7-1/2 in. gage with 3-3/4 in. spacing between rows and located 2 in. from the face of each flange. Each end-plate was 1-1/4 in. thick of specified A36 steel. A 3/4 in. thick, A36 steel, stiffener in the plane of the girder web was provided to stiffen the extended portions of the end-plate outside. The layout of the end-plate is shown in Figure 1.

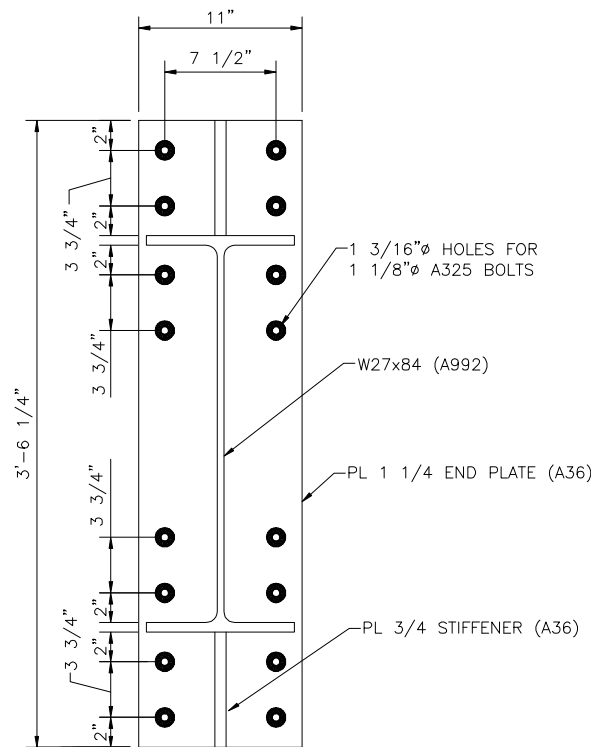


Figure 1. End-plate Layout

One-half of the bolts were instrumented with a “bolt” strain gauge to measure bolt strain during loading. The tension in the instrumented bolts was monitored during installation as the bolts were installed to the specified pretension force in the AISC *Specification for Structural Steel Buildings* (2005). Non-instrumented bolts were installed by the turn of the nut method based on number of turns required to pretension the instrumented bolts.

Two W14x22 filler beams attached to the web of the column and four W14x22 filler beams attached to the W27x84 girders supported a composite slab with special detailing in the area of the beam-column connection to minimize the impact of the composite slab on the performance of the connections. The layout of the test specimen is shown in Figure 2. Figure 3 is a photograph of the test setup.

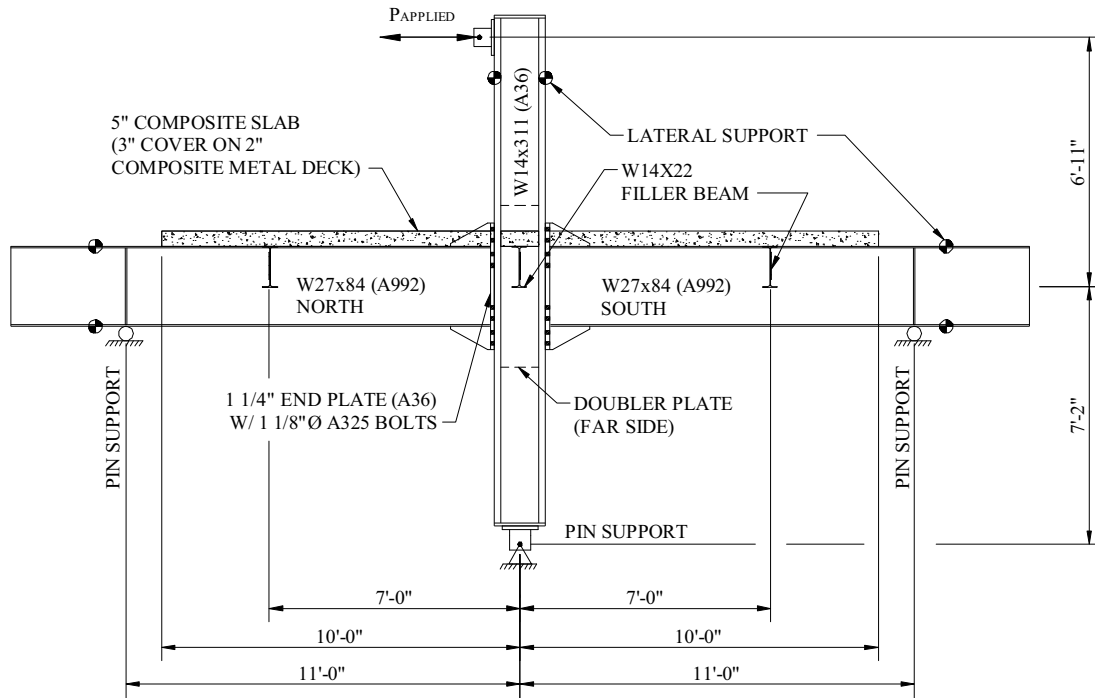


Figure 2. Elevation of Test Setup



Figure 3. Photograph of Test Setup

The beam-column sub-assembly included a 5 in. thick, 20 ft long by 6 ft wide normal weight composite slab. The slab was supported on the W27x84 girders and the six W14x22 filler beams. The filler beams supported the slab at the column centerline and in each direction at 7 ft from the column centerline. Twelve 3/4 in. diameter A108 shear studs ($F_U = 65$ ksi) with a 4-1/2 in. installed height were welded to the girders and the outer filler beams as shown in Figure 4. To protect the region of expected plastic hinging, studs were not welded to the girders for a distance of 1.5 times the beam depth (40.5 in.) from the end of the end-plate stiffener. Studs were not installed on the filler beams that were attached to the web of the columns. The 5 in. thick slab (3 in. cover on 2 in. ribbed deck) was placed on Vulcraft 2VLI, 20 gage, zinc coated composite steel deck. The deck was fastened to the beams by the stud welds only. The slab was reinforced with 4 x 4 - W2.9 x W2.9 welded wire fabric. A piece of 8 in. wide, 3/8 in. thick neoprene was used to form a gap between the slab and the end-plate and the column flanges. The gap provided a minimum clearance of 1/2 in. and the void was filled with spray foam insulation. The concrete slab was wet cured for 5 days and had a 40 days compressive strength of 3600 psi.

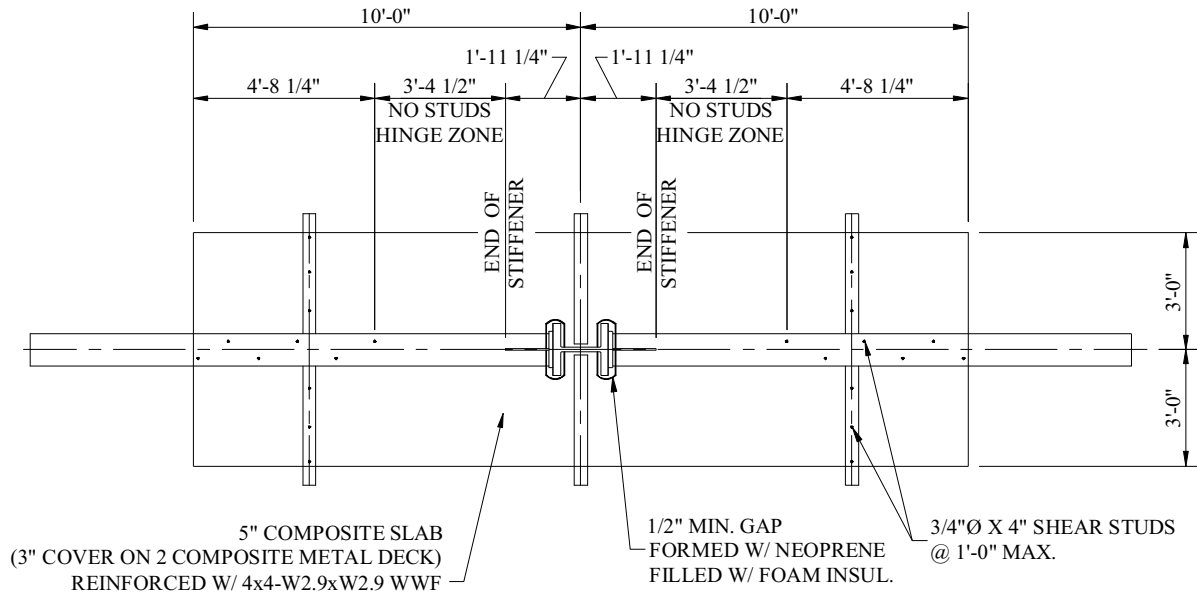


Figure 4. Plan View of Test Setup

End-plate welds were made using Gas Metal Arc Welding (GMAW) processes with 1/16 in. diameter Tri-Mark Metalloy 76 metal cored gas shielded carbon steel wire in accordance with AWS Specifications. The flange-to-end plate weld was made using a single-bevel-groove weld similar to AWS TC-U4b-GF. The beam flanges were prepared with a full depth 45 degree bevel with the root at the web side of the flange. The beam web was prepared with 45 degree half-depth bevels on each side. Weld access holes were not provided. The generic welding sequence for moment end-plate connections shown in Figure 5 was used. The web double bevel groove weld was placed first. Next 5/16 in. backing fillets were placed on the inside of each flange. The root of the bevel was then back-gouged and the flange groove welds placed. In the region of the flange-

web intersection, a partial penetration groove weld similar to AWS BTC-P4-GF was used. The stiffener was clipped to provide clearance from the flange weld and attached using double bevel groove welds.

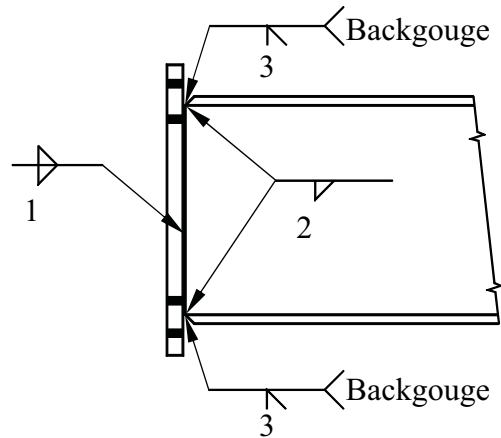


Figure 5. Welding Sequence

The design of the column panel zone was in accordance with the provisions of the AISC Seismic Provisions for Structural Steel Buildings (2002) and the recommendations of the AISC Prequalified Connections for Special and Intermediate Moment Frames for Seismic Applications (2005a). The panel zone of the W14x311 column was reinforced with a 3/4 in., A36 steel doubler plate on one side of the column web. The doubler plate was beveled full depth 15 degrees with a 3/16 in. root opening along the intersection with the column flange, and a complete joint penetration single bevel groove weld was placed using a GMAW process. A 1/4 in. fillet weld was placed between the doubler plate and column web. Continuity plates were not used.

Tensile coupons were taken from the bottom flange of each beam from portions of the beam that did not sustain significant stresses during the cyclic testing. A tensile coupon representative of the end-plate was taken from the same plate material as the end-plates. Tensile coupon test results of the beam and end-plate material are listed in Table 1.

Table 1. Tensile Coupon Test Results

Coupon	Thickness (in.)	Width (in.)	Area (in.)	Upper Yield Stress (ksi)	Dynamic Yield Stress (ksi)	Ultimate Stress (ksi)	Elongation (%)
North Beam	0.653	1.499	0.979	65.2	64.6	81.7	28.8
South Beam	0.652	1.499	0.977	64.7	64.3	82.1	28.1
End Plate	1.283	1.500	1.924	51.1	49.9	78.2	30.9

INSTRUMENTATION

One-half of the bolts used in the moment end-plate connection were instrumented with strain gauges. Two instrumented calipers were used to measure the separation between the north end-plate and the column. The calipers were placed across the thickness of the end-plate and column flange at the inside of the top and bottom beam flanges. To measure the deformations in the column panel zone, a pair of plunger type potentiometers was placed diagonally in the panel zone on the side of the column that was not reinforced with the doubler plate. Additionally, each side of the panel zone was instrumented with two 120 ohm, three gauge, 45 degree rosettes. One of the rosettes was placed at the center of the panel zone and the other placed in the lower left hand corner of the panel zone. Slip in the concrete slab relative to the beams was measured using two plunger type potentiometers that were placed approximately 3.5 ft and 9 ft from the centerline of the column on each beam.

LOADING PROTOCOL

The specimen was loaded according to the protocol specified in Appendix E of the *Protocol for Fabrication, Inspection, Testing and Documentation of Beam-Column Connection Tests and Other Experimental Specimens* Report No. SAC/BD-97/02 from the SAC Joint Venture (1997). The report specifies stepwise increasing deformation cycles based on the inter-story drift angle, θ , of the specimen. Load was applied to the column tip and the total inter-story drift angle was derived from the displacement of the column tip by dividing the column tip displacement by the height of the column (169 in.). Rigid body movements were eliminated from the net column tip displacement by subtracting the displacements at the column base and each beam tip.

DESCRIPTION OF PERFORMANCE

During the cycles of 0.015 radians of story drift, light flaking of the whitewash on the beam bottom flange was observed, indicating the onset of yielding in the bottom flange. Yielding of the bottom flange became more apparent during the cycles of 0.02 radians of story drift and cracking in the slab was observed. During the cycles of 0.03 radians of story drift, the bottom flange of each beam buckled as shown in Figure 6. Some yielding of the end-plate stiffener was observed as well as yielding in the panel zone on the doubler plate side of the column. Crushing of the concrete at the column in the area of the stiffener was observed as shown in Figure 7. Longitudinal cracks propagating from the stiffener parallel to the beams offset about 3 in. from the beam centerline were also observed as shown in Figure 7. Several of the bolts on both the inside and outside of the bottom flange had loosened to where they could be turned by hand. The specimen completed only 1/2 cycle at 0.04 radians of story drift before failure of the test frame was eminent. Two attempts to complete the first full cycle were made but large deformations of the pin support at pin at the column base prevented the achievement of the desired story drift. A third attempt to reach 0.04 radians of story drift was made by extending the ram at the south beam tip. In each case, loading was stopped short of

the desired drift angle for fear of failure of the test frame. At the time the test was aborted, the end-plates had shown no signs of distress. Very little separation of the end-plate from the column flange was observed and only minor flaking of whitewash was observed on the edges of the endplate adjacent to the bottom flange.

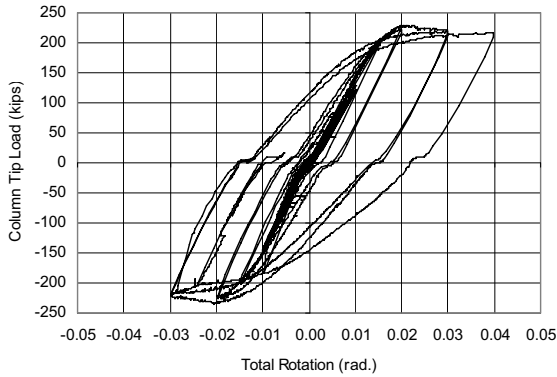


Figure 6. Yielding and Bottom Flange Buckle

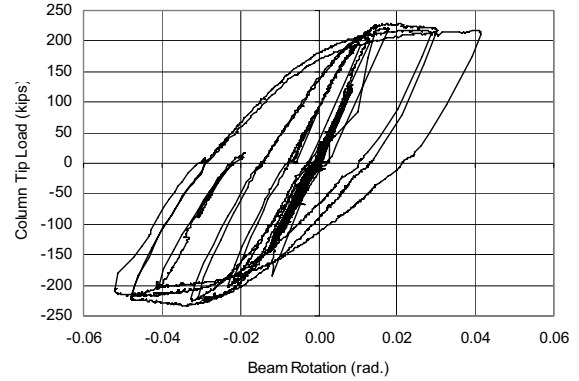


Figure 7. Cracking of Slab

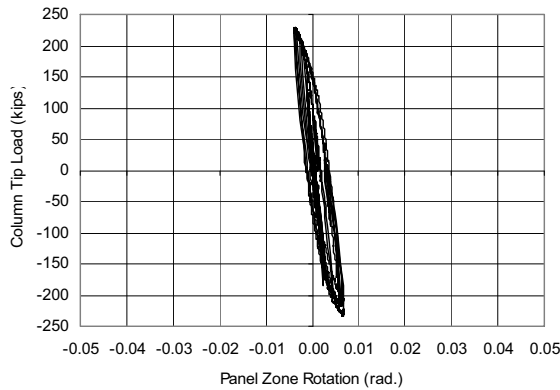
A peak column tip load of 229.3 kips was applied. The maximum net column tip displacement, δ_c , achieved was 6.750 in. which corresponds to an inter-story drift angle, $\theta = 0.04$ radians. The corresponding contribution of the beams, column and panel zone to the total total tip displacement is $\delta_{beam} = 5.568$ in., $\delta_{col} = 1.687$ in. and $\delta_{pz} = -0.506$ in. The corresponding rotations of the beams, column and panel zone are $\theta_{beam} = 0.051$ radians, $\theta_{col} = 0.010$ radians, and $\theta_{pz} = -0.030$ radians respectively. The total rotation response and the contributions of the individual components relative to the column tip load are shown in Figure 8. The strain in the bottom flange bolts of the south north beam is shown relative to the south beam centerline moment in Figure 9.



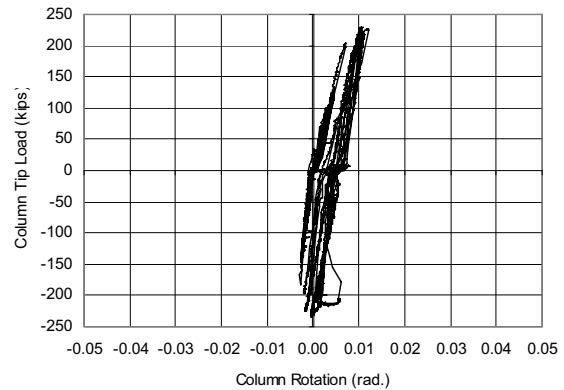
(a) Column tip Load vs Total Rotation



(b) Column Tip Load vs Beam Rotation



(c) Column tip Load vs Panel Zone Rotation

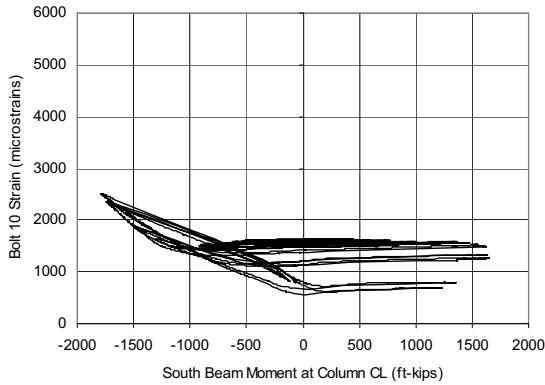


(b) Column Tip Load vs Column Rotation

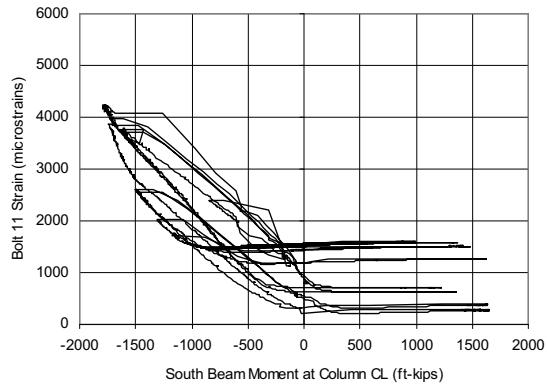
Figure 8. Specimen Rotation Response Relative to Column Tip Load

CONCLUSIONS

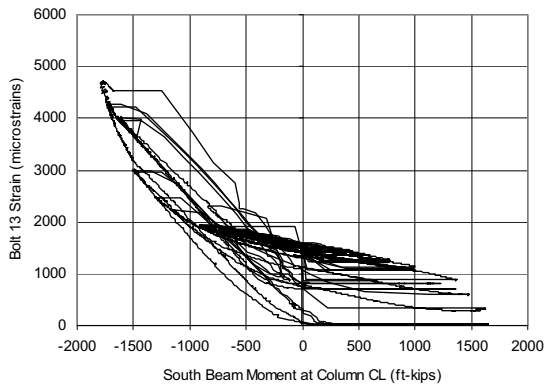
The test showed that when a ½ in. minimum gap is provided between the structural slab and the face of the column and when shear studs are eliminated for a distance of 1.5 times the beam depth from the expected hinge location, a composite slab does not negatively affect the performance of a bolted moment end plate connection. The test specimen was subjected to only ½ cycle at 0.04 radians instead of the desired 2 full cycles due to eminent failure of the test frame. Because both beam bottom flanges buckled during the cycles at 0.03 radians resulting in slight strength degradation and the connection did not exhibit signs of distress, it is believed that the specimen could have endured the full 2 cycles at 0.04 radians had the test frame not failed.



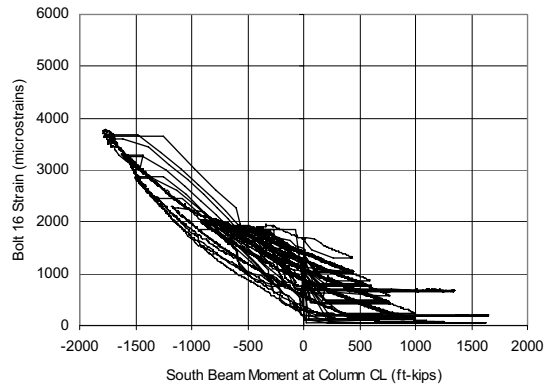
(a) Bolt 10 Strain vs S. Beam Moment



(b) Bolt 11 Strain vs S. Beam Moment



(a) Bolt 13 Strain vs S. Beam Moment



(b) Bolt 16 Strain vs S. Beam Moment

Figure 9. South Beam Bottom flange Bolt Strain vs Beam Moment

RECOMMENDATIONS

At moment end-plate and similar bolted moment connections, to eliminate the composite action between the slab and beam in the regions of the beam where plastic hinges are expected, the following slab and shear stud detailing is recommended:

- Shear studs should not be placed along the top flange of the connecting beams for a distance from the face of the column, one and a half times the depth of the connecting beam.
- Compressible expansion joint material, at least $\frac{1}{2}$ in. thick, should be installed between the slab and the column face.

- The slab reinforcement in the area within two times the depth of the connecting beam from the face of the column should be minimized.

REFERENCES

AISC (2002), *Seismic Provisions for Structural Steel Buildings*, American Institute of Steel Construction, Chicago, IL

AISC (2005), *Specifications for Structural Steel Buildings*, American Institute of Steel Construction, Chicago, IL.

AISC (2005a), *Prequalified Connections for Special and intermediate Moment Frames for Seismic Applications*, American Institute of Steel Construction, Chicago, IL.

Murray, T. M. and Sumner, E. A., (2004) *End-Plate Moment Connections – Wind and Seismic Applications*, Design Guide Series 4 – 2nd Edition, American Institute of Steel Construction, Chicago, Illinois, 2004, 158 pages.

Sumner, E. A. and T. M. Murray, "Behavior of Extended Moment End-Plate Connections Subject to Cyclic Loading," *Journal of Structural Engineering*, ASCE, Vol. 128, No. 4, April 2002, pages 501-508.

Sumner, E. A., T. W. Mays and T. M. Murray, "Heavy Moment End-Plate Connections Subject to Seismic Loading," *Behavior of Steel Structures in Seismic Areas – STRESSA 2000*, Balkema, Rotterdam, 2000, pp. 735-740.

The SAC Joint Venture (1997), *Protocol for Fabrication, Inspection, Testing and Documentation of Beam-Column Connection Tests and Other Experimental Specimens* Report No. SAC/BD-97/02.

PREQUALIFICATION TESTING OF BUILT-UP T-STUB CONNECTIONS FOR USE IN MOMENT RESISTING FRAMES

Elie G. Hantouche

University of Cincinnati, Cincinnati OH, USA
hantoueg@email.uc.edu

Gian A. Rassati

University of Cincinnati, Cincinnati, OH, USA
gian.rassati@uc.edu

James A. Swanson

University of Cincinnati, Cincinnati, OH, USA
james.swanson@uc.edu

Roberto T. Leon

Georgia Institute of Technology, Atlanta, GA, USA
roberto.leon@ce.gatech.edu

ABSTRACT

One of the developments to result from the experimentation following the 1994 Northridge earthquake is the requirement that all beam-to-column connections used in Special Moment Frames (SMF) and Intermediate Moment Frames (IMF) be prequalified by testing prior to their use. The appropriate section of the AISC Seismic Provisions reference ANSI/AISC 358, *Prequalified Connections for Special and Intermediate Steel Moment Frames for Seismic Applications*, wherein several types of connections are detailed based on prequalification testing that was performed during the SAC Project funded by FEMA or during subsequent testing. This paper outlines ongoing efforts to demonstrate bolted T-stub Connections, referred to as Double-Tee Connections in ANSI/AISC 358, as prequalified for both SMFs and IMFs. These efforts include analytical studies and testing at the University of Cincinnati and Georgia Institute of Technology to build upon the experimentation previously conducted to provide a more robust data set for analysis. Additionally, the researchers intend to demonstrate the acceptability of T-stub components that are built-up from plates in addition to the rolled T-stubs that have already been successfully tested.

INTRODUCTION

The 1994 Northridge earthquake caused numerous and unexpected brittle failures of welded connections. Damage occurred at the beam-to-column connections and

included fractures of full penetration welds, cracks in beam flanges, and cracks through the column sections. The connection failures were not only brittle, but also occurred at unpredictably low levels of plastic beam rotation. As a possible alternative, studies on the use of bolted connections (rigid and semi-rigid) for seismic resistance were conducted. Bolted connections have the advantage of eliminating the difficulties of field welding and facilitate shop welding with field bolting.

An extensive study of T-stub connections was performed in 2000 at the Georgia Institute of Technology by Swanson and Leon (2000) as part of Phase II of the SAC Project. Six full scale beam-to-column connection tests were performed using small and medium-size members. The connection designs were similar to the one presented in this paper; the beam was connected to the column by T-stubs cut from wide flange sections. In two specimens, the beam was made of a W21x44 section and in the other four specimens a W24x55 beam section was used. A W14x145 column section was used for the column in all experiments. 48 tests of individual T-stubs were also carried out as part of that project in order to study behavior, failure modes, and ductility of this bolted connection. The main parameters tested include the size of the T-stub, the spacing and gauges of the bolts, and the type and diameter of the bolts. The largest T-stubs tested were cut from a W33x169. A simplified theoretical stiffness model for the T-stubs was also presented.

A full-scale bidirectional test on a composite connection was conducted in 2001 at the Georgia Institute of Technology by Green et al. (2001) to examine the bidirectional behavior of a composite slab system with partially restrained connections. The test specimen had a 22' x 30' x 3-1/4" lightweight concrete slab on 3" composite decking. The column was a W14x159 and 3/8" thick shear tabs were fillet welded to the column. The beams and girders were W18x40 and W24x55 respectively. The T-stubs were cut from a W30x90. The connection behaved very well up to a uniaxial drift of about 2%. Composite action began to deteriorate and the connection strength and stiffness declined after a 2% drift level. As a result of this test, a suggestion that the full depth of the slab be maintained for a region 6 in around the joint has been incorporated in the commentary to Part II of the 2002 AISC Seismic Specification.

An experimental study of large bolted seismic steel beam-to-column connections was conducted at the University of California at Berkeley by Popov and Takhirov (2002). Two large bolted steel moment-resisting connections were investigated. These connections were single-sided beam-to-column assemblies that are representative of exterior connections composed of W36x150 beams and W14x283 columns. T-stubs were cut from W40x264 sections. During cyclic testing, the beam deformation was minimal and the overall deflection was controlled by the active participation of T-stub flanges. A separation between T-stub flanges and the column flanges was observed that was caused by plastic bending deformations in the T-stub flanges and plastic deformation in the high-strength bolts.

An experimental study on cyclic inelastic behavior and low-cycle fatigue of bolted T-stub connections was performed at the Tokyo Institute of Technology by Kasai and Xu (2003). A total of 42 component tests were carried out to study inelastic behavior of bolted T-stub connections. The variables studied include flange thickness, column bolt diameter, column bolt gage, edge-distance, column bolt pretension, and loading

patterns. Effects of various parameters on the stiffness, strength, ductility, and energy dissipation were reported. Two deformation modes under cyclic loading are categorized based on whether the column bolts yield or not.

An experimental assessment of the behavior of bolted T-stubs made up of welded plates was performed at the Deft University of Technology by Coelho et al. (2003). A total of 32 component tests were carried out to study the behavior in terms of strength, stiffness, deformation capacity, and failure modes. The parameters tested include the weld throat thickness, the size of the T-stub, the type and diameter of the bolts, the steel grade, the presence of transverse stiffeners, and the T-stub orientation.

This paper will outline ongoing efforts to demonstrate bolted T-stub Connections - referred to as Double Tee Connections in ANSI/AISC 358 – as prequalified for use in SMFs and IMFs. These efforts include analytical studies and testing at the University of Cincinnati and Georgia Institute of Technology to build upon the experimentation previously conducted to provide a more robust data set for analysis. Additionally, the researchers intend to demonstrate the acceptability of T-stub components that are built-up from plates in addition to the rolled T-stubs that have already been successfully tested. The planned study consists of three stages: (1) an experimental study on connection components, (2) an analytical study at the component level and at the global level, and (3) testing of six additional full-scale beam-column T-stub connections under cyclic loads.

T-STUB CONNECTION PROVISIONS DRAFT

General:

T-stub connections utilize components that are bolted to both the column flange and the beam flanges using high-strength bolts. The top and bottom T-stubs must be identical. T-stubs shall be cut from rolled sections or built-up from plate material that is joined using a CJP weld (the use of fillet welds is being discussed and investigated). The beam web is connected to the column with a single plate shear connection bolted to the beam web. A detail for this connection is shown in Figure 1. Yielding and hinge formation are intended to occur in the beam near the ends of the stems of the T-stubs. As is illustrated in Figure 2 (Swanson, 1999), double tee connections using rolled T-stubs have demonstrated performance that merits prequalification for use in Special Moment Frame (SMF) and Intermediate Moment Frame (IMF) systems within the limitation of the provisions.

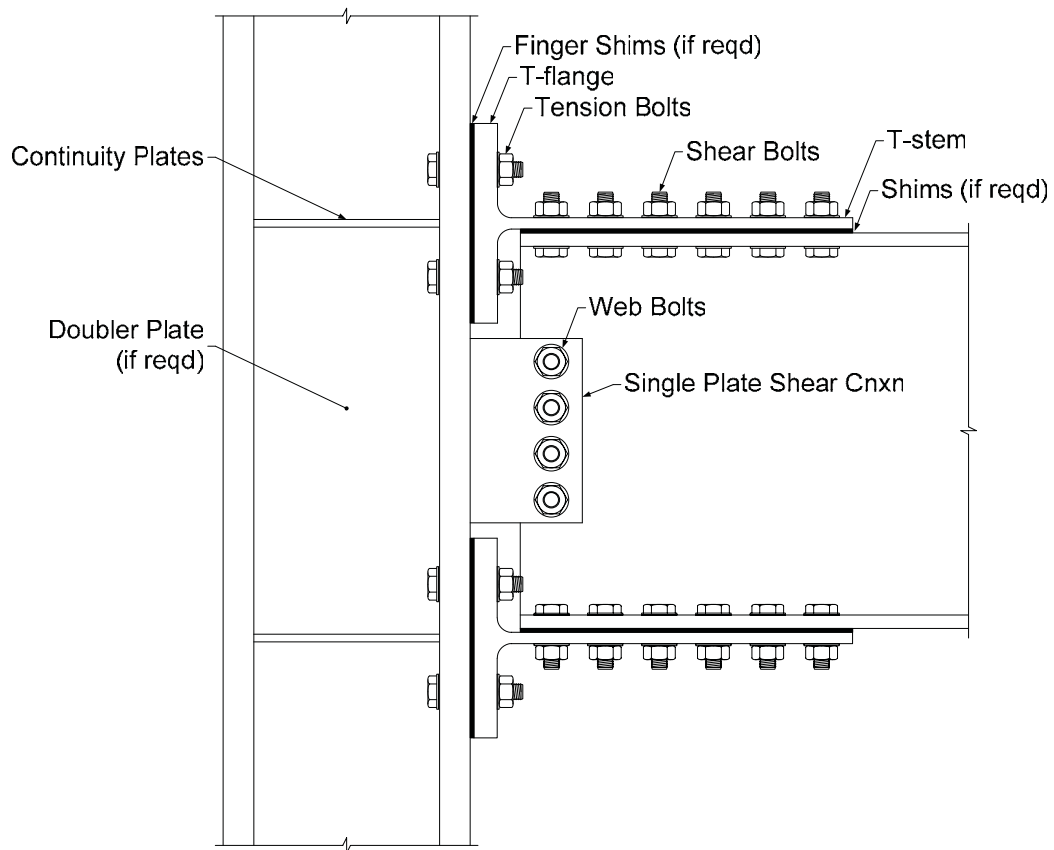


Figure 1 - Typical Double Tee Connection (Shown with Rolled T-stubs)

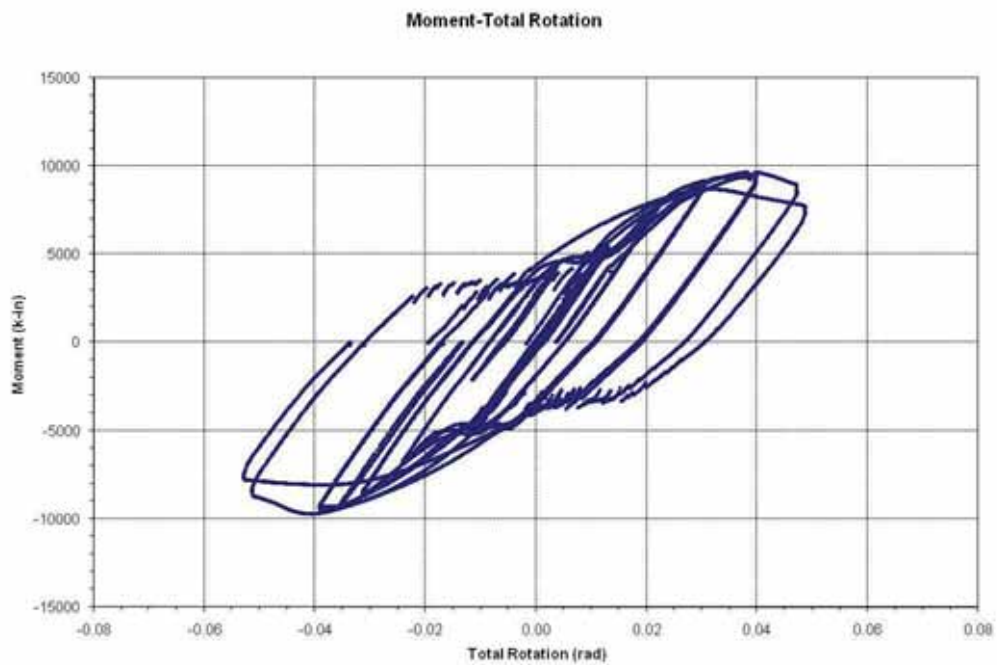


Figure 2 - Moment Versus Connection Rotation for a T-stub Connection

Current draft provisions limit beam size to a maximum of a W36x150 and columns to a maximum size of W36 when a slab is present or a W14 when it is not. The maximum flange thickness is limited to 1.00 in and the protected zone consists of the T-stubs and the portion of the beam between the face of the column and one beam depth past the last row of bolts. The beam must be connected to the flange of the column (though box columns are permitted). Lacking experimental data for connections without them, continuity plates are required in all cases.

One of the more interesting details of the provisions is the inclusion of T-stubs that are built up from plates. Though this concept still needs to be validated experimentally, it will add a considerable amount of flexibility to the detailing of T-stub connections. Currently, the stem and flange of built-up T-stubs must be connected using a demand critical CJP groove weld but the authors are hoping to validate the use of fillet welds in place of the CJP weld. T-stubs cut from rolled sections shall conform to either ASTM A992 or A913 Gr. 50. T-stubs built-up from plate material shall conform to either ASTM A36 or A572-50.

Research Objectives:

The main objective of this investigation is to prequalify T-stub connections for use in Special Moment Frames (SMFs) and Intermediate Moment Frames (IMFs) with larger beam members by providing fundamental performance data. Several prequalification parameters and their effect on responses will be evaluated. These include the influence of the hole fabrication process on the cyclic behavior of a plate and the influence of the type of welding used to build a T-stub. In the first case, drilling, punching, and CNC flame cutting of STD and SSL holes will be compared. Punched holes would provide an economical means of fabrication and these tests are meant to verify which fabrication methods provide sufficient strength and ductility for use in T-stub connections. In the second case, the strength, stiffness, and ductility of T-stubs fabricated with CJP welds will be compared to those fabricated using a pair of a fillet welds. If fillet welds behave comparably to CJP welds, they will considerably improve the ease and economy of fabrication of built-up T-stubs.

This series of tests will verify the proposed design of T-stub connections for SMFs and IMFs, as prepared by AISC CPRP and to ascertain the differences between the use of a rolled T-stub and of a built-up T-stub. The connection has been designed based on the member sizes in a current example of a RBS beam-to-column connection in a SMF in the seismic manual, and the design procedure followed is the one being developed by the CPRC.

Based on the results of the experimental investigation, an attempt will be made to prequalify connections that can be used as a basis for further research and practical applications. These include a comparison between the behavior of rolled T-stubs and built-up T-stubs. The importance of clarifying whether built-up T-stubs can withstand the deformation demands associated with the pre-qualification process is in the design and fabrication flexibility that such details would allow for T-stub connections.

Additionally, a parallel analytical study will be conducted, using the experimental results for validation, which will allow to further augment the database of existing connection data available, using full nonlinear material and geometric analysis, and accounting for pretension of fasteners and full contact interactions. An example of such a model, for a one-way beam-to-column connection, is presented in Figure 3 below.

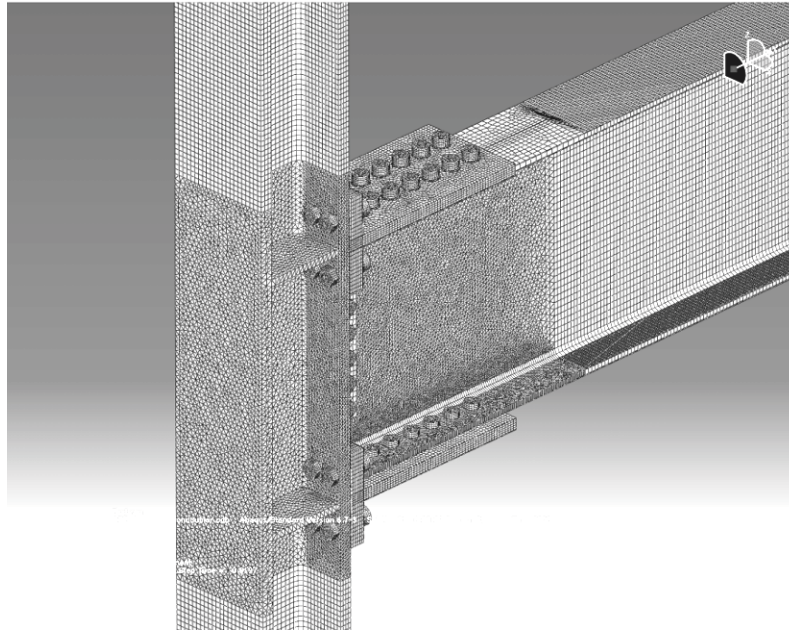


Figure 3 - Example of Analytical Model

Experimental Program

The experimental program is composed of two parts. The first part is comprised of component tests while the second will focus on the testing of at least six full-scale connection assemblies. The outcome of the first experimental part will guide the detailing of full-scale specimens to be tested in order to prequalify T-stub connections for SMF and IMF using larger beams.

To evaluate the influence of the hole fabrication process, 3/4" thick plates, 3" wide, and 48" long will be used, with 6, 13/16" standard or short-slotted holes punched, drilled, or CNC flame cut in the middle section. The plates will be clamped in a 400 kip universal testing machine and will be subjected to (1) a monotonically increasing load to failure, and (2) a cyclically variable load in tension, following the AISC Seismic load history, in order to evaluate the low-cycle fatigue response of the holes. Two specimens will be tested for each case, for a total of 10 monotonic tests and 10 cyclic tests (2 each for drilled, punched, flame cut, SSL punched, and SSL flame cut).

To evaluate the difference between CJP and fillet welds, T-stub specimens will be tested in a 400 kip universal testing machine both monotonically and cyclically. The T-stub specimen has a flange made with a PL10x6x2, welded by means of CJP or fillet

welds to a stem made with a PL12x6x3/4 or PL12x6x1-1/4. Four, 1-1/16" diameter STD holes are drilled into the flanges and 12, 13/16" STD holes are drilled into the stems. The T-flange is to be bolted using four A490 bolts to an existing stiffened W12x136 secured to the top table of the universal testing machine, and the T-stem is to be bolted to a requested stiffened W12x136 with a PL10x15x2 welded on its top flange, in which 12, 13/16" STD holes are drilled. Figure 4 shows the nominal data for the T-stub component tests. Two specimens each will be subject to either a monotonically increasing load to failure or a cyclically variable load in tension, in the spirit of the AISC Seismic load history. A total of 16 specimens will be tested, 8 monotonically, and 8 cyclically (for 3/4" stem, 2 CJP and 2 fillet, and for 1-1/4" stem, 2 CJP and 2 fillet).

The second part of the experimental program consists of at least six full-scale beam-column T-stub connections that will be tested under cyclic loads. These connections will be single-sided beam-to column assemblies that are representative of exterior beam-to-column connections, and they are composed two W24x76, two W30x108, and two W36x150 and all connected to W14x257 columns. Tables 1 and 2 show the member sizes and connection details for the specimens. T-stubs will be built-up from plates and welded using CJP welds or fillet welds. The T-stubs will be bolted to the beam flanges and the column flange. The shear tabs will be bolted to the beam webs and welded to the column flanges. Continuity plates will be provided and doubler plates will be provided if needed. The test specimens were designed so that the various modes of failure could be established and that in most instances, the controlling mode of failure would be the development of a plastic hinge in the beam.

Table 1 - Member Sizes

Specimen	Column	Beam	Length
BC-1	W14x257	W24x76	240"
BC-2	W14x257	W30x108	240"
BC-3	W14x257	W36x150	240"

Test Setup

The test setup was designed to accommodate specimens with beams in a vertical position. The overall specimen geometry and test setup are shown in Figure 5. ASTM A992 steel was specified for all beam and column sections and A572 Gr. 50 steel was specified for all plate material. The column is to be installed horizontally on top of the floor mountings, with one end attached to the laboratory strong wall. Elastic flexibility of the column profile in the connection area and for several feet in each direction is maintained. The beam is installed vertically, cantilevered from the column with a 330 kip actuator installed at the free end. The testing setup has a displacement range of $\pm 12"$. No axial load will be applied to the column. The beam end is placed at a distance of 16 ft from the column face. The loading sequence for beam-to-column moment connections as defined in the 2005 AISC Seismic Provisions will be used.

Displacement transducers, strain gage rosettes, and uniaxial strain gages will be placed in specific locations on the specimens to measure global and local responses.

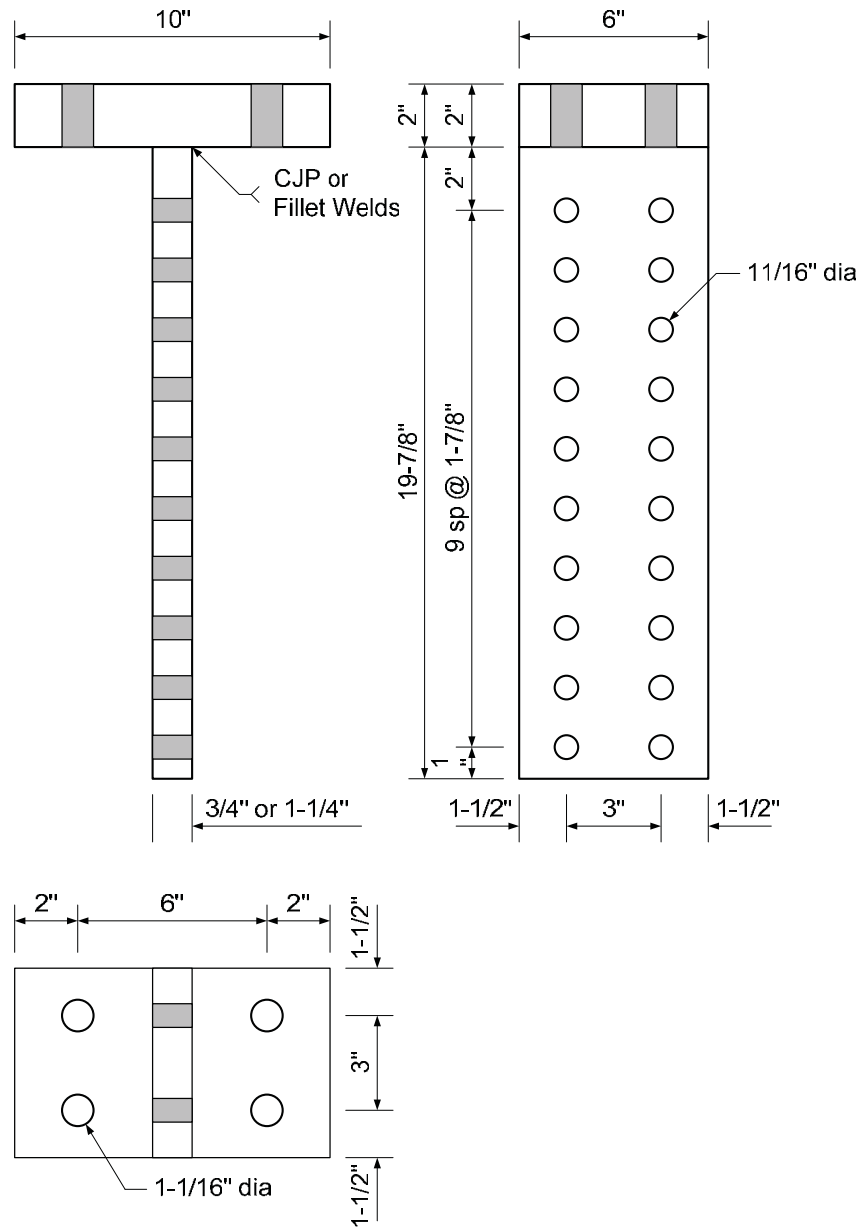


Figure 4 - Nominal Data for T-stub Component Tests

Anticipated Results and Conclusions:

The completion and documentation of this experimental program will augment the database of experimental results which can be used in the development of new models and in the evaluation of current ones. The comparison between rolled and built-up T-stubs will shed some light on the applicability of the latter. A pre-qualifiable T-stub

connection for SMF and IMF will provide designers with another viable option for practical application. The completion of the component tests will guide the detailing of 6 full-scale specimens of beam-to-column T-stub connections with the final objective of submission to CPRP for prequalification.

Table 2 - Connection Details

Specimen	T-stub Flange	T-stub Stem	Shear Bolts	Tension Bolts	Doubler Plate	Continuity Plates
BC-1	2-1/4"	7/8"	16 @ 7/8"	8 @ 1"	None	3/4"
BC-2	2-1/2"	1-1/4"	16 @ 1"	8 @ 1-1/4"	2 @ 1/2"	7/8"
BC-3	2-1/2"	1-3/4"	14 @ 1-1/4"	8 @ 1-1/2"	2 @ 5/8"	1"

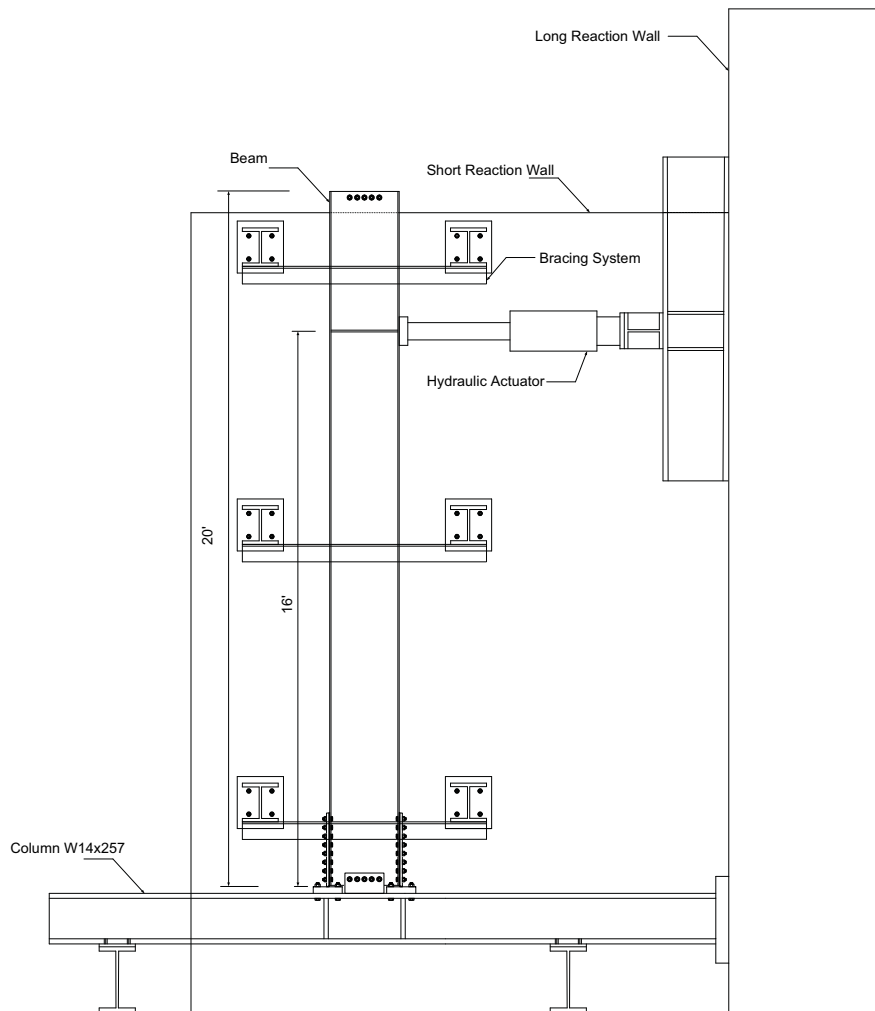


Figure 5 - Experimental Set Up

REFERENCES:

AISC (2005) "Manual of Steel Construction, Load and Resistance Factor Design," 13th Edition, American Institute of Steel Construction, Chicago, IL.

AISC (2005) "Prequalified Connections for Special and Intermediate Steel Moment Frames for Seismic Applications, American Institute of Steel Construction, Chicago, IL.

AISC (2005) "Seismic Provisions for Structural Steel Buildings, American Institute of Steel Construction, Chicago, IL.

Coehlo, A.M, Bijlaard, F.S, Gresnigt, N, and Da Silva, L.S (2004). "Experimental Assessment of the Behavior of Bolted T-stub connections made up of welded plates, *Journal of Constructional Steel Research*, Vol. 60, (pp. 269-311).

Green, T.P, Leon, R.T, Rassati, G.A (2004). "Bidirectional Tests on Partially Restrained Composite Beam-to-Column Connections, *Journal of Structural Engineering*, Vol. 130, (pp. 320-327).

Kasai, K., and Xu, Y., (2002). "Experimental Study on Cyclic Inelastic Behavior and Low-Cycle Fatigue of Bolted T-stub Connections", *Journal of Structures and Construction Engineering*, No.560, (pp. 169-179).

Swanson, J.A. (1999), "Characterization of the strength, stiffness, and ductility behavior of T-stub connections." PhD dissertation, Georgia Institute of Technology, Atlanta.

Swanson, J.A, and Leon, R.T, (2001). "Bolted Steel Connections: Tests on T-Stub Components", *Journal of Structural Engineering*, Vol. 126, No 1, (pp. 50-56).

Swanson, J.A, and Leon, R.T, (2001). "Stiffness Modeling of Bolted T-Stub Connection Components", *Journal of Structural Engineering*, Vol. 127, No 5, (pp. 498-505).

Popov, E.P, and Takhirov, S.M, (2002). "Bolted Large Seismic Steel Beam to Column Connections Part 1: Experimental Study, *Journal of Engineering Structures*, Vol. 24, No 24, (pp. 1523-1534).

EXPERIMENTAL BEHAVIOR OF LINK-TO-COLUMN CONNECTIONS IN ECCENTRICALLY BRACED FRAMES

Taichiro Okazaki

University of Minnesota, Minneapolis, MN, USA
tokazaki@umn.edu

Michael D. Engelhardt

University of Texas at Austin, Austin, TX, USA,
mde@mail.utexas.edu

Apostolos Drolias

University of Texas at Austin, Austin, TX, USA,
apdrolias@mail.utexas.edu

Eric Schell

University of Texas at Austin, Austin, TX, USA,
eschell@mail.utexas.edu

Jong-Kook Hong

University of California, San Diego, La Jolla, CA, USA
jkhong@ucsd.edu

Chia-Ming Uang

University of California, San Diego, La Jolla, CA, USA
cuang@ucsd.edu

ABSTRACT

Twenty-four large-scale specimens were tested at the University of Texas at Austin to study the seismic performance of link-to-column connections in eccentrically braced frames. The test parameters included the link length, connection detail, link section, and cyclic loading protocol. The test results suggest that link-to-column connections are susceptible to fracture at the link flange welds, regardless of the link length. A large number of specimens failed prematurely, before meeting the plastic link rotation requirement. However, two promising link-to-column connection details were developed, including a detail using all-around fillet welds between the link and the column flange, and a reinforced connection welding a pair of stiffeners in the first link web panel next to the column, parallel to the link web. Test specimens using either of these two details were able to preclude failure at the link-to-column connection until the plastic link rotation capacity was exceeded.

INTRODUCTION

Eccentrically braced frames (EBFs) are an efficient seismic load resisting system for satisfying the stiffness and ductility requirements in contemporary building code provisions. The *2005 AISC Seismic Provisions for Structural Steel Buildings* (AISC 2005) prescribes design rules for EBFs to ensure ductile performance of the link and to concentrate inelastic deformation of the frame in the links. The importance of link-to-column connections is recognized in the *Provisions* by stringent laboratory testing criteria for performance evaluation. However, to date, there is few test data that demonstrates that link-to-column connection can satisfy the performance requirements per these criteria. Therefore, the design and detailing of link-to-column connections remain a critical unresolved issue that substantially restricts the use of EBFs.

Link-to-column connections are required to transfer the large shear and moment developed in a fully plastic link, while accommodating large plastic rotation of the link. On the other hand, the force and deformation demand at the connection is governed by the geometry of the link. A shear yielding link develops very large shear force and less substantial moment, while undergoing a plastic rotation as much as 0.08 radians. A flexure yielding link develops very large moment and less substantial shear, while undergoing a plastic rotation of 0.02 radians. In addition, the stresses and strains at the link-to-column connection can depend on the length-to-depth ratio of the link, flange-to-web area ratio of the link, and yielding of the members outside of the link (Engelhardt and Popov 1992). Therefore, despite the apparent similarity to moment frame connections, the design and behavior of EBF link-to-column connections is affected by factors that are usually not concerned for moment frame connections.

Previously, tests by Engelhardt and Popov (1992) observed that long flexural yielding links are susceptible to premature fracture at the link-to-column connection. Tsai et al. (2000) observed link-to-column connections using square box columns to fail after reaching only half of the link rotation capacity prescribed in the *AISC Seismic Provisions*. Consequently, an extensive experimental research program was conducted at the University of Texas at Austin to study the seismic performance of EBF link-to-column connections. This paper discusses the overall perspective of the program, including results which have not been reported previously. Full details of the program are described by Okazaki (2004) and Drolias (2007).

TEST PLAN

The test setup shown in Fig. 1 was used to produce the cyclic force and deformation demand in typical EBFs. A total of twenty-four large-scale specimens were tested using this test setup. Table 1 summarizes the key parameters for each specimen, including the connection type, link section, link length, plastic link rotation capacity determined per the *2005 AISC Seismic Provisions*, and the loading protocol used for testing. The specimens were composed of a W12x120 column and a W18x40 or W10x68 link, each of A992 steel. The links were provided with one-sided stiffeners as required in the *2005 AISC Seismic Provisions*. Table 2 lists key properties of the link sections, where V_p is the plastic shear strength, M_p is plastic moment of the link.

The six connection details are shown in Fig. 2. The PN-connection (see Fig. 2(a)) represented the pre-Northridge design and construction; the MW-connection (Fig. 2(b)) incorporated recommended modifications in welding procedure (FEMA 2000), such as use of toughness rated electrodes, removal of backup bars and weld tabs; the FF-connection (Fig. 2(c)) was a variation of the “free-flange” connection originally developed for moment connections by Choi et al. (2003); the NA-connection (Fig. 2(d))

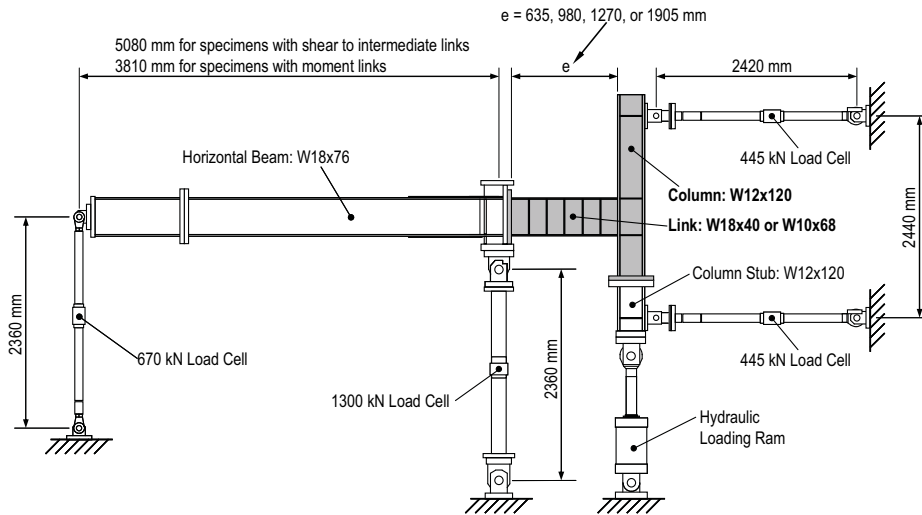


Fig. 1 Test Setup

Table 1 Test Specimens

Specimen	Connection Type	Link			Target γ_p (rad.)	Loading protocol
		Section	Length (mm)	$e/(M_p/V_p)$		
PNS	PN	W18x40	635	1.11	0.080	Old
PNI	PN	W18x40	1,270	2.22	0.043	Old
PNM	PN	W18x40	1,905	3.34	0.020	Old
MWS	MW	W18x40	635	1.11	0.080	Old
MWI	MW	W18x40	1,270	2.22	0.043	Old
MWM	MW	W18x40	1,905	3.34	0.020	Old
FFS	FF	W18x40	635	1.11	0.080	Old
FFI	FF	W18x40	1,270	2.22	0.043	Old
FFM	FF	W18x40	1,905	3.34	0.020	Old
FFS-R	FF	W18x40	635	1.11	0.080	Revised
FFSL-R	FF	W18x40	980	1.72	0.073	Revised
NAS	NA	W18x40	635	1.11	0.080	Old
NAI	NA	W18x40	1,270	2.22	0.043	Old
NAM	NA	W18x40	1,905	3.34	0.020	Old
NAS-R	NA	W18x40	635	1.11	0.080	Revised
NASL-R	NA	W18x40	980	1.72	0.073	Revised
AISC-1	AF	W18x40	980	1.72	0.073	Revised
AISC-2	AF	W18x40	980	1.72	0.073	Revised

AISC-3	AF	W18x40	980	1.72	0.073	Revised
AISC-4	AF	W10x68	980	1.33	0.080	Revised
AISC-5	UCSD	W18x40	980	1.72	0.073	Revised
AISC-6	UCSD	W10x68	980	1.33	0.080	Revised
AISC-7	UCSD	W10x68	980	1.33	0.080	Revised
AISC-8	UCSD	W18x40	980	1.72	0.073	Revised

Table 2 Link Properties Based on Measured Yield Stress

Link Section	V_p (kN)	M_p (kN·m)	M_p/V_p (mm)
W18x40	793	453	571
W10x68	622	463	744

was based on the no-weld-access-hole connection that are in use in Japan (Suita et al. 1999); the AF-connection (Fig. 2(e)), intended for shop fabrication, used double-sided fillet welds all-around the link flanges and web to connect the link to the column; the UCSD-connection (Fig. 2(f)) welded a pair of steel plates in the first link web panel next to the column, at both sides of the link web, to reinforce the MW-connection. The UCSD-connection was developed at the University of California, San Diego, based on detailed nonlinear finite element simulations. The FF, AF, and UCSD-connections were varied between specimens in order to accommodate different link lengths and sections, and in order to examine the effect of key design choices. Fig. 2(c), (e), and (f) show the connection designs for Specimens FFI, AISC-1, and AISC-5, respectively.

The PN-connection used a self-shielded flux core arc welding (SS-FCAW) process with an E70T-4 electrode for the complete joint penetration (CJP) groove welds connecting the link flange to the column flange. The MW, FF, and NA-connections used a SS-FCAW process with an E70T-6 electrode for the CJP welds between the link flange and column flange. The welding procedure was varied between AF-specimens. Specimen AISC-1 used a shield metal arc welding (SMAW) process with an E7018 electrode, while Specimens AISC-2 through AISC-4 used a gas shielded flux core arc welding (GS-FCAW) process with an E70T-9 electrode. US fabricators use GS-FCAW more commonly than SMAW.

The specimens had varying link length. The 2005 AISC *Seismic Provisions* define the plastic link rotation capacity, γ_p , depending on the link length: 0.08 radians for links shorter than $e = 1.6M_p/V_p$; 0.02 radians for links longer than $e = 2.6M_p/V_p$; and linear interpolation is used for links of $1.6M_p/V_p \leq e \leq 2.6M_p/V_p$. However, observations from earlier specimens and finite element simulations (Okazaki 2004) suggested that links near the range of $1.6M_p/V_p \leq e \leq 2M_p/V_p$ produce the most critical force and deformation demand to the link-to-column connection, by combining large shear, large flexure, and large plastic rotation requirements. Consequently, later specimens with a W18x40 link focused on this critical link length range ($e = 1.72M_p/V_p$).

Two different link sections were used for the specimens. W18x40 represented deep, beam-like sections, while W10x68 represented shallow, column-like sections. The value $e/(M_p/V_p)$ indicates whether the link behavior is dictated by shear or flexure. However,

the length-to-depth ratio varies substantially depending on the shape of the link section.

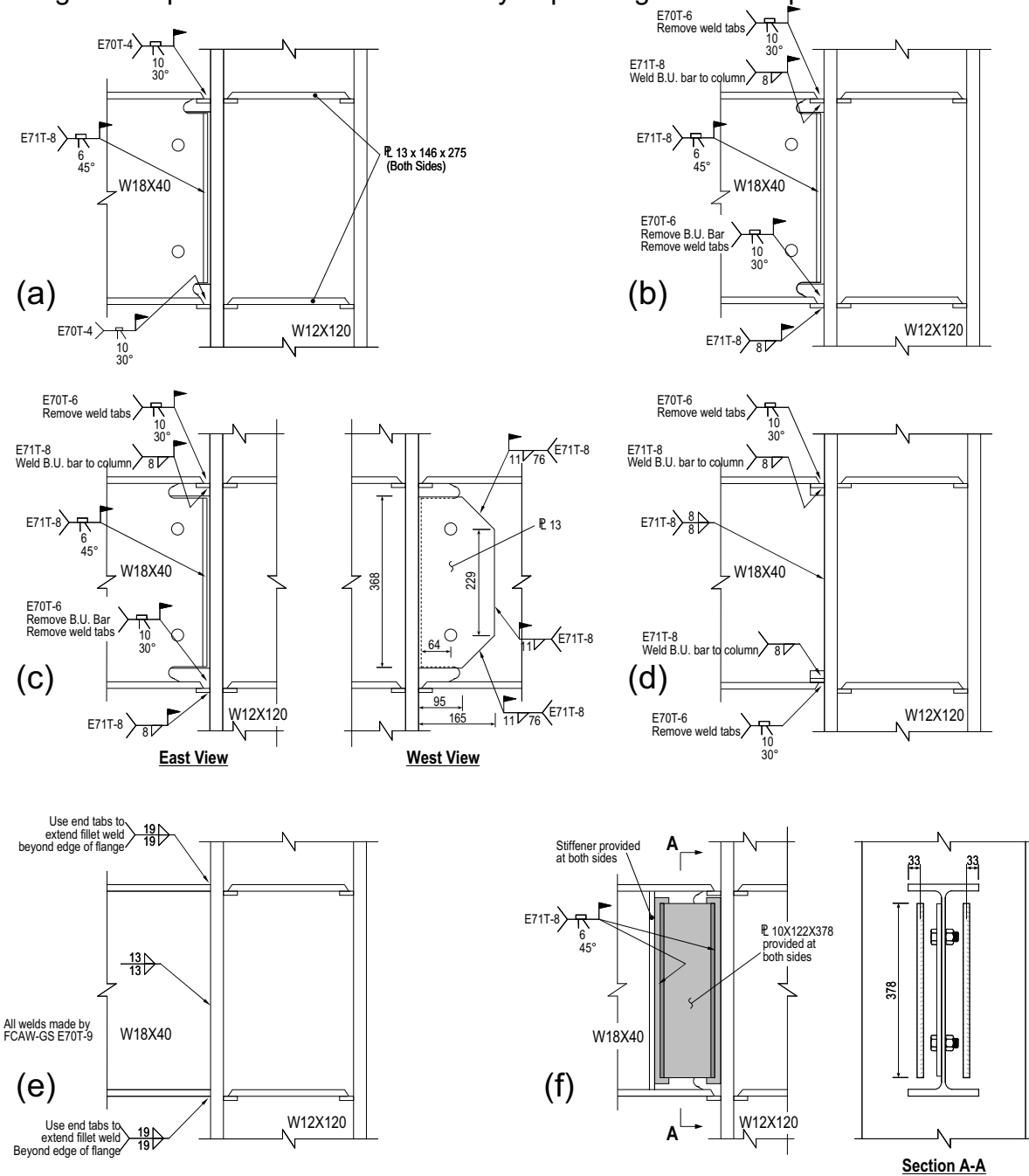


Fig. 2 Connection Types (link stiffeners not shown): (a) PN-Connection; (b) MW-Connection; (c) FF-Connection; (d) NA-Connection; (e) AF-Connection; and (f) UCSD-Connection

For the same $e/(M_p/V_p)$ value, a deeper section gives a smaller length-to-depth ratio than a shallower section, and hence develops larger strain in the link flanges to supply plastic hinge rotation at the link ends. Therefore, for a given $e/(M_p/V_p)$ value, W18x40 was expected to produce a more critical condition than W10x68.

Initially, the loading protocol prescribed in the *2002 AISC Seismic Provisions* (AISC 2002), indicated in Table 1 as the “Old” protocol, was used to introduce cyclic loading to the specimens. However, during the course of this program, it was realized that the Old protocol demanded too many inelastic cycles to shear yielding links before reaching the target plastic rotation of 0.08 rad. Consequently, Richards and Uang (2006) developed a new loading protocol based on an extensive numerical study, which has been adopted in the *2005 AISC Seismic Provisions*. The new protocol, indicated in Table 1 as the “Revised” protocol, was used in later specimens tested in this program.

TEST RESULTS

Table 3 summarizes key results obtained for each specimen. The table lists the plastic link rotation capacity determined per the *2005 AISC Seismic Provisions*, the maximum plastic rotation measured during the test, and a brief description of the observed failure mode. The maximum plastic rotation was defined based on the last full loading cycle in which the link shear force exceeded the nominal link shear strength (computed based on the nominal yield stress of 345 MPa) at the end of both the positive and negative excursion.

Table 3 indicates that a large number of specimens failed due to fracture of the link flange near the weld connecting the link flange to the column flange. Fracture at the link flange was commonly seen in specimens with all link lengths between short shear yielding links and long flexure yielding links. All PN and MW-connections failed due to this failure mode, permitting the link to develop half or less of its plastic rotation capacity. The FF and NA-connections were based on designs that perform well in moment frame connections. However, with the exception of Specimen FFI and NAS-R, the FF and NA-connections did not meet the plastic link rotation requirements.

Tables 3 Test Results

Specimen	Target γ_p (rad.)	Measured γ_p (rad.)	Observed failure
PNS	0.080	0.041	Fracture at link flange
PNI	0.043	0.018	Fracture at link flange
PNM	0.020	0.008	Fracture at link flange
MWS	0.080	0.051	Fracture at link flange
MWI	0.043	0.018	Fracture at link flange
MWM	0.020	0.008	Fracture at link flange
FFS	0.080	0.060	Fracture of link web around shear tab
FFI	0.043	0.046	Fracture at link flange, shear tab, and link web
FFM	0.020	0.016	Fracture at link flange, shear tab, and link web
FFS-R	0.080	0.031	Fracture at shear tab

FFSL-R	0.073	0.019	Fracture at shear tab
NAS	0.080	0.071	Fracture of link web at stiffeners
NAI	0.043	0.027	Fracture at link flange
NAM	0.020	0.017	Fracture at link flange
NAS-R	0.080	0.119	Fracture at link flange
NASL-R	0.073	0.058	Fracture at link flange
AISC-1	0.073	0.11	Fracture at link flange
AISC-2	0.073	0.095	Fracture at link flange
AISC-3	0.073	0.057	Fracture at link flange
AISC-4	0.080	0.096	Fracture of link web at stiffeners
AISC-5	0.073	0.10	Fracture of link web at stiffeners
AISC-6	0.080	0.095	Fracture of link web at stiffeners
AISC-7	0.080	0.094	Fracture of link web at stiffeners
AISC-8	0.073	0.056	Fracture at link flange and supplementary stiffener

A common failure observed from the FF-specimens was fracture between the shear tab/link web and the column flange. This unique failure mode, which was not seen in other connections, was due to the feature of FF-connections to draw stresses to the thick shear tab and link web, and thereby, to reduce stresses in the link flange groove welds. Specimen FFS failed in the link web along the shear tab to link web fillet welds, while no damage was observed near the column face. The poor performance of Specimens FFS-R and FFSL-R is attributed to the design that cut the link web short of reaching the column flange, as opposed to having the link web welded directly to the column flange as in the other FF-specimens. The observed behavior of FF-specimens indicates that link-to-column connections are also susceptible to fracture in the link web initiating at the top and bottom edge of the link web weld.

Specimens NAS and NAS-R were identical specimens tested under different loading protocols. The plastic rotation angle achieved by Specimen NAS-R, which was tested under the Revised protocol, was 50% greater than the angle achieved by Specimen NAS, which was tested under the Old protocol. This comparison agrees with previous tests (Okazaki and Engelhardt 2007) suggesting that the loading protocol has a significant influence on the experimental performance of EBFs.

Some of the specimens that exceeded the plastic rotation requirement ultimately failed due to fracture of the link web at the stiffener welds. A large number of recent tests (Okazaki and Engelhardt 2007) suggest that this is a failure mode that dominates short shear yielding links. Therefore, noting that failure of the link-to-column connection was avoided until the link developed its capacity limit, the performance of Specimens AISC-4 to AISC-7 was excellent. Specimen NAS was likely penalized by the overly conservative loading protocol.

ALL-AROUND FILLED WELDED CONNECTIONS

The concept of AF-Connections (see Fig. 2(e)) was motivated by observations made during a large number of isolated link tests (Okazaki and Engelhardt 2007). In these

tests, the each ends of the link was welded to heavy end plates by large double-sided fillet welds, and the end plates were bolted to the testing frame. After trial-and-error, successful performance of the link end connection was obtained by choosing a fillet weld size of 1.5 times the thickness of the connected link flange or web, using the SMAW process with an E7018 electrode, and using weld tabs to run-off the fillet welds beyond the edge of link flange.

Specimens AISC-1 to AISC-4 adopted the fillet-welded detail at the link-to-column connection, by welding the link directly to the column flange, and not using an end plate. The key parameters for the four specimens the fillet weld size (1.0 or 1.5 times the thickness of the connected plate), welding process (SMAW or GS-FCAW), and the use of partial joint penetration (PJP) groove welds for thicker link flanges. Specimen AISC-1 used fillet welds sized as 1.5 times the plate thickness, made using the SMAW process; Specimen AISC-2 was identical to Specimen AISC-1, except that the welds were made using GS-FCAW; Specimen AISC-3 was identical to Specimen AISC-2, except that the fillet welds size was reduced to 1.0 times the plate thickness. Fig. 3(a) shows the excellent cyclic behavior exhibited by Specimen AISC-2. After completing a cycle at ± 0.10 radians, the specimen failed due to fracture of the link flange as shown in Fig. 3(b). The results listed in Table 3 suggest that GS-FCAW is acceptable for the AF-Connection, although SMAW may provide better performance. The excellent performance of Specimens AISC-1 and AISC-2 and poor performance of Specimen AISC-3 suggest that a fillet weld size approximately equal to 1.5 times the link flange thickness is required to meet the plastic rotation requirements.

Specimen AISC-4 used a W10x68 link which had a thicker flange plate than a W18x40. The thicker flange was connected to the column flange using a PJP groove weld, reinforced by a fillet weld on the other side. The excellent performance of Specimen AISC-4 suggests that the combination of PJP groove weld and fillet weld is adequate for links with thicker flange plates.

UCSD CONNECTIONS

The last four specimens, AISC-5 to AISC-8, used the UCSD-connection (see Fig. 2(f)). The UCSD-connection was a MW-connection with added reinforcement. A pair of supplemental stiffeners was added to the first link panel next to the column, parallel to the link web. At the end of the first link panel, link stiffeners were placed at both sides of the link web, in order to support the supplemental stiffeners at both sides of the link web. The supplemental stiffeners were intended to increase the plastic strength of the link beyond the maximum forces expected at the column face, and thereby, to prevent excessive stresses to develop near the critical link flange welds.

The four specimens were designed with two different link sections (W18x40 and W10x68) and two different designs for the supplemental stiffeners. Specimens AISC-5 and AISC-6 used supplemental stiffeners that were at least as thick as the link web, and sufficiently thick to meet the plastic strength criteria described above. CJP groove welds were used to weld the supplemental stiffeners. In comparison, Specimens AISC-7 and AISC-8 reduced the thickness of the supplemental stiffeners (from Specimens

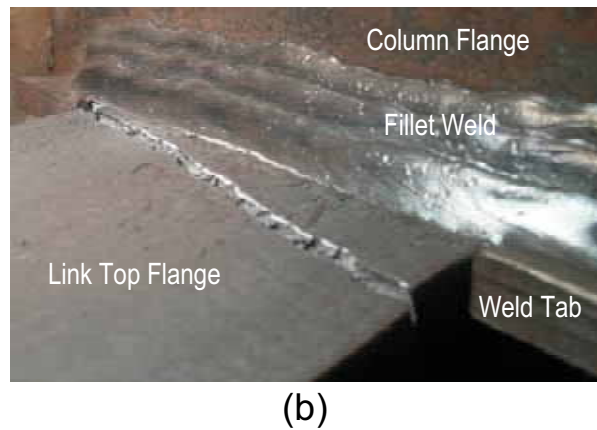
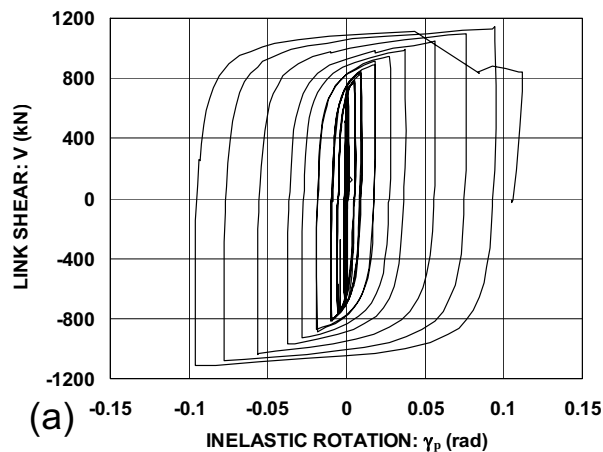


Fig. 3 Specimen AISC-2: (a) Hysteretic response; and (b) Fracture of link flange

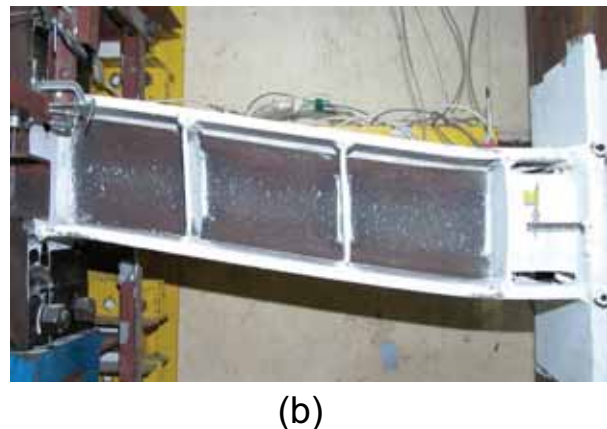
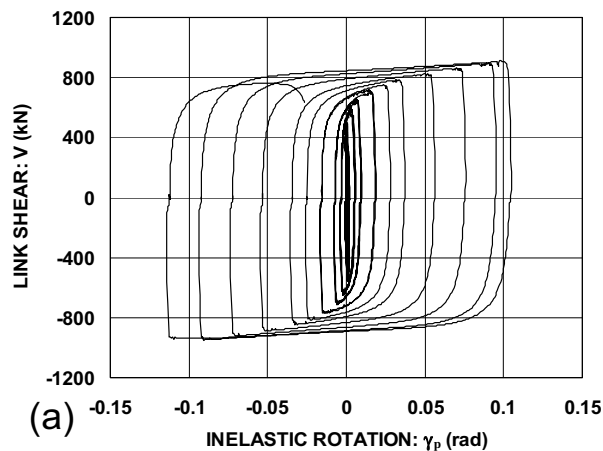


Fig. 4 Specimen AISC-6: (a) Hysteretic response; and (b) Link near end of test

AISC-6 and AISC-5, respectively) and used one-sided fillet welds. Fig. 4(a) shows the excellent cyclic behavior exhibited by Specimen AISC-6, while Fig. 4(b) shows the specimen near the end of the test. Fig. 4(b) indicates that due to reinforcement, yielding in the first link panel was precluded. Because plastic rotation was supplied by the link outside of the reinforced region, it might be justified to exclude the first link panel from the link length. The data in Table 3 and Fig. 4(a) are based on the link length including the first link panel. While the other three UCSD-specimens exceeded the plastic link rotation capacity by a large margin, Specimen AISC-8 failed prematurely due to fracture along the fillet welds connecting the supplementary stiffeners to the column flange. Therefore, while very promising results were obtained for the UCSD-connections, further study is recommended to refine the design methods.

SUMMARY

This paper summarizes an experimental research program on the seismic performance

of EBF link-to-column connections. Tests demonstrated that link-to-column connections are susceptible to fracture at the link flange, regardless of the link length. Connections designed and constructed according to the pre-Northridge practice failed when the link achieved only half of its plastic rotation capacity. Modifications in welding and configuration, which are recommended for moment frame connections, did not lead to satisfactory performance of link-to-column connections.

Two promising link-to-column connection details resulted from this program. The first detail uses all-around fillet welds between the link end and the column flange. The second detail reinforces the link by welding two steel plates in the first link web panel next to the column. Test results demonstrated that excellent performance can be achieved by these two connection details. Further studies are recommended to confirm the performance of the two connection details over a larger range of parameters, to refine the design methods, and to identify limits of application of the two details

ACKNOWLEDGEMENTS

Funding for this project was provided by the National Science Foundation (Grant No.CMS-0000031) and the American Institute of Steel Construction. The opinions expressed in this paper are those of the authors and do not necessarily reflect the views of the sponsors.

REFERENCES

- American Institute of Steel Construction, Inc. (AISC). (2002), *Seismic Provisions for Structural Steel Buildings*. Standard ANSI/AISC 341-02, AISC, Chicago, U.S.A.
- American Institute of Steel Construction, Inc. (AISC). (2005), *Seismic Provisions for Structural Steel Buildings*. Standard ANSI/AISC 341-05, AISC, Chicago, U.S.A.
- Choi, J.-H., Stojadinovic, B. and Goel, S. C. (2003), "Design of Free Flange Moment Connection", *AISC Engineering Journal*, Vol. 40, First Quarter (pp.1-44).
- Drolias, A. (2007). Experiments on Link-to-Column Connections in Steel Eccentrically Braced Frames", *Master's Thesis*, Department of Civil Engineering, University of Texas at Austin, Austin, Texas, U.S.A.
- Engelhardt, M. D. and Popov, E. P. (1992), "Experimental Performance of Long Links in Eccentrically Braced Frames", *Journal of Structural Engineering*, ASCE, Vol. 118, No. 11 (pp. 3067-3088).
- Federal Emergency Management Agency (FEMA). (2000), *Recommended Seismic Design Criteria for New Steel Moment-Frame Buildings*, FEMA-350, FEMA, Washington, D.C.
- Okazaki, T. (2004). "Seismic Performance of Link-to-Column Connections in Steel Eccentrically Braced Frames", *Ph.D. Dissertation*, Department of Civil Engineering, University of Texas at Austin, Austin, Texas, U.S.A.
- Okazaki, T. and Engelhardt, M. D. (2007). "Cyclic Loading Behavior of EBF Links Constructed of ASTM A992 Steel." *Journal of Constructional Steel Research*, Vol. 63, No. 6 (pp. 751-765).
- Richards, P. and Uang, C.-M. (2006). "Testing Protocol for Short Links in Eccentrically Braced Frames", *Journal of Structural Engineering*, ASCE, Vol. 132, No. 8 (pp. 1183-1192).
- Suita, K., Nakashima M., and Engelhardt M. D. (2000), "Comparison of Seismic Capacity between Post-Northridge and Post-Kobe Beam-to-Column Connections", *The third International Conference on Behaviour of Steel Structures in Seismic Areas (STESSA 2000)*, Montreal, Canada.
- Tsai, K.-C., Engelhardt, M. D., and Nakashima, M. (2000). "Cyclic Performance of Link-to-Box Column Connections in Steel Eccentrically Braced Frames", *The First International Conference on Structural Stability and Dynamics*, Taipei, Taiwan.

DEFORMATIONAL COMPATIBILITY IN WELD GROUPS

Larry S. Muir

Cives Engineering Corp., Roswell, GA

lmuir@cives.com

ABSTRACT

Both the AWS Welding Code and AISC Specification allow a strength increase for fillet welds based on the direction of loading. This strength increase can often be used to improve the economy of structural steel connections. However, deformational compatibility must also be maintained when designing concentrically loaded fillet weld groups with the elements loaded in different directions or with differing leg sizes. Several examples of common connections pertaining to this topic will be discussed.

INTRODUCTION

Since 1993 the AISC Specification has included a provision that allows for a directional strength increase for fillet welds. The provision in its full form produces acceptable results and is consistent with test results. Historically the procedure was used primarily to calculate the capacity of eccentrically loaded weld groups, though the procedure is equally suited to concentrically loaded weld groups. The directional strength increase and the load-deformation relationship of the weld elements are determined from an approximate equation based on an equation presented by Lesik and Kennedy (Lesik and Kennedy 1990).

In the 2005 AISC Specification the directional strength increase was moved from an appendix into the main body of the Specification. Also added were a number of equations to simplify the application of the strength increase to concentrically loaded weld groups. The equations added are (J2-5) and (J2-9b). The Specification states that (J2-5) is applicable a single line weld or weld group that are aligned linearly and (J2-9b) is applicable to weld groups with elements oriented both longitudinally and transversely to the load.

This paper will demonstrate that additional requirements must also be satisfied if either (J2-5) or (J2-9b) is to be applied. Those requirements are that all weld elements must be of the same strength and size. This paper will also demonstrate the proper application of J2.4(b) to concentrically loaded weld groups consisting of fillet weld elements of varying leg sizes.

AN EXAMPLE

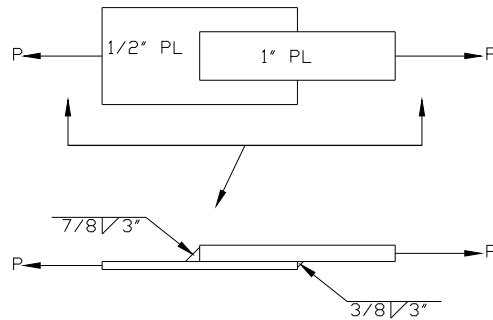


Figure 1

Assume two plates connected as shown in Figure 1 subjected to an axial load. Any eccentricity due to the line of action of the force is neglected for this example. With the maximum size transverse welds applied, the capacity of the welds is to be calculated. Based on section J2.4(a) of the AISC Specification the strength of each weld can be calculated as:

$$R_n = A_w 0.60 F_{EXX} (1.0 + 0.50 \sin^{1.5} \theta) \text{ where,}$$

F_{EXX} = the electrode classification number, ksi

A_w = the effective area of the weld, in.

θ = the angle of loading measured from the weld longitudinal axis, degrees

For convenience the term $(1.0 + 0.50 \sin^{1.5} \theta)$ will be called η . Since the welds are both loaded transversely, η , in accordance with the Manual, will be 1.5 for both welds. The capacity, assuming 70 ksi weld metal, is then calculated as:

$$R_n = (0.875 + 0.375)(\cos 45) 0.60(70 \text{ ksi})(1.5)(3") = 167 \text{ kips}$$

However, one crucial parameter has been missed. If we assume the plates to be infinitely rigid, then the deformation of the smaller weld and the larger weld must be equal. However, the 3/8" weld cannot accommodate the same degree of deformation as the 7/8" weld. This can be seen in Figure 2. AISC gives the deformation of a weld at fracture as:

$$\Delta_u = 1.087(\theta + 6)^{-0.65} w \leq 0.17w$$

η-Deformation Curves Based on Equation(J2-7)

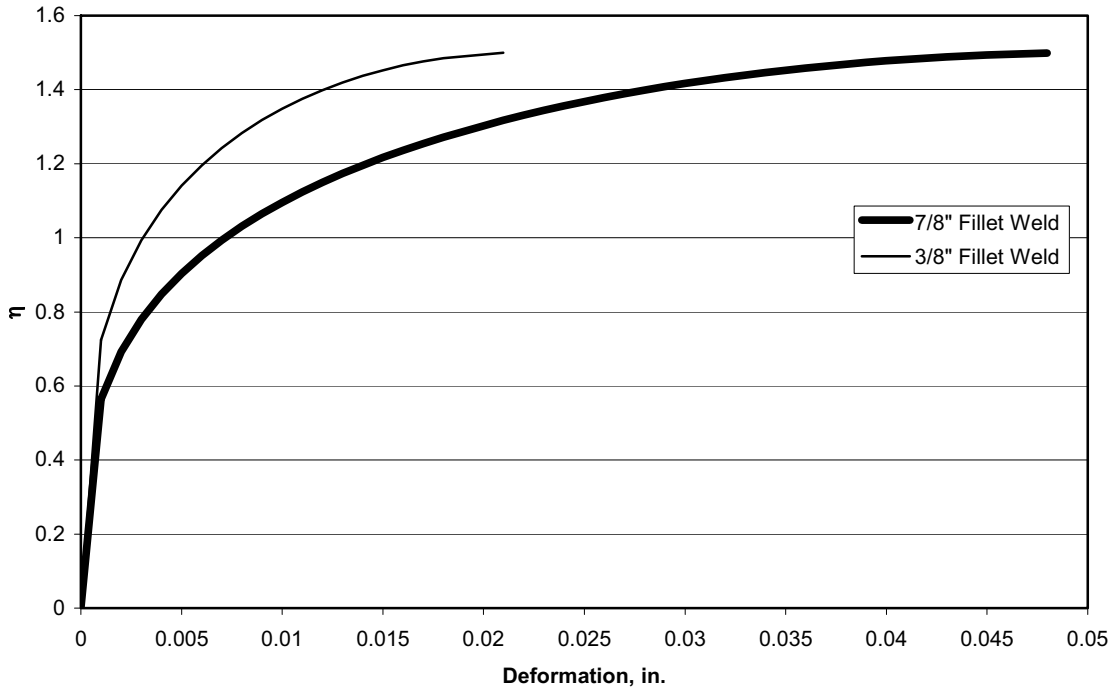


Figure 2

This can be simplified to $0.056w$ assuming transverse loading. For the 3/8" weld this results in a maximum deformation of 0.021". For the 7/8" weld this results in a maximum deformation of 0.049". Therefore the 3/8" weld will fracture prior to the 7/8" weld developing its full strength. Equation (J2-7) from the AISC Specification gives the strength of a weld element as:

$$F_{wi} = 0.6F_{EXX} (1.0 + 0.50 \sin^{1.5} \theta) f(p) \text{ where,}$$

$$f(p) = [p(1.9 - 0.9p)]^{0.3}$$

p = the ratio of the deformation to the deformation at maximum stress,

Δ_m .

$$\Delta_m = 0.209(\theta + 2)^{-0.32} w, \text{ for transverse loading } \Delta_m = 0.049w$$

For the 7/8" weld $\Delta_m = 0.043"$. With the limiting deformation based on the 3/8" weld of 0.021", $p = 0.021/0.043 = 0.488$. An effective η can be calculated as:

$$\eta_{eff} = (1.5)[0.488(1.9 - 0.9(0.488))]^{0.3} = 1.36$$

From this the capacity of the weld considering the deformational compatibility can be calculated as:

$$R_n = [0.875(1.36) + 0.375(1.5)](\cos 45)0.60(70 \text{ ksi})(3") = 156 \text{ kips}$$

This is somewhat smaller (6.6%) than the capacity of 167 kips predicted by (J2-4).

The problem become somewhat more complicated when combining longitudinally and transversely loaded welds of varying leg sizes, as shown in Figure 3.

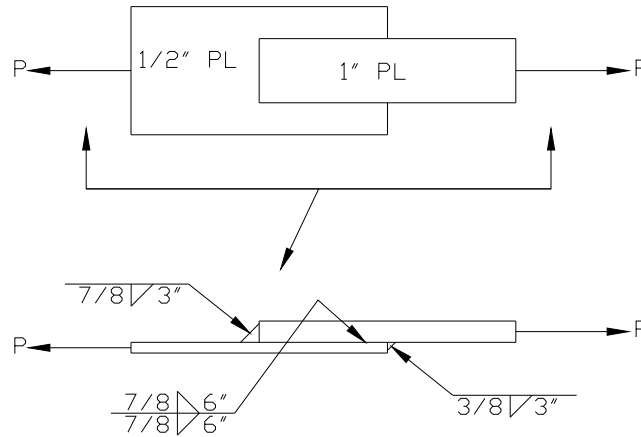


Figure 3

Since the additional welds are both larger than the limiting 3/8" weld and longitudinally loaded, it is obvious that the added welds will not limit the deformation. However, it is also obvious that they will not develop their full strength. AISC Equation (J2-9b) would predict the strength as:

$$R_n = [0.85(0.875)(12") + 1.5(0.875 + 0.375)(3")](\cos 45)0.60(70 \text{ ksi}) = 432 \text{ kips}$$

Equation (J2-9b) assumes η equal to 1.5 for the transversely loaded welds and 0.85 for the longitudinally loaded welds. However, again the deformational compatibility of the varying sizes of welds is neglected.

The effective η for the transversely loaded 7/8" fillet weld will not change due to the addition of the new welds, since these welds do not limit the deformation of the system. However, an effective η for the longitudinally loaded fillet welds must be calculated. This is done in a manner similar to that for 7/8" weld in the original configuration.

$$\Delta_m = 0.209(0 + 2)^{-0.32}(0.875) = 0.146"$$

With the limiting deformation based on the 3/8" weld of 0.021", $p=0.021/0.146 = 0.144$. An effective η can be calculated as:

$$\eta_{eff} = (1.0)[0.144(1.9 - 0.9(0.144))]^{0.3} = 0.664$$

From this the capacity of the weld considering the deformational compatibility can be calculated as:

$$R_n = [0.875(1.36)(3") + 0.375(1.5)(3") + 0.875(0.664)(12")](\cos 45)0.60(70 \text{ ksi}) = 363 \text{ kips}$$

This is about 16% less than the capacity predicted by (J7-9b).

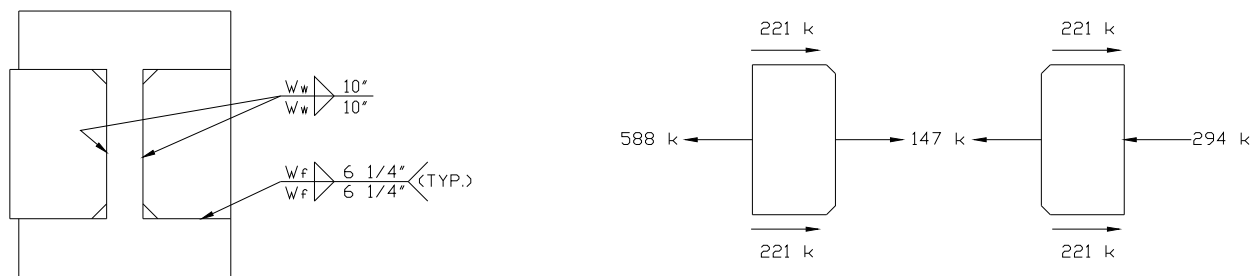
NEGLECTING THE DIRECTIONAL STRENGTH INCREASE

Prior to the inclusion of the directional strength increase in the Specifications, welds were obviously designed neglecting the increase. However, the deformation compatibility of the weld group was also neglected. The AISC Specification still allows this approach in Equation (J2-9a). It is commonly believed that neglecting the directional strength increase must surely be conservative, but this does not appear to be the case for the condition discussed. Neglecting the strength increase and the deformational compatibility, the capacity can be calculated as shown:

$$R_n = [(0.875)(12") + (0.875 + 0.375)(3")](\cos 45)0.60(70 \text{ ksi}) = 423 \text{ kips}$$

This is nearly as great as the capacity predicted by Equation (J2-9a) and exceeds the capacity predicted considering the deformation compatibility by 16.5%. This 16.5% increase is not negligible and is not justified.

A MOMENT CONNECTION EXAMPLE



(a) stiffeners welded to column

(b) free-body diagrams of stiffeners

Figure 4

The same problems arise in actual design situations, such as weak-axis moment connections. Assume the stiffeners for a moment connection to the weak-axis of a

column are welded as shown in Figure 4a. The corresponding free-body diagrams are shown in Figure 4b.

The required weld size at the flanges in accordance with (J2-9a) can be calculated as:

$$W_f = \frac{221 \text{ kips}}{(\cos 45)0.60(70 \text{ ksi})(2)(6.25\text{'})} = 0.595 \text{ Use } 5/8\text{' fillet welds}$$

The required weld size at the web in accordance with (J2-9a) can be calculated as:

$$W_w = \frac{147 \text{ kips}}{(\cos 45)0.60(70 \text{ ksi})(2)(10\text{'})} = 0.247 \text{ Use } 1/4\text{' fillet welds}$$

The required weld size at the flanges in accordance with (J2-9b) can be calculated as:

$$W_f = \frac{221 \text{ kips}}{(0.85)(\cos 45)0.60(70 \text{ ksi})(2)(6.25\text{'})} = 0.700 \text{ Use } 3/4\text{' fillet welds}$$

The required weld size at the web in accordance with (J2-9b) can be calculated as:

$$W_w = \frac{147 \text{ kips}}{(1.5)(\cos 45)0.60(70 \text{ ksi})(2)(10\text{'})} = 0.165 \text{ Use } 3/16\text{' fillet welds}$$

Now we can check the welds obtained using (J2-9a) considering the directional strength increase and the deformational compatibility. The weld to the web being smaller and inherently less ductile will obviously limit the maximum deformation. The maximum deformation of this weld can be calculated as:

$$\Delta_u = 1.087(90 + 6)^{-0.65}(0.25) \leq 0.17(0.25) = 0.014\text{' < } 0.043\text{'}$$

As has been demonstrated previously, the effective η for the longitudinally loaded welds at the flanges can be calculated as:

$$\Delta_m = 0.209(\theta + 2)^{-0.32} w = 0.209(0 + 2)^{-0.32}(0.625) = 0.105\text{'}$$

$$p = \frac{0.014\text{'}}{0.105\text{'}} = 0.133$$

$$\eta_{eff} = f(p) = [0.133(1.9 - 0.9(0.133))]^{0.3} = 0.649$$

The strength of the weld group can be calculated as:

$$R_n = [0.625(0.649)(6.25)(4) + 0.25(1.5)(10)(2)](\cos 45)0.60(70 \text{ ksi}) = 524 \text{ kips}$$

Since this is less than the required load of 588 kips, the welds designed according to (J2-9a) are not sufficient.

Next the welds designed in accordance with (J2-9b) will be investigated. Again the weld to the web will obviously limit the maximum deformation. The maximum deformation of this weld can be calculated as:

$$\Delta_u = 1.087(90 + 6)^{-0.65}(0.1875) \leq 0.17(0.1875) = 0.011" < 0.0319"$$

The effective η for the longitudinally loaded welds at the flanges can be calculated as:

$$\begin{aligned} \Delta_m &= 0.209(\theta + 2)^{-0.32} w = 0.209(0 + 2)^{-0.32}(0.75) = 0.126" \\ \rho &= \frac{0.011"}{0.126"} = 0.087 \\ \eta_{eff} &= f(\rho) = [0.087(1.9 - 0.9(0.087))]^{0.3} = 0.575 \end{aligned}$$

The strength of the weld group can be calculated as:

$$R_n = [0.75(0.575)(6.25)(4) + 0.1875(1.5)(10)(2)](\cos 45)0.60(70 \text{ ksi}) = 487 \text{ kips}$$

Again the capacity is less than the required load, so (J2-9b) is not suitable either.

In order to carry the required load some parameter of the weld group must change. Given that the weld to the web is very small and is limiting the overall deformation of the group, increasing its size is the obvious choice. If the size is increased from 3/16" to 5/16", the largest single pass weld, then the limiting deformation becomes:

$$\Delta_u = 1.087(90 + 6)^{-0.65}(0.3125) \leq 0.17(0.3125) = 0.017" < 0.053"$$

The effective η for the longitudinally loaded welds at the flanges will also increase to:

$$\begin{aligned} \Delta_m &= 0.209(\theta + 2)^{-0.32} w = 0.209(0 + 2)^{-0.32}(0.75) = 0.126" \\ \rho &= \frac{0.017"}{0.126"} = 0.135 \\ \eta_{eff} &= f(\rho) = [0.135(1.9 - 0.9(0.135))]^{0.3} = 0.652 \end{aligned}$$

The strength of the weld group increases to:

$$R_n = [0.75(0.652)(6.25)(4) + 0.3125(1.5)(10)(2)](\cos 45)0.60(70 \text{ ksi}) = 641 \text{ kips}$$

Since the original weld size was small, There is little difference economically between the original configuration using 3/16" welds and the new configuration using 5/16"

welds. However, the change in welds size represents a 66% increase. Using a 1/4" does not quite meet the capacity. If the optimal change was not quite so obvious, the relative benefits of all possible solutions must be weighed.

For instance, increasing the size of the weld to the flanges would be another option. If the 3/4" longitudinally loaded welds at the flanges were increased to 1-1/8", the effective η can be calculated as:

$$\Delta_m = 0.209(\theta + 2)^{-0.32} w = 0.209(0 + 2)^{-0.32}(1.125) = 0.188"$$

$$\rho = \frac{0.011"}{0.188"} = 0.058$$

$$\eta_{eff} = f(\rho) = [0.058(1.9 - 0.9(0.058))]^{0.3} = 0.513$$

The strength of the weld group can be calculated as:

$$R_n = [1.125(0.513)(6.25)(4) + 0.1875(1.5)(10)(2)](\cos 45)0.60(70 \text{ ksi}) = 595 \text{ kips}$$

The weld is now sufficient to carry the required load of 588 kips. However, this option is obviously not the most economical choice.

CONCLUSIONS

Load-deformation compatibility must be considered in the design of weld groups. Both AISC and AWS adopt an instantaneous center of rotation procedure, which can be used to maintain compatibility. In the AISC Specification this procedure is outlined in J2.4 (b), and in AWS D1.1 it is outlined in 2.5.4.3. However, both AISC and AWS also allow the designer to neglect load-deformation compatibility if the increased directional strength is also neglected. This was done to allow the use of the traditional method of adding weld strengths with no increase in directional strength and no consideration of deformation compatibility. It also avoids a significant decrease in the predicted capacity for welds that are loaded longitudinally with small returns loaded transversely.

The design examples in this paper have been designed in accordance with the procedures shown in the AISC Specifications and AWS Code. The author was unable to locate results of physical tests of fillet weld groups consisting of weld elements of varying leg size. In the absence of confirming tests, it would seem prudent to design fillet welds groups accounting for load-deformation compatibility, as it is included in the AISC Specification and AWS Code.

REFERENCES

AISC (1993), *Load and Resistance Factor Design Specification for Structural Buildings*, American Institute of Steel Construction, Inc., Chicago, IL.

AISC (2005), *Specification for Structural Steel Buildings*, American Institute of Steel Construction, Inc., Chicago, IL.

AWS (2004), *Structural Welding Code—Steel*, AWS D1.1/D1.1M:2004, 19th edition, American Welding Society, Miami, FL.

Lesik, D.F., and Kennedy, D.J.L. (1990), "Ultimate Strength of Fillet Welded Connections Loaded in Plane," *Canadian Journal of Civil Engineering*, Vol. 17, No. 1.

EARTHQUAKE SIMULATIONS ON SELF-CENTERING STEEL MRFS WITH POST-TENSIONED MOMENT CONNECTIONS

James M. Ricles

Lehigh University, Bethlehem, PA 18017, USA
jmr5@lehigh.edu

Choung-Yeol Seo

Lehigh University, Bethlehem, PA 18017, USA
cys4@lehigh.edu

Ying-Cheng Lin

Lehigh University, Bethlehem, PA 18017, USA
ycl206@lehigh.edu

Richard Sause

Lehigh University, Bethlehem, PA 18017, USA
rsause@lehigh.edu

ABSTRACT

The behavior of a self-centering moment resisting frame (SC-MRF) under earthquake loading is characterized by gap opening and closing at the beam-column interface. The beams are post-tensioned to the columns by high-strength post-tensioning (PT) strands to provide self-centering forces when gap opening occurs. Energy dissipation is provided by web friction devices (WFDs) placed on the beams. Using a performance-based design procedure, an SC-MRF is designed to have no damage under the Design Basis Earthquake (DBE), leading to an immediate occupancy following the DBE. In addition, under the Maximum Considered Earthquake (MCE) the structure is designed to have minimal damage and develop the life-safety performance level.

A seven-bay, four-story SC-MRF prototype building was designed with the above performance objectives and a 0.6-scale test frame model with two bays of the SC-MRF was constructed. This paper presents the connection details, performance-based design procedure and the expected seismic performance of the test frame based on nonlinear time history analysis.

INTRODUCTION

To avoid damage to moment resisting frames (MRFs) during the design earthquake, post-tensioned beam-to-column connections have been developed (Ricles et al. 2001, Garlock et al. 2005, Rojas et al. 2005, Wolski et al. 2008). The self-centering behavior of these connections results in a self-centering MRF (SC-MRF). In an SC-MRF, high-strength post-tensioned (PT) steel strands run parallel to the beams, and energy dissipation devices are placed in the beam-to-column connection. Energy dissipation devices that have been utilized in the past include bolted top and seat angles (Garlock et al. 2005), friction plates on the beam top and bottom flanges (Rojas et al. 2005), and a bottom flange friction device (BFFD) located beneath the beam in order to avoid interference with the floor slab (Wolski et al. 2008). Dissipating energy by friction is advantageous because it avoids the need to replace top and seat angles that have yielded and are susceptible to fracture under low-cycle fatigue. SC-MRFs with BFFDs in the connections were investigated by Iyama et al. (2008), who determined that the difference in the connections positive and negative moment capacity causes the inflection point in the beams to move away from midspan. As a result, the BFFD requires larger beam sections or longer reinforcing plates for the beam top flanges to avoid beam flange buckling, leading to an increase in fabrication costs.

A PT beam-to-column connection with a web friction device (WFD), referred to as a PT-WFD connection, is presented in this paper. In addition, a performance-based design procedure for SC-MRFs with PT-WFD connections is briefly presented. The results from time history analyses of a test frame are presented to assess the design procedure.

SC-MRFs WITH PT-WFD CONNECTIONS

A frame with PT-WFD beam-to-column connections is shown in Figure 1(a). The PT strands run parallel across multiple bays by passing the strands through the column flanges, where they are anchored on the outside column flange. The details for a PT-WFD connection with are shown in Figure 1(b). The WFD consists of two channels welded to the column flange and brass shim plates sandwiched between the channels and the beam web. The channels and brass shim plates are tightened by bolts (called *friction bolts*) that are placed through slotted holes in the beam web to generate a friction force in the WFD. Shim plates are placed between the beam flanges and the column flanges to maintain good contact between the beam flanges and column flanges. Reinforcing plates are welded to each beam flange to prevent the beam flanges from yielding excessively.

PT-WFD CONNECTION BEHAVIOR

The conceptual moment-relative rotation ($M-\theta_r$) for a PT-WFD connection under cyclic loading is shown in Figure 1(c). The connection has an initial stiffness similar to that of a fully restrained welded moment connection, where θ_r equals zero (events 0 to 1). Once the connection overcomes the moment due to post-tensioned (referred to as the decompression moment M_d) and the moment due to friction in the WFD (M_{Ff}), imminent gap opening (IGO) occurs at event 1, where the beam tension flanges separates from the column flange shim plate. The connection moment associated with IGO is designated as M_{IGO} . Following IGO, between events 1 and 2 the moment capacity of the connection continues to increase as the PT strands elongate, causing an increase in the PT force. Continued loading may eventually yield the PT strands at event 3. The WFD connection is designed to self-center under cyclic loading by preventing yielding in the PT strands as well as the beam web and the flanges. Upon unloading at event 2, θ_r remains constant as the moment contribution from the friction, M_{Ff} , changes direction due to the reversal of friction force F_f in the WFD between events 2 and 4. A complete reversal in the friction force results in a change of moment of $2M_{Ff}$ between points 2 and 4. Continued unloading between events 4 and 5 reduces θ_r to zero as the beam flange returns to being in contact with the column flange shim plate. Further unloading decreases the moment to zero, as the beam tension flange compresses fully against the column face shim plate between events 5 and 6. A load reversal results in similar behavior.

The moment capacity M of the PT-WFD connection is composed of a contribution from the axial force P in the beam and from the friction force F_f in the WFD, where

$$M = \underbrace{Pd_2}_{M_d} + \underbrace{F_f r}_{M_{Ff}} \quad (1)$$

In Eq. (1) P , F_f , d_2 , and r are equal to the axial force in the beam, friction force resultant in the WFD, the distance from the centroid of the beam section to the center of rotation (COR) that coincides at the reinforcing plate and the shim plate, and the distance between the COR and the friction force resultant, respectively. The axial force in the beam is comprised of the floor diaphragm force F_{fd} that is caused by the interaction of the SC-MRF with the floor system (Garlock et al., 2005) and the PT force T :

$$P = F_{fd} + T \quad (2)$$

where the PT force T is equal to

$$T = T_0 + 2d_2 \left(\frac{k_b k_s}{k_b + k_s} \right) \theta_r \quad (3)$$

In Eq. (3) T_0 , k_b , and k_s are equal to the initial PT force, the axial stiffness of the beam in one bay of the SC-MRF, and the axial stiffness of all of the PT strands in one bay of the SC-MRF, respectively.

PERFORMANCE-BASED DESIGN OF SC-MRFS

A performance based design (PBD) approach is used to design the SC-MRF system. Under the Design Basis Earthquake (DBE) the SC-MRF should achieve the *immediate occupancy* performance level defined in *FEMA 450* (FEMA 2000), where only limited structural and nonstructural damage has occurred. Under the Maximum Considered Earthquake (MCE) the SC-MRF should achieve the *collapse prevention* performance level (FEMA 2000). The MCE has a 2% probability of being exceeded in 50 years while the DBE is defined as 2/3 the intensity of the MCE, with an approximate 10% probability of being exceeded in 50 years (FEMA 2000).

Under the DBE, the structural components of the SC-MRF should not develop inelastic behavior, except for minimal yielding in the column base and the beam flanges at the end of the reinforcing cover plates. As a result, the building does not develop residual drift and is ready to be reoccupied after the DBE. Under the MCE, the PT strands should not yield. Some degree of inelastic behavior is anticipated in the panel zones, beams, and columns, however, the beams should not develop local buckling. Thus, under the MCE, the frame is anticipated to lose some of its self-centering capacity, but not collapse.

In order to meet the performance objectives described above, it is necessary to estimate the structural demands in the SC-MRF at the DBE and MCE levels. An amplified code-based procedure is used to estimate the structural demands where the total roof displacement of the inelastic structure is amplified from the elastic roof displacement. The elastic roof displacement for the DBE level is estimated using the design base shear V_{des} and the equivalent lateral force (ELF) procedure in accordance with the 2000 International Building Code (ICC 2000). Using the equal displacement principle, the roof displacement demand for the DBE and the MCE are estimated as follows (Garlock et al. 2005, Rojas et al. 2005):

$$\Delta_{roof,DBE} = C_{\xi} \cdot C_T \cdot R \cdot \Delta_{el-des} \quad (4a)$$

$$\Delta_{roof,MCE} = 1.5 \cdot C_{\xi} \cdot C_T \cdot R \cdot \Delta_{el-des} \quad (4b)$$

In Eq. (4) C_{ξ} , C_T , R , and the Δ_{el-des} are equal to the damping correction factor to correct for a damping ratio other than 5%; the period correction factor to correct for a design

period not equal to the actual first-modal period; the response modification factor; and the roof displacement from a linear elastic analysis of the frame under the equivalent lateral forces corresponding to V_{des} . The 1.5 factor in Eq. (4b) is based on the relationship between the DBE and MCE in accordance with FEMA (2000).

The amplified roof displacements are divided by the building height to estimate the maximum roof drift for the DBE, $\theta_{roof, DBE}$, and for the MCE, $\theta_{roof, MCE}$. Once the roof drift is known, the maximum story drift, θ_s , for a given hazard level is estimated as follows:

$$\theta_{s, DBE} = C_\theta \cdot \theta_{roof, DBE} \quad (5a)$$

$$\theta_{s, MCE} = C_\theta \cdot \theta_{roof, MCE} \quad (5b)$$

where $\theta_{s, DBE}$ and $\theta_{s, MCE}$ in Eq. (5) are associated with the DBE and MCE levels, respectively. C_θ in Eq. (5) is equal to 1.5, based on results of nonlinear dynamic analyses of SC-MRF's by Rojas et al. (2005). The relative rotation θ_r is utilized to design the PT-WFD connections in the SC-MRF, where at a given hazard level θ_r is estimated from the corresponding θ_s :

$$\theta_{r, DBE} = C_r \cdot \theta_{s, DBE} \quad (6a)$$

$$\theta_{r, MCE} = C_r \cdot \theta_{s, MCE} \quad (6b)$$

where C_r is equal to 0.8 based on results of nonlinear dynamic analyses performed by Rojas (2003); $\theta_{r, DBE}$ and $\theta_{r, MCE}$ are associated with the DBE and MCE levels, respectively. Rojas et al. (2005) and Garlock et al. (2005) previously estimated θ_r by subtracting the elastic component of the story drift from the total story drift. The θ_r from time history analyses by Rojas et al. (2005) however is much larger than the θ_r estimated using this approach.

DESIGN CRITERIA FOR PT-WFD CONNECTIONS

To ensure gap closing (and self-centering) on load reversal, the decompression moment of the connection, M_d , is set equal to or greater than $0.6M_{IGO}$ in accordance with the recommendations of Rojas et al. (2005). However, the energy dissipation of the PT-WFD connection must also be considered. The energy dissipation characteristics of WFD connections are quantified using the effective energy dissipation ratio, β_E , which is the actual energy dissipation of the connection for a given value of θ_r normalized by the energy dissipation of a corresponding bi-linear elastic-plastic connection with the same strength. Seo and Sause (2005) recommend $\beta_E \geq 0.25$ for SC-MRF systems to have displacement demands similar to those of elastic-perfectly plastic systems. In this

paper, the PT-WFD connections designed with $\beta_E > 0.25$ resulted in M_d equal to or less than $0.75M_{IGO}$. As a result, the PT-WFD connections were designed such that $0.6 < M_d/M_{IGO} < 0.75$. In addition, to ensure sufficient connection strength, $M_{IGO} > \alpha M_{des}$, where α is set equal to 0.95 (Iyama et al. 2008) and M_{des} is the design moment obtained from an ELF analysis of the SC-MRF using a model with fully restrained connections and a design base shear equal to V_{des} .

DESCRIPTION AND DESIGN OF TEST FRAME

A prototype building was selected for an experimental study to be performed. The building consists of a 4-story structure with two 2-bay perimeter SC-MRFs with PT WFD connections along each side of the building. The layout of the prototype building with the gravity and moment resisting frames are shown in Figure 2(a). The floor diaphragm system consists of a composite floor slab, with collector elements to transfer the inertia forces to selected bays of the SC-MRFs, while allowing the gaps to open in the PT-WFD connections. The building was designed in accordance with the criteria described previously. The design assumed that the structure is an office building on stiff soil at a site in Van Nuys near Los Angeles, California. A992 steel sections were used throughout the structure.

The building frame was designed using a response modification factor equal to 8, specified for steel special moment resisting frames (SMRFs) in IBC2000. The fundamental period T_1 of the prototype building was 1.5 sec. A 2-bay perimeter frame of the SC-MRF prototype building was chosen and scaled down by the scale factor of $\lambda = 0.6$ for the test frame, as shown in Figure 2(b). The design base shear of the test frame was 552 kN based on the portion of the floor plan tributary to two bays of the test frame. The beams and columns satisfied the ASIC seismic compactness criteria (AISC 2005). The fundamental period of the test frame, T_1 , from an eigenvalue analysis is 1.17 sec., which is approximately equal to the fundamental period of the prototype building of 1.5 sec, scaled by $\sqrt{\lambda}$ ($= 0.77$) in accordance with the similitude law to preserve the magnitude of acceleration between the prototype and model frame. The design demands (θ_{roof} , θ_s , and θ_r) based on the design procedure presented above are shown in Table 1 for the test frame.

PREDICTION OF TEST FRAME PERFORMANCE

The performance of the test frame under two ground motion sets was estimated by nonlinear time history analysis using an analytical model created using OpenSEES

(McKenna and Fenves 2008). The beams and columns of the test frame were modeled using nonlinear beam-column elements with fiber sections at discrete locations along the element length to consider the effects of moment-axial load interaction and shear deformations. The model of the panel zones used a tri-linear moment-rotation behavior, and a set of master-slave nodes to model shear force-deformation behavior, and the kinematics of the column panel zone. Gap opening between the beam flanges and the column face was modeled using two zero length elements located at the beam flanges at the beam-to-column interface. PT strands were modeled with truss elements having a trilinear elastic-plastic material where the first yielding point defines the linear elastic limit, which is approximately equal to 80% of the breaking strength of the strands. The WFD was modeled using a bi-directional rigid-plasticity based material model incorporated into a zero length section element (Iyama et al. 2008).

Seismic hazard levels with 10% and 2% probability of occurrence (PO) in 50 years were chosen for a performance-based estimate of structural performance under the DBE and the MCE levels. Identification of the relative contribution of each record is accomplished through a probabilistic seismic hazard disaggregation analysis (Baker and Cornell 2006). Two sets of 15 pairs of ground motion records were selected. The ground motion sets for 10% PO in 50 years and for 2% PO in 50 years are designated as 10PO50 gm and 2PO50 gm, respectively.

Structural response demand under earthquake loading is typically assumed to be lognormal. Thus, the geometric mean value of the response demands, X , is reported for the central tendency, and designated as \hat{X} . The geometric mean multiplied by the exponential of plus/minus one standard deviation of the natural logarithm of the response demands is reported for the response corresponding to the 16 and 84 percentile, and designated as ^-X and ^+X , respectively. For the residual story drift demands, count statistics are used to determine the statistical properties of the data.

The statistics for the maximum and residual story drift, θ_s^{\max} and θ_s^{res} as well as the design response demands, $\theta_{s,DBE}$ and $\theta_{s,MCE}$ of the test frame are shown in Figure 3, where the latter is indicated by straight vertical lines in Figure 3. The θ_s^{\max} represents the maximum value of a story for a given ground motion during the time history analysis. θ_s^{\max} , shown in Figure 3(a) and (b), tends to be larger in the upper stories and smaller at the lower stories. The maximum values of θ_s^{\max} tend to occur at the roof story, while the minimum values of θ_s^{\max} tend to occur at the 1st story. For the 10PO50 ground motions $\theta_{s,DBE}$ (= 3.8%) fell between $\hat{\theta}_s^{\max}$ and $^+\theta_s^{\max}$ at the roof story but is larger than $^+\theta_s^{\max}$ at the lower stories. Similar trends are observed for the results from the 2PO50 ground

motions, where $\theta_{s.MCE}$ (= 5.6%) fell within $\hat{\theta}_s^{\max}$ and $+\theta_s^{\max}$ in the upper two stories but was larger than $+\theta_s^{\max}$ at the lower stories.

The statistics of residual story drift, θ_s^{res} over the height of the test frame shown in Figure 3(c) show that a negligible residual story drift occurs under the 10PO50 ground motions, indicating the frame essentially self-centers under the DBE. Figure 3(d) shows that under the 2PO50 ground motions, the θ_s^{res} profile is irregular over the height of the structure, where $\hat{\theta}_s^{res}$ and $+\theta_s^{res}$ are generally smaller than 0.15% and 0.22%, respectively. The maximum value of θ_s^{res} for the 2PO50 ground motions is 1.1% at the roof story.

The statistics of the maximum of the average relative rotation for each floor, $\theta_r^{\max Ave}$, for the ground motions are shown in Figure 4(a) and (b). Similar to the story drift, $\theta_r^{\max Ave}$ is larger in the upper floors and smaller in the lower floors. Maximum values of $\theta_r^{\max Ave}$ occur at the roof, while the minimum values of $\theta_r^{\max Ave}$ among all floors occurs at the 1st floor. This result may be due to restraint of the gap opening in the 1st floor by the ground floor. In Figure 4(a), for the 10PO50 ground motions $\theta_{r.DB E}$ (= 3.0%) is between $\hat{\theta}_r^{\max Ave}$ and $+\theta_r^{\max Ave}$ for the two upper floors while for the lower two floors it is smaller than $+\theta_r^{\max Ave}$, but larger than $\hat{\theta}_r^{\max Ave}$. A similar trend was observed for the 2PO50 ground motions, except that $\hat{\theta}_r^{\max Ave}$ (= 4.8%) at the roof is slightly larger than $\theta_{r.MCE}$ (= 4.5%). The statistics for the residual relative rotation, θ_r^{res} , for the ground motion sets are shown in Figure 4(c) and (d). It is apparent that under the 10PO50 ground motions, θ_r^{res} is almost negligible, while under the 2PO50 ground motions some degree of θ_r^{res} is observed and is largest at the roof floor level.

The beams, columns, panel zones, and PT strands remain essentially elastic under the DBE. Under the MCE the beams undergo some inelastic behavior at the 1st floor level. The base of the column at the ground level in addition to the panel zones develop minor yielding. The medium value for PT force demand under the MCE is less than the yield strength of the PT strands.

SUMMARY AND CONCLUSIONS

To investigate the seismic behavior of a post-tension SC-MRF with web friction devices, a 0.6-scale SC-MRF test structure was developed from a prototype building designed using a performance based design procedure. Analytical studies of the test frame were performed to investigate its performance under the DBE and MCE hazard levels, and to

evaluate the design response demand estimates used in the design.

The results of the time history analyses indicated that the performance of the test frame is in general satisfactory under the DBE and MCE hazard levels. Although the performance of the test frame under the DBE and the MCE satisfied the design criteria, the response estimates used in the design procedure need to be improved for more accurate prediction for purposes of design. One source of improvement is the refinement of the factors used in the design equations to predict story drift and relative rotation demand from roof drift. For example, the design relative rotation is estimated from the design story drift multiplied by C_r . Based on the time history analysis results, a value of C_r equal to 1.0 instead of 0.8 is recommended. Also, it is observed that the design roof drift demand estimates are larger than the time history analysis results, indicating the equal displacement principle may be questionable. Further investigation is needed to improve the prediction of the design roof drift demand.

ACKNOWLEDGEMENTS

The research reported in this paper was conducted at the Advanced Technology for Large Structural Systems (ATLSS) Center at Lehigh University. The work was supported by the National Science Foundation under Grant No. CMS-0420974, within the George E. Brown, Jr. Network for Earthquake Engineering Simulation Research (NEESR) program and Award No. CMS-0402490 NEES Consortium Operation. The research was conducted at the Real-Time Multi-Directional (RTMD) Testing Facility located in the ATLSS Center at Lehigh University.

REFERENCES

- AISC (2005), *Seismic Provisions for Structural Steel Buildings*, American Institute of Steel Construction, Chicago, IL.
- Baker J.W. Cornell C.A. (2006), "Spectral Shape, Epsilon and Record Selection," *Earthquake Engineering & Structural Dynamics*, 35(9): 1077-1095.
- FEMA. (2000), *NEHRP Recommended Provisions for Seismic Regulations for New Buildings and Other Structures. Part 1 – Provisions and Part 2 – Commentary*, FEMA 450, Federal Emergency Management Agency, Washington, D.C.
- Garlock M., Sause R., Ricles J.M. (2005), "Behavior and Design of Post-tensioned Steel Frame Systems," *Journal of Structural Engineering*, ASCE; 133(3), 389-399.
- International Code Council. (2000), *International Building Code*, Falls Church, Virginia.

Iyama, J., Seo, C-Y., Ricles, J.M., and Sause, R., (2008), "Self-centering MRFs with Bottom Flange Friction Devices under Earthquake Loading," *Journal of Constructional Steel Research*, in press, doi:10.1016/j.jcsr.2008.02.018.

McKenna, F. and Fenves, G. (2008), *The OpenSees Command Language Manual: version 1.2 Pacific Earthquake Engineering Center*, Univ. of Calif., Berkeley. (<http://opensees.berkeley.edu>).

Ricles J.M., Sause R., Garlock M., Zhao C. (2001), "Post-Tensioned Seismic-Resistant Connections for Steel Frames," *Journal of Structural Engineering*, ASCE; 127(2):113-121.

Rojas P., Ricles J.M., Sause R. (2005), "Seismic Performance of Post-Tensioned Steel MRFs with Friction Devices," *Journal of Structural Engineering*, ASCE; 131(4):529-540.

Rojas P. (2003), "Seismic Analysis, Design, and Evaluation of Post-tensioned Friction Damped Connections for Steel Moment Resisting Frames," Ph.D. Dissertation, Department of Civil and Environmental Engineering, Lehigh University.

Seo, C-Y., Sause R. (2005), "Ductility Demands on Self-Centering Systems under Earthquake Loading," *ACI Structural Journal*; 102(2): 275-285.

Wolski M., Ricles J.M., Sause R. (2008), "Experimental Study of Self-centering Beam-column Moment Connections with a Bottom Flange Friction Device," *Journal of Structural Engineering*, submitted for publication.

Table 1. Design response demands (in radians)

$\theta_{roof,DBE}$	$\theta_{s,DBE}$	$\theta_{r,DBE}$	$\theta_{roof,MCE}$	$\theta_{s,MCE}$	$\theta_{r,MCE}$
0.025	0.037	0.03	0.037	0.056	0.045

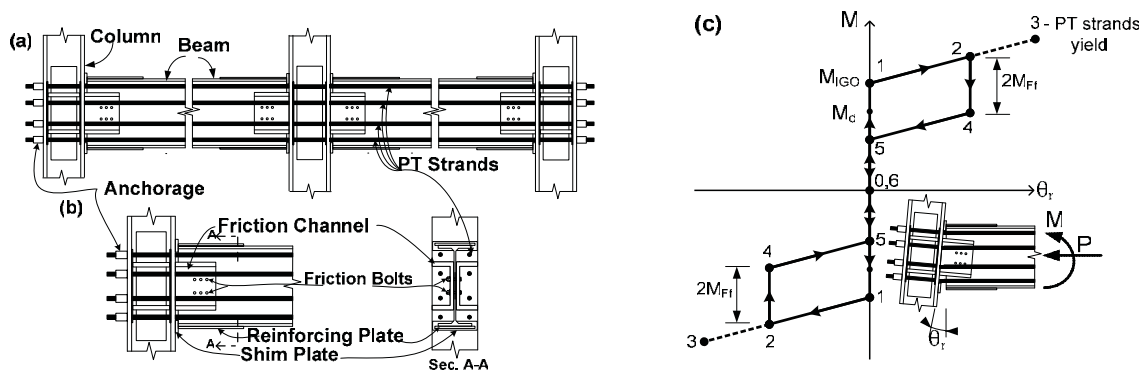


Figure 1 Schematic of (a) elevation of a 2-bay SC-MRF with PT strands, (b) PT-WFD connection, and (c) moment-relative rotation ($M-\theta$) of a PT-WFD connection.

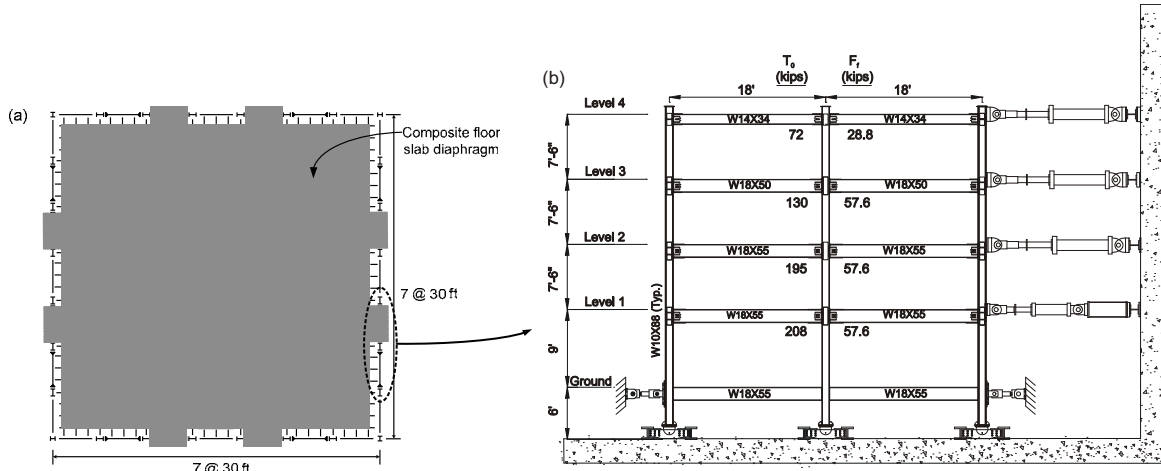


Figure 2 Schematic of (a) plan of prototype building, and (b) elevation of 0.6-scale 4-story 2-bay SC-MRF test frame.

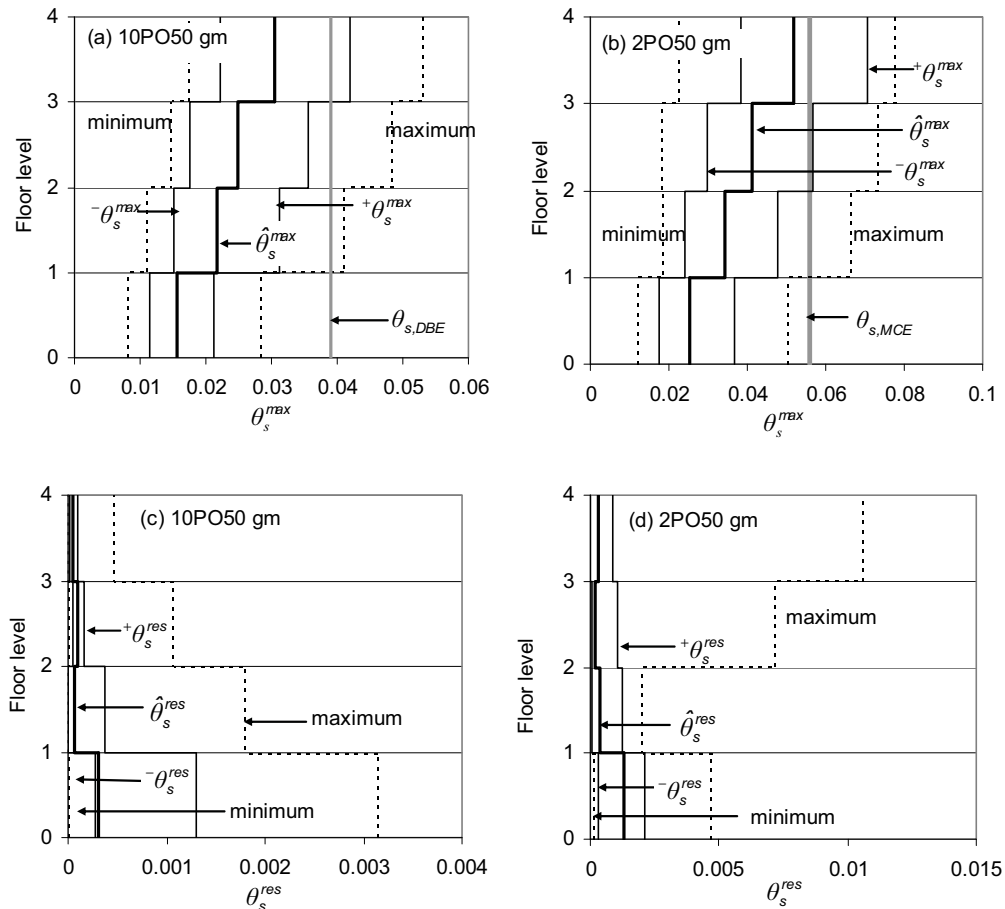


Figure 3 (a) and (b) statistics of maximum story drift envelop for 10PO50 and 2PO50 ground motions, and (c) and (d) statistics of residual story drift envelop for 10PO50 and 2PO50 ground motions.

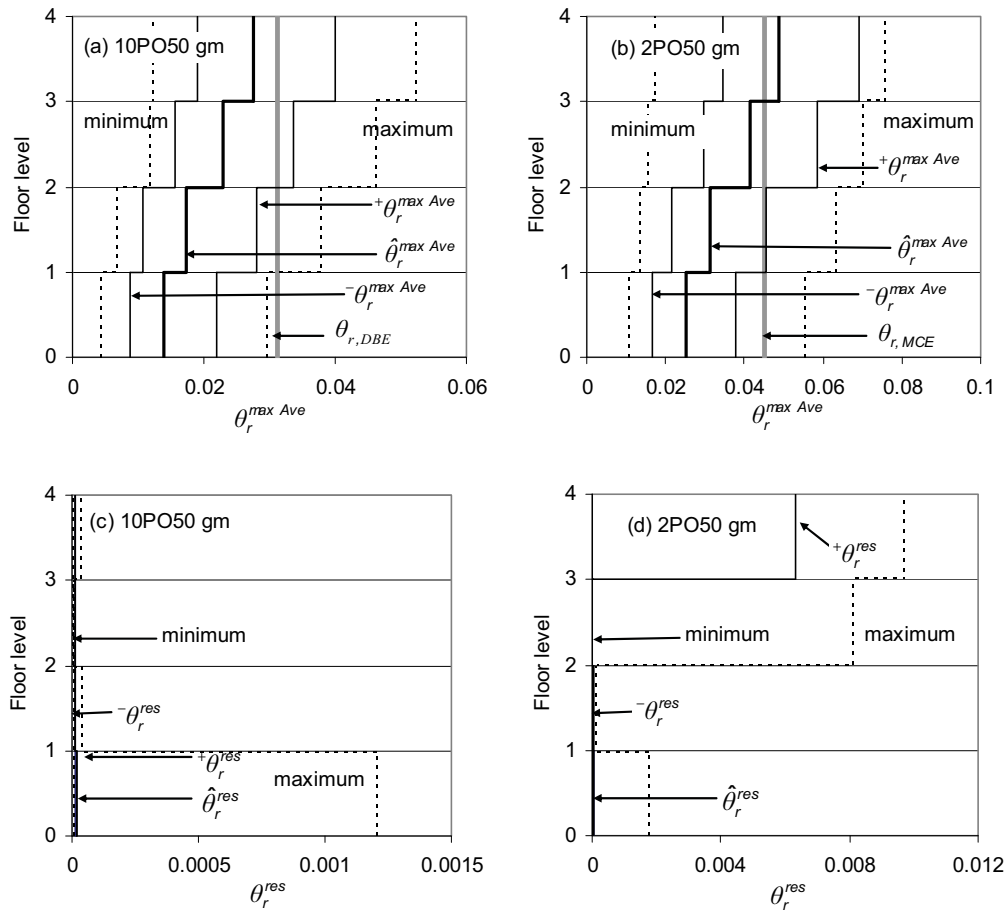


Figure 4 (a) and (b) statistics of maximum average relative rotation envelope for 10PO50 and 2PO50 ground motions, and (c) and (d) statistics of average residual relative rotation envelope for 10PO50 and 2PO50 ground motions.

HYBRID MOMENT RESISTING STEEL FRAMES

Finley A. Charney

Virginia Tech, Blacksburg, Virginia 24061, USA

fcharney@vt.edu

Ozgur Atlayan

Virginia Tech, Blacksburg, Virginia 24061, USA

atlayan@vt.edu

A new type of moment resisting steel frame, called a Hybrid Moment Resisting Frame, is described. Unlike a typical moment frame, where all member sizes and connection details fit a specific set of rules (e.g. for a special moment frame), the Hybrid Frame contains members and connections with a variety of detailing rules, including those typically associated with ordinary (OMF), intermediate (IMF), and special moment frames (SMF). Elements that have special detailing are designed to yield at force levels well below the design basis earthquake, and thereby provide some inelastic energy dissipation that helps to control dynamic amplification. Elements with ordinary detailing are designed to remain elastic during the design basis earthquake, and to provide enough positive stiffness to counteract P-delta effects. The resulting system is expected to perform better than the traditional special moment frame, and to be more economical than the special moment frame because a limited number of elements and connections have special detailing. The behavior of the system is demonstrated through incremental nonlinear dynamic response history analysis.

INTRODUCTION

The current specifications for seismic resistant design (ASCE, 2006; AISC, 2005a; AISC, 2005b) require that special detailing be used in moment resisting frame systems that are to be constructed in high seismic hazard regions. This detailing requires the use of designated flexural yielding regions with limited width-to-thickness ratios, highly ductile pre-qualified connection types, limited panel zone yielding, and adherence to a strong-column weak-beam design philosophy. The structure must be designed such that first significant yield occurs at lateral force levels that are at or above the Design Basis Earthquake (DBE) forces. The sequencing of plastic hinging is usually not explicitly designed, and hence, there is no guarantee that the slope of the structure's force-deformation response (pushover curve), including P-Delta effects, is continuously positive up to the maximum expected drift. This is a critical design issue because it is much more likely that dynamic instability will occur when the post-yield stiffness is negative (Gupta and Krawinkler, 2000). This fact has led to a significant revision in the 2003 NEHRP Provisions (FEMA, 2004) where it is required that the pushover curve be continuously positive up to 1.5 times the target displacement if the stability ratio, based

on initial elastic stiffness and on design level gravity loads, exceeds 0.10^1 . Another consequence of not explicitly designing the hinging sequence is that the expected over-strength, which is implicitly included in the system's Response Modification Coefficient, R , is not guaranteed. Indeed, there is nothing in the current design provisions that prevents a designer from developing a system for which a nonlinear static pushover analysis indicates that all of the hinges form nearly simultaneously.

In a Hybrid Moment Resisting Frame (HMRF), the hinging sequence is explicitly designed to assure a continuously positive post-yield pushover response. The HMRF shares many of the features of the Special Moment Resisting Frame (SMRF), with the following exceptions:

1. The yielding sequence is set such that the first plastic hinges form at load levels well below the design basis earthquake, and the last hinges form at load levels consistent with the maximum considered earthquake. The inelastic energy dissipation provided through early yielding is expected to improve the performance of the structure to earthquakes of intensity less than the design basis earthquake. The near-elastic response of the late-forming hinges is intended to guarantee a positive pushover response.
2. The detailing for the lateral load resisting components and their connections depends on the level of inelastic rotation that is expected in the various plastic hinges. The hinges that form first have the highest ductility demand, and are detailed according to the rules for special moment frames. It is noted that these hinges may have ductility demands that exceed those expected from traditional SMRF designs. The hinges that form last have the lowest ductility demand, and are detailed according to the rules for intermediate or ordinary moment frames.

The Hybrid Frame concept may be used for any structural system, such as concentrically braced frames, or buckling restrained braced frames. The concept of Hybrid Buckling Restrained Frames is particularly attractive because of the ability to tightly control the inelastic behavior of the yielding elements.

The advantages of Hybrid Frames will be demonstrated through two examples. The first example is of a Hybrid Braced Frame, and is used only to demonstrate the concepts and to introduce some of the features used in the analysis. The second example is of a 9-story steel moment resisting frame.

DEMONSTRATION OF CONCEPTS: A HYBRID BRACED FRAME

In this demonstration, a simple one-story braced frame is analyzed. This fictitious frame, shown in Figure 1, is intended to have the dynamic characteristics of a 15 story building, with a first mode period of vibration of 2.0 seconds. Two different versions of the frame are presented. The first frame, called the "Normal" frame, has six identical

¹ A similar requirement is expected to be adopted in the ASCE 7-10 Specification.

diagonal braces, each with an axial strength of 141 kips. The second frame, called the "Hybrid" frame has bracing bars of the following strengths: bar 1 = 47 kips, bar 2 = 94 kips, bars 3 and 4 = 141 kips, bar 5 = 188 kips and bar 6 = 235 kips. The lateral strength of the structure, exclusive of P-Delta effects, is 600 kips. The axial stiffness of each of the bars, whether in the Normal or Hybrid Frame is 68.9 kips per inch. The initial lateral stiffness of each frame is 207 kips/inch. It was assumed that the bars were elastic-plastic, without strain-hardening.

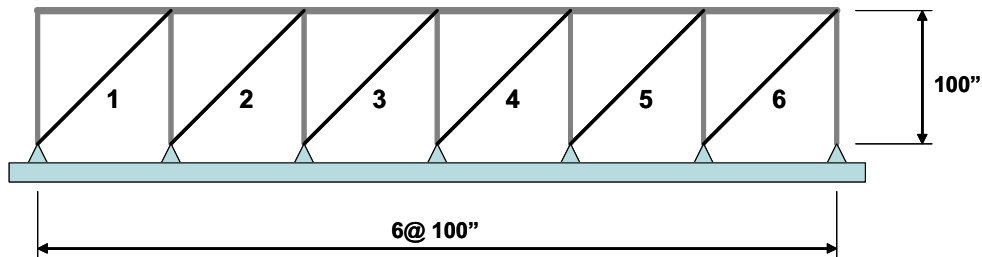


Figure 1. A Simple Braced Frame

Nonlinear static pushover plots of the Normal and Hybrid frames are shown in Figs. 2(a) and 2(b), respectively. Response curves with and without P-Delta effects are shown. Where included, the P-Delta analysis emulates a structure with an average story stability ratio of 0.10.

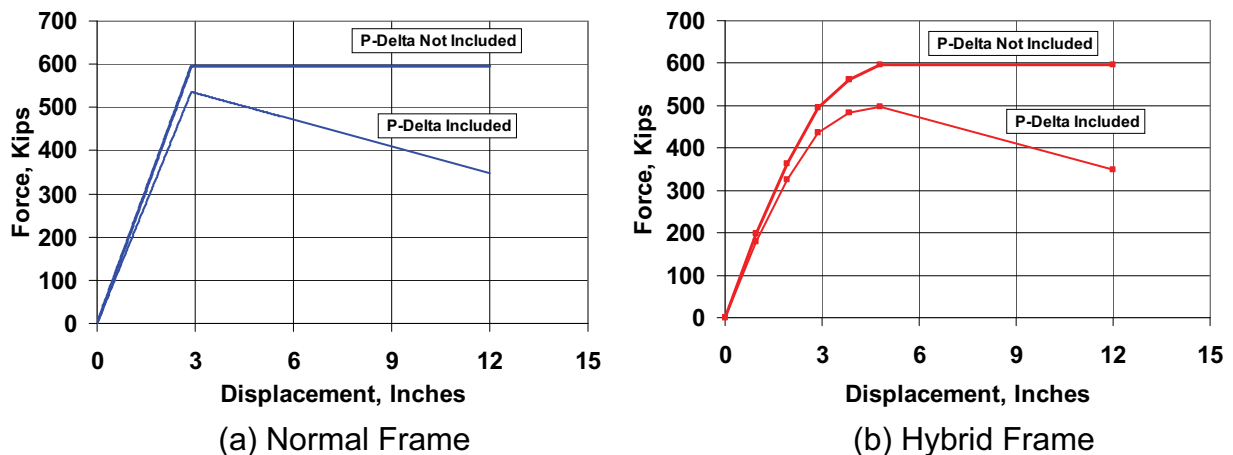


Figure 2. Nonlinear Static Pushover Curves for Braced Frame Structure

To investigate the dynamic behavior the Normal and Hybrid structures, with and without P-Delta effects included, were subjected to the 1940 Imperial Valley ground motion, with a peak ground acceleration of 0.35g. For each case, the structure was repeatedly subjected to this ground motion, with each analysis using an incrementally larger ground motion multiplier. The multipliers ranged from 0.2 to 2.0, in increments of 0.2. For this example, it is assumed that a multiplier of 1.0 corresponds to the Design Basis

Earthquake (DBE) and the factor of 1.5 corresponds to the Maximum Considered Earthquake (MCE).

Analysis was run using NONLIN-Pro (Charney and Barngrover, 2006), which uses the Drain 2D-X (Prakash et al., 1993) analysis engine. All analyses were run with an inherent damping ratio of approximately 0.02. One set of analyses was run without P-Delta effects, and the other with P-Delta effects. When P-Delta effects were considered, both the Normal and Hybrid structures were dynamically unstable when the ground motion multiplier exceeded 1.5.

Plots of the results for the models without P-Delta effects are shown in Figures 3(a) through 3(d). Figure 3(a) plots the ground motion multiplier on the vertical axis and the computed roof displacement on the horizontal axis. The displacements appear to be similar for the two systems, except that it is noted that the Hybrid frame displacements are about 12 to 15% less than the Normal frame displacements for the first two increments of loading. For all ground motion levels less than or equal to the MCE, the residual inelastic deformations Fig. 3(c), are significantly lower for the Hybrid frame, when compared to the Normal frame. (Residual deformations are the permanent lateral deformations that remain in the structure after ground shaking has ceased.) At the ground motion intensity level of 1.8, however, the residual deformations in the Hybrid frame exceed those in the Normal frame. The base shears for the Hybrid frame, shown in Fig. 3(b) are also lower than those for the Normal frame for the first two increments of ground motion intensity.

Ductility demands for Bar 1, Bar 6, and for the average of all bars are presented in Figure 3(d). For the Hybrid frame, Bar 1 is the weaker bar, and as expected, the ductility demand is the highest. At the DBE level (multiplier 1.0), the ductility demand for Bar 1 is 6.61. At the same intensity, the ductility demand for Bar 6 is only 1.32, and the average ductility demand for all Hybrid bars is 2.88. For the Normal frame, the ductility demand for all bars is the same at each intensity level, and is 2.15 at the multiplier of 1.0.

It appears from the results that the Hybrid frame is performing as expected. Displacements at low level ground motions are reduced due to the early yielding and associated hysteretic behavior of Bars 1 and 2. Delayed yielding of the stronger bars provides a component of elastic stiffness that controls residual deformations.

When P-Delta effects are included, the performance of the Hybrid frame is further improved when compared to the Normal frame. This is illustrated in Figures 4(a) through 4(d), where it may be seen that the total displacements, Fig. 4(a), are significantly less in the Hybrid frame at all ground motion levels up to the DBE. This improved performance is due to the significant reduction in residual deformations, shown in Fig. 4(c). As mentioned earlier both the Hybrid and Normal frames displayed dynamic instability when the ground motion multiplier exceeded 1.5. This is due to the negative stiffness of the pushover curves (see Fig. 2) at larger displacements.

It is interesting to note from Fig. 4(b) that at ground motion multipliers between 0.6 through 1.0, the base shears for the Hybrid frame are somewhat greater than for the normal frame. This is not a disadvantage for the Hybrid frame, because the lower base shears for the Normal frame are associated with P-Delta related strength loss.

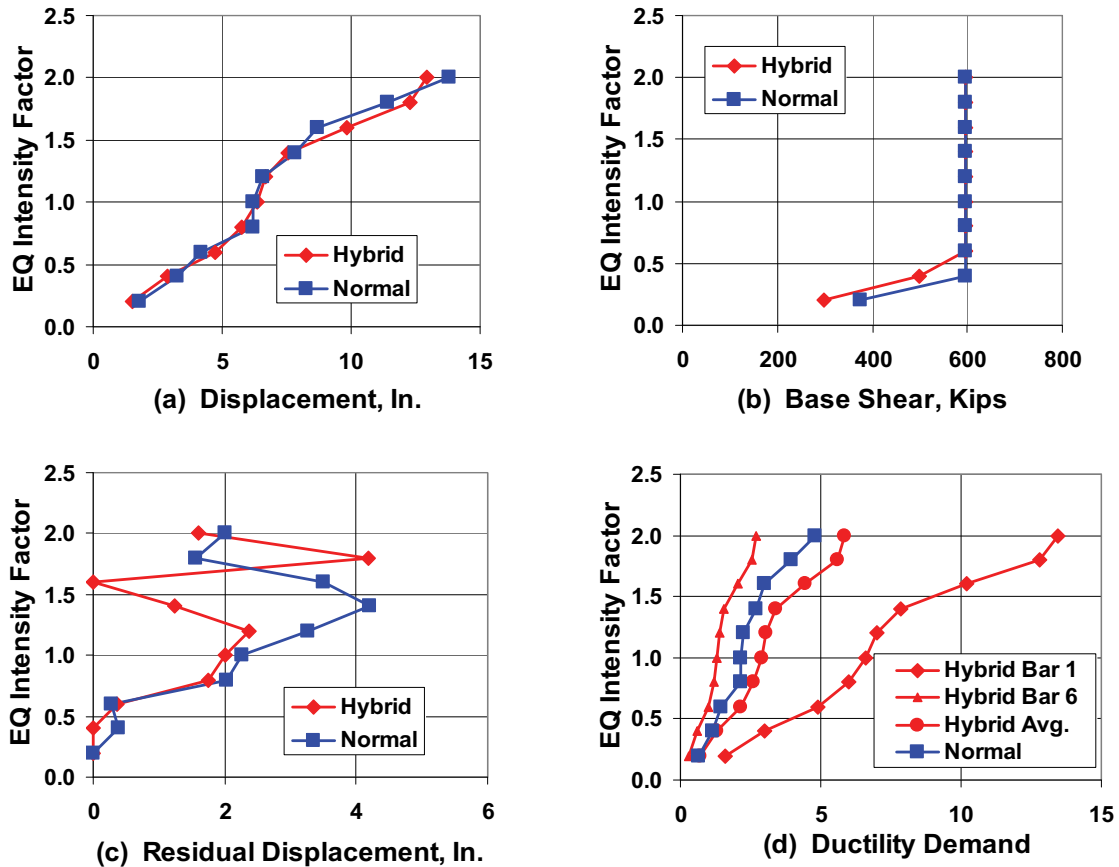


Figure 3. Results of Frame Analysis Without P-Delta Analysis

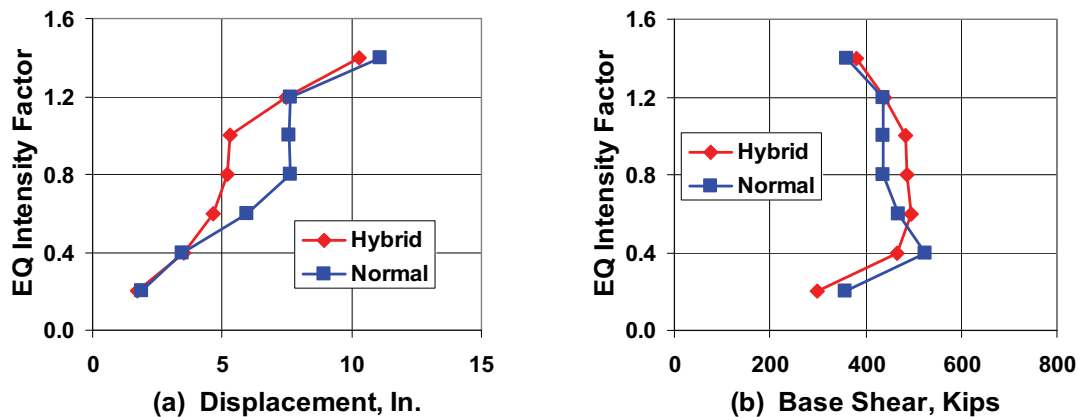


Figure 4. Results of Frame Analysis With P-Delta Analysis

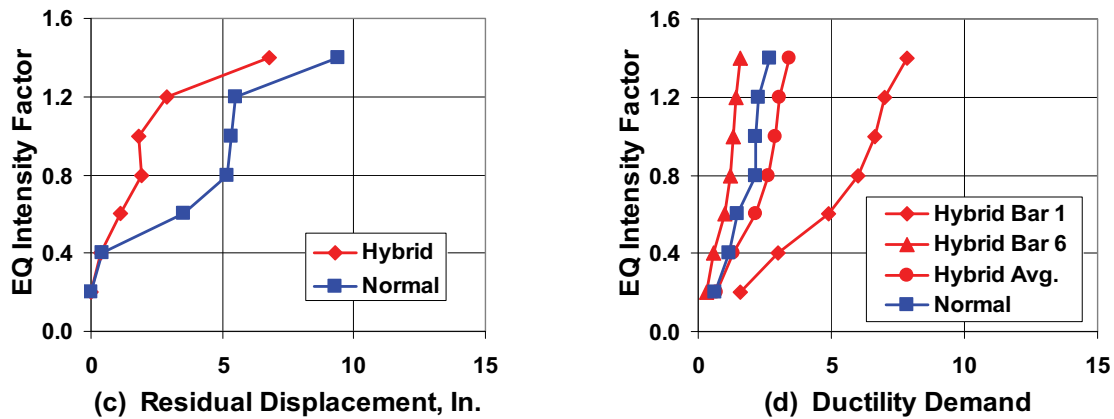


Figure 4. Results of Frame Analysis With P-Delta Analysis (continued)

ANALYSIS of A HYBRID MOMENT RESISTING FRAME (Preliminary Results)

The Hybrid Moment Frame concept is demonstrated by the analysis of a five-bay nine-story frame building, located near Seattle, Washington. The geometry of this building is identical to that studied in the SAC Steel Project (FEMA, 2000). The ASCE 7 design parameters used for the design are summarized in Table 1. Four different Hybrid frame configurations were used in this study. Figure 5 shows the member sizes used for different Hybrid frame combinations. (Member sizes for the girders are shown above each girder, with Combination 1 at the bottom and Combination 4 at the top.) Combination 1 is a Normal frame design without any change in the plastic hinge capacities throughout the story. For this design the response reduction factor R , was taken as 6, and the deflection amplification factor, C_d , was taken as 5. The two exterior girders of the Hybrid Frame (bays 1 and 5) were designed as special moment frames (SMF), the two interior girders (bays 2 and 4) were designed as intermediate moment frames (IMF) and the middle girder (bay 3) was designed as an ordinary moment frame (OMF). After the sections of the 1st hybrid combination (the Normal frame) were found, the plastic capacities were changed throughout the story. The plastic capacities of the exterior girders were decreased by 25%, 37.5% and 50% for the 2nd, 3rd and 4th hybrid frame combinations. Since the main idea of the Hybrid frame is to keep the total strength of the story the same, the plastic capacity of the middle girder was increased by 50%, 75% and 100%. The bay 2 and bay 4 girder capacities were kept the same for all combinations. In summary, as the combination number gets bigger, the frame becomes more hybrid with a greater variation in beam sizes across the width at each story. The column sections were kept the same for all the combinations but the panel zone doubler plate thicknesses were changed as necessary. Reduced beam sections were used for all the girders except for the girder in the middle bay, which was designed according to the rules for an OMF. The strong column - weak beam requirement was satisfied at the joints of the columns on column lines 1, 2, 5, and 6.

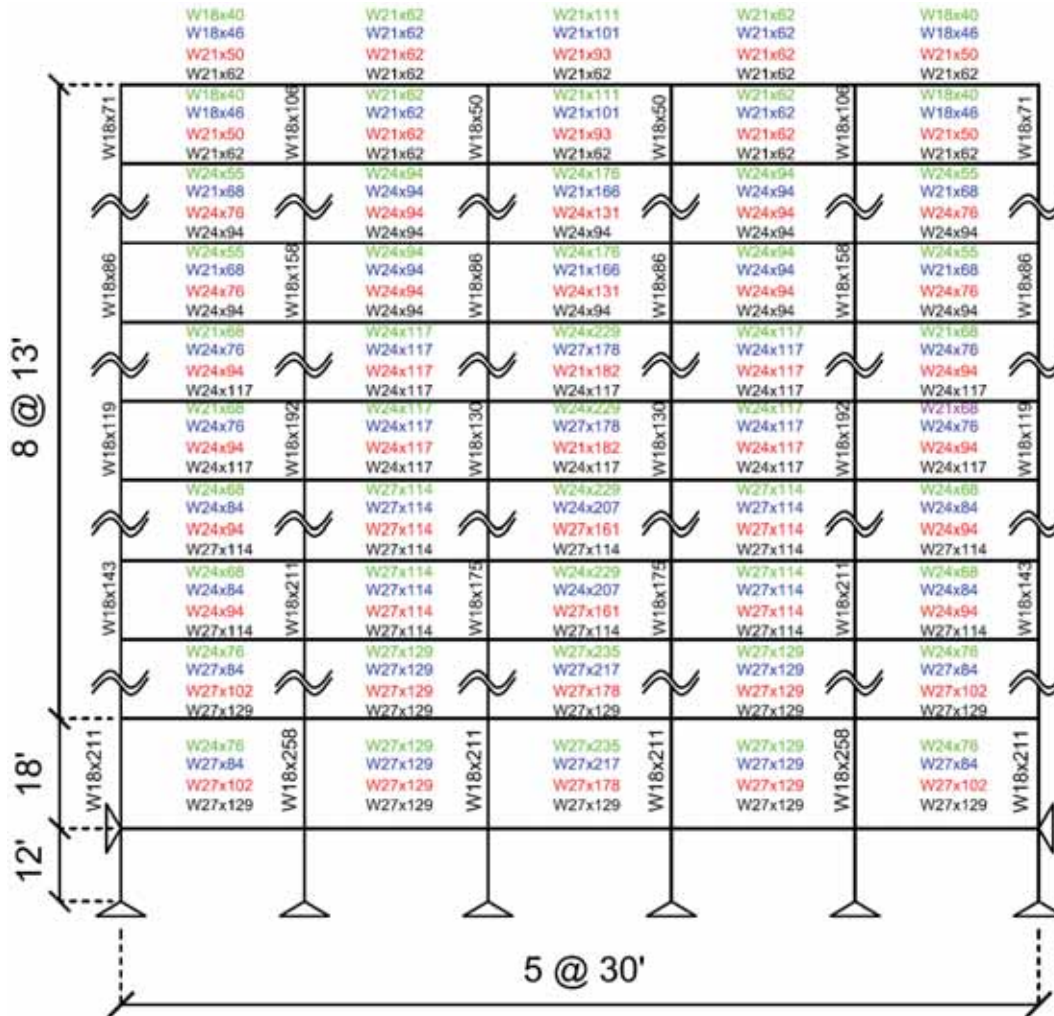


Figure 5. Member Sizes Used for Hybrid Frames 1 to 4 (bottom to top)

Table 1. ASCE 7-05 Design Parameters for Hybrid Frame

Design Parameter	Value
0.2 second spectral acceleration S_s	1.25 g
1.0 second spectral acceleration S_1	0.5 g
Site Class	D
0.2 second design acceleration S_{ds}	0.83 g
1.0 second design acceleration S_{d1}	0.5 g
Seismic Use Group	II
Importance Factor	1.0
Seismic Design Category	D
Effective Seismic Weight W	10,500 kips

Structural Analysis

All structural analysis was conducted using Perform-3D (CSI, 2006), using a planar model consisting of one of the two perimeter frames that are parallel to the design ground motion. Panel zones were explicitly represented by use of Krawinkler's model (Charney and Marshall, 2006). P-Delta effects were included in all analysis, using a special linear "ghost frame" which captures the entire gravity load tributary to the leaning columns. The inherent damping was determined by setting the critical damping ratio to 2% at the natural period of the structure and at a period of 0.2 sec as it was done in the SAC Report (FEMA, 2000). Two types of analysis were performed for each frame; nonlinear static pushover analysis (NSP) and incremental dynamic analysis (IDA). Pushover curves for the four different Hybrid Frames are shown in Figure 6.

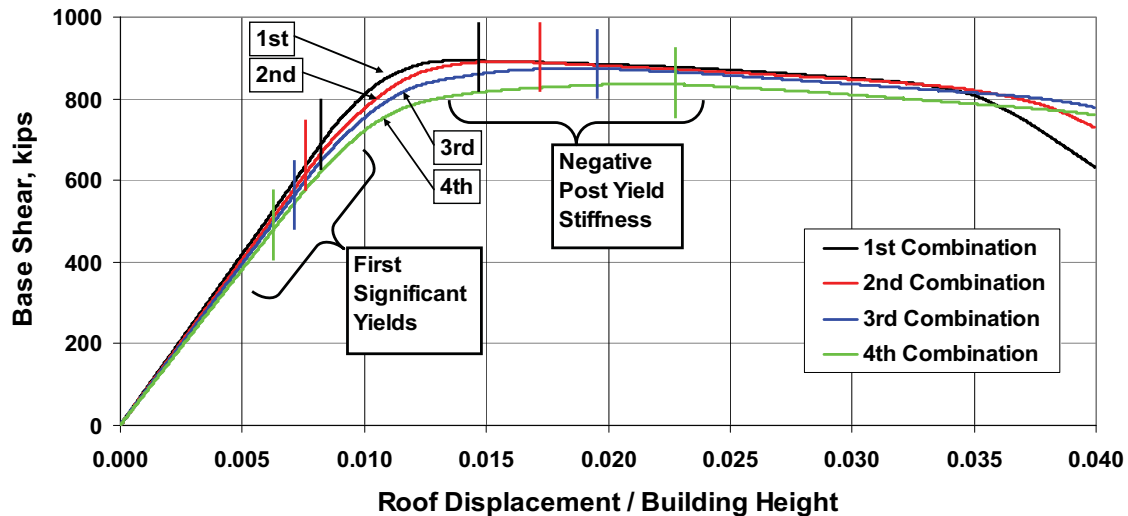


Figure 6. Static Pushover Curves for Hybrid Frames

Note that the point of the first significant yield and the point at which the post-yield curve becomes negative are shown on the figure. As expected, combination 4 starts yielding first, and combination 1 yields at last. The more reduction in the plastic capacity of the exterior bays, the earlier the structure starts yielding. In addition, the negative post yield stiffness of the pushover curves is reached later as the frames become more hybrid.

Incremental dynamic analysis, sometimes called dynamic pushover analysis, consists of a sequence of nonlinear response history analyses of the structure, with each analysis in the sequence subjecting the structure to the same basic ground motion, but at a higher intensity than the previous analysis in the sequence (Vamvatsikos, 2002). In this study, IDA analysis was conducted for the structure subjected to ten different earthquake records, and at intensities of 0.2 to 2.0 times the ground motion scaled to match the design basis earthquake. The ground motions were scaled to match the ASCE-7 design basis spectrum at the structure's fundamental period of vibration. This scaling procedure is recommended for IDA analysis by Shome and Cornell (Shome et al., 1998). The ground motions used in the analysis are summarized in Table 2. It is noted that these ground motions, developed by Somerville (Somerville, 1996), are the same as those used in the original SAC research (FEMA, 2000).

Table 2. Ground Motion Records Used in Analysis

EQ No.	SAC Name	EQ Name	Time Step (sec.)	Newmark Integration Time Step	Scale Factor	Scaled PGA
EQ00	SE 21	Mendocino, 1992	0.020	0.005	0.403	0.311
EQ01	SE 23	Erzincan, 1992	0.005	0.005	0.657	0.313
EQ02	SE 25	Olympia, 1949	0.020	0.005	2.111	0.435
EQ03	SE 27	Seattle, 1965	0.020	0.001	6.214	1.087
EQ04	SE 29	Valpariso, 1985	0.025	0.0025	2.088	1.178
EQ05	SE 31	Valpariso, 1985	0.025	0.001	3.934	1.262
EQ06	SE 33	Deep Interplate	0.020	0.001	4.281	0.888
EQ07	SE 36	Miyagi-oki, 1978	0.020	0.001	1.189	0.523
EQ08	SE 37	Shallow Interplate 1	0.020	0.005	1.054	0.632
EQ09	SE 40	Shallow Interplate 2	0.020	0.001	1.747	0.879

Figures 7 and 8 illustrate the roof displacement response histories of Hybrid frames subjected to EQ07 and EQ05 with scale factors of 2.0 and 1.8 times the anchored design spectrum scaling, respectively. These two earthquakes are the most severe ones out of all the earthquakes used in this study. As can be seen from Figure 7, the 1st, 2nd and 3rd Hybrid frame combinations reach dynamic instability whereas the 4th combination, which is the most hybrid, resists the collapse with 60 in. of residual displacement at the roof level. All the Hybrid frame combinations collapse when they are subjected to EQ05 with 1.8 IDA scaling. However, as the frames become more hybrid, they resist the collapse more, i.e. collapses occur at a later time. Figure 9 shows the roof displacement when the frames are under EQ09 with IDA scaling of 2.0.

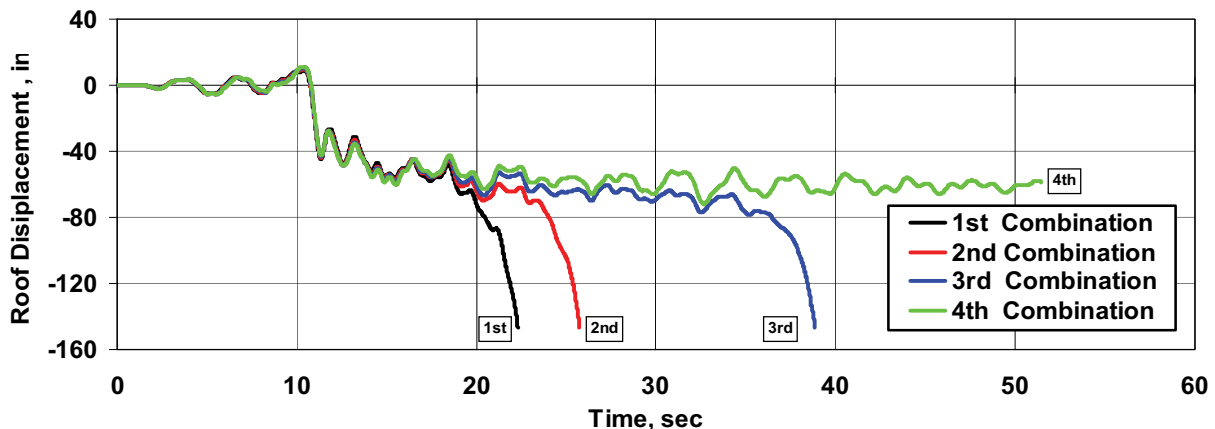


Figure 7. Roof Displacement Response History of Hybrid Frames subject to EQ07 with scale of 2.0 times the anchored design spectrum scale.

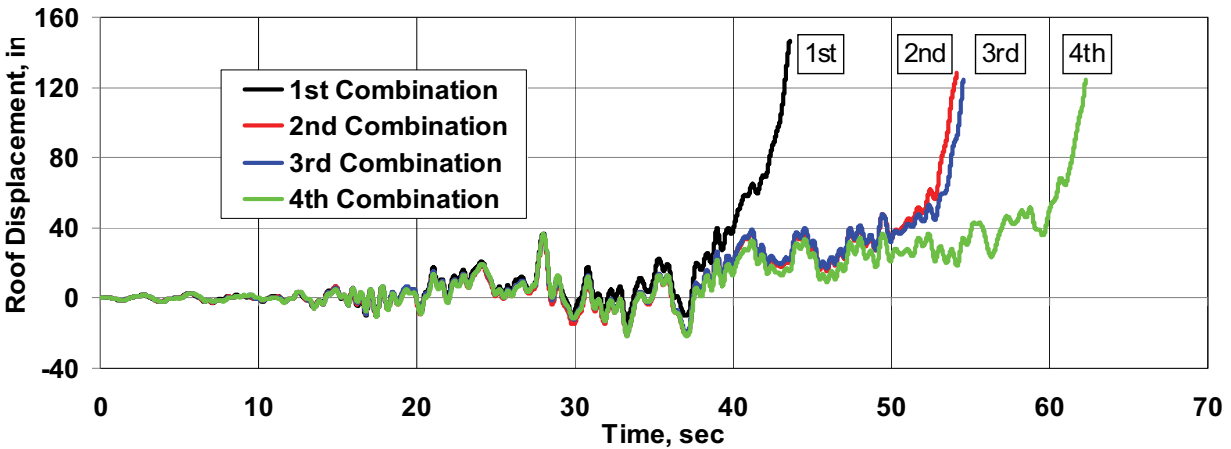


Figure 8. Roof Displacement Response History of Hybrid Frames subject to EQ05 with scale of 1.8 times the anchored design spectrum scale.

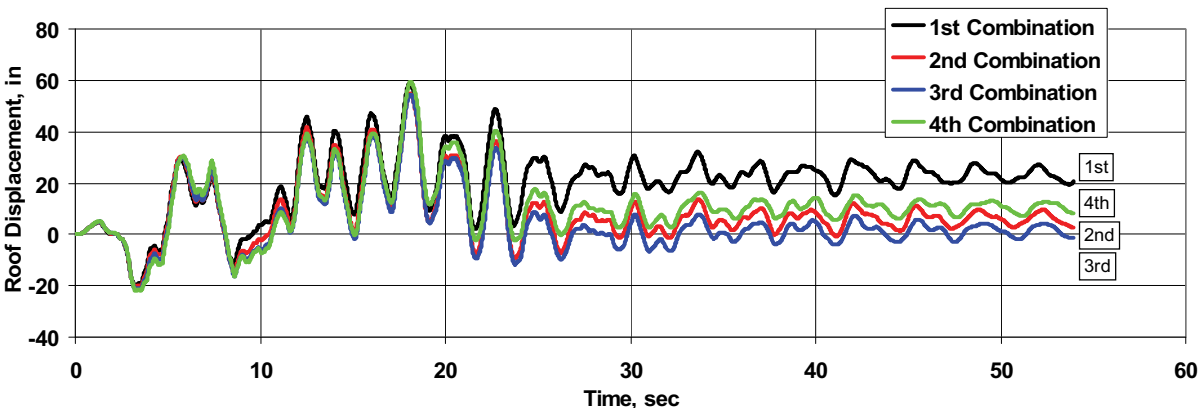


Figure 9. Roof Displacement Response History of Hybrid Frames subject to EQ09 with scale of 2.0 times the anchored design spectrum scale.

Although none of the frames collapse, the residual displacement is the most for the 1st combination which is actually a normal frame. However, this time the 3rd combination instead of the 4th combination Hybrid frame gives better results in terms of residual displacements (see Fig.9). If an IDA scale factor of 1.8 was used, then the 4th combination would give less residual displacement than the 3rd one. Due to the uncertainties of nonlinear dynamic analysis, this kind of result is possible.

According to the results of IDA analysis, Hybrid frames always give better results when the structures are subjected to severe earthquakes, and almost always, as the frame gets more hybrid, the results becomes better. This structural behavior can be explained with the effect of the relatively late occurrence of negative post yield stiffness in Hybrid frames.

The effect of early yielding of Hybrid frames in pushover curves was observed at low scaled gentle earthquakes. Figure 10 shows an example of this behavior when the frames are subjected to EQ00. As the frames become more hybrid, the maximum

displacements decrease which is a predicted result of early yielding which will provide some hysteretic damping to the structure. Similar results were obtained from EQ01 which is also a gentle earthquake.

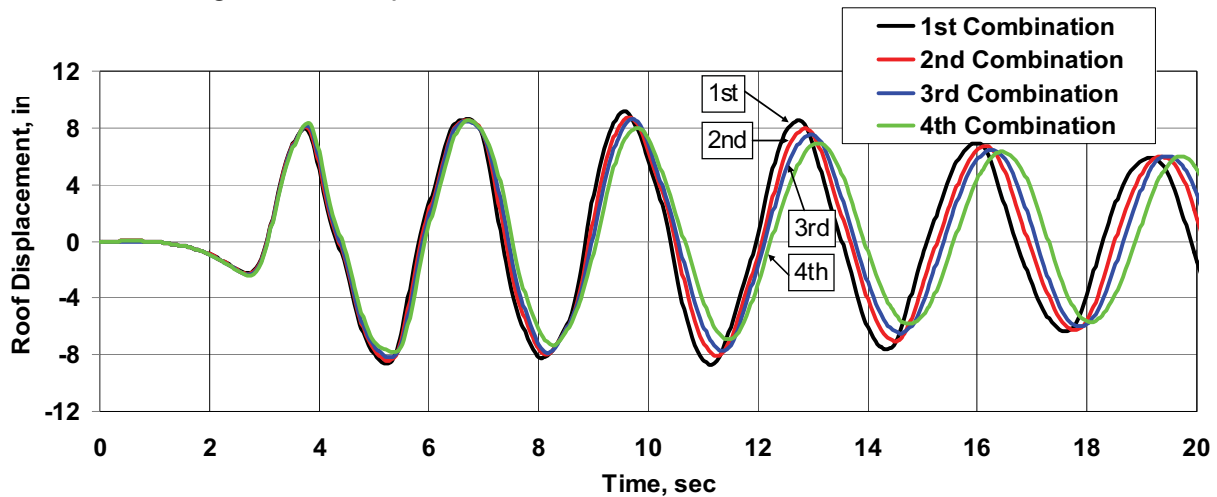


Figure 10. Roof Displacement Response History of Hybrid Frames subject to EQ00 with scale of 0.4 times the anchored design spectrum scale.

SUMMARY and CONCLUSIONS

While the work reported in this paper is preliminary, it appears that there are significant benefits associated with the concept of Hybrid frames. By carefully controlling the sequence of yielding, there is a clear indication of improvement in response at all levels of ground shaking, particularly at higher levels where dynamic instability may be more prevalent. At lower levels of shaking, the improvement is less significant, although there is a trend towards reduced displacements and base shears. This behavior is associated with the energy dissipation provided by early yielding of the low-strength plastic hinges.

For the frames studied, there is a significant increase in ductility demand, compared to traditional special moment frames, for those elements and connections that are expected to yield early. Although it is expected that traditional special moment frame detailing will suffice for these locations, additional research needs to be done to determine how much ductility can actually be provided by such connections. It may be necessary to develop special connection details for these areas. The use of special low-strength steels should also be investigated.

Additionally, the Hybrid frames described herein were designed on an ad-hoc basis, as no specific rules have been established for assigning the sequence of yielding. It is expected that improved performance can be obtained if the sequence of hinging is more formally optimized. The use of an energy based procedure is being explored for use in the development of an optimum hinging sequence.

Finally, additional work needs to be done to determine if significant economy is obtained by the Hybrid frames. Such economy would be expected even if the performance of the hybrid frames was equivalent to the normal frames. This advantage in economy is due to the reduction in the number of special moment connections in the structure.

REFERENCES

AISC (2005a). *Seismic Provisions for Structural Steel Buildings, ANSI/AISC 341-05*, American Institute of Steel Construction, Chicago, IL.

AISC (2005b). *Prequalified Connections for Special and Intermediate Moment Frames for Seismic Applications, ANSI/AISC 358-05*, American Institute of Steel Construction, Chicago, IL.

ASCE (2006). *Minimum Design Loads for Buildings and Other Structures (ASCE 7-05)*, American Society of Civil Engineers, Reston, VA.

Charney, F.A., and Barngrover, B. (2006). Nonlin-Pro Base Program Description and User's Guide, Advanced Structural Concepts, Inc., Blacksburg, VA.

Charney, F. A., and Marshall, J. D. (2006). "A comparison of the Krawinkler and Scissors Models for Including Beam-Column Joint Deformations in the Analysis of Moment-Resisting Steel Frames." *Engineering Journal*, 43(1), 31-48.

CSI (2006). *Perform-3D User's Guide, Nonlinear Analysis and Performance Assessment of Structures*, Computers and Structures, Inc., Berkeley, CA.

FEMA (2000), FEMA-355C, *State of the art report on systems performance*, Federal Emergency Management Agency, Washington, D.C.

FEMA (2004). *NEHRP Recommended Provisions for Seismic Regulations for New Buildings and Other Structures (FEMA 450-1)*, Federal Emergency Management Agency, Washington, D.C.

Gupta, A., and Krawinkler, H. (2000), "Dynamic P-Delta Effects for Flexible Inelastic Steel Structures", *Journal of Structural Engineering*, 126(1): 145-154.

Prakash, V., Powell, G.H., and Campbell, S. (1993) Drain 2DX Base Program Description and User's Guide, University of California, Berkeley, CA.

Shome, N., Cornell, C. A., Bazzurro, P., and Carballo, J. E. (1998). "Earthquakes, records and Nonlinear Responses." *Earthquake Spectra*, 14(3), 469-500.

Somerville, P.G. (1996). Ground motion prediction for performance based seismic engineering, *Proceedings of the 65th Annual Convention, Structural Engineers' Association of California*, Maui, October 1-4, 1996, p. 67-86.

Vamvatsikos, D. (2002). *Seismic Performance, Capacity, and Reliability of Structures as Seen Through Incremental Dynamic Analysis*, Ph.D. Thesis, Stanford University.

BEHAVIOR OF HIGH-STRENGTH STEEL WELDED BEAM-TO-COLUMN JOINTS WITH BEAMS OF UNEQUAL HEIGHT

Sandra Jordão^a, L. Simões da Silva^b, Rui D. Simões^c

^{a,b,c}University of Coimbra, Coimbra, Portugal

^asjordao@dec.uc.pt, ^bluisss@dec.uc.pt, ^crads@dec.uc.pt

ABSTRACT

Joints have a significant role on the global behavior of a steel structure. Although the most current joint typologies are already covered by several design codes, there are others, such as internal joints with beams of unequal height, which are not yet normalized. The aim of this paper is to contribute to a methodology based on the “component method” of EC 3 for this new type of node with high-strength steel S690. Finite element models calibrated with experimental results were developed, as well as analytical models tailored for the new type of joint and high-strength steel. Some modifications of state-of-the-art formulations (design rules) are proposed.

1. INTRODUCTION

The structural behavior of joints is complex in nature, due to the variety of components, geometry and phenomenon involved (plasticity, contact, non linearity, instability, etc) (Simões da Silva e Gervásio, 2007). Nevertheless, due to the huge role that connections have in construction, both in terms of structural behavior and cost (50% of the cost of the structure (Evers and Maatje, 1999)), the effort in research on this theme has grown considerably over the last 30 years (Nethercot, 2007). The subjects have been diverse, but a considerable cut has been into the development of the procedures related to the component method. In that view, there are still some important issues that haven't been addressed so far. One of them is the behavior of internal joint with beams of different heights, and the other is the updating of the Eurocode rules for high strength steel. The present paper addresses these two subjects. The procedure includes the development of finite element models (Fig. 3) calibrated with experimental results (FEM-CER) (Fig. 4), which are used in the development of analytical models for the new type of joint and S690.



Fig. 1. Test S690E2 (M-/M-) Fig. 2. Test S690E4 (M-/M+) Fig. 3. FEM (E2, E4)

Thirteen full scale tests were performed (5 for S355 and 8 for S690). IPE400, HEB200 and HEB240 profiles were used for beams and column, respectively. Two types of joints were considered: i) internal node with beams of different heights (INBDH), with two different loading conditions corresponding to different shear levels in the web panel (Fig. 1 and Fig. 2); ii) external node and internal node symmetrical, to provide reference data for situations that are already in EC3 (Jordão, 2008).

2. ANALYTICAL MODEL

2.1 Analytical Jaspert Model

The rotational behavior of a welded joint can be expressed as the sum of the distortion of the web panel, associated with shear, and the load introduction rotation, associated with the forces directly transmitted through the beam flanges (Fig. 4). Atamaz and Jaspert (Atamaz and Jaspert, 1989) and Jaspert (Jaspert, 1991) defined models for each rotational component (Fig. 5 and Fig. 6) in terms of resistance and deformability, which became the basis of the component method.

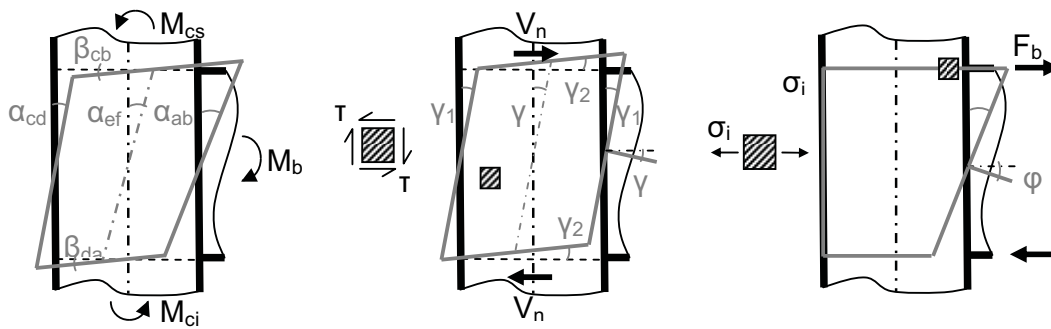


Fig. 4. Rotational behavior of a welded joint: Total, Shear and Load introduction.

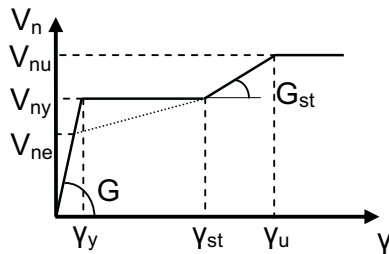


Fig. 5. Shear curve

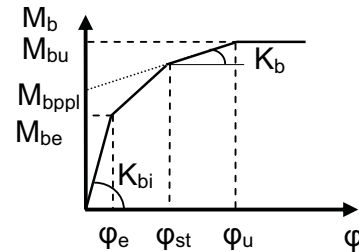


Fig. 6. Load introduction curve

The models consider the geometrical and material properties of the joint, and the von Mises yield criterion is used to account for the stress interactions. The models are valid up to failure except when instability is the failure mode. In this case the model does not mimic the negative slope end portion of the curve. The components of the stress state on the column web panel are: i) normal stresses, associated with the forces from the beams (σ_i) (localized effect); ii) shear stresses, associated with shear forces on the web panel (τ) (constant through out the web panel); and iii) normal vertical stresses, associated with column bending and axial force (σ_n), (constant through out the web panel). The relevant interactions are: τ with σ_n , and τ with σ_i .

2.2 Analytical Jaspert Modified Model

In order to deal with INBDH, the web panel is divided into two subpanels, corresponding to two areas with different shear values (Analytical-Jaspert Modified model - AJM) (Jordão, 2008) and (Jordão et al., 2007). The same assumptions already adopted in the Analytical-Jaspert model are used to account for the interaction between the internal forces on the column web panel. In the case of INBDH, the relevant combinations between σ_i , τ and σ_n lead to a higher number of possibilities that have to be accounted for. Fig. 7 and Fig. 8 show a schematic for E2.

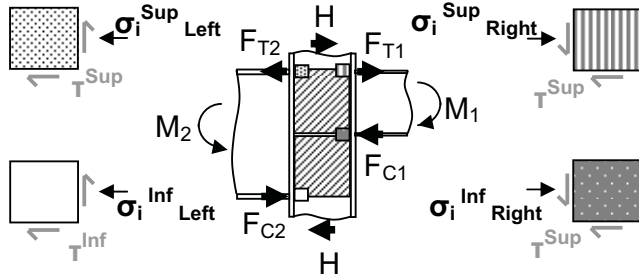


Fig. 7. $\sigma_i - \tau$ interaction

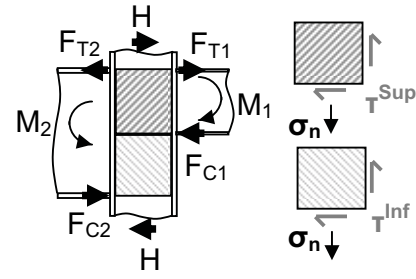


Fig. 8. $\sigma_n - \tau$ interaction

For each case, the load introduction (AJMLI) and shear (AJMShear) curves for AJM model are established. Homologous curves were obtained from FEM-CER (LI and Shear) (Fig. 9). AJMLI and AJMShear curves are added, yielding the AJM moment/rotation curve (AJMSum), for the right and left joints, upper and lower panels (Fig. 9).

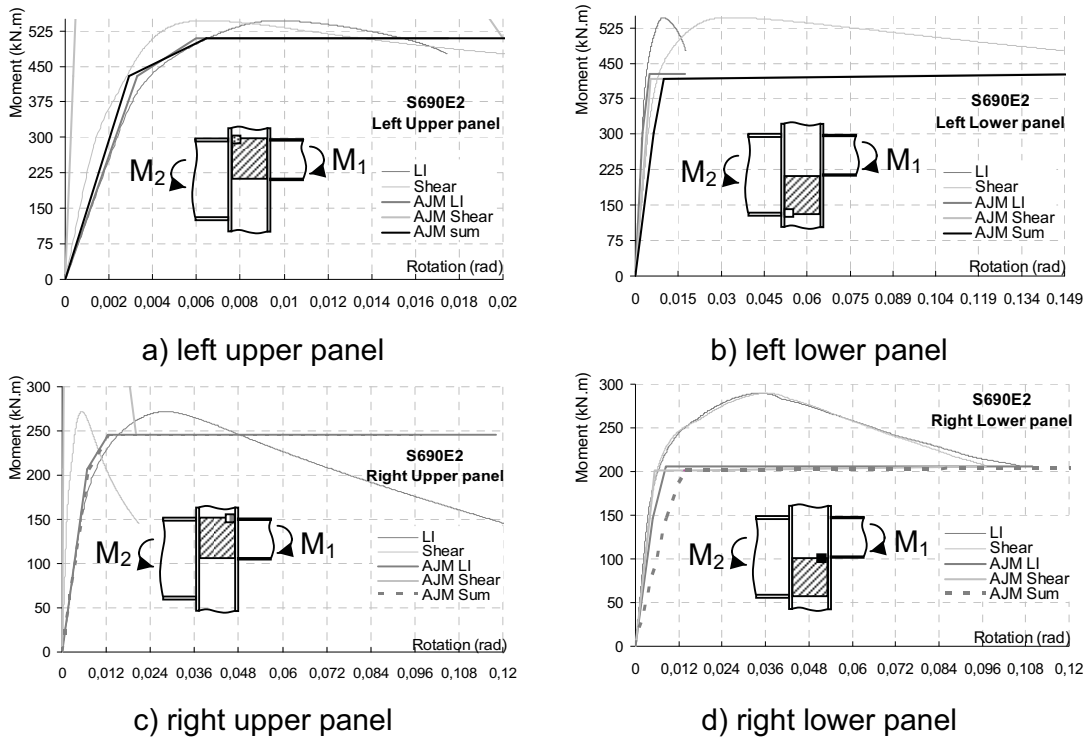


Fig. 9. M- θ curve (AJM) as the sum of LI and shear curves

Since it is sought to obtain a single curve for each side of the joint, a procedure must be established to concatenate the two curves obtained for each joint. For the left side it is assumed that the upper and the lower panels contribute equally to the global response, so the average is used (Fig. 10a)). For the right side the response of the joint is determined by the upper panel alone (Fig. 10b)). These figures illustrate the comparison of AJM vs FEM-CER. The good adjustment shows that the AJM model is suited for INBDH. A description of these topics may be found in (Jordão, 2008).

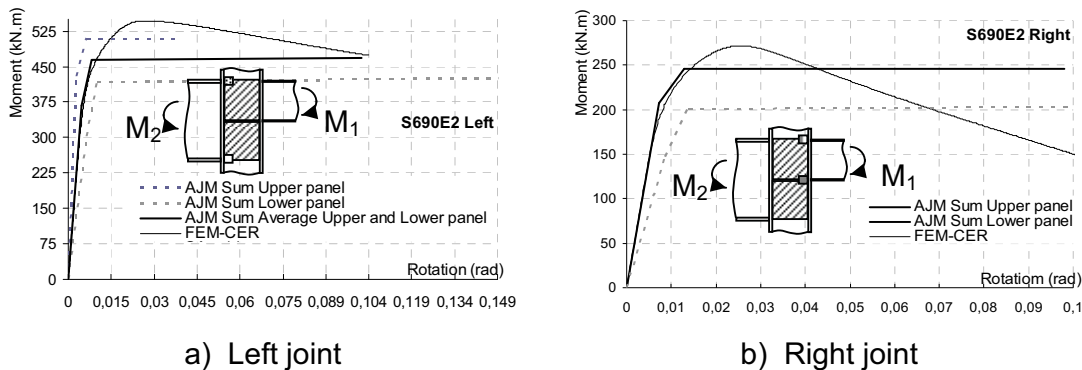


Fig. 10. M-θ curve (AJM): average of M-θ curve for upper and lower panels

An identical study was performed for S355 models (Jordão, 2008). The same level of adjustment was reached at elastic and post-yielding range, but better agreement was reached at maximum load. This raises the question whether AJ, AJM and EC3 models are adequate for S690. This issue is discussed in the following sub section.

3. APPLICATIONS OF THE ANALYTICAL MODEL

3.1 State-of-the-art analytical models: Extension for S690 steel grade

For joints with high strength steel, two different levels of evaluation can be established. Firstly, comparing the FEM-CER and the AJ model will show whether the AJ model still yields good results for high strength steel. Secondly, comparing equivalent joint typologies for S355 and S690 steels should highlight the qualitative differences that occur because of the use of different steel grades. This assessment is carried out using only the typologies that are currently covered by EC3 (E1: external and E3: internal symmetrical), in order to avoid the influence of coupled effects due to the new node configuration.

The results for S690 models are presented along with homologous results, from a similar study undertaken on S355 steel grade prototypes (Jordão, 2008). The reason for this parallel presentation is that the AJ model was established and calibrated for mild steel, and the comparative analysis will bring in information that may be used to interpret any maladjustment between FEM-CER and AJ models for S690 steel grade joints. A comparison is set between the FEM-CER and the AJ model and the FEM-CER and the EC3 model, for S355 and S690 steel grades, E1 (Fig. 11a) and Fig. 11b)) and E3 (Fig. 11c)) and Fig. 11d)) joints.

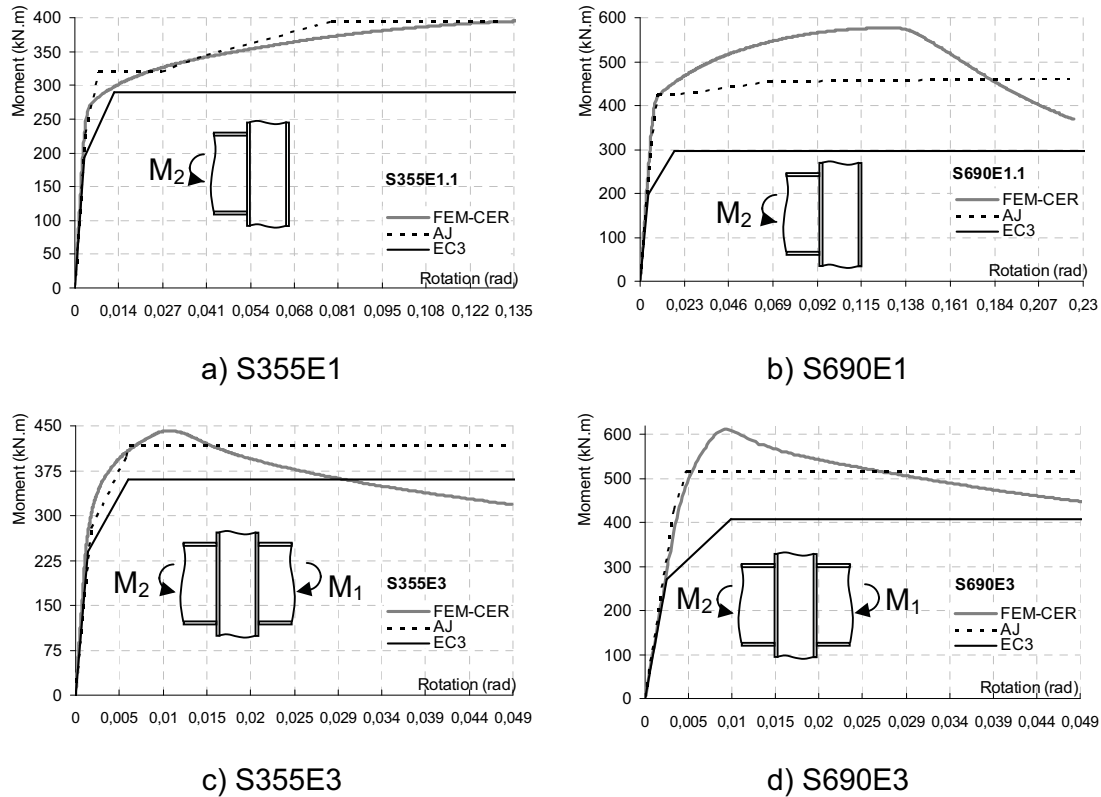


Fig. 11. FEM-CER vs AJ

In terms of AJ vs FEM-CER and EC3 vs FEM-CER, for both E1 and E3 S355 steel grade joints, the agreement is good for the whole curve. For steel grade S690 joints the agreement is similar, except for the maximum load, where a more conservative value is reached. The AJ model estimates the maximum load of the joint and the corresponding failure mode. For test E1 (external node), the difference between the maximum load and the predicted load, is $\Delta=21\%$ ($\Delta=0.1\%$), corresponding to shear failure. The values in brackets correspond to the S355 tests, for comparison. For test E3 (internal node with symmetrical loading), this difference is $\Delta=17\%$ ($\Delta=7.5\%$) and is governed by instability. The EC3 model predicts the plastic resistance of the joint. A similar comparison reveals $\Delta=29\%$ ($\Delta=0.1\%$) and $\Delta=20\%$ ($\Delta=3\%$) for tests E1 and E3, respectively. In order to assess the reason for this poor agreement in terms of maximum loads, for the S690 steel grade models, both instability and shear formulations are analyzed. Eq. 1 describes the shear area (EC3) for welded sections

$$A_{vc} = \eta h_{wc} t_{wc} = \eta A_{wc} \quad (1)$$

where h_{wc} is the height and t_{wc} is the thickness of the column web, respectively, and η is equal to 1.2 for steel grades S460 and below, and is given by 1.0 for higher steel grades (EC3, 2004). The calculations using the AJ model show that the value 1.0 leads to very poor agreement, so a new formula is proposed, that accounts for the actual shear area, and for the throat thickness of the weld explicitly (Eq. (2)).

$$A_{vc} = (h_{wc} - 2t_{fc}) t_{wc} + 4.a_c^2 + (2.a_c \sqrt{2} + t_{wc}) t_{fc} / 2 \quad (2)$$

t_{fc} is the thickness of the column flanges and a_c is the weld throat. Solving Eq. (1) with respect to η shows that this parameter is the ratio between A_{vc} and A_{wc} , so a parametric study on the influence of a_c on the η and on the shear area was performed (Table 2, Fig. 12 and Fig. 13).

a_c	$0.5.t_{wc}$ (lower bound)	$0.7.t_{wc}$ (used in prototypes)	t_{wc} (upper bound)
η	1.22	1.27	1.35

Table 1. Parameter η as function of a_c

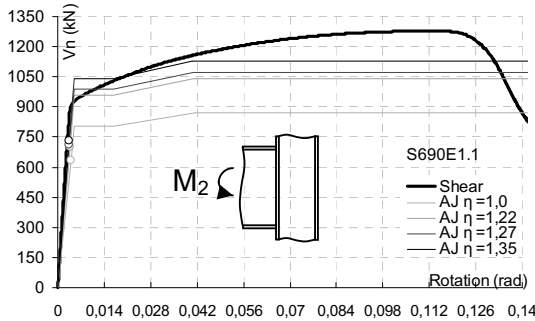


Fig. 12. η effect on shear rotation curve

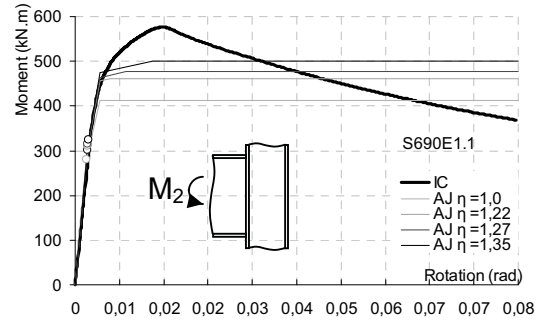


Fig. 13. η effect on LI rotation curve

Figs. 12 and 13 indicate that η influences the complete load-rotation curves, except for the elastic part of the LI curve. It also shows that the best adjustment is for values of η in the range 1.22 to 1.35. Thus, for S690 steel grade welded sections, (Eq. (2)) should be adopted for the evaluation of the shear area.

The failure mode for tests E3 is instability of the column web in compression. Comparison between the FEM-CER and AJ results have shown larger differences for S690 when compared to S355. This may results from the estimate of the elastic critical load of the compressed web, taken by Jaspart (Jaspart, 1991) as:

$$P_{vc} = (h_{wc} - 2t_{fc})t_{wc}k \frac{\pi^2 E}{12(1-\nu^2)} \left(\frac{t_{wc}}{h_{wc} - 2t_{fc}} \right)^2 \quad (3)$$

that underestimates the theoretical solution by 27.3% for simply-supported conditions. Additional differences may also results from the definition of the “buckling length”, taken as $h_{wc} - 2 t_{fc}$, which neglects the influence of the size of the weld for welded profiles or the root radius for rolled sections. The application of the EC3 model to S690 is much more conservative, when compared to S355. This is linked to the plate buckling curves adopted in Part 1.8 of EC3 that penalize high strength steels excessively. To illustrate this clearly, a S355 vs S690 results comparison must be set. Since S355 profiles are rolled and S690 profiles are welded, it is first necessary to calculate equivalent rolled sections for S690 joints (Jordão, 2008). The S690/S355 gain in nominal yield strength is 48.6%. Using the equivalent S690 “rolled” sections, the S690/S355 gain in the shear and the tension components is 42%, and in the compression component is 30%. This is due to the fact that λ_p (plate slenderness) (Eq. (4)) is highly penalized when $f_{y,wc}$ increases, leading to a considerable reduction in ρ (compression resistance reduction factor to account for plate buckling of the column web panel) (for example, $\lambda_p=0.89$ and $\rho=0.85$ for S355,

and $\lambda_p=1.14$ and $\rho = 0.71$ for S355), that reduces the advantage of $f_{y,wc}$ on the resistance (Eq. (5)). The authors propose that new plate buckling curves should be derived for S690. Further investigation is due to clear this matter.

$$\bar{\lambda}_p = 0.932 \sqrt{\frac{b_{eff,c,wc} \cdot d_{wc} \cdot f_{y,wc}}{E \cdot t_{wc}^2}} \quad (4)$$

$$F_{c,wc,Rd} \leq \omega \cdot \rho \cdot b_{eff,c,wc} \cdot t_{wc} \cdot f_{y,wc} \quad (5)$$

3.2 β -parameters: Extension for internal nodes with beams of different heights

Part 1-8 of EC3 (EC3, 2005), presents formulation for β parameters for internal nodes symmetrical. For INBDH the code indicates that: “the actual distribution of shear stresses in the column web panel should be taken into account”. In order to do so, the forces entering the web panel have to be considered in terms of magnitude and position. Fig. 14a) and Fig. 14b) show the load schematics for the two types of node. From those it is possible to withdraw formulation for β parameters for INBDH. Table 3 shows a comparison between the β formulation for EC3, and INBDH nodes.

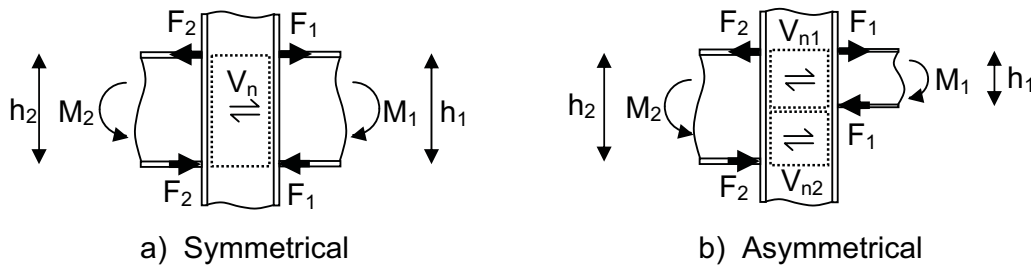


Fig 14. Load in the web panel in symmetrical and asymmetrical internal nodes

EC3 node configurations	$V_n = \beta_1 F_1$	$\beta_1 \frac{M_1}{z} = \frac{M_1}{z} - \frac{M_2}{z}$	$\beta_1 = \left 1 - \frac{M_2}{M_1} \right $	$\beta_2 = \left 1 - \frac{M_1}{M_2} \right $
INBDH	$V_n = \beta_2 F_2$	$\beta_1 \frac{M_1}{z_1} = \frac{M_1}{z_1} - \frac{M_2}{z_2}$	$\beta_1 = \left 1 - \frac{M_2 z_1}{M_1 z_2} \right $	$\beta_2 = \left 1 - \frac{M_1 z_2}{M_2 z_1} \right $

Table 2. Parameter β : formulation for EC3 node configurations and INBDH

The β values calculated with INBDH formulation, concern only the upper panel. In the lower panel, the forces from the right beam cancel each other out, so the lower panel may be considered equivalent to an external node ($\beta=1$). To assess the quality of INBDH β formulation, a comparison was set between the initial stiffness of AJM and of EC3 model (β calculated with NBDH formulation). For all the joints studied, the referred comparison, established for the lower panel with $\beta = 1$, yields a fair agreement (ex. in Fig. 15a) for S690E4), which confirms that the lower panel may be considered similar to an external node. In the case of E2 models, the forces entering the panel are similar on both sides, meaning that the shear value is null, so β should be also null. When considering this value, the agreement between the initial stiffness of the two models is reasonable (example in Fig. 15b) for S690E2).

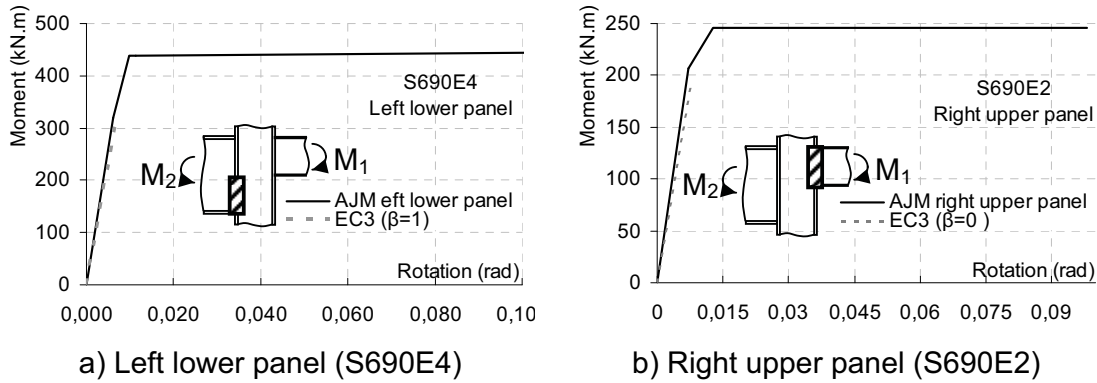


Fig. 15. Comparison between the initial stiffness of AJM and EC3 model

In the case of E4 joints, the shear value, in both the upper and lower panels is high, so these are the best cases to completely test the INBDH β formulation. Fig. 16a) shows an example for the left upper panel, where a reasonable adjustment is achieved. In the case of the right upper panel (Fig. 16b)), the value yielded from the new formulation leads to an initial stiffness that lies far from the one of AJM. This is due to the fact that the difference between the moments on both beams is considerable, which leads to non significant values for the right joint. The EC3 formulation prevents this situation by limiting the β value to 2.

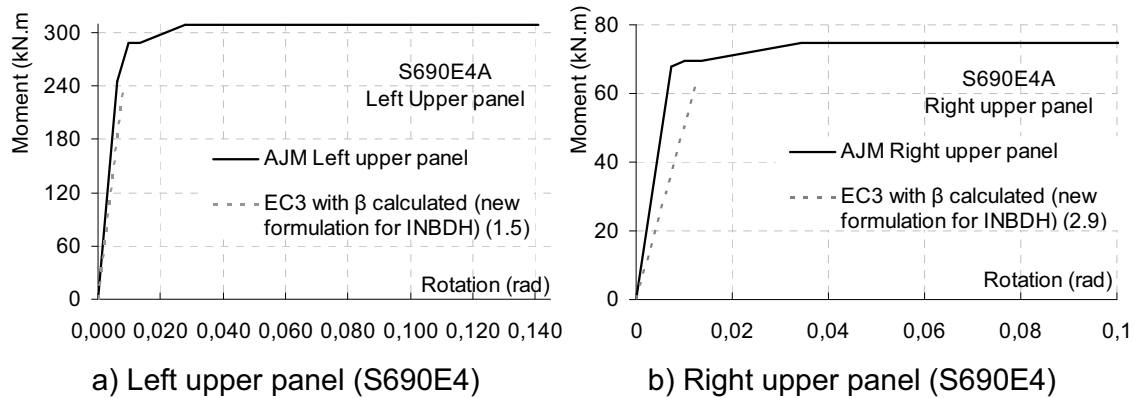


Fig 16. Comparison between the initial stiffness of AJM and EC3 model

Table 4 shows the results of the comparison between the initial stiffness of AJM and EC3 curve (β evaluated by INBDH formulation). The letters *c* and *a* stand for calculated, (β calculated by INBDH formulation) and adjusted (value that β parameter should read so that the initial stiffness of AJM and EC3 curves would be the same). If *a* and *c* are alike it means that INBDH formulation yields good results.

	S690E2A		S690E2B		S690E4A		S690E4B	
	c	a	c	a	c	a	c	a
Left ^{Upper}	0	0	0	0	1.5	1.25	1.5	1.2
Left ^{Lower}	1	1	1	1	1	1	1	1
Right ^{Upper}	0	0	0	0	2.9	1.6	2.9	1.4

Table 3. Parameter β (INBDH formulation): calculated and adjusted values

The adjustment is reasonable for all the cases, except for the right upper panel, due to the high difference between the moments on the joints, as explained above. The implementation of the β formulation (INBDH) yields two different values for the joint in the left (upper and lower panel). Since it is sought to obtain a single value for β for each joint, a procedure must be established to concatenate the two β values obtained for the joint in the left. The approach used consists in determining the value of β that would make the initial stiffness of EC3 curve be similar to that of the AJM or FEM-CER, and relate that value to those obtained for left joint/upper panel and left joint/lower panel. The referred procedure is illustrated in Fig. 17 for S690E4A, and Table 5 summarizes the homologous results for the other studied models.

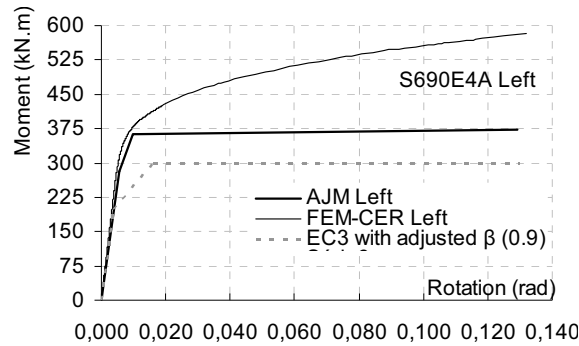


Fig. 17. β parameter for the left joint by adjusting the initial stiffness of EC3 curve to that of AJM

	S690E2		S690E4	
	c	a	c	a
Left ^{Upper}	0	0	1.5	1.2
Left ^{Lower}	1	1	1	1
Average	0.5	0.5	1.3	1.1
Left ^{Joint} (adjusted)	0.57		0.95	
Drift from average (%)	12	12	27	14

Table 4. β parameters for the left joint: upper and lower panels and the whole joint

For the configurations E2 (M-/M-), the β value obtained for the whole joint on the left, has a difference of 12% to the average of the β values obtained for the upper and lower panels, for both calculated and adjusted values.

For the configurations E4 (M+/M-), the β value obtained for the whole joint on the left, has a difference of 14% or 27% to the average of the β values obtained for the upper and lower panels, for calculated and adjusted values, respectively.

The β value obtained for the whole joint on the left seems to have a steady relation to the average of the β values, obtained for the upper and lower panels, except for the calculated values in E4 model. It is not yet possible to establish a relation between the parameters for the whole joint and those of the sub-panels. Further investigation is due.

4. CONCLUSIONS

Based on experimental and numerical evidence resulting from a series of tests on welded joints (external nodes, internal nodes with beams of similar height and internal nodes with beams of different height) in steels grades S690 and S355, it was possible to propose a model to predict the behavior of the column web panel with beams of different height. This model is an extension of the Analytical-Jaspart model that led to the EC3 rules for the evaluation of the behavior of the column web panel.

It is worth highlighting that the modified model (AJM) yields good results for S355 steels, reflecting the quality of the Analytical -Jaspart model for these steel grades.

Secondly, the adjustment for S690 steels is not so good. It is clear that some adjustments are necessary in terms of the shear resistance of the web panel and the evaluation of the stability of the compressed web. The implementation of final design rules to improve these aspects requires further work, notably a thorough parametric study to widen the limits of application.

An extension to the EC3 β parameters formulation is proposed for the case of internal nodes with beams of different heights. The application of the Analytical-Jaspart modified model allowed testing the quality of the referred extension. Some importance conclusions have been drawn concerning this topic, but clearly, further work is needed.

The problems presented are currently actively being looked into by the authors, and further developments and conclusions are expected.

REFERENCES

Simões da Silva, L., Gervásio, H. - Manual de dimensionamento de estruturas metálicas : Métodos avançados. Ed.: CMM, 2007.

Evers, H., Maatje, F.: Cost based engineering and production of steel constructions. II Encontro Nac. Construção Metálica Mista, pp.: 323-330. Coimbra, Portugal, 1999.

Nethercot, D. A.: Semi-rigid and partial strength joint action: Then, now, when? 3RD Int. Conf. on Steel and Composite Structures, pp.: 3-9 Manchester, UK, 2007,

Jordão, S.: Behaviour of internal welded joints with beams of different heights, steel grade S690, Phd Thesis, Univ. of Coimbra, Portugal, 2008 (in Portuguese).

Jordão, S., Simões da Silva, L. and Simões, R.: Experimental behaviour of internal joints with beams of different heights, steel grade S690, pp.: 91-105 ICSAS07 6th Int. Conference on Steel & Aluminium Structures, Oxford, UK, 2007.

Atamaz, W. et Jaspart, J.-P.: Étude du comportement jusqu'à la ruine des nœuds complètement soudés. IREM 89/7 : *Lausanne IREM*; *MSM N 194* : Liège, 1989.

Jaspart, J.-P.: Etude de la semi-rigidité des nœuds poutre-colonne et son influence sur la résistance et la stabilité des ossatures en acier. Phd.Thesis Univ. Liège, 1991.

European Committee for Standardization (CEN). EN 1993-1-8: Eurocode 3: Design of steel structures – Part 1-8: Design of joints, May 2005.

EXPERIMENTAL PROGRAM FOR EVALUATION OF MOMENT BEAM-TO-COLUMN JOINTS OF HIGH STRENGTH STEEL COMPONENTS

Dan Dubina

"Politehnica" University of Timisoara, Timisoara, Romania
Romanian Academy, Centre for Advanced and Technical Sciences, Timisoara
dan.dubina@ct.upt.ro

Aurel Stratan

"Politehnica" University of Timisoara, Timisoara, Romania
aurel.stratan@ct.upt.ro

Nicolae Muntean

"Politehnica" University of Timisoara, Timisoara, Romania
nicu.muntean@ct.upt.ro

Florea Dinu

"Politehnica" University of Timisoara, Timisoara, Romania
Romanian Academy, Centre for Advanced and Technical Sciences, Timisoara
florea.dinu@ct.upt.ro

ABSTRACT

Seismic resistant building frames designed as dissipative structures must allow for plastic deformations in specific members, whose behavior has to be predicted by proper design. In dual frames (i.e. moment-resisting frames in combination with concentrically braced frames or eccentrically braced frames) members designed to remain predominantly elastic during earthquakes, such as columns for instance, are characterized by high strength demands. Dual steel structural systems, optimized according to a Performance Based Design Philosophy, in which high strength steel is used in "elastic" members and connection components, while mild carbon steel in dissipative members, can be very reliable and cost effective. Based on this idea, a targeted testing program on the purpose to evaluate the performance of moment resisting joints of high strength steel and mild carbon steel components, under monotonic and cyclic loading was carried out. The results of this program are summarized in the present paper.

INTRODUCTION

Previous studies realized by authors (Dubina and Dinu, 2007, Dubina et al., in print) showed the advantages of using High Strength Steel (HSS) in combination with Mild Carbon Steel (MCS) in so called dual-steel structures, to enhance robustness and better control of the response of seismic resistant building frames.

To get a rational design of a seismic resistant structure – i.e. both safe and economic – the dissipative elements have to approach the plastic capacity under design forces, in order to reduce the demand on non-dissipative members. The best way to accomplish this is not by changing size of sections in dissipative and non-dissipative members because it also changes their stiffness, but to realize them of MCS and HSS, correspondingly (see also, in present volume, Dubina et al., 2008). This principle applies both for members and connection components.

In order to check the validity of the principle, a large experimental research program was carried out at the "Politehnica" University of Timisoara, CEMSIG Research Centre (<http://cemsig.ct.upt.ro>) in order to study the performance dual-steel configuration for beam-to-column joints under monotonic and cyclic loading. Present paper summarizes the part of this program referring to joint specimens, while test results on weld details and T-stub specimens of dual steel are presented in a companion paper (Dubina et al, 2008).

SEISMIC PERFORMANCE OF DUAL-STEEL BUILDING FRAMES

Both eccentrically braced frames (EBF) and concentrically braced frames (CBF) dual-frames have been analyzed. The EBF building has eight storeys and CBFs buildings have sixteen storeys. They are made from European H-shaped profiles. The buildings have three bays of 6 m with equal storey heights of 3.5 m, except the first storey which is of 4.5 m height. Each building structure uses different combinations of mild carbon steel S235 and high strength steel S460 (see Figure 1):

- EBF structure uses mild carbon steel S235 for all members, except the central columns of the first two storeys which are HSS S460. The structure was design for a behavior factor $q = 6$.
- CBF structure uses mild carbon steel S235 for all members, except the interior columns of the first four storeys and intermediate beams, which are HSS S460. The structure was design for a behavior $q = 4.8$.
- BRB structure uses mild carbon steel S235 for all members, except the interior columns of the first four storeys, which are HSS S460. The structure was design for a behavior factor $q = 6$.

The design was carried out according to EN 1993-1, EN 1998-1 and P100-1/2006 (Romanian seismic design code, aligned to EN 1998-1). A 4.0 kN/m^2 dead load on the typical floor and 3.5 kN/m^2 for the roof were considered, while the live load amounted 2.0 kN/m^2 . The buildings are located in Bucharest, characterized by the following seismic parameters: design peak ground acceleration - $0.24g$; soft soil conditions, with control period of the ground motion $T_C = 1.6$ sec and interstorey drift limitation of 0.008 of the storey height. The first period of vibration amounted to 1.05 seconds for EBF structure, and 1.94 seconds for CBF and BRB. In order to isolate inelastic deformations to removable dissipative members only (links or braces), they may be realized using low yield strength steel. Recent research (Dubina et al., 2007) suggested that a similar effect can be obtained by using mild carbon steel in dissipative members and high strength steel in non-dissipative members. In assessing the potential benefits of using HSS in dual frame configurations considered in the study, steel grade was increased from S235 to S460 both in the columns and beams of exterior moment frame bays. These new structures are

denoted by the prefix S46. Figure 1. shows the eccentrically and centrally braced frame configurations.

In order to assess the structural performance, nonlinear dynamic analyses were performed. A set of seven ground motions were used in the analysis (Figure 2). Three performance levels were considered: serviceability limit state (SLS), ultimate limit state (ULS) and collapse prevention (CPLS) limit state. Intensity of earthquake action at the ULS is equal to the design one (intensity factor $\lambda = 1.0$). Ground motion intensity at the SLS is reduced to $\lambda = 0.5$ (similar to $v = 0.5$ in EN 1998-1), while for the CPLS limit state was increased to $\lambda = 1.5$ (FEMA 356, 2000).

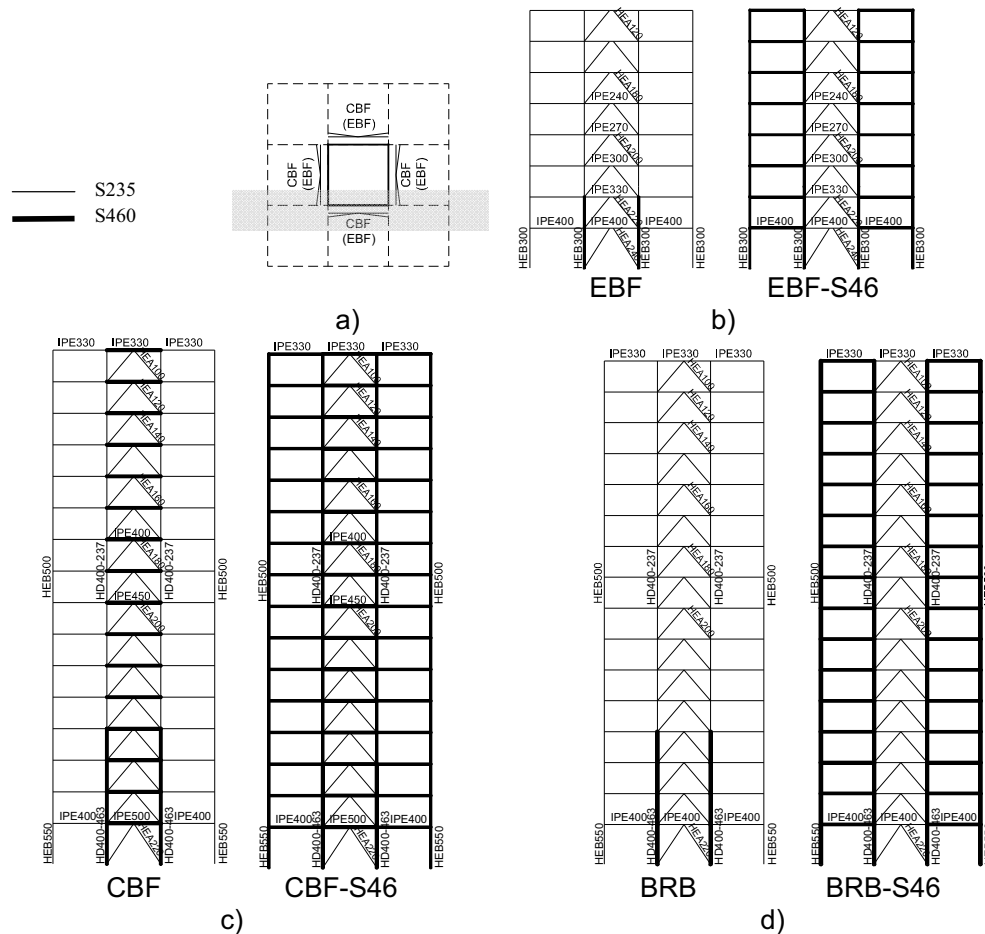


Figure 1. Frame configurations: (a) plan view; (b) elevation of EBF and EBF-S46 structures; (c) elevation of CBF and CBF-S46 structures; (d) elevation of BRB and BRB-S46 structures

The results of numerical simulations are summarized in Table 1. When referring to plastic rotation demands in beams, it has to be considered that the values refer in fact to the beam-column joints as well, if no specific constructional detailing are applied (e.g. dog-bone, beam haunch, etc). It is important to observe the contribution of HSS members in reducing the ductility demand, both for members and joints. However, for beam-to-column joints, at CPLS, this demand still remains significant, particularly for CBF. This fact justifies the interest for experimental study of dual-steel beam-to-column joints (e.g. of both HSS and MCS components).

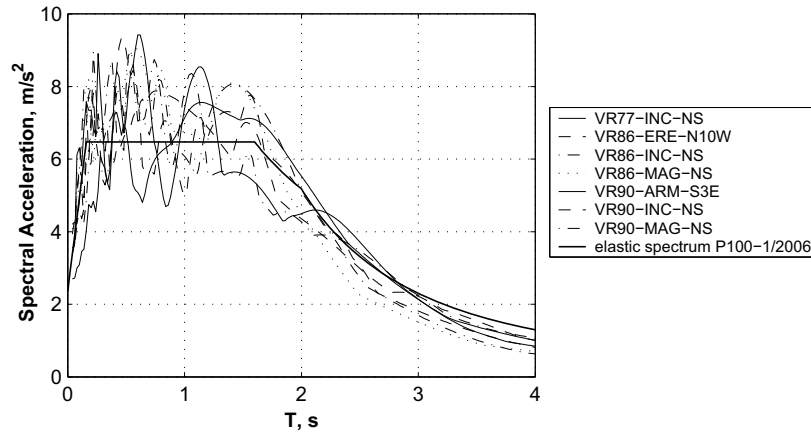


Figure 2. Elastic acceleration response spectra of the semi artificial accelerograms and design spectra (P100-1/2006, $a_g=0.24g$, $TC=1.6s$)

Table 1. Plastic rotation demands (in rad) at ULS and CPLS for the eccentrically and concentrically braced frames, average and maximum of all records

		EBF	EBF-R46	CBF	CBF-S46	BRB	BRB-S46
		Beams or joints					
ULS	Average	0.014	0.004	0.014	0.003	0.010	0.002
	Maxim	0.016	0.007	0.043	0.016	0.012	0.008
CPLS	Average	0.022	0.014	0.016	0.015	0.012	0.004
	Maxim	0.034	0.021	0.051	0.027	0.020	0.014
		Columns					
ULS	Average	0.007	0.002	0.005	-	0.001	-
	Maxim	0.009	0.004	0.026	0.0001	0.004	-
CPLS	Average	0.0014	0.008	0.007	0.001	0.0011	0.001
	Maxim	0.024	0.017	0.050	0.0022	0.006	0.005

DESCRIPTION OF TESTING PROGRAM

Two typologies of beam to column joints were tested: welded and bolted extended end-plate. In both cases stiffeners were used to strengthen the connection zone, alleviating stresses in the critical area of beam to column and beam to end-plate zone (see Figure 3). Beams were realized from mild carbon steel (S235), while columns from both MCS and HSS (S355 and S460). End-plates were realized from three steel grades (S235, S460 and S690) with end-plate thickness computed so as to correspond to mode 2 failure. MAG welding was used, with G3Si1 (EN 440) electrodes for welds between MCS components, and ER 100S-G/AWS A5.28 (LNM Moniva) for welds between MCS and HSS components. An overview of tested specimens is presented in Table 2. Both monotonic and cyclic loading was applied.

EN 1998-1 requires for dissipative moment resistant frames a minimum plastic rotation of beam-to-column joints of 0.035 rad, the contribution of column web being limited to 30%. The reason of this limitation is to prevent premature fracture due to

low cycle fatigue in the heat affected zones (HAZ) in the welded connections (e.g. beam-to column, beam-to-end-plate). However, test results currently proved larger contribution of column web (Dubina et al., 2005) and there are authors who recommended extending this contribution to 50% of total inelastic rotation (Lu L.W. et al., 2000). When HSS columns are used, it can be expected to have a larger elastic component of total rotation capacity of the joint. Also, in case of HSS end-plates, one expects to have a larger capacity to follow in elastic range the distortion of column web in shear and, consequently, a larger margin of safety in regard with low fatigue fracture in HAZ. Having in mind these facts (see also Girao and Bijlaard, 2007), the joint specimens were designed with strong beams (even the SCWB principle was altered) so that the weakest components would be column web and end-plate.

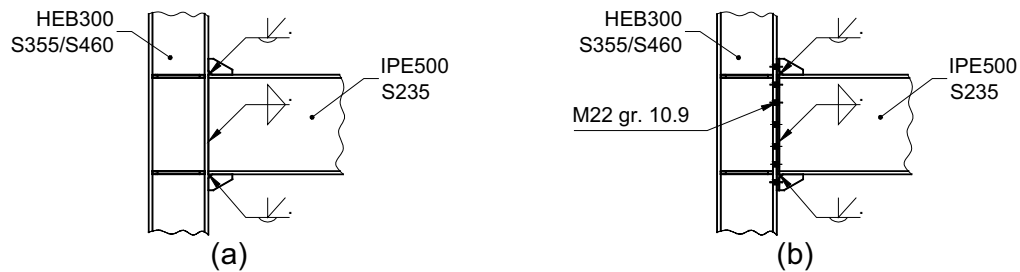


Figure 3. Main characteristics of welded joints (a) and bolted joints (b)

Table 2. Nominal characteristics of joint specimens

Joint type	Label	Column	Beam	End plate
Welded	C355WC	HEB300 (S355)	IPE500 (S235)	-
	C460WC	HEB300 (S460)	IPE500 (S235)	-
Bolted	C355EP12	HEB300 (S355)	IPE500 (S235)	t = 12 mm (S690)
	C460EP12	HEB300 (S460)	IPE500 (S235)	t = 12 mm (S690)
	C355EP16	HEB300 (S355)	IPE500 (S235)	t = 16 mm (S460)
	C460EP16	HEB300 (S460)	IPE500 (S235)	t = 16 mm (S460)
	C355EP20	HEB300 (S355)	IPE500 (S235)	t = 20 mm (S235)
	C460EP20	HEB300 (S460)	IPE500 (S235)	t = 20 mm (S235)

TEST RESULTS

Materials were supplied by ARCELOR-MITTAL and UnionOcel, Czech Republic. Table 4 and 5 show the measured average values of yield stress f_y , tensile strength f_u and elongation at rupture A . Bolts were tested in tension as well, showing an average ultimate strength of 1182.8 N/mm². It can be observed that there is an important difference between nominal and measured material characteristics. On the other hand, an unexpected ductility of S460 is remarked. With these values, the joint properties have been calculated according to EN 1993-1.8 and are presented comparatively with the designed ones in Table 5. Due to the fact in EN 1993-1.8 there are no specific provisions for the T-stub component corresponding to the outer part of the end plate (1st bolt row), which was stiffened according to the provisions of AISC (AISC, 2005), a similar procedure as the one for 2nd bolt row was applied. In

fact, the outer "stiffener" was assimilated with beam web. This procedure was confirmed experimentally in the companion paper (Dubina et al., 2008).

Table 3. Material properties – flat steel (end-plates, stiffeners) – UnionOcel

Nominal steel grade	f_y , N/mm ²	f_u , N/mm ²	A, %	Actual steel grade
S235	266	414	38	S235
S460	458	545	25	S460
S690	831	859	13	S690

Table 4. Material properties – sections, ARCELOR-MITTAL

Nominal steel (ordered)	Element	Supplier specifications			Tests			Actual steel grade (supplied)
		f_y , N/mm ²	f_u , N/mm ²	A, %	f_y , N/mm ²	f_u , N/mm ²	A, %	
S235 JR + M (EN 10025-2/2004)	Flange	342	434	31.46	375	470	38	S355
	Web	-	-	-	418	525	25	
S355 JO + M (EN 10025-2/2004)	Flange	453	540	24.86	448	560	32	S460M or ML
	Web	-	-	-	465	603	29	
S460 M (EN 10204/2004/3.1)	Flange	478	598	23.97	464	550	33	S460M or ML
	Web	-	-	-	451	600	30	

Table 5. Properties of joints: nominal / actual material characteristics

Specimen	Joint properties		Weakest component			
	$M_{j,Rd}$ [kNm]	$S_{j,ini}$ [kNm/rad]	Bolt row 1 [kN]	Bolt row 2 [kN]	Bolt row 3 [kN]	Bolt row 4 [kN]
C355W	455.8 / 584.1	183184 / 183184	CWPS 941.7 / CWPS 1206.9			
C460W	545.6 / 584.1	183184 / 183184	BFWC 1127.3 / CWPS 1206.9			
C355EP12	447.7 / 563.3	92768 / 92768	EPB 430.5 / EPB 512.8	EPB 430.5 / EPB 512.8	CWPS 80.7 / CWPS 181.2	--- / ---
C460EP12	532.5 / 563.3	92768 / 92768	EPB 430.5 / EPB 512.8	EPB 430.5 / EPB 512.8	EPB 257.1 / CWPS 181.2	BFWC 93.9 / ---
C355EP16	456.4 / 562.2	106830 / 106830	EPB 462.6 / EPB 508.7	EPB 462.6 / EPB 508.7	CWPS 16.6 / CWPS 189.4	--- / ---
C460EP16	549.4 / 562.2	106830 / 106830	EPB 462.6 / EPB 508.7	EPB 462.6 / EPB 508.7	EPB 267.3 / CWPS 189.4	CWPS 19.8 / ---
C355EP20	445.2 / 557.1	112209 / 112209	EPB 421.2 / EPB 489.8	EPB 421.2 / EPB 489.8	CWPS 99.4 / CWPS 227.2	--- / ---
C460EP20	525.0 / 557.1	112209 / 112209	EPB 421.2 / EPB 489.8	EPB 421.2 / EPB 489.8	EPB 229.3 / CWPS 227.2	CWPS 140.6 / ---
Beam plastic resistance $M_{pl,b} = 515.6 / 822.8$ kNm S355 column plastic resistance $M_{pl,c} = 663.5 / 852.3$ kNm S460 column plastic resistance $M_{pl,c} = 859.7 / 852.3$ kNm			$M_{j,Rd}$ - Moment resistance; $S_{j,ini}$ - Initial stiffness; EPB - end plate in bending; CWPS - column web panel in shear; Beam flange and web in compression - BFWC			

Table 6. Behavior of tested joints

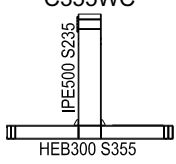
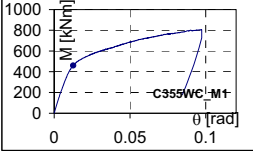
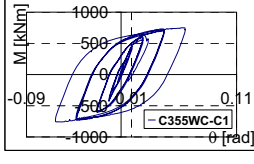
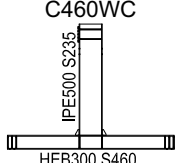
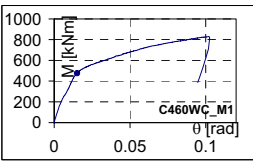
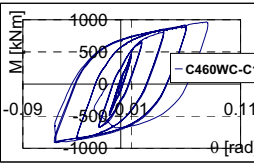
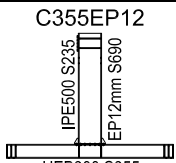
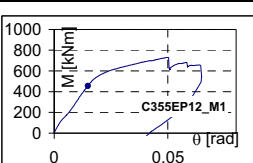
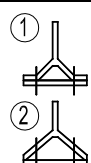
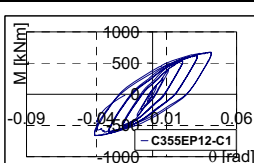
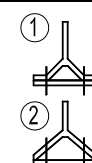
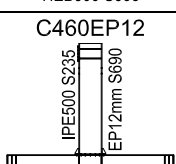
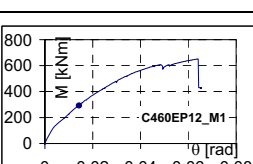
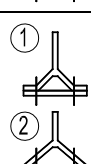
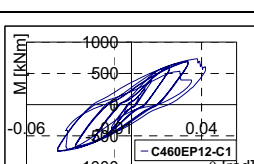
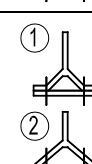
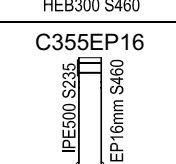
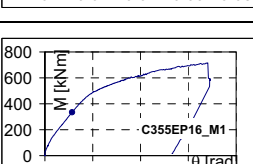
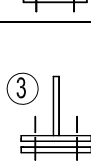
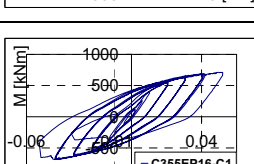
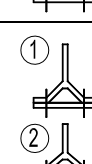
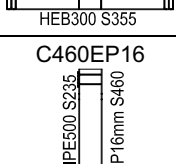
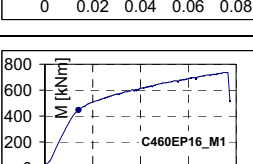
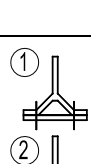
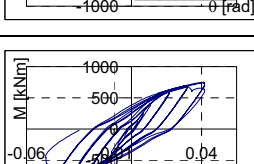
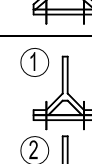
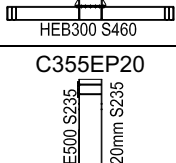
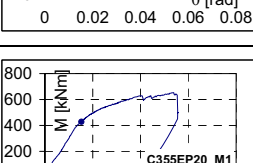
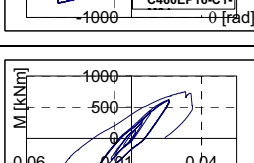
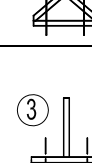
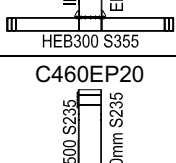
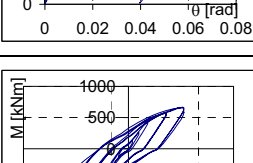
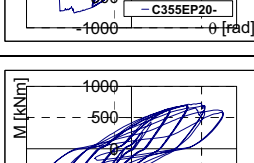
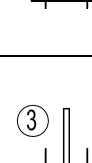
Joint Type	Test Results					
	Monotonic			Cyclic		
	M- θ curve	Failure Mode	θ_u	M- θ curve	Failure Mode	θ_u
<p>C355WC</p> 		Web column buckling then weld failure	0.097		Web column buckling then weld failure	0.060
<p>C460WC</p> 		Web column buckling then weld failure	0.098		Web column buckling then weld failure	0.076
<p>C355EP12</p> 			0.061			0.039
<p>C460EP12</p> 			0.064			0.038
<p>C355EP16</p> 			0.068			0.051
<p>C460EP16</p> 			0.075			0.039
<p>C355EP20</p> 			0.052			0.018
<p>C460EP20</p> 			0.032			0.050

Table 6 shows synthetically the behavior of tested joints. Associated to that table, there are Table 7 and Table 8 with the characteristics of the moment – rotation ($M-\theta$) relationship for monotonic and cyclic loading, respectively. It can be observed that column web panel has a major contribution to joint plastic rotation, both under monotonic and cyclic loading. The remainder of plastic rotations was due to end-plate deformations. Analytical predictions by EN 1993-1-8 of the yield moment computed using measured material characteristics were generally conservative with respect to experimental values for monotonic loading. In the case of cyclic loading, experimental values of the yield moment were slightly larger than analytical ones, which is attributed to the procedure used to determine experimental yielding (following procedure from ECCS, 1986).

In Figure 4 is shown the state of strain in the column web panel of bolted specimens under monotonic loading, obtained using the digital image correlation technique. It can be observed that the web panel has a major contribution to plastic deformations of the joints, conclusions that can be also observed from Table 8.

In Table 9, a brief description of failure modes of joints is presented and in Figure 5, a selection of photos during testing of specimens. C355WC-C1, C460EP16-M1 and CP460EP16-C1 are shown. It is also useful to remark the fact that residual rotation was in the range of 0.04 – 0.06 rad for bolted joints and around 0.08 rad for welded ones.

Table 7. Characteristics of joints under monotonic loading

Specimen	θ_y , rad	θ_u , rad	θ_{panel}^{web} , rad	M_y , kNm	M_{max} , kNm
C355WC-M1	0.011	0.097	0.097(100%)	519	787.8
C460WC-M1	0.011	0.098	0.098(100%)	521	830.1
C355EP12-M1	0.013	0.061	0.037(61%)	598.7	729.2
C460EP12-M1	0.016	0.064	0.046(72%)	524.9	650.3
C355EP16-M1	0.015	0.068	0.061(90%)	556.9	716.2
C460EP16-M1	0.011	0.075	0.075(100%)	516.3	736.1
C355EP20-M1	0.012	0.052	0.042(81%)	527	652.3
C460EP20-M1	-	-	-	-	-

Table 8. Characteristics of joints under cyclic loading

Specimen	θ_y , rad	θ_u^+ , rad	θ_u^- , rad	θ_{panel}^{web} , rad	M_y , kNm	M_{max}^+ , kNm	M_{max}^- , kNm
C355WC-C1	0.009	0.060	0.059	0.059(100%)	543.1	748.8	756.2
C460WC-C1	0.010	0.076	0.059	0.076(100%)	658.4	959.3	916.3
C355EP12-C1	0.013	0.039	0.039	0.030(77%)	567.3	670.8	661.2
C460EP12-C1	0.015	0.038	0.038	0.027(71%)	664.9	733.8	741.8
C355EP16-C1	0.012	0.051	0.049	0.036(70%)	564.3	706.8	679.6
C460EP16-C1	0.014	0.039	0.045	0.026(58%)	620	737.6	761.8
C355EP20-C1	0.012	0.018	0.035	0.035(100%)	617.6	635.2	685.2
C460EP20-C1*	0.015	0.031	0.032	0.022(69%)	600	659.6	651.7
C460EP20-C2	0.014	0.050	0.048	0.033(66%)	616	731.3	683.9

* Displacement amplitude of cycles, after attainment of yield displacement d_y , of $\pm 2d_y$, $\pm 4d_y$, ..., according to ECCS Recommendation (ECCS, 1986). All other specimens have been tested with cycles of d_y , $\pm 2d_y$, $\pm 3d_y$, $\pm 4d_y$...

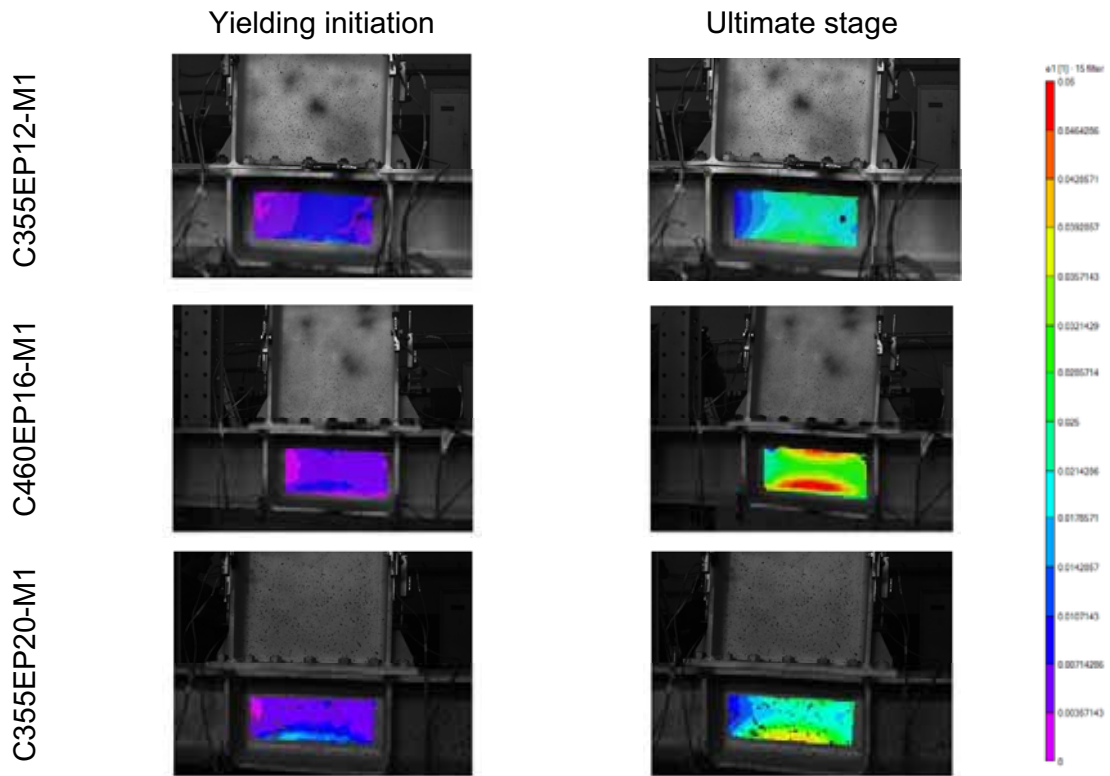
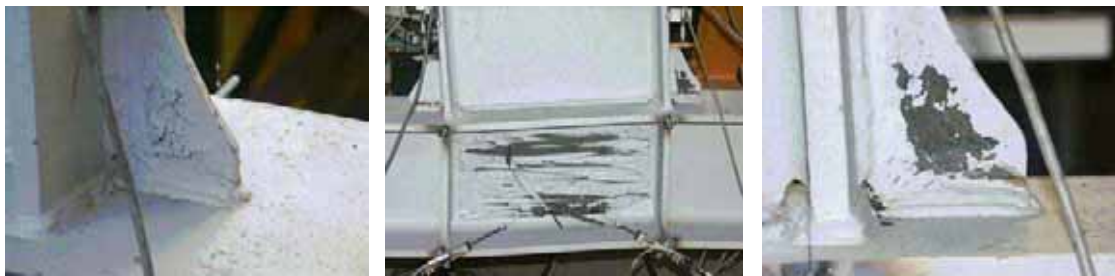


Figure 4. State of strain in the column web at yield and failure using digital image correlation technique



C355WC-C1



C460EP16-M1



C460EP16-C1

Figure 5. Joint tested specimens

Table 9. Brief description of failure modes of joint specimens

C355WC-M1	Buckling of compressed stiffener between column and beam flanges; shearing of panel zone; buckling of beam flange; weld cracks initiated at stiffener in tension (max displacement 200mm)
C355WC-C1	2e _y – shearing of panel zone; 4(6) e _y – weld cracks initiated at stiffener in tension
C460WC-M1	Buckling of compressed stiffener between column and beam flanges; shearing of panel zone; buckling of beam flange; weld cracks initiated at stiffener in tension (max force 3490kN)
C460WC-C1	2e _y – shearing of panel zone; 4(6) e _y – weld cracks initiated at stiffener in tension
C355EP12-M1	End plate visible deformations in tension zone; shearing of panel zone; T-stub in mode 2 and bolt failure
C355EP12-C1	3e _y – end plate visible deformations on both directions; 4e _y – small weld cracks at stiffeners; shearing of panel zone; T-stub in mode 2 and bolt failure
C460EP12-M1	End plate visible deformations in tension zone; shearing of panel zone; T-stub in mode 2 and bolt failure
C460EP12-C1	3e _y – end plate visible deformations on both directions; 4e _y – small weld cracks at stiffeners; shearing of panel zone; T-stub in mode 2 and bolt failure
C355EP16-M1	Small end plate visible deformations in tension zone; shearing of panel zone; bolt failure in mode 3
C355EP16-C1	3e _y – end plate visible deformations on both directions; 4e _y – small weld cracks at stiffeners; shearing of panel zone; T-stub in mode 2 and bolt failure
C460EP16-M1	End plate visible deformations in tension zone; shearing of panel zone; T-stub in mode 2 and bolt failure
C460EP16-C1	Important end plate visible deformation in tension zone; shearing of panel zone; T-stub in mode 2 and bolt failure
C355EP20-M1	Small end plate visible deformation in tension zone; shearing of panel zone; bolt failure in mode 3
C355EP20-C1	Small end plate visible deformation in tension zone; shearing of panel zone; bolt failure in mode 3
C460EP20-C1	3(4) e _y – small end plate visible deformation in tension zone; shearing of panel zone; bolt failure in mode 3
C460EP20-C2	3(4) e _y – small end plate visible deformation in tension zone; shearing of panel zone; 4e _y – bolt failure in mode 3; 5e _y – weld cracks initiated at stiffeners

CONCLUDING REMARKS

It is clear that due to the significant difference between design and actual values of materials that tested specimens are practically other than initially planned. However, the intention to test and evaluate performance of joint specimens of S460 columns has been realized. By increase of beam strength, its contribution to the joint deformability was practically inhibited, but the end-plates have been as planned. Since the analysis and interpretation of results still is in progress, hereafter some preliminary conclusions are presented only:

- A very good ductility of HSS component was observed;
- Excepting one case, all cyclic specimens demonstrated their rotation capacity, at least equal to the limit of 0.035 rad specified in EN 1998-1;
- The contribution of web panel larger than 30% does not affect the robustness of joints
- Thick end-plates, even of MCS, reduce the ductility of joints without significant increase of moment capacity.
- No significant degradation of capacity was observed from monotonic to cyclic results.
- The analytical prediction of joint moment resistance based on component method of EN 1993-1.8 seems to be good enough in this case, and the procedure used for the outer bolt row is confirmed.
- The control of upper limit of yield strength is of real importance and fabricators must find a way to introduce that on the material specification, additionally to the lower limit, otherwise the real response of the structure can be very different from the one predicted through design.

ACKNOWLEDGMENT

This research was supported by the contract no. 29/2005 "STOPRISC", funded by Romanian Ministry of Education and Research, within the frame of "Excellence Research" Program, CEEX – Matnantech.

REFERENCES

AISC 2005, Seismic Provisions for Structural Steel Buildings. *American Institute of Steel Construction*, Inc. Chicago, Illinois, USA.

Dubina, D. and Dinu, F., 2007, High strength steel for seismic resistant building frames", *Proc. of 6th Int. Conf. Steel and Aluminium Structures – ICSAS'07*, Ed. R. G. Beale, Oxford Brooks Univ.

Dubina, D., Stratan, A. Dinu, F. (in print). "Dual high-strength steel eccentrically braced frames with removable links". *Earthquake Engineering & Structural Dynamics*, Published Online: 10 Jul 2008.

Dubina, D., Stratan, A., Ciutina, A., 2005, Components and Macro-Components of Rotation Capacity of Moment Connections, *Proc. of 20th CTA Congress Advances in Steel Constructions*, ACS ACAI, Milano.

Dubina, D., Stratan, A., Muntean, N., Grecea, D., 2008, Dual Steel T-stub behaviour under monotonic and Cyclic loading, (in present volume).

ECCS 1986, Recommended testing procedure for assessing the behaviour of structural steel elements under cyclic loads, ECCS no. 45.

FEMA 356, 2000, Prestandard and commentary for the seismic rehabilitation of buildings, Washington (DC), *Federal Emergency Management Agency*.

Girao Coelho, A.M., Bijlaard, F.S.K., 2007, Ductility of High performance Steel Moment Connections, *Advanced Steel Construction*, Vol.3, No.4.

Lu, L.W. et al., 2000, Critical issues in achieving ductile behavior of welded moment connections, *Journal of Constructional Steel Research*: 55.

POST-TENSIONED COLUMN BASES FOR SELF-CENTERING MOMENT RESISTING FRAMES

Hoseok Chi

Purdue University, West Lafayette, Indiana 47907, USA
hchi@purdue.edu

Judy Liu

Purdue University, West Lafayette, Indiana 47907, USA
jliu@purdue.edu

ABSTRACT

A post-tensioned (PT) column base connection is presented for use in a self-centering steel moment resisting frame. The PT column base consists of post-tensioned high-strength bars, buckling restrained steel plates, keeper plates, and reinforcing plates. Moment-rotation response of the PT column base connection is characterized by gap opening behavior at the column-grade beam interface. Properly designed PT column base connections show self-centering capability without inelastic deformation in columns. Thus, potential plastic hinges at the bottoms of first story columns can be eliminated by the gap openings at column bases. Nonlinear dynamic analyses for a prototype self-centering steel moment resisting frame were carried out to evaluate the performance of the PT column base connections.

INTRODUCTION

Self-centering moment resisting frame (SC-MRF) systems have the potential to eliminate structural damage due to earthquakes. Numerical and experimental studies have demonstrated the viability of steel SC-MRFs and, in particular, the performance of the beam-column connections (Garlock, 2002; Garlock et al. 2005). These studies assumed columns that were continuous at ground level, extending into a basement, and able to develop their full plastic moment capacity at their base. While these SC-MRFs demonstrated the ability to return to their original vertical positions, or self-center, the yielded column bases may be considered to be damaged. This study explores the use of post-tensioning as a solution for self-centering, damage-free column bases for SC-MRFs. Non-linear dynamic analyses are used to evaluate various levels of post-tensioning and the addition of energy dissipating devices. Specific issues, such as shear resistance, flange buckling, and anchorage detailing requirements, are addressed. Plans for experimental validation are discussed.

EVALUATION OF COLUMN BASE ALTERNATIVES

The development of the column base detail is based on non-linear analysis of SC-MRF. Different details are explored; these include the original, continuous column, a pinned base, a post-tensioned column base, and a post-tensioned column base with energy-dissipating devices. For all cases, adequate shear resistance is assumed. These column base configurations are analyzed for six different design basis earthquakes (DBE). The configurations are labeled as: (a) post-tensioning only, (b) post-tensioning with energy dissipating devices, (c) theoretically-pinned bases, and (d) the original model.

Self-Centering Frame and Column Base Modeling

This study is based on a 4-bay, 6-story SC-MRF used in previous research by Garlock (2002). All of the same beam and column sizes are used. These include W14x398 columns at the first story and W36x194 for the first story beams. The DRAIN-2DX model used for analysis includes a leaning column representing the gravity frames, as well as spring and link elements representing the collector beams, as shown in Fig. 1. Springs at the column base represent the rotational stiffness at the ground level, provided by the continuous columns into the basement and the grade beams. This model is referred to as the “original model.”

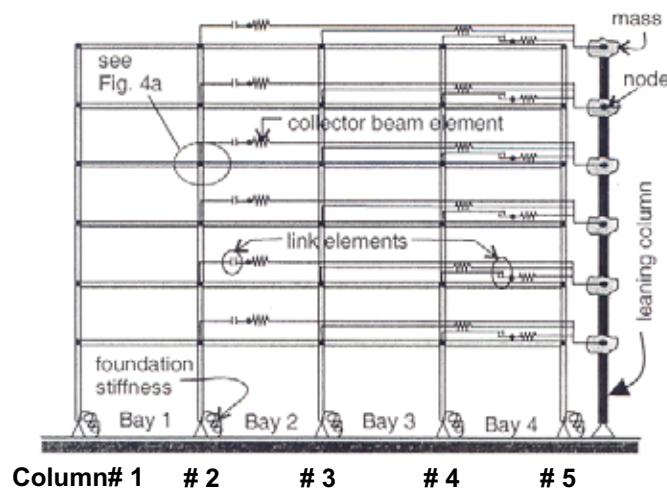


Fig. 1: Model of 4-bay, 6-story SC-MRF with “original” column bases (Garlock, 2002)

For the self-centering, post-tensioned column bases, the grade beams and basement columns are modeled explicitly. The post-tensioning bars are assumed to start above ground level and continue into the basement, as shown in Fig. 2. Gap-opening in the column bases occurs at the top of the grade beam. This configuration is chosen because preliminary non-linear dynamic analyses of a frame, with bars in the first story, results in column shortening and reduction in post-tension force. These effects are due to the compressive forces from post-tensioning in addition to overturning.

The columns, gap-opening elements, and post-tension bars are modeled as by Garlock (2002). The moment-rotation response is as shown in Fig. 2. For these analyses, it is assumed that shear is adequately resisted by keeper elements. When considered, fictitious energy dissipating devices, in the form of truss elements with bilinear force-deformation response, are placed at the column flanges. A moment-rotation response for a column base with energy dissipating devices, extracted from the analysis for a particular ground motion, is shown in Fig. 3.

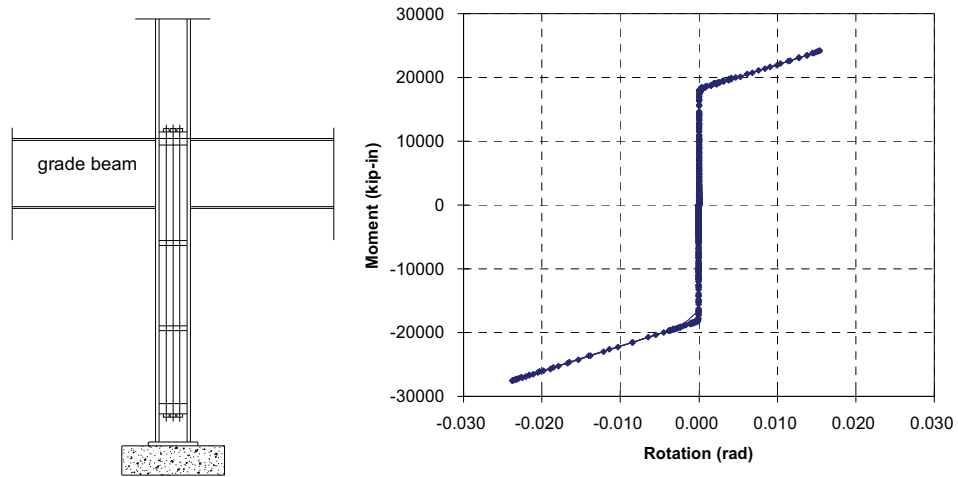


Fig. 2: (Left) Schematic of Post-tensioned Column Base: (Right) Moment-rotation Response of Column Base without Energy Dissipating Devices

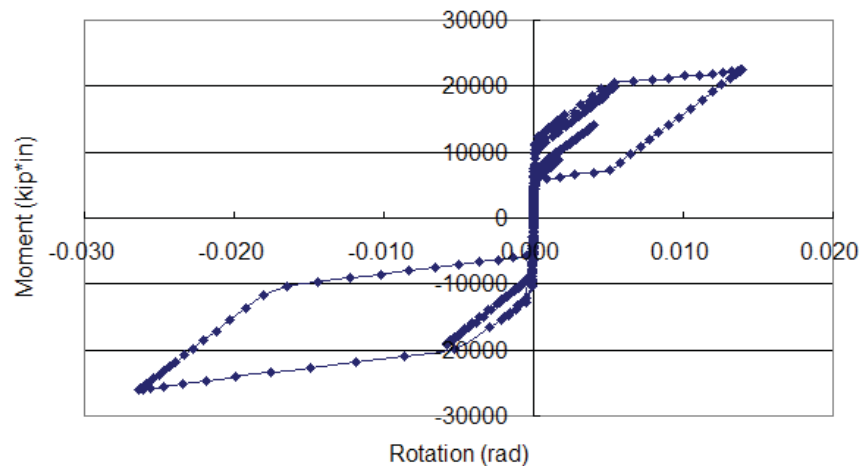


Fig. 3: Moment-rotation Response for the Post-tensioned Column Base with Energy Dissipating Devices

Level of Post-Tensioning

A few levels of post-tensioning are considered initially. The resulting decompression moments correspond to roughly 25%, 50% and 75% of the nominal yield moment of the column. Analysis has shown that the column bases will not decompress under wind loads.

Responses to the Kobe design basis earthquake (DBE) demonstrate that the level of post-tensioning at the column base has little effect on the maximum interstory drift response. A larger post-tension force does reduce the residual drift, but these drift values are acceptable for all levels of post-tensioning. Furthermore, yielding occurs at the tops of the first story columns regardless of the post-tension force. Based on these results, the decision was made to use the post-tension force corresponding to a column base decompression moment of approximately 25% of the yield moment of the column.

Response to Design Basis Earthquakes

Six ground motions are considered. These records have been scaled to the design basis earthquake (DBE) level, based on the procedure by Somerville et al.(1997). These are shown in Table 1. The responses to the DBE are evaluated with respect to maximum interstory drift, residual drift, and yielding in the columns. Overall, configuration (b), the post-tensioned (PT) column bases with energy dissipating devices, performs the best, with the least interstory drift, 0.037 radians maximum in the first story, and the least residual drift (Fig. 4). A residual drift limit is set at 0.002 radians, deemed an acceptable out-of-plumb value based on the AISC Code of Standard Practice (2005). Configurations (a) and (d) also produce acceptable values of residual drift. The theoretically-pinned bases (c) result in unacceptable drift values.

While yielding still occurs in the columns, the demand is significantly less for configuration (b) than for others in most cases, and comparable to the demand for configuration (a) in some cases. A graph of maximum strain normalized to yield strain, ϵ/ϵ_y , demonstrates this effect of the energy dissipating devices (Fig. 5). Yielding occurs either at the top or base of the first story column in each case; the lowest normalized strain is shown for configuration (b).

REFINEMENT OF POST-TENSIONED COLUMN BASE DETAIL

From non-linear dynamic analysis results, configuration (b), the post-tensioned column based with energy dissipation devices, is the most promising. However, issues such as yielding of the column at the top of the first story and adequate shear resistance must be addressed. Furthermore, nonlinear dynamic analysis for the maximum considered earthquake (MCE) reveals high interstory drift values as well as unacceptable drift values for some DBE. Further development of the post-tensioned column base includes changes in column size for the interior columns, detailing of keeper plates for shear resistance, detailing of energy dissipation devices, and detailing of the PT bar

anchorage. A post-tensioned column base detail including these elements is shown in Fig. 6.

Table 1. Ground Motions

Ground motion	Scale factor (DBE)	PGA (g)	PGV (in/s)
ARTI, ARTIFICIAL	1	0.39	19.4
CC99CHY, Chi-Chi, Taiwan 1999	1.036	0.31	15.9
LA21, KOBE, 1995	0.429	0.55	24.1
LP89G03, LOMA PRIETA, 1989	1.495	0.55	26.3
SE36, MIYAGI-OKI, 1978	0.541	0.42	26.3
NR94TAR, NORTHRIDGE, 1994	1.091	1.08	33.2

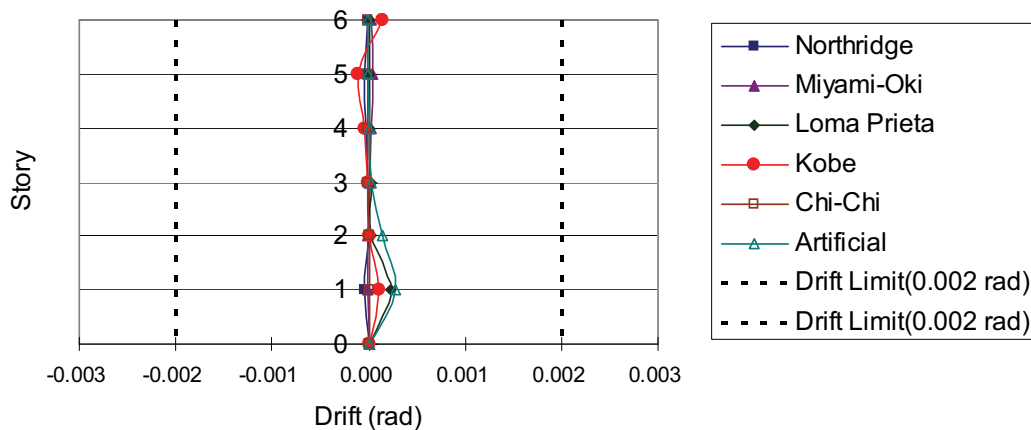


Fig. 4: Residual Drift for PT Column Bases with Energy Dissipating Devices

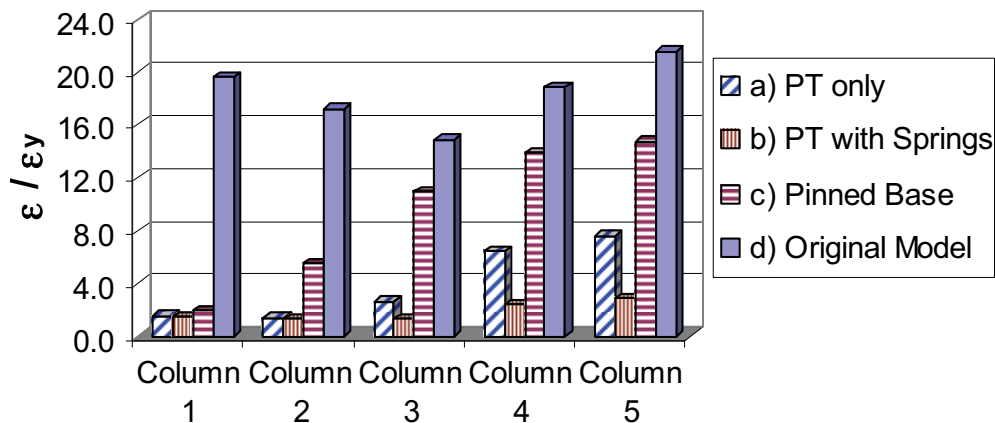


Fig. 5: Normalized Maximum Strain in the First Story Columns for Each Configuration, Response to Loma Prieta DBE

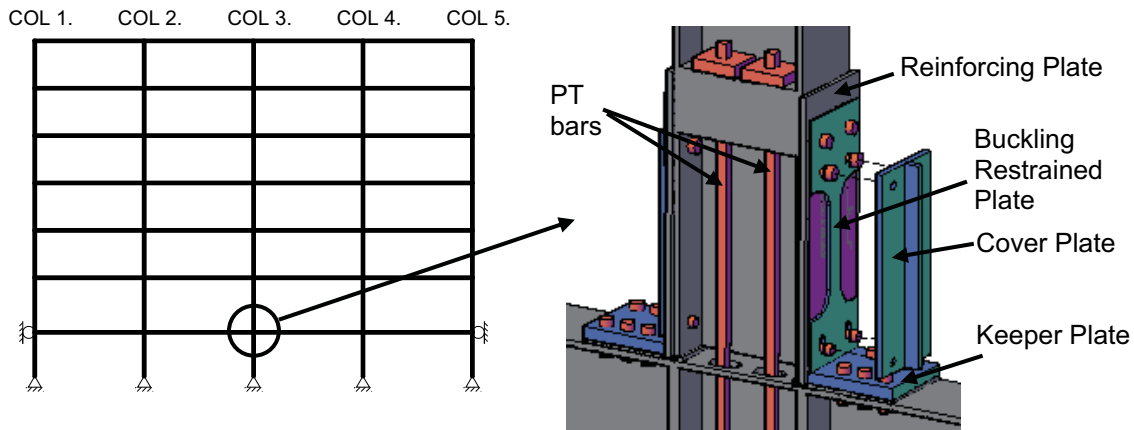


Fig. 6: Post-Tensioned Column Base Detail

PT Column Base Design

The column base is designed considering that (1) no decompression occurs at the PT column base connections for the design wind load, (2) no PT bars yield under the DBE, (3) buckling and fracture do not occur in the energy dissipation plates under the DBE, and (4) No shear slip occurs at the interfaces of columns and grade beams under the MCE. However, the yielding of the PT bars is allowed for the MCE. If necessary, the ED plates and PT bars, which might be damaged under the MCE, could be easily replaced. In design of the prototype frame, the initial PT force is 350 kips, which corresponds to the decompression moment of 23% of the nominal plastic moment capacity (M_p).

Member sizes are modified in order to meet the design drift limit of 0.02 radians for the DBE. Because of the relatively flexible post-tensioned column bases, deep sections are used for the interior columns (#2-4, Fig.1). W36x328s were selected for these first story columns.

Reinforcing plates are used not only to distribute bearing stresses, but also to distribute shear stresses along the length in column webs. After the gap opening under the MCE, the interior column (W36 shape) flange and web may suffer buckling because of the high compressive forces and relatively thin flange and web compared a more commonly used W14 shape. W14s are still recommended for the exterior columns. Reinforcing plates may be needed at the interior column bases to prevent local buckling under the MCE for strong and weak axis gap opening even if the section is seismically compact.

Nonlinear dynamic analyses for this SC-MRF with PT column base connections are performed for six different ground motions scaled to DBE and MCE levels. Mean drift of first story column is 0.022 radians for the DBE and 0.032 radians for the MCE. Residual drift for the DBE is within the limit of 0.002 radians. Time history of roof displacement for the Northridge record is presented for the DBE and MCE in Figure 7. The SC-MRF with

PT column base connections shows self-centering capability without damage (i.e., plastic hinges).

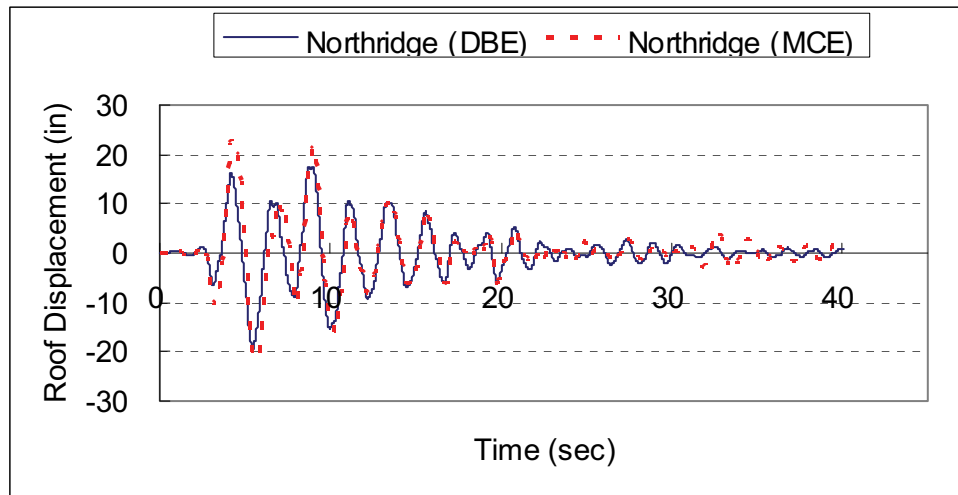


Fig. 7: Roof Displacement for Northridge Record Scaled to the DBE

The shear resistance at a PT column base is provided by friction (i.e., V1 in Figure 8) between the grade beam and first story column and bearing (i.e., V2 in Figure 8) on the beveled keeper plate, as shown in Figure 8. The axial force developed in the column is the main contributor to V1. The axial force is the sum of the initial gravity load, initial PT force, and increased PT forces due to gap opening. A friction coefficient between steel surfaces of 0.3 is assumed. Additional shear resistance, V2, is provided by the keeper plates. The keeper plates are bolted (i.e., slip critical connection) to the grade beam flanges. When the shear demand exceeds V1, the column flange bears against the keeper plate, and the bearing force is transferred to the grade beam flange by friction.

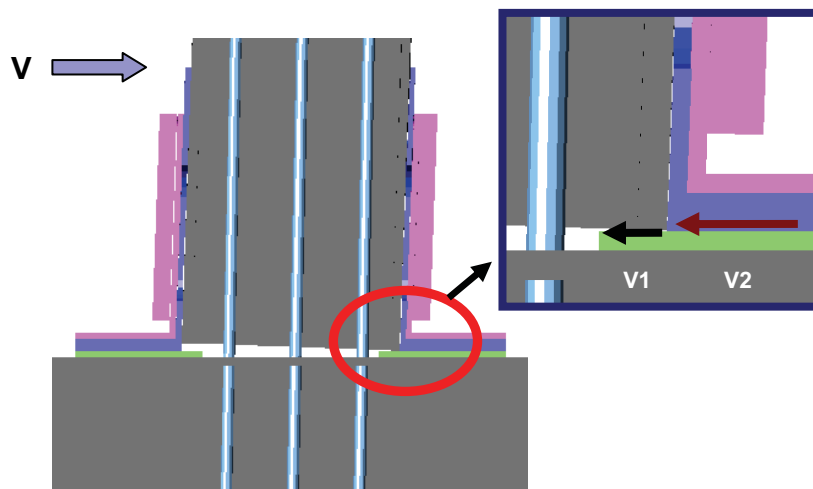


Fig. 8: Shear Resistance in Post-Tensioned Column Base

Seismic energy can be dissipated at PT column bases by yielding of the buckling restrained steel plates. A representative force-deformation response of the steel plate from the time-history analysis is plotted in Figure 9. The buckling restrained steel plate can show a stable hysteretic behavior without buckling or fracture. The steel plates are restrained by cover plates so that buckling of the plate is prevented under cyclic loading. The proper length of the steel plate was selected such that the maximum axial strain in the plate remains below an ultimate strain value for a maximum gap opening at 4% drift. The possibility of low cycle fatigue will be examined through an experimental study. The energy dissipation devices are bolted to column flanges and grade beam flanges. Therefore, the steel plates can be easily replaced if damaged.

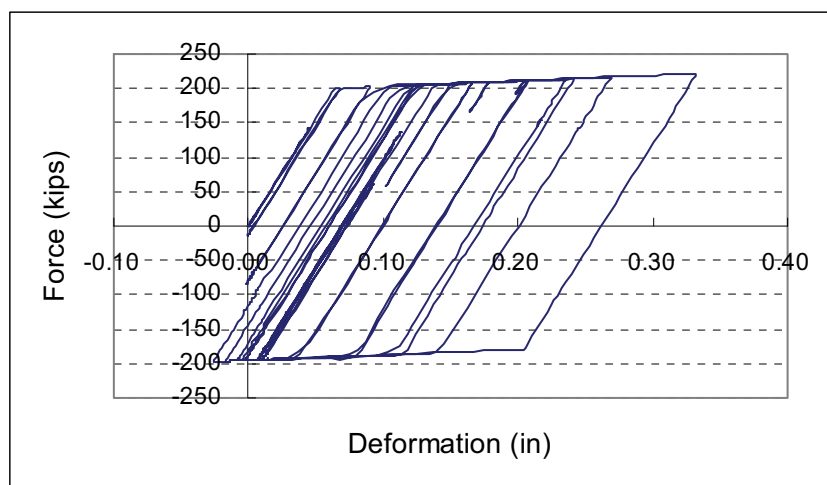


Fig. 9: Force-Deformation Response in Energy Dissipation Device

Detailing Issues of PT Column Base

Binding of the PT bars at the holes in the grade beam can cause additional bending stresses in the bars. Therefore, a properly sized slotted hole is needed. For example, if the slot is 2 times the diameter of the bar, the developed extreme fiber stress is approximately 7% of the yield stress of the bar.

Anchorage detailing is also critical for the PT column base design, because excessive deflection and stresses of the anchorage can cause inadequate behavior of the PT column base. A possible stiffened anchorage detail, with vertical stiffeners as well as a side plate connected on three sides to the column flanges and horizontal anchorage plate, is shown in Fig. 10.

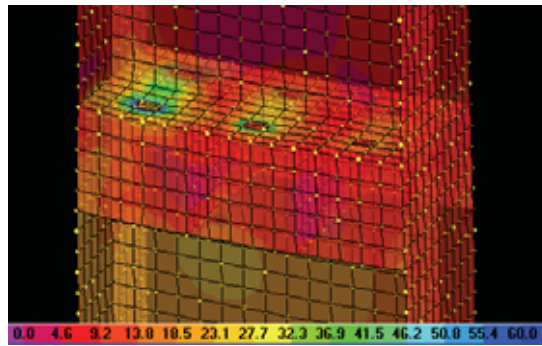


Fig. 10 Stress (Von Mises) Distribution for a Stiffened Anchorage at 3% Drift

EXPERIMENTAL EVALUATION

An experimental study to investigate the behavior of the PT column bases for both strong and weak axis gap opening is in progress. A schematic of the test setup is presented in Figure 11. Specimens will be subjected to gravity loads and increasing cyclic, quasi-static lateral displacements. Experimental variables include the initial PT force, initial axial force (i.e., gravity load), and use of energy dissipation devices. Investigated limit states include PT bar yielding and keeper plate slip. The cyclic behavior of the PT column base connections for both strong and weak axis bending will be studied. The shear resistance by the keeper plates at column bases will also be evaluated.

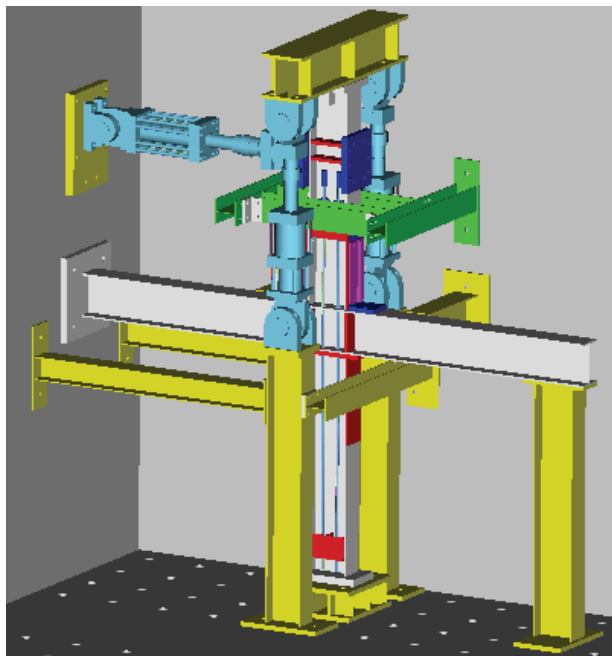


Fig. 11: Test Setup for the PT Column Base

CONCLUSIONS

The results shown here suggest that, considering strains and residual drift, a PT column base with energy dissipating devices may be the best option for an SC-MRF. The recommended level of post-tensioning results in a decompression moment of approximately 25% of the column yield moment.

Work on the PT column bases includes design and detailing of the anchorages for the post-tensioning strands, the energy dissipating devices, and the keeper elements for resisting shear demands. Experimental validation, detailed analysis of the PT column base detail, and nonlinear analysis of an SC-MRF frame with PT column bases continues. Results will demonstrate the viability of the PT column base as a solution for self-centering moment resisting frames.

REFERENCES

- AISC (2005), "Code of Standard Practice for Steel Buildings and Bridges," AISC303-05, Chicago, IL.
- Garlock, M. (2002). "Full-Scale Testing, Seismic Analysis, and Design of Post-Tensioned Seismic Resistant Connections for Steel Frames," Ph.D. Dissertation, Civil and Env. Engineering Dept., Lehigh University, Bethlehem, PA.
- Garlock, M, Ricles, J., and Sause, R. (2005). "Experimental Studies on Full-Scale Post-Tensioned Steel Connections", *Journal of Structural Engineering*, ASCE, 131(3).
- Somerville, P., Smith, N., Punyamurthula, S., Sun, J., and Woodward-Clyde Federal Services. (1997). Development of Ground Motion Time Histories for Phase 2 of the FEMA/SAC Steel Project. SAC/BD-97/04 SAC Joint Venture.

ACKNOWLEDGMENTS

This material is based on work supported by the National Science Foundation, Award No. CMS-0420974, in the George E. Brown, Jr. Network for Earthquake Engineering Simulation Research (NEESR) program. Advice from project members Prof. Richard Sause and Prof. James Ricles from Lehigh University and Prof. Maria Garlock from Princeton University is gratefully acknowledged.

EXPERIMENTAL STUDY ON STIFFENING METHODS FOR PLATE-TO-CIRCULAR HOLLOW SECTION CONNECTIONS

Andrew P. Voth

Department of Civil Engineering, University of Toronto, Canada
andrew.voth@utoronto.ca

Jeffrey A. Packer

Department of Civil Engineering, University of Toronto, Canada
jeffrey.packer@utoronto.ca

ABSTRACT

Branch plate-to-circular hollow section (CHS) connections experience significant deformation under branch plate axial load resulting in low connection capacity if an ultimate deformation limit state is employed. To increase the connection capacity, strengthening methods such as “through plate connections” or concrete/grout filling have been proposed. An experimental study has been undertaken on 12 plate-to-CHS connections, with either longitudinal, transverse or skewed branch and through plates and with branches loaded in either tension or compression, to investigate the through plate connection stiffening method.

INTRODUCTION

The limit states design resistance for plate-to-hollow structural section (HSS) connections subject to branch plate axial load is generally relatively low due to connection flexibility. As such, an imposed deformation limit of 3% of the connecting face width for rectangular hollow section (RHS) connections or 3% of the diameter for CHS connections (Lu et al., 1994; Wardenier et al., 2008b; IIW, 2008) frequently governs the connection design capacity rather than punching shear or fracture criteria. Though a deformation limit is practical and necessary, the potential strength of the hollow section member is being under-utilized, particularly with the increase in use of heavily-loaded plate-to-HSS connections in tubular arch bridges, roof trusses and cable-stayed roofs. With the increased demand on these connections types the need to develop connection strengthening and stiffening methods becomes apparent.

CHS-to-CHS connections in offshore platform structures have previously been strengthened with internal annular ring stiffeners (Lee and Llewelyn-Parry, 1999, 2004, 2005; Willibald, 2001) and doubler or collar plates (Choo et al., 1998). One method of strengthening plate-to-CHS or plate-to-RHS connections is to pass the branch plate through the chord member and weld the plate to both sides of the tube, producing a “through plate connection”. Plate-to-RHS connections have previously been studied (Kosteski and Packer, 2003) and design recommendations have since been incorpo-

Table 1. Design resistances of uniplanar branch plate-to-CHS connections under branch axial load according to CIDECT (Wardenier et al., 2008b)

Design Resistance		
Chord Plastification:	$N_1^* = Q_u \cdot Q_f \cdot \frac{f_{y0} t_0^2}{\sin \theta_1}$	
Type of Connection:		
Transverse Plate		
	Function Q_u :	
	X-type	$2.2 \left(\frac{1 + \beta}{1 - 0.7\beta} \right) \cdot \gamma^{0.15}$
	T-type	$2.2(1 + 6.8\beta^2) \cdot \gamma^{0.2}$
	Chord Punching Shear Check: (when $b_1 \leq d_0 - 2t_0$):	
		$N_1^* = 1.16 t_0 f_{y0} b_1$
Longitudinal Plate		
	Function Q_u :	
	X-type	$5(1 + 0.40\eta)$
	T-type	
	Chord Punching Shear Check:	
		$N_1^* \sin \theta_1 = 1.16 \cdot t_0 f_{y0} \frac{h_1}{\sin \theta_1}$
Function Q_f :		
$Q_f = (1 - n)^{c_1}$	$n = \left \frac{N_0}{N_{pl,0}} \right + \left \frac{M_0}{M_{pl,0}} \right ^a$ (class 1 and 2 sections)	Chord in compression: $a = 1$ Chord in tension: $a = 2$
	$n = \left \frac{N_0}{N_{pl,0}} \right + \left \frac{M_0}{M_{el,0}} \right ^a$ (class 3 sections)	
Value of c_1	Branch axial load: Compression, $c_1 = 0.25$ Tension, $c_1 = 0.20$	
Range of Validity:		
Chords must be class 1 or 2 [CEN, 2005], but also $d_0/t_0 \leq 50$ For X-type connections: $d_0/t_0 \leq 40$	Transverse plate: $\beta \geq 0.4$ Longitudinal plate: $1 \leq \eta \leq 4$	$\theta_1 \geq 30^\circ$ $f_{y1} \leq f_{y0}$ $f_y/f_u \leq 0.8$ $t_1 \leq t_0$ $f_{y0} \leq 460 \text{ MPa}$

rated into CIDECT Design Guide No. 9 (Kurobane et al., 2004) and the forthcoming AISC Design Guide on HSS Connections (Packer et al., 2008). However, design recommendations for through plate-to-CHS connections are absent in published literature,

indicating a need for further research. The experimental program presented herein investigates the behaviour of through plate-to-CHS connections by comparison with their branch plate counterparts.

CURRENT DESIGN GUIDELINES FOR BRANCH PLATE CONNECTIONS

Branch plate-to-CHS connection behaviour is highly dependent on the orientation and dimensions of the branch plate and the connecting chord member. The ultimate connection resistance is determined by checking the branch plate connection capacity under two possible failure modes that have been identified for both transverse and longitudinal branch plate connections: chord plastification resulting in excessive deformation, and chord punching shear failure (given that both the branch plate and weld are adequately designed and are non-critical). Design formulae for both of these failure modes are given in Table 1 in accordance with a recent re-appraisal by Wardenier et al. (2008a), now incorporated in CIDECT Design Guide No. 1 (Wardenier et al., 2008b).

EXPERIMENTAL PROGRAM

The experimental program consisted of 12 plate-to-CHS connections tested under quasi-static tension or compression branch load with plates oriented at 0° (longitudinal), 45° (skewed) and 90° (transverse) to the longitudinal axis of the CHS chord. All connections were fabricated from ASTM A500 Grade C tubes (ASTM, 2007) with nominal dimensions of 219 x 4.8 mm and specified yield stress of 317 MPa, plus plate with a nominal thickness of 19 mm and specified yield strength of 300 MPa. All specimens were fabricated with nominal 10 mm fillet welds and were proportioned to have a nominal width ratio (β) or depth ratio (η) of 0.457 and a width-to-thickness ratio of the chord (2γ) of 48.8. It should be noted that not all experimental connections complied with the validity range for CIDECT design equations in Table 1; the X-type connections violate the width-to-thickness ratio of the chord (2γ) by exceeding a valued of 40 and the longitudinal plate-to-CHS connections have a nominal depth ratio less than unity. In addition, the chord is neither class 1 or 2 according to Eurocode 3 (CEN, 2005). Measured material and geometric properties are summarized in Tables 2 and 3 respectively with geometric variables shown in Figure 1.

Table 2. Measured material properties

	E (GPa) ^a	f _y (MPa) ^a	f _u (MPa) ^a	ε _u (%) ^a
CHS	211.5	389 ^b	527	30.0
Plate (t ₁ = 19.0 mm)	210.5	326	505	37.7

^a Properties determined by average measurements from multiple tensile coupons

^b Yield strength calculated using 0.2% offset method for cold formed materials

Each specimen was instrumented with eight LVDTs (Linear Variable Differential Transformers) to measure the deformation along the longitudinal centreline and circumfer-

ence of the CHS chord and five strain gauges that were spaced evenly across the plate surface 35 mm above the CHS surface to measure the plate strain distribution. Connection deformation was defined as the change in distance between point A and a point on the plate where the displacement instrumentation was attached (point B); see Figure 1.

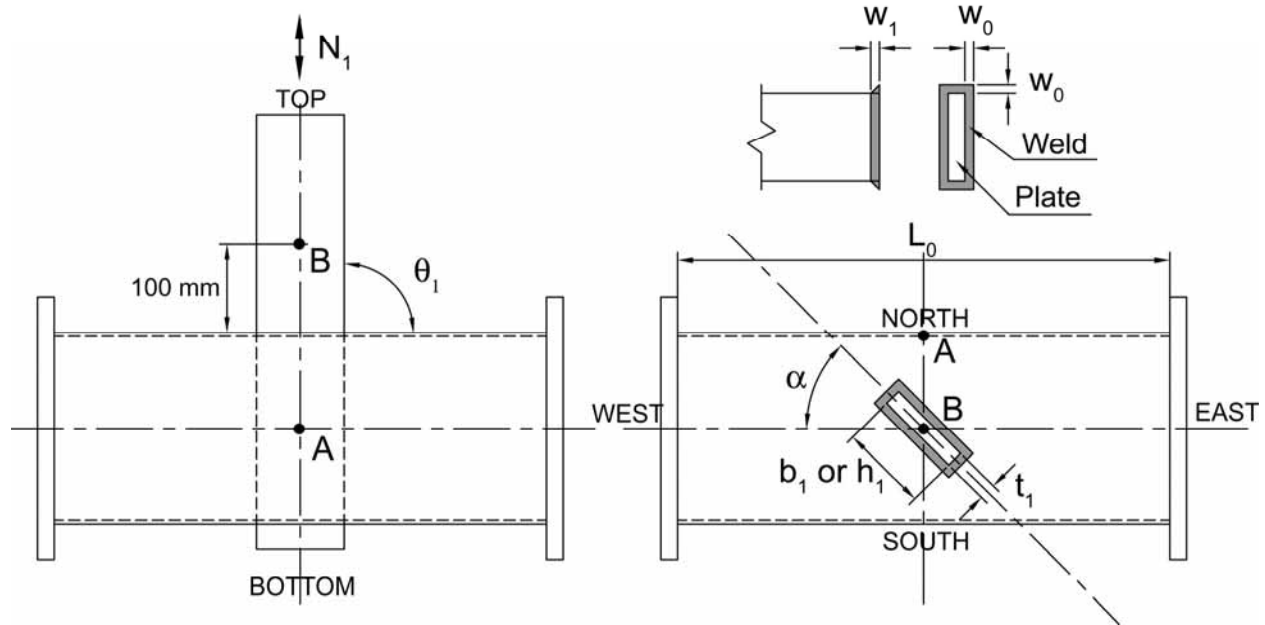


Figure 1. Geometric connection properties

Table 3. Average measured geometric properties

Specimen ID	Constant Properties	b_1 or h_1 (mm)	L_0 (mm)	θ_1 ($^\circ$)	α ($^\circ$)	w_0 (mm)	w_1 (mm)	Connection Type		
CB0EA	CHS: $d_0 = 219.17$ mm $t_0 = 4.49$ mm $A_0 = 2973$ mm ^{2 a}	99.9	559	90	0	11.5	11.8	T-type branch plate in tension		
CB45EA		100.2	558		45	11.0	10.6			
CB90EA		100.3	558		90	10.8	14.0			
CB0EB		100.1	558		0	12.4	11.4	T-type branch plate in compression		
CB90EB		100.3	558		90	11.4	12.9			
CT0EA		100.4	559		0	10.1	10.4		T-type through plate in tension	
CT45EA		100.3	559		45	11.0	9.7			
CT90EA		100.2	558		90	9.6	12.4			
CT0EB		Plate: $t_1 = 19.0$ mm	100.2		559	0	11.1	11.3	T-type through plate in compression	
CT90EB		100.1	558		90	10.6	9.8			
XB90EA			100.2		559	45	0	10.2	9.3	X-type branch plate in tension
XB45EA			100.1		920		12.3	10.1		

^a Measured area calculated using stub column length and measured weight, and by assuming a steel density of 7850 kg/m³

EXPERIMENTAL RESULTS

All connections tested, under both tension and compression branch loads, exhibited punching shear failure (PS) around the weld toe in the CHS member as their ultimate failure mechanism after significant deformations and CHS ovalization. Specimens CB90EA, CT90EA and CT90EB also experienced some tear out (TO) away from the welds which could be classed as a combined punching shear and tear out failure (see Figure 2(d)). Table 4 summarizes the experimental results as well as compares these results to the current CIDECT design recommendations based on the two limit states of chord plastification (N_{1*CP}) and chord punching shear (N_{1*PS}). Predictions for both limit states (failure modes) are calculated using effective geometric properties (β' or η'). The load-deformation curves for all experimental tests are shown in Figure 2. The ratio of the load at 3% d_0 ($N_{3\%}$) to the governing chord plastification resistance (N_{1*CP}) of all connections has a value ranging from 1.2 to a maximum of 5.7 (CT0EB) demonstrating that the current design guidelines tend to underestimate the connection capacity. Comparing the experimental fracture load (N_u) and the current design guidelines for punching shear resistance (N_{1*PS}), several connections have values close to or less than unity (hence unsafe predictions) suggesting that a reduction factor to produce an effective punching width in design may be appropriate, as is the case for some plate-to-RHS connections (e.g. with transverse plate).

Table 4. Experimental and CIDECT (Wardenier et al., 2008b) predicted connection capacity

Specimen ID	Failure Mode	K_n (kN/mm)	$N_{y, Bi-linear}$ (kN)	$N_{3\%}$ (kN)	N_u (kN)	N_{1*CP} (kN)	N_{1*PS} (kN)	$N_{3\%}/N_{1*CP}$	N_u/N_{1*PS}
CB0EA	PS	41.3	>50 ^a	161	286	48.0	249	3.35	1.14
CB0EB	PS	64.8	– ^a	-84.9	-258	-48.2	-253	1.76	1.02
CB45EA	PS	78.4	113	223	233	– ^b	248	–	0.94
CB90EA	PS, TO	98.2	177	283	320	101	247	2.80	1.30
CB90EB	PS	140	– ^a	-127	-311	-103	249	1.23	1.25
CT0EA	PS	141	203	259	406	47.8	244	5.42	1.66
CT0EB	PS	148	-182	-273	<-387 ^c	-48.0	-248	5.69	1.56
CT45EA	PS	199	260	347	352	– ^b	248	–	1.42
CT90EA	PS, TO	304	304	447	459	98.6	242	4.53	1.90
CT90EB	PS, TO	414	-340	– ^d	-400	-101	246	–	1.63
XB90EA	PS	30.6	– ^a	124	226	47.8	244	2.59	0.93
XB45EA	PS	28.1	– ^a	114	250	72.3	476	1.58	0.53

^a No clear yield load was found using bi-linear approximation

^b Design method not applicable

^c Failure of overall experimental setup before ultimate load

^d Method not applicable

In this experimental program the chord length was short, with a L_0/d_0 value usually of 2.55. This generally produces a stiffer and stronger connection response relative to specimens with a longer chord length. The effect of chord length is one of many con

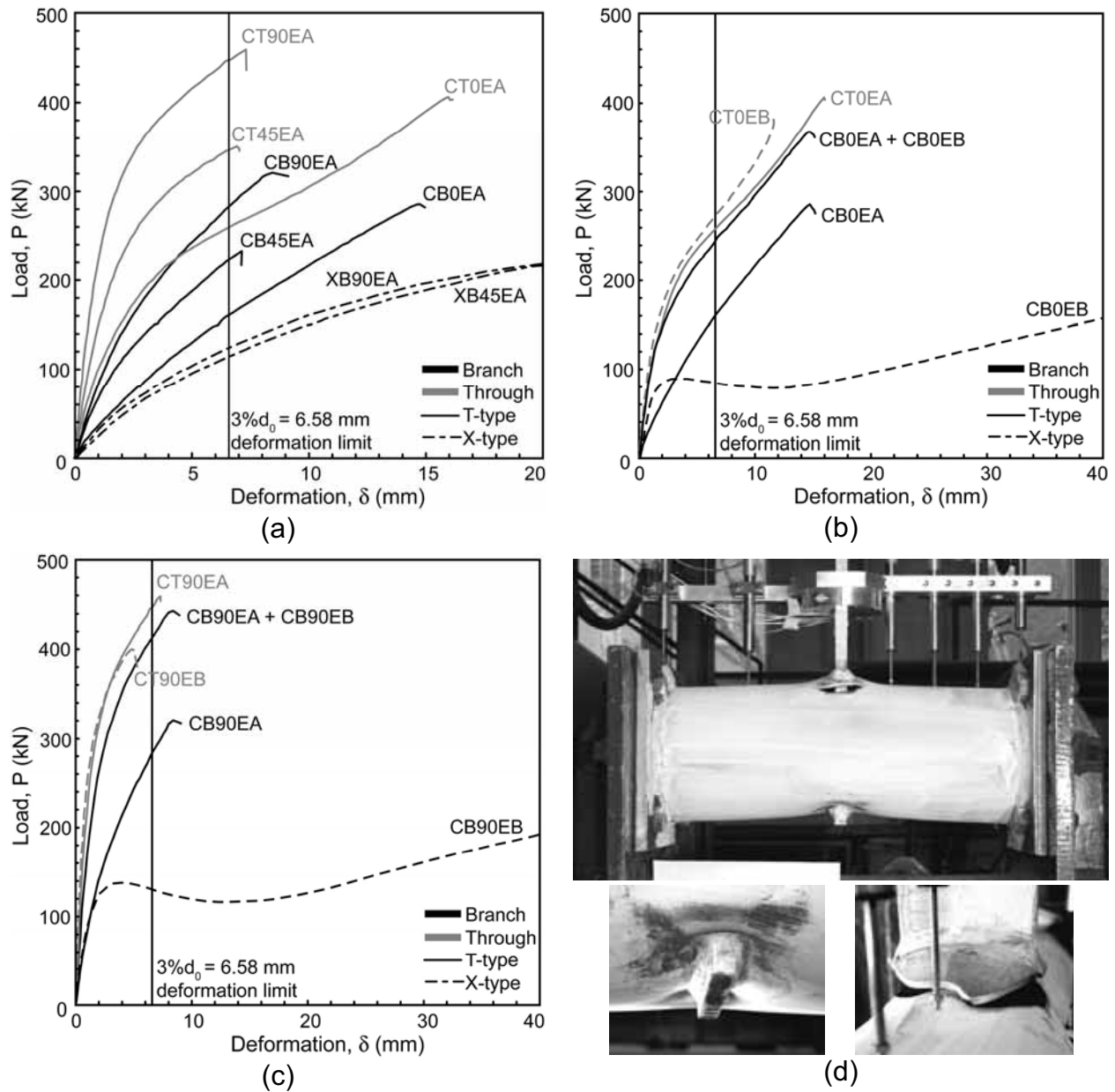


Figure. 2 Load-deformation curves for: (a) T- and X-type connections in tension, (b) longitudinal connections in compression and tension, (c) transverse connections in compression and tension, and (d) typical failure mode (specimen CT90EA)

nection variables now being assessed in a larger numerical parametric study using non-linear finite element analysis.

Influence of Plate Skew Angle and Load Sense

From Figure 2(a) and Table 4 it is observed that the connection load at 3% d_0 increases as the plate skew angle (α) increases. The current CIDECT (Wardenier et al., 2008b) design guidelines follow this general trend; the chord plastification design load is higher

for transverse plate-to-CHS connections than it is for longitudinal plate-to-CHS connections, but intermediate (skew) angles are not covered. The two experimental results for skewed angle connections show that the connection capacity, (based on the $3\%d_0$ limit), for a branch or through plate 45° skew plate connection, is approximately the average of the 0° (longitudinal) and 90° (transverse) connection capacities. Though this general trend exists, a linear interpolation function can not be assumed yet between the longitudinal and transverse connections and therefore further investigation is required.

Comparing branch plate connections tested in compression and tension in Figures 2(b) and 2(c) there are two very different load carrying mechanisms present: a connecting face tension model (CB0EA or CB90EA) and a connecting face compression model (CB0EB or CB90EB). Though tension connections may have similar ultimate failure loads as their counterparts in compression, the deformation at ultimate load is significantly different, with the connection subjected to compression potentially being five times more ductile than the connection subjected to tension. Alternatively, if the load at the $3\%d_0$ deformation limit is compared, the branch plate connection under tension has far more capacity than the connection under compression (Table 4 and Figures 2(b) and 2(c)).

Comparison of Branch and Through Plate-to-CHS Connections

Through plate-to-RHS connections have been previously shown to have approximately double the capacity of similar branch plate-to-RHS connections (Kosteski and Packer, 2003); however, through plate-to-CHS connections do not exhibit this behaviour. Comparing the $N_{3\%}$ load of branch and through plate connections (see Table 5), a through plate-to-CHS connection has approximately 1.6 times the capacity of a similar branch plate connection test in tension (or 3.2 times the capacity of a similar branch plate connection test in compression). The fracture load (N_u) of a through plate-to-CHS connection is approximately 1.4 times that of a similar branch plate connection regardless of skew angle or loading sense due to ultimate fracture occurring in the same manner for all connections tested.

For through plate-to-RHS connections, the flat connection face has approximately the same deformation pattern and behaviour when loaded in either tension or compression. Furthermore, there is little interaction between the loaded RHS face and the neighbouring side walls. The combination of two identical flat plate mechanisms, such as in a through plate connection, results in double the strength. For through plate-to-CHS connections a similar philosophy can be applied by combining two different mechanisms: a tension mechanism and a compression mechanism, each on one connection "face". A summation of the load at a given displacement for compression-loaded and tension-loaded branch plate connections (see Figures 2(b) and 2(c)) results in a combined load-deformation curve that closely matches that of a through plate connection, confirming that combining the two individual mechanisms (tension and compression) is an appropriate way to model through plate connection behaviour and capacity. This methodology for through plate-to-CHS connections suggests that separate connection resistance ex-

pressions for branch plate compression and tension loading should be used, rather than defining the capacity based on the lower compression behaviour as at present (Wardenier et al., 2008b).

Table 5. Comparison of branch and through plate-to-CHS connections

		CT0EA/ CB0EA	CT45EA/ CB45EA	CT90EA/ CB90EA	CT0EB/ CB0EB	CT90EB/ CB90EB
$N_{3\%}$ (kN) of:	through plate	259	347	447	-273	-400 ^a
	branch plate	161	223	283	-84.9	-127
$\frac{N_{3\%} \text{ of through plate}}{N_{3\%} \text{ of branch plate}}$		1.61	1.56	1.58	3.22	3.15
N_u (kN) of:	through plate	406	352	459	< -387	-400
	branch plate	286	233	320	-258	-311
$\frac{N_u \text{ of through plate}}{N_u \text{ of branch plate}}$		1.42	1.51	1.43	> 1.50	1.29

^a Ultimate fracture load used in lieu of $N_{3\%}$ as fracture occurs before $3\%d_0$ limit is reached

CONCLUSIONS

An experimental program, consisting of 12 branch and through plate-to-CHS connections, under both tension and compression loading, has been completed. The results of this experimental program yield the following insights:

- T-type through plate-to-CHS connections have approximately 1.6 times the capacity of similar branch plate connections, at the $3\%d_0$ deformation limit load.
- Current design guidelines for T- and X-type plate-to-CHS connections are conservative.
- T-type branch plate-to-CHS connections have significantly different behaviour under branch tension and compression loading; however, T-type through plate-to-CHS connections under branch tension and compression loading behave in almost the same manner. In addition, the summation of the load-displacement characteristics of T-type branch plate-to-CHS connections under branch tension and compression loading produces similar behaviour to a T-type through plate-to-CHS connection. This underlines the need to separate the resistance of branch plate-to-CHS connections for branch tension versus compression loading, which is one of the goals of this research project.

ACKNOWLEDGEMENTS

Financial support has been provided by CIDECT (Comité International pour le Développement et l'Étude de la Construction Tubulaire), the Steel Structures Education Foundation (SSEF, Canada), the Natural Sciences and Engineering Research Council of Canada (NSERC) and Deutsche Forschungsgemeinschaft (DFG, Germany). Generous donations of CHS, plate and fabrication of test specimens were made by Atlas Tube Inc.,

IPSCO Inc. and Walters Inc. (Ontario, Canada) respectively. The authors are grateful to Dr. Silke Willibald for assistance with the project experimental phase.

NOMENCLATURE

- A_0 = chord member cross sectional area
- E = Young's modulus, modulus of elasticity
- K_n = connection load-displacement curve initial stiffness
- L_0 = chord length (see Figure 1)
- M_0 = chord member applied bending moment
- $M_{el,0}$ = chord member elastic moment capacity
- $M_{pl,0}$ = chord member plastic moment capacity
- N_0 = chord member applied axial force
- N_1 = branch member applied axial force
- $N_{3\%}$ = branch member load at a connection displacement of $3\%d_0$
- N_1^* = connection resistance, expressed as an axial force in branch member
- $N_{1\text{ CP}}^*$ = connection resistance against chord plastification, expressed as an axial force in branch member
- $N_{1\text{ PS}}^*$ = connection resistance against punching shear, expressed as an axial force in branch member
- $N_{pl,0}$ = squash load of chord member = $A_0 f_{y0}$
- N_u = connection ultimate load
- $N_{y,\text{Bi-linear}}$ = connection yield load calculated using classical bi-linear approximation
- b_1 = branch member width
- b_1' = branch member effective width ($b_1' = b_1 + 2w_0$)
- d_0 = chord member external diameter
- f_u = ultimate stress
- f_y = yield stress
- f_{y0}, f_{y1} = yield stress of chord member, branch member
- h_1 = branch member depth
- $h_1' = (h_1/\sin\theta_1 + 2w_0)\sin\theta_1$
- t_0, t_1 = thickness of chord member, branch member
- w_0, w_1 = measured weld size (leg length) along chord member, branch member (see Figure 1)
- α = plate skew angle (see Figure 1)
- β = connection nominal width ratio ($\beta = b_1/d_0$)
- β' = connection effective width ratio ($\beta' = b_1'/d_0$)
- ϵ_u = ultimate strain
- γ = chord radius-to-thickness ratio ($\gamma = d_0/2t_0$)
- η = branch member nominal depth-to-chord diameter ratio ($\eta = h_1/d_0$)
- η' = branch member effective depth-to-chord diameter ratio ($\eta' = h_1'/d_0$)
- θ_1 = inclination angle between branch member and chord member
- CIDECT = Comité International pour le Développement et l'Étude de la Construction Tubulaire

REFERENCES

- ASTM (2007), *Standard Specification for Cold-Formed Welded and Seamless Carbon Steel Structural Tubing in Rounds and Shapes*, ASTM A500/A500M-07. ASTM International, West Conshohocken, Pennsylvania, USA.
- CEN (2005), *Eurocode 3: Design of Steel Structures Part 1.8: Design of Joints*, EN1993-1-8: 2005(E). European Committee for Standardisation, Brussels, Belgium.
- Choo, Y.S., Li, B.H., Liew, J.Y.R., Vegte, G.J. van der and Zettlemoyer, N. (1998), "Static Strength of T-joints Reinforced with Doubler or Collar Plates", *Proceedings of the 8th International Symposium on Tubular Structures*. Balkema, Rotterdam, The Netherlands (pp. 139-145).
- IIW Subcommittee XV-E (2008), "Static Design Procedure for Welded Hollow Section Joints - Recommendations", IIW Doc. XV-1281-08 and IIW Doc. XV-E-08-386, *International Institute of Welding Annual Assembly*, Graz, Austria.
- Kosteski, N. and Packer, J.A. (2003), "Longitudinal Plate and Through Plate-to-Hollow Structural Section Welded Connections", *Journal of Structural Engineering*, ASCE, Vol. 129, No. 4 (pp. 478-486).
- Kurobane, Y., Packer, J.A., Wardenier, J. and Yoemans, N. (2004), *Design Guide for Structural Hollow Section Column Connections*. CIDECT and Verlag TÜV Rheinland GmbH, Köln, Germany.
- Lee, M.M.K. and Llewelyn-Parry, A. (1999), "Strength of Ring-Stiffened Tubular T-joints in Offshore Structures – A Numerical Parametric Study", *Journal of Constructional Steel Research*, Vol. 51 (pp. 239-264).
- Lee, M.M.K. and Llewelyn-Parry, A. (2004), "Offshore Tubular T-joints Reinforced with Internal Plain Annular Ring Stiffeners", *Journal of Structural Engineering*, ASCE, Vol. 130, No. 6 (pp. 942-951).
- Lee, M.M.K. and Llewelyn-Parry, A. (2005), "Strength Prediction for Ring-Stiffened DT-joints in Offshore Jacket Structures", *Engineering Structures*, Vol. 27, (pp. 421-430).
- Lu, L.H., Winkel, G.D. de, Yu, Y. and Wardenier, J. (1994), "Deformation Limit for the Ultimate Strength of Hollow Section Joints", *Proceedings of the 6th International Symposium on Tubular Structures*. Balkema, Rotterdam, The Netherlands (pp. 341-347).
- Packer, J.A., Sherman, D.R. and Lecce, M. (2008), *HSS Connections Design Guide*. American Institute of Steel Construction, Chicago, Illinois, USA.
- Wardenier, J., Vegte, G.J. van der and Makino, Y. (2008a), "Joints between Plates or I Sections and a Circular Hollow Section Chord", *Proceedings of the 18th International Offshore and Polar Engineering Conference*. International Society of Offshore and Polar Engineers, Cupertino, California, USA.
- Wardenier, J., Kurobane, Y., Packer, J.A., Vegte, G.J. van der and Zhao, X.-L. (2008b), *Design Guide for Circular Hollow Section (CHS) Joints Under Predominantly Static Loading: Second Edition*. CIDECT and Verlag TÜV Rheinland GmbH, Köln, Germany.

Willibald, S. (2001), "The Static Strength of Ring-Stiffened Tubular T- and Y-Joints", *Proceedings of the 9th International Symposium on Tubular Structures*. Balkema, Rotterdam, The Netherlands (pp. 581-588).

STRAIN-BASED DESIGN OF STRUCTURAL CONNECTIONS

Peter Marshall

National University of Singapore, Singapore
mhpsyseng@aol.com

Xudong Qian

National University of Singapore, Singapore
cveqx@nus.edu.sg

ABSTRACT

This paper presents a CTOD-based limit strain approach ($\epsilon_{lim} = CTOD/l_{FE}$) to represent the progressive fracture failure frequently observed in welded connections. The proposed strain limit includes the element size to yield consistent predictions for a practical range of finite element sizes. This strain-based approach agrees, via different case studies, with the AWS fillet weld code provisions and with experimental results reported. On a micro-scale level, the strain-based approach predicts a consistent failure mode and load-deformation curve compared to the more rigorous microscopic Gurson material model.

INTRODUCTION

Background and Incentive

Ductile tearing at prior discontinuities in a welded connection often imposes critical threats to the safety of steel structures by causing rapid load reductions and therefore unstable structural failures. Detailed numerical approaches with micro-scale element sizes often embed assumptions on the crack growth path and direction (e.g., the discrete crack model) or require calibration of numerous material parameters (e.g., the damage mechanics model). Such approaches impose frequently a huge demand on the computational time for a practical joint dimension and become infeasible to be widely adopted in the present design offices. In contrast, integrity assessment procedures via a simple, strain-based engineering approach which can be easily implemented into commercial finite element packages offer computationally tractable solutions to practicing engineers, using T×T×T level or slightly more refined models. However, such approaches should demonstrate reasonable capabilities in predicting the load-deformation curves for structural connections of different geometries, material properties and fracture toughness characteristics. Meanwhile, they should also prove their consistency with the micro-scale material models which characterize ductile fracture through void growth, nucleation and coalescence at material length scales.

T×T Level Fatigue Analysis for Welded Connections

The T×T finite element analysis has found wide applications in the fatigue analysis of tubular and non-tubular welded connections to compute the hotspot stresses/strains. The last few decades observe significant developments in catalogues of empirical S-N curves for different structural details, upon which the fatigue life can be estimated through simple, linear-elastic finite element analysis performed using thin shell T×T or T×T×T solid elements, coupled with an idealized damage accumulation rule, e.g., Miner's rule (Marshall, 2006). The hotspot stress/strain concept places many different connection geometries on a common basis, by measuring both the membrane and shell bending stresses. A standard experimental procedure records the hotspot stress using strain gauges positioned adjacent to the weld toe, but not in the local weld toe notch, the effect of which is included in the empirical S-N curve. For smooth concave weld profiles adjoining the base metal, the notch effects remain similar to that for the edge of a butt weld.

Originally developed for offshore applications, the hotspot stress approach has now extended to the fatigue assessment of tubular highway bridges and plated structures such as marine hulls and orthotropic bridges. Marshall et al. (1998) presented a finite element stress analysis using T×T shell models for a 160,000-ton bulker which typically repairs up to 60 fatigue cracks at each 5-year dry-docking. Design guidelines (Hobbacher, 2003) has formulated standard procedures in using T×T or T×T×T finite element approach to compute hotspot stresses for plate-type details in ship hulls. The fatigue assessment of the connection details in floating, production, storage and offloading (FPSO) ships adopts more conservative S-N curves and safety factors due to the long-term operational requirement and the high intensity of stress fields caused by the more severe weld toe notches (Salama et al., 2004). The American Welding Society (AWS) Structural Welding Committee is in the process of developing a synchronized hotspot approach for the fatigue analysis of tubular and non-tubular connections (Marshall and Wardenier, 2005).

The treatment of fatigue analysis via the T×T level model might remain as a coarse estimation to many researchers. However, the linear-elastic finite element stress analysis yields a progressively higher stresses with increasing mesh refinement. Consequently, the adoption of a more detailed mesh than the T×T level model requires the use of a correspondingly higher notch stress S-N curve (Hobbacher, 2003).

A Strain-Based Approach for Progressive Failure

This study proposes a practical strain-based engineering approach to represent the progressive ductile fracture failure, frequently incurred in testing welded joints, using a finite element procedure. The proposed strain limit follows rationally a linear relationship with the material fracture toughness, measured by the critical crack-tip opening displacement (CTOD), and an inverse relationship with respect to the element size.

The following section summarizes briefly the common strain limit approaches adopted to define ultimate strength of welded structural connections. The next section

demonstrates the feasibility of the proposed strain limit approach in different applications. The last section summarizes the key conclusions drawn from the current study. A companion paper will explore the validity of the strain limit approach from a micro-scale material model.

A STRAIN LIMIT APPROACH

Towards the objective to represent progressive ductile fracture failure through finite element methods, the first intuition is to limit the strength of a structural connection at a constant strain level applied to the T×T shell or T×T×T 3-D elements, consistent with the modeling approach for fatigue analysis. In contrast to the linear-elastic fatigue analysis, this type of finite element approach often requires accurate representation on both the elastic-plastic material properties and the large deformation response of the element. This simple strain limit incorporated in the continuum-mechanics-based finite element analysis offers a computationally tractable solution to estimate the ultimate strength of the welded structural details influenced by the crack initiation and propagation.

However, determination of a correct constant strain limit remains the key to the success of such an approach and becomes extraordinarily challenging for a wide range of geometries under a large spectrum of loading. From previous evidences, the practical strain-limit ranges from 5 to 10 times the yield strain, or approximately 2% for welded details under membrane-type of plastic deformation and for demand-critical welded connections under earthquake loads. For the ultimate strength of tubular joints subjected to significant shell bending, researchers normally adopt a higher tensile strain limit of 15%, extending their behavior beyond the observation of the first crack at 2-3% of strain level. This proves to be consistent with the experimental measurements on the reduced-scale tubular specimens. However, thicker sections in offshore platforms may require a lower strain threshold due to the limited material toughness and size effects, if specialized node steel is not used in the chord.

The load-deformation relationship described in AWS (AWS, 2008) for the fillet welds provides a means to calibrate a uniform strain limit applied to different loading directions (See Fig. 1). Figure 2a shows the application of the calibrated strain limits to a girder-to-tube joint failure in the SP8X platform. The modeling of fillet welds (of 0.31"-0.37" in size) between the girder and the circular hollow section (CHS) member employ 3 spring elements calibrated from Fig. 1 to represent the load-deformation characteristics of fillet welds in 3 global directions. The girder and CHS adopt 8-node T×T shell elements. This "phenomenological" finite element model reproduces the unzipping failure observed in the real joint as shown in Fig. 2b (Qian and Marshall, 2007).

Engineering critical assessment (ECA), as described in BS 7910 (2005), provides an alternative approach to the constant strain limit by defining a maximum permissible flaw size through a fracture toughness parameter, measured by K_{IC} , δ_c or J_{IC} . The maximum load capacity due to the presence of a crack derives from the failure assessment diagram (FAD), which defines the interaction of two competing failure modes: the overload failure and the ductile fracture.

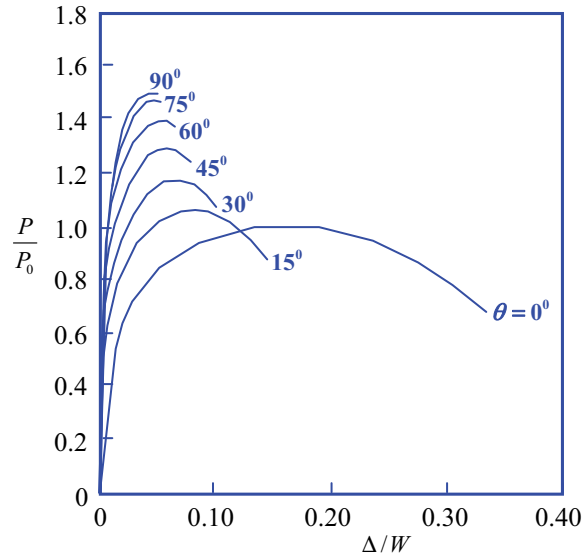


Fig. 1: AWS (2008) load-deformation relations for fillet welds.

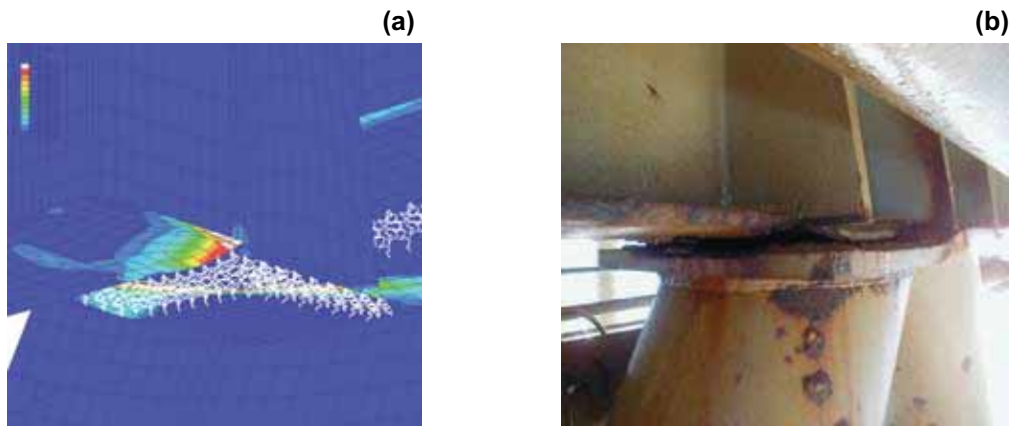


Fig. 2: (a) Stitch model for fillet welds in a girder-to-CHS joint; (b) Unzipping failure for the real joint.

A “DEATH STRAIN” APPROACH

Representation of the progressive failure through a finite element procedure can be done by “killing” of the highly strained/stressed elements along the crack propagation path. Packer (2005) proposes an approach to enforce the “death” of an element via modifying the stress-strain relationship. Figure 3 shows the stress-strain relationship used in a gusset-tube welded connection, of which the experimental study is reported by Cheng and Kulak (2000). The numerical procedure assigns the “death strain” properties to the base metal in the tube. The “death strain” analysis reproduces the observed shear-lag progressive fracture failure mode for L/D of 1.57. Figure 4 compares the load-deformation curves obtained from a conventional finite element approach and the death strain analysis for a shorter gusset-tube connection under axial tension. The

“death strain” analysis provides a consistent estimation on the ultimate capacity of the gusset-tube connection compared to the AISC shear lag formulation.

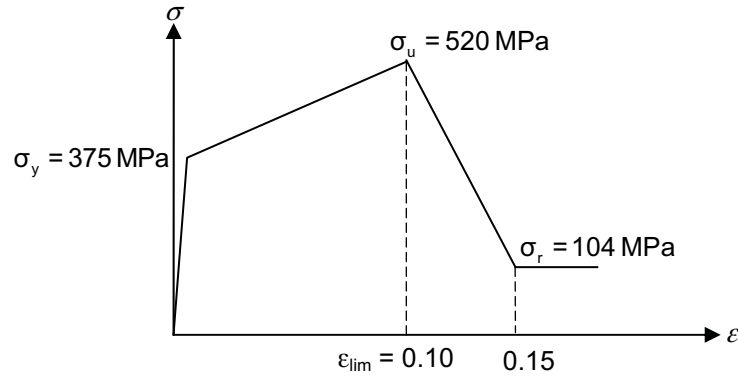


Fig. 3: Stress-strain relationship used in the analysis of the gusset-tube connection.

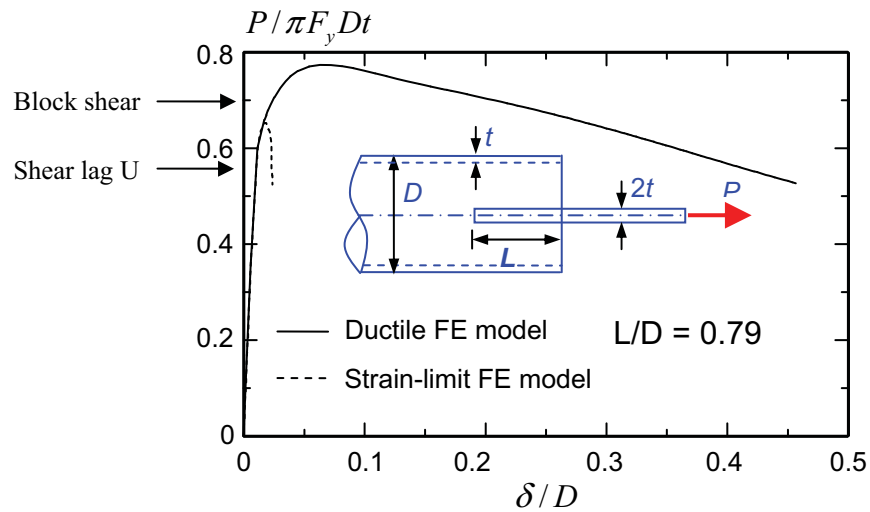


Fig. 4: Comparison of FE analysis without “death strain” and that with “death strain” implementation for a gusset-to-tube connection.

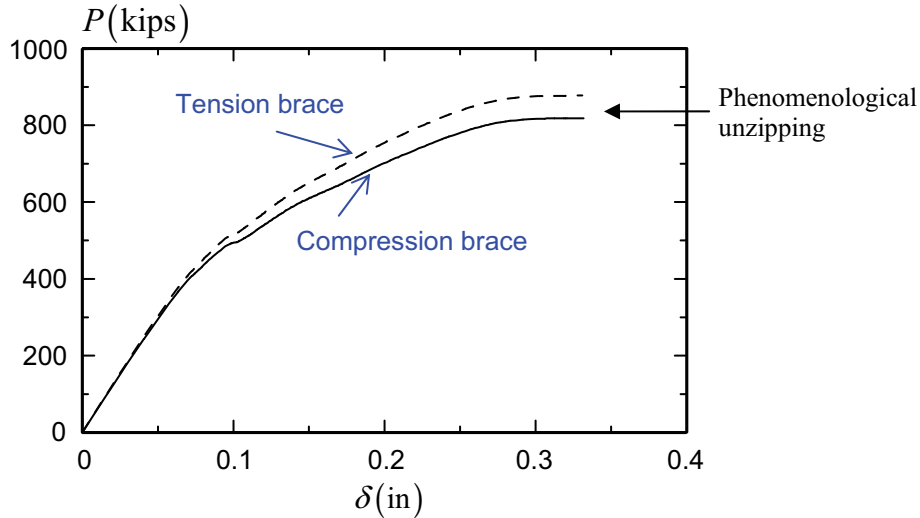


Fig. 5: Load-deformation curves for the girder-to-CHS connection in SP8X platform.

Figure 5 shows another application of the “death strain” analysis to the girder-to-CHS connection previously shown in Fig. 2. The finite element model includes a total of 24,000 20-node elements and 125,000 nodes, with the element size around the fillet welds about $T/2 \times T/2$. The analysis takes about 72 hours in a 64-bit SUN Linux workstation with 2 GB RAM. The predicted ultimate capacity is consistent with the simpler phenomenological representation utilized in Fig. 2.

CTOD-BASED DEATH STRAIN

The above examples demonstrate that the “death strain” approach provides a feasible scheme to represent the progressive ductile tearing in welded connections. However, quantification of the limiting strain, ϵ_{lim} , in Fig. 3, depends on the element size, elastic-plastic material properties and the material toughness level. A reasonably accurate definition of this strain limit, therefore, requires coupling of a material parameter that includes the effects of material properties and toughness, and a length scale parameter that represents the size of the finite element used. The crack-tip opening displacement (CTOD) evolves as a natural choice of the material parameter since it characterizes the fracture toughness for different types of steels. Figure 6 presents the proposed strain limit with respect to element size. A constant strain level of 20% prevents the unbounded increase in the strain limit for very small elements.

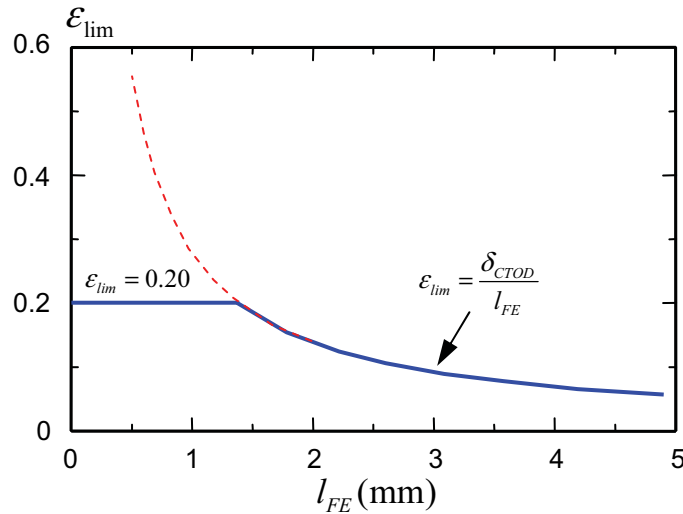


Fig. 6: Proposed strain limit for the “death strain” approach.

Verification of this strain limit employs two examples. Figure 7 shows the load deformation curves obtained from a cruciform joint, where the fillet welds remain perpendicular to the loading axis. The critical displacements and ultimate load levels cluster closely around the AWS target (Fig. 1), with the very refined mesh ($l_{FE} < 1\text{mm}$) showing slightly more brittle responses. Models with larger elements ($l_{FE} \geq 1\text{mm}$) in Fig. 7 demonstrate the marginal element-size dependence of the FE analysis. Figure 8 compares the load-deformation curve for a B×2B single-edge notched bend, SE(B) specimen computed by the proposed strain-limit approach and the experimental results reported by Gubeljak et al. (2002). The “death strain” finite element analysis shows consistent load-deformation relationship with the experimental record. Rapid load reductions did not occur in the experiment, nor was it predicted in the numerical analysis, for this ductile material.

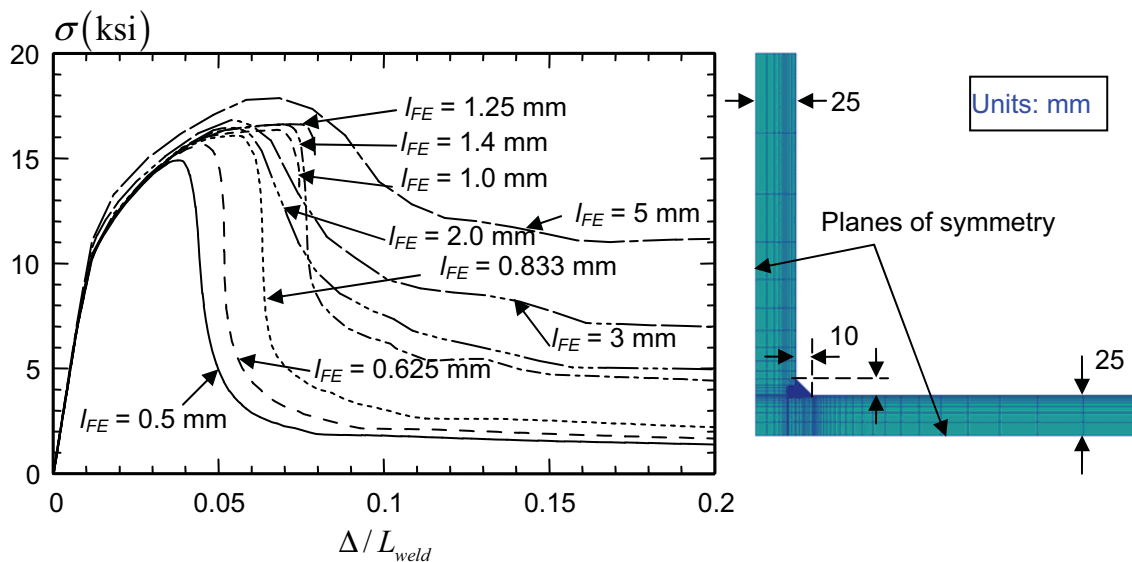


Fig. 7: Load-deformation curves for a cruciform joint with welds modeled by different element size.

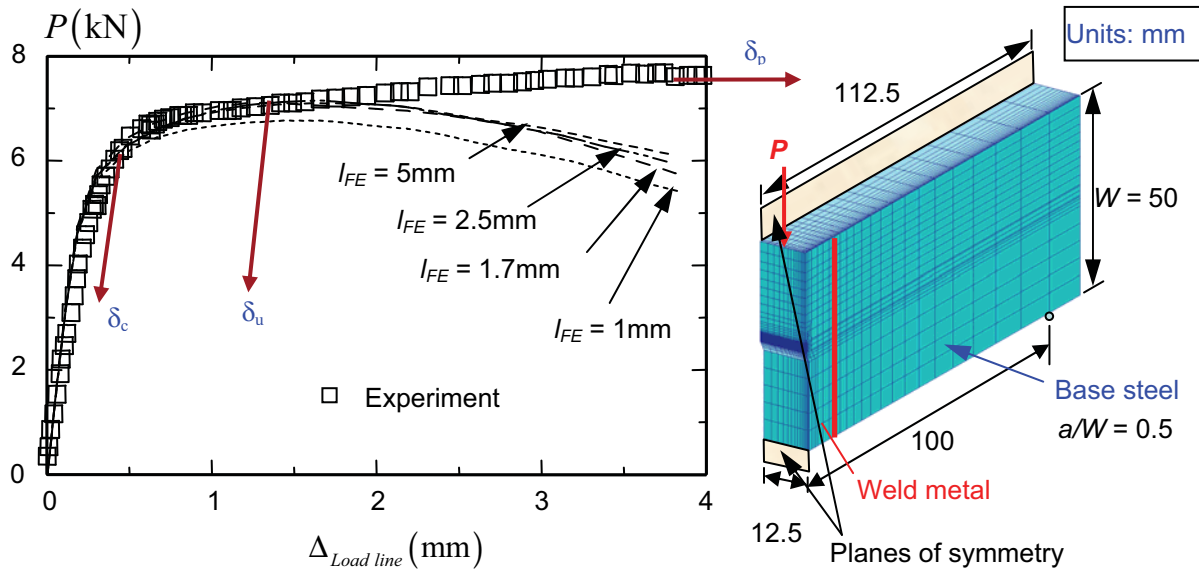


Fig. 8: Load-deformation curves for a SE(B) specimen modeled using different element sizes.

GURSON DUCTILE FRACTURE MODELS

The Gurson model (Gurson, 1977) represents a more rigorous, but more computationally demanding approach to simulate the ductile fracture procedure through void growth, nucleation and coalescence. The Gurson model modifies the von mises yield criterion via the void volume fraction, which grows with increasing volume change under plastic deformation. The yield criterion in the Gurson model follows,

$$\phi = \left(\frac{\sigma_e}{\sigma_0} \right)^2 + 2q_1 f \cosh \left(\frac{3q_2 \sigma_m}{2\sigma_0} \right) - (1 + q_3 f^2) = 0 \quad (1)$$

where σ_e denotes the effective Mises stress, σ_m refers to the hydrostatic (mean) stress, σ_0 defines the current flow stress and f specifies the current void fraction in the material. Faleskog et al. (1998) report the q -factors used to model the strong effect of strain-hardening on the void growth rate. The growth of the void volume fraction, f , follows,

$$df_{growth} = (1 - f) d\varepsilon_{kk}^p, \quad (2)$$

The nucleation of the void volume follows a mathematical model that assumes a normal distribution of the nucleation strain as shown in Eq. 3, with ε_e^p denoting effective plastic strain.

$$df_{nucleation} = \frac{f_N}{s_N \sqrt{2\pi}} \exp \left[-\frac{1}{2} \left(\frac{\varepsilon_e^p - \varepsilon_N}{s_N} \right)^2 \right] d\varepsilon_e^p \quad (3)$$

where ε_N defines the nucleation strain, s_N denotes the standard deviation of ε_N and f_N refers to the void volume fractions of the nucleating particles.

Figure 9 illustrates the calibration of the Gurson material parameters for a blunt-notched tensile bar (reported by Chi et al., 2006), together with the calibrated material properties. Figure 10 shows the load-deformation curve and failure mode for the cruciform fillet welds, comparable to the other methods shown earlier in this paper.

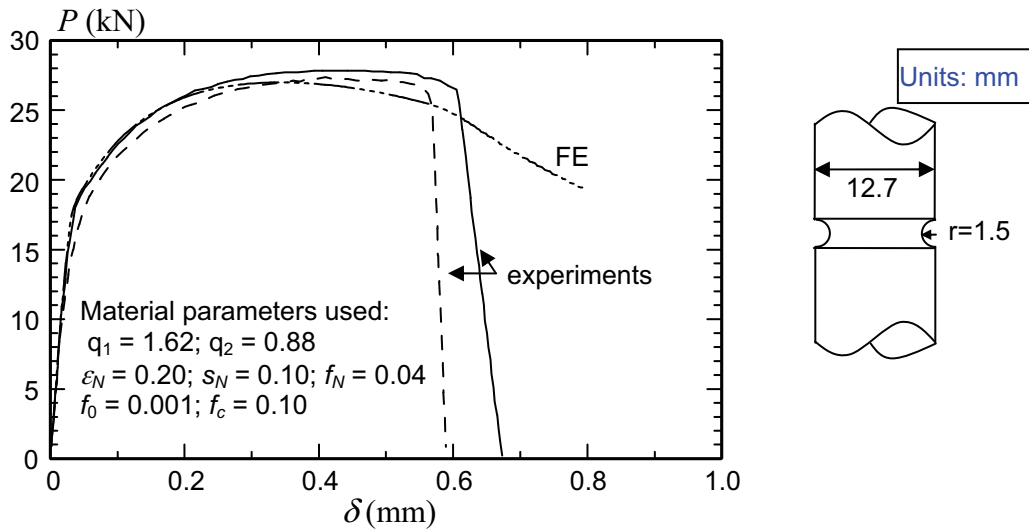


Fig. 9. Calibration of the Gurson model parameters from a blunt-notched tension bar.

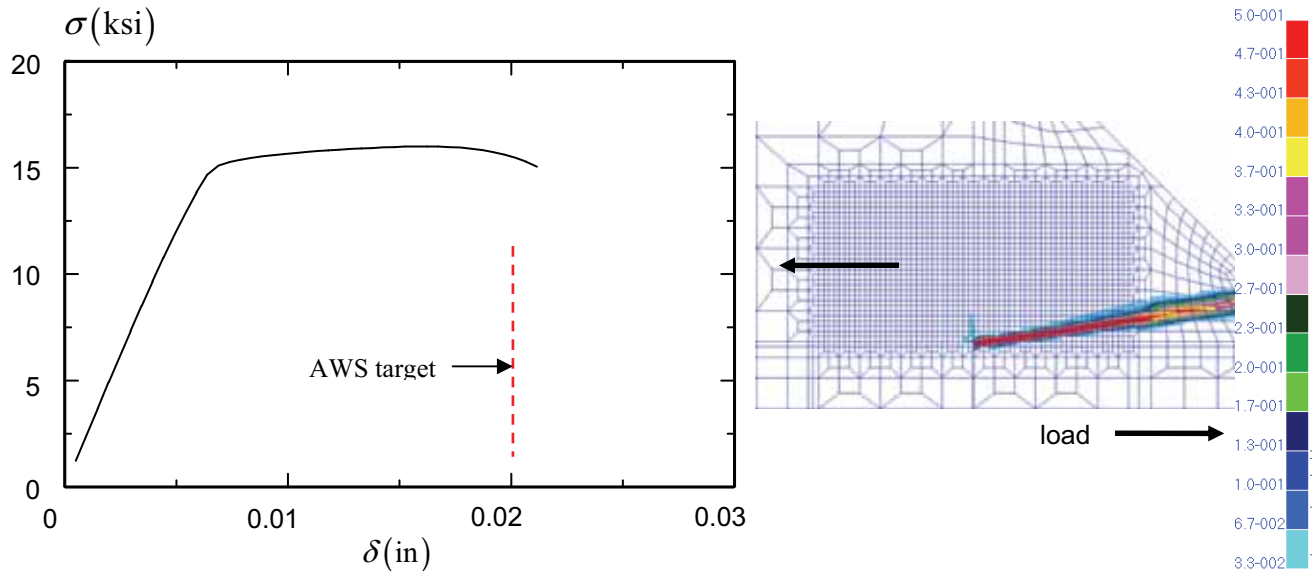


Fig. 10: Load-deformation curves and failure modes for the cruciform joint computed using the Gurson material model.

SUMMARY AND CONCLUSIONS

This paper proposes a simple numerical treatment of the progressive ductile fracture failure frequently observed in welded structures. The CTOD-based “death strain” approach defines a strain limit coupling the critical crack-tip opening displacement with the size of the finite element used. The Gurson mathematical model offers a more rigorous approach to represent the ductile tearing process caused by void growth, nucleation and coalescence. Case studies of various welded structural details support the following conclusions:

- 1) Unlimited deformation capacity, which remains as the default assumption in conventional finite element analysis, yield unsafe (upper-bound) predictions on the ultimate strength
- 2) The “death strain” approach becomes very conservative in estimating the ultimate strength when applied in models with very small element sizes ($< 1\text{mm}$). The proposed “optimum” element size for this approach ranges from 2-5mm for different types of connection details studied.
- 3) Applying a calibrated Gurson material model to a variety of configurations reproduces the load-deformation and failure modes at the load level corresponding to the proposed CTOD-based “death strain” limit in models with different element sizes.

REFERENCES

- American Society of Testing and Materials. (2001). E 1820-01 *Standard Test Method for Measurement of Fracture Toughness*.
- American Welding Society. (2008), *Structural Welding Code – Steel*, AWS D1.1/D1.1M:2008.
- British Standards Institution. (2005), BS 7910:2005, *Guide to Methods for Assessing the Acceptability of Flaws in Metallic Structures*.
- Cheng, J. J. R. and Kulak, G. L. (2000), “Gusset Plate Connection to Round HSS Tension Members”, *AISC - Engineering Journal*, Vol 37, No. 4, pp. 33-139.
- Chi, W. M., Kanvinde, A. M., and Deierlein, G. G. (2006), “Prediction of Ductile Fracture in Steel Connections Using SMCS Criterion”, *ASCE – Journal of Structural Engineering*, Vol 132, No. 2, pp. 171-181.
- Faleskog, J., Gao, X., and Shih, C. F. (1998). “Cell Model for Nonlinear Fracture Analysis – I. Micromechanics Calibration” *International Journal of Fracture*, Vol 89 pp. 355-373.
- Gubeljak, N., Legat, J. and Kocak, M. (2002). “Effect of Fracture Path on the Toughness of Weld Metal”. *International Journal of Fracture*, Vol 115, pp. 343-359.

- Gurson, A. L. (1977). "Continuum Theory of Ductile Rupture by Void Nucleation and Growth: Part I-Yield Criteria and Flow Rules for Porous Ductile Media." *Journal of Engineering Material Technology*, Vol 99 No. 1, pp. 2-15.
- Hobbacher, A. (2003), Recommendations for Fatigue Design of Welded Joints and Components. International Institute of Welding (IIW) Doc. XIII-1965-02/ XV-1127-03.
- Marshall, P. W. (2006), "Punching Shear and Hot Spot Stress: Back to the Future?", Kurobane Lecture, *Proceedings of the 11th International Symposium on Tubular Structures, ISTS 11*, Quebec.
- Marshall, P. W. et al. (1998), "Bulk Carrier Structural Integrity: Predicting Fatigue Life with Influence Functions.", *Proceedings of RINA Conference: Design and Operation of Bulk Carriers*, London.
- Marshall, P. W. and Wardenier, J. (2005), "Tubular and Non-Tubular Hot Spot Stress", *Proceedings of 15th International Conference on Offshore and Polar Engineering, ISOPE-2005*, Seoul
- Packer, J. A. (2005), "Tubular Brace Member Connection in Braced Steel Frames" *Proceedings of 11th International Symposium in Tubular Structures*, Quebec.
- Qian, X., Choo, Y. S., Liew, J. Y. R. and Wardenier, J. (2005). "Simulation of Ductile Fracture of CHS Joints Using the Gurson Model", *ASCE – Journal of Structural Engineering*, Vol 131. No. 5, pp. 768-780.
- Qian, X. and Marshall, P. W. (2007). "Unzipping Analysis of a Full-Scale Offshore Structure Connection." *Proceedings of the 5th International Conference on Advanced Steel Structures*. Singapore.
- Salama, M. M. (2004), *Proceedings of OMAE FPSO-04*, ASME International Petroleum Technology Institute, Houston.

STRUCTURAL RESPONSE OF K AND T TUBULAR JOINTS UNDER STATIC LOADING

Luciano R. O. de Lima, Pedro C. G. da S. Vellasco, Sebastião A. L. de Andrade
Structural Engineering Department, UERJ, Rio de Janeiro, Brazil
lucianolima@uerj.br; vellasco@uerj.br; seb.andrade@uol.com.br

José G. S. da Silva
Mechanical Engineering Department, UERJ, Rio de Janeiro, Brazil
jgss@uerj.br

Luís F. da C. Neves
Civil Engineering Department, Coimbra, Portugal
luis@dec.uc.pt

Mateus C. Bittencourt
Civil Engineering Post-Graduate Program, UERJ, Rio de Janeiro, Brazil
matebittencourt@yahoo.com.br

Abstract: The intensive worldwide use of tubular structural elements, mainly due to its associated aesthetical and structural advantages, led designers to be focused on the technologic and design issues. Consequently, their design methods accuracy plays a fundamental role when economical and safety points of view are considered. Additionally, recent tubular joint studies indicate further research needs, especially for some joint geometries. In this work, a nonlinear numerical analysis based on a parametric study is presented, for K and T tubular joints where both chords and braces are made of hollow tubular sections. Starting from test results available in the literature, a model has been derived, taking into account the weld geometry, material and geometric nonlinearities. The proposed model was validated by comparison to the experiments, analytical results suggested on the Eurocode 3 (2003) and to the classic deformation limits proposed in literature.

INTRODUCTION

Structural hollow sections (Figure 1) are widely used by designers, due to their aesthetical and structural advantages (Packer et al., 1992). On the other hand, the adoption of tubular sections frequently leads to more expensive and complex connections, since there is no access to the interior of the connected parts. This problem can be solved by special blind bolted connections or, more frequently, by the extensive use of welded joints. In addition to the fabrication costs, a proper connection design has to be performed since their behaviour frequently governs the overall structural response. This paper deals with the structural behaviour of SHS “T” joints and CHS “K” joints widely used in trusses under static loading (Figure 2). The effects of shear, punching shear and bending are considered to predict the possible joint failure mechanisms.

The circular hollow section (CHS) K-joint configuration is commonly adopted in steel offshore platforms (e.g. jackets and jack-ups) which are designed for extreme environmental conditions during their operational life. The ultimate and service strengths of such structures significantly depend on the component (member and joint) responses. Consequently, in the past few years various research programmes on tubular joints funded by oil and gas companies and national governments were initiated.



Figure 1. Examples of tubular structures with T and K tubular joints

Traditionally, design rules for hollow sections joints are based on either plastic analysis or on a deformation limit criteria. The use of plastic analysis to define the joint ultimate limit state is based on a plastic mechanism corresponding to the assumed yield line pattern. Typical examples of these approaches can be found on Packer et al (1992), Cao et al (1998), Packer (1993), Choo et al. (2006) and Kosteski et al (2003). Each plastic mechanism is associated to a unique ultimate load that is directly related to this particular failure mechanism. The typically adopted yield lines were: straight, circular, or a combination of those patterns.

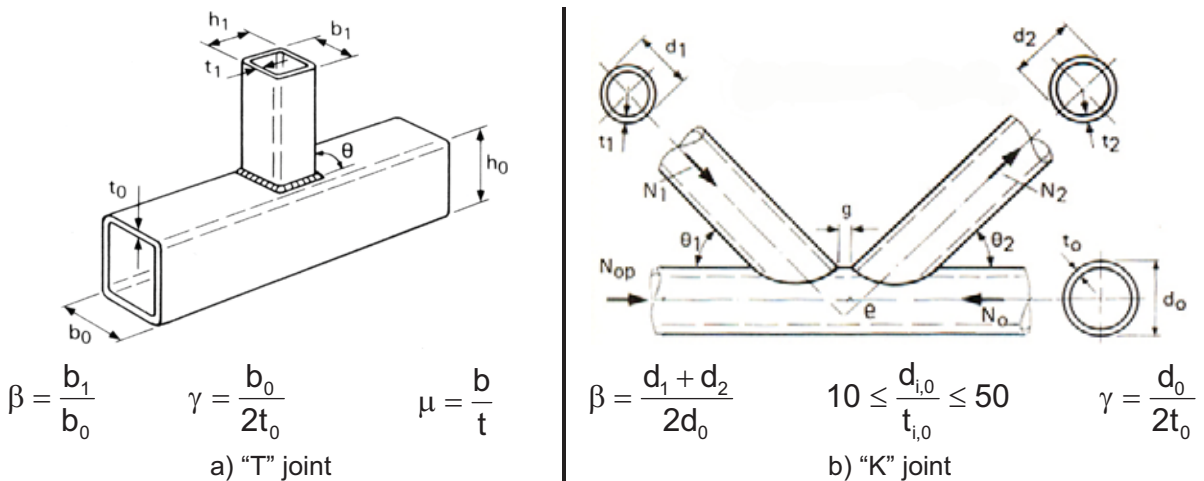


Figure 2. Joint geometry and governing parameters, Eurocode 3 (2005)

Deformation limits criteria usually associate the ultimate limit state of the chord face to a maximum out of plane deformation of this component. The justification for a deformation limit criterion instead of the use of plastic analysis for the prediction of the ultimate limit state is that, for slender chord faces, the joint stiffness is not exhausted after the complete onset of yielding, and can assume quite large values

due to membrane effects. This phenomenon is clearly shown in the curves obtained from the material and geometrical nonlinear finite element analysis performed in the present study. It is evident that, if the maximum load is obtained from experimental curves, the absence of a “knee” in the curve could complicate the identification of this ultimate limit state point. Additionally, there is still the need of further comparisons to experimental and plastic analysis results based on a deformation criteria.

For T tubular joints, Korol and Mirza (1982) proposed that the ultimate limit state should be associated to a chord face displacement of 1.2 times its thickness. This value is approximately equal to 25 times the chord face elastic deformation. Lu et al (1994) proposed that the joint ultimate limit state should be associated to an out of plane deformation equal to 3% of the face width, corresponding to the maximum load reached in their experimental study. This 3% limit was proposed as well by Zhao (1991), and is actually adopted by the International Institute of Welding to define this particular ultimate limit state.

Similarly, for K tubular joints, the deformation limit proposed by Lu et al. (1994) and reported by Choo et al. (2003) may be used to evaluate the axial and/or rotational capacity of a joint subjected to the corresponding brace axial or moment loads. The joint strength is based on a comparison of the deformation at the brace-chord intersection for two strength levels: the ultimate strength, N_u which corresponds to a chord indentation, $\Delta_u = 0.03d_0$, and the serviceability strength, N_s that is related to $\Delta_s = 0.01d_0$. Lu et al. (1994) stated that the first peak in the load-deformation diagram should be used if it corresponds to a deformation smaller than the limit $\Delta_u = 0.03d_0$. According to Lu et al. (1994), if the ratio of N_u/N_s is greater than 1.5, the joint strength should be based on the ultimate limit state, and if $N_u/N_s < 1.5$, the serviceability limit state controls the design. In the case of CHS joints, $N_u/N_s > 1.5$ and the appropriate deformation limit to be used to determine the ultimate joint strength should be equal to $0.03d_0$.

EUROCODE 3 PROVISIONS (Eurocode 3, 2005)

For connections between CHS joints, such as the ones represented in Fig. 1 and Fig. 2, the methodology proposed by the Eurocode 3 (2003) part 1-8 is based on the assumption that these joints are pinned. Therefore the relevant design characteristic (in addition to the deformation capacity) is the chord and braces strength, primarily subjected to axial forces according to Eurocode 3 (2003) provisions. Equation (1) and (2) define, according to Eurocode 3 (2003), the chord face plastic load for the investigated T and “K” joint, respectively, with the geometric parameters defined in Figure 2. $N_{1,Rd}$ is the brace axial load related to the development of the chord face yielding or punching limit states.

$$N_{1,Rd} = \frac{k_n f_{y0} t_0^2}{(1-\beta) \sin \theta_1} \left(\frac{2\beta}{\sin \theta_1} + 4\sqrt{1-\beta} \right) \quad (1)$$

where k_n is 1,0 for tensioned members, f_{y0} is the chord yield stress, t_0 the chord thickness, β is a geometrical parameter defined in Figure 2 and θ_1 the angle between the chord and the brace.

$$N_{1,Rd} = \frac{k_g k_p f_{y0} t_0^2}{\sin \theta_1} \left(1.8 + 10.2 \frac{d_1}{d_0} \right) / \gamma_{M5} \quad \text{and} \quad N_{2,Rd} = \frac{\sin \theta_1}{\sin \theta_2} N_{1,Rd} \quad (2)$$

where f_{y0} is the chord yield stress, t_0 the chord thickness, θ_1 and θ_2 are the angle between the chord and the braces, k_p and k_g can be obtained from eq. (3).

$$k_g = \gamma^{0.2} \left(1 + \frac{0.024\gamma^{1.2}}{1 + \exp(0.5g/t_0 - 1.33)} \right); k_p = 1 - 0.3 n_p(1 + n_p) \leq 1.0; n_p = \frac{N_{p,Sd}}{A_0 f_{y0}} + \frac{M_{0,Sd}}{W_0 f_{y0}} \quad (3)$$

NUMERICAL MODEL – CALIBRATION AND RESULTS

Tubular joints are most commonly modelled by shell elements that represent the mid-surfaces of the joint member walls. The welds are usually represented by shell (see Figure 3) or three-dimensional solid elements, may be included or not in the model. It is common practice to analyse this type of joints without an explicit consideration of the welds. This is made simply modelling the mid-surfaces of the member walls using shell elements, Lee (1999) and Lie et al. (2006). Despite this fact, some authors stated that this effect may be significant especially for K-joints with a gap, since the weld does not have a negligible size when compared to the gap size, Lie et al. (2006). In the present investigation the weld for T joint was firstly modelled by using a ring of shell elements (SHELL 181 - four nodes with six degree of freedom per node), Figure 3, similarly to the configuration proposed by Lee (1999) and Van der Vegte et al. (2007). Afterwards, solid elements (SOLID45 - eight nodes with three d.o.f. at each node) were used to considerate the joint welds to properly assess its influence.

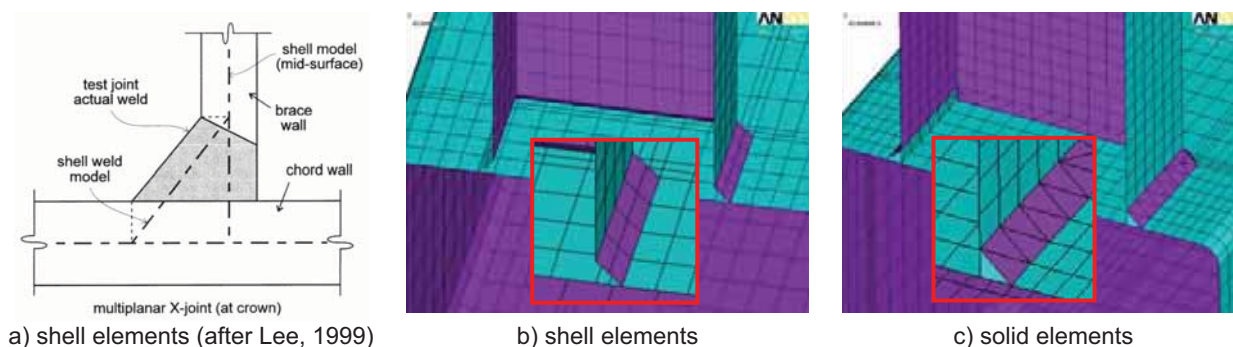


Figure 3. Modelling of the welds

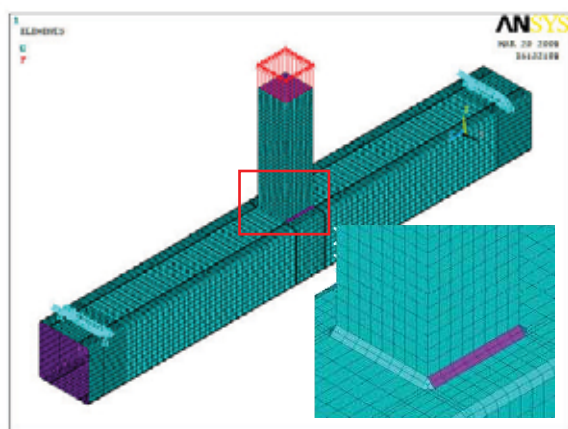
For an ultimate strength analysis, this approach is generally acknowledged as sufficiently accurate to simulate the overall joint structural response. The decisions on the choice of element and the better strategy to represent the welds (if included), should be made in advance since it determines the model layout and the required mesh density.

The finite element models in the present study were generated using automatic mesh generation procedures. A finite element model adopted four-node thick shell elements, therefore considering bending, shear and membrane deformations. For the “T” joint model calibration, the numerical results found in Lie *et al.* (2006) (T1 & T2 models) were used. Their mechanical and geometrical properties are depicted in Table 1. For the T1 joint, the parameters of Figure 2 assumes values of $\beta = 0.57$, $\mu_0 = 23.3$, $\mu_1 = 12.5$ and $\gamma_0 = 11.67$. It should be noted that a value of $\beta = 0.57$ is not critical.

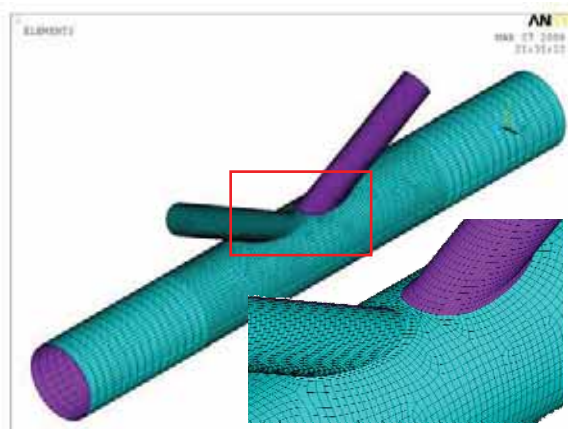
The complete model was made of 9482 nodes and 9284 elements (see Figure 4) and the analysis was performed using the Ansys 10.0 (2005) program. The model calibration was performed on a RHS T-joint considering material and geometric nonlinearities (see Figure 5). The material non-linearity was considered by using a Von Mises yield criterion associated to a three-linear stress-strain relationship to incorporate strain hardening of 5% and 10%, respectively. The geometrical non-linearity was introduced in the model by using a Updated Lagrangean formulation. A refined mesh was used near the weld, where a stress concentration is likely to occur. An effort was made to create a regular mesh with well proportioned elements to avoid numerical problems. The load was applied in terms of force in the extremity of the brace.

Table 1. Mechanical and geometrical properties – T1 and T2 models (Lie *et al.*,2006)

Specimen	b_0 (mm)	h_0 (mm)	t_0 (mm)	b_1 (mm)	h_1 (mm)	t_1 (mm)	t_w (mm)	f_y (MPa)	f_u (MPa)	f_w (MPa)
T1	350	350	15	200	200	16	12	380.3	529.0	600
T2	350	350	15	200	200	12	12	380.3	529.0	600

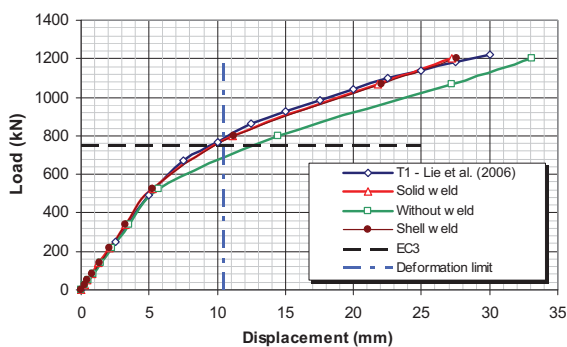


a) "T" tubular joint

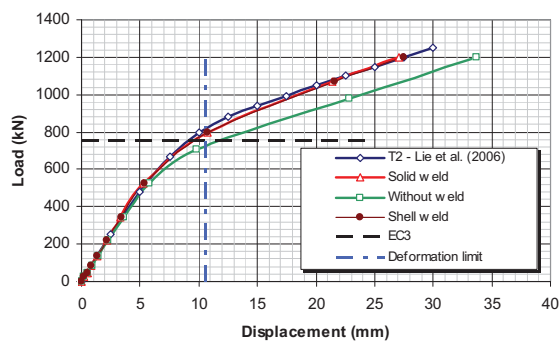


b) "K" tubular joint

Figure 4. Finite element model performed in Ansys 10.0 software (2005)



a) T1 tubular joint



b) T2 tubular joint

Figure 5. Results comparison – "T" tubular joints

Considering the "K" joint model based on Choo *et al.* (2006), different boundary conditions may impose significant effects on the joint strength, altering chord axial stress magnitudes, chord bending stress magnitudes and introducing additional brace bending loads on the brace versus chord intersection. At present,

there are insufficient data from experiments to provide a good basis to characterise the ideal boundary conditions that could represent the effects imposed by adjacent structural members on the particular investigated joint, (Choo et al., 2006).

Lee (1999), states that the best way to model the boundary conditions of a K joint to simplify the test layout procedures is to consider the pinned brace ends with the translations in all coordinate directions fixed at the nodes. The load was applied by means of displacements at the nodes present at the right end of the chord while the left end was left unrestrained in the horizontal direction (see Figure 6).

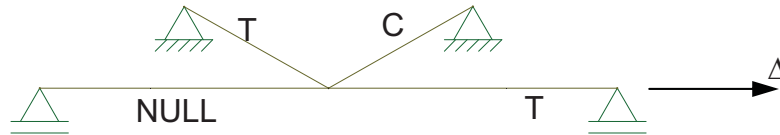


Figure 6. Applied boundary conditions on the “K” tubular joint numerical model

The geometrical and mechanical properties of the “K” joint model are presented in Table 2. These parameters lead to values of $\beta = d_1 / d_0 = 0.40$, $\gamma = 18 < 25$, $0.2 < d_i / d_0 = 0.4 < 1.0$, $10 < d_0 / t_0 = 18 < 50$ and $10 < d_i / t_i = 14.4 < 50$. It must be emphasized that these parameters satisfy the Eurocode 3 limits (Eurocode 3, 2005). For this numerical model a full material (a bilinear material model was considered with a 5% strain hardening) and a geometric nonlinear analysis was also performed.

Table 2. Mechanical and geometrical properties – K joint

d_0 (mm)	t_0 (mm)	$d_1 = d_2$ (mm)	$t_1 = t_2$ (mm)	$\theta_1 = \theta_2$ (°)	e (mm)	g (mm)	f_y (MPa)	f_u (MPa)	f_w (MPa)
406	11.28	162.4	11.28	30	0	378.4	355	430	600.0

The results allow the assessment of the Eurocode 3 (2003) performance not only in terms of maximum load (however the maximum numerical load is compared to the plastic load calculated from the Eurocode 3, 2003), but also in terms of the load versus displacement curve. This may lead to the derivation of conclusions in terms of the stiffness and post-limit behaviour of the chord face, namely for the assessment of the performance of deformation limits criteria for the chord face resistance, or for the evaluation of the available joint over-strength achieved by membrane action.

Figure 7(a) presents the load versus axial displacement curves for the brace members. From this figure it may be observed that, in the elastic range, an excellent agreement of the curves was obtained. Figure 7(b) presents the load versus axial displacement curve for the chord member.

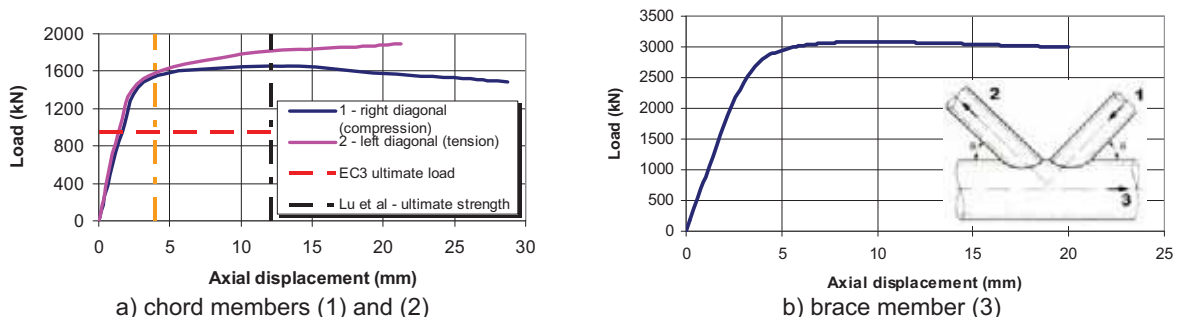


Figure 7. Load versus displacement curves

According to the deformation limit proposed by Lu et al. (2004), and reported by Choo et al. (2006), $N_s = 1550\text{kN}$ and $N_u = 1650\text{kN}$. Using Eurocode 3 (Eurocode 3, 2005) provisions, the joint ultimate load, also represented in Fig. 7 is equal to 946kN being an inferior limit to the numerical model results. The joint ultimate load was controlled by the chord local buckling at the compression brace member region (see Figure 8, where the Von Mises stress distribution of the model that did not explicitly considered the welds are presented).

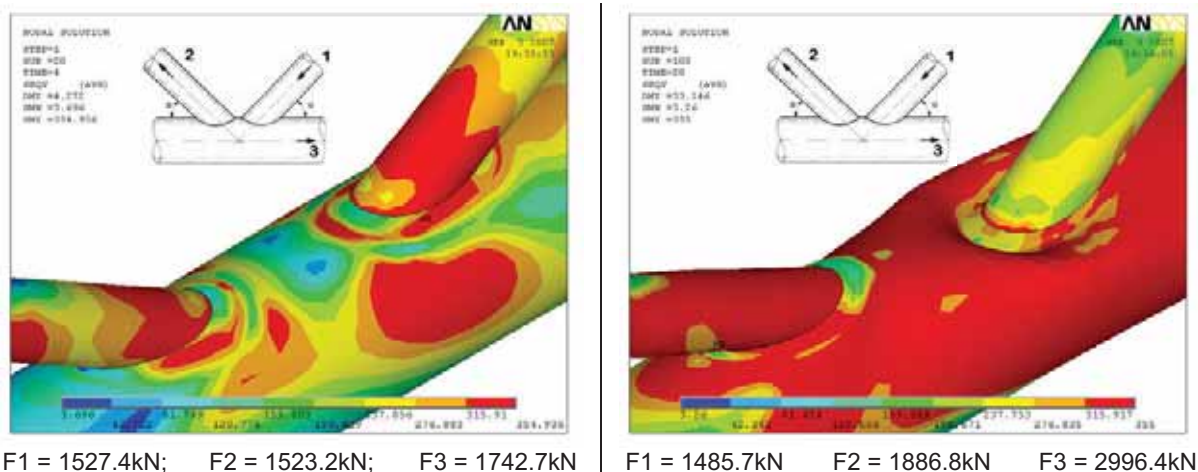


Figure 8. Von Mises stress distribution (in MPa) – deformed scale factor equal to 2

PARAMETRICAL ANALYSIS

To evaluate the influence of the parameter β on the “T” joint global behaviour, five models were used in a parametric analysis, keeping the same chord for all models ($350 \times 350 \times 15$). The same mechanical properties early used were adopted i.e.: the braces width were: 90, 180, 260, 280 and 300 mm, that correspond to values of β of 0.25, 0.50, 0.75, 0.80 and 0.857, respectively. The results are presented in Figure 9. As expected, increasing the value of β leads to a strong increase in the strength of the connection specially if $\beta \leq 0,75$. However, if $\beta \geq 0,75$, an increase of this parameter leads to an increase of strength with a magnitude much smaller than expected. This is due to the fact that for large values of β , the limit state related to bending does not control, while shear and punching shear begins to be the governing limit states.

The individual load versus displacement curves are presented in Figure 9. Through the observation of these curves, it may be concluded that the numerical results have in general a good agreement with the Eurocode 3 (2003) provisions. The joint resistance was derived at a load magnitude corresponding to a limit deformation of the chord face deformation of 3% of the chord width, i.e., 10.5 mm according to the proposal of Lu et al. (1994). However, the last model where $\beta = 0.857$, presented different results when compared to Eurocode 3 (2003) provisions.

Three additional models were included in the parametric analysis to evaluate the influence of the ratio diameter by thickness on chord of “K” joint global behaviour, more, keeping the same brace characteristics for all models ($\phi 406 \times 11.28$). The same mechanical properties early used were also adopted. The chord diameters were 125,

205 and 245 mm, corresponding to β values of 36, 31.2 and 27, respectively. The results are presented in Figure 10. As expected, increasing the value of β leads to a substantial increase in the connection load carrying capacity.

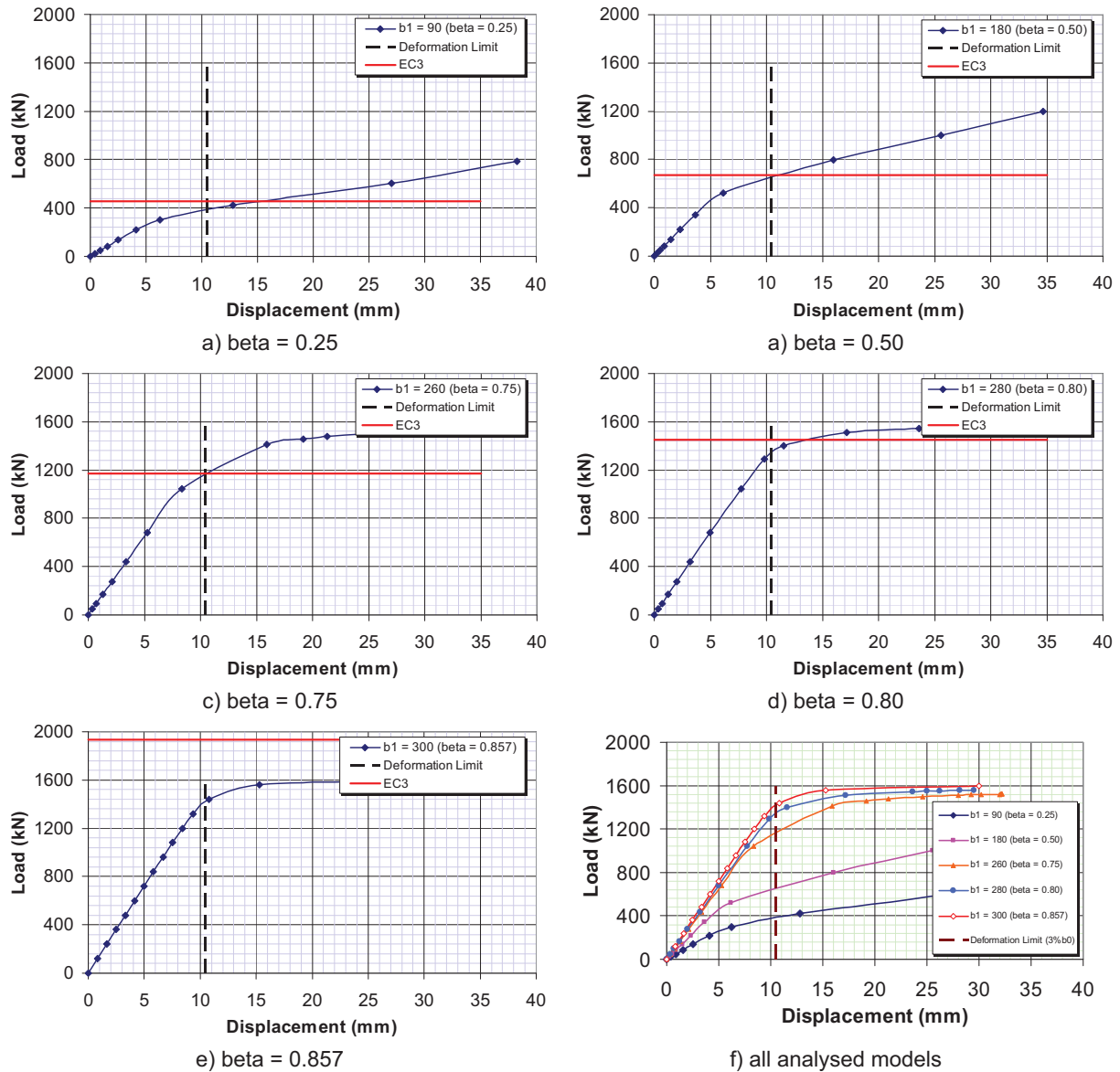


Figure 9. Load versus displacement curves – "T" tubular joints

Figure 10, depicts the individual curves for brace members (left and right) where it is possible to assess the joint resistance according to Choo et al. (2006). It may be observed that the joint resistance evaluated according to Eurocode 3 (2003) provisions represents a lower limit for the analysed joints.

FINAL REMARKS

A finite element geometrical and material non linear model was developed to simulate the T and K joints behaviour using four-node thick shell elements. This strategy enable the assessment of the proper influence of bending, shear and membrane deformations.

Deformation limits criteria were used to obtain the joint ultimate load. This criterion usually associates the ultimate limit state of the chord face to a maximum out of plane deformation of this particular component. The reason for using a deformation limit criterion instead of the use of plastic analysis for the prediction of the ultimate limit state is that, for slender chord faces, the joint stiffness is not exhausted after the complete yielding onset due to membrane effects.

The results of the analysis were used to assess the EN 1993-1-8 [4] performance not only in terms of maximum load, but also in terms of the global load versus displacement curves to fully characterise the joint structural response in terms of stiffness and ductility capacity.

Through the observation of the analytical curves, it could be concluded that the numerical results achieved a good agreement with the Eurocode 3 [4] provisions for the joint resistance combined with a serviceability limit criterion associated to the joint chord face deformation.

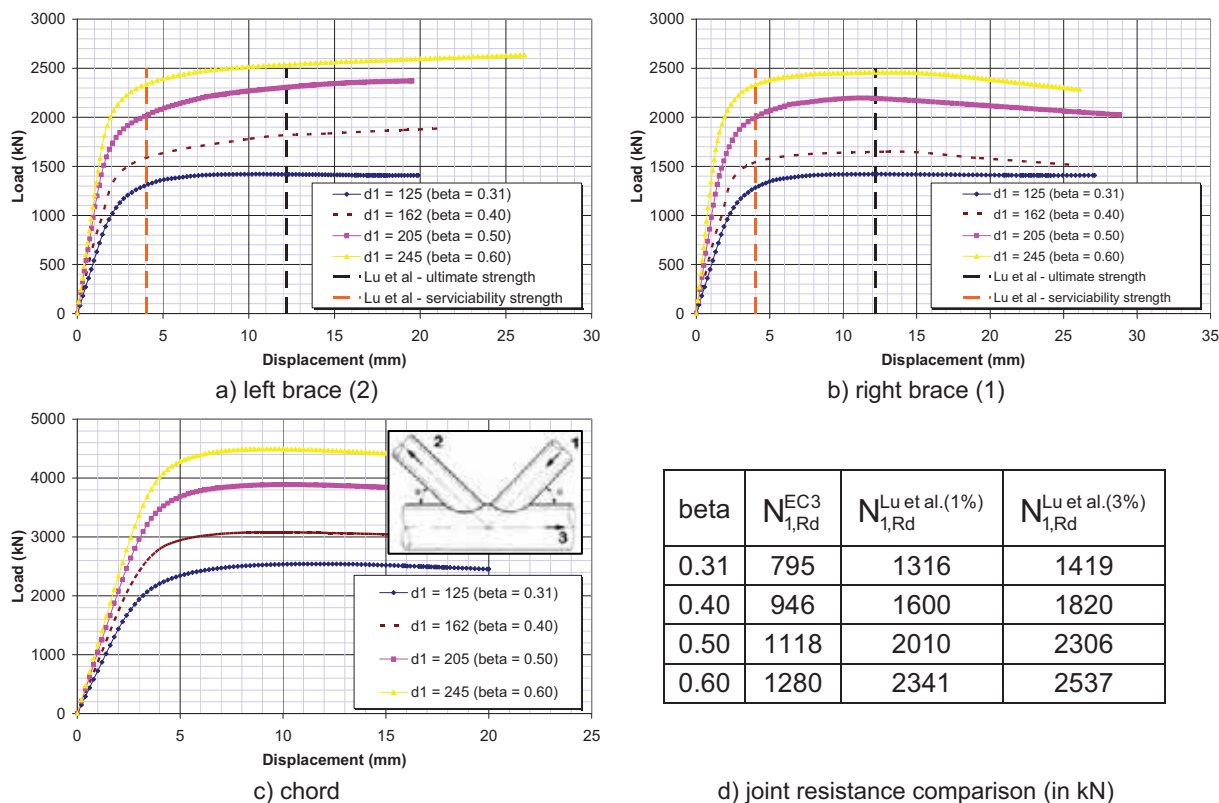


Figure 10. Load versus displacement curves – “K” tubular joints

Acknowledgements: The authors would like to thank the Brazilian and Rio de Janeiro State Science and Technology Developing Agencies CNPq, CAPES and FAPERJ for the financial support provided to enable the development of this research program.

REFERENCES

- ANSYS 10.0 ® (2005), ANSYS - Inc. Theory Reference.
- Cao, J.J., Packer, J.A., Young, G.J. (1998), "Yield line analysis of RHS connections with axial loads", *Journal of Constructional Steel Research*, Vol. 48, (pp 1-25).
- Choo, Y. S., Qian, X. D., Liew, J. Y. R, Wardenier, J. (2003), "Static strength of thick-walled CHS X-joints - Part I. New approach in strength definition", *Journal of Constructional Steel Research*, Vol.59 (pp. 1201-1228).
- Choo, Y. S., Qian, X. D., Wardenier, J. (2006), "Effects of boundary conditions and chord stresses on static strength of thick-walled CHS K-joints", *Journal of Constructional Steel Research*, Vol.62 (pp. 316-328).
- Eurocode 3, prEN 1993-1.8 (2003), Design of steel structures – Part 1.8: Design of joints, CEN, European Committee for Standardisation, Brussels.
- Korol, R., Mirza, F. (1982), "Finite Element Analysis of RHS T-Joints", *Journal of the Structural Division*, ASCE, Vol.108, (pp. 2081-2098).
- Kosteski, N., Packer, J.A., Puthli, R.S. (2003), "A finite element method based yield load determination procedure for hollow structural section connections", *Journal of Constructional Steel Research*, Vol. 59, (pp. 427-559).
- Lee M. M. K. (1999), "Strength, stress and fracture analyses of offshore tubular joints using finite elements", *Journal of Constructional Steel Research* Vol. 51 (pp. 265-286).
- Lie S. T., Lee C. K., Chiew S. P. and Yang, Z. M. (2006), "Static Strength of Cracked Square Hollow Section T Joints under Axial Loads. I: Experimental", *ASCE Journal of Structural Engineering*, Vol. 132, (pp. 368-377).
- Lie S. T., Lee C. K., Chiew S. P. and Yang, Z. M. (2006), "Static Strength of Cracked Square Hollow Section T Joints under Axial Loads. II: Numerical", *ASCE - Journal of Structural Engineering* Vol. 132, (pp. 378-386).
- Lu, L. H., de Winkel, G.D., Yu, Y., Wardenier, J. (1994), "*Deformation limit for the ultimate strength of hollow section joints*". Proceedings of Sixth International Symposium on Tubular Structures, Melbourne.
- Packer, J. A., (1993), "Moment Connections between Rectangular Hollow Sections", *Journal of Constructional Steel Research*, Vol. 25 (pp. 63-81).
- Packer, J. A., Wardenier, J., Kurobane, Y., Dutta, D. and Yoemans, N. (1992), *Design Guide for Rectangular Hollow Section (RHS) Joints Under Predominantly Static Loading*, CIDECT - Construction with Hollow Steel Sections, Verlag TÜV Rheinland.
- Van Der Vegte G. J., Koning C. H. M., Puthli R. S. and Wardenier J. (2007), "Numerical Simulation of Experiments on Multiplanar Steel X-Joints", *International Journal of Offshore and Polar Engineering*, Vol. 1, (pp. 200).
- Zhao, X., Hancock, G., (1991), "T-Joints in Rectangular Hollow Sections Subject to Combined Actions", *ASCE - Journal of the Structural Division*, Vol.117, (pp. 2258-2277).

ROTATION CAPACITY OF WELDED T & X BEAM-COLUMN JOINTS WITH RHS

Jerzy K. Szlendak

Bialystok Technical University, Bialystok, Poland
szlendak@pb.bialystok.pl

ABSTRACT

Rotation capacity of joints is often studied by the researchers as the estimation of the ductility of its components. In the case of welded RHS joints different parts of joints could be classified as the elements with ductility: large (face wall of chord), medium (side walls of chord) and small (welds). It should be noticed that the rotation capacity is very "sensitive" for any imperfections of joint geometry as well as material, type and defects of welds, welding process etc. It is one of the reasons why during the tests for two test samples with the same mechanical and geometrical properties very often is obtained substantially different rotation capacity. In the paper a new semi-empirical formula is derived to predict the rotation capacity of welded T and X beam-column joints with RHS. It is based on the presented test results. Finally, some preliminary conclusions are given.

INTRODUCTION

Design prediction of the rotation capacity of joints is difficult (Brodka, 1998) and with regard to indispensable, from practical design reason, simplifications the difference between the theoretical predicted and experimental obtained value of rotation could be considerable. Results obtained from experiments have shown that in the tension corner, just before the failure the crack of weld was observed. Only very ductile joints failed by the very large deformation of the chord face without the crack of the welds.

THEORETICAL MODEL

In the theoretical estimation of rotation capacity is assumed that it occurs due to:

- elongation of the tension fillet weld between the branch and chord member as illustrated in Fig. 1,
- deformations of face and side walls of the chord member as illustrated in Fig. 2,
- distortion of webs. In case of RHS joints where exists two webs (side walls) this influence could be neglected.



Figure 1. Fillet weld after failure



Figure 2. Deformations of face and side walls

Rotation from elongation of the tension fillet weld

One of a way to predict the deformation of joint, at the moment of failure, due to the elongation of the welds is the calculation of elongation of the perpendicular to the chord branch tension weld as illustrated in Fig. 1. The welds together with the branch section as the rigid punch rotate when the branch is loading by the bending moment. Outside of the branch by the tension side of the joint, plate GIEN as illustrated in Fig. 3, in the plastic hinge mechanism counteract to this rotation (Szlendak, 1982).

Angle φ_2 and deflection „w” arise from the elongation of this plate. It is assumed that before the load was applied the weld has the triangle shape with the angle 45° . If bending moment M_y is applying to the branch the weld is tension and its section change the shape for isosceles triangle with the angles γ i ϑ . If the small deflection „w” is assumed then the angle γ is

$$\gamma = (\pi/2) + \varphi_1 + \varphi_2 \quad (1)$$

where

$$\varphi_1 = 2w/(\eta b_0) \quad (2)$$

$$\varphi_2 = w/x \quad (3)$$

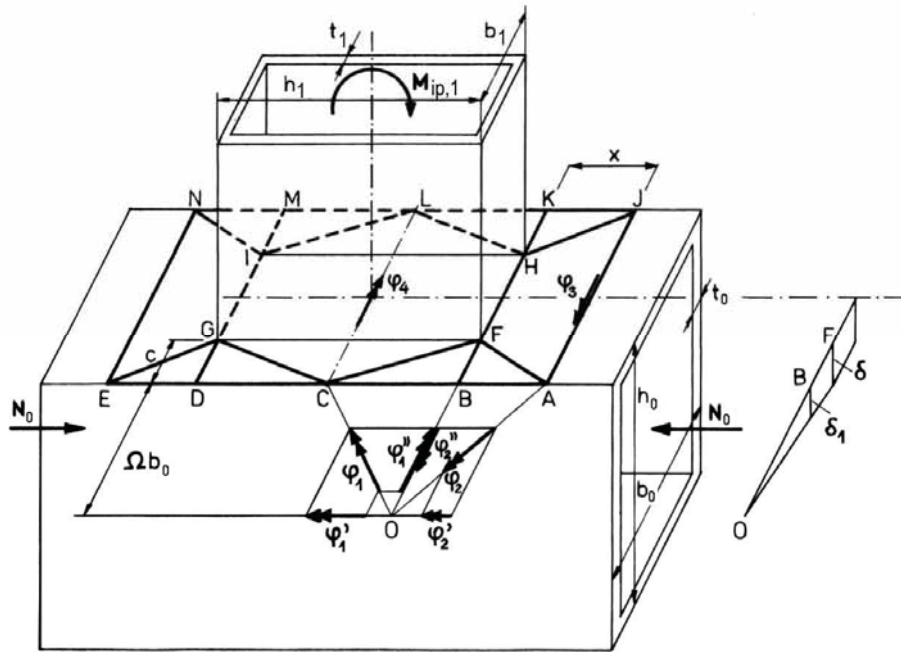


Figure 3. Plastic yield line kinematical mechanism of failure

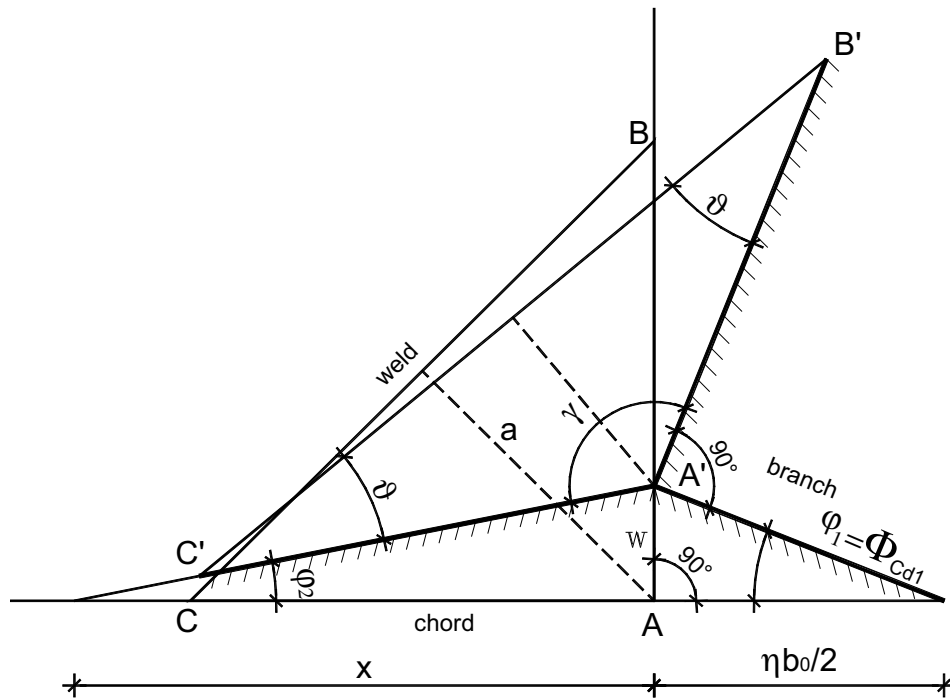


Figure 4. Deformation of the branch tension weld

It is assumed that the range of deformation of chord loaded plate x has the same value as was derived by (Szlendak, 1982).

When $\beta \leq \lambda_0 - 2.5/\lambda_0$

$$x = \frac{b_0(\Omega b_0 + c)}{\sqrt{2 + \frac{4}{3}\lambda_0^2\Omega^2}} \quad (4)$$

For $\Omega \neq 0$, as illustrated in Fig. 3, in plastic hinges A-E and J-N axial-bending stresses arise. In particular case when $\Omega = 0$ only bending stress occurs in hinges. Such model is introduced in EC Standard (EC 3 Part 1.8, 2005). Then equation 4 is

$$x = \frac{b_0}{2} \sqrt{1 - \beta} \quad (5)$$

However, when $(\lambda_0 - 2.5)/\lambda_0 < \beta \leq 1$

$$x = \frac{b_0(\Omega b_0 + c)}{\sqrt{1 + 2\lambda_0\Omega + \frac{1}{6\lambda_0\Omega}}} \quad (6)$$

The second particular case occurs when $\Omega = \infty$ then only axial stress arises, and equation 6 is

$$x = \frac{b_0}{2} \frac{1}{\sqrt{\frac{\lambda_0}{2}}} \quad (7)$$

When $0 < \Omega < \infty$ the equations to calculate range of chord loaded plate deformation x have been developed by (Szlendak, 1982). They are very complicated and rather useless to evolve the simple prediction of joints rotation capacity. So, it is assumed that for parameter $\beta \leq \lambda_0 - 2.5/\lambda_0$, when joint behavior is dominated by bending (axial stress influence could be neglected) equation 5 should be used.

However, when $(\lambda_0 - 2.5)/\lambda_0 < \beta \leq 1$ and axial stresses in plastic hinges A-E and J-N are dominated then equation 7 is correct.

If substitute 5 or 7 to 3 value of angle φ_2 could be obtained. After substituting it to 1 value of angle γ could be derived. This finally leads to value of angle ϑ

$$\vartheta = (\pi - \gamma) / 2 \quad (8)$$

Elongation of fillet weld is

$$\varepsilon = \frac{B'C' - BC}{BC} \quad (9)$$

where

$$BC = 2a, \text{ a } B'C' = 2\sqrt{2}a \cos((\pi - \gamma) / 2) \quad (10)$$

then

$$\varepsilon = \sqrt{2} \cos((\pi - \gamma)/2) - 1 \quad (11)$$

After substituting γ to 11 is

when $\beta \leq \lambda_0 - 2.5/\lambda_0$

$$\varepsilon = \sqrt{2} \cos(\pi/4 - (w/b_0)(\frac{1}{\eta} + \frac{1}{\sqrt{1-\beta}})) - 1 \quad (12)$$

and when $(\lambda_0 - 2.5)/\lambda_0 < \beta \leq 1$

$$\varepsilon = \sqrt{2} \cos(\pi/4 - (w/b_0)(\frac{1}{\eta} + \frac{\sqrt{\lambda_0}}{2})) - 1 \quad (13)$$

Rotation capacity of joint is

$$\Phi_{cd1} = \varphi_1 = 2w/\eta b_0 \quad (14)$$

If one substitutes 14 to 12 is

when $\beta \leq \lambda_0 - 2.5/\lambda_0$

$$\varepsilon = \sqrt{2} \cos(\pi/4 - (\eta\Phi_{cd1}/2)(\frac{1}{\eta} + \frac{1}{\sqrt{1-\beta}})) - 1 \quad (15)$$

and after transformation

$$\Phi_{cd1} = \frac{\pi - 4 \arccos(\frac{1+\varepsilon}{\sqrt{2}})}{2(1 + \frac{\eta}{\sqrt{1-\beta}})} \quad (16)$$

However, when $(\lambda_0 - 2.5)/\lambda_0 < \beta \leq 1$

$$\Phi_{cd1} = \frac{\pi - 4 \arccos(\frac{1+\varepsilon}{\sqrt{2}})}{2(1 + \eta \sqrt{\frac{\lambda_0}{2}})} \quad (17)$$

If elongation of tension weld ε will be known then from 16 and 17 could be obtained the joint rotation. This elongation is predicted from experimental results of 52 welded T RHS joints tested by (Kanatani et al., 1981). From these results only such have been chosen where the chord RHS is very compact and width of branch is equal to width of chord ($\beta = 1$). Then deformations of face and side walls of the chord member and distortion of webs could be neglected. Many experiments of welded T RHS joints have been done but only (Kanatani et al., 1981) register the rotation of joints up to failure. Other researchers finished their tests earlier, often obtained very large rotations, but before the rotation capacity $\Phi_{Cd, eks}$ have been reached

In Table 1 the geometrical and mechanical properties of joints No 177 and 178 (Szlendak and Broniewicz, 1995) are presented. During the experiments (Kanatani et al., 1981) experimental rotation capacities $\Phi_{Cd, eks}$, as illustrated in Table 2, column 6, have been registered. After substituting medium value of their rotation angle to 17 elongation ε of the tension weld could be predict. It was equal about 5%.

Table 1. Geometrical and mechanical properties of joints tested by (Kanatani et. al., 1981)

Geometrical properties					Yield stress		Parameters			weld thick a mm
No joints	chord $b_0 \times h_0$ mm	branch $b_1 \times h_1$ mm	chord thick. t_0 mm	branch thick. t_1 mm	chord f_{y0} MPa	branch f_{y1} MPa	β	η	λ_0	
(1)	(2)	(3)	(4)	(5)	(6)	(7)	(8)	(9)	(10)	(11)
177	200x200	200x200	12	6	378	383	1	1	16.7	4
178	200x200	200x200	12	6	378	392	1	1	16.7	9.1

Table 2. Experimental and theoretical rotation capacity of joint Φ_{Cd} tested by (Kanatani et. al., 1981)

No joints	β	η	λ_0	weld thick. a mm	exper. rotation $\Phi_{Cd, eks}$ mrad	theor. rotation weld Φ_{Cd1} mrad	theor. rotation face Φ_{Cd2} mrad	theor. rotation Φ_{Cd} mrad	ratio rotation exper./ teoret. (6)/(9)
(1)	(2)	(3)	(4)	(5)	(6)	(7)	(8)	(9)	(10)
177	1	1	16.7	4	20.4	26.4	10.0	36.5	0.56
178	1	1	16.7	9.1	32.3	26.4	10.0	36.5	0.89

So, theoretical value of the rotation capacity Φ_{Cd1} is

$$\Phi_{Cd1} = \frac{\pi - 4 \arccos\left(\frac{1.05}{\sqrt{2}}\right)}{2\left(1 + \eta\sqrt{\frac{\lambda_0}{2}}\right)} \quad (18)$$

and after transformation when $(\lambda_0 - 2.5)/\lambda_0 < \beta \leq 1$

$$\Phi_{Cd1} = \frac{102.7}{1 + \eta\sqrt{\frac{\lambda_0}{2}}} \text{ [mrad]} \quad (19)$$

and from 16 when $\beta \leq \lambda_0 - 2.5/\lambda_0$

$$\Phi_{Cd1} = \frac{102.7}{1 + \frac{\eta}{\sqrt{1-\beta}}} \text{ [mrad]} \quad (20)$$

Estimated above first part of the rotation capacity Φ_{Cd1} has been obtained on deterministic way. After subtract this value from the overall value of rotation capacity $\Phi_{Cd,eks}$ probabilistic value of rotation is obtained. For the simplicity it is assumed as second part of the rotation capacity which occurs only from deformations of face and side walls of the chord member. Distortion of webs is neglected.

Rotation due deformations of face and side walls of the chord

Analysis of 47 experimental results welded T RHS joints tested by (Kanatani et al., 1981) leads to prediction of this second part of the rotation capacity. Five tests from 52 pieces set have been rejected due to other mode of failure or test mistake. It has been noticed that dominant influences on rotation capacity have three geometrical parameters β, η i λ_0 . Influence of weld thickness has also been noticed, as illustrated in Table 1 and 2. Test results have shown (Szlendak, 2007) that thin fillet welds, less then thickness of the branch wall section should be avoided. However, from the too small tests of joints with different thickness of fillet welds influence of this parameter is neglected.

For the joints with width of branch section equal or almost equal to width of chord section, so when $(\lambda_0 - 2.5)/\lambda_0 < \beta \leq 1$ the bellow equation for prediction rotation capacity Φ_{Cd2} is proposed

$$\Phi_{Cd2} = k_C f_C(\beta, \eta, \lambda_0) \quad (21)$$

where: k_C – coefficient and f_C – unknown function.

From many different functions f_C the following one has been chosen

$$f_C = \beta^{y_1} \eta^{y_2} \lambda_0^{y_3} \quad (22)$$

For $\beta \leq \lambda_0 - 2.5/\lambda_0$ i.e. the joints width of branch section is smaller then width of chord section, modification of the influence of parameter β is necessary as

$$f_C = [(1/\beta) - 1]^{y_4} \eta^{y_5} \lambda_0^{y_6} \quad (23)$$

Probabilistic variable $x_i = \frac{\Phi_{Cd,eks} - \Phi_{Cd1}}{\Phi_{Cd,2}}$ is used for evaluation of above parameters.

Results of 47 failure tests by (Kanatani et al., 1981), collected as part of data bank (Szlendak and Broniewicz, 1995), have been used to obtain values of parameters k_C and y_i . Confidence level $(1 - \alpha)$ is equal to 0.95.

For 9 test results when $(\lambda_0 - 2.5)/\lambda_0 < \beta \leq 1$ values of unknown exponents are equal to $\gamma_1 = -1/2$, $\gamma_2 = -1$, $\gamma_3 = 1$ and $k_c = 0.6$. After substituting them to 21 is

$$\Phi_{cd2} = 0.6 \frac{\lambda_0}{\eta} \sqrt{\frac{1}{\beta}} \text{ [mrad]} \quad (24)$$

Moreover for 37 test results when $\beta \leq \lambda_0 - 2.5/\lambda_0$ values of unknown exponents are equal to $\gamma_4 = 1/2$, $\gamma_5 = -1$, $\gamma_6 = 3/2$ and $k_c = 0.93$. After substituting them to 23 is

$$\Phi_{cd2} = 0.93 \frac{1}{\eta} \sqrt{\frac{\lambda_0^3 (1-\beta)}{\beta}} \text{ [mrad]} \quad (25)$$

Rotation capacity of welded T RHS joints

Rotation capacity of joint is the sum of the rotation Φ_{cd1} from 19 and 20 and the rotation Φ_{cd2} from 24 and 25. Finally, rotation capacity of welded T RHS joints is

when $\beta \leq \lambda_0 - 2.5/\lambda_0$

$$\Phi_{cd} = \frac{102.7}{1 + \frac{\eta}{\sqrt{1-\beta}}} + 0.93 \frac{1}{\eta} \sqrt{\frac{\lambda_0^3 (1-\beta)}{\beta}} \text{ [mrad]} \quad (26)$$

and when $(\lambda_0 - 2.5)/\lambda_0 < \beta \leq 1$

$$\Phi_{cd} = \frac{102.7}{1 + \eta \sqrt{\frac{\lambda_0}{2}}} + 0.6 \frac{\lambda_0}{\eta} \sqrt{\frac{1}{\beta}} \text{ [mrad]} \quad (27)$$

In Fig. 5 theoretical estimation Φ_{cd} from equations 26 and 27 is compared with experimental results $\Phi_{cd,eks}$ from tests by (Kanatani et al., 1981). As the test results are taken the medium values for group of joints where the geometrical properties are practically identical.

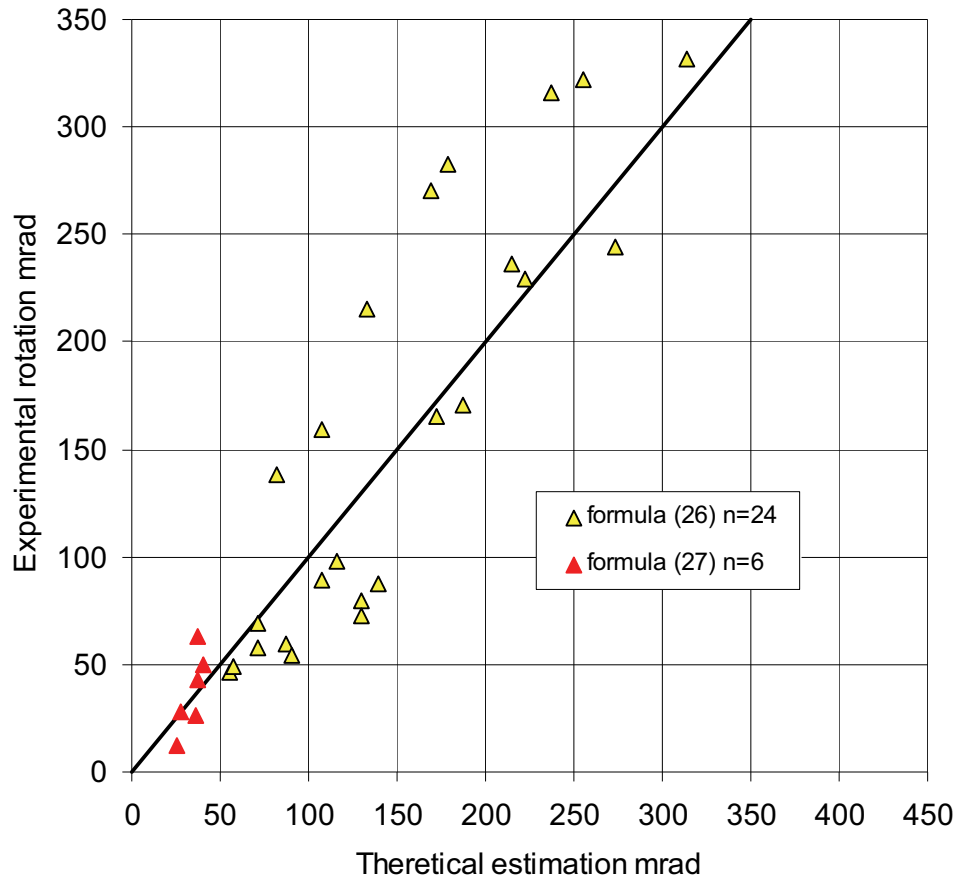


Figure 5. Comparison of theoretical estimation obtained from formulas (26) and (27) with medium value of experimental results by (Kanatani et al., 1981)

CONCLUSIONS

1. Test results have shown, as in example illustrated in Table 2 and more data published in (Szlendak, 2007), that even for two test samples with the same mechanical and geometrical properties very often is obtained substantially different rotation capacity. So, the comparison given in Fig. 5 seems to be satisfactory.
2. It will be valuable if further study gives data about the elongation of flexible parts of discussed here joints. They ought to be measured separately. So, then the component method could be adopted to solve the problem of rotation capacity of such joints.

NOTATION

- a throat thickness of fillet weld
 f_c function

f_y	yield stress of (f_{y1} – branch member, f_{y0} – chord member)
k_C	coefficient
x	range of yield line mechanism outside branch
y_i	unknown exponents ($i = 1 \div 6$)
β	branch width to chord width ratio ($\beta = b_1 / b_0$)
η	branch depth to chord width ratio ($\eta = h_1 / b_0$)
λ_0	slenderness of chord face ($\lambda_0 = b_0 / t_0$)

ACKNOWLEDGEMENT

This research project No W/IIB/ /08 was financially supported by Bialystok University of Technology

REFERENCES

- Kanatani, H., Fujiwara, K., Tabuchi, M. and Kamba T. (1981), "Bending tests on T-joints of RHS chord and RHS or H-shape branch", *Report of CIDECT*, Program 5AF-80/15.
- Szlendak, J. (1982), "Ultimate load of welded beam-column connections with rectangular hollow sections", *Ph.D. thesis*, Warsaw Technical University, (in Polish).
- Szlendak, J. and Broniewicz, M. (1995), "Data bank of connections. Beam to column welded connections, Part 1: RHS column to RHS beam", *Bialystok Technical University*, (in Polish).
- Brodka, J. (1998), "Evaluation of rotation capacity of steel semi-rigid joints", Proc. of Conf. *Semi-rigid joints in steel structures*, Workshop II, Rzeszow, Poland (in Polish).
- European Committee for Standardization (CEN) (2005), Eurocode 3: *Design of steel structures: Part 1.8: Design of joints*, European Standard EN 1993-1-8.
- Szlendak, J. K. (2007), "Design models of beam-column welded joints in steel structures made with rectangular hollow sections", *D.Sc. thesis*, Bialystok University Press (in Polish).

LOAD BEARING CAPACITY OF SPLICED COLUMNS WITH SINGLE ROW BOLTED BUTT-PLATES

J.C.D. Hoenderkamp, H. H. Snijder
Eindhoven University of Technology, The Netherlands
j.c.d.hoenderkamp@tue.nl h.h.snijder@tue.nl

ABSTRACT

A butt-plate splice makes part of the column and therefore must be designed for second order bending moments and shear forces in addition to the axial force. Building Codes may require or recommend minimum strength and/or stiffness for such splices. The presence of a splice can have influence on the bearing capacity of the column and on the force distribution in the overall structure. This paper suggests an expression for the calculation of the rotational stiffness of single row bolted butt-plate column splices and a procedure for obtaining the reduced bearing capacity of such a spliced column under compression. The methods are based on the assumption of a virtual moment arm in the splice which is a function of a linear stress gradient across the column section due to Eurocode 3 defined column imperfections.

INTRODUCTION

In general, a column splice for the transfer of axial loads can be manufactured in two ways: with butt-plates welded perpendicular to the cut section of the two columns or with cover plates on the flanges and web. The cover plates can create a gap between the two column ends or allow direct contact. The splices should preferably be located at floor level but for practical reasons this usually occurs at 0.5 m to 1.0 m above floor level, i.e. about one quarter up a story high column. The axial loads can be transferred in different ways through the column-to-column connection: by direct bearing through the butt-plates or through the flanges and web or by compression and tension in the cover plates. In all cases there will be shear forces in the splice.

Eurocode 3 Part 1.8 (2006) gives design rules for column splices requiring minimum capacities for bending moment and shear force in case of load transfer through the cover plates and a minimum normal compressive force to be accounted for in case of bearing.

The splice is part of the column and must be designed for 2nd order bending moments and shear forces in addition to the axial force. A strength requirement for the column splice derived on this basis has been presented earlier. In addition, a stiffness requirement for column splices with small imperfections was suggested on the basis of allowing a maximum reduction of 5% in the Euler buckling load. A limited number of experimental tests on HE100A columns has shown that butt-plate splices can have a negative influence on the buckling load of columns. (Snijder & Hoenderkamp, 2008).

In this paper the theory on rotational stiffness of column splices will be extended to include larger imperfections such that butt-plate separation is allowed to occur. It will also give a method of analysis to quantify the influence of the splice on the load bearing capacity of the column.

LITERATURE

Code Requirements

In Eurocode 3 Part 1.8, a distinction is made between bearing and non-bearing column splices. Where the members are not prepared for full contact in bearing, the moment resistance should be not less than 25% of the moment capacity of the weaker section applied in both directions and the design shear force should be taken not less than 2.5% of the squash capacity also to be applied in two directions. Where the members are prepared for full contact in bearing, cover plates, bolts and welds should be able to transmit 25% of the maximum compressive force in the column. The background to these requirements could not be traced.

A study of design methods for column splices subject to concentric axial loading as suggested by the National Building Codes of Europe, Great Britain, Germany, The Netherlands, United States, Canada, Australia and Japan (Snijder & Hoenderkamp, 2005, 2008) yields a profusion of different empirical approaches which lead to a variety of design procedures with different load combinations which must be applied to the connection. The study was extended to requirements and rules on fabrication published in Great Britain, The Netherlands and Australia. The majority of the studied codes only address design requirements for strength with the exception of BS5950 and NEN6772 which also refer to splice stiffness. A BS5950 requirement states that for direct contact bearing splices, the stiffness in the connection must be maintained. In a BCSCA-SCI publication on simple connections it is stated that an accurate elastic analysis of the connection should be used to verify that it is at least as stiff as the member. It further suggests that even where a splice connection is entirely in compression, it is advisable to maintain full continuity of stiffness through the connection. NEN 6772 requires that the stiffness of a splice must be included in the analysis of the building structure.

Only half of the building codes studied require second order effects be taken into account in the design of the column splice. A number of codes state that the connection materials such as plates, bolts and welds must secure that the two column sections remain in place.

Research

The influence on the stability of columns of specific column imperfections which are introduced by the application of column splices was further investigated (Lindner & Gietzelt, 1988; Lindner, 1998, 1999, 2002, 2008) based on earlier research (Popov & Stephen, 1977; Sheer et al., 1987). It was concluded, that in case slip is prevented in the splice, e.g. by pre-stressing the bolts, standard column stability checks would suffice to cover column splice imperfections. In case slip is not prevented, a less favourable buckling curve must be used. It has been advised to transfer at least 10% of the normal force by the connectors to secure both column parts in location. Full scale buckling tests on butt-spliced columns for weak axis buckling were carried out on HE240A (S235)

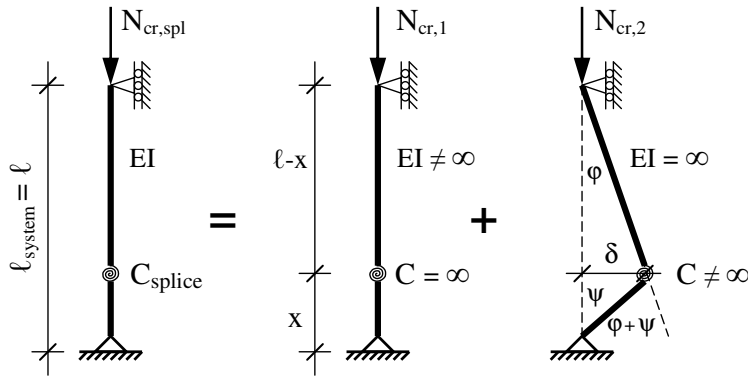


Figure 1: Column model for critical load of spliced column

sections. Results were compared with load bearing capacities confirming that spliced columns can be checked as normal columns for stability. Splice stiffness was not addressed.

A research project at the Eindhoven University of Technology on the design of column splices for strength and stiffness was instigated by the Dutch steel fabricators who specifically objected to the rather severe requirement to supply a minimum of 25% of the moment capacity of the column section through the splice material.

CRITICAL LOAD OF SPLICED COLUMNS

The critical load of a spliced column $N_{cr,spl}$ can be estimated by combining the critical loads for the two subsystems as shown in Figure 1. In the subsystem 1, the splice rotational stiffness C is assumed to be infinite while the column has a finite bending stiffness EI . In subsystem 2 on the right, the splice rotational stiffness C is finite while the column is assumed to have infinite bending stiffness EI . The Euler buckling load for column 1, $N_{cr,1}$, where the splice stiffness is taken as $C = \infty$, is:

$$N_{cr,1} = \frac{\pi^2 EI}{\ell^2} \quad (1)$$

Equilibrium in the deformed state gives the critical load $N_{cr,2}$ of subsystem 2, where the bending stiffness is taken as $EI = \infty$

$$N_{cr,2} = \frac{C\ell}{x(\ell - x)} \quad (2)$$

Now the critical load for the spliced column with finite values for the splice rotational stiffness C and column bending stiffness EI can be obtained by using the Dunkerley formula (Dunkerley, 1894) as follows:

$$\frac{1}{N_{cr,spl}} = \frac{1}{N_{cr,1}} + \frac{1}{N_{cr,2}} \quad (3)$$

Substituting Eqs. (1) and (2) into Eq. (3) and simplifying yields the following equation for the critical load of the spliced column:

$$N_{cr,spl} = \frac{C\ell}{\frac{C\ell^3}{\pi^2 EI} + x(\ell - x)} \quad (4)$$

ROTATIONAL STIFFNESS OF COLUMN SPLICES

Full Contact between Butt-Plates

A generally accepted method for calculating the rotational stiffness of a column splice under compression is not available to the knowledge of the authors. In order to get an indication of the rotational stiffness of a column splice under compression the authors have adopted a simplified design procedure which employs an equation from Eurocode 3 Part 1.8 (EN1993-1-8:2004, 2006) for the initial rotational stiffness of beam-to-column connections subject to bending

$$C = \frac{Ez^2}{\mu \sum \frac{1}{k_i}} \quad (5)$$

in which z is a moment arm represented by the distance between a compression point and the center of the bolt group in the tension area; μ is given a unit value for initial stiffness; and k_i is a stiffness factor to be determined according to Eurocode 3. The suggested method requires adjustment to the values for z and k_i in order to take the column-column end plate splice configuration with a single central row of bolts as shown in figure 2a into account.

The stiffness factors k_i in Eqn. (5) are to be determined for all individual components that are active in resisting the forces in the connection. In a column splice subject to compressive stresses only as shown in Figure 2 there exists just one stiffness component: axial compression. It is suggested that the stiffness factor becomes

$$k = \frac{A}{\ell} \quad (6)$$

in which A is the sectional area of the column and ℓ is its length. The equation for the initial rotational stiffness of the column splice can be simplified and rewritten as

$$C = \frac{EAz^2}{\ell} \quad (7)$$

The axial load on the column splice in Figure 2a with the associated second order bending moment due to the imperfection at the splice $e_{spl,l}$ will cause a typical linear stress distribution in the column section as shown in Figure 2b. It is suggested that the moment arm z be obtained from the linearly extended stress distribution across the steel section as shown in Figure 2b. A full compressive stress distribution holds true for small load eccentricities at the splice, i.e. no tensile stresses in the splice where N_{Ed} is the

$$\frac{N_{Ed}}{A} \geq \frac{N_{Ed} e_{spl,l} h / 2}{I} \quad (8)$$

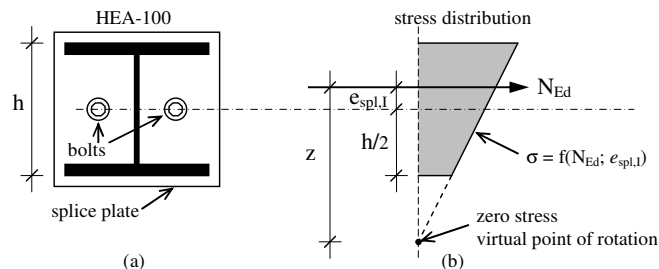


Figure 2: Alternative moment arm

design axial compressive load, I is the second moment of area and h is the height of the section. Then

$$e_{spl,l} = e^* \sin \frac{\pi x}{l} \leq \frac{i^2}{h/2} \quad (9)$$

in which e^* is the maximum column imperfection at mid height defined by Eurocode 3 and can be expressed as follows (Snijder & Hoenderkamp, 2008)

$$e^* = \frac{1-\chi}{\chi} \frac{n-1}{n} \frac{M_{pl,Rd}}{N_{pl,Rd}} \quad (10)$$

where $N_{pl,Rd}$ is the design plastic resistance of the gross cross-section (squash load), $M_{pl,Rd}$ is the design plastic resistance for bending and the radius of gyration is

$$i = \sqrt{\frac{I}{A}} \quad (11)$$

Reduction factor χ is a function of Φ and the relative slenderness of the column $\bar{\lambda}$

$$\chi = \frac{1}{\Phi + \sqrt{\Phi^2 - \bar{\lambda}^2}} \quad (12)$$

$$\varphi = 0.5 \{1 + \alpha(\bar{\lambda} - 0.2) + \bar{\lambda}^2\} \quad (13)$$

$$\bar{\lambda}^2 = \frac{N_{pl,Rd}}{N_{cr,spl}} \quad (14)$$

where α is an imperfection factor dependent on the pertaining instability curve. The bearing capacity of the spliced column can be expressed as follows

$$N_{b,Rd,spl} = \chi N_{pl,Rd} \quad (15)$$

For this ultimate column load the factor n now becomes

$$n = \frac{N_{cr,spl}}{N_{b,Rd,spl}} \quad (16)$$

From the geometry in Figure 2b it can quite easily be shown that the moment arm is

$$z = \frac{i^2}{e_{spl,l}} + e_{spl,l} \quad (17)$$

This moment arm can now be used in Eq. (7) to obtain the initial rotational stiffness of the splice subject to axial force and bending moment. It should be noted here that the moment arm and thereby the rotational stiffness of the splice are independent of the size of the axial load.

Separation of Butt-Plates

If the eccentricity of the axial load is increased beyond a distance $2f^2/h$, the combined axial and bending stress on one side of the connection (the tension flange) will result in a tensile stress if the butt-plates were welded together. Since they are bolted together in the center of the splice, the plates will separate at the tension flange.

The coming apart of the plates will change the stressed I-shaped cross-section of the spliced column into a T-shape as the intended tensile flange is not participating anymore in resisting the eccentric axial load. Upon gradual separation of the end plates, the location of the neutral axis of the T-section will move towards the compression

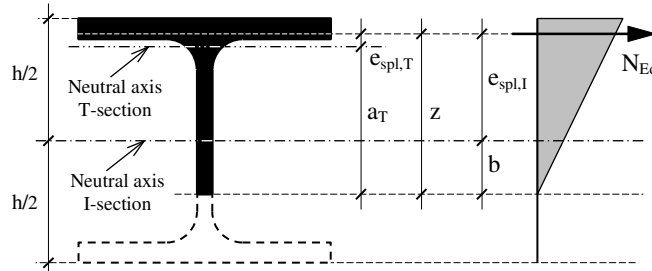


Figure 3: Stress distribution after butt-plate separation

flange. When the neutral axis is at a point on a T-shaped cross-section where the applied eccentric load will cause a triangular stress distribution in that section, the separation of the plates will stop, see Figure 3. Here the tensile stress due to bending is equal to the axial compression from the axial load. Increasing the load eccentricity $e_{spl,I}$ will cause a further shift of the neutral axis of the T-section towards the compression flange until again the tensile stress due to bending is equal to the axial compression from the axial load. For the point of zero stress

$$\frac{N_{Ed}}{A_T} - \frac{N_{Ed} e_{spl,T} a_T}{I_T} = 0 \quad (18)$$

from which follows

$$e_{spl,T} = \frac{I_T}{A_T a_T} = \frac{i_T^2}{a_T} \quad (19)$$

where A_T is the sectional area of the T-section, I_T is its second moment of area, i_T is the radius of gyration and a_T is the location of the neutral axis measured from the point of zero stress. The moment arm can be expressed as follows

$$z = e_{spl,T} + a_T = \frac{i_T^2}{a_T} + a_T \quad (20)$$

The eccentricity of the axial load measured from the neutral axis of the I-section is

$$e_{spl,I} = \frac{i_T^2}{a_T} + a_T - b = z - b \quad (21)$$

in which b is the distance between the neutral axis of the I-section and the point of zero stress in the T-section, see Figure 3. The rotational stiffness of the splice now is

$$C = \frac{EA_T z^2}{\ell} \quad (22)$$

It should be noted here that using the simple looking equations (19-21) can be quite cumbersome. It is suggested to start the calculation procedure by giving distance b specific values, e.g. $(h/2) - t_f$ or 0.0. For a column splice with end plates and a single row of bolts in the center the minimum value for b is 0.0 mm. For this case A_T , I_T , a_T , $e_{spl,T}$ and $e_{spl,I}$ can quite simply be determined as the geometric properties of T-sections obtained from half I-sections given in the literature.

The two stages with trapezoidal and triangular stress distributions across the section of an HEA100 are shown in Figure 4. Up until a load eccentricity of $2i^2/h = 34.34$ mm (point A) the cross-section is subject to compressive stresses only as is shown in figure 2b. For a load eccentricity $0.0 \leq e_{spl,I} \leq 34.34$ mm there will be a trapezoidal stress

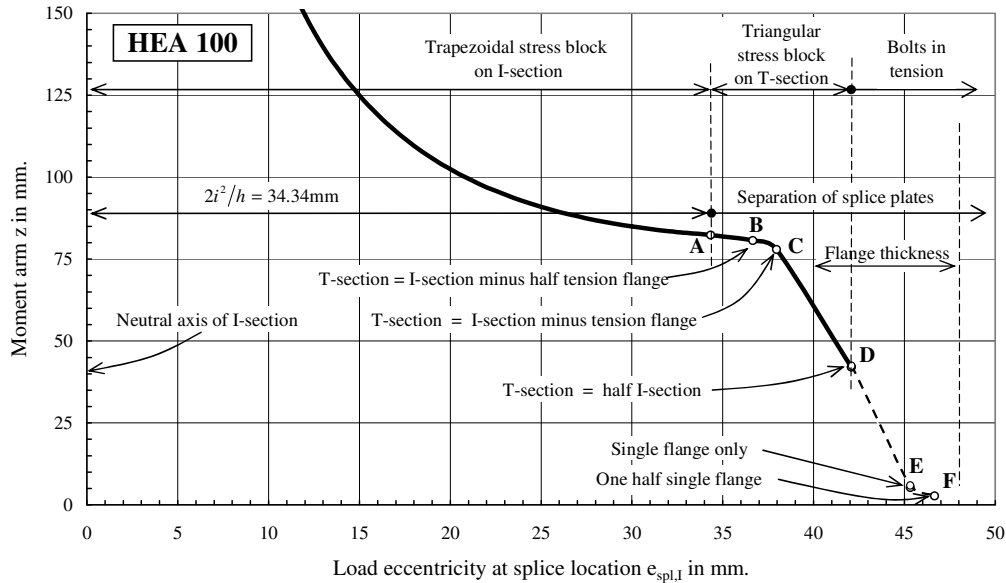


Figure 4: Moment arm versus load eccentricity

distribution across the I-section. The length of moment arm z is given by Eq. (17) and changes from infinity to 82.34 mm.

For load eccentricities larger than 34.34 mm the splice plates will separate and the axial load and bending moment must be resisted by a reduced cross section. The bending moment that can be resisted by the reduced section due to the axial load is smaller than the bending moment on the full I-section as the neutral axis of this T-section is now closer to the axial load, i.e. $e_{spl,T} < e_{spl,I}$ as shown in Figure 3.

For very large eccentricities beyond 42.08 mm (point D) tensile stresses will be introduced into the bolts and the rotational stiffness of the splice mainly becomes a function of individual stiffness factors k_i of the various components resisting the axial force and bending moment which must be used in Eq. (5). This is beyond the scope of this study.

The curve in Figure 4 shows that the moment arm z reduces rapidly with increasing load eccentricity. The curve has been further extended with a dotted line for the condition without bolts.

Table 1 shows intermediate calculation steps for six selected points, A-F, on the $e_{spl,I}$ versus z curve in Figure 4. The table is enlarged for a specific column to show the influence of the imposed column imperfections and thereby the rotational stiffness of the splice on its load carrying capacity. For a 3.39 m long HE100A, S235 column without splice $\alpha = 0.34$, $N_{cr,1} = 629.8$ kN and $N_{pl,Rd} = 499.1$ kN which yields an axial load capacity $N_{b,Rd}(\text{no splice}) = 333.1$ kN.

DESIGN OF BUTT-PLATE SPLICED COLUMNS

In order to obtain the load carrying capacity of a butt-plate spliced column the rotational stiffness of the splice C must be known. This stiffness is a function of the eccentricity at the splice $e_{spl} \times n/h - 1$ which is to be obtained from a code defined maximum imperfection

Table 1: Influence of imposed imperfections on load capacity of 3.39 m long HE100A spliced column

	Eq. nr.	Full HE100A I-section	Full section minus half tension flange	Full section minus full tension flange	One half HE100A section	Compression flange only	Half compression flange
Location on graph	-	A	B	C	D	E	F
$b_{imposed}$, mm	-	48	44	40	0	-40	-44
i_T^2 , mm ²	-	1644.1	1420.4	757.6	116.9	5.333	1.333
a_T , mm	-	48.00	54.67	66.59	39.09	4.00	2.00
$e_{spl,T}$, mm	19	-	25.98	11.38	2.991	1.333	0.6667
$e_{spl,I}$, mm	(9)*, 21	34.34	36.65	37.97	42.08	45.33	46.67
z , mm	(17), 20	82.34	80.65	77.97	42.08	5.33	2.67
C , kNm	(7), 22	892.1	694.7	498.5	116.5	1.44	0.18
$N_{cr,2}$, kN	2	1403.9	1092.9	784.3	183.3	2.265	0.283
$N_{cr,spl}$, kN	3	434.7	399.6	349.3	142.0	2.257	0.283
% of $N_{cr,1}$ (no splice)	-	69.0	63.4	55.5	22.5	0.40	0.04
$\bar{\lambda}$	14	1.071	1.118	1.195	1.875	14.868	41.987
χ	12	0.553	0.525	0.481	0.235	0.004	0.001
$N_{b,Rd,spl}$, kN	15	275.7	261.9	239.9	117.2	2.207	0.281
% of $N_{b,Rd}$ (no splice)	-	82.8	78.6	72.0	35.2	0.66	0.08

* equation numbers in brackets refer to Full HE100A I-section (point A) only.

at column mid height e^* , the critical load of the spliced column $N_{cr,spl}$ and load on the structure N_{Ed} . Both the imperfection and critical load of the spliced column are functions of the rotational stiffness of the butt-plate connection. Therefore an iterative procedure is necessary to obtain the load carrying capacity of the spliced column $N_{b,Rd,spl}$:

1. The column without splice is first designed for a maximum imperfection at mid height. This requires a load check for the column with a maximum second order eccentricity $e^* \times n/n-1$ defined by Eurocode 3. Obtain $N_{cr,1}$, $N_{pl,Rd}$, λ , χ , $N_{b,Rd}$. This yields e^* and then $(e_{spl} \times n/n-1)_i$ at splice location.
2. For the spliced column the rotational stiffness of the connection C_i is a function of the load eccentricity $(e_{spl} \times n/n-1)_i$ at the splice. For $(e_{spl} \times n/n-1)_i \leq 2f^2/h$ the moment arm z must be obtained for an I-section. For $(e_{spl} \times n/n-1)_i > 2f^2/h$ the moment arm z must be obtained for a T-section. $N_{cr,2,i}$ and the reduced critical load for the spliced column $N_{cr,spl,i}$ can now be calculated and will yield values for λ_i , χ_i and $N_{b,Rd,spl,i}$. This will lead to an increased eccentricity $(e_{spl} \times n/n-1)_{i+1}$ at splice location.
3. If $(e_{spl} \times n/n-1)_i / (e_{spl} \times n/n-1)_{i+1} \geq 0.99$ the iteration procedure can stop. At this point the second order imperfection as defined by Eurocode 3 has now been applied to the spliced column. The percentage reduction in $N_{b,Rd,spl}$ will always be smaller than for $N_{cr,spl}$.
4. If $(e_{spl} \times n/n-1)_i / (e_{spl} \times n/n-1)_{i+1} < 0.99$, a new reduced rotational stiffness for the splice C_{i+1} must be obtained from eccentricity $(e_{spl} \times n/n-1)_{i+1}$ and calculate $N_{cr,spl,i+1}$ to continue the iterative procedure.

Table 2: Iterative design procedure for two butt-plate spliced columns

Column	HE100A, 3.39 m long						HE100A, 4.53 m long		
	Eq. nr.	No splice	1	2	3	4	No splice	1	2
e_{applied} , mm	-	0.0	13.77	16.92	18.11	18.55	0.0	29.46	46.1
z , mm	17	∞	133.2	114.1	108.9	107.2	∞	85.27	?
C , kNm	7	∞	2333	1713	1560	1511	∞	716	
$N_{cr,2}$, kN	2	∞	3671	2695	2455	2378	∞	843	
$N_{cr,sp}$, kN	3	629.8	537.6	510.5	501.2	497.9	352.8	248.7	
% $N_{cr,1}$ (no splice)	-	100	<i>85.4</i>	<i>81.1</i>	<i>79.6</i>	79.1	100	<i>70.5</i>	
$\bar{\lambda}$	14	0.890	0.964	0.989	0.998	1.001	1.189	1.42	
χ	12	0.667	0.620	0.604	0.598	0.596	0.484	0.38	
$N_{b,Rd,sp}$, kN	15	333.1	309.6	301.5	298.6	297.6	241.5	186.9	
% $N_{b,Rd}$ (no splice)	-	100	<i>92.9</i>	<i>90.5</i>	<i>89.6</i>	89.3	100	<i>77.4</i>	
e^* , mm	10	9.17	10.15	10.48	10.60	10.65	13.14	16.2	
n	16	1.89	1.74	1.69	1.68	1.67	1.46	1.33	
$e_{sp} \times n/n-1$, mm	-	13.77	16.92	18.11	18.55	18.71	29.46	46.1	
M_{sp} , kNm	-	4.59	5.24	5.46	5.54	5.57	7.11	8.62	
% $M_{pl,Rd}$ (no splice)	-	23.5	26.9	28.0	28.4	28.6	36.5	44.2	

The iterative procedure of the calculations is shown in Table 2 for two different lengths of HEA100 columns. The input eccentricity, $e = 13.77$ mm, for the first iteration is obtained from the first order imperfection defined by Eurocode 3 at mid height, $e^* = 9.17$, dividing through by $\sqrt{2}$ and multiplying by $n/(n-1)$ to make it a second order imperfection at $x = \ell/4$. $M_{pl,Rd} = 19.5$ kNm.

The procedure for the shorter column converges to a design load of 297.6 kN which is still 89.3% of the same column without splice. The design of the 4.53 m long column quickly diverges as the eccentricity rapidly increases at an increasing rate.

For second order eccentricities larger than 42.08 mm the bolts will be subjected to tensile forces and the rotational stiffness of the splice then is a function mainly of the bending stiffness of the butt plates. It should be noted here that the eccentricity of the first iteration, $e = 29.46$ mm still causes only compressive stresses in the splice. The adjusted rotational stiffness of the splice reduces the critical and ultimate loads thereby increasing the second order eccentricity to 46.1 mm that must be applied in the next iteration. The resulting moment arm z is now only 2 mm. This can be read from the graph in Figure 4. The load on the column must now be drastically reduced.

DISCUSSION

It could be argued that for situations where the entire cross-section at the column splice is subject to compressive stresses, there will be no reduction in stiffness, i.e. for $(e_{sp} \times n/n-1)_{\text{final}} < 2\bar{r}^2/h$ the rotational stiffness of the splice has an infinite value and the axial load capacity need not be reduced from the no-splice condition. The condition of a complete compressive stress distribution across the full I-section at the splice would

also allow the column to be designed without any minimum requirements for the connection. However, if friction is not allowed to be taken into account, a minimum splice would only require to be designed for the shear force at splice location.

It was found that none of the eight building codes studied has adopted such a design approach for column splices with butt-plates. (Snijder & Hoenderkamp, 2005, 2008)

CONCLUSIONS

A method of analysis for spliced columns with single row bolted butt-plates has been presented. Imperfections defined by Eurocode 3 allowed the rotational stiffness of the splice in addition to reduced values for critical and ultimate loads to be obtained with an iterative procedure. The method does not allow tensile forces in the bolts to be included. The study of the behavior of butt-plate splices has shown that there are boundaries to the eccentricities that can be applied to the connection.

If the design procedure converges to a reduced design load, no additional materials need be applied to the column splice.

Columns with butt-plate splices always need to have their ultimate axial load reduced because Eurocode 3 requires the columns to be designed with specifically defined imperfections.

REFERENCES

Dunkerley S. (1894), On whirling and vibration of shafts. *Philosophical Transactions of the Royal Society of London*, Ser. A, 185, (pp. 279-360).

EN1993-1-8:2004, *Eurocode 3*. (2006), *Design of steel structures, Part 1.8: Design of joints*.

Lindner J. and Gietzelt R. (1988), Kontaktstöße in Druckstäben, *Stahlbau*, 57, (pp. 39-49 and 384), (in German)

Lindner J. (1998), Contact Splices in Compression Members, *Proceedings of the Nordic Steel Construction Conference 98*, Bergen, Norway, September 14-16, Vol.1, (pp. 167-176).

Lindner J. (1999), Traglastversuche an Kontaktstößen mit Kopfplatten, *Stahlbau*, 68, (pp. 929-934), (in German)

Lindner J. (2002), Zur Tragfähigkeit von Kontaktstößen, *Bauen mit Stahl, Dokumentation 654*, Vortragsreihe I, Deutscher Stahlbautag 2002 Neues aus Forschung, Entwicklung und Normung, (pp. 12-17), (in German)

Lindner J. (2008), Old and new solutions for contact splices in columns, *Journal of Constructional Steel Research*, Vol. 64, pp. 833-844, doi:10.1016/j.jcsr.2008.01.026

Popov E.P., and Stephen R.M. (1977), Capacity of Columns with Splice Imperfections, *Engineering Journal*, AISC, Vol. 14, No. 1, (pp. 16-23).

Scheer J., Peil U. and Scheibe H.-J. (1987), Zur Übertragung von Kräften durch Kontakt im Stahlbau, *Bauingenieur*, 62, (pp. 419-424), (in German)

Snijder H.H. and Hoenderkamp J.C.D. (2005), *Column splices in steel structures – literature research* (in Dutch), Eindhoven University of Technology, Faculty of Architecture Building and Planning, Report O-2005.19.

Snijder H.H. and Hoenderkamp J.C.D. (2008), Influence of end plate splices on the load carrying capacity of columns, *Journal of Constructional Steel Research*, Vol. 64, pp. 845-853, doi:10.1016/j.jcsr.2008.01.020

STRUCTURAL INTEGRITY – WHAT DOES THIS MEAN FOR CONNECTION DESIGN?

Kurt Gustafson

American Institute of Steel Construction, Chicago, Illinois, USA
kgustafson@aisc.org

Cynthia J. Duncan

American Institute of Steel Construction, Chicago, Illinois, USA
duncan@aisc.org

Thomas Schlafly

American Institute of Steel Construction, Chicago, Illinois, USA
schlafly@aisc.org

ABSTRACT

This paper summarizes the efforts that have been made since the World Trade Center tragedy to address its impact on how a steel structure should be designed. The development of the two proposals suggested for incorporation into the 2009 International Building Code, by the NCSEA Joint Industry Committee, is discussed. One proposal considers “Risk Assessment” requirements for certain building categories; and the other incorporates “Minimum Requirements” for structural integrity in many other structures. A major part of the latter proposal deals with “tie-forces” in structures. The impact of the NCSEA proposed tie-force requirements on typical structural steel connections, if they are adopted, will be assessed. An overview of the existing codes containing provisions for structural integrity and a summary of ongoing research in the U.S. on the topic is also included.

INTRODUCTION

Everything that a structural engineer does involves structural integrity, but this has become a “buzz word” in the construction community as a result of the World Trade Center (WTC) tragedy. Following the collapse of the twin-towers, there has been significant discussion as to whether total collapse could have been prevented and if the country could afford the economics associated with producing a virtually indestructible structure. The likely answer is that we will not be able to afford structures that will withstand every possible disaster, but is there a middle-ground somewhere, in which concepts of enhanced integrity can be balanced in harmony with the economics of the construction? The efforts to address the WTC tragedy and other past collapses are summarized, as well as their effect on connection design. As the United States attempts to further codify structural integrity, it is also helpful to review what other code

bodies are incorporating into their standards, as well as examine what additional research may be required.

STRUCTURAL INTEGRITY: RECENT BUILDING CODE ACTIVITIES

In the aftermath of the Twin-Towers collapse, the National Institute of Standards and Technology (NIST) conducted an exhaustive study of each of the towers construction, a damage assessment of the effect of the airliners impact, an assessment of probable interior damage, and an assessment of the resulting fire impact on the structure. NIST generated an extensive report of the study with conclusions as to the probable collapse mechanisms of the towers. The Final Report of the Collapse of the World Trade Center Towers was issued in September 2005. The Executive Summary of findings included this statement:

“The two aircraft hit the towers at high speed and did considerable damage to primary structural components (core columns, floors, and perimeter columns) that were directly impacted by the aircraft or associated debris. However, the towers withstood the impacts and would have remained standing had it not been for the dislodged insulation (fireproofing) and the subsequent multi-floor fires. The robustness of the perimeter frame- tube system and the large size of the buildings helped the towers withstand the impact. The structural system redistributed loads from places of aircraft impact, avoiding larger scale damage upon impact. The hat truss, a feature atop each tower which was intended to support a television antenna, prevented earlier collapse of the building core. In each tower, a different combination of impact damage and heat-weakened structural component contributed to the abrupt structural collapse.”

The abstract of the Report summarizes: “The report concluded with a list of 30 recommendations for action in the areas of increase structural integrity, enhanced fire endurance of structures, new methods of fire resistant design of structures, enhanced active fire protection, improved building evacuation, improved emergency response, improved procedures and practices, and education and training.”

Many in the structural engineering community failed to see the direct connection between the conclusions of the report as to the robustness of the structural frames to withstanding the tremendous impact, and the following recommendation for needed action in the area of increased structural integrity. Pressure was placed on the building code community to address the recommendations of the concluding NIST Report. It was evident to many that this had become a political issue; not one to address a deficiency related to the collapse of the towers, but to the way structures are designed or constructed.

The International Code Council (ICC) formed an Ad-Hoc Committee on Terrorism Resistant Buildings (TRB Committee), which developed a proposal pertaining to not only the general structural integrity issue; but also disproportionate collapse. In other words, the latter part was to address the stability of a structure if structural supports were removed. This document was intended to be adopted into the 2007 IBC Supplement. This was commonly designated as ICC Proposal S5. The general structural integrity provisions of the S5 proposal primarily addressed adding horizontal

and vertical ties between structural components. The minimum tie force requirements for structural steel systems presented in this S5 proposal largely emulated requirements from British Standards adopted after the Ronan Point collapse in 1968.

Ronan Point was a 22 story precast concrete, high-rise apartment structure in London, England, which consisted of stacked construction of precast bearing walls and floor slabs. Connections of the slabs and walls, though not well documented, were thought to be minimal. A minor gas explosion near one of the exterior walls at the 18th level pushed out one of the exterior wall panels; in turn causing a chain reaction, culminating in collapse of the entire corner of the structure from ground to roof. As summarized from Rouse and Delatte, *Lessons from the Progressive Collapse of the Ronan Point*, Proceedings of the 3rd ASCE Forensics Congress, October 19-21, 2003, San Diego, California, it was reported that subsequent investigations of the collapse revealed that Architect Sam Webb, at the request of the Newham's Housing Committee, had done exhaustive studies of the structural system used to construct Ronan Point. The Webb report revealed that there were significant deficiencies in the design and construction of the buildings associated with the particular type of panelized, stacked construction. The use of this type of system had grown out of the need to replace the housing stock destroyed during the Second World War. A change in national policy in Great Britain allowed the density to double. A lack of skilled construction workers led to the use of these newly developed prefabricated construction techniques (known as system buildings) for high-rise apartment buildings. Webb's report indicated that this panelized system was not developed for use in buildings that exceeded six stories in height. The study also revealed that the building could just as well have collapsed from high winds; as the design wind loads used were severely inadequate. In addition, the level of workmanship quality was found to be extremely poor in the construction of these structures. However, public reaction to this event had resulted in a call for significant revision of British building standards that enveloped all types of structural systems; not only for the panelized, wall bearing types of systems. As a result, engineers in the United Kingdom developed approaches that included provisions for continuous ties in buildings.

During this past year, in recent meetings with British researchers and engineers, an ASCE/SEI Committee on Progressive Collapse delved into the issue of the British Standards tie-force requirements. The Committee indicated that there does not appear to be documentation as to the magnitude of the required tie-force recommendations. This Committee could not find a clear scientific explanation for the basis of the required tie-forces proposed.

In the years that followed the Ronan Point collapse, the precast concrete industry in the U.S. performed studies of ways in which precast concrete structures could be constructed in a more robust manner, such that these types of wall bearing structures would be less likely to collapse in a manner similar to Ronan Point. Detailing provisions were incorporated into ACI 318 (ACI, 2005), intended to better tie the structures together and provide for **enhanced** redundancy and ductility of the structure. These are labeled as Requirements for Structural Integrity.

The S5 proposal emulated the British tie-forces requirements as a basis for the tie-forces required for steel structures in the U.S. However, the S5 proposal did not extend the same requirements to cast-in-place concrete construction, the proponents stating that this was because the ACI 318 Standard had included detailing requirements designated for Structural Integrity. It is not clear if the TRB Committee attempted to correlate the tie-force requirements they had proposed for steel structures, to the tie-forces associated with the ACI detailing requirements. In addition to the tie-force requirements, the S5 proposal had also included requirements for progressive collapse evaluation; assuming that members of a structure would be lost in an unknown event. This would be similar to GSA (General Services Administration) and DOD (Department of Defense) requirements for government buildings considered to be subject to terrorist attack.

There was significant opposition to the S5 proposal developed by this TRB Committee from a broad spectrum of the structural design community, and from numerous standards development organizations; including AISC. These opponents to the S5 proposal largely agreed that there was no substantiation of a need to reevaluate the way buildings are designed in the U.S; that buildings properly designed and constructed in accordance with the consensus industry standards are not subject to collapse like a “house of cards,”, as the S5 proponents had often stated.

The National Institute of Building Sciences (NIBS), which monitors building code issues, held hearings in Washington D.C. in May 2006 to discuss and determine what action to take regarding the ICC Ad-Hoc Committee’s Proposal S5. Representatives of ASCE, NCSEA, as well as those of the material standards organizations, including AISC, all spoke in opposition to the S5 Proposal. At the hearings, NCSEA (National Council of Structural Engineers Associations) committed to forming a Joint Industry Committee to develop an alternate proposal that would address structural integrity, intended for submission in the 2009 IBC cycle. The proponents of Proposal S5 indicated that they would continue to leave their proposal active for ICC consideration, pending the completion of a Proposal by the NCSEA Joint Industry Committee. The S5 Proposal was subsequently disapproved by ICC for incorporation into the 2007 IBC Supplement.

The NCSEA Joint Industry Committee on Structural Integrity was formed, comprised of members of the design community working in conjunction with industry Standards development organizations, and government representatives to develop a reasonable approach to “enhanced” building design. This Committee effort resulted in two proposals submitted for ICC consideration. One of the proposals considers “Risk Assessment” requirements for certain building categories; the other incorporates “Minimum Requirements” for structural integrity for many other structures. The suggested “Minimum Requirements” proposal deals mainly with “tie-forces” in structures.

The horizontal tie-force requirements for frame structures of the NCSEA proposal in many ways are similar to those in the S5 proposal for structural steel framing; however,

there are also some distinct differences. Similar to the S5 proposal, the minimum tie-force requirements of the NCSEA proposal is calculated based on the span of the framing component (beam), and the gravity loads that the member was designed to support. In other words, the horizontal tie-force was correlated to a percentage of the design end reaction of the spanning member. However unlike the S5 proposal, the NCSEA proposal used the same method to assess tie-force requirements for both structural steel and concrete structures. Also like the S5 proposal, the horizontal tie force was not required to be considered simultaneously with the gravity load vertical reaction. Unlike the S5 proposal, the NCSEA proposal recognizes the two load approaches permitted for structural steel, as covered in both the ASCE 7 Standard and the AISC Specification. The NCSEA proposal defines equivalent load approaches for ASD and LRFD, while the S5 proposal limits the design check to using the LRFD approach. Like the S5 proposal, the determination of the required tie force in the NCSEA proposal is rather arbitrary, and has no definitive scientific basis. Unlike the S5 proposal, the NCSEA proposal assesses the tie-force requirement on a nominal strength basis; rather than comparison to a design strength. The NCSEA Committee reasoned that since this horizontal tie-force is intended to evaluate a failure mechanism, rather than a serviceability consideration, it would be more appropriate to use the nominal limit states as criteria against which to check the horizontal tie-force.

The two NCSEA Proposals were submitted to ICC for consideration of adoption to the 2009 IBC. The TRB Committee also resubmitted their competing proposal for consideration in the 2009 Cycle. These were designated by ICC for the 2009 cycle as follows:

- G108 – NCSEA Risk Assessment
- S101 – NCSEA Minimum Requirements for Structural Integrity
- S59 – TRB Disproportionate Collapse

This discussion may be somewhat immaterial at this point in time, since at the ICC Hearings in February 2008, the ICC Structural Committee disapproved both S59 and S101. Also, the ICC General Committee disapproved G108. Therefore, there are no Committee 'Approved' active proposals on the structural integrity or progressive collapse issues pending for the 2009 ICC cycle.

As previously stated, there is widespread agreement with the ASCE/SEI findings of lack of scientific basis for the arbitrary tie-force requirements. However, regardless of the magnitude of a horizontal tie-force, we will herein explore the capacity of typical steel connections to resist axial tension forces. In this study, we make comparisons of the horizontal capacity limit states in relation to the vertical capacity limit states.

The first connection examined is the common conventional configuration, single-plate shear connection. The example is for a 5/16-in.-thick, ASTM A36 shear plate, with four 3/4-in.-diameter A325N bolts in SSLT holes. The geometry is as used in the 13th edition Manual Tables. The check is to determine the vertical reaction capacity for the connection. Capacity limit states checks of Bolt Shear, Shear Yielding, Shear Rupture,

Bolt Bearing, and Block Shear Rupture for this particular connection, indicates that the vertical reaction capacity is controlled by Bolt Shear at the available strength level; 63.6 kips (LRFD) and 42.4 kips (ASD). Looking in Table 10-9a on page 10-107 of the 13th Edition *Steel Construction Manual* (AISC, 2005b) is the easy way to confirm these numbers. Just as a side-note, the nominal strength level is controlled by Shear Yielding, but this is not evident by looking in the Manual Tables, as only the controlling limit state available capacity is shown.

The horizontal capacity for the same four bolt single-plate connection can also be checked for the applicable limit states of Bolt Shear, Tensile Yielding, Tensile Rupture, Bolt Bearing, and Block Shear Rupture per the Specification. (We have side-stepped the Specification limitation that slots are not permitted in the direction of the load, for now.) In this particular connection, it is again found that Bolt Shear is the controlling limit state at the available strength level; 63.6 kips (LRFD) and 42.4 kips (ASD). In this case one cannot check the numbers in Manual tables, because the Tables do not address axial loads.

In summary, using the example of a single-plate shear connection, the available capacity to resist horizontal loads is identical to the capacity to resist vertical loads. Detailed comparisons have not yet been made of other combinations of plate thickness and yield strength, bolt type, and whether threads are excluded from the shear plane or not. Checks on the beam web side of the single-plate connection have also not been made. If more detailed comparisons are investigated, there may be variations as to the controlling limit states, and the ratio of horizontal-to-vertical capacity. However, it is not expected that we will likely find very great deviations in this ratio for most single-plate connections of the conventional configuration.

The second type of connection examined is the all bolted double-angle connection. The example is for 2L 4 x 3 ½ x ¼, with three rows of ¾-in.-diameter A325N bolts. The geometry is as used in the 13th Edition Manual Tables. First, the vertical reaction capacity for the connection is checked. Capacity limit states checks of Bolt Shear, Shear Yielding, Shear Rupture, Bolt Bearing, and Block Shear Rupture, for this particular connection, indicates that the vertical reaction capacity is controlled by Block Shear Rupture at the available strength level; 76.4 kips (LRFD) and 50.9 kips (ASD). This time looking in Table 10-1 on page 10-22 of the 13th Edition Manual is the easy way to confirm these numbers. This time also, the nominal strength level is controlled by Shear Yielding.

In the case of double angle connections, the assessment of axial tensile capacity is a very complex matter. Present strength level approaches necessitate very thick angles to accommodate relatively small axial tensile loads. These approaches do not really reflect the desirable performance attributes of the connection to deform and shed load at the inelastic level, prior to failure. The ¼-in.-thick angles in this example will have very little capacity to resist axial load at the limitations set by the prying model approach. If it is necessary to accommodate the same load as determined for the vertical capacity in an axial tensile load direction; we would need to increase the angle thickness such that

flexibility of the connection to vertical loads would be severely compromised. It may also be apparent that the rolled angles will often not be thick enough to accomplish this requirement. In this particular example, if we need to resist a horizontal tie-force equivalent to the **vertical shear capacity** of the connection, and if the prying model approach is used, the thickness of the angles would need to be 7/8 in.

Another variation of the double-angle connection, where the outstanding legs are welded along the vertical edge to the support (knifed connection), is really not appropriate for use to accommodate axial loads. The eccentricity of the force to the weld results in a torsion on the weld; rather than a direct shear. This type of connection should not be used to resist axial tensile loads.

The formation of the NCSEA Joint Industry Committee was a necessary reaction to address the TRB proposals, which many in the design and standards development organizations felt were unwarranted, and without substantiation as to basis or need. However, there are ongoing discussions in the ASCE/SEI and NCSEA groups in an attempt to define effective criteria and procedures to assess general structural integrity and progressive collapse. Whether tie-force requirements are an effective or necessary approach, or whether concentrating more on ductility and performance approaches would be preferred, is being discussed and evaluated.

Regardless whether tie-forces will be required by future building codes, it would seem prudent to consider further testing and evaluation as to the performance and ultimate capacity of these connections to resist axial tensile loads. The British have developed an approach to the design of the all-bolted double-angle connection to resist axial tensile forces, which in effect results in the angles tending to straighten out and resisting the force by primarily tension in the angles.

BCSA Appendix B (BCSA) describes the approach to the design of double angles to resist tensile axial tie-forces. The large displacements exhibited by the angles, as confirmed by tests; tend to straighten the angles, effecting a reduction in the eccentricity. This results in a large portion of the axial tension being resisted directly by tension in the angles.

NIST has been conducting analytical studies, followed by testing of the ultimate performance of different types of steel connections. The preliminary studies were mainly related to seismic connection types. During the NCSEA Joint Industry Committee meetings, there were discussions with NIST representatives pertaining to the ultimate performance of simple steel shear connections in progressive collapse scenarios. We also discussed the contribution of the slab/deck diaphragm in assisting to arrest collapse mechanisms. In the NCSEA Structural Integrity Proposal, the tie force requirement assumed an unknown contribution of the diaphragm in arresting collapse mechanisms. The tie-force requirement was permitted to be reduced by 50% if a described diaphragm was provided. In subsequent modeling by NIST of collapse mechanisms for steel framing, the three dimensional frames were modeled both with

and without diaphragm. The results of their study supported the 50% reduction included in the NCSEA Proposal.

There is still a lot of dissension as to what should be done to enhance the integrity of built structures. There is also a lot of dissent as to whether all structures should be designed to the same level of resistance to terrorist attack, or to accidental occurrences; and if so, can the economy afford the luxury of building structures that are virtually indestructible.

Everything that a structural engineer does involves structural integrity, but this has become a 'buzz word' in the construction community as a result of the World Trade Center tragedy. In the realm of structural steel construction, everything that the AISC Specification, Seismic Provisions, Steel Construction Manual, as well as other developed AISC documents, promotes structural integrity in general. Besides providing requirements to assess a steel structure capacity to adequately resist Building Code mandated gravity and lateral loads, the Stability Analysis requirements stipulate actual procedures to assess the stability of the structure as a whole and for each of its elements. These stability analysis requirements provide a significant advancement in the way the structural performance of the whole steel structure is looked at. The ductility of connections in assessing the performance of the structure is also covered as general requirements in the AISC Specification. In support of these requirements, the Steel Construction Manual provides direct guidance as to how the ductility performance of typical 'Simple Connections' are assessed. This is also a prime factor in the way connections perform in resisting abnormal loads.

The AISC Specification until recently included minimum capacity requirements for steel connections of 6 kips (ASD) and 10 kips (LRFD). These minimal capacities now seem somewhat meaningless, since as the common use of high strength bolts has become almost universal in structural steel connections. The AISC Specification has not required that connections for main steel members contain a minimum of two bolts, but the standard connection details in the Manual have always used two bolts as a minimum. This may be somewhat of a moot point however, since the OSHA requirements stipulate that steel members must be secured with at least two bolts prior to release from the load line.

Although not specifically identified as requirements for structural integrity, these are prime factors in providing for the basic integrity of structural steel construction. A history of successful performance of steel structures constructed in accordance with the AISC Specification, and using properly designed common connection details as included in the Manual, seem to attest to the structural integrity of such constructions. There also seems to be no basis for the claims that there is a significant deficiency in the way structural steel structures are designed and constructed; or that a 'house of cards' could be built when constructed in accordance with the AISC Specification.

However, while there does not seem to be a problem with the general integrity of properly designed and constructed structural steel buildings, we always should be

looking for ways to improve the performance of our structures. Whether progressive collapse is to be considered an issue in the design of structures, whether being directed to a specific classification of occupancies, or as a general consideration, is an ongoing discussion.

STRUCTURAL INTEGRITY IN OTHER STANDARDS AND CODES

In an effort to find some agreeable and more explicit solution to codifying structural integrity for steel structures on a national level in the United States, it may be helpful to look further at what provisions already exist in various standards and codes in the U.S. and in other countries. Although the International Building Code (IBC) (ICC, 2006) does very little to address structural integrity, the ASCE standard that is the referenced load standard in the U.S., *Minimum Design Loads for Buildings and Other Structures* (SEI/ASCE 7) (ASCE, 2005), includes a section on the subject. A couple of other U.S. material standards include limited provisions on the subject, as well as some code bodies outside of the U.S., such as the *British Standard for Structural Steelwork* (CEN, 2006), discussed earlier, the Eurocode, and the Canadian standard, *Limits States Design of Steel Structures* (CAN/CSA-S16-01) (CSA, 2007). Much of the coverage in these standards is vague and general, and not specifically addressing how connection designs would be ultimately affected.

In the U.S., the SEI/ASCE 7 standard, as well as the material standards for concrete (ACI, 2005) and cold-formed wall studs, address structural integrity in some manner. SEI/ASCE 7 addresses structural integrity peripherally in Section 1.3, which is a general safety-related section including provisions for handling “self-straining forces” and “counteracting structural actions.” The subject is addressed more specifically in Section 1.4, “General Structural Integrity,” where it says “Buildings and other structures shall be designed to sustain local damage with the structural system as a whole remaining stable and not being damaged to an extent disproportionate to the original local damage.” The section concludes, “This shall be accomplished by providing sufficient continuity, redundancy, or energy-dissipating capacity (ductility)...” The latter could be accomplished by providing the proper flexibility in the connections. It is interesting to note, however, that the IBC has not adopted this section because it is considered to be too vague and unenforceable to be appropriate for a building code. The assumption is that by correctly applying the adopted structural standards, in other words, SEI/ASCE 7 and associated material standards, buildings will have some level of inherent structural integrity.

Efforts to directly incorporate structural integrity provisions into material standards have been limited. As mentioned earlier, the concrete code, *Building Code Requirements for Structural Concrete* (ACI 318) (ACI, 2005) incorporated criteria in response to the Ronan Point collapse, including a requirement for minimum tensile strength of connections at diaphragms (Section 7.13). The *AISI Wall Stud Design Standard* (AISI, 2004) integrates structural integrity with a requirement that perhaps incorporates some level of redundancy in the structure. The standard says, “When sheathing braced

design is used, the wall stud shall be evaluated without the sheathing bracing for the following load combination: $1.2D + (0.5L \text{ or } 0.2S) + 0.2W$ (Eqn. C3-1).” Also, in the *AISC Specification for Structural Steel Buildings* (AISC, 2005a), it could be said that the requirements in Sect. J1.10 to use pretensioned or slip-critical joint or welds in certain situations, such as in column splices in all multi-story structures over 125 ft or when there are live loads producing impact or reversal, is providing some amount of robustness or structural integrity in the structure.

Outside the U.S., the Eurocode and the Canadian Code, CAN/CSA-S16-01, currently include provisions that address structural integrity to some extent. For example, there are statements made in Eurocode 0, 1 and 3 (CEN, 2002; CEN, 2005; CEN, 2006) that imply an effort to attain some level of structural integrity, but the terminology is not used explicitly. Eurocode 1 (CEN, 2006) criteria, mentioned in Davison and Tyas (2008), is vague and general, with three options provided for limiting the extent of localized failure in accidental situations. Eurocode 0, Part 2.1, gives a general requirement that the “structure shall be designed and executed in such a way that it will not be damaged...to an extent disproportionate to the original cause; while Part 2.6 provides a similar requirement to AISC Sect. J1.10, as discussed above, for joints loaded in shear subject to impact, vibration and/or load reversal. There is a specific connection requirement in Eurocode 3, Part 1-8, Sect. 3.10.4(5) that stipulates a minimum of two bolts or rivets “to attach a lug angle to a gusset or other supporting part.” In contrast to the Eurocode, CAN/CSA-S16-01 introduces the topic directly, including how it relates to connection design, in Sect. 6.1.2, “Structural Integrity,” as follows:

The general arrangement of the structural system and the connection of its members shall be designed to provide resistance to widespread collapse as a consequence of local failure. The requirements of this Standard generally provide a satisfactory level of structural integrity for steel structures. Supplementary provisions may be required for structures where accidental loads such as vehicle impact or explosion are likely to occur (see Clause 1.3)

Although the verbiage is again general, it is stating that use of the Standard will provide the necessary amount of structural integrity. Clause 1.3 states that supplementary provisions may be required in special situations, including steel structures “exposed to severe environmental conditions or possible severe loads.” CAN/CSA-S16-01 carries the theme of Sect. 6.1.2 by inserting the term “integrity” throughout the document. For example, the term appears in the following sections: (1) Sect. 4.2.2(j), where structural design documents shall include “all load-resisting elements essential to the integrity of the completed structure and the details necessary to ensure the effectiveness of the load-resisting system...”; (2) Sects. 4.3.3 and 4.3.4, related to erection diagrams and procedures, where erection diagrams must show “all steel load-resisting elements essential to the integrity of the completed structure, size and types of bolts, field welds,...”; (3) Sect. 21.5, where in bearing joints in compression members “there shall be sufficient fasteners or welds ...to provide a satisfactory level of structural integrity”; (4) Sect. 27.1.2, where the general requirements for seismic design using capacity design shall maintain structural integrity; and (5) Sects. 29.1 and 29.3, where temporary bracing and connections must provide structural integrity. This model may be a possible direction for future editions of the AISC Specification.

AISC AND RESEARCH ON STRUCTURAL INTEGRITY

Research in the U.S. is being conducted by governmental and private groups. AISC has recognized the need for sound responses based on valid investigation and evidence. We believe steel frames do provide ductility and resistance to many damage scenarios and can be made to resist others with little extra cost. What cannot be allowed to happen is to have arbitrary and unfounded demands based on perception become part of the design regime. Our mission is to assure we have the knowledge to respond to needs in a reasoned fashion. Damage scenarios can be selected. These damage scenarios can be associated with frame responses and then with component demands. Components can be evaluated to determine their resistance to those demands.

AISC participated with NIST in modeling calibration tests of full size seismic type connection configurations. AISC has assigned a task group to establish a strategy for structural integrity investigation and is commencing work with two projects within that strategy. The primary exercise conducted to provide background for a strategy was an analytic evaluation by Dr. Foley of Marquette University. Dr. Foley considered a number of damage scenarios in multiple frame heights. The study reached some conclusions about integrity but perhaps more importantly gave an idea of the issues that need future investigation, a vision of methods that might be used to develop effective levels of integrity, component requirement modeling needs and other areas that need development before a sound response to the need for integrity is defined. Structural integrity is a wide ranging issue that will demand investigation from the frame to the component level and with the structure provided by a research strategy. Potential areas of work include: effects of various damage scenarios on various frame types and sizes, how slab and deck effects performance, ways to model slab effects, determining what demands are placed on components, defining a load protocol for testing that will give results that correlate to damage scenarios, and determining what the ultimate strength of components is when subjected to an appropriate load protocol. AISC hopes to be able to support some efforts to resolve elements of the total issue.

In 2007, AISC awarded the Faculty Fellowship to Dr. Kodur for work on fire resistance in steel structures, certainly another related topic. In April, AISC announced the 2008 AISC Faculty Fellowship was awarded to Dr. Jeff Berman of the University of Washington for "Improving the Threat Independent Life-Safety of Steel Gravity Framing Systems." Dr. Berman will work on this project for the next 4 years. We have also initiated discussion with Dr. Larry Fahnestock of the University of Illinois Urbana Champaign to support some of his work on "Assessment of Structural Integrity and Mitigation of Progressive Collapse in Steel Buildings." There are many tasks to be completed in pursuit of all the knowledge needed so we anticipate more projects in the future.

REFERENCES

- ACI (2005), *Building Code Requirements for Structural Concrete*, ACI 318-05, American Concrete Institute, Farmington Hills, MI.
- AISC (2005a), *Specification for Structural Steel Buildings*, ANSI/AISC 360, American Institute of Steel Construction, Chicago, IL.
- AISC (2005b), *Steel Construction Manual*, 13th Edition, American Institute of Steel Construction, Chicago, IL.
- ASCE (2005), *Minimum Design Loads for Buildings and Other Structures*, ASCE/SEI 7-05, American Society of Civil Engineers, Reston, VA.
- AISI (2004), *Wall Stud Design Standard*, American Iron and Steel Institute, Washington, DC.
- BCSA, "Appendix B, Large Displacement Analysis Double Angle Web Cleats," British Constructional Steelwork Association, Ltd., London.
- CEN (2002), *Eurocode 0: Basis of Structural Design*, EN 1990, Comité Européen de Normalisation, Brussels, Belgium.
- CEN (2005), *Eurocode 3: Design of Steel Structures – Part 1-8: Design of Joints*, EN 1993-1-8, Comité Européen de Normalisation, Brussels, Belgium.
- CEN (2006), *Eurocode 1 : Actions on Structures - Part 1-7: General Actions - Accidental Actions*, EN 1991-1-7, Comité Européen de Normalisation, Brussels, Belgium.
- CSA (2007), *Limit States Design of Steel Structures*, CAN/CSA-S16-01, including Supplement No. 1 dated 2005 and reaffirmed in 2007, Canadian Standards Association, Mississauga, Ontario, Canada.
- Davison, J.B. and Tyas, A. (2008), "Robustness of Steel Connections," *Proceedings, Connections Workshop VI*, Chicago, IL.
- ICC (2006), *International Building Code*, International Code Council, Fall Church, VA.

PERFORMANCE OF SEISMIC MOMENT RESISTING CONNECTIONS UNDER COLUMN REMOVAL SCENARIO

Fahim Sadek, H. S. Lew, Joseph A. Main, John L. Gross

Building and Fire Research Laboratory, National Institute of Standards and Technology,
Gaithersburg, MD, U.S.A.

fahim.sadek@nist.gov, hsl@nist.gov, joseph.main@nist.gov, john.gross@nist.gov

ABSTRACT

Beam-to-column moment connections in steel frame construction have been studied extensively for seismic applications. The behavior of such connections, however, has not been studied under the monotonic loading conditions expected in progressive collapse scenarios, in which connections are subjected to combined bending and tension. This paper presents an experimental and analytical assessment of the performance of beam-column assemblies with two types of moment resisting connections under vertical column displacement. The connections considered include (1) a welded unreinforced flange-bolted web connection and (2) a reduced beam section connection. The study provides insight into the behavior and failure modes of the connections, including their ability to carry tensile forces that develop in the beams. The results indicate that these connections can sustain larger rotations under monotonic loading conditions than under the cyclic loading conditions developed for seismic applications. Validated models of the connections are developed that capture the primary response characteristics and failure modes.

INTRODUCTION

While structural safety in buildings is implicitly assured through reliability-based load and resistance factors, such provisions in current building codes and standards do not include load combinations to account for abnormal loading events that may lead to progressive collapse. Progressive collapse is the collapse of a disproportionately large portion of a structure that results from localized initial damage (e.g., failure of a column). An accurate characterization of the nonlinear, large-deformation behavior associated with the transfer of forces through the connections in this scenario is critical in assessing the potential for progressive collapse.

The National Institute of Standards and Technology (NIST) has initiated a research program to study the behavior of structures that when exposed to abnormal loads, might lead to progressive collapse. At present, design and evaluation of structures for progressive collapse potential are typically based on acceptance criteria obtained from seismic research (e.g., FEMA 350, 2000). As will be shown in this paper, using this approach to predict the response to monotonic loading similar to that expected during progressive collapse underestimates the rotational capacities of the connections.

To understand the behavior of structural systems near their ultimate strength limit states and to develop reliable tools to quantify the reserve capacity and robustness of structural systems, the NIST study involves analysis of three-dimensional models of structures with various materials and systems to assess the vulnerability of different types of structural systems to progressive collapse. The three-dimensional analyses use experimentally validated subsystem models of the various components and connections of the structure.

The study reported herein covers the development of finite element models of steel moment resisting connections with experimental validation. This paper describes two tests of steel beam-column assemblies with selected moment resisting connections under vertical displacement of a center column, representing a column removal scenario. These tests help fill the gap in defining the response characteristics of these connections under monotonic loading, and also contribute to establishing a database of connection behavior that can be used to assess the robustness of structural systems. Finite element models of the tested assemblies are developed and validated with the purpose of understanding the response characteristics and providing input to three-dimensional system-level models of complete structural systems to be analyzed in future studies.

DESCRIPTION OF BUILDING DESIGNS

Prototype steel framed buildings were designed in the NIST study for the purpose of examining their vulnerability to progressive collapse. The buildings are 10-story office buildings with plan dimensions of 100 ft x 150 ft (30.5 m x 45.7 m). The buildings were designed and detailed for two Seismic Design Categories (SDC) to examine the effectiveness of seismic design and detailing in resisting progressive collapse. One building was designed for SDC C, which resulted in a design using intermediate moment frames (IMFs) for the lateral load resisting system and the other for SDC D, which resulted in a design using special moment frames (SMFs) as defined in the American Institute of Steel Construction (AISC) Seismic Provisions (2002).

Moment frames, located around the perimeter of both buildings, provided the lateral load resistance. Connections used in the moment frames were selected from the prequalified steel connections specified in FEMA 350 (2000): (1) Welded Unreinforced Flange-Bolted Web (WUF-B) connections for the IMFs in the SDC C building, and (2) Reduced Beam Section (RBS) connections for the SMFs in the SDC D building.

Beam-column assemblies consisting of two-span beams connected to three columns (see Figure 2) were selected from the second floor of the moment resisting frames of each of the two buildings for the experimental and computational studies presented herein. The beams had a span length (center to center of columns) of 20 ft (6.10 m). The beams selected from the building in the SDC C zone were W21x73 sections, and were connected to W18x119 columns using WUF-B connections. The beams selected from the building in the SDC D zone were W24x94 sections, and were connected to W24x131 columns using RBS connections. ASTM A992 structural steel ($F_y = 50$ ksi, 345 MPa) was used in all beams, columns, and doubler plates in the panel zone.

ASTM A36 steel ($F_y = 36$ ksi, 248 MPa) was used for the shear tabs and continuity plates at connections. ASTM A490 high strength bolts were used for the bolted connections, and welding requirements followed the recommendations in FEMA 353 (2000).

BEAM-COLUMN ASSEMBLY WITH WUF-B CONNECTIONS

Description of WUF-B Connection

The WUF-B connection is similar to the connection commonly used prior to the 1994 Northridge earthquake. After significant research, it was determined that, with several improvements and appropriate quality assurance, this connection can perform reliably. FEMA 355D (2000) provides extensive information on the testing and performance of the WUF-B connections under seismic loading. The acceptable values for inter-story drift angle or rotation capacity of the WUF-B connection was specified in FEMA 350 (2000) based on a statistical analysis of the results from cyclic tests of full-scale connections. The rotation capacity, in radians, corresponding to collapse prevention, characterized by the inability of the connection to maintain its integrity under gravity loading, was estimated to be $\theta_U = 0.060 - 0.0006d_b$, where d_b is the beam depth in inches. For the W21x73 section used with the WUF-B connection, $\theta_U = 0.047$ rad.

The WUF-B connection used in this study is shown in Figure 1. As shown, the beam web is connected to the column flange using a shear plate (shear tab), which is fillet welded to the column using 5/16 in (8 mm) weld and bolted to the beam web using three 1 in (25 mm) diameter, high strength bolts. The bolt holes are standard holes with an edge distance of 2.75 in (70 mm). The beam flanges are joined to the column flange using complete joint penetration (CJP) groove welds. Weld access holes are cut from the beam flanges per the recommendations of FEMA 350 (2000). Continuity plates are provided for both interior and exterior columns as shown in Figure 1. No doubler plates were required for either column.

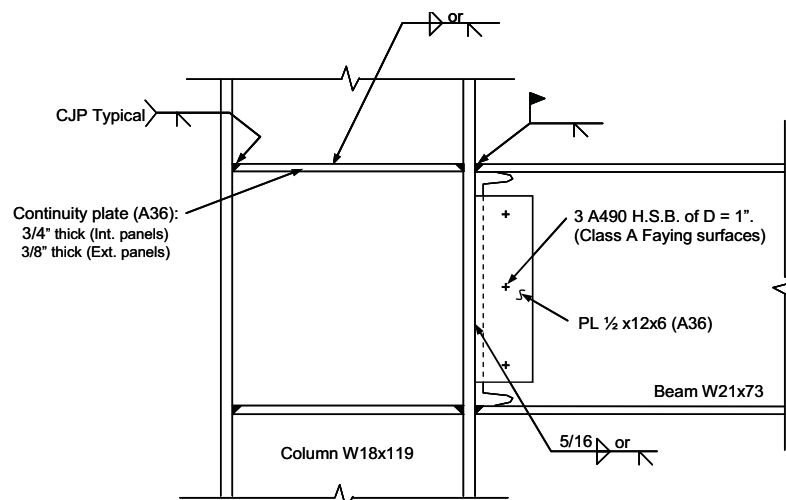


Figure 1. WUF-B Connection Details – Second Floor of Building in SDC C zone

Experimental Setup and Test Results

A schematic of the test specimen is shown in Figure 2 along with details of the instrumentation. Figure 3 shows a photograph of the test specimen along with a close-up of the connections to the center column. As shown in the figures, the double-span beam was supported on two exterior columns, which were anchored to the strong floor of the testing laboratory. Two diagonal braces were rigidly attached to the top of each exterior column to simulate the bracing effect provided by the upper floor. The center column was free at its bottom to simulate a column removal scenario, but its out-of-plane motion was restrained. In addition, the beams were restrained from out-of-plane motion at mid-span by lateral bracings. A hydraulic ram with a capacity of 500 kips (2224 kN) and a 20 in (508 mm) stroke was attached to the top of the center column to apply a vertical load to the specimen. Load was applied under displacement control at a rate of 1 in/min (25 mm/min). The uncertainty in the measured data from the load cells, deflection (D) and strain (S) gages, and inclinometers (I) was within $\pm 1\%$. For more details, see Sadek et al. (2008).

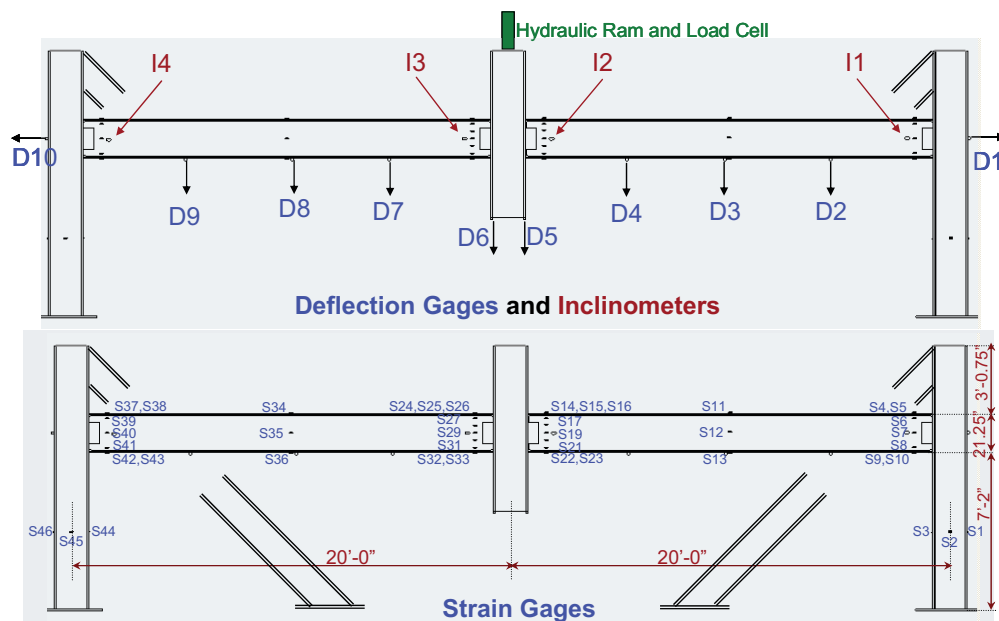


Figure 2: WUF-B Test Specimen Schematic and Instrumentation Layout



Figure 3: Photographs of the WUF-B Test Specimen

The specimen experienced large deflections and rotations prior to failure. The connection failed at a vertical displacement of the center column of about 19.5 in (495 mm), with a corresponding beam end rotation of about 0.088 rad. At that displacement, the applied vertical load was about 200 kips (890 kN). The failure was characterized by the following sequence (see Figure 4): (1) local buckling of the top flanges of the beams at the center column, (2) successive shear fractures of the lowest and middle bolts connecting the beam web to a shear tab at the center column, and (3) fracture of the bottom flange near the weld access hole immediately thereafter.



Figure 4: Failure mode of the WUF-B Test Specimen

Plots of the applied vertical load versus vertical displacement of the center column and the beam axial force versus the vertical displacement of the center column are shown in Figure 7. The beam axial forces are estimated based on the measured strains on the beams. Also presented are the results of the computational models. As the plots indicate, the specimen was unloaded at a vertical displacement of about 18 in (457 mm) to adjust the stroke of the hydraulic ram and then was reloaded again to failure. Figure 7 indicates that the assembly remained in the elastic range up to a vertical displacement of the center column of about 2 in (50 mm). At the early stages of the response, the behavior was dominated by flexure indicated by the compressive axial forces in the beams. With increased vertical displacement, tensile axial forces developed in the beams and the behavior was dominated by catenary action. At the time of failure, the axial tension in the beams was about 150 kips (667 kN).

Finite Element Models and Results

Two finite element models of the beam-column assembly with WUF-B connections were developed to study the behavior of the connections and to compare the calculated response with that measured during the test. The first was a detailed model of the assembly with approximately 300 000 elements, while the second was a reduced model with about 150 elements. The analyses were conducted using LS-DYNA, an explicit formulation, finite element software package (Hallquist, 2007). Overviews of both models are shown in Figure 5.

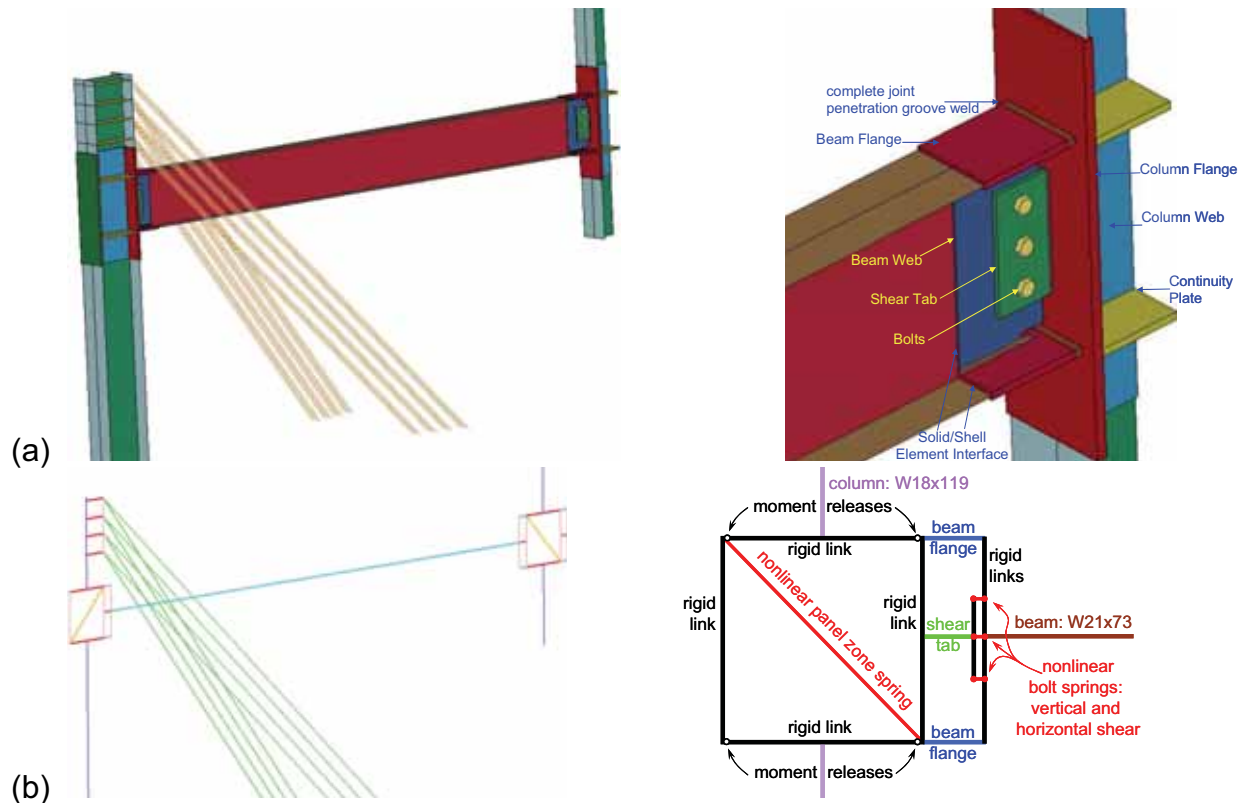


Figure 5: (a) Detailed and (b) Reduced Models of the WUF-B Test Specimen

The detailed model, Figure 5(a), consisted of finely meshed solid elements representing the beams, columns, continuity plates, shear tabs, bolts, and welds in the vicinity of the connection. Contact with friction was defined between the bolts, shear tabs, and beam webs to model the transfer of forces through the bolted connection. Away from the connection zones, the beams and columns were modeled with shell elements. Spring elements were used to model the braces at the top of the exterior columns. All nodes were fixed at the bases of the exterior columns. The steel for the various elements was modeled using a piecewise-linear plasticity model based on coupon tensile test data obtained for all steel sections and plates.

The reduced model used beam elements with Hughes-Liu formulation (Hallquist, 2007) to model the beams and columns. An arrangement of beam and spring elements, connected with rigid links, was used to model the WUF-B connection as shown in Figure 5(b). Nonlinear spring elements represented the bolts, while beam elements represented the shear tab and the top and bottom flanges of the beam. Spring elements were also used to model the diagonal braces and the shear behavior of the panel zone. For the panel zone, the diagonal springs had an elasto-plastic load deformation curve based on the geometry and strength of the panel zone (for more details, see Sadek et al., 2008). Two analyses were conducted in which the bases of the end columns were modeled as fixed and pinned.

Based on the analysis of the detailed model, the beam-column assembly responded initially in a purely flexural mode before catenary action developed. The beam

remained essentially elastic except for the sections in the vicinity of the connections next to the center and end columns where significant yielding was observed. The failure mode of the connection based on this analysis was very similar to that observed in the experiment, see Figure 6. The results from the reduced model were consistent with those from the detailed model, albeit without the same level of detail.

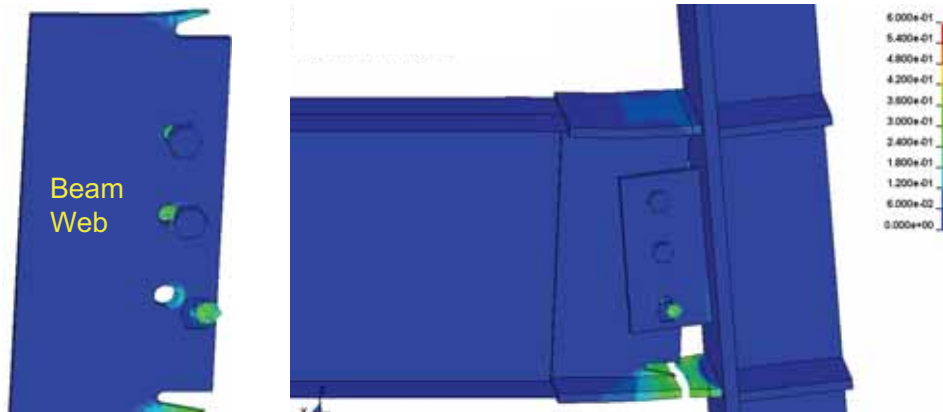


Figure 6: Failure Mode from the WUF-B Detailed Model

Figure 7 shows plots of (a) the applied vertical load and (b) the beam axial force against the vertical displacement of the center column from the experimental results and the two finite element models. The plots indicate a good agreement between the experimental and computational results and provide validation for the detailed and reduced models.

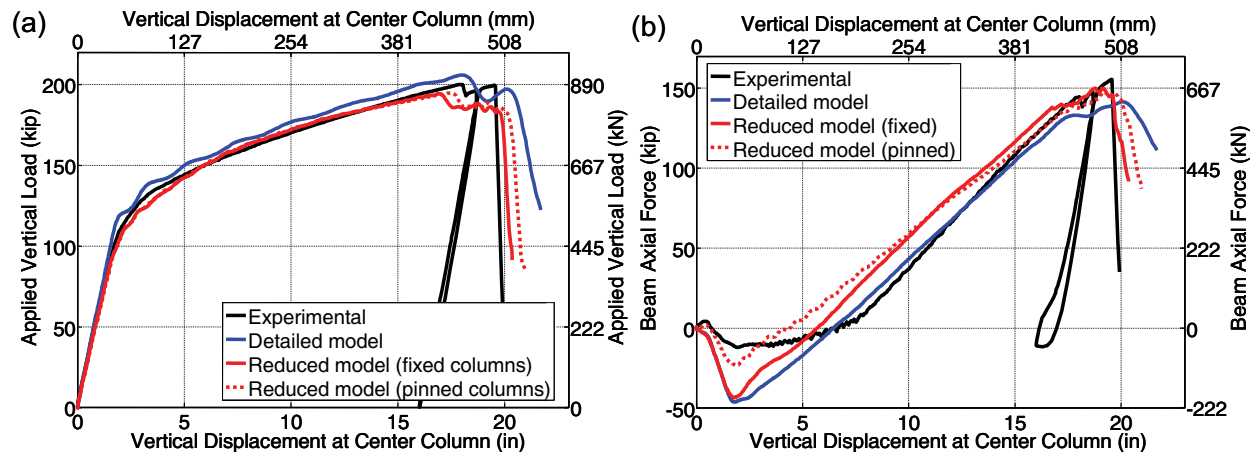


Figure 7: (a) Applied Vertical Load and (b) Beam Axial Force versus Vertical Displacement at Center Column of the WUF-B Specimen

BEAM-COLUMN ASSEMBLY WITH RBS CONNECTIONS

Due to the similarities between the test layout, boundary conditions, and loading system of the WUF-B and RBS specimens, only a brief overview of the RBS test is presented herein. The reader is referred to Sadek et al., 2008 for further details.

Description of RBS Connection

The RBS connection is created by cutting away a portion of the top and bottom flanges of the beam at a distance from the beam-column interface so that yielding would be concentrated in this reduced area. The RBS connection was developed as a result of extensive research following the 1994 Northridge earthquake and has been used for seismic design since then. FEMA 355D (2000) provides extensive information on the testing and performance of the RBS connections under seismic loading. The rotation capacity of the RBS connection, in radians, corresponding to collapse prevention, was specified in FEMA 350 (2000) based on full-scale cyclic tests as $\theta_U = 0.080 - 0.0003d_b$. For the W24x94 section used with the RBS connection, $\theta_U = 0.073$ rad.

The RBS connection used in this study is shown in Figure 8. As shown in the figure, the beam flanges and web are connected to the column flange using CJP groove welds. The connection is created by circular radius cuts in both top and bottom flanges of the beam. Continuity plates are provided for both center and end columns, while doubler plates were required only for the center column.

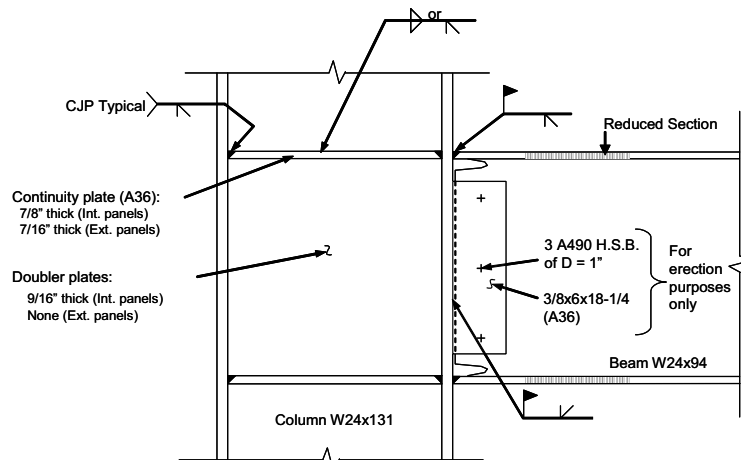


Figure 8. RBS Connection Details – Second Floor of Building in SDC D zone

Test Results

The connection failed at a vertical displacement of the center column of about 33.5 in (851 mm), corresponding to a beam end rotation of about 0.155 rad. At that displacement, the applied vertical load was about 400 kips (1780 kN). The failure was characterized by the fracture of the bottom flange in the middle of the reduced section of one of the connections near the center column. As shown in Figure 9, the fracture propagated through the web until the specimen could no longer carry the applied load.

Plots of the vertical load versus vertical displacement of the center column and the beam axial force versus the vertical displacement of the center column are shown in Figure 12. Also shown are the results of the computational models. Similar to the WUF-B specimen, in the early stages of loading, the response of the beam was primarily in flexure. As the loading progressed with increased vertical displacement of

the center column, the beam response was dominated by tensile axial forces. At the time of failure, the beam axial tensile forces were about 550 kips (2447 kN).



Figure 9: Failure mode of the RBS Test Specimen

Finite Element Models and Results

Similar to the WUF-B specimen, two finite element models were used to estimate the response of the RBS specimen. The detailed model consisted of shell elements representing the columns, beams, continuity and doubler plates, and welds. Finer meshes were used in the vicinity of the reduced section. The reduced model consisted of beam and spring elements. Each reduced beam section was modeled using five beam elements with varying section properties. Both fixed and pinned bases were considered for the end columns.

The detailed model showed that the beam-column assembly responded initially in a flexural mode before catenary action developed. The failure mode of the connection was very similar to that observed in the experiment, see Figure 10. The results from the reduced model were consistent with those from the detailed model.

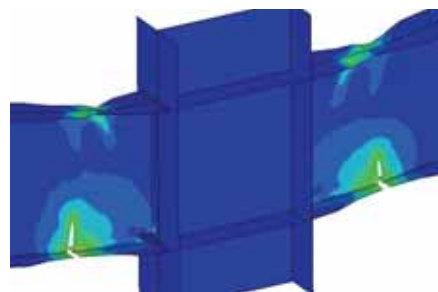


Figure 10: Failure mode from the RBS Detailed Model

Figure 11 shows plots of (a) the applied vertical load and (b) the beam axial force against the vertical displacement of the center column from the experimental results and the two models. The agreement between the experimental and computational results is good and validates the detailed and reduced models. The plots also indicate that the results using the reduced models with pinned and fixed boundary conditions at end column bases generally bracketed the experimental results.

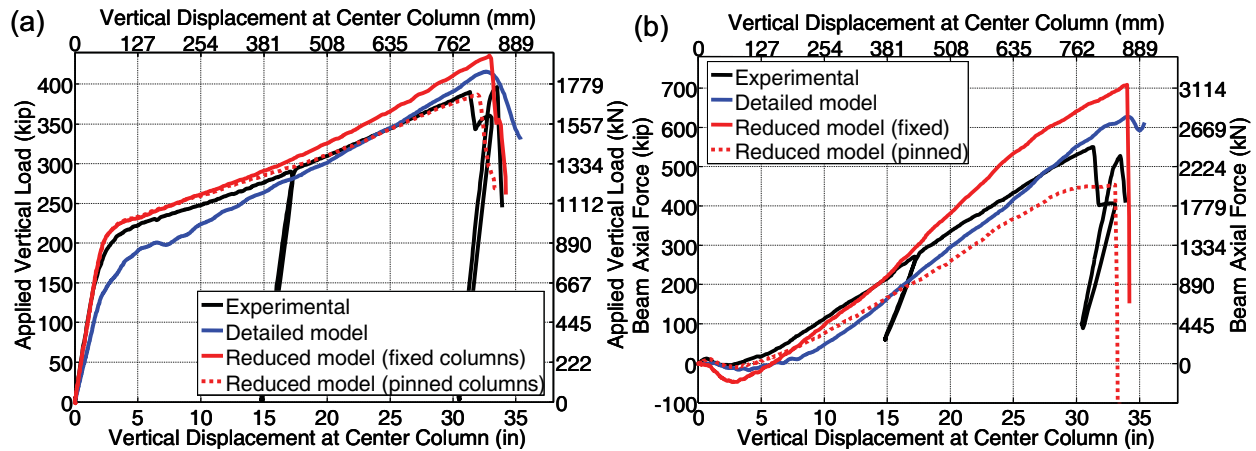


Figure 11: (a) Applied Vertical Load and (b) Beam Axial Force versus Vertical Displacement at Center Column of the RBS Specimen

DISCUSSION AND COMPARISONS

This study indicates a good agreement between the experimental results and the computational predictions. Both detailed and reduced models were capable of capturing the primary response characteristics and failure models. The validated reduced models developed in this study will be valuable in the analysis of complete structural systems for assessing reserve capacity and robustness of building structures. The analyses confirm that the loads under a column removal scenario are primarily resisted by axial tensile forces in the beams. These tensile forces increase until the connection can no longer sustain the axial force.

For the WUF-B and RBS connections, the rotations at peak load were about 0.088 rad and 0.155 rad, respectively based on the experimental results in this study. The rotational capacities of these connections based on seismic testing data are approximately 0.047 rad and 0.073 rad for the WUF-B and RBS connections, respectively. These results show that the rotational capacities of these connections under monotonic column displacement are about twice as large as those based on seismic test data. Contributors to this difference may include: (1) cyclic loading leads to significant degradation in the strength and stiffness of the connection, while no such degradation is expected under monotonic loading, and (2) the applied loads are resisted by different mechanisms in the two cases, with the connection in pure flexure for seismic loading but subjected to both flexure and tension under vertical column displacement, with tension being the dominant load.

SUMMARY AND CONCLUSIONS

This paper presented an experimental and computational assessment of the performance of beam-column assemblies with two types of moment-resisting connections (WUF-B and RBS) under monotonic vertical displacement of a center column. The study provided insight into the behavior and failure modes of the connections. The results indicate that these connections can accommodate

substantially larger rotations (prior to significant strength degradation) under monotonic loading conditions than under the cyclic loading conditions considered in seismic tests. Both detailed and reduced models are capable of capturing the primary response characteristics and failure modes of the connections. The reduced models, in particular, would be valuable in the analysis of complete structural systems for assessing reserve capacity and robustness of building structures.

REFERENCES

AISC (2002), *Seismic Provisions for Structural Steel Buildings*, American Institute of Steel Construction, Chicago, IL.

FEMA 350 (2000), *Recommended Seismic Design Criteria for New Steel Moment-Frame Buildings*, SAC Joint Venture and Federal Emergency Management Agency, Washington, D.C.

FEMA 353 (2000), *Recommended Specifications and Quality Assurance Guidelines for Steel Moment-Frame Construction for Seismic Applications*, SAC Joint Venture and Federal Emergency Management Agency, Washington, D.C.

FEMA 355D (2000), *State of the Art Report on Connection Performance*, SAC Joint Venture and Federal Emergency Management Agency, Washington, D.C.

Hallquist, J. (2007), *LS-DYNA Keyword User's Manual*, Livermore Software Technology Corporation, Livermore, CA, Version 971.

Sadek et al. (2008), *An Experimental and Analytical Study of the Robustness of Moment Resisting Steel Connections*, National Institute of Standards and Technology, Gaithersburg, MD, under preparation.

ACKNOWLEDGEMENTS

The experimental program was conducted at the Engineering Research and Development Center (ERDC) of the U.S. Army Corps of Engineers with partial support from ERDC, the Defense Threat Reduction Agency, the U.S. Air Force, and the American Institute of Steel Construction. Mr. Stephen D. Robert and Mr. Vincent Chiarito of ERDC led the experimental work. The authors acknowledge their contributions. The authors acknowledge the discussions with Professor Sherif El-Tawil of the University of Michigan in the development of finite element models. The authors acknowledge the through review by Drs. Long T. Phan and William E. Luecke of NIST.

Certain commercial software or materials are identified to describe a procedure or concept adequately. Such identification is not intended to imply recommendation, endorsement, or implication by NIST that the software or materials are necessarily the best available for the purpose. The policy of NIST is to use metric units in all its published materials. Because the paper is intended for the U.S. construction industry which uses inch-pound units, units are presented in the inch-pound and metric systems.

ROBUSTNESS OF STEEL CONNECTIONS

J. Buick Davison

Department of Civil & Structural Engineering, University of Sheffield,
Sir Frederick Mappin Building, Mappin Street, Sheffield, S1 3JD, UK
j.davison@sheffield.ac.uk

Andrew Tyas

Department of Civil & Structural Engineering, University of Sheffield,
Sir Frederick Mappin Building, Mappin Street, Sheffield, S1 3JD, UK
a.tyas@sheffield.ac.uk

ABSTRACT

For almost forty years UK building regulations have required the beams and columns of framed structures to be adequately tied together to avoid progressive collapse. Simple prescriptive rules have been routinely applied to RC and steel structures with little difficulty. In recent years, an increased emphasis on performance-based engineering has focussed attention on the real behaviour of structures under extreme loading, for example steel structures in fire. The mechanism of load transfer in damaged structures and the ability of connections to sustain loads in extreme events remains a key research area. This paper reports on work conducted at the University of Sheffield in two areas. First, a series of experimental work on the robustness of simple steel joints to provide data to support the development of component based models capable of predicting joint behaviour with sufficient accuracy for inclusion in frame analysis. Second, the rationale for a recently commenced project on the response of steel joints to suddenly applied loading arising from damage at a remote location in a structure.

THE IMPORTANCE OF ROBUSTNESS

An American government working party report (Defense Threat Reduction Agency, 1999) stated that “Progressive structural collapse is a primary, if not the leading, cause of injury and death in building failures, regardless of the source of loading...For this reason, predicting and designing to prevent progressive collapse of a building under a specified attack scenario is (and should be) a primary objective...” Among their recommendations was “The nature and mechanism of progressive collapse is a subject that merits further study by the academic community.” Although building codes admonish designers to ensure that collapse does not occur, they do not provide guidance on how this can or should be accomplished.

The situation in the United Kingdom is similar. A Standing Committee on Structural Safety report (SCOSS, 1999) acknowledged that, whilst the requirement for structures

to be robust against accidental damage is not disputed, there is presently no established basis for determining how much redundancy is required in order to provide an acceptable level of safety in the event of damage, or to estimate how the forces in a damaged structure are redistributed. The same report pointed out that inherent robustness of buildings may have been compromised by advances in structural analysis and design, which have enabled the designer to model a structure more accurately. This, it argued, has reduced the usual over-design of structural frames in the pursuit of economy of construction, and may have resulted in buildings with reduced robustness.

Eurocode 1 (BSI, 2006) suggests three strategies to limit the extent of localised failure: (1) applying prescriptive design and detailing rules that provide acceptable robustness for the structure (2) designing key members to withstand accidental actions (3) accepting localised failure and ensuring that the integrity of the rest of the structure is not compromised (the *alternate load path* method)

The British Standard for Structural Steelwork (BSI, 2007) section on structural integrity (a term used interchangeably with robustness) adopts approach 1 where possible and prescribes a set of conditions that, if satisfied, allow the designer to assume that the robustness against progressive collapse required by the Building Regulations (ODPM, 2004) is assured. These conditions centre on the need to provide tensile ties at each storey level, and suggest that simple design checks for the capacity of the tie beams and beam-column connections are sufficient to ensure the robustness of the frame to column loss. Similar rules are provided in informative Annex A of Eurocode 1 Part 7 (BSI, 2006), which according to a European report (Leonardo da Vinci Pilot Project, 2005) “were developed from the UK Codes of Practice and regulatory requirements introduced in the early 70s following the partial collapse of a block of flats [Ronan Point] in east London caused by a gas explosion”.

However, a post-September 11th Institution of Structural Engineers’ report (I Struct E, 2002) states, “It is insufficient merely to tie structural elements together. Tying alone does not inherently provide a ductile structure or one with good energy absorption capability.” Robustness is achieved through the use of a structure that can absorb energy; the role of connections is of particular importance. The report notes that “Knowledge of vulnerability of building structures to progressive collapse is incomplete and research is needed to improve understanding of the phenomenon.” Recent research by Izzuddin et al (2007) has highlighted the need for a rational approach to design procedures to prevent progressive collapse as well as the need for experimental work on the behaviour of joints under combined axial and bending (Vlassis et al., 2007).

The collapse of buildings at the World Trade Center has been a reminder of the potential of fire to cause devastating failures of high-rise buildings by initiating a progressive collapse. Research (Armer and O’Dell, 1997; Sanad et al, 2000) has shown that in general composite floors can have a significantly greater fire resistance than is suggested by conventional tests on isolated elements. It is implicitly assumed in fire engineering design approaches that joints retain their structural integrity, yet evidence from the collapse of the World Trade Center buildings (FEMA, 2002), especially Building

5, and full-scale tests at Cardington (BRE, 2004) indicates that joints may be particularly vulnerable during both heating and cooling. If joint failure occurs, the assumed response of the structure will not be able to develop fully, thereby compromising safety levels.

ROBUSTNESS OF STEEL JOINTS IN FIRE

Design codes generally consider that steel connections will be heated more slowly than beams or columns in fire situations, and are therefore less likely to be the critical components in fire safety design. However, connections may often be the weakest link in a structural frame in fire conditions because, at ambient temperature, connections are designed to transfer shear and/or moment, whereas in fire they can be subjected to additional compressive or tensile forces due to restraint to thermal expansion or to catenary action arising from large deflections. At very high temperatures, beams lose most of their bending capacity, and develop axial tensile forces which, in combination with large deflections, may support the lateral loads by second-order effects. In consequence, the connections may eventually be subjected to large rotations and significant tensile forces (Yu and Liew, 2005). Under such conditions there is a clear possibility of connection fracture, which may lead either to fire spread to upper floors, or to progressive collapse of the building. The ability of steel connections to resist combined forces under such circumstances has never been investigated. Recently completed tests at the University of Sheffield were designed to understand the behaviour of common steel connections when subjected to significant catenary forces. Four connection types - flush endplate, flexible endplate, fin plate and web cleat connections - were studied. The test arrangement is shown in Figure 1.

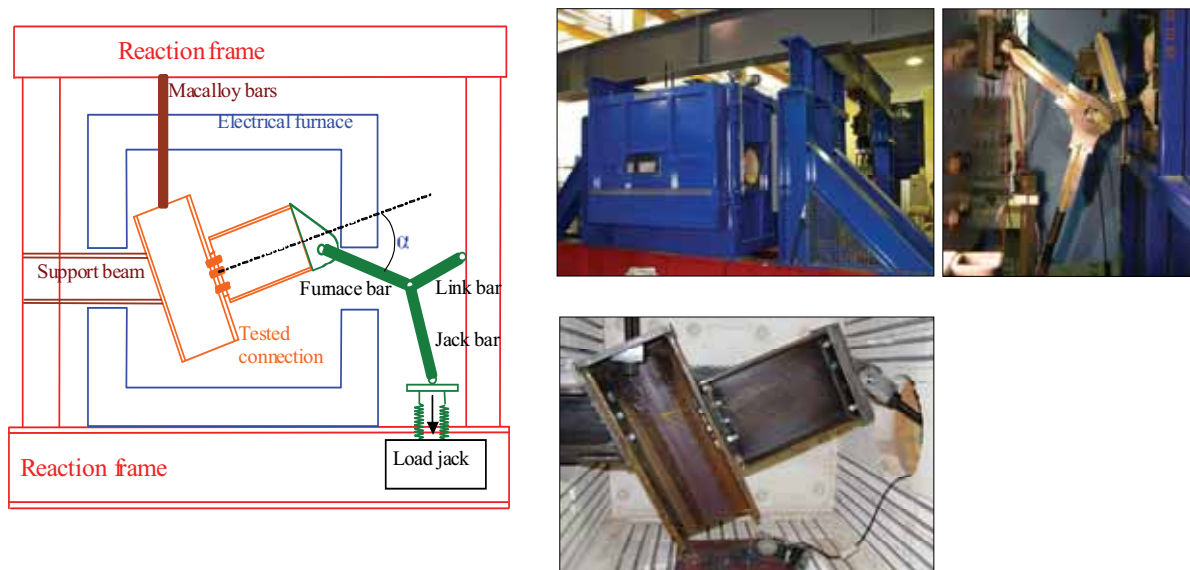


Figure 1 The test setup.

Steady-state temperature tests were undertaken in an electric furnace, with the specimen heated to a specified temperature and tested at a constant temperature. The beam-to-column connection was placed in the middle of the furnace supported by a UC203×86 and two $\Phi 25\text{mm}$ 1030 grade Macalloy bars. To allow very large rotation of the beam, an articulated load system was designed using three $\Phi 26.5\text{mm}$ 1030 grade Macalloy bars all connected to a central pin. The angle between the furnace bar and the axis of the beam determined the ratio of shear and tensile forces applied to the connection with measurement of the forces achieved with strain-gauges attached to the three load bars. Measurement of specimen deformations was made using a digital camera looking through a 100 x 200mm observation hole in the front of the furnace.

Specimens

To fit into the internal space of the furnace, a UC254×89 was used for the column and UB305×165×40 sections were used for the beam. Figure 2 shows as an example the geometry of the tested 8mm thick fin plate connections. A custom made connector was bolted to the end of the beam and the load was applied to the connector through a pin hole. The effective distance of the load to the connection was 490mm. All bolts used were M20 Grade 8.8. The steel used was nominally S275 for the beams (although it tested at 355N/mm^2), and the column was S355.

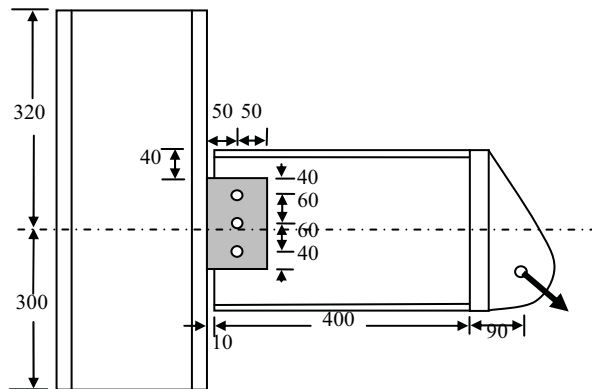


Figure 2. The geometry of the test specimen.

Test Results

Table 1 summarises the results of the tests on fin plates (Yu et al., 2007) and web cleats (Yu et al., 2008a) - results for partial depth endplates can be found in Hu et al. (2008), and flush endplates in Yu et al. (2008b). Examining the ambient temperature tests, it is clear that the resistance of the joint is significantly affected by the inclination of the applied tying force, in the case of the web cleat connection for example reducing from 243 to 186kN, which compare rather poorly with the test value of over 400kN in axial tension obtained for similar connections by Owens and Moore (1992). The experimental results have been used to assist development of mechanical (component-based) models to describe the behaviour of simple connections when subjected to combined axial and bending forces. The methods are described in Yu et al. (2008a) and

an example of the accuracy of the method can be seen in Figure 3 which compares the test results and mechanical model for web cleat connections.

Specimen geometry	Temperature (°C)	Load angle (Degree)	initial α (Degree)	ending α (Degree)	Force (kN)	Rotation (Degree)
FINPLATES						
1. 3-8.8-20	20	55	53.85	32.41	145.95	8.107
2. 3-8.8-20	450	55	51.47	41.37	70.48	6.093
3. 3-8.8-20	550	55	53.44	42.68	34.81	6.558
4. 3-8.8-20	650	55	53.09	44.02	17.99	6.255
5. 3-8.8-20	20	35	33.80	34.06	185.11	7.805
6. 3-8.8-20	450	35	39.04	33.52	84.47	6.237
7. 3-8.8-20	550	35	40.94	31.51	37.46	7.121
8. 3-8.8-20	650	35	40.50	30.60	19.30	7.367
9. 6-8.8-20	550	35	41.56	32.21	81.12	6.853
10. 6-8.8-20	550	55	55.99	46.60	67.01	4.782
11. 3-10.9-20	20	35	36.53	29.80	213.0	10.62
12. 3-10.9-20	550	35	40.85	23.90	56.82	11.50
13. 3-8.8-24	20	35	37.38	29.67	203.1	8.339
14. 3-8.8-24	550	35	42.10	29.06	74.02	7.855
WEB CLEATS						
1. 3-8.8-20	20	55	55.0	34.4	186.34	16.57
2. 3-8.8-20	450	55	55.8	43.5	93.74	9.39
3. 3-8.8-20	550	55	56.0	42.2	52.91	10.52
4. 3-8.8-20	650	55	56.5	34.4	25.70	14.15
5. 3-8.8-20	20	45	45.7	32.0	212.54	17.12
6. 3-8.8-20	450	45	46.7	37.3	99.42	10.29
7. 3-8.8-20	550	45	47.0	36.8	56.35	11.53
8. 3-8.8-20	650	45	48.1	34.5	28.18	15.94
9. 3-8.8-20	20	35	37.4	21.2	243.17	16.71
10. 3-8.8-20	450	35	41.1	29.1	112.85	10.75
11. 3-8.8-20	550	35	41.4	26.6	61.21	12.56
12. 3-8.8-20	650	35	40.9	21.6	31.57	14.86
13. 6-8.8-20	550	35	40.2	27.2	85.01	10.95
14. 6-8.8-20	550	55	55.7	41.0	66.78	9.19

Table 1 Robustness test results for simple connections in fire

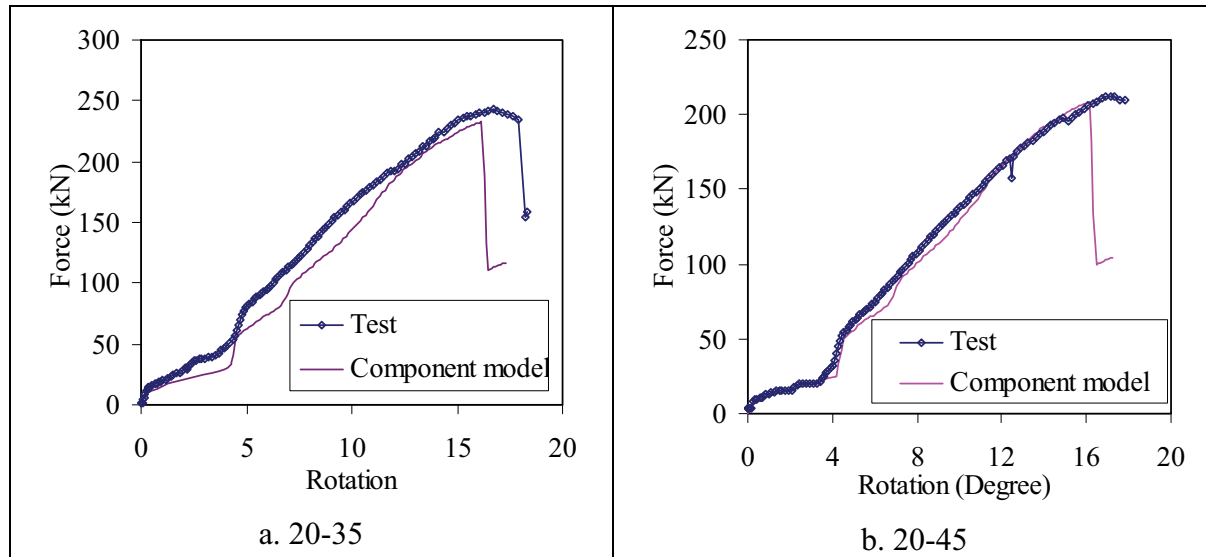


Figure 3 Comparison of component model and test results for web cleat connections

ROBUSTNESS OF STEEL JOINTS SUBJECT TO RAPIDLY APPLIED LOADING

Although current UK design guidelines emphasise the importance of catenary action in providing robustness against damage in framed buildings, and the consequent requirement for tensile capacity of members and connections, little is known about the ability of joints to tie a structure together. Such information is vital to assess the energy-absorption capacity of connections and thus demonstrate the ability of popular connection arrangements to contribute to the robustness of the structure. Owens and Moore (1992) present the most relevant information on the ability of steel connections to prevent progressive collapse. The paper detailed a series of essentially static tests conducted to demonstrate the inherent strength in simple connections, compare their ultimate capacity with the steel design code requirements and propose simplified design methods. Munoz-Garcia et al. (2007) conducted a series of analyses on the steel connections used by Owens and Moore using LS-DYNA (Hallquist, 1998), an explicit finite element analysis code, to assess their ability to resist rapidly applied tensile loads. Characteristics such as strength, energy absorption and response to different times of loading were studied. The effect of material strain rate sensitivity was accounted for using the Cowper and Symonds formulation. Results from these analyses showed that the response of steel connections is affected by the velocity of loading, generally making the connection fail in a brittle way despite the general belief that the structural performance of steel is enhanced as the rate of loading increases. Munoz-Garcia's work also examined the response of structural bolts to dynamic loading; a series of experiments was conducted (Munoz et al., 2005) to investigate the influence of strain rate on structural bolts used in normal construction and a comparison was made of the experimental results with numerical models in LS-DYNA.

From these tests it was concluded that thread stripping is the expected failure mechanism when a dynamic force is applied in a bolt that only possesses one nut, regardless of the strength of either the bolt or nut or its diameter. Nevertheless this

failure can possibly be avoided by using close tolerance bolts (Kirby, 1995). When two nuts are attached to a bolt, a cross section failure occurred in the threaded portion between the underside of the nut and the unthreaded part of the bolt, while the shank remained elastic. This failure mechanism increased the resistance in the bolt by a minimum of 16 % in relation to the load measured during thread stripping. Both failure mechanisms showed low ductility with a maximum strain value of 4.6 % and therefore very low energy dissipation and are thus not recommended for dynamic loading. The results obtained from these tests showed similar trends to the ones obtained by Mouritz (1994), who performed tests on mild steel bolts subject to tensile loads exerted at strain rates ranging from 10^{-5} to 10^2 s^{-1} . He found that threads are significantly weaker than the shank loaded in tension, and that the relative strengths of the threads compared with the shank decreases as the strain rate was increased. The static ultimate strength was higher than the dynamic ultimate strength for 8.8 bolts. This result suggests that even though some of the steel of the bolt presents a slight dynamic enhancement, the overall response of the nut and bolt assembly is reduced due to brittle failure at localized regions of the bolt.

Experimental Study of the Response of Connections to Dynamic Loading

The overall aim of this project is to conduct a detailed experimental study of the response of steel connections to rapid dynamic loading. The scenario envisaged is that implicit in current UK structural codes of practice for a unhardened civilian structure exposed to a severe accidental or malicious loading; that is, it is accepted that such an event would be likely to cause severe local damage to a structure, potentially removing one or more load carrying members, and resulting in a redistribution of load to other members. Numerical work conducted at the University of Sheffield (Liu, 2005) indicates that this redistribution is likely to occur over a few 10s to a few 100s of milliseconds. Loading rates that might be imposed on a structure directly from a large adjacent explosion are specifically excluded.

The specific objectives of this work are to: (i) develop an experimental methodology for dynamic testing of steel beam-column connections at different strain rates (ii) conduct a series of static and dynamic (at different strain rates) axial tension and moment/shear tests to failure, on simple, semi-rigid and full-moment steel beam-column connections (iii) investigate typical modes of failure, measure the energy absorption capability of the tested connections, and compare the results from static and dynamic tests, and (iv) use experimental data to produce recommendations for dynamic capacities of connections. Dynamic loading tests will be carried out on a range of connection types typically used in the UK - partial depth end-plate, fin-plate, web-cleats, flush end-plate and extended end-plate - with loads applied either in direct tension, or combined shear-bending. The investigation will be split into three distinct phases, each lasting approximately one year: Phase 1: Commissioning test arrangement. Towards the end of this period, a short series of 5-6 tests will be conducted, to demonstrate the efficacy of the test methodology, and provide initial data on the connection response.

Phase 2: Intensive series of 60 tests providing data on the failure modes and capacities of a range of steel beam-column connections at various loading rates.

Phase 3: A short series of more heavily instrumented tests will be conducted, with the aim of providing more detailed quantitative data on the response of the connections. Instrumentation will include strain gauges on bolts and other connecting ply.

All dynamic testing will be conducted at the University of Sheffield's Civil Engineering Dynamics (CEDUS) laboratories at Buxton. Test specimens will comprise a stub length of Universal Beam section, connected to a short length of heavy Universal Column, using standard connection types. The loading for these tests will be generated using heavy drop hammer equipment. Using different drop heights and masses, and placing rubber pad dampers between the hammer and the impact face, can respectively vary energy and loading rate. Dynamic axial load will be applied to the end of the beam stub, using two methods: (i) moment/shear loading (ii) direct axial tension loading.

The experimental work will focus on recording the transient loads, strains and deflections experienced by the components of the connections. Instrumentation is planned to include:

Applied load: strain gauges will be placed on the beam stub to capture the magnitude and spatial distribution of loading.

Connection response: Full field displacement measurements of the connections will be obtained from the analysis of consecutive digital images. Images will be recorded using high-speed video recording. Two high resolution cameras with acquisition rates of up to 5000 fps will be used in a stereoscopic configuration. Analysis of the collected images will produce 3D displacement/strain/strain rate maps for the varied connections using a correlation technique that determines the correspondence between several particles (in this application paint dots attached in a random pattern to the joint area) in successive images. The technique relies on identifying particle clusters or "facets", and how the characteristics of these facets change from image to image (Okamoto et al., 1995). Facet based correlation algorithms work by optimising the best combination of mappings between identified particles in order to represent translation, shearing and rotation and can obtain a matching accuracy of better than 0.01 pixels in 3D for materials which are subject to translations, rotations and shearing (Siebert et al., 2005). A flat, white light source will illuminate the area of interest on the joint, which will be speckle painted, and 2 high speed video cameras in a stereoscopic configuration, will record the data for analysis using stereoscopic and facet based image correlation software. This system will be employed to generate time-dependent maps of displacement and strain across the connection and provide a means of identifying times and positions of failures of the various components in the connections. In phase 3, strain gauges will be placed on the bolts, and the connecting ply to provide additional quantitative data on the load-carrying/failure mechanisms. Displacement transducers will be employed to capture the deformation of the connection at single points, in order to provide independent verification of the image based system.

The data from the experimental work will identify qualitative and quantitative differences in connection behaviour under static and dynamic loading. It is expected that this comparative study will enable the project team to draw general conclusions on the dynamic capacity of connections.

CONCLUDING REMARKS

The construction of robust steel-framed buildings (i.e. capable of remaining standing when damaged locally) relies on the ability of connections between individual structural members to withstand large deformations and maintain load resistance. An experimental study of the robustness of steel connections in fire conditions has provided valuable data to validate component based models for use in finite element analysis for structural fire engineering. These models may also be used at ambient temperatures. To further understanding of the behaviour of joints under accidental loading conditions, an experimental investigation of the ability of steel joints to resist rapidly applied loading is currently underway.

ACKNOWLEDGEMENTS

Research on the robustness of steel joints in fire was funded by EPSRC (EP/C510984/1), whose support is gratefully acknowledged, and conducted by Dr Hong Xia Yu and Andy Hu, with supervision provided by Professors Burgess and Plank. EPSRC have recently awarded the Universities of Sheffield (grant no. EP/F004338/1) and Bradford (Professor Tait, grant no. EP/F002599/1) grants to undertake an experimentally based study. This support is also gratefully acknowledged.

REFERENCES

- Armer, G. S. T. and O'Dell, T. (1997) *Fire, static and dynamic tests of building structures*, Second Cardington Conference, England 12–14 March 1997, E & FN Spon, London, ISBN 0-419-21680-4
- BRE (2004), *Results and observations from full-scale fire test at BRE Cardington 19/01/03*, Client Report No 215-741, download available from <http://www.mace.manchester.ac.uk/project/research/structures/strucfire/>
- BSI (2006), BS-EN 1991-1-7, Eurocode 1 - Actions on structures - Part 1-7: General actions - Accidental actions.
- BSI (2007), BS 5950-1:2000 Structural use of steelwork in building - Part 1: Code of practice for design - Rolled and welded sections, including amendment No.1 August 31.
- Defense Threat Reduction Agency (1999), *Blast Mitigation for Structures*, Status Report on the Defense Threat Reduction Agency, National Academy Press, Washington D.C.
- Federal Emergency Management Agency (2002) *World Trade Centre Building Performance Study*, FEMA 403, May, New York, download available from <http://www.fema.gov/rebuild/mat/wtcstudy.shtm>

Hallquist, J.O. (1998), *LS-DYNA theory manual*, Livermore Software Technology Corporation, May 1998

Hu, Y., Burgess, I.W., Davison, J.B. and Plank, R.J. (2008) "Tying resistance of flexible endplates in fire", Eurosteel, 3-5 September, Graz, Austria.

Institution of Structural Engineers (2002), *Safety in tall buildings and buildings of large occupancy*, July, London.

Izzudin, B.A., Vlassis, A.G., Elghazouli, A. and Nethercot, D.A. (2007) "Progressive collapse of multi-storey buildings due to sudden column collapse - Part 1: Simplified assessment framework", *Engineering Structures*, in press, available on line.

Kirby, B.R. (1995). "The behaviour of high-strength grade 8.8. bolts in fire." *Journal of Constructional Steel Research*, Vol. 33, No. 1-2 (pp. 3-38).

Leonardo da Vinci Pilot Project (2005), *Implementation of Eurocodes: Handbook 3 Action effects for buildings - Guide to basis of structural reliability and risk engineering related to Eurocodes supplemented by practical examples*, Leonardo da Vinci Pilot Project CZ/02/B/F/PP-134007, www.eurocodes.co.uk

Liu, R. (2005), *Robustness of Steel framed Buildings*, PhD Thesis, University of Sheffield.

Mouritz, A. P. (1994), "Failure mechanisms of mild steel bolts under different tensile loading rates", *International Journal of Impact Engineering*, Vol. 15, No. 3 (pp. 311-324).

Munoz-Garcia, E., Davison, J.B. and Tyas, A. (2005), "Analysis of the response of structural bolts subjected to rapid rates of loading", *4th European Conference on Steel and Composite Structures*, Eurosteel 2005, Maastricht, 8-10 June (pp. 4.10-17).

Munoz-Garcia, E., Davison, J.B. and Tyas, A. (2007), "Performance of Steel beam to column Connections under rapidly applied tensile loading", submitted for publication to *ASCE Journal of Structural Engineering*.

ODPM (2004), *The Building Regulations 2000 (2004 edition), Structure - Approved Document A*, www.planningportal.gov.uk

Okamoto K, Hassan Y.A., and Schmidl W.D. (1995), "New tracking algorithm for particle image velocimetry", *Experiments in Fluids* Vol. 19, No. 5 (pp. 342-347).

Owens, G.W. and Moore, D.B. (1992) "The robustness of simple connections", *The Structural Engineer*, Vol. 70, No. 3, 4 February (pp. 37-46).

Sanad, A, M., Rotter, J. M., Usmani, A. S. and O'Connor, M. A. (2000), "Composite beams in large buildings under fire — numerical modelling and structural behaviour", *Fire Safety Journal*, Vol. 35, No. 3 (pp. 165-188).

SCOSS (1999), *1997-99 Review and Recommendations*, The Twelfth Report of The Standing Committee on Structural Safety, published by SETO.

Siebert, T., Becker, T. and Splitthof, K. (2005) *High speed digital image correlation techniques*. SAE Special Publication Papers, SP 2033, 2006-01-0528.

Vlassis, A.G., Izzudin, B.A., Elghazouli, A. and Nethercot, D.A. (2007) Progressive collapse of multi-storey buildings due to sudden column collapse - Part II: Application, *Engineering Structures*, in press, available on line.

Yu, H. X. and Liew, R. J. Y. (2005), "Considering catenary action in designing end-restrained steel beams in fire", *Advances in Structural Engineering*, Vol. 8, No. 3 (pp. 309-324).

Yu, H.X., Davison, J.B., Burgess, I.W. and Plank, R.J. (2007) "Experimental Investigation of the Robustness of Fin Plate Connections in Fire", Proceedings ICASS 2007, Singapore (pp. 722-727).

Yu, H.X., Burgess, I.W., Davison, J.B. and Plank, R.J. (2008a) "Tying Capacity of Web Cleat Connections in Fire- Experimental and Theoretical Investigation", in preparation.

Yu, H.X., Burgess, I.W., Davison, J.B. and Plank, R.J. (2008b), "Experimental investigation of the behaviour of flush endplate connections in fire", Steel in Fire 08, May 28-30, NTU, Singapore.

ROBUSTNESS OF STRUCTURES – BEHAVIOUR OF COMPOSITE JOINTS

Jean-François Demonceau

University of Liège, Liège, Belgium
jfdemonceau@ulg.ac.be

Jean-Pierre Jaspart

University of Liège, Liège, Belgium
jean-pierre.jaspart@ulg.ac.be

ABSTRACT

Recent events such as natural catastrophes or terrorism attacks have highlighted the necessity to ensure the structural integrity of buildings under exceptional loading. Accordingly, a European RFCS project entitled “Robust structures by joint ductility” has been set up in 2004, for three years, with the aim to provide requirements and practical guidelines to ensure the structural integrity of steel and composite structures under exceptional loading through an appropriate robustness. In this project, the importance of the structural joints has been shown; indeed, these experience additional high-tying forces after the loss of a column, as a result of the development of membrane forces in the beams located just above the damaged column. Moreover a reversal of moments occurs in some joints. In this paper design models for the evaluation of the mechanical properties of joints in such extreme situations are presented. References are made to recent tests on joints in isolation recently achieved in the framework of the above-mentioned RFCS project.

INTRODUCTION

A structure should be designed to behave properly under service loads (at SLS) and to resist design factored loads (at ULS). The type and the intensity of the loads to be considered in the design process may depend on different factors such as:

- the intended use of the structure (type of variable loads...);
- the location (wind action, snow, level of seismic risk...);
- and even the risk of accidental loading (explosion, impact, flood...).

In practice, these individual loads are combined so as to finally derive the relevant load combination cases. In this process, the risk of an exceptional (and therefore totally unexpected) event leading to other accidental loads than those already taken into consideration in the design process in itself is not at all covered. This is a quite critical situation in which the structural integrity should be ensured, i.e. the global structure should remain globally stable even if one part of it is destroyed by the exceptional event (explosion, impact, fire as a consequence of an earthquake, ...). In conclusion, the structural integrity will be required when the structure is subjected to

exceptional actions not explicitly considered in the definition of the design loads and load combination cases.

According to Eurocodes (prEN 1991-1-7, 2004, ENV 1991-2-7, 1998) and some different other national design codes (BS 5950-1:2000, 2001, UFC 4-023-03, 2005), the structural integrity of civil engineering structures should be ensured through appropriate measures but, in most of the cases, no precise practical guidelines on how to achieve this goal are provided. Even basic requirements to fulfil are generally not clearly expressed. Different strategies may therefore be contemplated:

- Integrate all possible exceptional loads in the design process in itself; for sure this will lead to non-economic structures and, by definition, the probability to predict all the possible exceptional events, the intensity of the resulting actions and the part of the structure which would be affected is seen to be “exceptionally” low.
- Derive requirements that a structure should fulfil in addition to those directly resulting from the normal design process and which would provide a robustness to the structure, i.e. an ability to resist locally the exceptional loads and ensure a structural integrity to the structure, at least for the time needed to save lives and protect the direct environment. Obviously the objective could never be to resist to any exceptional event, whatever the intensity of the resultant actions and the importance of the structural part directly affected.

In the spirit of the second strategy, a European RFCS project entitled “Robust structures by joint ductility – RFS-CR-04046” has been set up in 2004, for three years, with the aim to provide requirements and practical guidelines allowing to ensure the structural integrity of steel and composite structures under exceptional events through an appropriate robustness. As part of the project, Liège University is mainly concerned by the exceptional loading “loss of a column further to an impact” in steel and composite buildings. In particular, the importance of the structural joints has been shown; indeed, these ones are initially designed to transfer shear forces and hogging bending moments, but experience additional high tying forces after the loss of a column, as a result of the development of membrane forces in the beams located just above the damaged or destroyed column. Moreover a reversal of moments occurs in the joints located just above the damaged column.

In this paper design models for the evaluation of the mechanical properties of joints in such extremes situations (Demonceau, 2008) are presented, as a part of a more global study, realised at Liège University, aimed at deriving design requirements for robust composite building frames. References are first made to recent experimental tests on joints in isolation and joints in frames recently achieved at Stuttgart University and at Liège University in the framework of the above-mentioned RFCS project. Then, the developed design models are presented.

PERFORMED EXPERIMENTAL TESTS

Introduction

Within the previously mentioned European project, an experimental test campaign was defined, as illustrated in Figure 1. In a first step, an experimental test on a

substructure simulating the loss of a column in a composite building frame was performed at Liège University; the objective of this test was to observe the development of the membranar forces within the structure and their effects on the joint behaviour. Then, in a second step, the composite joint configuration met within the tested substructure was tested in isolation at Stuttgart University with the objective to derive the response of this joint configuration subjected to combined bending moments and tensile loads. Finally, in a third step, all the components met within the substructure joints were tested in isolation at Trento University.

In order to reach a full adequacy between the experimental results, all the steel elements used for the tested specimens come from the same producer and from the same production.

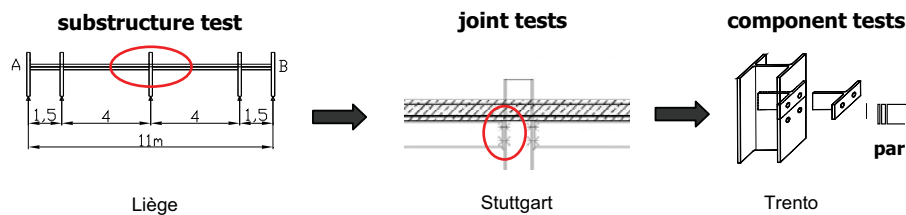


Figure 1. Test campaign within the RFCS project “Robust structures by joint ductility”

Within the present section, only the joint tests in isolation are briefly described. More information concerning the substructure test is available in (Demonceau, 2008) and about the component tests in (Stuttgart University, 2008).

Experimental composite joint tests in isolation

The test campaign realised at Stuttgart University was performed in strong collaboration with Liège University. The tested joint configuration (coming from the substructure designed and tested at Liège University) is presented in Figure 2. The tested joint configuration was designed so as to exhibit a ductile behaviour at collapse and with account of the M-N combined loading (Demonceau, 2008). The materials were ordered as follows: S355 steel for the profiles and the end-plates, ductile S450C steel for the rebars and C25/30 for the concrete.

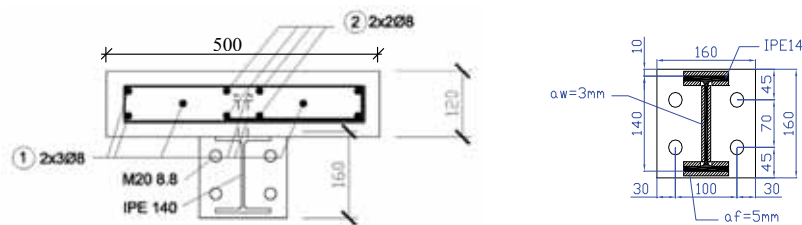


Figure 2. Joint configuration tested at Stuttgart University

In total, five tests on this joint configuration have been performed. The objective of these tests is to derive the full M-N resistance interaction curve of the tested joints (in the tensile zone), as illustrated in Figure 3. They are distinguished by the loading sequences followed during the tests as described here after.

Three tests under hogging moments: one test with the joint first loaded under hogging bending moments until reaching the ultimate resistance in bending and secondly, after having slightly reduced the applied bending moment, loaded under tension loads until the collapse of the joint (TEST 1) and two tests with the joint, first, loaded under hogging bending moments with the loading stopped just before reaching the ultimate resistance to bending and, secondly, loaded under tension loads until the collapse of the joint (TEST 2 & TEST 3).

Two tests under sagging moments: one test with the joint first loaded under sagging bending moments until reaching the ultimate resistance in bending and secondly, after having slightly reduced the applied bending moment, loaded under tension loads until the collapse of the joint (TEST 4) and one test with the joint, first, loaded under sagging bending moments with the loading stopped just before reaching the ultimate resistance to bending and, secondly, loaded under tension loads until the collapse of the joint (TEST 5).

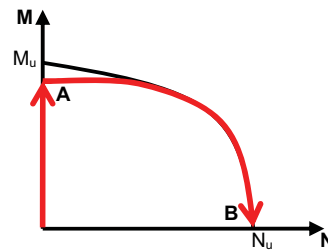


Figure 3. M-N resistant resistance curve of the joint to be characterised through the performed tests

TEST 1 and TEST 4 were initially performed to characterise the behaviour of the tested joint under hogging and sagging moments. The obtained results are presented in Figure 4 where the bending moment vs. joint rotation obtained through these tests are presented. The M-N interaction curves obtained through the performed tests are presented in Figure 5. During the tests, the collapse of the rebars in tension was observed at point A of Figure 6 during TEST 1 and at point A' during the other tests. After the collapse of the rebars, the tested joints can be considered as steel ones. It can be observed that, after the resistance loss, the remaining steel components are able to sustain additional tension loads. To pass from the pure bending moment loading to the maximum tensile load, only ductile components such as the end-plate and the column flange in bending or the rebars in tension were activated, as expected through the joint design.

All the observations made during the experimental tests are presented with more details in (Stuttgart University, 2008). In the next section, the so-obtained experimental results are used to validate the developed analytical models.

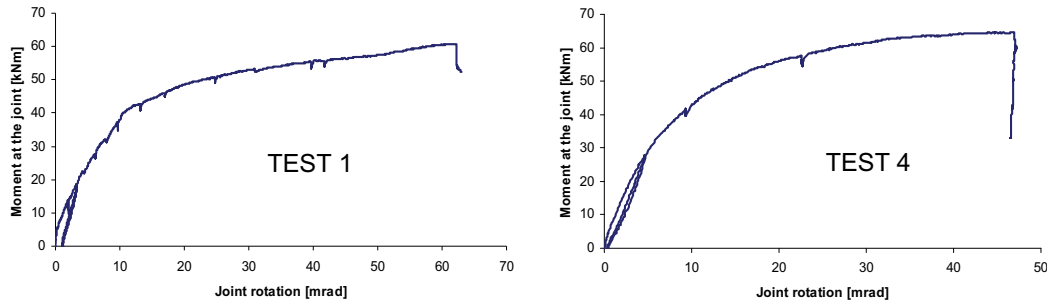


Figure 5. Bending moment vs. joint rotation curves obtained through TEST 1 and 4

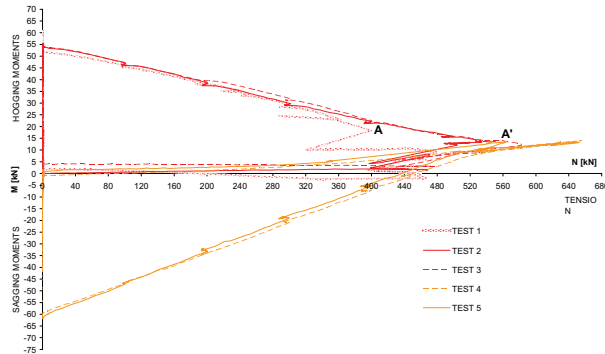


Figure 6. M-N interaction curve obtained through the performed experimental tests

DEVELOPED DESIGN MODELS

Introduction

As previously mentioned, joints which are initially designed to transfer shear forces and hogging bending moments experience additional high tying forces after the loss of a column, as a result of the development of membrane forces in the beams located just above the damaged or destroyed column. Moreover a reversal of moments occurs in the joints located just above the damaged column, i.e. joints initially subjected to hogging bending moments are subjected to sagging ones.

In the present section, analytical models to predict the response of composite joints subjected to sagging moments and to combined bending moments and axial loads are described. More details about these methods are available in (Demonceau, 1998).

Design model for composite joints subjected to sagging bending moments

Within the Eurocodes, the analytical method recommended for the joint design is the “component method”. This method, as actually proposed, is not yet able to predict the behaviour of composite joints subjected to sagging bending moments. Indeed, no method is available to characterise one of the activated components under such loading: the concrete slab in compression.

In recent research, methods to characterise this component in term of « resistance » are proposed. Their aim is to define a rectangular cross section of concrete participating to the joint resistance.

The procedure which is proposed in this section combined two methods proposed respectively by Fabio Ferrario (Ferrario, 2004) and by J.Y. Richard Liew (Liew et al, 2004). The combination of these two methods permits to reflect in a more appropriate way how the concrete resists to the applied load in the vicinity of the joint. Also, a formula for the characterisation of this component in term of “stiffness” is proposed. The so-defined analytical method is first described and then validated through comparison to the experimental test presented in the previous section.

In the PhD thesis of Fabio Ferrario (Ferrario, 2004), a formula is proposed to compute the width of the concrete $b_{eff,conn}$ which has to be taken into account for the joint component “concrete slab in compression”:

$$b_{eff,conn} = b_c + 0,7h_c \leq b_{eff}$$

where b_c is the width of the column profile flange, h_c the height of the column profile cross section and b_{eff} , the effective width of the concrete/composite slab to be considered in the vicinity of the joint; b_c represents the contribution of the concrete directly in contact with the column flange while $0,7.h_c$ the contribution of the developed concrete rods in the “strut-and-tie” behaviour (see Figure 7).

In the article of J.Y. Richard Liew et al, the width of the concrete is taken as equal to the width of the column flange ($b_{eff,conn} = b_c$) and the development of the concrete rods in compression through the “strut-and-tie” model is neglected.

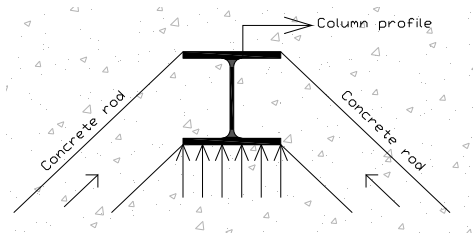


Figure 7. Plane view of the slab in the vicinity of the joint - development of concrete rods in compression under sagging moment

The definition of the width given in (Ferrario, 2004) is used in the developed procedure as this definition reflects in a more appropriate way the mechanism developing in the concrete slab according to the observations reported during experimental tests (Ferrario, 2004 and Demonceau, 2008).

Another difference between the two methods is linked to the definition of the height of concrete to be considered and, accordingly, to the position of the centre of compression within the joint. In (Ferrario, 2004), the centre of compression is assumed to be at mid-height of the concrete slab while in (Liew et al, 2004), the following procedure is given to compute the position of this point:

- the characterisation of the components in tension and eventually in shear is performed according to the rules recommended in the Eurocodes;
- then, the height of the concrete/composite slab contributing to the joint behaviour is computed by expressing the equilibrium of the load developing in the concrete/composite slab in compression with the components in tension or in shear and assuming a rectangular stress distribution in the concrete (equal to $0,85 f_{ck}/\gamma_c$ in a design). For instance, in the example illustrated in Figure 8, the concrete height to be considered is equal to:

$$z = \frac{F_{Rd,1} + F_{Rd,2} + F_{Rd,3}}{b_{eff,conn} \cdot (0,85 \cdot f_{ck} / \gamma_c)} \leq h_{concrete}$$

where $h_{concrete}$ is the total height of the concrete slab (in case of a composite slab, $h_{concrete}$ is equal to the concrete above the ribs);

- finally, the characterisation of the joint is performed assuming that the centre of compression is situated at the middle of the height of the contributing part of the concrete slab (z).

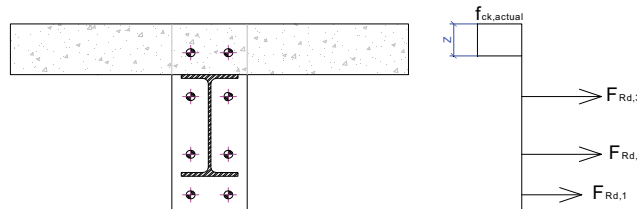


Figure 8. Height of the concrete to be considered in the characterisation of the new component

It is the latter procedure which is considered in the proposed method as it reflects in a more appropriate way the actual behaviour of the joint according to the observations made during experimental tests (Demonceau, 2008).

The resistance of the component “concrete slab in compression” can be computed through the following formula:

$$F_{Rd,CSC} = b_{eff,conn} \cdot z \cdot (0,85 \cdot f_{ck} / \gamma_c)$$

The two previously mentioned references only deal with the characterisation of the component “concrete slab in compression” in term of resistance but no formulas are proposed to characterise the latter in term of stiffness; however, the latter is requested in order to be able to predict the initial stiffness of the joint (and to derive the moment-rotation curve).

If reference is made to (Weynand, 1999), a formula is proposed to predict the stiffness of a concrete block against a rigid plate. In the present case, the steel column encased in the concrete slab can be considered as a rigid plate; so, the formula proposed in (Weynand, 1999) can be extended to the present situation to compute the stiffness of the component under consideration:

$$k_{csc} = \frac{E_c \cdot \sqrt{b_{eff,conn} \cdot z}}{1,275 \cdot E_a}$$

where E_c is the secant Young modulus for the concrete, E_a , the elastic Young modulus for the steel and k_{csc} , the stiffness of the component “concrete slab in compression” to be considered in the component method.

With the so-defined procedure for the characterisation of the component “concrete slab in compression”, the composite joint tested at Stuttgart University under sagging moments (i.e. TEST 4) has been characterised through the component method and the so-obtained prediction has been compared to the experimental results as presented in Figure 9.

Within the analytical computations, the actual material properties (without safety factors), determined through coupon tests for the steel materials and through cylinder compression tests for the concrete, are used. The resistant bending moment M_{Rd} and the initial stiffness $S_{j,ini}$ are computed in full agreement with the component method recommended in the Eurocodes while the ultimate moment M_u , the post-limit stiffness $S_{j,post-limit}$ and the rotation capacity ϕ_u are computed according to the method proposed in the PhD thesis of Jean-Pierre Jaspart (Jaspart, 1991) (which is in full agreement with the component method), as no methods are actually proposed in the codes to compute these properties.

In Figure 9, it can be observed that two analytical curves are reported; they are distinguished by the shape of the non-linear part of the curves. In fact, the non-linear part of the curves is computed according to the rule recommended in the Eurocodes and is a function of a shape coefficient called Ψ . The proposed value for joints with bolted end-plates is equal to 2.7. If this value is used, it can be observed in Figure 9 that the comparison with the experimental test result is not satisfactory. Indeed, the initial stiffness and the resistant and ultimate bending moments are in good agreement while the post-elastic stiffness is under-estimated. The observed difference is associated to the membranar forces within the joint components in bending (i.e. the column flange and the end-plate in bending) which develop when significant deformations are observed for the latter; this phenomenon is not yet included in the component method as actually proposed in the codes. If the shape coefficient is modified to take implicitly into account of this phenomenon (for instance, Ψ equal to 1), it can be observed that a very good agreement is obtained between the so-obtained analytical prediction and the experimental result. Further developments are requested on this topic; the latter are already initiated at the University of Liège.

The proposed analytical model has also been validated through comparisons to other experimental results in (Demonceau, 2008).

Design model for composite joints subjected to combined bending moments and axial loads

The presence of axial loads in the beams has an influence on the rotational stiffness, the resistance moment and the rotation capacity of the joints. As the analytical method proposed in the Eurocodes, i.e. the component method, is dedicated to the

characterisation of the joint subjected to bending moment only, the proposed field of application is limited to joints in which the axial force N_{Ed} acting in the joint remains lower than 5 % of the axial design resistance of the connected beam cross section $N_{pl,Rd}$:

$$\left| \frac{N_{Ed}}{N_{pl,Rd}} \right| \leq 0,05$$

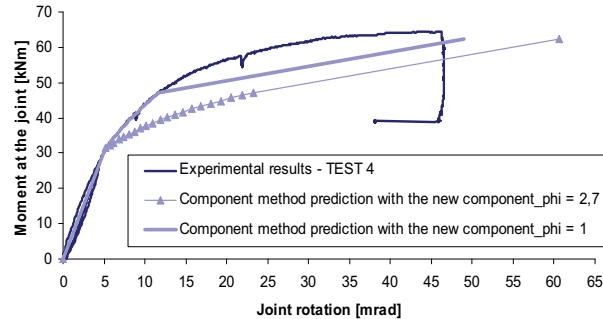


Figure 9. Comparisons analytical predictions vs. experimental result (TEST 4)

This limitation is a fully arbitrary one and is not at all scientifically justified. It has also to be underline that this criterion only depends of the applied axial load N_{Ed} and of the plastic resistance of the beam $N_{pl,Rd}$ which is quite surprising as what is considered here is the influence of the applied axial load on the joint response.

If this criterion is not satisfied, the Eurocodes recommend considering the resistant resistance diagram defined by the polygon linking the four points corresponding respectively to the hogging and sagging bending resistances in absence of axial force and to the tension and compression axial resistances in absence of bending.

In a previous study (Cerfontaine, 2003), it was illustrated that the proposed method is quite questionable. So, in (Cerfontaine, 2003), an improved design procedure, based on the component method concept, has been developed to predict the response of steel joints subjected to combined axial loads and bending moments.

In (Demonceau, 2008), the developed design procedure by F. Cerfontaine is extended to composite joints and validated through comparisons to the experimental test results obtained at Stuttgart University, as illustrated in Figure 10.

The computation details to obtain the analytical M-N resistance interaction curve are presented in (Demonceau, 2008). In Figure 10, it can be observed that two analytical curves are reported: one named “plastic resistance curve” which is computed with the elastic strengths of the materials and one named “ultimate resistance curve” which is computed with the ultimate strengths of the materials.

In Figure 10, it can be seen that the computed analytical curves are in very good agreement with the experimental results. Indeed, the experimental curves are

between the plastic and ultimate analytical resistant curves what is in line with the loading sequence followed during the tests.

Also, it is shown in Figure 10 that the maximum tensile load which can be supported by the joint is underestimated by the analytical procedure. This difference can be justified by the fact that the proposed analytical procedure does not take into account of the presence of membranar forces within the components “column flange in bending” and “end-plate in bending” associated to the big deformations of these components appearing when high tensile loads are applied to the joint. This phenomenon was already identified when investigating the behaviour the joint subjected to sagging bending moments.

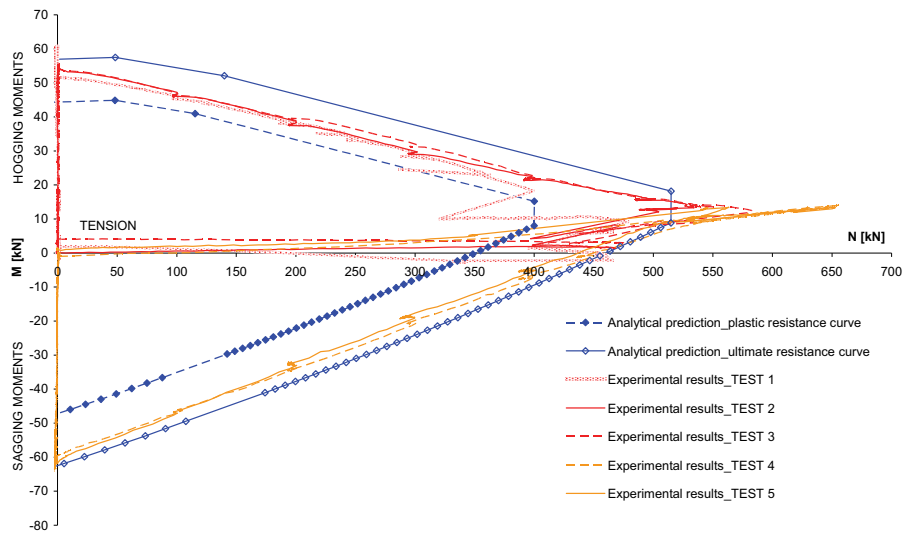


Figure 10. Comparison of the resistance interaction curves

CONCLUSIONS

Within the present paper, experimental and analytical investigations conducted within a European project to investigate the behaviour of composite joints when significant membranar forces developed in a structure further to a column loss were presented. In particular, two analytical models dedicated to the prediction of the response of composite joints subjected to sagging moments and to combined bending moments and axial loads, situations not accurately covered by the actual codes, were briefly described and validated through comparisons with experimental results.

REFERENCES

- BS 5950-1:2000 (2001), “Structural use of steelwork in building – Part 1: Code of practice for design – Rolled and welded sections”.
- Cerfontaine, F. (2003), Study of the interaction between bending moment and axial force in bolted joints (in French). PhD thesis presented at Liège University.

Demonceau, J.-F. (2008), "Steel and composite building frames: sway response under conventional loading and development of membranar effects in beams further to an exceptional action", PhD thesis presented at Liège University.

ENV 1991-2-7 (1998), "Eurocode 1: Basis of design and action on structures – Part 2-7 : Accidental actions due to impact and explosions", final draft, June 1998.

Ferrario F., 2004, "Analysis and modelling of the seismic behaviour of high ductility steel-concrete composite structures", PhD thesis presented at Trento University.

Jaspart J.P. (1991), "Study of the semi-rigidity of beam-to-column joints and its influence on the resistance and stability of steel buildings", PhD thesis, Liège University, in French.

Liew R.J.Y., Teo T.H. and Shanmugam N.E., 2004, "Composite joints subject to reversal of loading – Part 2: analytical assessments", Journal of Constructional Steel Research, pp. 247-268.

prEN 1991-1-7 (2004), "Eurocode 1 – Action on structures – Part 1-7: General actions – Accidental actions", final project team draft (stage 34), 9 July 2004.

Stuttgart University (2008), "Robust structures by joint ductility - Final report of the RFCS project N° RFS-CR-04046", to be published.

UFC 4-023-03 (2005), "Unified Facilities Criteria (UFC) - Design of buildings to resist progressive collapse", Department of Defence, USA. 25 January 2005.

Weynand K. (1999), "Column bases in steel building frames. COST C1 – Semi-rigid behaviour of civil engineering structural connections", Luxembourg.

FIRE DESIGN OF BOLTED STEEL BEAM-TO-COLUMN JOINTS

Aldina Santiago and Luís Simões da Silva

University of Coimbra, Coimbra, Portugal
aldina@dec.uc.pt; luiss@dec.uc.pt

Paulo Vila Real

University of Aveiro, Porto, Portugal
pvreal@civil.ua.pt

ABSTRACT

In this paper, the main approaches used for developing a practical consistent methodology to predict the behaviour of bolted steel beam-to-column joints under a natural fire are presented and discussed. This methodology incorporates the influence of the transient temperature variation on the time-varying forces that act on the joint and gives design guidance on how to avoid the failure of the joint throughout the fire event (heating and cooling phase). Validation of the proposed model is carried out by comparison against the available results obtained from an experimental programme of steel sub-frames under a natural fire undertaken at the University of Coimbra, Portugal (Santiago *et al.*, 2008).

1. INTRODUCTION

Under a natural fire conditions, the behaviour of steel joints within a structure highly depends on the redistribution of internal forces with time as a result of the global behaviour of the structure. In this situation, the actual behaviour clearly deviates from the results of isolated joint tests, being subjected to a full 3D stress state (N , M_y , M_z , M_t , V_z and V_y), resulting from local, distortional or global instability of the connected members that could lead to the failure of the tensile components (such as bolts or end-plates).

This paper gives a brief description of a consistent methodology to predict the behaviour of bolted steel beam-to-column joints under a natural fire. This methodology incorporates the influence of the transient temperature variation on the time-varying forces that act on the joint and gives design guidance on how to avoid the failure of the joint throughout the fire event. Validation of the proposed model is carried out by comparison against experimental results (Santiago *et al.*, 2008).

2. BEHAVIOUR OF JOINTS IN FIRE

Based on the studies previously described, it is confirmed that it was in the last fifteen years that the subject of steel joints under fire conditions suffered its main developments. Several experimental tests were performed in different typologies of joints and under different boundary and loading conditions, and analytical and numerical models were developed, which tried to reproduce adequately the behaviour

of such tested joints. However, some of these experimental tests were concentrated on predicting the behaviour of isolated joints at high temperatures under monotonic bending loading, while other tests used this known bending-rotational behaviour as boundary conditions, in order to study the behaviour of the heated connected beams. Despite the evident importance of modelling the behaviour of beam-to-column joints under a natural fire, as part of a frame structure, low experimental studies concerned with this matter have yet been published in the open literature.

In a research project developed at the University of Coimbra (Santiago *et al.*, 2008; Santiago, 2008), some fire tests on a sub-frame beam-to column were carried out, as shown in Fig. 1). The structural definition consisted of two thermally insulated HEA300 cross-section columns (S355) and an unprotected IPE300 cross-section beam (S355) with 5.7 m free span, supporting a steel-concrete composite slab. The mechanical loading applied at room temperature corresponded to the self-weight and the concentrated loads equal to 20 kN at 700 mm from the mid-span cross-section; the thermal loading corresponded to a heating-cooling curve applied to the beam and joints. The parametric study is focused on the beam-to-column joint configuration (Table 1).

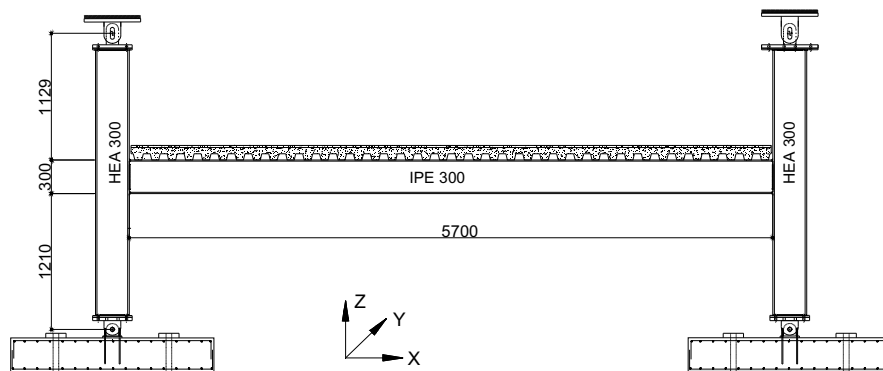


Figure 1. Structural model (mm).

Table 1. Beam-to-column joint configuration.

Test ID	Joint typology	End-plate dimensions (mm) and steel grade	Bolts / Weld
FJ01	Flush end-plate	(320×200×10); S275	2 bolt row M20, 8.8
FJ02		(320×200×16); S275	2 bolt row M20, 10.9
FJ03		(320×200×16); S275	2 bolt row M20, 8.8
EJ01	Extended end-plate	(385×200×16); S275	3 bolt row M20, 8.8
HJ01	Header plate	(260×150×8); S275	4 bolt row M20, 8.8
WJ01	Welded	-----	$a_f = a_w = 10 \text{ mm}$

3. COMPONENT METHOD IN FIRE

3.1 Overview

Over the past three decades, a considerable effort was undertaken to give consistent predictions of the steel joints at room temperature using the component method (Jaspart, 2002); however due to the large number of parameters that need to be taken into account when modelling the joint's response in fire, very little research work has been conducted in fire situation; exception should be mentioned to the work developed by the University of Coimbra (Simões da Silva *et al.*, 2001), the University of Sheffield (Block *et al.*, 2007) and the Imperial College London (Ramli Sulong *et al.*, 2007). From the available methods (Simões da Silva *et al.*, 2005), the component-based approach is also chosen in this work to model the connection behaviour because of its computational efficiency and capacity to provide a reasonable representation of the full range of response starting from the actual geometrical and mechanical properties.

3.2 Proposed component method

Considering the evidences reached from the experimental tests and the numerical simulations (Santiago *et al.*, 2008 and Santiago, 2008), some important aspects were identified as relevant for the formulation of any component methodology to analyse steel joints under fire: i) components characterization; ii) material properties dependency with temperature; iii) variable combination of bending moment and axial force; iv) non-conservation of linear cross-sections; v) loading-unloading-reloading that characterise the changing temperatures; vi) effective length of the components.

The spring model chosen in this work corresponds to the one developed by Cerfontaine (Cerfontaine, 2004) to analyse joints under bending moment and axial force at room temperature. Figure 2 depicts the proposed model to a flush end-plate joint; the number and location of each component depends on the joint typology. For a bolted joint, the compression components (beam flange in compression and column web in compression) are located at the level of the beam flanges axis and the tension components (column web in tension, column flange in bending, end-plate in bending, bolts in tension and beam web in tension) are located at the level of the bolt rows axis. Additionally, the shear column components are located independently of the tension-compression system, as suggested by Cerfontaine. However an important difference should be highlighted; in the Cerfontaine model, the axial force and bending moment is monotonic increased and proportional throughout the analysis; but under a natural fire, the axial force changes from compression to tension and the bending moment from hogging to sagging.

For the performed experimental tests, the columns were maintained at low temperatures, and its deformability, compared with the global deformability of the joint, was much reduced (Santiago, 2008). So, on the application of the proposed model, the column web components could be disregarded: column web in shear, compression and tension.

The application of the proposed model is feasible when the component response is introduced as a force – displacement curve. Due to the reduced number of studies

on the component characterization at high temperatures, a bilinear law was assumed in this study: the plastic resistance and initial stiffness at room temperature were calculated according the EN 1993-1-8-2005; once the component was loaded beyond its yield capacity, post-limit stiffness defined on literature was adopted (Santiago, 2008). For each step, the degradation of the strength and stiffness of each component material with temperature was considered using the reduction factors proposed by EN 1993-1-2-2005, and the component temperatures corresponded to the experimental measurements, as shown in Fig. 3. The effective length of each component remains constant throughout the analysis and corresponds to the value calculated by the EN 1993-1-8-2005 at room temperature.

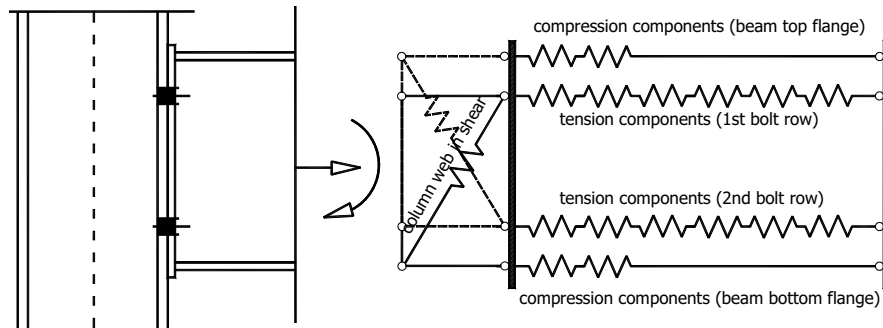


Figure 2. Proposed model to a flush end plate joint.

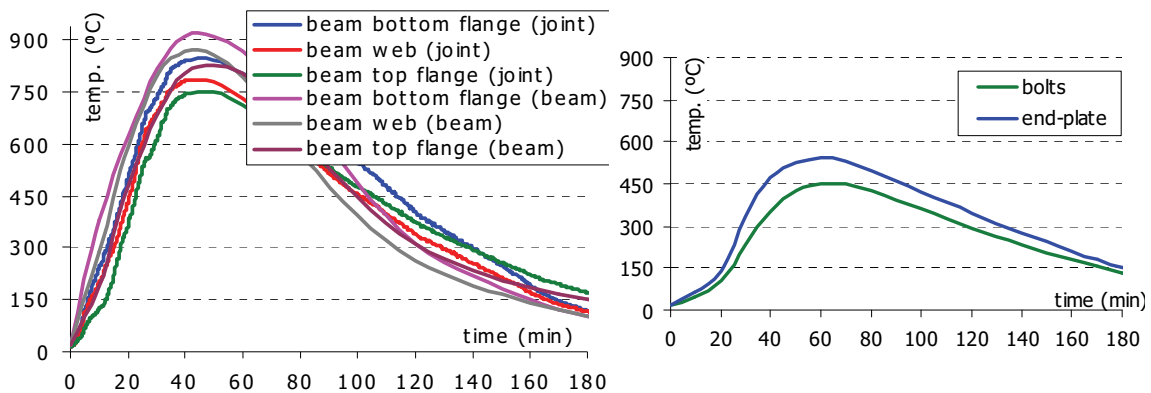


Figure 3. Temperature applied to the FJ03 model.

The variable combination of bending moment and axial force, derived from the finite element models, was introduced in the spring model as axial forces at the level of each component (Santiago, 2008).

To respond to the changing loading-unloading-reloading characteristic, a modified Masing rule has also been implemented into the model. The Masing rule assumes that a material like steel unloads with a stiffness equal to the initial stiffness of the loading curve, and then follows a hysteresis curve meeting the mirror image of the point at which unloading started in the opposite quadrant. However, if the temperature changes between loading and unloading, this process becomes more complicated because the components response is temperature dependent. In this case, the

assumption that the plastic strain is not affected by the temperature distribution should be employed (Franssen, 1990). The main underline of this assumption it that each force-displacement curves at different temperature unloads to the same plastic deformation, Δ_p , as shown in Fig. 4..

One of the main problems of this approach originates from the fact that the tensile and compressive forces in the connection do not share the same line of action. So, it was assumed that the compression springs are plastically deformed and unload until the end-plate loses contact with the column flange, the compression springs are deactivated and the tension springs start taking load from this deformed position. However, if the tension springs are deformed plastically and unload to initial position, it is assumed that all subsequent compression forces in the tension spring is taken by the compression spring row adjacent to the unloading tension spring row.

Another problem inherent to a fire situation is the large deformations developed on the beam. After large deformations, the well known Bernoulli's hypothesis, according to which plane cross-sections remain plane in the deformed state of the beam, is not valid, as observed in the experimental tests (Santiago *et al.*, 2008). The component method presented in the EN 1993-1-8 assumes that the cross-section remains always plane, even at large deformations. Here, the same simplifying assumption was adopted.

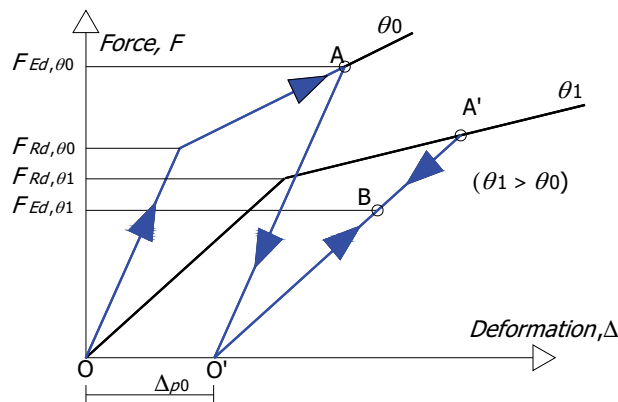


Figure 4. Force-displacement paths for loading with increasing temperature.

3.3 Application to a bolted end-plate beam-to-column joints

The connection element has been validated against the experimental results (Santiago *et al.*, 2008). The active components were chosen according the variation of the axial stresses integrated in a beam cross section near the connection and the axial stresses of the bolts; Figure 5 illustrates it for the flush end-plate joint FJ03: The active beam components were divided in five periods: $t < 12$ min - compression in the lower zone and tension in the upper zone; $12 \leq t < 27$ min - compression in the lower and upper zones; $27 \leq t < 90$ min - compression in the lower and tension in the upper zone; $t \geq 90$ min - tension in the lower and upper zones.

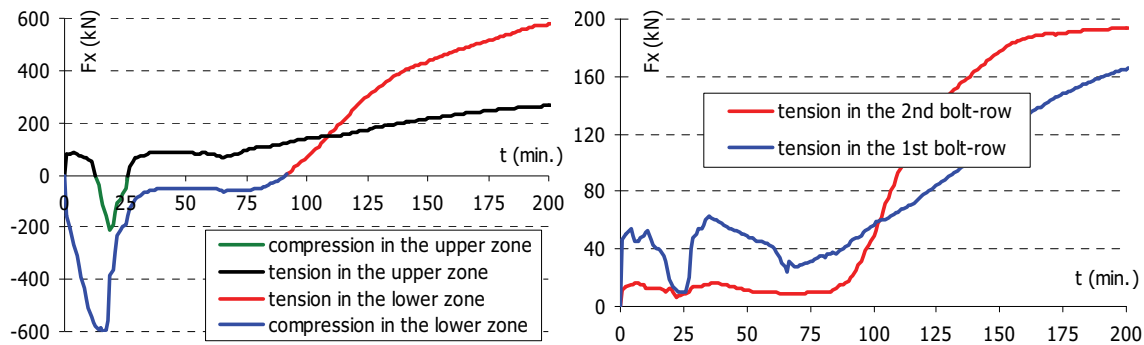


Figure 5. Forces introduced in the component model (joint FJ03).

Applying the axial forces and the bilinear force-displacement response of the active components at each temperature (Figure 6), the main quantities relevant for the FJ03 joint, for some representative times, are set out in Tables 2 and 3. For $t < 27$ min; no active component reached its capacity. Between $27 \leq t < 90$ min. the beam bottom flange exhibits a decrease of the compressive force and the upper connection zone changes from compression to tension. This change of forces is shown in the active components during this period: the components reached their highest temperature leading to a relevant decrease of their resistances and to the yielding of the beam bottom flange in compression and beam web in tension (top).

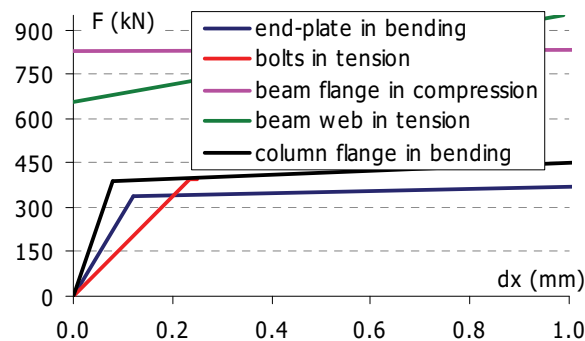


Figure 6. Force-displacement response of each component at room temperature.

Table 2. Proposed model applied to the bolted joint FJ03 ($27 \leq t < 90$ min)

	t (min)	temp. (°C)	$F_{Rd,t}$ (kN)	$F_{Ed,t}$ (kN)	Δ_t (mm)	note
beam bottom flange in compression	27.0	700.0	188.4	189.0	0.396	yield
	42.0	849.5	69.8	51.1	0.396	elastic
	89.0	686.5	215.0	27.2	0.396	elastic
1 st bolt-row in tension	27.0	206.4	370.4	41.2	0.027	elastic
	42.0	378.7	318.5	110.8	0.090	elastic
	89.0	414.5	294.8	77.8	0.067	elastic
end-plate in bending (top)	27.0	291.1	336.2	33.0	0.015	elastic
	42.0	518.2	243.2	87.1	0.057	elastic
	89.0	502.5	259.7	113.9	0.069	elastic
column flange in bending (top)	27.0	95.4	390.7	41.2	0.008	elastic
	42.0	302.7	390.7	110.8	0.028	elastic
	89.0	404.9	390.7	77.8	0.023	elastic
Beam web in tension (top)	27.0	636.0	250.8	33.0	0.000	elastic
	42.0	790.9	79.1	87.1	0.423	yield
	89.0	572.6	362.9	113.9	1.609	elastic

From Figure 5 it is observed that between $90 \leq t < 165$ min, only the tension components are active. According to the proposed methodology, there was one component that reached its plastic resistance: end-plate in bending (bottom) at $t = 131$ min, $F_{Rd,t} = 336.2$ kN and $F_{Ed,t} = 358.2$ kN, with a corresponding displacement of $\Delta_t = 0.93$ mm (see Table 3)). The last active component that reached its maximum capacity was the 2nd bolt-row in tension at $t = 165$ min, $F_{Rd,t} = 376.7$ kN and $F_{Sd,t} = 377.1$ kN, with a corresponding displacement of $\Delta_t = 13.6$ mm. It should be referred that on the experimental test, this component failed at $t = 190$ min. For each bolted end-plate beam-to-column joints, Table 4 gives the components that reached their plastic capacity.

4. RECOMMENDATIONS FOR DESIGN RULES

In the previous section, a methodology for the evaluation of the response of steel joints under fire loading based on the component method was developed and applied. It was able to reproduce with sufficient accuracy the transient response of the steel joints throughout the fire development and to identify the failure modes of the joint. This procedure provides an adequate basis for incorporation in advanced calculation methods through the development of specialized joint finite elements. However, for conceptual and pre-design, the proposal of simple design recommendations is a desirable goal. Although the number of tests carried out in this research work is clearly insufficient to validate wide-ranging simplified rules, it is nevertheless enough to propose a framework and a methodology for future simplified rules.

Focusing on bolted end-plate beam-to-column joints, simplified design rules should take into account two distinct design points (on top of the fulfilment of the cold-design criteria): (i) design period A that corresponds to the critical period during the heating phase; and (ii) design period B that corresponds to the critical cooling time. Based on the times when the active components yield or fail (bolts in tension): period A is in the range $20 \leq t \leq 40$ min and period B in the range $t \geq 100$ min. Naturally, the choice of these two design periods depends on the fire scenario that must be considered as a relevant parameter in the simplified design recommendations. To propose these periods, only the fire scenario adopted in this research work was considered.

Table 3. Proposed model applied to the bolted joint FJ03 ($90 \leq t < 165$ min).

	t (min)	temp. (°C)	$F_{Rd,t}$ (kN)	$F_{Ed,t}$ (kN)	Δ_t (mm)	note
1 st bolt-row in tension	90.0	389.1	313.2	86.4	0.072	elastic
	131.0	256.5	364.0	183.8	0.128	elastic
	165.0	159.3	376.7	275.6	0.173	elastic
end-plate in bending (top)	90.0	467.1	286.6	118.9	0.067	elastic
	131.0	300.9	336.2	186.5	0.083	elastic
	165.0	192.9	336.2	234.9	0.093	elastic
column flange in bending (top)	90.0	379.2	390.7	86.4	0.024	elastic
	131.0	241.3	390.7	183.8	0.043	elastic
	165.0	161.2	390.7	275.6	0.059	elastic
Beam web in tension (top)	90.0	515.8	478.0	118.9	1.609	elastic
	131.0	292.3	653.7	186.5	1.609	elastic
	165.0	153.2	653.7	234.9	1.609	elastic
2 nd bolt-row in	90.0	389.1	313.2	35.9	0.030	elastic

tension	131.0	256.5	364.0	299.2	0.209	elastic
	165.0	159.3	376.7	377.1	13.60	yield
end-plate in bending (bottom)	90.0	455.0	276.7	0.0	0.000	elastic
	131.0	314.1	336.2	358.2	0.930	yield
	165.0	196.6	336.2	497.9	5.105	plastic
column flange in bending (bottom)	90.0	379.2	390.7	35.9	0.010	elastic
	131.0	241.3	390.7	299.2	0.070	elastic
	165.0	161.2	390.7	377.1	0.081	elastic
Beam web in tension (bottom)	90.0	515.8	653.7	0.0	0.000	elastic
	131.0	292.3	653.7	358.2	0.000	elastic
	165.0	153.2	653.7	497.9	0.000	elastic

Table 4. Sequence of yield or failure (bolts) of the components to each bolted end-plate beam-to-column joints.

acting forces	Top – T Bottom - C	Top – C Bottom - C	Top – T Bottom - C	Top – T Bottom - T
	Heating			Cooling
FJ01	-----	$t = 22$ (beam bottom flange in compression)	$t = 32$ (end plate in bending - top)	$t = 99$ (end plate in bending - bottom)
FJ02	-----	$t = 22$ (beam bottom flange in compression)	$t = 44$ (beam web in tension - top)	$t = 123$ (column flange in bending - bottom) $t = 141$ (column flange in bending - top) $t = 170$ (failure of the 2 nd bolt-row in tension is imminent: $F_{Ed,t} = 0.99 F_{Rd,t}$)
FJ03	-----	$t = 27$ (beam bottom flange in compression)	$t = 42$ (beam web in tension - top)	$t = 131$ (end-plate in bending - bottom). $t = 165$ (2 nd bolt-row in tension)
EJ01	-----	$t = 34$ (beam web in tension - bottom)	-----	$t = 110$ (end-plate in bending - 3 rd bolt-row) $t = 141$ (beam web in tension - 3 rd bolt-row) $t = 190$ (3 rd bolt-row in tension)

The second step in the proposed simplified procedure consists on the evaluation of approximate levels of bending moment and axial force corresponding at the two design periods A and B (see Fig. 7).

Finally, the tensile capacity of the main brittle component, which could lead to the structural failure, should be compared with the active forces. In this case, special reference will be made to the bolts in tension during the cooling phase:

$$F_{ten,t,Ed} \leq F_{ten,t,Rd} = 0.9f_{ub} A_s k_{b,\theta} \quad (1)$$

where $F_{ten,t,Ed}$ is the tensile force in the bolt; $F_{ten,t,Rd}$ is the design tension resistance of a single bolt in fire; f_{ub} is the ultimate stress of the bolts; A_s is the tensile stress area of the bolt and $k_{b,\theta}$ is the reduction factor for bolt resistance at temperature θ . This comparison is made in Fig. 8. The tensile bolt forces are represented by thick lines, the bolt resistances are drawn using dashed lines and the failure of the bolts is represented by a circle. This allows for the identification of the bolt failure.

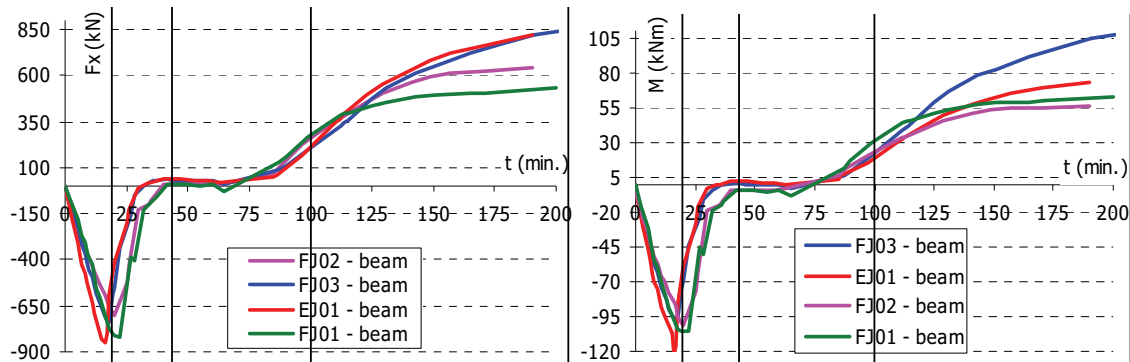


Figure 7. Numerical curves of the axial force and bending moments on the joints during the fire.

Of course, the tensile forces in the bolts were obtained performing an exhaustive numerical model. The identification of the degree of lateral and rotational restraint of the beam and the evaluation of approximate levels of bending moment and axial force at the two design periods A and B could be an alternative to obtain these tensile forces. As example, expressions proposed by Yin and Wang could be used to approximate these values (Yin and Wang, 2005). Although appropriate calculation and benchmarking would be mandatory.

Moreover, to avoid failure of the joint throughout the fire development, it was shown that a crucial factor is the ability of the connection to redistribute the applied internal forces. In particular, the deformability of the end-plate *vis a vis* the forces in the bolts plays a most relevant role. In EN 1993-1-8-2005 it is stated that a bolted end plate joint may be assumed to have sufficient rotation capacity for plastic analysis, provided that both of the following conditions are satisfied: (i) the moment resistance of the joint is governed by the resistance of either the column flange in bending or the end plate in bending and (ii) the thickness t of either the column flange or the end plate (not necessarily the same basic component as in (i)) satisfies:

$$t \leq 0.36\phi \sqrt{\frac{f_{u,b}}{f_y}} \quad (2)$$

where ϕ is the bolt diameter, $f_{u,b}$ is the tensile strength of the bolt and f_y is the yield strength of the relevant basic component. The application of this expression to the tested joints, results in the following bolt requirements (Table 5). It is observed that only the joint FJ01 meets the ductility criteria.

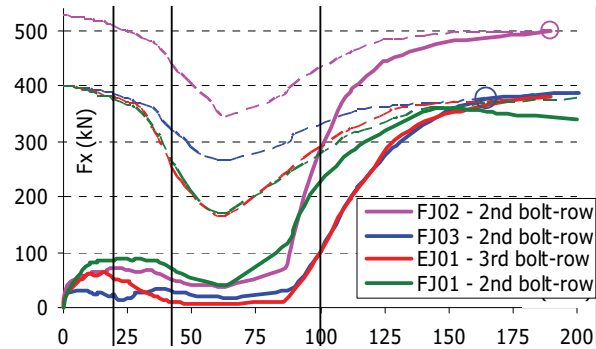


Figure 8. Bolts in tension.

Table 5. Ductility criteria (EN 1993-1-8-2005).

	f_{ub} (MPa)	f_{yp} (MPa)	ϕ (mm)	t_p (mm)	joint failure mode	bolt required
FJ01	810	275	M20	10	end-plate deformation	M20 ✓
FJ02	1076	275	M20	16	stripping-off of the threads of the bolts	M24 ✗
FJ03	810	275	M20	16		M24 ✗
EJ01	810	275	M20	16		M27 ✗

5. CONCLUSIONS AND GENERAL RECOMMENDATIONS

In this paper, a component method and a design verification to analyse beam-to-column joints under a fire were proposed and compared with experimental tests. Based on the results and considerations achieved during this research work, some design suggestions were proposed:

i) The application of a thin end-plate demonstrated to be a good option to reduce the large bolt strain and consequently the bolt failure (FJ01). However, even no bolt failure was observed, large deformations on the end-plate were developed and bearing failure around the bolts could be happen.

ii) Special attention should be made when it is intended to increase the joint resistance. The application of a bolt class with higher resistance reduces the bolt deformations and reveals to be a good choice to increase the joint resistance. However, a joint typology with a higher resistance at room temperature only increases the resistance to the hogging moment, but not to sagging moment that controls the cooling phase. Additional bolt rows in the lower zone of the connections should be considered in order to increase the joint resistance during the cooling phase.

ACKNOWLEDGMENTS

Financial support from the Portuguese Ministry of Science and Higher Education (*Ministério da Ciência e Ensino Superior*) under contract grant POC/ECM/55783/2004 is gratefully acknowledged

REFERENCES

- Block, F., Burgess, I. Davison, B. and Plank, R.J. (2007), "The development of a component-based connection element for end-plate connections in fire". *Fire Safety Journal*, vol. 42(6-7) (pp. 498-506).
- Cerfontaine, F. (2004), "Etude de l'interaction entre moment de flexion et effort normal dans les assemblages boulonnés" (in french), Thèse de Docteur en Sciences Appliquées, Faculté des Sciences Appliquées, University of Liège, Belgium.
- EN 1993-1-2-2005. European Committee for Standardization – CEN. Eurocode 3: Design of Steel Structures. Part 1.2: General Rules – Structural Fire Design, Brussels.
- EN 1993-1-8-2005. European Committee for Standardization – CEN. Eurocode 3: Design of steel structures. Part 1.8: Design of joints, Brussels.
- Franssen, J-M (1990) "The unloading of building materials submitted to fire". *Fire Safety Journal*, vol.16, (pp. 213-227).
- Jaspart, J.P. (2002) "Design of structural joints in building frames" *Progress in Structural Engineering and Materials*, vol. 4 (pp. 18-34).
- Ramli Sulong, N.H., Elghazouli, A.Y. and Izzuddin, B.A. (2007), "Behaviour and design of beam-to-column connections under fire conditions". *Fire Safety Journal*, 42 (6-7), (pp.437-451).
- Santiago, A., Simões da Silva L., Vila Real P., Gameiro Lopes A. and Vaz G. (2008), "Experimental evaluation of the influence of connection typology on the behaviour of steel structures under fire", *Engineering Journal*, AISC (submitted).
- Santiago, A. (2008), "Behaviour of beam-to-column steel joints under natural fire". Doctoral Thesis, Department of Civil Engineering, University of Coimbra.
- Simões da Silva L., Santiago A. and Vila Real P. (2001), "A component model for the behaviour of steel joint at high temperatures". *Journal Constructional Steel Research*, vol. 57(11) (pp. 1169-1195).
- Simões da Silva, L., Santiago, A., Vila Real, P. and Moore, D. (2005), 'Behaviour of steel joints and fire loading'. *International Journal of Steel and Composite Structures* vol. 5(6) (pp. 485-513).
- Yin, Y.Z. and Wang, Y.C. (2005), "Analysis of catenary action in steel beams using a simplified hand calculation method, Part 1: theory and validation for uniform temperature distribution". *Journal of Constructional Steel Research*, vol. 61 (pp. 183-211).

COMPOSITE CONNECTIONS IN EN 1994-1-1 EUROCODE 4

David Anderson

University of Warwick, Coventry, CV4 7AL, UK
da@eng.warwick.ac.uk

ABSTRACT

During the 20-year overall period of developing the Eurocodes, connections became of increasing importance in the work of the drafting teams. The final (EN) version of Eurocode 3 includes extensive provisions for the design of moment-resisting steel connections. Eurocode 4 for composite steel-concrete structures complements Eurocode 3 and includes provisions for composite connections. This paper describes their development, identifies principal background documents and explains the presentation finally adopted. In conclusion, further research needs are prioritised.

INTRODUCTION

Design recommendations for composite connections (Figure 1) were developed progressively during the drafting process. The first published draft of Eurocode 4 (Commission of the European Communities, 1985) stated that joints between beams and columns should be designed to have one of four types of behaviour. These were: simple, semi-rigid or rigid, as defined by Eurocode 3 for steel joints, or monolithic, as implied by Eurocode 2 for in-situ reinforced concrete. If semi-rigid joints were to be used, "the effect of joint rotation on the overall structural behaviour should be determined from the expected moment-rotation characteristics of the joints". No guidance was given on how these characteristics were to be found. Not surprisingly, it was then stated that the detailed recommendations of this Eurocode were limited to structures with simple, rigid or monolithic joints.

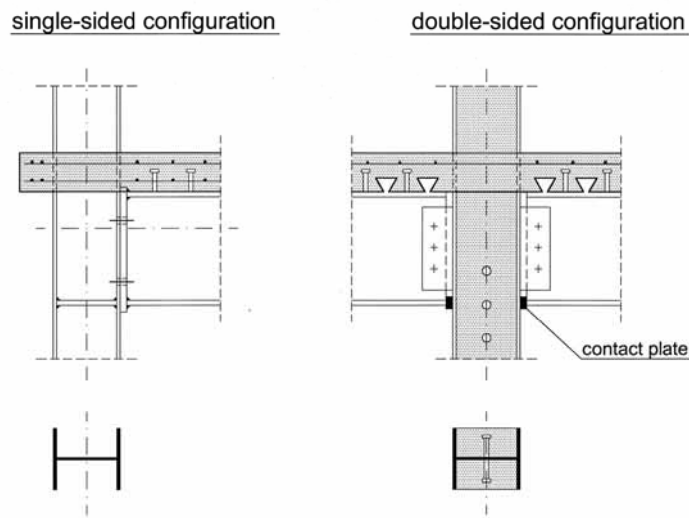


Figure 1 Examples of composite connections (Hanswille)

By the next published draft (CEN, 1992), matters had moved on considerably. The scope of the Eurocode's rules meant that any semi-rigid or rigid beam-to-column connection would be subject to hogging, but not sagging, bending moment. With this in mind, a composite connection was defined as one in which reinforcement was intended to contribute to the resistance. The expectation was that the reinforcement would be within the usual top slab of a composite beam (Figure 1).

For the first time in Eurocode 4, some design provisions were given for composite joints, in a two-page section entitled "Composite connections in braced frames for buildings". Again, not surprisingly given the shortness of this section, very little was useful to a designer seeking advice on how to proportion a composite joint and to allow for its effect on the structure.

In contrast, provisions for steel joints, particularly end-plate connections, were now available in some detail in Eurocode 3. This followed substantial research, a good overview of which is provided by the proceedings of the first international workshop on connections in steel structures, held in Cachan, France (Bjorhovde et al, 1988). Around the same time, Moore (1988) had provided a critical review of the then-current provisions for end-plate connections intended for Eurocode 3.

Eurocode 3 had adopted the component method as the basis for calculating the structural properties of joints (Jaspart et al, 1999). A joint is considered as a set of individual basic components; the relevant structural characteristics of each component are evaluated; the components are then assembled to determine the properties of the joint as a whole. The section on composite connections in the 1992 draft of Eurocode 4 (CEN, 1992) was intended to supplement or modify the provisions of Eurocode 3 for steel joints. It was recognised that joint properties would be affected by reinforcement (implicitly understood to be in the slab of a composite beam) and concrete encasement to the column. However, no advice was given on how to proceed further, other than mention of yielding of reinforcement being of importance and the need to justify improvements due to encasement by testing. Eurocode 3 had classified joints by rotational stiffness and moment resistance, comparing joint properties with those of the connected members. Eurocode 4 clarified the properties to be used for composite members.

A handbook (Johnson and Anderson, 1993) gave background to the very limited provisions of this draft Eurocode. It was stated that no detailed rules had been given because methods to predict structural properties were not then sufficiently established to justify inclusion in a Eurocode. For moment resistance and stiffness, this was to change during the 90s, when much effort in both research and development was given to composite joints.

BACKGROUND DOCUMENTS

The year 1991 saw the commencement of the COST C1 programme. This concerned connections for civil engineering structures and was supported, financially and in other ways, by the European Commission. The funding enabled members to meet to discuss their work in research and development, with the aim of formulating common approaches for connection design. The working group on steel and composite joints

set up a sub-group on composite joints, made up of COST members and members of the relevant technical committee of the European Convention for Constructional Steelwork (ECCS). Two substantial reports were produced:

- Composite steel-concrete joints in braced frames for buildings (Anderson et al., 1996)
- Design of composite joints for buildings (Anderson et al., 1999).

The first document aimed to increase understanding of composite connections and made considerable reference to original publications of research. It treats the following topics:

- classification of composite joints, in terms of influence on the response of other elements of the frame
- flexural behaviour, with reference to physical tests on full-size configurations
- the component method as applied to composite joints
- component characteristics
- calibration of proposed design methods against test results.

If Eurocode 4 was to give detailed provisions for composite joints, components additional to those for steel joints would need to be identified. This was done, and proposals for their properties presented.

The second report was intended for designers seeking code-type provisions for composite joints and guidance on how such connections would affect the design of other frame elements. The provisions were compatible with the 1992 draft of Eurocode 4 (CEN, 1992) and were seen as a model for inclusion in the future final (EN) version of Eurocode 4. Provisions for steel joints using the component method had been made available as an Annex J to Eurocode 3, and for this reason the model provisions for composite joints were referred to as Annex J to Eurocode 4. The calculation procedures were shown by sample calculations for six different joint configurations.

SCI/BCSA CONNECTIONS GROUP

In parallel with the COST C1 activities, within the UK a Connections Group had produced a series of design guides for structural steel connections. This was under the auspices of the Steel Construction Institute (SCI) and the British Constructional Steelwork Association (BCSA). Their work included the development of standard connections, which enabled connection properties to be presented in tables. Guidance on composite connections was published in the late 90s (Couchman and Way, 1998). Step-by-step design procedures were presented and illustrated by a worked example. Standard steelwork joints with flush end plates (Stainsby and Cruickshank, 1995) were developed into composite connections with slab reinforcement being anchored beyond the column (for an internal joint, this would usually be by running the reinforcement into the adjacent span). Like the ECCS Recommendations, the guidance from the Connections Group set the design of the joints in the wider context of frame design. Unlike ECCS though, no guidance was given on the calculation of stiffness. Under service loading, it was assumed that the connections could be treated as rigid. Beam design at ultimate limit state assumed plastic hinges would form in the connections.

ROTATION CAPACITY

This validity of this approach to beam design depends on the connections having rotation capacity in hogging bending sufficient to develop whatever sagging moment is to be taken in the mid-span region. Ductile behaviour in the steelwork parts of the connection was provided by using relatively thin end plates in S275 steel and strong bolts and welds (Bose and Hughes, 1995). For composite connections, tests had shown that rotation capacity could be limited by rupture of the reinforcing bars and a method to predict this had been developed (Anderson et al, 2000). Very substantial rotation capacity will be required if the plastic moment of the composite beam in sagging bending is to be approached in the span (Nethercot et al., 1995; Najafi and Anderson, 1997). The Connections Group's recommendations (Couchman and Way, 1998) limited the design sagging resistance moment to 85% of the fully-plastic value. Minimum areas of reinforcement were given to achieve the required rotation capacity.

EN 1994-1-1 EUROCODE 4

Introduction

Although the conversion of the draft Eurocodes into EN European Standards was undertaken by small groups of experts, each group working as a Project Team, this was in consultation with a much wider bodies of experts chosen from each CEN member country. Although model clauses for composite joints were available (Anderson et al, 1999), the national experts and the Project Team judged them too lengthy for inclusion in the EN. For steel connections, a separate document EN 1993-1-8 (CEN, 2005) was being prepared, but this was not appropriate for the more specialised topic of composite joints. It was therefore decided that in EN 1994-1-1 (CEN, 2004), the provisions for composite joints should just modify or supplement EN 1993-1-8. This means that any user must first be familiar with that part of Eurocode 3. Given the much more common occurrence of steel joints compared to composite connections (and the usual order of the curriculum in teaching), this is a reasonable assumption.

Composite joints are treated in Section 8 Composite joints in frames for buildings and in an informative Annex A Stiffness of joint components in buildings.

Scope

The earlier European reports (Anderson et al, 1996, 1999) had concerned beam-to-column connections in buildings. These were a basis for Section 8 and Annex A, so these have been restricted to such structures. The joint configurations in these reports comprise mainly the following (Figure 1):

- connections with steel flush end plates, in which the upper part of the steel connection contributes to the resistance of the tension zone of the joint
- the so-called "contact plate" connection, in which there is no steelwork connection in the tension zone. The reinforcement in the slab alone provides the

tensile resistance to bending. In the compression zone, bearing between the lower flange of the beam and the flange of the column is through a plate component placed between these two flanges.

These are the configurations envisaged when writing Section 8. The steel members were expected to be I- and H-sections. The columns could be cased in concrete. Steel connections with flush end-plates are well-established as a form of moment-resisting connection (Stainsby and Cruickshank, 1995), with a substantial increase in resistance and stiffness when forming part of a composite connection (Couchman and Way, 1998). The contact plate connection is a form that had already been used in continental Europe.

Analysis, Modelling and Classification

As in Eurocode 3, joints are to be modelled as simple, continuous or semi-continuous (Figure 2). The appropriate model is determined by comparing the joint's structural properties with those of the connected members. The global analysis may be elastic or elastic-plastic and so the stiffness of the joint is relevant. The code recognises it is conventional to treat a stiff joint as rigid, even though there is really some flexibility. Composite joints are usually quite stiff and the choice of joint model is between continuous and semi-continuous. In the global analysis, allowance is to be made for cracking and creep of concrete. The classification of joints would be too complicated if member stiffness was to include these effects. In classification therefore, their effect may be neglected. This overestimates member stiffness, making it more likely that a joint will be classified as semi-continuous and its effect on the global analysis treated in a more advanced manner with less approximation.

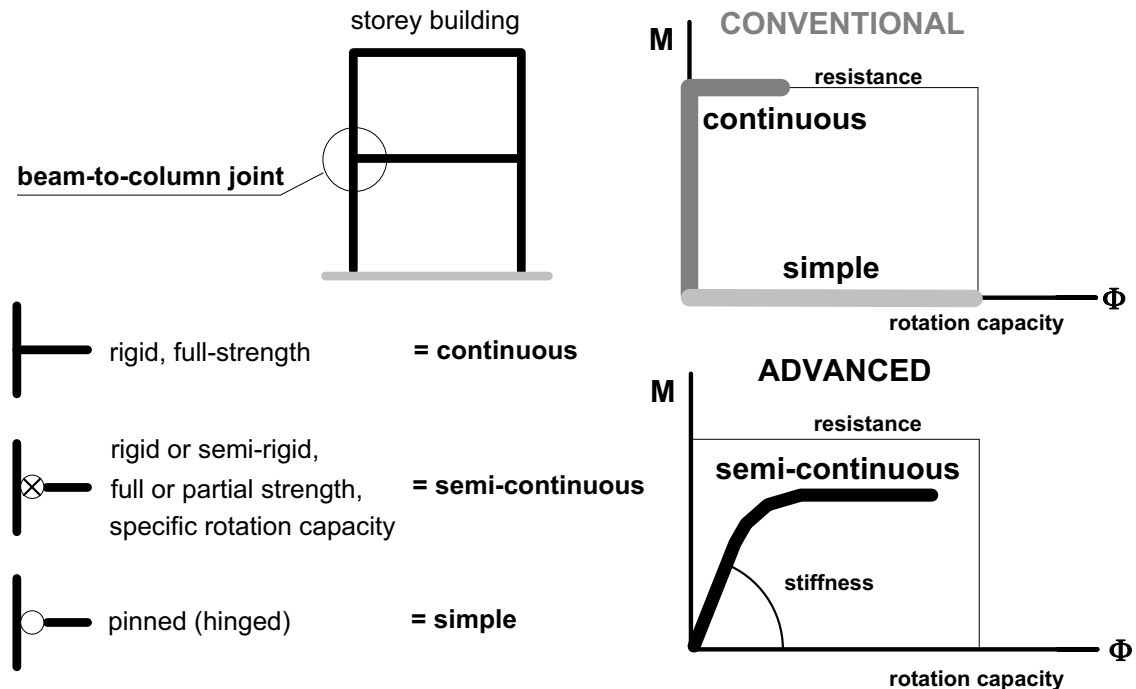


Figure 2 Types of joint model (Huber)

Joint stiffness reduces as its moment resistance is approached. To allow for this in global analysis, Eurocode 3 permits the rotational stiffness to be taken as an initial value divided by a modification factor. For common steel beam-to-column joints, Eurocode 3 gives a value of 2.0. For composite joints, Eurocode 4 modifies this value to 1.5, based on an assessment of how such joints behave.

Design Methods

The basis is to treat a row of reinforcing bars in tension in a manner similar to a bolt-row in tension in a steel connection, but using the structural properties of the reinforcement. By stating this in the Eurocode, much shorter provisions have been possible, compared with the previous model clauses (Anderson et al., 1999). The moment of resistance and the rotational stiffness are to be determined “by analogy to the provisions for steel joints” given in Eurocode 3. The project Team for EN 1994-1-1 and the national experts believed that further detail in Eurocode 4 was unnecessary. Calculation methods had already been demonstrated in the Background Documents and the UK Connections Group’s publication referenced above. A guide on EN 1994-1-1 (Johnson and Anderson, 2004) also provides a fully-worked example in accordance with the code.

Rotation capacity has been treated differently. Eurocode 3 gives checks which, if satisfied, enable the designer to assume adequate rotation capacity for plastic global analysis. Rotation capacity may also be determined by testing or calculation models based on the results of tests. For composite joints, the calculation method (Anderson et al., 2000) had been justified by comparison with tests but was regarded as too new for inclusion in Eurocode 4. Eurocode 3 permits a joint to be classified by stiffness on the basis of previous satisfactory experience (a provision incidentally that, as it is not modified by Eurocode 4, is also applicable to composite joints). Eurocode 4 extended this approach to rotation capacity. The structural analysis is required to reflect the anticipated behaviour of joints but there are no values given for required rotation capacity or limits on redistribution due to semi-continuous joint action.

Components for composite joints

Eurocode 4 introduces two basic components additional to those in Eurocode 3:

- longitudinal steel reinforcement in tension
- steel contact plate in compression.

It also gives provisions for reinforced components, to cover situations in which the steel column web is encased in concrete:

- column web panel in shear
- column web in transverse compression.

Background to the properties of these components is given in the report from the COST C1 programme (Anderson et al., 1996) and by Huber (Huber, 1999). The

provisions on resistance can, in the main, be seen to be reasonable by inspection and are treated as normative and placed in the main body of the code. However, stiffness was treated in an informative annex. Its content was based on the best available research, which was recent, and its application was untried outside specialist design teams.

To calculate joint stiffness, it was judged necessary to treat the influence of slip by including a procedure that reduces the stiffness of the joint in the tension zone (Aribert, 1996). This forms part of the calculation method for rotation capacity given outside the Eurocode (Anderson et al., 2000). No provisions were given in the Eurocode for the influence of the shear connection on the joint's resistance. In Eurocode 4, it is assumed that full shear connection will be provided in hogging bending.

CONCLUSION

The use of composite joints has several advantages in design. Compared to nominally pinned connections, there will usually be:

- a reduction in the section size for beams
- reduction in the deflections of beams
- reduction in crack widths.

In the past, designers will have created composite joints by providing slab reinforcement to limit cracking, but without taking advantage of the additional resistance and rotational stiffness. One purpose of the provisions in Eurocode 4 was to enable the designer to quantify these additions.

Research continues and further comparisons between codes and tests (physical or by sophisticated simulations) are valuable, particularly when they concern less frequently tested forms of construction. Examples are:

- single-sided configurations and double-sided configurations under un-balanced loading, which introduce forces into the column (Figure 3)

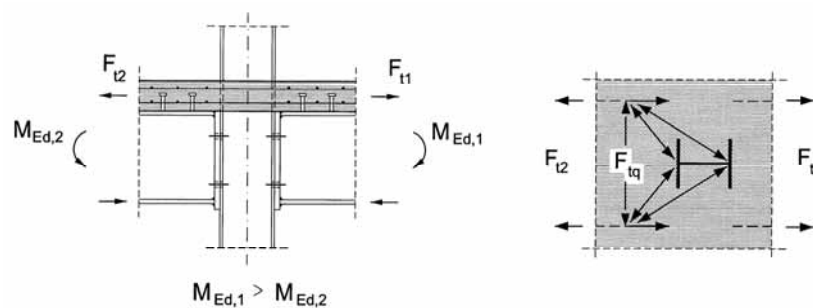


Figure 3 Unbalanced loading (Hanswille)

- double-sided configurations with beams of unequal depth
- tests which investigate quantitatively the influence of reinforcement ductility on rotation capacity
- connections to beams with partial shear connection in hogging bending.

Such research opens the possibility of improved design methods and additional forms of composite joint. Perhaps though the most important investigation is to find what practical use is being made of existing methods. Are code provisions clear and easy to use? Most importantly, to what extent are composite joints, whose potential benefits have often been stated by researchers, contributing to economical construction in buildings and other structures?

ACKNOWLEDGEMENTS

The author acknowledges with thanks the provision of figures by Professor G. Hanswille and Dr G. Huber.

REFERENCES

Anderson, D., Bode, H., Huber, G., Jaspart, J.P., Kronenberger, H.J. and Tschemmernegg, F.(1996), *Composite steel-concrete joints in braced frames for buildings*. COST C1 Semi-rigid behaviour of civil engineering structural connections, Office for Official Publications of the European Communities, Luxembourg.

Anderson, D., Aribert, J.M., Bode, H., Huber, G., Jaspart, J.P., Kronenberger, H.J. and Tschemmernegg, F.(1999), *Design of Composite Joints for Buildings*. Publication 109, European Convention for Constructional Steelwork (ECCS), Brussels.

Anderson, D., Aribert, J.M., Bode, H and Kronenberger, H.J. (2000), "Design rotation capacity of composite joints", *The Structural Engineer*, Vol. 78, No. 6 (pp.25-29).

Aribert, J.M. (1996), "Influence of slip of the shear connection on composite joint behaviour", in Bjorhovde, R., Colson, A. and Zandonini, R. (eds) *Connections in Steel Structures III Behaviour, Strength and Design*. Pergamon, United Kingdom.

Bjorhovde, R., Brozzetti, J. and Colson, A. (1988), *Connections in Steel Structures: Behaviour, Strength and Design*. Elsevier Applied Science, London and New York.

Bose, B. and Hughes, A.F. (1995), "Verifying the performance of standard ductile connections for semi-continuous steel frames", *Proceedings of the Institution of Civil Engineers, Structures and Buildings*, Vol. 110, November (pp.441-457).

CEN (1992), *European PreStandard ENV 1994-1-1: 1992 Eurocode 4: Design of composite steel and concrete structures Part 1-1: General rules and rules for buildings*. European Committee for Standardization, Brussels.

CEN (2004), *European Standard EN 1994-1-1: 2005 Eurocode 4: Design of composite steel and concrete structures Part 1-1: General rules and rules for buildings*. European Committee for Standardization, Brussels.

CEN (2005), *European Standard EN 1993-1-8: 2004 Eurocode 3: Design of steel structures Part 1-8: Design of joints*. European Committee for Standardization, Brussels.

Commission of the European Communities (1985), *Eurocode No. 4: Common Unified Rules for Composite Steel and Concrete Structures*. Report EUR 9886 EN, Brussels.

Couchman, G. and Way, A. (1998), *Joints in Steel Construction: Composite Connections*. Publication 213, Steel Construction Institute, Ascot.

Huber, G. (1999), *Non-linear Calculations of Composite Sections and Semi-continuous Joints*. Ernst & Sohn, Berlin.

Jaspart, J.P., Steenhuis, M. and Anderson, D. (1999), "Characterisation of the joint properties by means of the component method", in Maquoi, R. (ed.), *COST C1 Control of the semi-rigid behaviour of civil engineering structural connections: Proceedings of the international conference, Liege, 17 to 19 September 1998*. Report EUR 18854 EN, Office for Official Publications of the European Communities, Luxembourg.

Johnson, R.P. and Anderson, D. (1993), *Designers' Handbook to Eurocode 4 Part 1.1: Design of composite steel and concrete structures*. Thomas Telford, London.

Johnson, R.P. and Anderson, D. (2004), *Designers' Guide to EN 1994-1-1 Eurocode 4: Design of composite steel and concrete structures Part 1.1: General rules and rules for buildings*. Thomas Telford, London.

Moore, D. B. (1988), "The design of end-plate connections", in Armer, G.S.T. and Moore, D.B. (eds.), *Frame and Slab Structures*. Butterworths, London.

Najafi, A.A. and Anderson, D. (1997), "Ductile steel-concrete composite joints", in *Composite Construction - Conventional and Innovative*. IABSE, Zurich.

Nethercot, D.A., Li, T.Q. and Choo, B.S. (1995), "Required Rotations and Moment-Redistribution for Composite Frames and Continuous Beams", *Journal of Constructional Steel Research*, Vol. 35 (pp.121 – 164).

Stainsby, R. and Cruickshank, N. (1995), *Joints in Steel Construction: Moment Connections*. Publication 207, Steel Construction Institute, Ascot.

APPLICATION OF THE EC3 DESIGN RULES TO END-PLATE CONNECTIONS WITH 4 BOLTS IN ONE ROW

Klaus Weynand and Ralf Klinkhammer

Feldmann + Weynand GmbH, Aachen, Germany
k.weynand@fw-ing.de

Dieter Ungermann and Stephan Schneider

Technical University of Dortmund, Dortmund, Germany
dieter.ungermann@uni-dortmund.de

Otto Oberegge, Hans-Peter Hockelmann and Nicole Ritterbusch

Fachhochschule Köln, Köln, Germany
otto.oberegge@fh-koeln.de

ABSTRACT

Eurocode 3 provides detailed application rules for the design of bolted end-plate connections. The rules in Eurocode 3 apply for bolt pattern with any number of bolt rows. However, the rules are limited-except for some few cases-to configurations with two bolts in one horizontal row only, i.e. one bolt on each side of the beam or column web. However, if for example wide flange H-sections are connected with bolted end-plates, it is sometimes economic to place four bolts in one row, which is a common and even standardized configuration in Germany. In general, Eurocode would also apply to this type of connection. The present paper gives an overview on the state of the art and it reports on recent developments.

1. INTRODUCTION

Eurocode 3 (CEN, 2005) provides detailed application rules for the design of joints with bolted end-plate connections. The rules to determine the resistance and stiffness of the end-plate are based on the so-called equivalent T-stub model. The rules in Eurocode 3 apply for bolt pattern with any number of bolt rows. But the rules are limited - except for some few cases - to configurations with two bolts in one horizontal row only, i.e. one bolt on each side of the beam or column web.

Sometimes, it could be more economic to place four bolts in one row, if for example wide flange H-sections are connected with bolted end-plates. This is a common and even standardized configuration in Germany. In general, Eurocode would also apply to this type of connection, as the principles for the design are very general, but application rules can be found neither in Eurocode 3 nor in the literature.

The present paper reflects the actual state of the art concerning the design of joints with end-plate connections having four bolts in one row in Europe and especially in Germany. Available models are described. Finally the paper reports on analytical, experimental and numerical investigations carried out in the frame of an actual national research project to derive and improve application rules for the design of end-plate connections with four bolts in one row based on the design principles of Eurocode 3.

2. STATE OF THE ART

Part 1.8 of Eurocode 3 (CEN, 2005) provides rules for the design of joints in steel structures. As far as joints with end-plates are concerned, Eurocode 3 provides detailed application rules for the determination of the design moment-rotation characteristic which is determined from the properties of the joint's basic components, i.e. the joint properties are calculated by means of the component method: The joint is separated in its basic components. For each component, rules are given to determine its design resistance and elastic stiffness (initial stiffness). Relationships between the properties of the basic components and the structural properties of the overall joints are given for the design moment resistance and rotational stiffness.

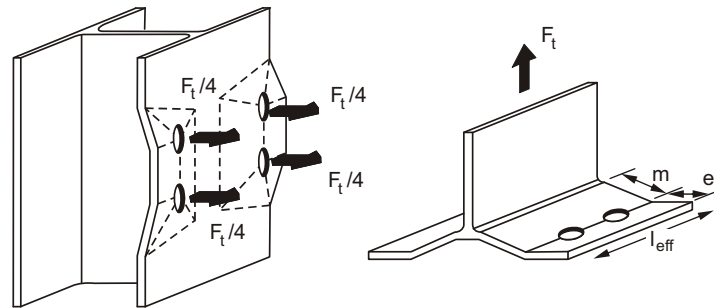


Figure 1 T-stub model: (a) real component and (b) effective T-stub

Rules to determine the properties of some components as for example “end-plate in bending” or “column flange in bending” are based on the equivalent T-stub model. This model considers a simple T-stub as a basic component where the web is loaded by a tensile force. The equivalence between this T-stub and the real component in the joint, for example the end-plate in bending, is expressed through an effective length of this T-stub in such a way that the properties of the T-stub are the same as those of the real component, see Figure 1. The rules in Eurocode 3 apply for bolt pattern with any number of bolt rows. A very important advantage of the model given in Eurocode 3 is its general applicability to most of typical end-plate details. This means that for example the position of the bolts or the use of stiffeners incl. intermediate stiffeners may be chosen by the designer in order to fit with the requirements given for example by the fabricator. In the mean-time user-friendly software tools are available to design such joints fully in accordance with Eurocode 3 (Weynand et al., 2008). Safety and economy aspects of the application of the Eurocode model have been discussed in many publications. However, as said before, the rules are limited – except for some few cases (e.g. in the extended part of an end-plate) – to configurations with two bolts in one horizontal row only, i.e. one bolt on each side of the beam or column web, see Figure 2a.

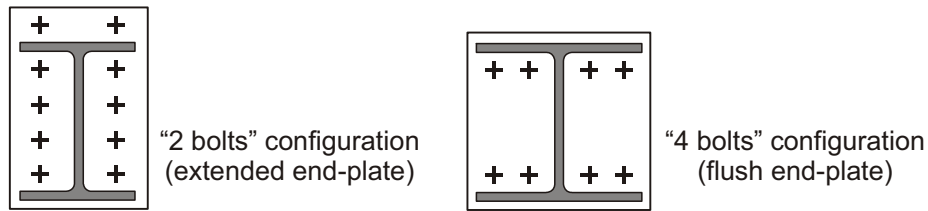


Figure 2 End-plates with (a) two bolts and (b) four bolts in one row

It can be stated that this limitation of the Eurocode application rules may appear as a barrier for designers in such countries (for example Germany) where end-plates with four bolts in one horizontal row, see Figure 2b, are typically used in practice. There are different reasons why such “4 bolts” configurations are chosen. If for example wide flange H-sections are connected with bolted end-plates, it is sometimes economic to place four bolts in one row in a moment resistant joint. All bolts have a maximum level arm to the center of compression and hence a maximum contribution to the design moment resistance. In other cases where compact sections with small profile height are selected but extended endplate can not be used because of geometrical limitations, a “4 bolts” configuration is the only solution to develop a significant moment in the connection. Finally, at least in Germany, the use of such configurations is very popular because they are part of a set of standardized joints (DSTV, 1978). This publication provides a significant number of standardized end-plate connections including not only the complete geometrical layout of the joints but also - in combination with most standard hot-rolled I or H sections - the design moment resistance and the design shear resistance. The resistance values are derived from a simple mechanical model, the so-called “DSTV model”, which is described more in detail in section 3. As explained in section 3 the model leads to rather high resistances of the joints but it is strictly limited to the specified range of validity.

For the designer, the most important benefit of such standardized joints is the fact, that no further calculations are needed when including such joints in the design of a steel structure. Similar publications exist in other countries, for example the well known so-called “green book” in UK (SCI and BCSA, 1995), but these design aids do not include “4 bolts” configurations. With regard to the application of the DSTV book (DSTV, 1978) in Germany, it should be noted that the use of the standardized joints need even no further checks by a proof-engineer as the design values got a general approval by the German building authorities. On the other side, the use of standardized joints give few freedom to the designer to optimize the layout or to fit better with fabrication and erection requirements.

Since the recent generation of design codes is based on the ultimate limit state design and as the new codes follow no more the concept of pure elastic design and allowable stresses, an updated version of the German book on standardized joints (DSTV, 1978) was required. In order to be prepared for the introduction of the new European design codes (Eurocodes), the Eurocode design model was used for the re-calculation of the design resistances, but with regard to the “4 bolts” configurations, Eurocode 3 provides no application rules. Nevertheless, in general, Eurocode would also apply to this type of connection, as the principles for the design of joints are very general. So, an extended model for the determination of the design moment resistance of “4 bolts” configurations has been derived in order to prepare

an update of the “old” design aids. This model is described in section 4. The extended model used for the new design tables (Weynand et al., 2002) is fully based on the principles given in Eurocode 3 and it follows very close the Eurocode 3 Part 1.8 application rules for “2 bolts” configurations. However, no experimental test were available at this time and some conservative assumption were made which led – at least in comparison to the resistance values of the “old” DSTV model – sometimes to rather low values. On the other side, the model gives certainly less restrictions with regards to the end-plate and bolt pattern geometries or material properties. With the purpose of further developing this model a new national research project has been founded. The main objective of the project is to improve the economy of the extended model by mean of increasing the resistance values. The project is carried out by the authors of the present paper. A progress report is given in section 5.

3. THE “DSTV” MODEL

The publication on standardized joints (DSTV, 1978) includes a model for the determination of the design moment resistance of joints with bolted end-plate connections. Even if no check is made, the joints are assumed to be rigid. The model considers four types of end-plates as shown in Figure 3. To validate the model, experimental tests carried out at the University of Karlsruhe were available (Steinhart and Schlaginhaufen, 1961).

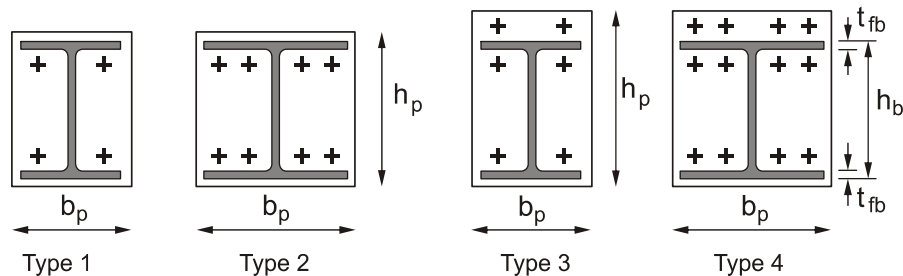


Figure 3 Types of end-plates considered by the DSTV model

It is assumed that the moment M_b acting in the beam is transferred through the flanges by a tensile force F_t and a compression force F_c

$$F_t = -F_c = \frac{M_b}{h_b - t_{fb}} \quad (1)$$

The tensile force is transferred by the bolts close to the beam flange in tension and the compression force is transferred through contact of the flange in compression.

The design moment resistance considers checks at ultimate limit state as well as serviceability criteria. The model and its range of validity is based on the assumption that both the plastic resistance of the end-plate and the ultimate tensile resistance of the bolts are reached nearly at the same time. Therefore a specific ratio t_p/d is required. Based on relationships between the internal forces shown in Figure 4, plastic moment resistances in sections “I” and “II” and shear capacity of the plate are calculated and compared with the tensile resistance of the bolts. Equilibrium

considerations lead to a maximum tensile force F_t and finally to the design moment resistance.

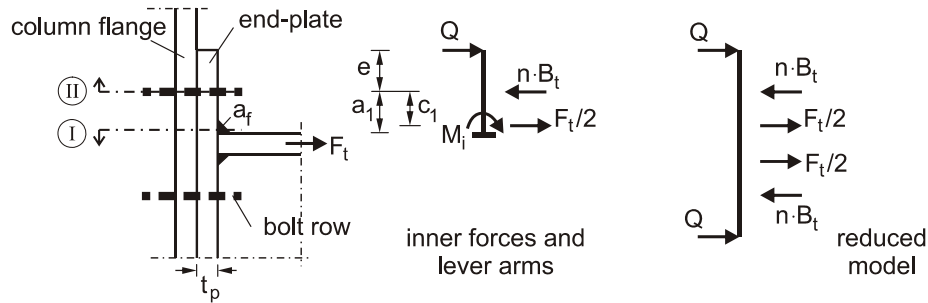


Figure 4 DSTV model for extended end-plates

In order to obtain a moment resistance close to the maximum value found in the experimental tests, an empirical inner lever arm c_1 has been introduced.

$$c_1 = a_1 - \frac{1}{3} a_f \sqrt{2} - \frac{1}{4} (d_w + t_p) \quad (2)$$

This reduced lever arm mainly account for the influence of the weld thickness and the washer.

The model does not check any component of the column which requires usually a number of stiffeners (a) to ensure that no failure occur in the column flange or column web and (b) to validate the assumption of rigid joints. As this model has been calibrated against experimental tests, design resistances obtained from this model are rather high and hence quite economic. But due to the fact, that bolt failure will always be relevant (due to the basic assumptions of the model mentioned before), the joints may not be considered as ductile. Furthermore, the model can not be used for other geometries or material properties as its validity outside the tested range has never been shown.

4. A PRELIMINARY DESIGN MODEL FOR “4 BOLTS” CONFIGURATIONS

As explained in section 2, the development of an extended model for the design of “4 bolts” configuration was required to prepare a new issue of the joint design tables published by the German Steelwork Association DSTV. Basis for the model is the design model of Eurocode 3, i.e. regarding the determination of the end-plate and column flange properties, the extended model refers to the T-stub model. This would –in contrast to the “old” DSTV model – allow for arbitrary plate thicknesses and bolt diameters as well as for any material introduced in the code and therefore allow to design ductile connection by means of thin end-plates as well as stiff connections by means of thick end-plates.

Two concepts have been investigated to be a basis for the extended model:

(a) T-Stub with four bolts

A quite general extension would be to develop a T-stub model with 4 bolts, i.e. 2 bolts on each side of the T-stub web as shown in Figure 5. The equations the describe the behavior of such a model are certainly much more difficult for

Mode 2 than those for the 'standard' T-stub with two bolts, because prying forces occur and the bolt forces in the inner and outer bolts are dependent on the stiffness of the T-stub system.

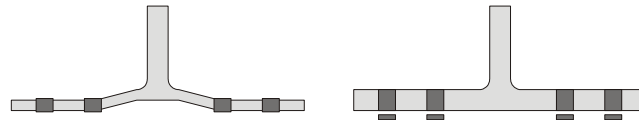


Figure 5 T-stub with 4 bolts (a) Mode 1: flange yielding and (b) Mode 3: bolt failure

But such an approach seem not very expedient because a significant stiffness of the plate is required in order to activate sufficient tensile forces in the outer bolts. In other word, if Mode 1 (pure flange yielding) is the decisive failure mode, the outer bolts will not be activated at all, i.e. the outer bolts will not contribute to the resistance of the joint. Tests carried out at the university of Aachen (Sedlacek and Stangenberg, 2000) confirm this. Even though the project shows some promising approaches, the results appear much to complex for a simple design model, not to forget the problem of defining the equivalent length of the T-Stub which is not yet solved.

(b) Consideration of individual T-stubs

Having in mind that the outer bolts may only be activated if they are located close to a stiffener (beam flange or horizontal stiffener in the column web) it seems much more convenient to determine the bolts forces and plate resistances through the consideration of individual T-stubs, i.e. to “cut” the plate into separate T-Stubs as shown in Figure 6. Note that the same approach is made if – in a “2 bolts” configuration – two bolt rows are separated by a stiffener. The difference is that in the later case, the individual T-stubs behave fully independent while in the situation shown in Figure 6 an interaction between the inner T-Stub and the outer T-Stub must be taken into account.

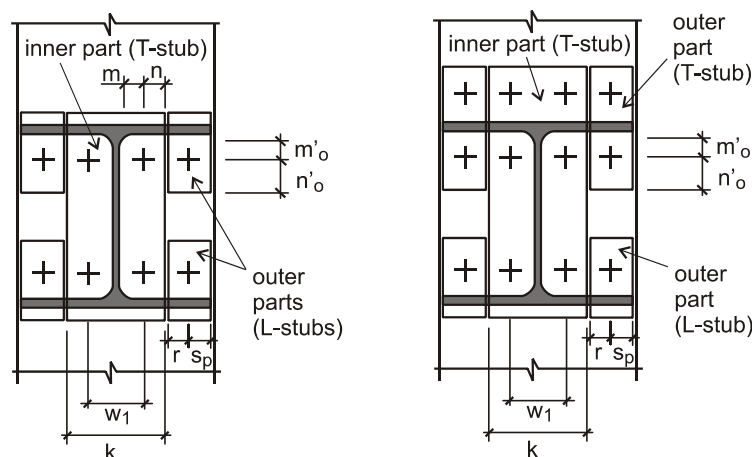


Figure 6 Individual T- or L-stubs (inner and outer part)

For the preparation of the new issue of the DSTV book, the second approach has been chosen. This approach is certainly more simple to apply and it is obviously fully

in accordance with the Eurocode 3 model. However, several specific aspects need to be taken into account.

Of course, the properties of the inner part of the end-plate will be determined exactly as a classical “2 bolts” configuration. Note that, as long as the failure mode will include a yielding of the plate, the approach is more conservative (and hence less economic) because the real yield lines of the plate will of course not end at the edge of the inner part.

With regard to the outer part, different situations must be considered when the plate is either an extended or a flush end-plate.

- (a) Outer part in an extended end-plate: In this situation, the real component can be modeled like the classical T-stub. The web of the equivalent T-Stub is the outer part of the beam flange (or the column web stiffener).
- (b) Outer part in a flush end-plate: Here, the real component can be modeled like a L-stub. Compared to the classical T-stub, further failure mode should be checked if plate yielding may occur, see Figure 7.

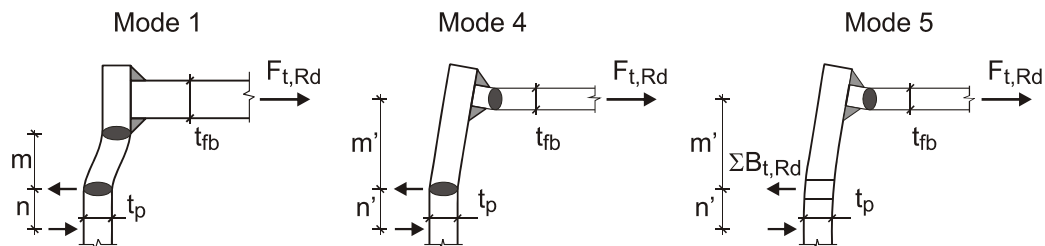


Figure 7 L-Stub model for outer bolts and additional failure modes

Finally, when determining the joint design moment resistance from the individual components, the compatibility in terms of deformation between the inner part and the outer part must be taken into account. It is assumed that the deformation, at the height of the horizontal bolt row, of the inner part is the same than that of the outer part, which is correct at the intersection of both parts but not at the bolt axis. Hence this is a conservative assumption for the following considerations.

According to the component approach, the behavior of each component is express by its load-deformation characteristic. The stiffness may be expressed by is stiffness coefficient k (k_i for the inner T-Stub, k_o for the outer T- or L-Stub). Due to the load-deformation behavior of the individual parts (inner and out part), 4 cases must be studied as follows, see Figure 8:

	Inner part ductile	Inner part NOT ductile
Outer part ductile	<u>Case 1:</u> $\max \delta_i, \max \delta_o \rightarrow \infty$ $\Rightarrow F_{row} = F_i + F_o$	<u>Case 2:</u> determine $\max \delta_i$ $\Rightarrow F_{row} = F_i(\delta_i) + F_o(\delta_i)$
Outer part NOT ductile	<u>Case 3:</u> determine $\max \delta_o$ $\Rightarrow F_{row} = F_i(\delta_o) + F_o(\delta_o)$	<u>Case 4:</u> $\delta^* = \min(\max \delta_i, \max \delta_o)$ $\Rightarrow F_{row} = F_i(\delta^*) + F_o(\delta^*)$

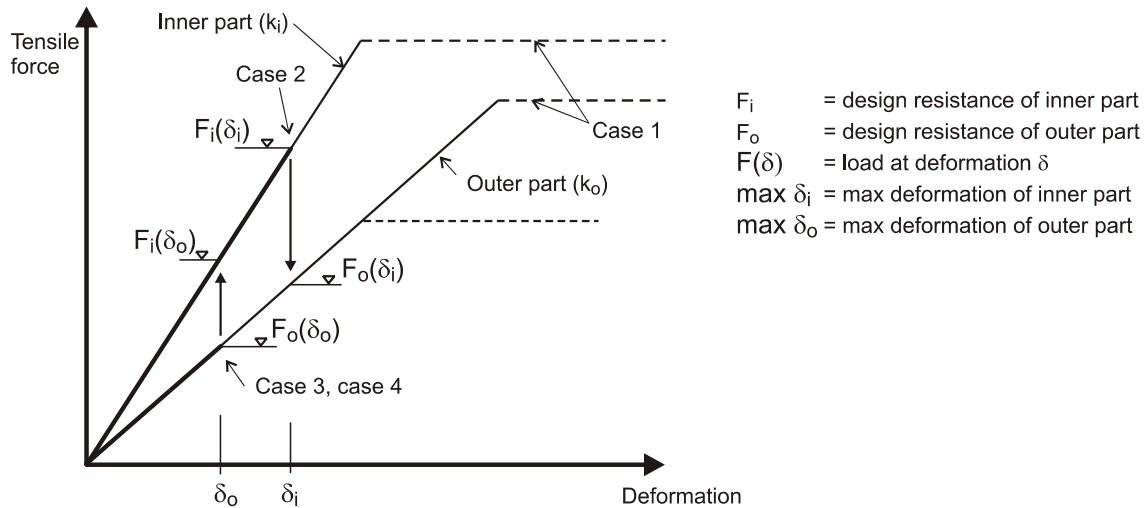


Figure 8 Deformation compatibility between inner part and out part

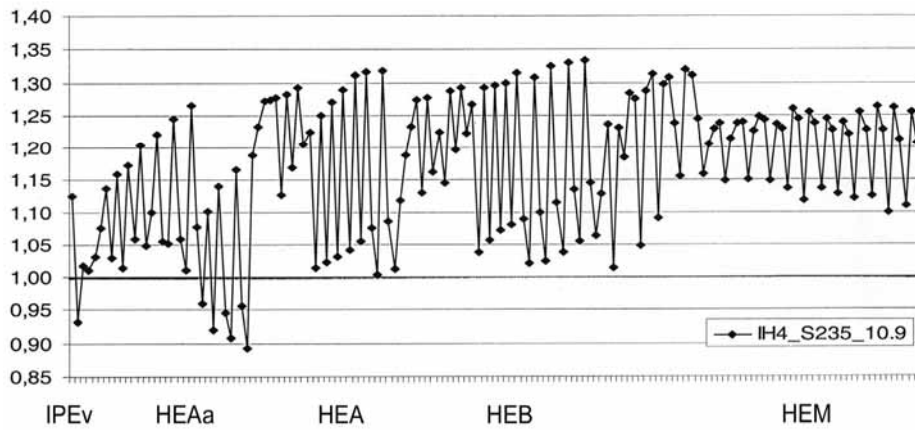


Figure 9 Comparison of design moment resistance M_{EC3} / M_{DSTV} for extended end-plates with 4 bolts in one row (T-stub in outer part)

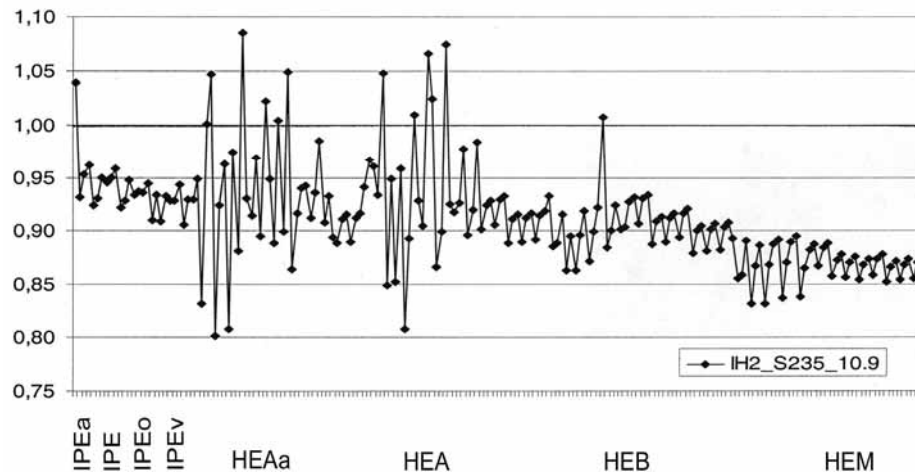


Figure 10 Comparison of design moment resistance M_{EC3} / M_{DSTV} for flush end-plates with 4 bolts in one row (L-stub in outer part)

Comparison between the design moment resistance of the old model compared to the extended Eurocode model have been made. Note that this can not be understood as a safety consideration because we compare here only two models; any statement concerning safety would require also a direct comparison with test results. Figure 9 shows the results of this evaluation for extended end-plates. It can be seen that the Eurocode model gives quite economic results. However, for flush end-plate, see Figure 10, the results obtained with the extended Eurocode model are in average lower than those of the old model.

5. RECENT INVESTIGATION TO IMPROVE THE EXTENDED DESIGN MODEL

As shown in Figure 10, the results of the new model are in many cases certainly lower than those given in the “old” DSTV design tables. Furthermore, according to the old DSTV model, the bolts must be preloaded and an additional serviceability check is needed to avoid any gap between the end-plate and the column flange. If this check would be taken into account as well, the values of the new model must be reduced again, which would lead in some cases to M_{EC3} / M_{DSTV} values between 0.55 and 0.70. As details of the old tests made in 1960 are no more available, it was not possible to improve the model with respect to these observations. Therefore a new national research program has been launched recently and it will be finalized end of 2008. Final results are not yet available. However first results from full scale test carried out at the University of Dortmund and component test carried out at the Cologne University of Applied Sciences shown quite interesting results.

In total 22 full scale tests will be carried out. As the distribution of the bolts forces are of high importance, the forces in the bolts are measured. As it can be seen from Figure 11, strain gauges have been placed inside the bolts. As an example, 0 shows the deformed flush end-plate of a full scale test after failure. Beside the experimental investigations, numerical studies are performed. 0 also illustrate the finite element model of the same test.

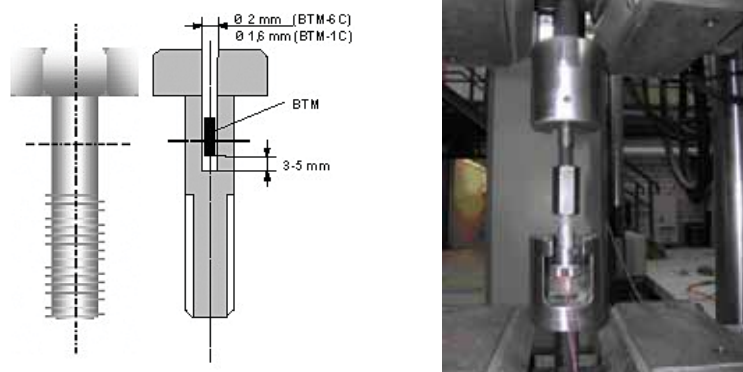


Figure 11 (a) Schematic diagram to measure bolt forces (taken from: Preusser Messtechnik) and (b) test to calibrate the measurements for bolts forces

More detailed results and further developments of the preliminary model presented in section 4 will be published as soon as the current project is finalized. Support from the AiF (German Federation of Industrial Research Associations, AiF project 15059N) is gratefully acknowledged.



Figure 12 New experimental test carried out at University of Dortmund and deformed finite element model

6. CONCLUSIONS

The present paper gives an overview on the state of the art regarding the design of joints with bolted end-plates with four bolts in one horizontal row. With regards to the application of Eurocode, a preliminary extended universal model is presented. Comparisons of this model to an older model with rather strong limitations in its application show already economic results for extended end-plates. To improve the economy for flush end-plates, a new research project has been launched. The work program includes full scale tests and component tests as well as parameter studies using finite element simulations.

7. REFERENCES

- CEN (2005), "Eurocode 3, Part 1.8", EN 1993-1-8, Design of steel structures - Design of joints, Brussels, Belgium
- DSTV/DAST (1978), *Typisierte Verbindungen im Stahlhochbau*, Stahlbau-Verlags GmbH, 2nd issue, Cologne, Germany
- SCI, BCSA (1995), *Joints in Steel Construction - Moment Connections*, Publication number 207/95, ISBN 1 85942 018 4, Ascot, UK.
- Sedlacek, G., Stangenberg, H, (2000), *Plastische Bemessung von Stirnplattenanschlüssen mit vier Schrauben in einer Reihe*, AiF Forschungsbericht 11446, Institute of Steel Construction, RWTH Aachen, Germany.
- Sedlacek, G., Weynand, K., Klinkhammer, R. (2002), *Typisierte Anschlüsse im Stahlhochbau*, Stahlbau Verlags- und Service GmbH, 2nd issue, Düsseldorf, Germany.
- Steinhart and Schlaginhausen, (1961), *HV-verschraubte Kopfplattenverbindungen bei biegefesten Stabwerken (Deutsch-Schweizer Gemeinschaftsversuche)*, Stahlbau-Verlags GmbH, Cologne, Germany.
- Weynand, K., Klinkhammer, R. (2002), *Extended design model for the application of EC3 to 4 bolts configurations*, Internal background document for the approval of the 2nd issue of DSTV design table for standardized joint, Aachen, Germany, (not published).

Weynand, K., Klinkhammer, R., Oerder, R. , Jaspart, J.-P. (2008), CoP - The Connection Program, Program for the design of joints according to EN 1993-1-8, www.fw-ing.de/software.

DESIGN OF INNOVATIVE SMA PR CONNECTIONS BETWEEN STEEL BEAMS AND COMPOSITE COLUMNS

Roberto T. Leon

Georgia Institute of Technology, Atlanta, GA 30332-0355, USA
rleon@ce.gatech.edu

Jong Wan Hu

Georgia Institute of Technology, Atlanta, GA 30332-0355, USA
gtg741p@mail.gatech.edu

ABSTRACT

This study describes the development of innovative connections between steel beams and concrete-filled tube columns that utilize a combination of low-carbon steel and super-elastic shape memory alloy components. The intent is to combine the recentering behavior provided by the shape memory alloys to reduce building damage and residual drift after a major earthquake with the excellent energy dissipation of the low-carbon steel. The analysis and design of structures requires that simple yet accurate models for the connection behavior be developed. The development of a simplified 2D spring connection model for cyclic loads from advanced 3D FE monotonic studies is described. The implementation of those models into non-linear frame analyses indicates that the recentering systems will provide substantial benefits for smaller earthquakes and superior performance to all-welded moment frames for large earthquakes.

INTRODUCTION

In recent years, concrete filled steel tube (CFT) columns have become widely accepted and used in multistory buildings as well as bridges. These elements provide the synergetic advantages of ductility and toughness associated with steel structures and high compressive strength associated with confined concrete components. The advantages of CFT columns over other so-called mixed or hybrid systems (fully encased or partially encased systems) include both the fact that the concrete prevents local buckling of the steel tube wall and the that the confinement action of the steel tube extends the usable strain and increases the strength of the concrete. In addition, CFT columns have improved fire resistance and significant cost reductions in comparison with traditional steel construction. Composite CFT columns are especially efficient as the vertical elements in moment resisting frames located in high seismic areas because they have a high strength to weight ratio, provide excellent monotonic and dynamic resistance under biaxial bending plus axial force, and improve damping behavior (Tsai et al. 2004).

Recently, work at Georgia Tech on shape memory alloys (SMA) has explored the

applications of these materials to the design of connections in steel structures subjected to large cyclic loads (Penar 2005). SMA materials can undergo large deformations with little permanent residual strain through either the shape memory effect or the super-elastic effect. The deformations can be recovered with changes in either temperature or stress as shown in Figure 1. In this research, the recentering properties of flag-shaped super-elastic SMA will be combined with the large energy dissipation of conventional low-carbon steels to develop a new type of connection for use in low-rise structures with CFT columns.

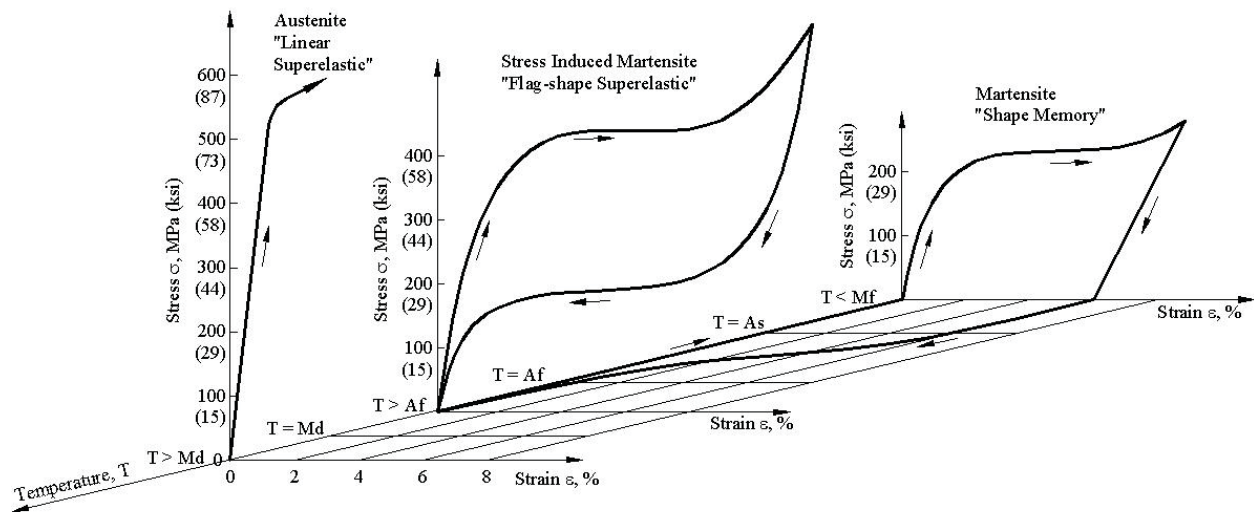


Figure 1. Characteristics of shape memory alloys (Penar 2005)

The proposed new connections are shown in Figure 2. These connections use three types of conventional PR connections (end plates, T-stubs and clip angles) but incorporate SMA and steel bars as the primary yielding elements. It is hypothesized that such combinations of CFT columns and SMA connections will achieve excellent ductility, upgraded energy dissipation and recentering capabilities. Connections to both rectangular and circular CFTs were developed; only the former will be discussed here.

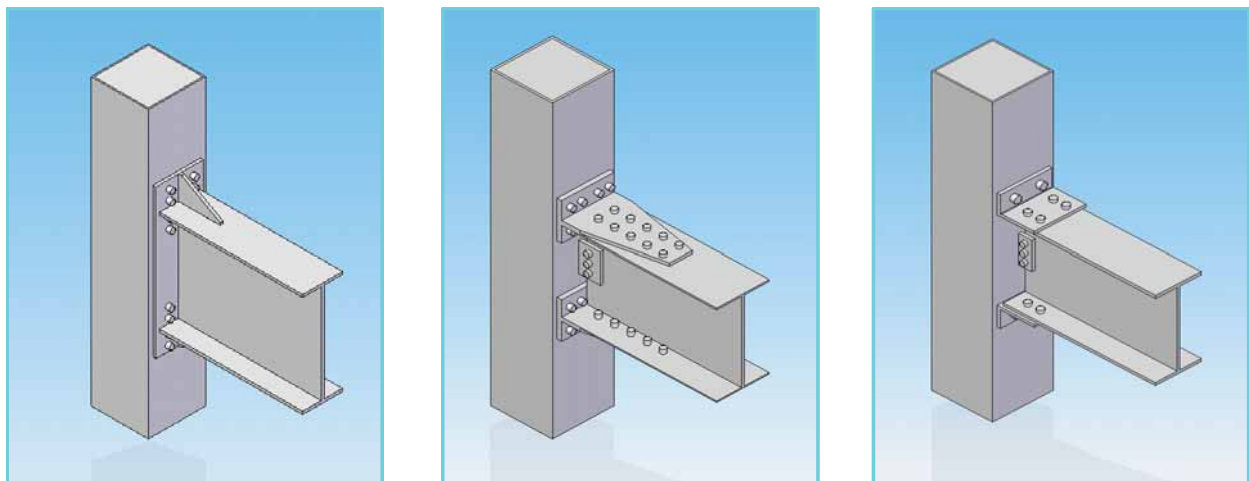


Figure 2. Proposed new connections to rectangular CFT columns

This paper is divided into two parts: (1) the development of a simplified 2D joint model suitable for numerical analyses using an open-source program, and (2) studies of the non-linear behavior of prototype 4 and 6-story composite moment frames using the OPENSEES program (Mazzoni 2006).

SMA PR-CFT CONNECTION DESIGN AND JOINT MODEL

All connections in this study were designed as full strength (FS), meaning that they can transfer the full plastic beam moment calculated according to the LRFD Standard (AISC 2001). The connection design, however, did not aim to achieve full restraint (FR or full end rigidity); it intended to utilize PR behavior to obtain ductile connection behavior. Joint components such as tension bars, bolts, welded stiffeners, and end-plates were designed with the intent of preventing or reducing loss of stiffness and strength due to brittle failure modes. Therefore, the dominant modes of the steel or SMA components will be ductile ones, ranging from very ductile such as tensile yielding of steel to moderately ductile such as minor local buckling. The connection selected for discussion in this paper is an end plate one (Figure 3). The connections were fabricated with an assembly of various steel members cut from standard shapes available in the current design specification (AISC 2001). A572 Grade 50 steel was used for all members and joint components. A490 high strength bolt material was used for steel bars, with matching materials for washers and nuts. Super-elastic (SE) Nitinol bars, with the characteristics shown in Figure 1, were located where the largest deformations were likely to occur and where their recentering effect would be maximized. Extended stiffener plates welded between the connected beam flange and the end-plate were required to maintain stiffness.

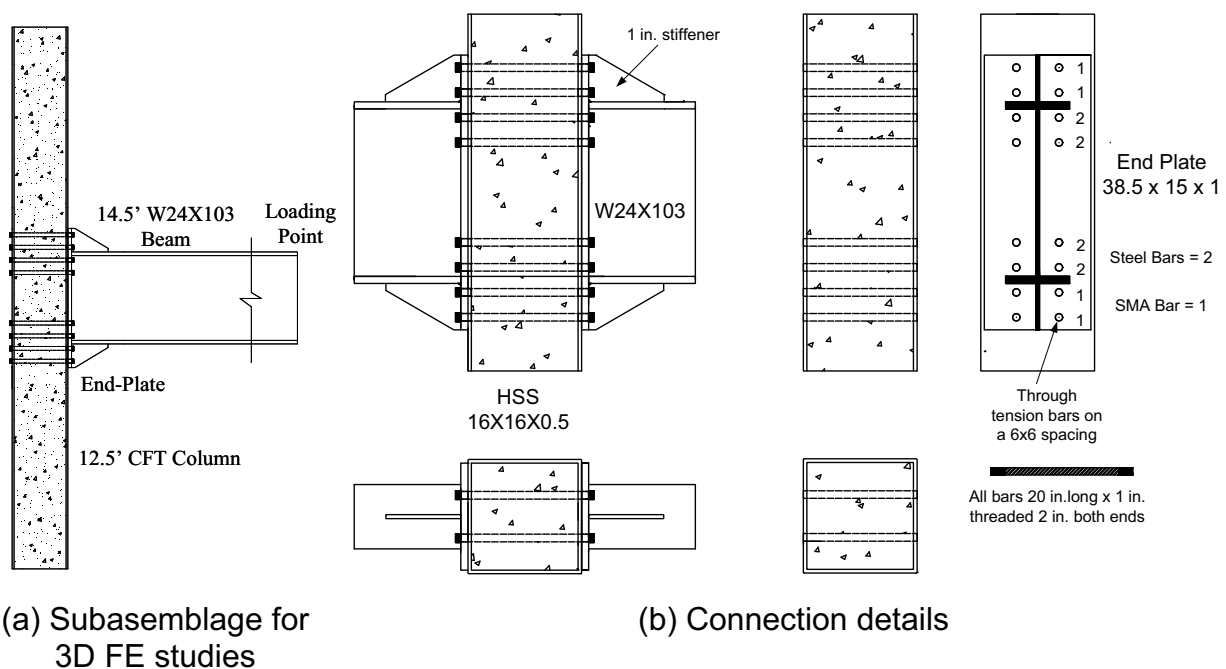


Figure 3 – End plate SMA PR-CFT connection

The ABAQUS Version 6.6-1 (ABAQUS, 2006) finite element code was used to analyze the proposed PR-CFT connections. These numerical 3D, symmetric models consisted of refined 3D solid elements incorporating the full nonlinear material/ geometric properties, contact elements, surface interaction with friction, constraint conditions using equation points, concrete crack conditions and elastic foundation springs. These advanced modeling methods were intended to provide a detailed and accurate understanding of the overall behavior of the connections, including the stress distributions on the contact surfaces in spite of the high computational cost typically associated with this type of approach. The results of a typical analysis are shown in Fig. 4. These results were used to verify that the end plate was thick enough to behave as a rigid element, that prying forces could be accurately measured, and that the transition points in the load deformation curves for individual components could be modeled by simple springs.

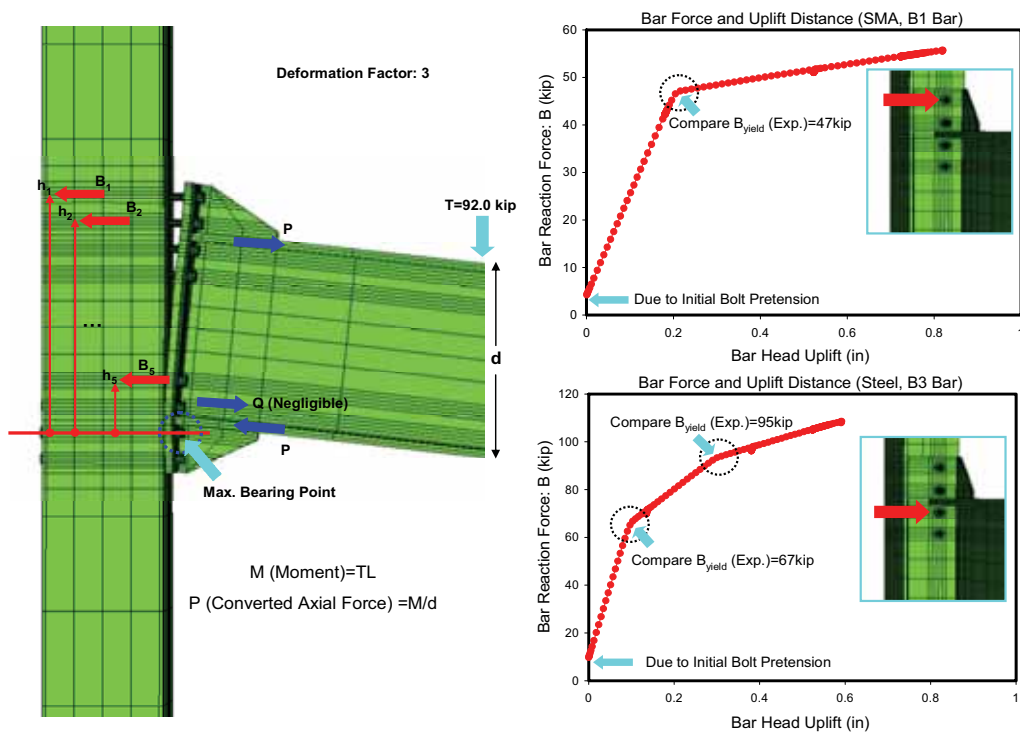


Figure 4 – Results of 3D FE analysis showing deflected shapes and behavior of both SMA and steel tension bars

After careful calibration of the 3D models to test data from SAC tests (FEMA 2000) and investigation of local behavior such as concrete crushing under the heads of the tension bars, the data from these monotonic studies was used to develop simplified 2D joint elements for use in OPENSEES. This program allows the implementation of user-defined elements such as the one proposed here (Figure 5). This element includes four equivalent spring elements (S1) to reproduce the behavior of the tension bars, four internal spring elements (S2) to reproduce the axial deformation of the CFT column,

four internal shear springs (S3) to reproduce the shear deformation of the CFT column and the beam, and one shear panel element (C) which is intended to reproduce the failure of the panel zone under severe loading. End-plates are modeled as rigid-plates in the joint element, and the beam and CFT columns are modeled as a nonlinear beam-column element with 2D fiber sections attached to the joint element.

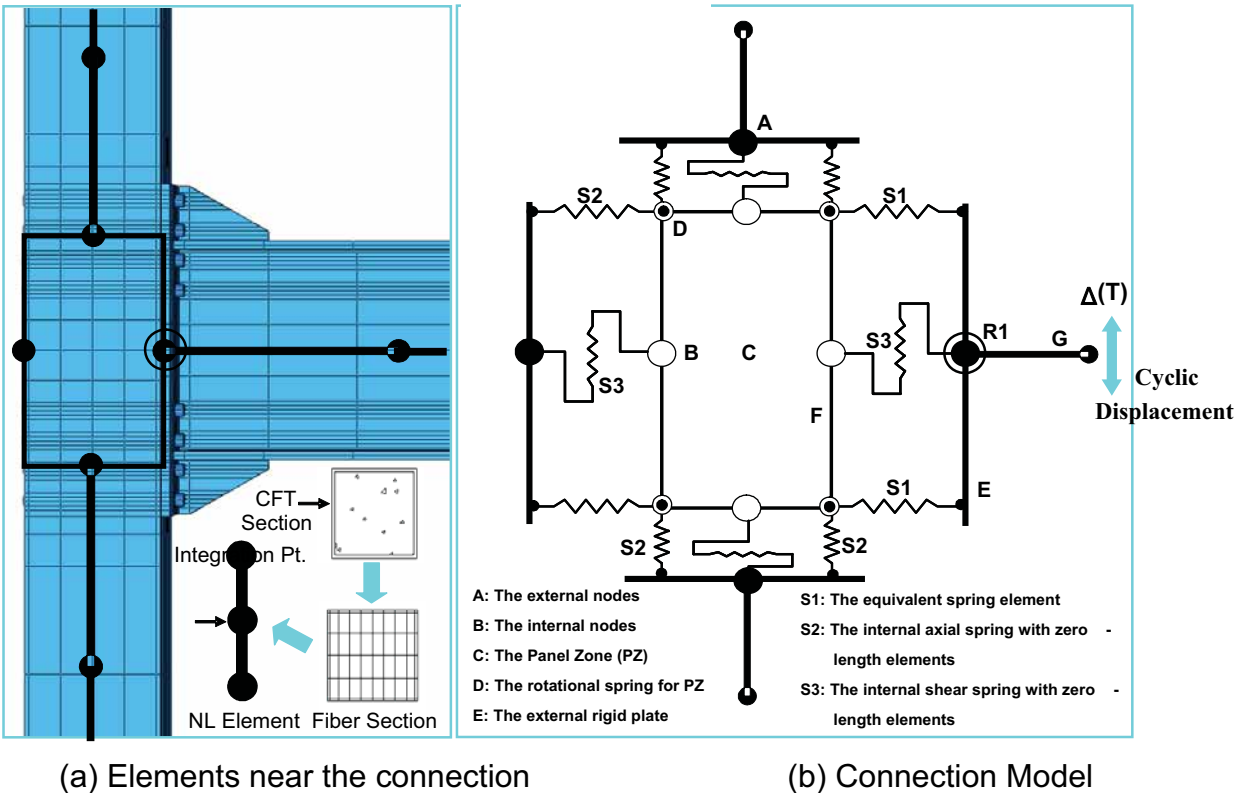


Figure 5 – Connection model and joint element

Force-deformation characteristics for these components were modeled by equivalent spring elements (Figure 5) installed in the joint element. The cyclic behavior was bounded by the monotonic FE results and applicable material properties. The cyclic behavior does not incorporate large strength and stiffness degradation because the designs were meant to result in connections that exhibited good hysteretic behavior. The 3D FE studies had shown that attempting to model large loss of strength and stiffness would lead to numerical problems and the need for sophisticated damage accumulation models in order to accurately predict the connection behavior. That type of model would not have been suitable for the 2D simplifications desired here. Because the deformation of the panel zone often contributes significantly to the drift of moment frames, care was taken to include in the model a reasonable composite panel zone component. The required information for this model, such as initial stiffness, yield shear, and ultimate shear strength were generated by using the equations proposed by Wu (Wu et al. 2007). The design equations for the panel zone consider both the increased shear stiffness due to composite action and stiffness losses due to bar holes. The shear strength is taken the superposition of shear strengths of the steel tube and the confined

concrete core and was modeled using the hardening material model in OPENSEES.

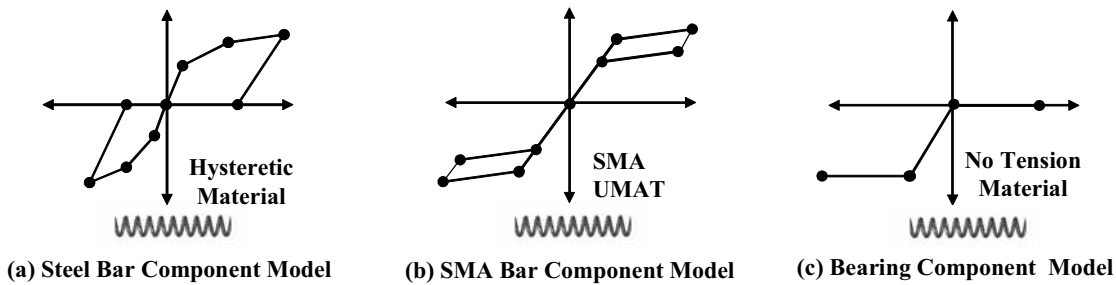


Figure 5 - Properties of typical equivalent springs

Initially, and for calibration purposes, the 2D joint models were subjected to loads applied to the tip of the beam corresponding to the position of a loading actuator (Fig. 3). A comparison between the monotonic results from the 3D FE model and the cyclic results of the joint element model is given in Figure 6. The data corresponds to the case of an end plate with 4 SMA and 4 steel bars top and bottom. The curves show good agreement in terms of initial stiffness, ultimate strength, and envelopes for the force-displacement behavior curves. In general, the 3D monotonic curves show less available strain because of numerical problems associated with the concrete model. For the cyclic behavior, the recentering effect can be observed during unloading due to the super-elastic (SE) SMA materials.

Results for the recentering effect depending on the types of bars used are given in Figure 7 for the same type connection as shown in Figure 6. The joint element model

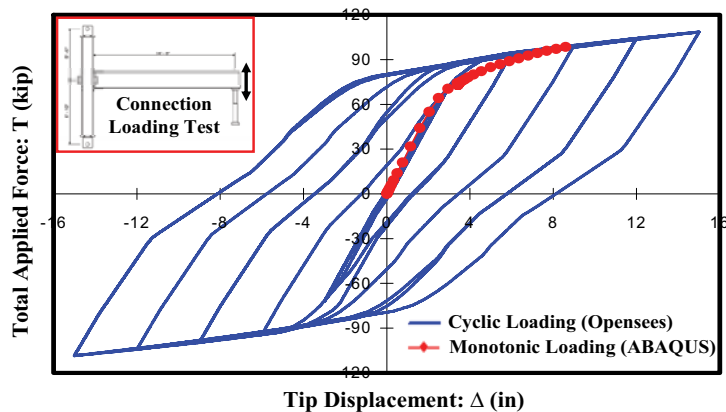


Figure 6. Comparison of monotonic and cyclic results

The joint equipped with only superelastic SMA tension bars (Fig. 7(a)) shows excellent recentering; however, plastic deformation of the beam causes some growing residual displacements in the moment vs. rotation curve. On the other hand, the behavior of the connection with steel tension bars only (Fig. 7(b)) shows much fatter hysteresis loops, indicating an increase in the energy dissipation capacity and provide improved resistance. The joint equipped with both steel tension bars and SMA tension bars (Fig. 6) takes advantage of both effects; full recentering behavior requires that the lower shelf of the stress-strain for the flag-shaped superelastic SMA provide enough restoring force to yield the steel bars in compression.

Finally, a comparison of connection behavior for two different connection types (a fully welded (FR/FS) connection and one with steel and SMA tension bars) is given in Figure 8. For the static monotonic curves (Fig. 8(a)), the initial slope of the welded connection

is steeper than that of the smart PR-CFT connection. However, the welded connection evidences smaller hardening after yielding under cyclic loads (Fig. 8(b)). The welded connection also shows much more permanent deformation during unloading with cycling.

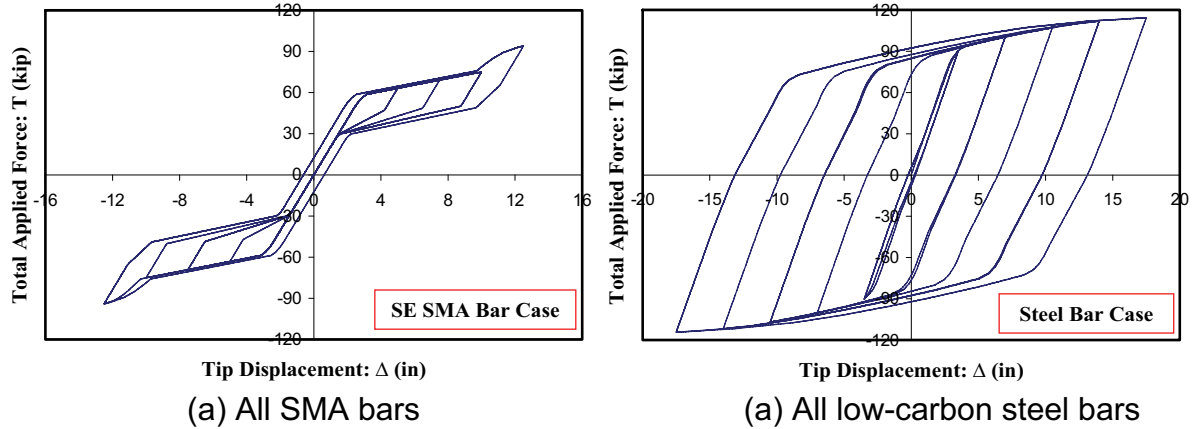


Figure 7. Comparison of connection behavior for all SMA or all steel bars

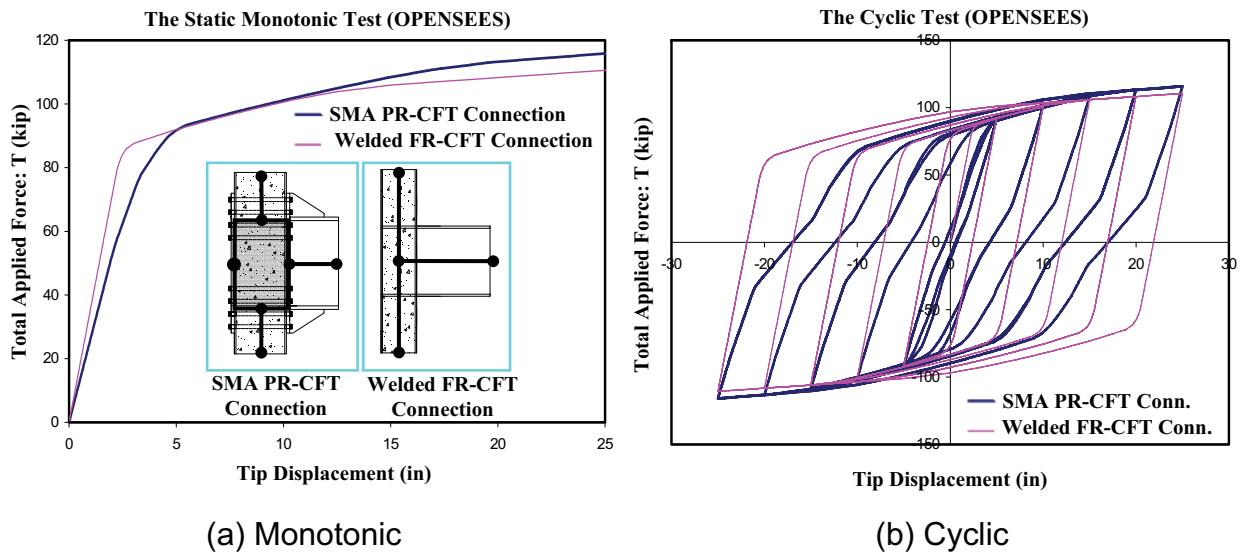


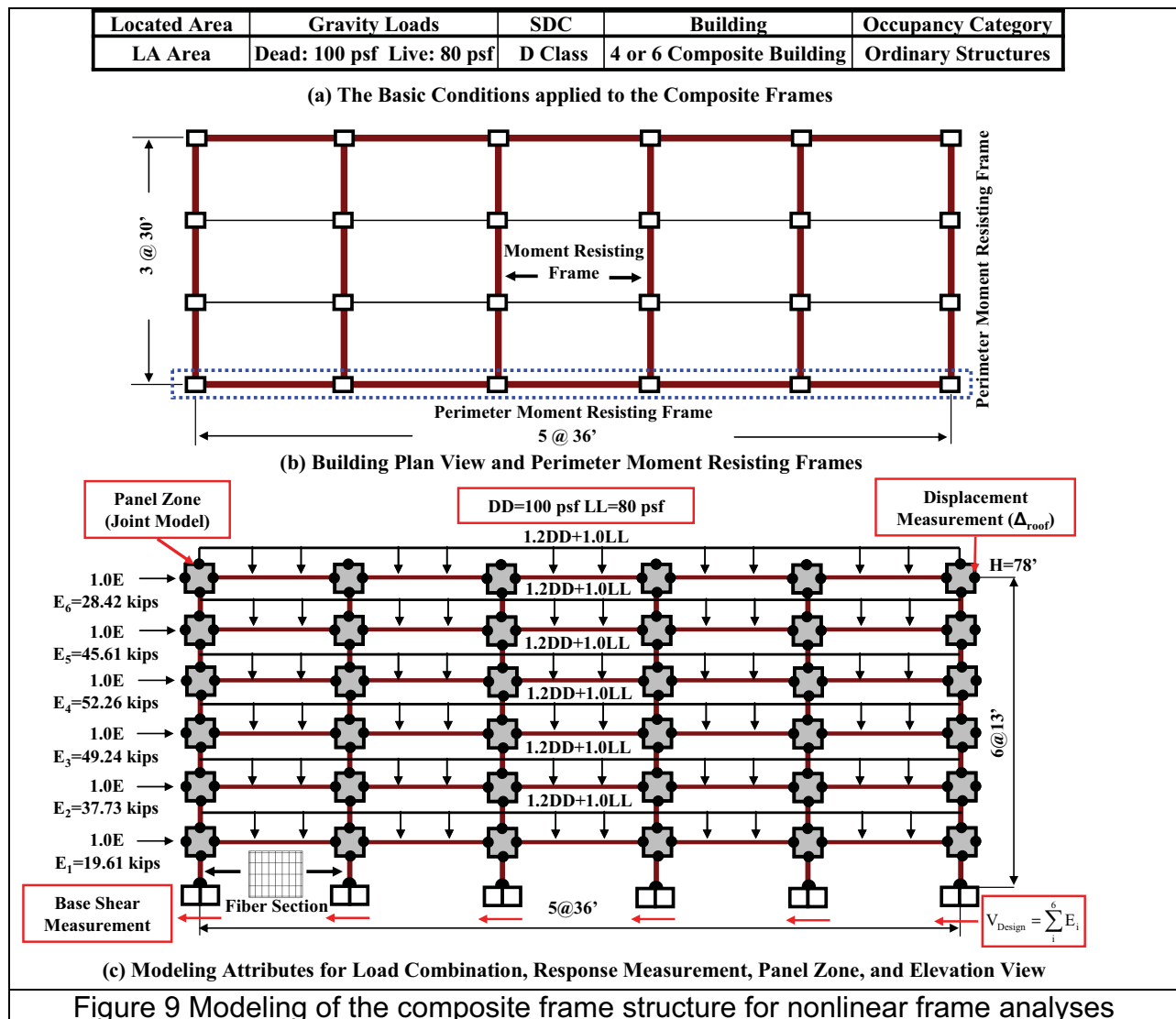
FIGURE 8. Comparison of PR vs. FR connection behavior

NUMERICAL MODELS FOR COMPOSITE MOMENT FRAMES

This section describes the building configuration, the numerical modeling attributes, and nonlinear frame analyses conducted for the composite moment frames. The design dead and live loads for the composite moment frames and the steel FR frames designed for comparison, are assumed as 100 psf and 80 psf, respectively. A seismic design category (SDC) D was assigned to the buildings, based upon the occupancy class and the seismicity of the site (LA and Seattle areas). All composite moment frames were designed in accordance with the ASCE 7-02 (ASCE 2002) and AISC 2005

Seismic Provisions (AISC 2005) for gravity loads and lateral loads, respectively.

The configuration of the 6 story composite building are illustrated in Figure 9 (b) and (c). The total height is 78 ft., with uniform 13 ft. floor heights. This building has 3 bays by 5 bays, with perimeter moment frames in the EW direction and interior moment frames in the NS direction. Except for moment resisting frames, all beams to column connections are assumed as pinned connections. The panel zones were designed in accordance with AISC 2005 for the steel FR frames and by the Wu et al. (Wu, 2007) procedure for the SMA PR-CFT connections. SMA PR-CFT connections were modeled using the joint element corresponding to the connection details shown in Figure 4.



Both monotonic and cyclic pushover analysis using equivalent lateral loads and nonlinear dynamic analysis under a set of 20 ground motions (10 ground motions for the Los Angeles (LA) area and 10 ground motions for the Seattle (SE) area) were performed. For the nonlinear pushover analyses, load factors and combinations

conform to the ASCE 7-02 and LRFD (AISC 2001) specification. Load combination 5 (LC 5: 1.2DD+1.0LL+1.0E) dominated over other load combinations. The resulting monotonic/cyclic pushover curves plotted as the interstory drift ratio (ISDR) at the roof level vs. the normalized base shear (V_{Base}/V_{Design}) are shown in Figure 10. Note that in Figure 8(a), both the FR and FR connections have similar strength but different stiffnesses. Current design specification do not recognize the lengthening of the period due to PR connections and thus the design base shears for both types of frames was similar. The rapid deterioration of the welded frames is attributable to the relatively low ductility assumed for the WUF-B connections in the FR frames. In addition, the degradation is tied to the larger loss of stiffness in the columns in these frames due to yielding and the consequent larger effect of P- Δ moments.

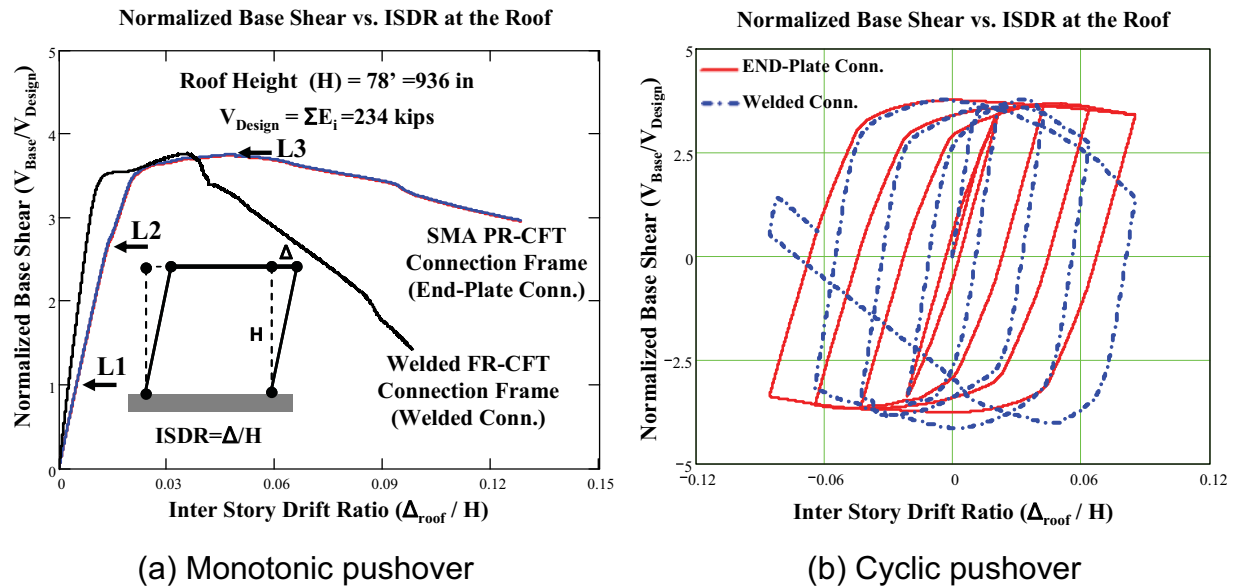


Figure 10. Comparisons of nonlinear pushover analyses (SMA PR vs. Welded FR)

The nonlinear dynamic analyses were performed by using two suites of 20 earthquake ground motions with 2% probability of exceedance in 50 years for the western area (LA21 to LA30 and SE21 to SE30, Somerville et al., 1997). In addition to dead loads and live loads, a combination of masses corresponding to 1.0DD+0.2 LL were applied to generate the inertial force due to the acceleration; 2.5 % Rayleigh damping was used in the first mode. Both geometric and material nonlinearities were considered during all nonlinear analyses. Figure 11 shows a typical result of these analyses, which indicates a significant reduction of the maximum drift for PR frames under a large pulse-type earthquake (LA21), but a similar level of residual deformation; the latter is due to the large amount of yielding at the column bases, which the SMA cannot overcome. More distinct differences in dynamic characteristics after first damage are shown for the LA26 ground motion.

CONCLUSIONS

The smart PR-CFT connections developed in this study are an innovative structural element that takes advantage of the synergistic characteristics of the composite system, flexible PR connections, and use of new materials. The structural advantages and characteristics for these composite moment frame were verified by the nonlinear analyses, which showed that these frames evidenced smaller residual displacements than those with welded connections due to the recentering effect. In addition, composite frames with PR connections showed a gradual strength degradation. Overall, the envelope of the monotonic curves corresponded to that of the cyclic curves when the same models were compared.

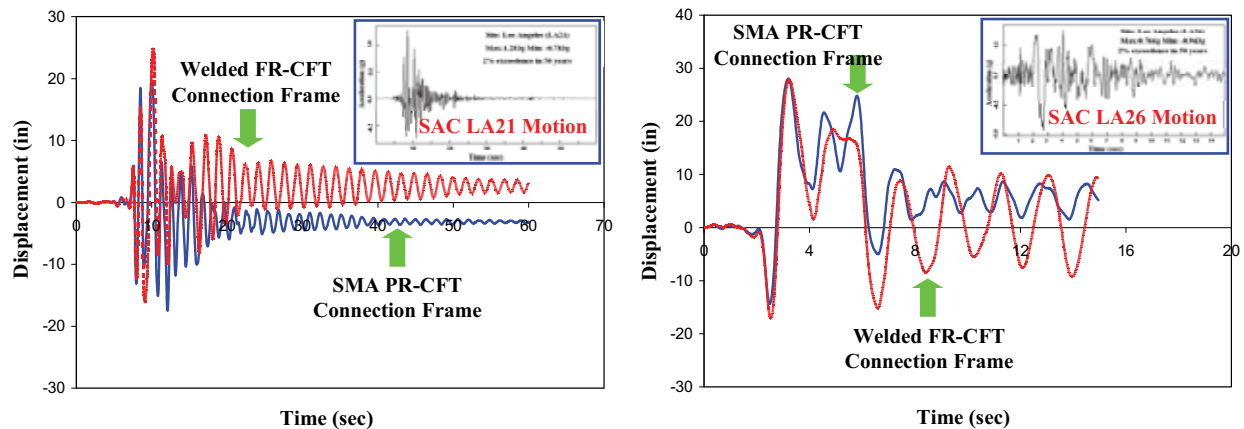


Figure 11 - Comparison of nonlinear dynamic analyses (SMA PR vs. Welded FR)

ACKNOWLEDGEMENTS

This work was supported partially through NSF Grant CMMI-0619047. The opinions and conclusions expressed here are solely those of the authors.

REFERENCES

1. ABAQUS v. 6.6-1, 2006. Hibbit, Karlsson & Sorensen, Inc., Pawtucket, RI.
2. American Institute of Steel Construction (AISC), 2001. Manual of Steel Construction, Load and Resistance Factor Design (LRFD), 3rd Ed., Chicago, IL.
3. American Institute of Steel Construction (AISC), 2005. Seismic Provisions for Structural Steel Buildings (ANSI/AISC 341-05), Chicago, IL.
4. American Society of Civil Engineers (ASCE), 2002. Minimum Design Loads for Buildings and Other Structures, ASCE 7-05
5. Federal Emergency Management Agency (FEMA), 2000. State of the Art Report, FEMA 355C, SAC Joint Venture, Washington, D.C.
6. Mazzoni, S., McKenna, F., and Fenves, G. L., 2006. OPENSEES Command Language Manual, CEE, University of California, Berkeley.
7. Penar, B. W., 2005. Recentering Beam-Column Connections using Shape Memory Alloys, Master's Thesis, The Graduate School, Georgia Institute of Technology.

8. Somerville, P.G., Smith, N., Punyamurthula, S., and Sun, J., 1997. Development of Ground Motion Time Histories for Phase 2 of the FEMA/SAC Steel Project, SAC Background Document, Report No. SAC/BD 97/04.
9. Tsai, K. C., Weng, Y. T., and Ling, M. L., 2004. Pseudo Dynamic Tests of a Full-Scale CFT/BRB Composite Frame, ASCE 2004 Structures Congress, ASCE
10. Wu, L. Y., Chung, L. L., Tsai, S. F., Lu, C. F. and Huang, G. L., 2007. Seismic Behavior of Bidirectional Bolted Connections for CFT Columns and H-Beams, Engineering Structures, v.29, pp. 395-407

CAPACITY OF WELDED JOINTS THAT COMBINE WELDS IN DIFFERENT DIRECTIONS

Logan J. Callele

Waiward Steel Fabricators, Edmonton, AB, T6B 2Y5, Canada
logan.callele@waiward.com

Gilbert Y. Grondin

University of Alberta, Edmonton, AB, T6G 2W2, Canada
ggrondin@ualberta.ca

Robert G. Driver

University of Alberta, Edmonton, AB, T6G 2W2, Canada
rdriver@ualberta.ca

ABSTRACT

Several independent research projects have demonstrated that the strength and ductility of fillet welds are a function of the angle between the weld axis and the line of action of the applied load. It has been demonstrated that transverse welds are about 50% stronger than longitudinal welds, but have considerably lower ductility. This difference in behaviour can have a significant impact on the design of welded connections with multiple weld orientations within the same joint. Tests on welded double lapped joints have recently been conducted to investigate the strength of connections with multiple weld segments of different orientations. The tests indicate that these joints possess capacities significantly lower than the sum of the individual weld segment strengths. The connection capacity depends on the load versus deformation characteristics of the individual weld segments. A general approach for the design of welded joints that combine welds in various directions is recommended.

INTRODUCTION

It has been well established that both the strength and the ductility of fillet welds are a function of the angle, θ , between the weld axis and the loading direction and that transverse welds are about 50% stronger than longitudinal welds of the same size. Research on eccentrically loaded fillet weld connections by Butler *et al.* (1972) and Lesik and Kennedy (1990) has focused on the influence of the loading orientation on the full load versus deformation response of fillet welds. This behaviour is shown in Figure 1 for transverse and longitudinal fillet welds, where Δ is the deformation of the weld and d is the leg size of the fillet. These distinctly different behaviours imply that if both longitudinal and transverse welds are used in a single connection, the longitudinal welds may not be able to develop their full capacity before the ductility of the transverse weld is exhausted. The lower ductility of the transverse weld therefore limits the capacity of

the connection. Referring to Figure 1, in a connection composed of transverse and longitudinal fillet welds, the curves of Butler *et al.* (1972) predict that the longitudinal weld would contribute 94% of its own capacity to the connection capacity, whereas those of Lesik and Kennedy (1990) predict that the longitudinal weld would contribute 80% of its capacity. From research on connections that combine fillet welds and bolts, Manuel and Kulak (2000) suggested that the longitudinal welds reach 85% of their capacity when combined with transverse welds.

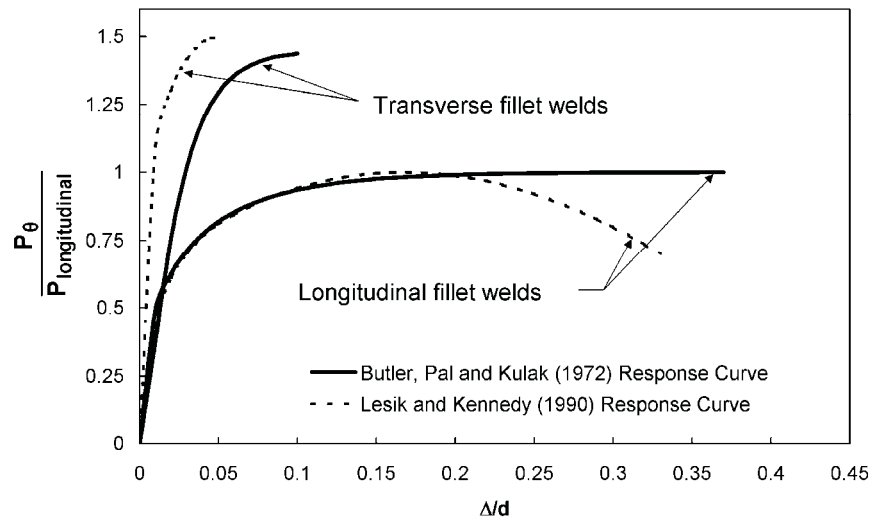


Figure 1. Fillet Weld Load versus Deformation Response from Previous Research

It is common for welded connections to have more than one fillet weld orientation within the same joint, so the distinct differences in response would be expected to be an important consideration for design. Since the research programs by Butler *et al.* (1972), Lesik and Kennedy (1990), and Manuel and Kulak (2000) were all based upon fillet welded connections fabricated using the shielded metal arc welding (SMAW) process, the more common flux cored arc welding (FCAW) process should be investigated in the development of a design procedure for connections with multiple weld orientations. Two recent research projects at the University of Alberta (Ng *et al.*, 2004; Deng *et al.*, 2006) investigated the accuracy of the current fillet weld design provisions in North American design specifications for joints with a single weld orientation and welds made with the FCAW process.

The design provisions in AISC (2005) specifications have adopted the recommendation of Manuel and Kulak (2000) when transverse and longitudinal fillet welds are used in the same joint. The investigation presented below verifies whether this provision is applicable and examines a broader range of weld orientations within the same joint.

EXPERIMENTAL PROGRAM

Eight connections that combine transverse and 45° fillet welds (“TF” specimens) and 11 with transverse and longitudinal fillet welds (“TL” specimens), as shown in Figure 2, were tested. The default nominal weld leg size is 12.7 mm (1/2 in.), deposited in three

passes, and the symbol “a” is used to denote specimens where 7.9 mm (5/16 in.) fillets, in one pass, were used instead. Four TF specimens and four TFa specimens were tested. The TL specimens are also distinguished in their designation by the longitudinal weld length (in mm): four TL50 specimens, four TL50a specimens and three TL100 specimens. Complementary tests were conducted to supplement the information from Deng *et al.* (2006) so that the main specimens could be analyzed. The complementary tests were double lap plate connections with longitudinal fillet welds only (“L” specimens) or transverse fillet welds (“T” specimens). Three each of L100, L150, and T specimens were fabricated for a total of nine extra specimens.

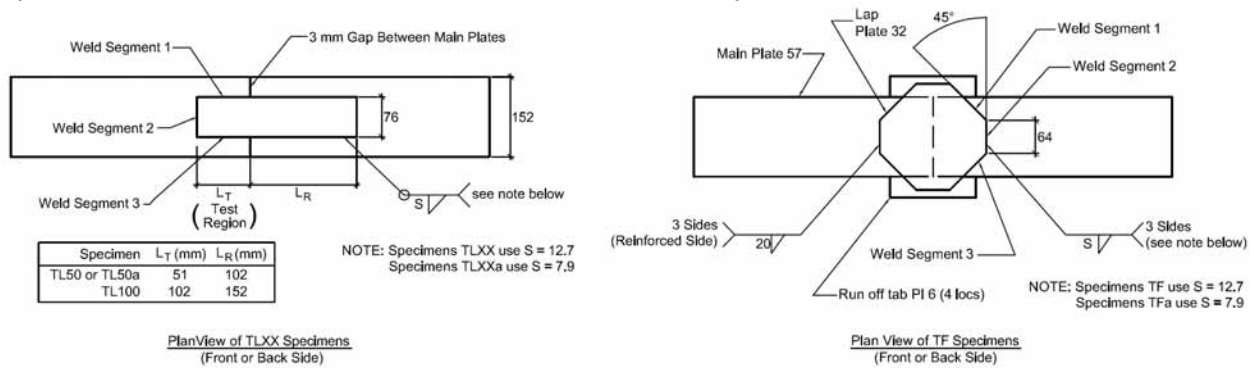


Figure 2. Test Connections that Contain Multiple Fillet Weld Orientations

All 28 specimens were fabricated with AWS E70T-7 wire and with plates that were thick enough to ensure that the plates would remain elastic during testing. Test specimens TL50, TL50a, TF, and TFa were fabricated from one heat of E70T-7 wire, while the remaining specimens were fabricated from a different heat. To establish the ultimate strength of the weld metal, three all-weld-metal tension coupons from each heat were fabricated and tested. The plates used in the fabrication of all specimens met the requirements of ASTM A572 grade 50 and CAN/CSA-G40.21 350W steel.

Prior to testing, all fillet weld main plate legs (MPL) and lap plate legs (LPL) were measured. Figure 3 defines the MPL and LPL and their relationship to the minimum throat dimension (MTD), which neglects both the root penetration and the weld reinforcement as is typically done in design. The throat area of a weld segment is taken as the MTD times the segment length.

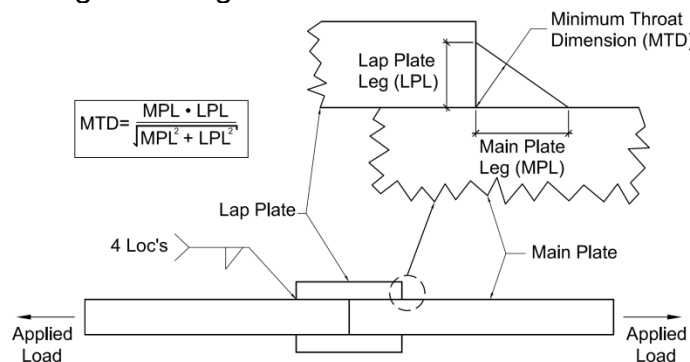


Figure 3. Fillet Weld Dimensional Definitions

The testing of each specimen took place by loading the connection in concentric tension until rupture of one or all of the fillet welds occurred. The tests were carried out quasi-statically in a universal testing machine under displacement control. Linear variable differential transformers (LVDTs) were used to measure the fillet weld deformations in the direction of the applied load. For further information on the test setup and procedures, refer to Callele *et al.* (2005).

The fillet weld deformations measured in the complementary tests were used to establish fillet weld load versus deformation response curves for each weld orientation. These response curves, along with those of Deng *et al.* (2006), are used to predict the capacities of the multi-orientation fillet weld connections.

EXPERIMENTAL RESULTS

The test results for the TL and TF specimens are shown in Table 1. The throat areas are given for each specimen transverse and non-transverse (i.e., longitudinal for the TL specimens and 45° for the TF specimens) weld segments on the side of the joint that failed. For example, if all the welds on the front lap plate of the specimen failed, but none failed on the back lap plate, then the throat area reported is two times the front fillet weld throat area.

Table 1. Test Results and Predicted Capacities

Specimen	Ultimate Load (kN)	Throat Area (mm ²)		Weld Metal UTS (MPa)	Predicted Capacities	
		Transverse Weld Segment	Non-transverse Weld Segment		Summation (kN)	Compatibility (kN)
TF-1	2000	1120	2540	575	2800	2310
TF-2	2510	1230	2320	575	2710	2270
TF-3	2230	1120	2200	575	2540	2120
TF-4	2430	1320	2360	575	2820	2370
TFa-1	1540	800	1560	575	2240	1870
TFa-2	1730	740	1510	575	2130	1770
TFa-3	1840	770	1550	575	2200	1830
TFa-4	1700	860	1520	575	2260	1900
TL50-1	1480	1440	1800	575	1970	1790
TL50-2	1660	1410	1820	575	1950	1780
TL50-3	1570	1460	1740	575	1950	1790
TL50-4	1700	1440	1850	575	1990	1810
TL50a-1	1300	990	1220	575	1670	1520
TL50a-2	1190	1010	1280	575	1720	1570
TL50a-3	1210	1000	1240	575	1690	1540
TL50a-4	1470	1080	1370	575	1850	1680
TL100-1	2360	1600	4010	569	3140	2750
TL100-2	2220	1460	3780	569	2920	2560
TL100-3	1980	1550	3710	569	2950	2600

DISCUSSION

Two methods of analyzing the tested connections are discussed: the strength summation approach and the compatibility approach. Strength summation takes the capacity of the connection as the sum of the capacities of each individual weld segment. This assumes that all of the weld segments have sufficient ductility to allow the segments to reach their individual capacities simultaneously. The compatibility approach accounts for the differences in ductilities of the various weld segments and limits the contribution of the more ductile segments based on the relative ductility between the least ductile segment, which is the segment that has an orientation closest to 90° to the applied load, and the other segments. The test data on connections having a single weld orientation, including the complementary tests of this research and those of Deng *et al.* (2006), are used to assess the expected capacity of each weld segment. The joint capacities predicted using the strength summation approach are presented in Table 1. Figure 4 compares the test and predicted capacities using the strength summation approach and presents the associated mean test-to-predicted ratio and coefficient of variation. It is clear that the strength summation method provides a non-conservative prediction of the strength of these connections.

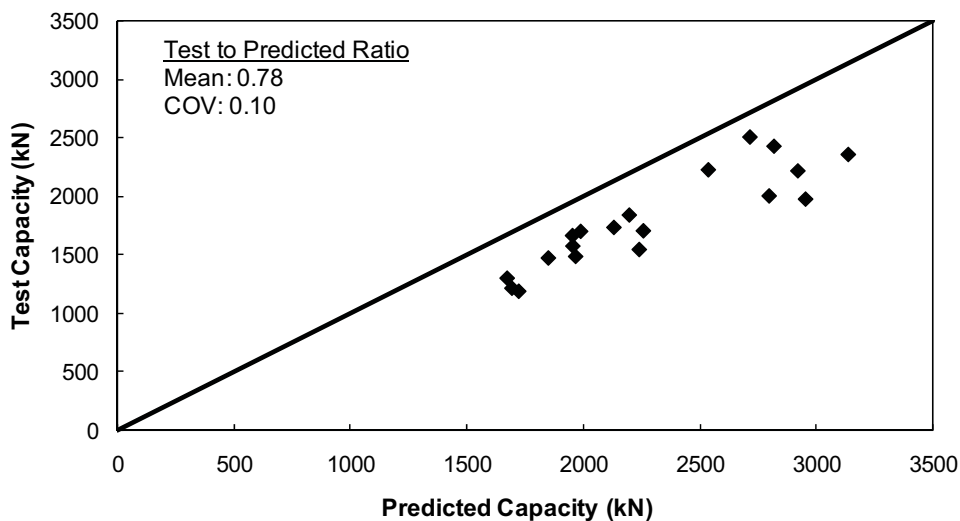


Figure 4. Results of Strength Summation Approach

The compatibility approach accounts for the reduction of ductility as the angle θ increases. Figure 5 shows fillet weld deformations from the complementary tests in this research, as well as tests of Deng *et al.* (2006) and Miazga and Kennedy (1989). The figure reports the deformations in terms of Δ_{ult}/d^* , where Δ_{ult} is the deformation of the fillet weld at its ultimate capacity and d^* is equal to $d(\sin\theta + \cos\theta)$. The weld deformations reported by Miazga and Kennedy (1989) were normalized by dividing by the fillet weld leg size, d , whereas the weld deformations reported by Deng *et al.* (2006) were normalized by dividing by the leg size, d , for orientations 0° and 90° only, whereas the deformations for welds with an orientation of 45° were normalized by dividing by $\sqrt{2}d$ (the weld dimension in the direction of loading). Since the direction of loading is believed to be the more meaningful normalization quantity (except for longitudinal

welds), the use of d^* allows a direct comparison between the test data of Miazga and Kennedy (1989) and Deng *et al.* (2006) and also provides a continuous function for use in further analysis of the test results.

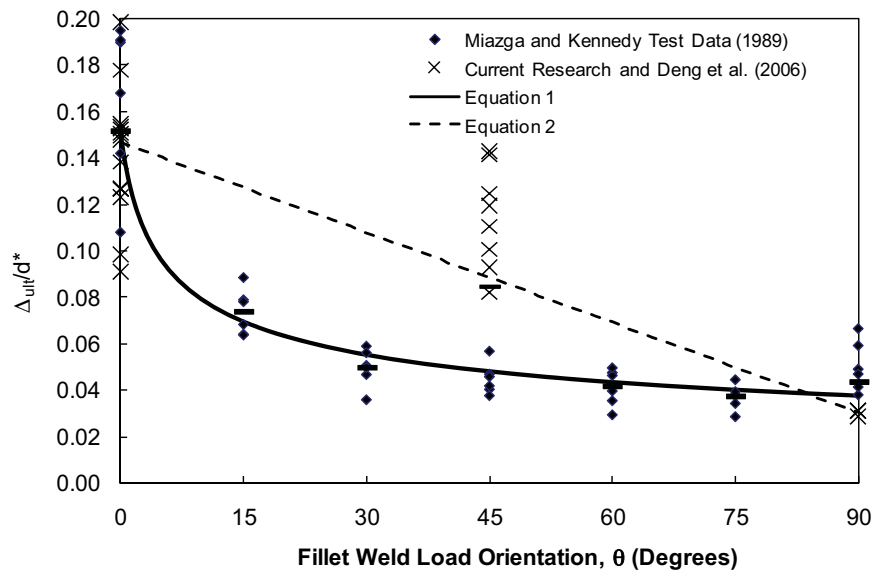


Figure 5. Fillet Weld Ductilities as a Function of Orientation

Figure 5 shows significant scatter in Δ_{ult}/d^* at weld orientations of 0° and 45° . The inconsistency in the two research programs at 45° suggests the need to look at two different predictions on the variation in weld ductility with loading angle. A power relationship provides a good fit to the data of Miazga and Kennedy (1989) as follows:

$$\frac{\Delta_{ult}}{d^*} = 0.20(\theta + 2)^{-0.36} \quad (1)$$

However, a linear relationship may be more appropriate when considering the results of the current research and that of Deng *et al.* (2006):

$$\frac{\Delta_{ult}}{d^*} = 0.146 - 0.0013\theta \quad (2)$$

Load versus deformation curves for fillet welds loaded in any orientation are required for the compatibility approach. A relatively simple relationship between the load as a fraction of the ultimate load and the deflection as a fraction of the ultimate deflection that gives results very close to the more complex relationship developed by Lesik and Kennedy (1990) is:

$$\frac{P_\theta}{P_{U\theta}} = [\rho(2 - \rho)]^{25}, \quad \text{when } \rho > 0.07 \quad (3)$$

$$\frac{P_\theta}{P_{U\theta}} = 8.7\rho, \quad \text{when } \rho \leq 0.07 \quad (4)$$

where,
$$\rho = \frac{\Delta}{\Delta_{ult}} \quad (5)$$

With estimates of both fillet weld ductility (Equations 1 and 2) and the load versus deformation response (Equations 3 and 4), the compatibility approach can now be used to predict the capacities of the TF and TL specimens. The maximum force that each weld segment can develop is calculated in the same manner as in the strength summation approach, except that in the compatibility approach the capacity of the more ductile weld segments is reduced by $P_{\theta}/P_{U\theta}$, with Δ taken as Δ_{ult} of the least ductile weld segment. $P_{\theta}/P_{U\theta}$ is hereafter referred to as the strength reduction factor, M_w , of the segment. The symbol “M” is selected because it applies only to multi-orientation fillet welds. It can be taken as 1.0 for joints with a single weld orientation. The reduced strengths of the more ductile welds are summed with the full strength of the least ductile weld to predict the total connection capacity.

Predicted capacities of the TL and TF specimens using the compatibility approach are shown in Table 1 and a comparison between the test and predicted values is shown in Figure 6. The mean test-to-predicted ratio of 0.90 represents a significant improvement over the strength summation approach, although the capacities still tend to be overestimated. To assess whether or not the compatibility approach is appropriate for design, it is necessary to perform a reliability analysis on the test data with an equation that takes into account the strength reductions.

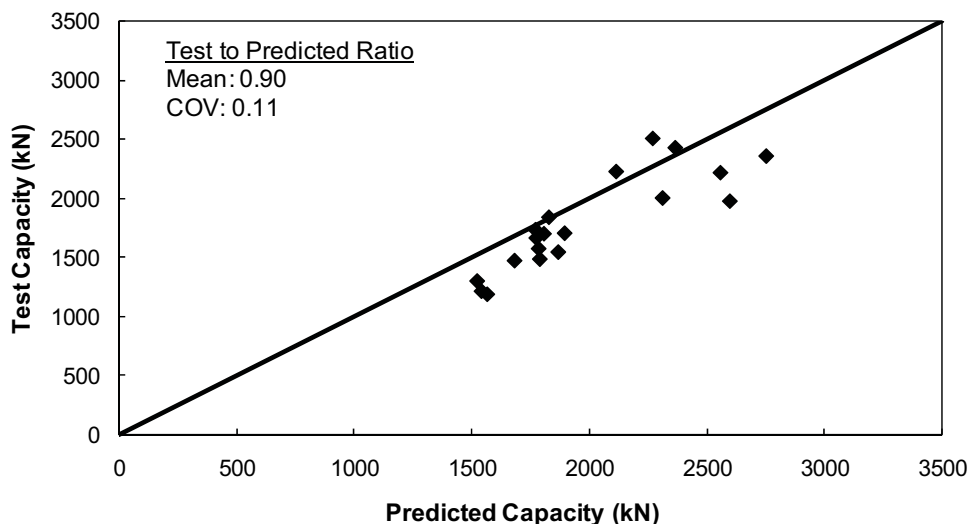


Figure 6. Results of Compatibility Approach

In order to use the compatibility approach in design it is desirable to simplify the procedure for determining M_w for different weld segment orientations. Figure 7 compares the variation of M_w in a connection where a transverse weld is the least ductile orientation, using the response curve of Equations 3 and 4 along with the

predicted weld deformations of either Equation 1 or 2. To simplify the evaluation of M_w , the following equation is proposed:

$$M_w = \frac{0.85 + \theta_1/600}{0.85 + \theta_2/600} \quad (6)$$

where θ_1 and θ_2 are the angles of the weld axis under consideration and the least ductile weld segment, respectively.

In addition to simplifying the design procedure greatly, Equation 6 tends to balance the significantly different curves for M_w obtained from Equations 1 and 2 shown in Figure 7. It is also consistent with the current Equation J2-9b in the AISC LRFD Specification (AISC, 2005) that is specifically for combined transverse and longitudinal welds, but eliminates the need for Equation J2-9a that acknowledges neither the higher strength of transverse welds nor the difference in ductility of welds with different orientations. Although the calculated value of M_w from Equation 6 for a longitudinal weld segment (0.85) is slightly greater than the values from Equations 1 and 2, the equation is shown subsequently to provide an adequate margin of safety for design.

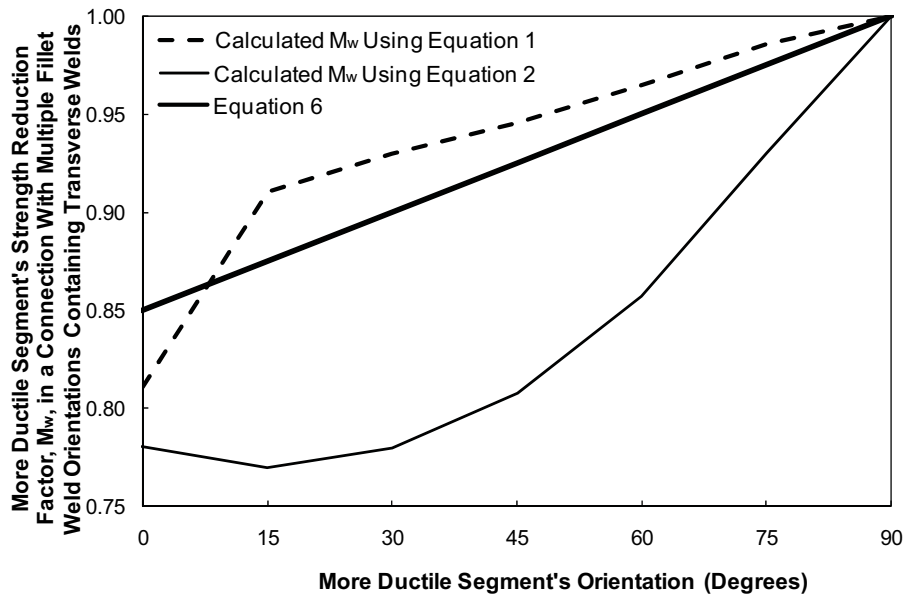


Figure 7. Strength Reduction Factor Variation In Connection with A Transverse Weld

A reliability analysis was performed on the TL and TF specimen test data to determine the reliability index obtained using the proposed design procedure and current resistance factors. The full details of this analysis can be found in Callele *et al.* (2005). For determining predicted values, both the Canadian design standard (CSA, 2001) and the AISC Specification (AISC, 2005) are considered, combined with the strength reduction factor, M_w , defined in Equation 6. The former design equation becomes:

$$V_r = 0.67 \phi_w A_w X_u (1.00 + 0.50 \sin^{1.5} \theta) M_w \quad (7)$$

and the latter:

$$V_r = 0.60 \phi A_w F_{EXX} (1.00 + 0.50 \sin^{1.5} \theta) M_w \quad (8)$$

Because the product $0.67 \phi_w$, where $\phi_w = 0.67$, in Equation 7 is equal to the product 0.60ϕ , where $\phi = 0.75$, in Equation 8, predicted connection capacities—and therefore the resulting reliability index—are identical for the two equations. The summation and compatibility methods result in reliability indices of 4.1 and 4.5, respectively. Considering the tendency of welded connections to fail in a rather brittle mode, a value of 4.5 is considered more suitable as a target, and the compatibility method, which reflects the well-accepted differences in ductility in welds with different orientations, is considered appropriate for design. Equations 7 and 8 provide a simple and general way of accounting for this difference of ductility in any concentrically loaded welded joint having more than one weld orientation. Although tests of joints where the least ductile weld is not transverse to the load direction were unavailable, an extension to these cases in order to generalize the procedure is reasonable since the concept of compatibility is consistently applied.

CONCLUSIONS AND RECOMMENDATIONS

By comparing test-to-predicted ratios and reliability indices, the compatibility approach for the prediction of the capacity of joints with fillet welds oriented at different angles to the applied load has been shown to be superior to predictions based on simple strength summation. The approach has been verified by comparison with the results of 19 tests on welded joints combining weld segments in different orientations. Equation 6, combined with either Equation 7 or 8, is recommended as a simple procedure suitable for design that accounts for fillet welds oriented at different angles within the same joint. These design equations allow the evaluation of the capacity of any multi-orientation fillet welded connection that is concentrically loaded.

ACKNOWLEDGEMENTS

This study was funded by the American Institute of Steel Construction and the Natural Sciences and Engineering Research Council of Canada.

REFERENCES

- AISC. (2005), "Specification for Structural Steel Buildings," ANSI/AISC 360-05, American Institute of Steel Construction, Chicago, IL.
- Butler, L.J., Pal, S., and Kulak, G.L. (1972), "Eccentrically Loaded Welded Connections," *Journal of the Structural Division*, ASCE, Vol. 98, No. ST5, May, pp. 989-1005.

Callele, L.J., Grondin, G.Y., and Driver, R.G. (2005), "Strength and Behaviour of Multi-orientation Fillet Weld Connections," Structural Engineering Report 255, Dept. of Civil and Environmental Engineering, University of Alberta, Edmonton, AB.

CSA. (2001), "Limit States Design of Steel Structures," CSA S16-01, Canadian Standards Association, Toronto, ON.

Deng, K., Grondin, G.Y., and Driver, R.G. (2006), "Effect of Loading Angle on the Behavior of Fillet Welds," *Engineering Journal*, AISC, Vol. 43, No. 1, pp. 9-23.

Lesik, D.F. and Kennedy, D.J.L. (1990), "Ultimate Strength of Fillet Welded Connections Loaded in Plane," *Canadian Journal of Civil Engineering*, Vol. 17, No. 1, pp. 55-67.

Manuel, T.J. and Kulak, G.L. (2000), "Strength of Joints that Combine Bolts and Welds," *Journal of Structural Engineering*, ASCE, Vol. 126, No. 3, March, pp. 279-287.

Miazga, G.S. and Kennedy, D.J.L. (1989), "Behaviour of Fillet Welds as a Function of the Angle of Loading," *Canadian Journal of Civil Engineering*, Vol. 16, No. 4, pp. 583-599.

Ng, A.K.F., Deng, K., Grondin, G.Y., and Driver, R.G. (2004), "Behavior of Transverse Fillet Welds: Experimental Program," *Engineering Journal*, AISC, Vol. 41, No. 2, pp. 39-54.

INCORPORATION OF FULL SCALE TESTING AND NONLINEAR CONNECTION ANALYSES INTO THE SEISMIC UPGRADE OF A 15-STORY STEEL MOMENT FRAME BUILDING

James O. Malley, Mark Sinclair and Tim Graf
Degenkolb Engineers, San Francisco, CA, USA
malley@degenkolb.com

Colin Blaney and Moisey Fraynt
Crosby Group, Redwood City, CA, USA
colin@crosbygroup.com

Chia-Ming Uang and James Newell
University of California, San Diego, La Jolla, CA, USA
cuang@ucsd.edu

Tamer Ahmed
State of California Dept. of General Services, West Sacramento, CA, USA
tamer.ahmed@dgs.ca.gov

ABSTRACT

This paper summarizes the seismic analysis and rehabilitation design of a 15-story steel moment resisting frame building constructed with connection details that were found to be vulnerable to fracture in the 1994 Northridge earthquake. This building is located in Oakland, California, less than five miles from the Hayward Fault. Previous testing of the existing moment connections demonstrated that the beam flange to column flange complete joint penetration groove welds were vulnerable to fracture, and consequently the building presented a risk to life safety in the event of a major earthquake. Seismic rehabilitation to meet the requirements of the State of California, Department of General Services resulted in a retrofit scheme including a combination of moment connection strengthening and addition of viscous dampers. Due to the deep W27 column and very large W36 beam sections present in the special moment resisting frames (SMRF), a series of four full-scale tests were conducted in order to evaluate the performance of the proposed rehabilitation schemes. Sophisticated analysis techniques were performed in the rehabilitation design, including nonlinear time history analyses. These models included a nonlinear fiber element that approximated the fracture behavior observed in the existing connection tests and incorporated results from the test program to model the strengthened connection behavior.

INTRODUCTION

Building Description

The Caltrans District 4 Office Building, located in the downtown section of Oakland, California, is a 15-story steel moment frame structure designed to meet the 1988 Uniform Building Code (ICBO, 1988) and constructed in 1991. The building has one basement level, a first story lobby/public space level, four levels of above grade parking, and ten stories of office space. The building is rectangular in plan with a large atrium above the parking levels. Full-height moment frames are located along the perimeter frame lines as well as two interior transverse moment frames adjacent to the atrium on either side. See Figure 1 for a typical floor plan.

Performance of Existing Moment Connections

The design of the building's original SMRF utilized typical pre-Northridge moment connections as indicated in Figure 2.

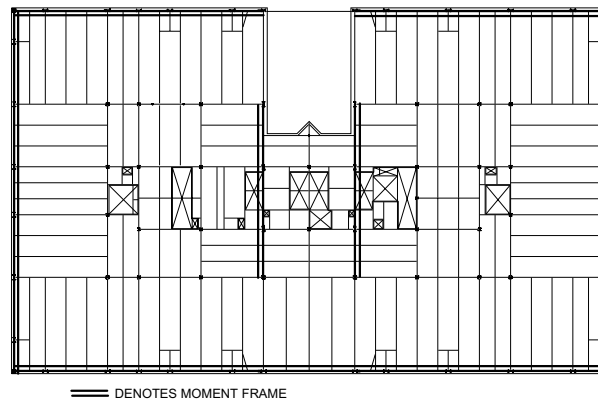


Figure 1. Typical floor plan.

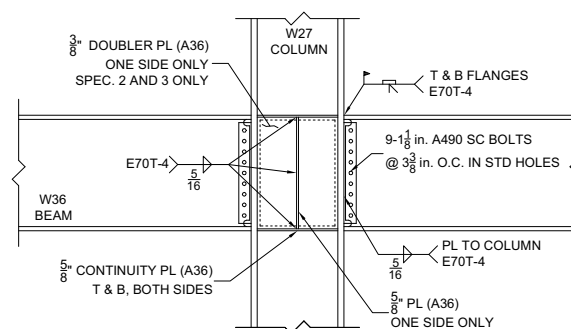


Figure 2. Pre-Northridge moment connection.

Recognizing the potential vulnerability of the existing SMRF system, the State of California commissioned laboratory testing on a few moment connections similar to that of the existing building. These tests were performed by the University of California,

Berkeley at the Pacific Earthquake Engineering Research Center (Kim, et al., 2003). Results of the testing program indicated very poor connection behavior for all specimens. Connection performance was far less than that predicted by adaptation of FEMA 351 (FEMA, 2000a). The hysteretic behavior for one single-sided test specimen with a W27×281 column and W36×210 beam is shown in Figure 3 and demonstrates the potential vulnerability of the existing connections. Initial fracture at the beam top flange occurred at approximately 0.58% drift and the maximum applied load was equivalent to 48% of the beam plastic moment capacity, M_p .

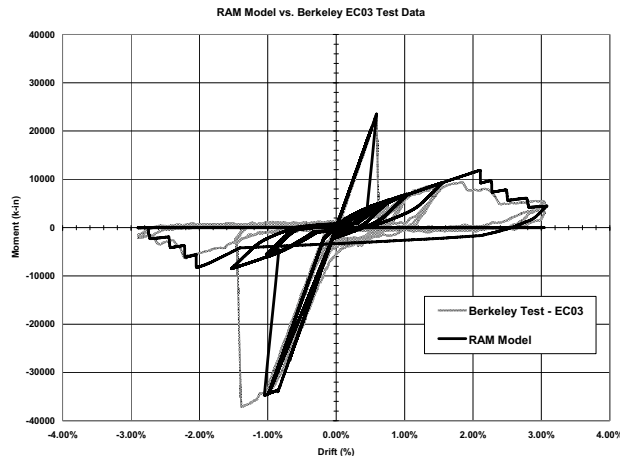


Figure 3. Existing connection fiber model compared to test results.

Performance Criteria

In accordance with the state guidelines (Guidelines, 1994, Rev. April, 2001), the building needed to be seismically upgraded to meet Risk Level III. The description for levels III is as follows: Minor, repairable structural damage with moderate non-structural damage. Minor risk to life-safety with return to occupancy within weeks and building system interruptions for days to months.

The project design criteria were written to incorporate the recommendations of both FEMA 351 and FEMA 356 (FEMA, 2000b) in order to meet the state guidelines. The state guidelines were interpreted to result in the following expected performance:

- A significant number of existing connection fractures may occur for DBE design earthquake; however, local collapse of framing is not expected.
- Repair of the lateral system (e.g. existing moment frame connections) may be required to restore the building to Risk Level III.
- After the DBE, a complete lateral system will still exist that should have sufficient capacity to permit occupancy of the building within weeks, while detailed inspection and any required repair of the lateral system is performed, or continues.
- FEMA 351 was used as the basis for design to establish Risk Level III drift limits. Structural life safety drift limits were established using 75% of the collapse prevention limits in FEMA 351. Appendix A was used to determine the expected

variability of the drift response for the MCE and to calculate a project specific Demand Variability Factor.

- FEMA 356 life safety limits were used to establish column plastic hinge deformation limits.

Seismic Ground Motion Design Criteria

Site-specific response spectra were developed for this site to represent the Design Base Earthquake (DBE, BSE-1) and the Maximum Considered Earthquake (MCE, BSE-2), in accordance with FEMA 356. These spectra were based upon deterministic considerations of both the San Andreas and Hayward faults and represent anticipated earthquakes of Richter magnitude 7.0 and 7.25. The site-specific response spectra are shown in Figure 4. Seven pairs of time-histories for use in the nonlinear response history analysis were also developed and scaled in accordance with FEMA 351 requirements. Directivity effects were not considered since the building is oriented approximately 45 degrees to the Hayward fault.

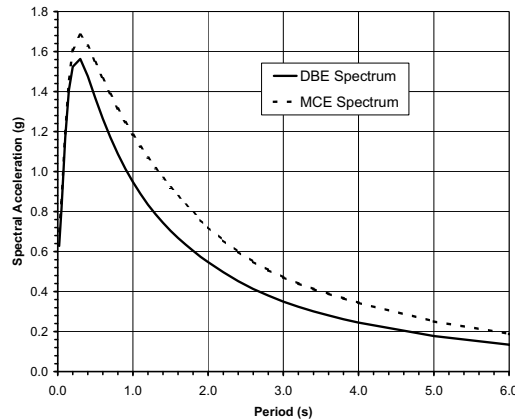


Figure 4. Project design response spectra.

Selected Retrofit Scheme

The retrofit scheme was designed in two phases, a study phase and a working drawings phase. Four strengthening schemes were developed during the study phase of the project – an all-connection-strengthening scheme, a connection-strengthening-plus-dampers scheme, a buckling restrained brace scheme, and a base isolation scheme. Each scheme was designed to meet the design criteria and the schemes were compared on the basis of construction cost and associated “soft” costs such as construction phasing, long-term and short-term staff relocation and other facility down time. Items also considered long-term architectural impacts to the building as well as projected cost for repair after a significant seismic event.

The retrofit scheme chosen by the owner was the connection-strengthening-plus-dampers scheme. The transverse frames are shown in Figure 5, the configuration is similar in the longitudinal direction. The particulars of the scheme are as follows:

- Connection upgrades and dampers have been placed at the same locations to minimize number of work locations.
- Maximum practical damper sizes have been used to reduce number of work locations.
- The damper layout avoids interference with major points of entry and interior building flow.
- Of 1218 existing moment-resisting connections in building, 746 connections will be strengthened (61% of connections) with several types of connection strengthening including welded double haunches, welded bottom haunches with top reinforcement, double gusset plates, gusset plate and haunch, and others.
- Column splices will be strengthened in locations where connection strengthening occurs.
- 228 dampers will be added at perimeter locations only, 56 – 670k Dampers ($C = 240 \text{ k (sec/in)}^{0.4}$, $\delta = 0.4$), 148 – 450k Dampers ($C = 160 \text{ k (sec/in)}^{0.4}$, $\delta = 0.4$), and 24 – 225k Dampers ($C = 80 \text{ k (sec/in)}^{0.4}$, $\delta = 0.4$).
-

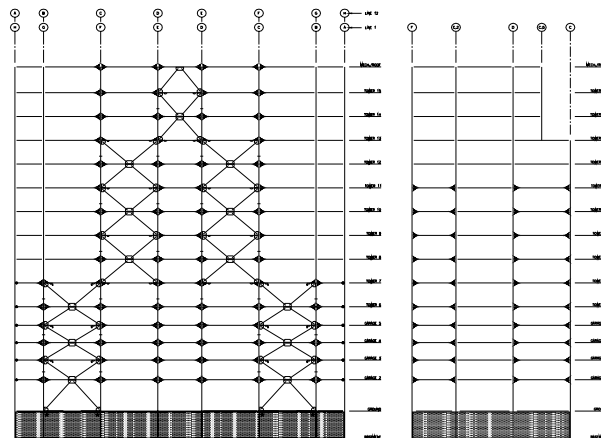


Figure 5. Transverse strengthening scheme showing exterior and interior frames.

ANALYSIS TECHNIQUES

Two types of analysis were used on the project. A simplified analysis was performed during the initial study phase of the project based on the Equivalent Linearization Procedure (FEMA 440, 2004), and full nonlinear dynamic time-history analysis (NLDTHA) was performed during the working drawings phase.

In the working drawings phase of the project two Perform models were constructed, one two-dimensional model for each primary direction of motion. In each model the moment frames were modeled completely and the gravity columns and (Guidelines, 1994, Rev. April, 2001) orthogonal moment frame columns were modeled for secondary effects. Rigid diaphragms were assumed.

The moment frames were built with compound elements comprised of both elastic and inelastic components. Beam elements were built from an elastic beam section and a

nonlinear moment-rotation hinge for strengthened connections or a nonlinear fiber section for the existing connections. The fiber section used to model the existing connection was a user-defined cross-section in which axial only fibers, with a chosen area and nonlinear material property, were assigned locations along a vertical axis. The cross section acted nonlinearly in tension, compression, and bending but was considered to remain elastic in shear. The existing connection fiber model was comprised of three different types of fibers: one fiber representing the top flange, one fiber representing the bottom flange, and one fiber for each of the bolts in the shear tab shown in Figure 6. Using the fiber section allowed the existing connection model to closely mimic tested behavior. The key aspects of using the fiber section to model the existing connection were that the fiber model captures:

- The top and bottom flanges fracturing at different moments, both which are significantly below the expected moment strength of the beam.
- The post-flange-fracture effect where the bending capacity of the connection relies on the couple between the shear tab bolts in shear and the fractured flange in bearing, and the individual fracture of each shear tab bolt at the expected bolt ultimate strength.

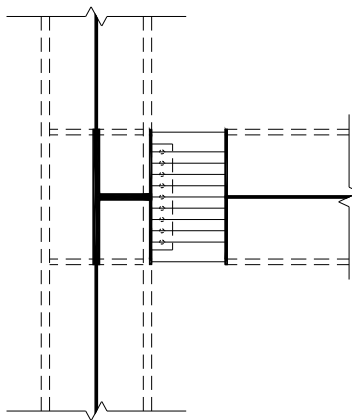


Figure 6. Graphical representation of beam connection fiber model.

Other modeling aspects include:

- Column elements were built from an elastic column element and a nonlinear axial moment interaction (PMM) hinge. Column splices were included in the model as nodes and forces were monitored at these locations.
- The basement walls were assumed to remain elastic, so they were modeled using elastic shear wall elements.
- The base of the model consisted of nonlinear compression-only soil springs created from nonlinear deflection curves provided by the geotechnical engineer.
- The dampers were modeled using an elastic bar and a nonlinear damper element that modeled the backbone of the viscous damper using five linear segments.

Two-dimensional frame analyses were used for both phases of the analysis since the building has been found to be torsionally very regular and due to model run-time constraints. Torsion was accounted for in the design of the retrofit scheme by

increasing drifts computed from the two-dimensional analyses by a factor determined from a nonlinear modal time history analysis of the full 3D SAP model including the dampers.

Connection Model Validation

To validate the existing fiber connection model, the existing connection test specimen was modeled using the fiber section and subjected to the same loading protocol, as shown in Figure 7 (Kim, et al., 2003). The correlation between the model and the test specimen is shown in Figure 3. The composite steel deck and concrete slab was not included in the existing test specimen or in the fiber model. The potential contribution to the connection flexural strength is relatively small due to the large beam size, and so the effect was not expected to substantially change the analysis results.

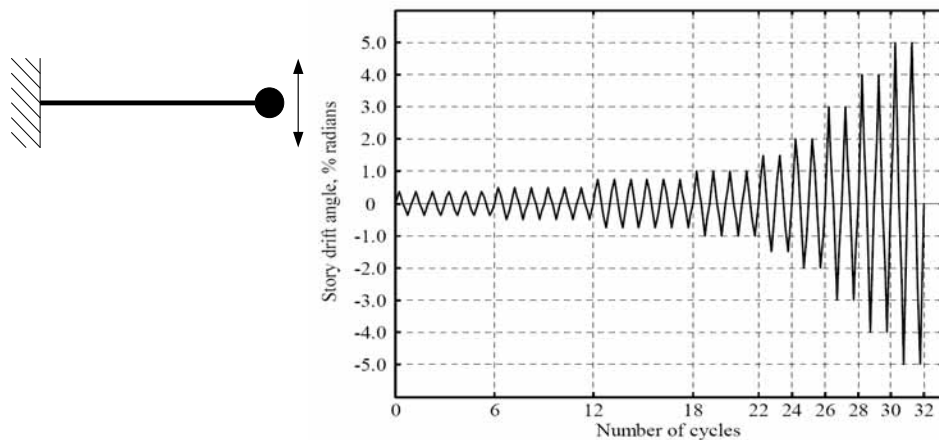


Figure 7. Model and displacement protocol used to test fiber connection.

The fiber model revealed that a second type of slab interaction occurred within the steel frame. Post-fracture lengthening of the bay occurred due to the diagonal length between beam flanges. This mechanism, which is shown in Figure 8, could result in overall frame lengthening of several inches over the dimension of the building at large drift ratios. This behavior was not observed in subassembly connection tests as the beam end is unrestrained, and so no additional lateral resistance was generated. In the initial version of the PERFORM model, very large axial loads were generated in the beam due to the slab, which was modeled as a rigid diaphragm. The effect was removed from the PERFORM model by releasing the axial load in the beams since there was no test data available to validate the strength and stiffness characteristics of this mechanism. This slab-beam coupling mechanism would not have generated sufficient resistance to substantially alter the evaluation of the building or the scope of the subsequent strengthening scheme; however, it might improve the outcome in other more marginal cases. Further research is required to more clearly understand this behavior.

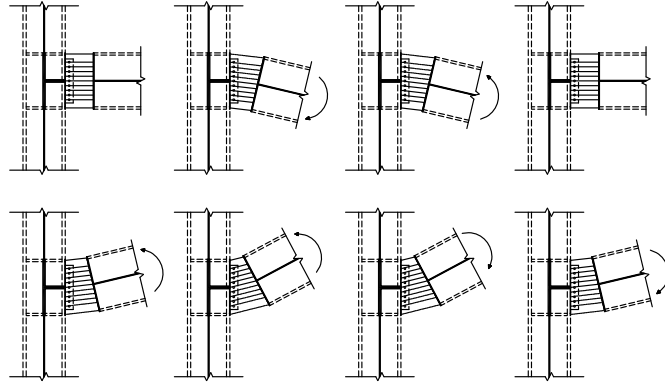


Figure 8. Ratcheting effect observed in existing connection test model.

ANALYSIS RESULTS

The drift performance of the building is shown in Figure 9. Results for three conditions are shown, (1) the existing structure with fracturing connections, (2) the structure with all connections fixed – representing either an all-connection strengthening scheme or the performance where fracture of the connections does not occur, and (3) the structure with the selected retrofit scheme consisting of dampers and 60% connection strengthening. In the NLDTHA of the building in the existing condition, connection fractures were observed to propagate from the bottom of the building upward, resulting in high drift demands in the lower portion of the building compared to the upper portion (Figure 9). Beams with existing connections in the upper portion of the building retained a significant portion of their original stiffness by reverting to a “pin-fixed” condition with the top flanges remaining intact and both bottom flanges fracturing within one beam span.

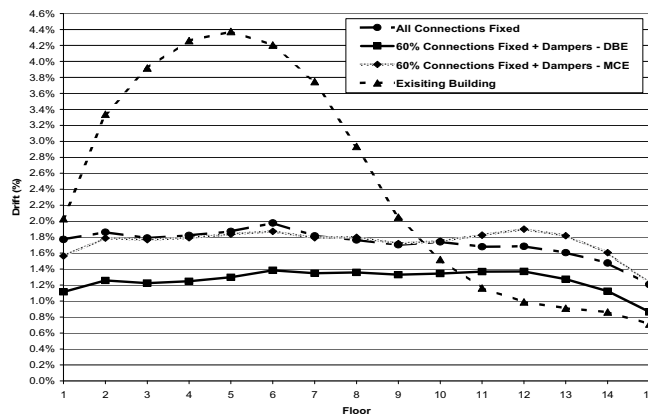


Figure 9. Average drift results for all existing connections, all connections fixed, and 60% connections fixed plus dampers (DBE/MCE).

CONNECTION STRENGTHENING

In addition to the sophisticated analysis techniques used for building performance, the testing program and the procedure to design the connections was also necessary to validate the strengthening connections. FEMA 351 and AISC/NIST Design Guide 12 (AISC, 1999) present several pre-qualified connection upgrades for SMRFs including Welded Bottom Haunch (WBH), Welded Top and Bottom Haunch (WTBH), Welded Cover Plate Flange (WCPF) and a few proprietary connections such as the Bolted Bracket (BB), Slotted Web Connection (SW), and the SidePlate Connection (SP). The pre-qualified connections are limited to W12 and W14 column sections and W36×150 and smaller beam sections. Deep column sections and large beam sizes were beyond the scope of previous testing and as such, connection strengthening schemes involving deep columns and very large beam sections must be experimentally tested for validation of the proposed rehabilitation scheme. Four full-scale, double-sided steel moment connection tests were commissioned so that the proposed strengthening scheme could be properly validated. Specimens included a representative width of composite steel deck and concrete slab. The schemes included a single welded haunch (WBH), a double welded haunch (WTBH), a double haunch on one side of the column and a double gusset plate on the other, and a Bolted Bracket (BB). The BB was considered because its installation could be performed without welding. This would shorten the construction schedule and reduce welding fume containment issues.

A detailed description of the test specimens and laboratory findings can be found in Blaney, et al., 2006 and Newell and Uang, 2006.

CONCLUSIONS

The Caltrans District 4 Office Building is a steel moment resisting frame building with connections similar to those that fractured in the 1994 Northridge, California earthquake. After studying various schemes, a combination of moment connection retrofits and the addition of viscous dampers was chosen to meet the performance goals established by the State of California. The early weld fracture observed in the existing connection test specimens (Kim, et al., 2003) has typically not been observed in other moment frame connection tests. The reasons for this behavior have not been fully understood but may be related to the deep column and heavy beam sections. The drift performance of the Caltrans building with existing connections modeled clearly shows that this condition presents a significant risk to life safety for the building occupants. Nonlinear time history analyses were successfully completed using to verify the performance of the existing and retrofitted structure. Existing connection fracturing behavior was successfully captured using a fiber model. The extra steps taken beyond typical engineering practices were intended to provide better assurance that the project's performance goals would be met during the design basis seismic event. Test results for the deep column sections and large beam performed well utilizing the WTBH retrofitted

connections. This included a column with a relatively weak panel zone in relation to the adjacent beams.

ACKNOWLEDGMENTS

Funding for this project was provided by the State of California, Department of General Services. The opinions presented in this paper are those of the authors, and do not necessarily reflect those of the State of California or the Department of General Services.

REFERENCES

AISC/NIST, 1999, "Steel Design Guide Series 12, Modification of Existing Welded Steel Moment Frame Connections for Seismic Resistance", Chicago, IL.

Blaney C. P., Fraynt M., Uang C. M., Newell J. D., and Ahmed T. A., "Experimental and Analytical Evaluation of Project-Specific Rehabilitated Steel Moment Connections for a 15-Story Building", Proceedings 100th Anniversary Earthquake Conference Commemorating the 1906 San Francisco Earthquake, 2006

Federal Emergency Management Agency, 2000a, "Recommended Seismic Evaluation and Upgrade Criteria for Existing Welded Steel Moment-Frame Buildings", FEMA 351. Washington, D.C.

ICBO, 1988, "Uniform Building Code", International Conference of Building Officials, Whittier, CA.

Kim, T., Stojadinovic, B., and Whittaker, A., 2003, "Physical and Numerical Performance Evaluation of Steel Moment Resisting Frames, Part 1: Existing Building Connection Studies", Pacific Earthquake Engineering Research Center, University of California, Berkeley, CA.

Newell, J., and Uang, C.M., 2006, "Cyclic Testing of Steel Moment Connections for the Caltrans District 4 Office Building Seismic Upgrade, Report No. SSRP-05/03", Department of Structural Engineering, University of California, San Diego, La Jolla, CA.

State of California, Real Estate Services Division, "Guidelines for the Seismic Retrofit of State Buildings", 1994, Rev. April 2001.

Yu, Q.S., Uang, C.M., and Gross J., 2000, "Seismic Rehabilitation Design of Steel Moment Connection with Welded Haunch", Journal of Structural Engineering, January 2000, pp 69-78.

STRENGTH REDUCTION FACTORS FOR STORAGE RACKS

Carlos Aguirre A.
Federico Santa Maria University, Valparaíso, Chile
carlos.aguirre@usm.cl

ABSTRACT

Present Seismic Codes include Strength Reduction Factors and Displacement Amplification Factors. In this paper, they were obtained from non linear analysis of some typical rack structures subjected to selected earthquake records. The moment rotation relationship for a typical connection was obtained in a previous experimental research work performed at Federico Santa Maria University Laboratory.

The results show that drift displacements became much larger than the limits prescribed in codes, it follows the design is normally controlled by displacements. The Strength Reduction Factor obtained from the analyses are smaller than the factor prescribed in the Chilean and in UBC Earthquake Code, which means that the design under those codes factors, could become unsafe in some cases.

BACKGROUND

Storage racks are extremely flexible structures, especially under the action of lateral loads. The behaviour in seismic zones is strongly dependent on the properties of the connections; they determine the behaviour of the structure and the performance of the structural system in the event of a destructive earthquake occurrence.

Rack structures in seismic zones are requested to comply with the local building codes, so they must be engineered to meet the code requirements of the building structures. Even though rack structures are quite different to buildings they use to be placed inside a building, so it is necessary to control the lateral deflections in order to avoid the hammering with the surrounding structure, and eventually the collapse of both structures. The storage rack structure studied in this paper has been used successfully in Chile for several years and they have survived the March 3, 1985 Chilean earthquake. The beam is connected to the column by using hooks that are fabricated with the beam; these hooks are inserted into columns slots, so they can be easily disconnected from the column. Details and connecting elements are shown in Fig. 1, the thickness of the elements is usually 2 mm. In Figure 1a, there is a detail of the beam to column connection and in figure 1b is shown the curve of the joint subjected to a cyclic load, obtained in a previous research work at Santa Maria Laboratory (Irisarri, 1998) and a characteristic curve to be used in non linear analysis of the rack structures. The details of these findings were presented in a previous paper during the Connections-V Workshop held in Amsterdam on 2004.

Most of the seismic codes define the earthquake loads in terms of reduced spectra. The

reduction factor depends on the structural ductility and over strength properties of the structure. Figure 2 shows the different kinds of behaviour, the actual one is the real response of the structure (it is also shown an equivalent idealized bilinear model) and the typical linear analysis performed at engineering offices.

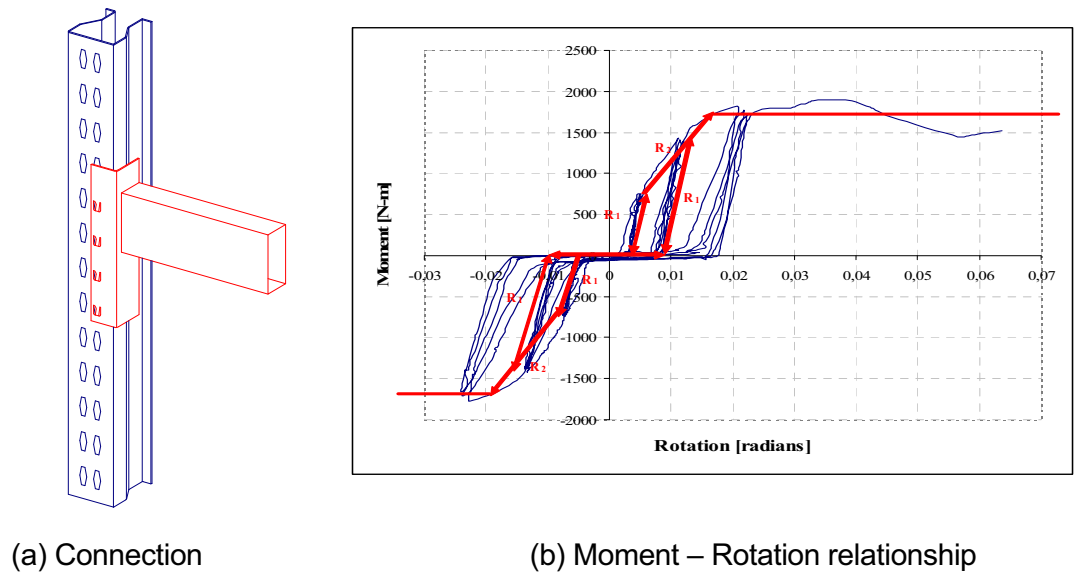


Figure 1 – Test conducted at Santa Maria University

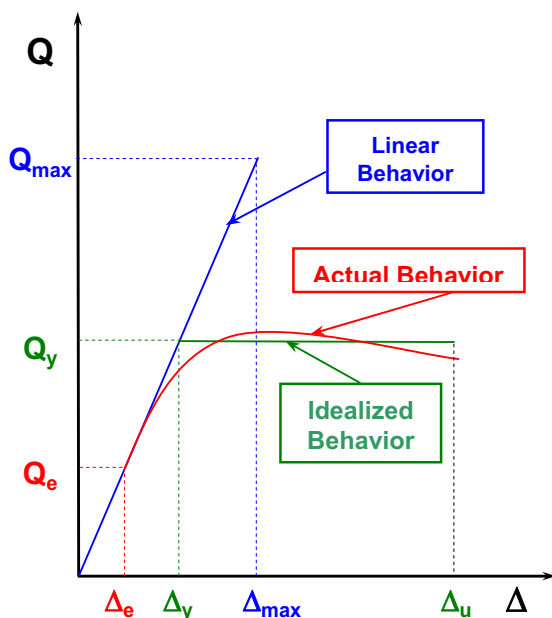


Figure 2 - Behavior of the Structure

Manufacturers Institute (2005), is 10 m for Racks constructed on public places. There were conducted some preliminary elastic analyses, assuming standard support conditions, that means the base of the columns were modelled as simple supports, simple supports plus beams 20 cm above the ground and fixed supports. The standard weight of the pallets is 1000 Kgf, so it is possible to have 2000 Kgf in each

Even though this approach simplifies the analysis, it does not allow to estimate the actual behavior of the structure. For these reason, the codes used to define two factors, the Strength Reduction Factor (R Factor) and the Displacements Amplification Factor (C_d Factor, is the name given at NEHRP, 2001).

PRELIMINARY ANALYSES

It was selected a typical storage rack and two heights: three and six storage levels, that means 4.5 m and 9 m respectively. The height limit establish for the Rack

level. A summary of the periods obtained from those analyses is presented on Table 1. It can be seen that storage racks are extremely flexible structures, with periods about 1 to 3 seconds and larger in higher racks, which means there is a need to have a special care to avoid hammering with the surrounding structure.

Table 1 – Period of Storage Racks

Structure	Period (seconds)
Three levels frame	0.94 – 1.18 – 1.50
Six levels Frame	2.07 – 2.34 – 2.74

PROCEDURE

There were conducted some elastic and non linear analyses on each structure under the same seismic load. In a first step the earthquake demand was determined, dynamic non linear analyses of the structures were conducted, under some selected ground motion records occurred during the last 25 years, the characteristics of the records are shown on Table 2.

Table 2 - Characteristics of the records

Earthquake	Year	Component	Richter Magnitude	Mercalli Intensity	Duration (s)	A _{max}
Viña del Mar	1985	S20W	7.8	VI – VII	116	0.35 g
Llo-Lleo	1985	N10E	7.8	VIII	116	0.67 g
México	1984	EW	8.1	VIII – IX	62	0.17 g
Northridge	1994	Sylmar EN	6.8	VIII – IX	60	0.84 g
Kobe	1995	JMA N-S	6.9	VIII – IX	48	0.82 g

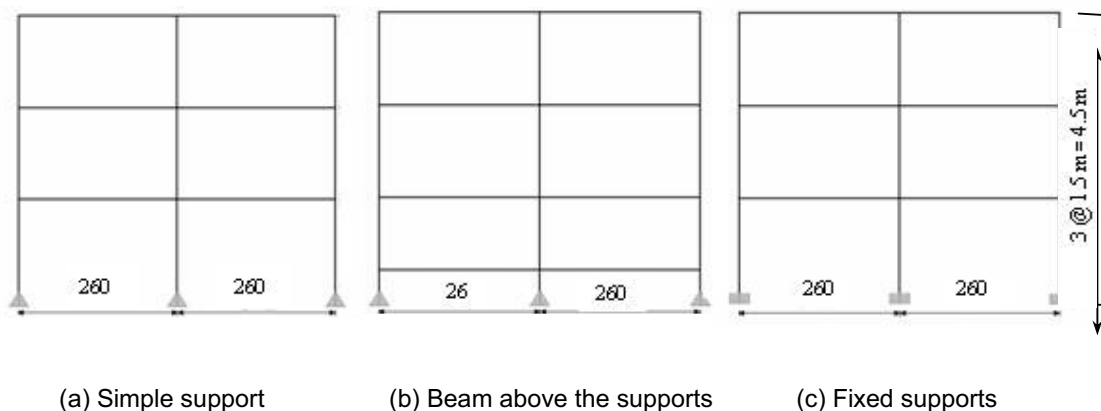
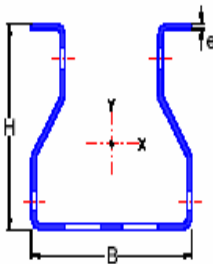
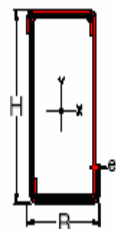


Figure – 3 Frame geometry and column base support

The geometry and support conditions for the 3 levels rack is shown on figure 3. The

same conditions were applied for the six levels rack (9 meters height), so 6 structures were analyzed. The section properties are shown on Table 3. In a second step, the capacity of each structure was determined, two approaches were applied: push over analyses first and non linear dynamic analyses under scaled records after.

Table 3 – Section Properties

GEOMETRIC PROPERTIES			
Dimension	Column		Beam
B [mm]	100.0		21.5
H [mm]	100.0		100.0
e [mm]	3.0		2.0
A [cm ²]	10.0		8.03
I _x [cm ⁴]	138.04		122.53
I _y [cm ⁴]	129.81		28.51
W _x [cm ³]	27.61		24.51
W _y [cm ³]	22.23		10.93
Weight [Kg/m]	7.84		6.28
			

EARTHQUAKE DEMAND

Lateral Elastic Displacements - The lateral displacements envelopes when the behaviour is elastic are shown in Figure 4.

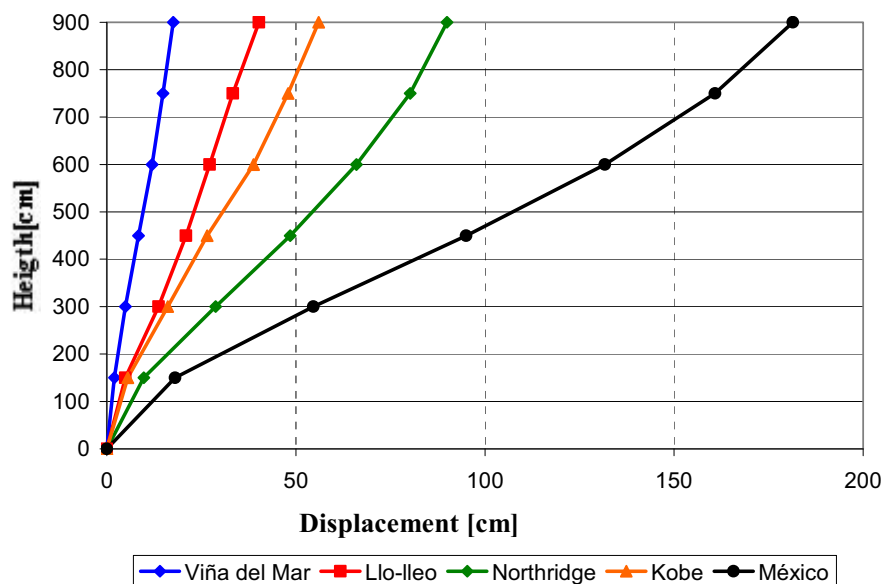


Figure 4 – 6 Levels rack displacements envelopes – Fixed Support at Base

The maximum displacement for the six levels rack was obtained with the Mexico earthquake record and it is 18% of the height of the rack structure; this figure is much larger than the limit prescribed at the Chilean NCh 2369 (INN, 2002) and the RMI

(RMI, 2005) Standards. For the less flexible three level racks, the maximum displacement was obtained with Northridge or Lolleo earthquake records. All the drift values obtained from analysis with different ground motion record exceed the maximum drift limit (0.015H) stipulated by the Chilean Code.

Figure 5, shows the displacement response at the top of the rack for the simple supported frames under the Chilean Earthquake record obtained in Viña del Mar city. The same figure shows the maximum allowable drift according to the Chilean NCh 2369 Code. In both cases the maximum drift is exceeded, but due to the frequencies content the three levels rack is more sensitive to the Viña del Mar earthquake record.

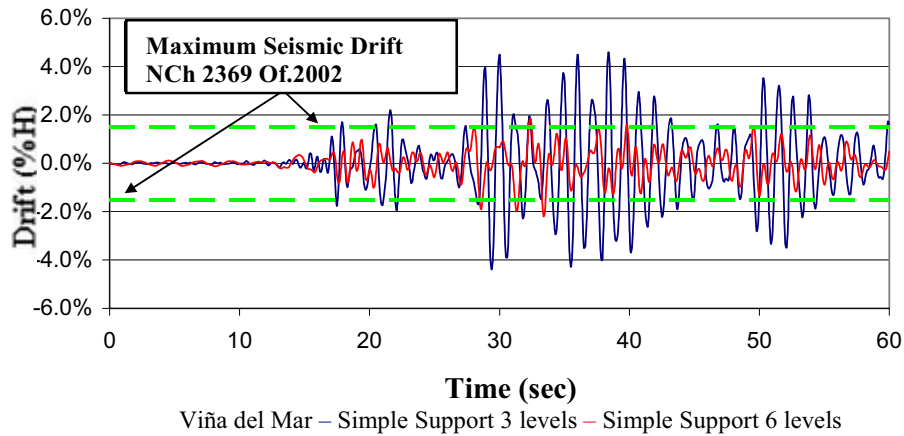


Figure 5 – Displacements at the top level

The maximum drift, for every structure subjected to different earthquakes are presented on Figure 6.

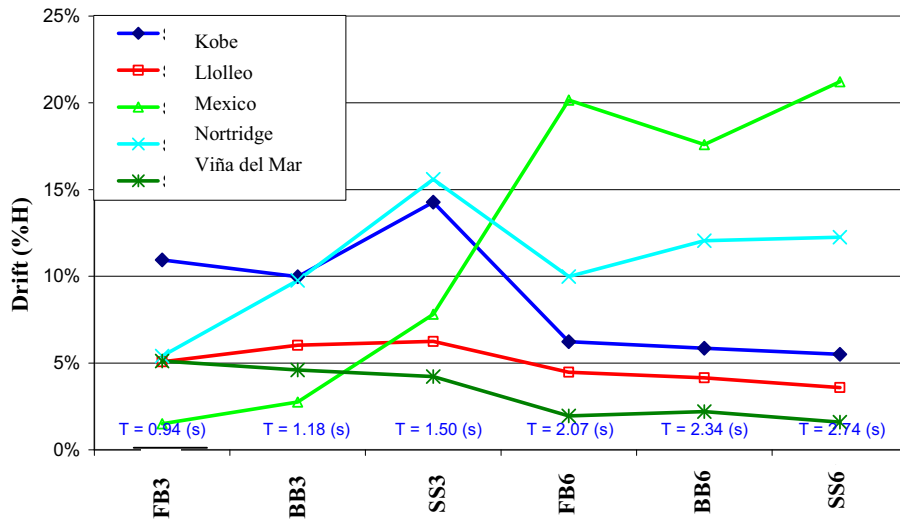


Figure 6 – Maximum drift at the top level

The structures are presented from small to large periods, fixed base for 3 levels

(FB3) has the smallest period and simple support for 6 levels (SS6) has the largest period.

Bending Moments and Rotations on the Elastic Connection – The envelopes of moment in connections shows that the strength capacity of the connection (20000 Kg-cm) is exceeded with all the records. The rotation capacity of the connection (0.03 radians) is also exceeded with all the ground motions, except with the Mexico earthquake.

Non Linear Dynamic Analysis. In order to consider the non linear behaviour, it was necessary to include the non linear properties of the connection. The moment – rotation relationship, obtained from cyclic tests by Irisarri (1998) is shown on Figure 7. A tri-linear model can be used. There is an initial gap due to the fitting of the hooks into the slots. The change in the curve slope is because of the yielding of the first hook. Two equivalent models were explored, one of them is by adding a multi linear plastic element between the column and the beam, another possibility is to include a hinge in the beam.

The program does not accept the same value in different points of the curve, so it was necessary to provide a small slope near the origin (10 kg-cm moment when the rotation is 0.002 radians), to the initial gap.

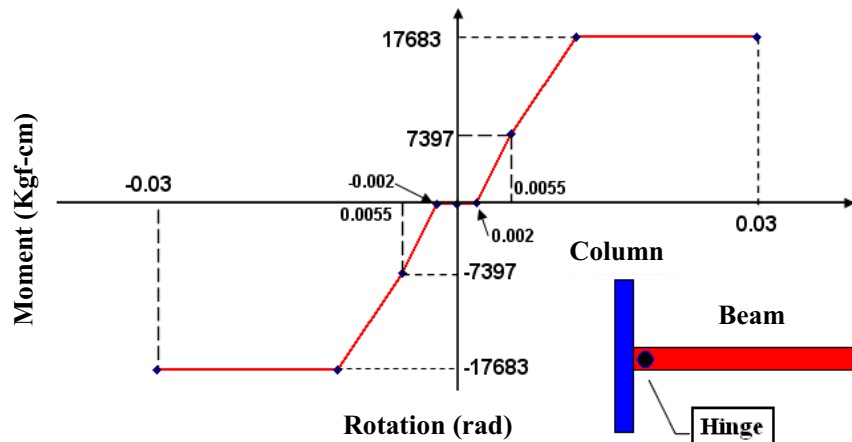


Figure 7- Moment rotation relationship

Non Linear Displacements.

Envelopes for the lateral displacements are shown on Fig. 8. The maximum displacement for the six levels rack with beam at the bottom occurred with Mexico record. This earthquake is the worst condition for the 9 levels rack. The non linear drift is about 3%, which is also larger than the codes limits (INN, 2002; RMI, 1997). Kobe, Northridge and Mexico produce the collapse of the racks. Envelopes of displacements and base shears are shown on Fig. 9.

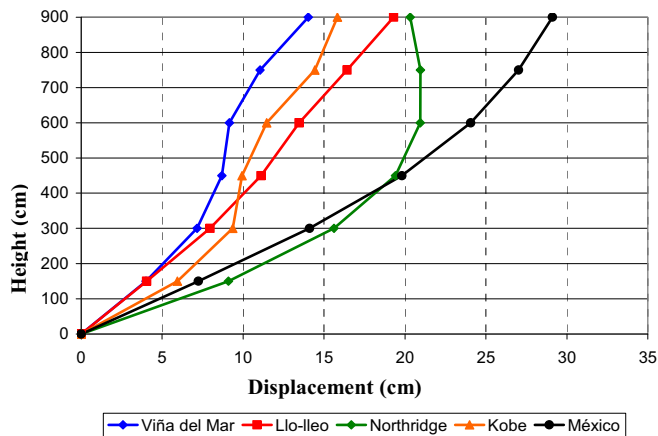
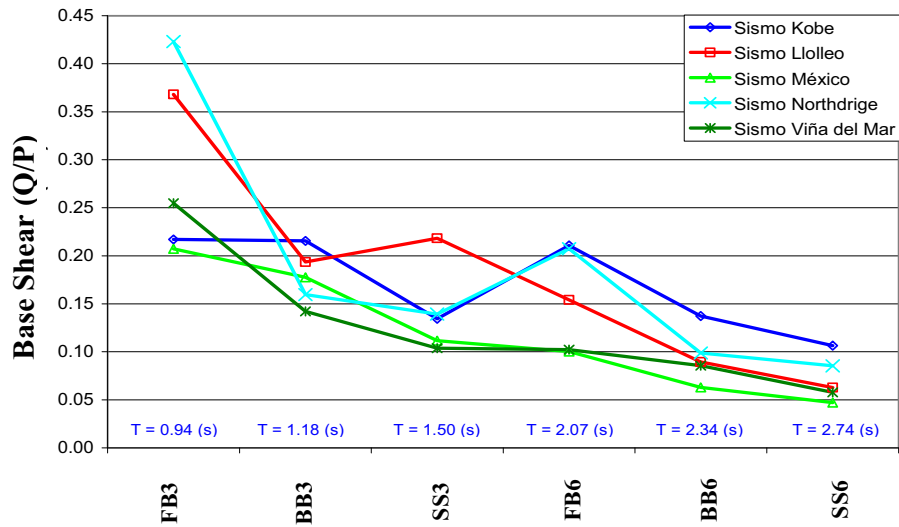
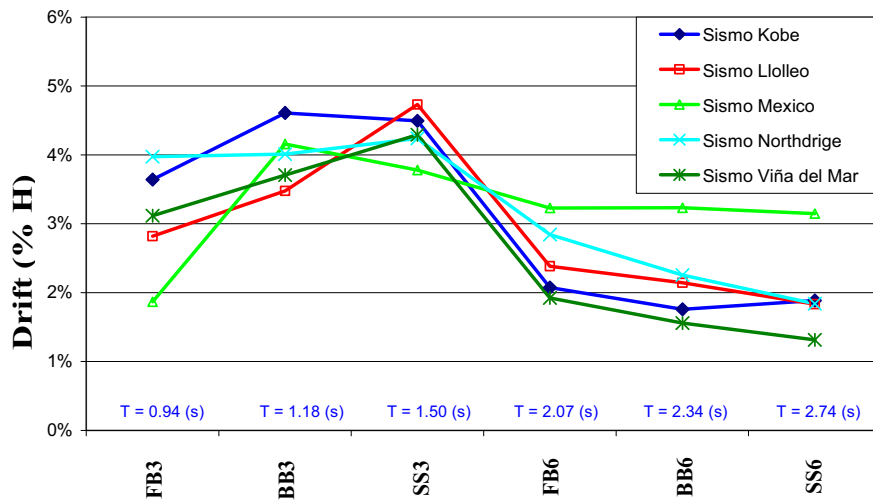


Figure 8 · Displacement Envelope – 9 meters-rack. Beam at the base



(a) Lateral Displacements



(b) Base Shear

Figure 9 – Displacements and Base Shear Envelopes

Pushover Analyses. Triangular and uniform lateral load pattern were applied to the structures above mentioned. SAP 2000 and connection Irisarri's bilinear model (1998) were used. In this model, the yielding starts at $\theta_y=0.012$ radians and the ultimate rotation is $\theta_u=0.03$. The plastic moment is 2000 Kg-cm.

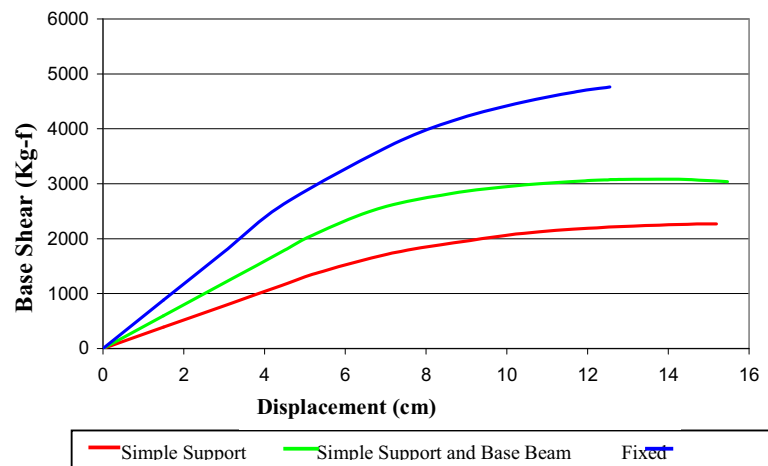


Figure 10 – Pushover Curves

Typical shear displacements curves for the six level racks, considering the 3 support conditions at the base are shown on Fig. 10. A summary of the largest displacements and base shear are given on Table 4.

Table 4 – Maximum Shear and Displacements

SUPPORT CONDITION	Δ_{max} (cm)	% H	Q_y (kgf)
Simple Support (4.5 m)	15.20	3.3 %	2150
Beam at the Base (4.5 m)	15.46	3.4 %	2850
Fixed (4.5 m)	12.6	2.8 %	4180
Simple Support (9.0 m)	22.5	2.50 %	1910
Beam at the Base (9.0 m)	25.9	2.88 %	2560
Fixed (9.0 m)	26.6	2.95 %	3200

Scaled Records – A second approach to determine the capacity was by scaling the amplitudes of the ground motion records, as far as the collapse or the structure or the 0.03 radians rotation limit is reached in some connection. In the case of Kobe, Northridge and Mexico was not necessary to increase the amplitude of the ground motion record. There were performed 30 analyses (6 structures, 5 records), 11 of them did not reach the ultimate condition and 10 of them belong to Chilean records. The only exception was the 3 levels rack with fixed base under the Mexico earthquake. Fig.11 shows one of the cases processed with the Chilean Earthquake.

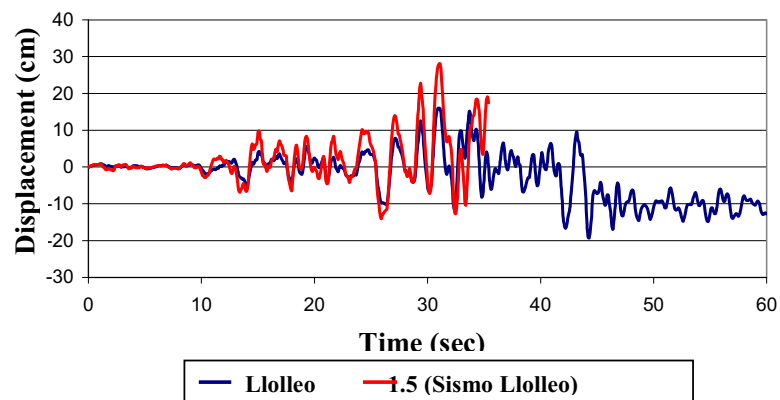


Figure 11 Time history response for Llolleo record on the top of the 9 meters rack

The only exception was the 3 levels rack with fixed base under the Mexico earthquake. Fig.11 shows one of the cases processed with the Chilean Earthquake.

DESIGN FACTORS

In order to obtain the design R and C_d factors, it is necessary the following definitions, associated to Fig. 2:

$$\mu = \frac{\Delta_u}{\Delta_y} \qquad R_\mu = \frac{Q_{max}}{Q_y} \qquad \Omega = \frac{Q_y}{Q_e}$$

Ductility Ratio - Strength Factor due to Ductility - Over strength Factor

1. – Displacement Amplification Factor. – It was obtained from the pushover analyses, the results and the **Displacement Amplification Factor [C_d]**, according to equation (4) (Uang, 1991) are shown in Table 5.

$$C_d = \mu \cdot \Omega \quad (4)$$

Table 5 – Displacement Amplification Factor

Height (m)	Over Strenght Factor (Ω)	Ductility Ratio (μ)	C_d
3 Levels	1.85	1.90	3.49
6 Levels	1.60	1.82	2.91

NEHRP Recommended Provisions (BSSC, 2001) suggest $C_d=3.5$ for Rack Structures, which seems to be appropriate for the 3 levels rack, for taller racks is less which is a conservative approach.

2. – Strenght Reduction Factor. – It was determined by two approaches: Pushover Analyses and non Linear Analyses with Scaled Records. It can be shown the following equation can be used to determine the **Strenght Reduction Factor [R]**

$$R = R_\mu \cdot \Omega \quad (5)$$

2.1. – Pushover Analyses Results. The average R factor for the 3 levels rack was 2.32, for the 6 levels rack the average was 2.83; the codes normally required a value around 4. The Over Strength is smaller for larger racks but the ductility ratio is larger for large racks.

2.2. – Scaled Non Linear Analyses Results. In most of the cases the ultimate strength condition of the structure was obtained with the original record. In those cases where there was no failure, the record was scaled until the structure reached the ultimate condition.

A summary of results is presented on Fig. 12 for both types of analyses. It can be seen that Pushover R Factors are smaller than R factors obtained with non linear analysis.

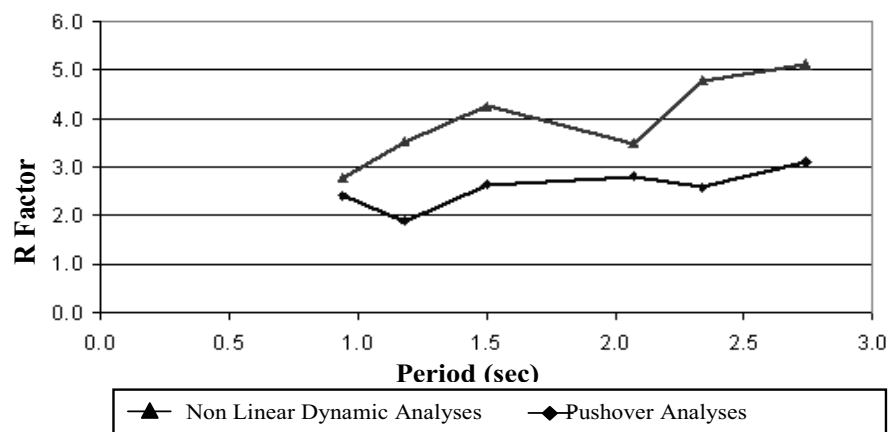


Figure 12 – Strenght Reduction Factors

There are several reasons that explain the differences: first under monotonic loading the plastic moment reaches by the connection is 20000 Kg-cm larger than the plastic moment obtained under cyclic loading, which is 17683 Kg-cm, because of the cyclic deterioration of the plastic moment.

CONCLUDING REMARKS

1. The average displacement produced for Chilean Earthquakes is 4% of the rack height. México (1985), Northridge (1994) and Kobe (1995) earthquakes produce an average displacement 10% of the total rack height. Those figures are larger than the limits of the codes, so the design is controlled by the lateral deflections.
2. Chilean Earthquakes do not take the rack to the strength limit condition that means the connections never reach the maximum rotation (0.03 radians).
3. No matter the R factor value, the lateral displacements obtained from time history exceed the limit values. As a consequence displacements control the seismic design. P – Δ effects should be included in the analysis.
4. The Average Base Shear reaches 40% of the weight of the structure.
5. The Strength Reduction Factor obtained with Chilean earthquakes is about 2, which is half of the maximum R factor specified in the Chilean code. More destructive earthquakes give larger R factors. The factor is sensitive to earthquake characteristics and to the structure properties.
6. The Chilean Codes don't specify an R value for rack storage structures. The American "NEHRP Recommended Provisions for Seismic Regulations for New Buildings and Other Structures, 2001" suggest $C_d = 3.5$. The analyses show that C_d becomes 3.49 for 3 levels racks and 2.91 for six levels racks.
7. It seems appropriate to include a beam above the support because it reduces the lateral displacements and improves the dissipation mechanism, because of the larger redundancy.

REFERENCES

- Building Seismic Safety Council (2001) – "NEHRP Recommended Provisions for Seismic Regulations for New Buildings and Other Structures", USA
- Instituto Nacional de Normalización INN (2002) – "Diseño Sísmico de Estructuras e Instalaciones Industriales" Norma Chilena NCh 2369-Of.2002
- Irisarri Harding, Alejandro (1998) – "Conexiones Semirígidas en Estructura de Acero y su influencia en el Análisis". Memoria Para Optar al Título de Ingeniero Civil, Departamento de Obras Civiles, Universidad Técnica Federico Santa María, Valparaíso, Chile. .
- Rack Manufactures Institute RMI (1997) – "Specification for the Design, Testing and Utilization of Industrial Steel Storage Racks", USA
- Uang C. M (1991). – "Establishing R (or R_w) and C_d Factors For Building Seismic Provisions". Journal of Structural Engineering, ASCE, 117(1), 19-28.

Key words: Steel Design, Rack Structures, Non Linear Behaviour, Semi-Rigid Connections.

A RELIABILITY-BASED METHODOLOGY FOR EVALUATING CONNECTION DESIGN OF SELF-CENTERING FRAMES

Maria E. Moreyra Garlock
Assistant Professor, Princeton University, Princeton, NJ, 08544
mgarlock@princeton.edu

Gordana Herning
Graduate Student, Princeton University, Princeton, NJ, 08544
gherning@princeton.edu

Erik VanMarcke
Professor, Princeton University, Princeton, NJ, 08544
evm@princeton.edu

ABSTRACT

Self-centering moment-resisting frames (SC-MRFs) have the potential to eliminate structural damage under a design basis earthquake (DBE) and return to its original vertical position (i.e. self-center) following a major earthquake. This study has two objectives: (1) examine the effectiveness of an existing SC-MRF design procedure to frames of varying building heights; and (2) propose a reliability-based methodology for improving the existing design procedure. Based on the response of 3 new prototype frames, the first part of the study shows that the existing design procedure for SC-MRFs can be improved. A reliability study, based on Monte Carlo simulations of thousands of synthetic ground motions, is proposed for improving the existing procedure since it is able to determine the probability of exceeding any given limit state.

INTRODUCTION

The self-centering behavior in self-centering moment-resisting frames (SC-MRFs) is achieved through the connections by post-tensioning (PT) the beams with either high strength strands or bars (Ricles et al. 2001, Garlock et al. 2005). The behavior of a SC-MRF is characterized by a gap opening and closing at the interface of the beam tension flange and column flange under earthquake loading (θ_r shown in Figure 1). Energy dissipation is provided by supplemental elements that deform under the gap opening behavior. Examples of hysteretic energy dissipating devices are top-and-seat angles (Garlock et al. 2003, 2005), friction devices (Rojas et al. 2005), steel bars (Christopolous et al 2002), or plates (Chou et al. 2006). The shape of the hysteretic energy dissipated by the connection is a “flag shape”, as shown in Figure 1(a), regardless of the energy dissipating device used. The amount of energy dissipation is proportional to the area inside the moment (M) – θ_r curve.

Existing design procedures for these SC-MRFs are based on a study of a six story

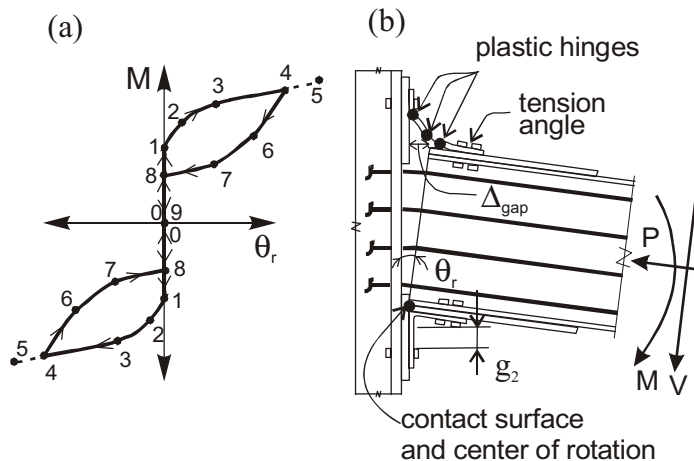


Fig. 1 (a) moment – relative rotation behavior of SC-MRF connection; and (b) SC-MRF connection detail with top-and-seat angles for energy dissipation

prototype that was subject to six ground motions (Garlock et al. 2007). At the time of that study, it was not possible to subject the frame to thousands of ground motions due to the limited capabilities of computing systems. Currently, advances in these systems can now run thousands of these analyses in a few hours. This study examines two aspects of SC-MRF designs: First, the existing design procedure is used to design a 3-story, a 9-story, and a 20-story frame. These frames are then subject to the same six ground motions that were used to develop

the design procedure and then analyzed to observe the effects of building height on the design procedure. Second, a reliability-based methodology is proposed to develop or improve design procedures for SC-MRFs. Using Monte Carlo simulation, the nonlinear prototype SC-MRF models are subject to thousands of ground motions. A series of conditional seismic reliability assessments of the structure are performed and the peak gap opening, θ_r , response is recorded. This data is then used to quantitatively express the effect that this parameter has on the seismic response. Monte Carlo sampling (based on randomness of given uncertainties such as yield stress) is used to calculate the probability of a limit state (e.g. strand yielding) given a demand (e.g. θ_r). The results of the ground motion demand and capacity are used to determine limit state reliability. This paper presents only the methodology and some example data based on preliminary results. Further limit state reliability studies are in progress and will be used to develop a reliability-based seismic design procedure for SC-MRF connection details.

PROTOTYPE BUILDINGS

Three, nine and twenty story prototype buildings were designed for a high-risk seismic zone and stiff soil conditions using a performance-based design procedure described in Garlock et al. (2007). All members are assumed to have a nominal yield stress of 50 ksi and gravity loads consistent with an office building. For details see Garlock et al. (2007, 2008). Floor plans, elevations, member sizes, and connection details of the three prototypes are shown in Figure 2. The shaded regions of the plan represent composite action of the beam and slab. The floor beams that frame into the MRFs are *collector beams* that transfer the floor inertial force to the SC-MRF (Garlock and Li 2008). The 3- and 9-story prototypes each have eight collector beams framing into one MRF, while the 20-story building has seven. The collector beam lateral stiffness for the 3 and 9 story is 65 kips/inch and a yield force of 98 kips. The 20 story prototype has stiffness of 86 kips/inch and a yield force of 108 kips. The fundamental periods for the 3, 9, and 20 story prototypes are 1.1, 3.3, and 3.4 seconds, respectively.

The interior column size was controlled by strong column – weak beam criterion. The exterior column size was uniformly set at two sizes smaller than the interior column size. The beam size was governed by either (1) beam compactness criteria, or (2) beam local buckling criteria based on combined moment and axial load stresses, or (3) decompression moment criterion required for self-centering. The last criterion requires that $M_d \geq 0.6 M_a$, where M_d is the minimum decompression moment (point 1 in Fig. 1(a)), and M_a is the moment at which the energy dissipating devices change stiffness (point 2 in Fig 1(a)). The beam sections in most lower stories of the 9 and 20 story prototype were controlled by the criterion that prevents connection decompression under wind forces, i.e. $M_d > M_{wind}$.

NONLINEAR STRUCTURAL MODEL

Nonlinear models of the prototypes were developed using OpenSees (McKenna and Fenves 2006). The 3-story prototype model is shown in Figure 3. This frame is one of the four perimeter SC-MRFs which comprise the lateral load resisting system of the prototype. The detailed connection model is also shown in Figure 3. The current model was validated with nonlinear time history analyses by comparison with the response of a simpler rotational spring model as described in Dobossy et al. (2006). Yielding in columns is assumed to be confined to the discrete areas just outside of the column panel zone. Potential yielding in the beams is assumed to be in the beam region just beyond the reinforcing plate. In the columns, length of inelastic elements is 1/10 of the column depth. In beams, inelastic elements are located between the end of the reinforcing plate and the point where the interior collector beam frames into the SC-MRF beam. Elastic-plastic force deformation behavior was used to represent top-and-seat angles, which were selected as the energy dissipating devices.

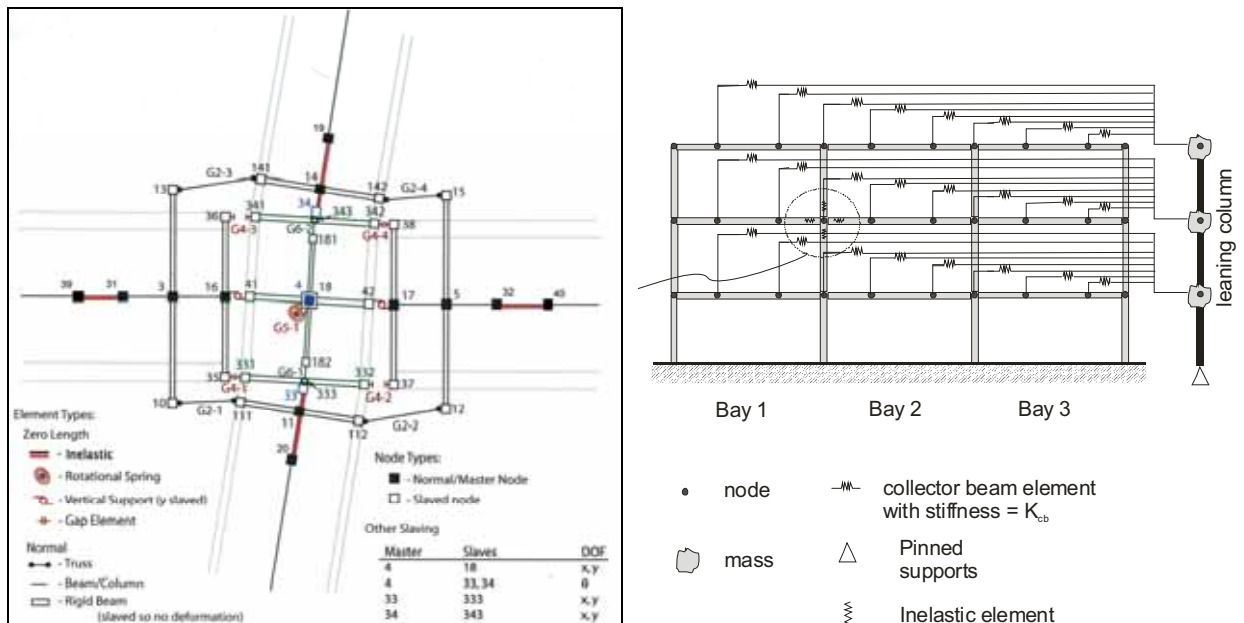


Fig. 3 – Nonlinear model of SC-MRF.

GROUND MOTIONS

This preliminary study examines the response of the prototype frames to two types of ground motions: (1) natural ground motions; and (2) artificially generated ground motions. The two natural ground motions are based on previous studies of a six story prototype (Garlock et al. 2008): 1989 Loma Prieta earthquake recorded at *Gilroy* array #3, and 1995 *Kobe* earthquake recorded at the JMA station. One ground motion is *artificially* generated to be compatible with the IBC 2000 (International 2000) design response spectrum. The Kobe and Gilroy natural ground motions were scaled to a level compatible with 5% damped IBC 2000 design spectrum. These three ground motions are plotted in Figure 4 for the design basis earthquake (DBE), which is scaled to 2/3 of the maximum considered earthquake (MCE) - a seismic event that has a 2% probability of exceedance in 50 years. Another 3 ground motions were scaled to the MCE. We will refer to these six ground motions as “*code-scaled*” to differentiate them from the probabilistic study set.

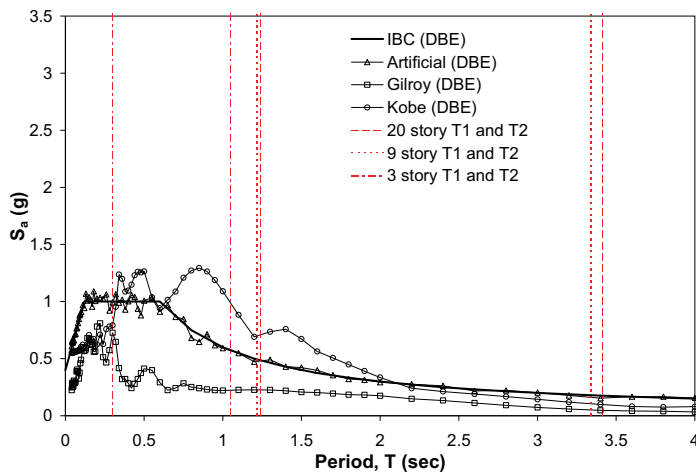


Fig. 4 – Code-scaled DBE ground motions.

To perform a seismic reliability analysis of the structure, it is necessary to identify the seismic hazard that is present at the particular location where the structure is being analyzed. For the same local soil conditions, the shaking intensity of the ground at the site depends on magnitude, M , source to site distance, R , and number of standard deviations of the ground motion deviates from the predicted (median) value, ϵ , which is a variable representing

the uncertainty (Bazzurro and Cornell, 1999). In this preliminary reliability study we use the Sebetta and Pugliese (1996) attenuation relationship to generate the ground motions and then scaled them so that the PGA equals a target PGA of 0.8g for the MCE. Monte Carlo simulation is used to generate about 5000 DBE ground motions and about 3000 MCE ground motions. Current work is developing another method for ground motion generation that is based on S_a (instead of PGA) and an attenuation function that has been calibrated for our site.

CODE-SCALED ANALYSIS RESPONSE

Previous studies compared the proposed design procedure of SC-MRFs to a six story frame (Garlock et al 2007). This paper examines how accurately such a procedure predicts the response of frames with different story heights. Figure 5 shows the maximum story drift at each floor and compares it to the design prediction. Table 1 examines the maximum roof displacement and the maximum relative rotations obtained

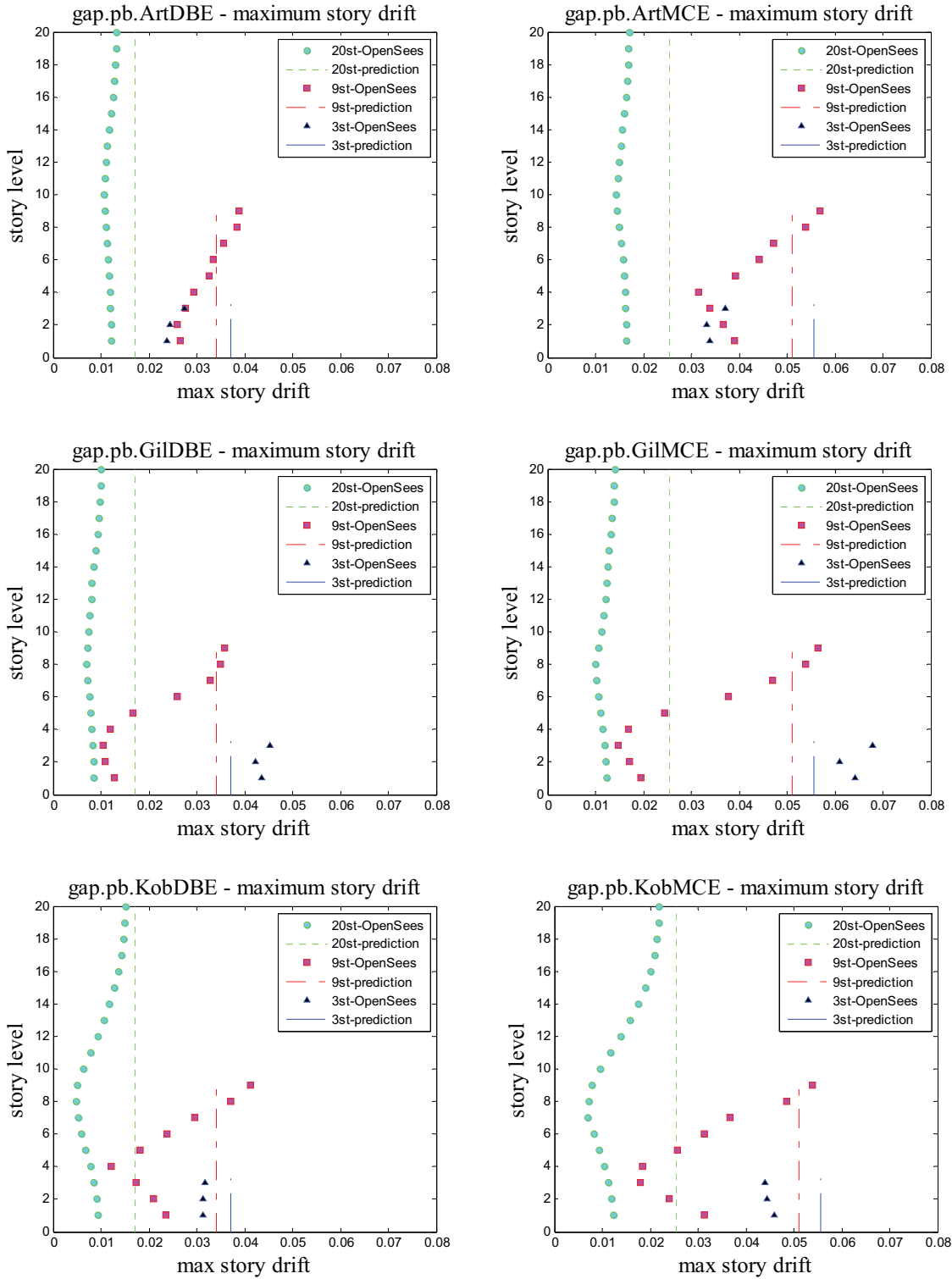


Figure 5: Maximum story drift (θ) at the DBE and MCE levels.

from the code-scaled analyses. Some *general* trends that can be seen from Table 1 and Figure 5 are: (1) the predicted maximum roof displacement is low compared to the 3-story frame response and high compared to the 9 and 20 story response; and (2) the maximum predicted relative rotation is low for the 3 story response and high for the 20 story response; and (3) the predicted maximum story drift is high for the 3 and 20 story frames and low for the 9 story frame.

Two general conclusions can be drawn from observing this table and figures. First, the ground motion characteristics play an important role in defining the response of the frame and therefore conclusions on the response cannot be drawn from a small sample of ground motions. Second, given the same ground motion, the correlation of the response to the predicted response of the frame will be different if the building height of the building is different. This implies that the design of the frame should consider building height characteristics and a large set of realistic ground motions should be used in the seismic assessment.

Table 1: Maximum roof displacement and relative rotations for the code-scaled ground motions: comparison to the design (predicted) values that are shaded.

		Max roof displacement, Δ_{roof} (in)		Maximum relative rotation θ_r (rad)	
		DBE	MCE	DBE	MCE
3 story	design	11.6	17.3	0.025	0.042
	Kobe	14.5	20.6	0.034	0.044
	Gilroy	19.7	28.6	0.035	0.062
	Artificial	11.4	15.4	0.026	0.041
9 story	design	32.7	49.1	0.026	0.042
	Kobe	16.3	22.8	0.033	0.039
	Gilroy	22.9	31.7	0.026	0.033
	Artificial	37.5	46.1	0.028	0.042
20 story	design	36.1	54.2	0.013	0.021
	Kobe	20.4	30.6	0.009	0.014
	Gilroy	23.1	33.8	0.006	0.010
	Artificial	33.2	44.5	0.010	0.015

LIMIT STATE RELIABILITY ANALYSIS

To improve the ground motion representation and also to evaluate the effects of design parameters, including story height, the authors propose a reliability study of the SC-MRFs. In such a study the prototype frames are subject to Monte Carlo simulations of realistic synthetically generated ground motions (described before) where peak responses are recorded. Using the probabilistic demand and capacity curves generated through the simulations, the combined probability of the demand exceeding the capacity is calculated. With such a procedure that can capture a realistic range of ground motion characteristics, we have a statistically robust dataset that can be used to validate or improve the design recommendations given previously for SC-MRFs (Garlock et al. 2007). This section presents an example of the methodology that is currently being employed by the authors. The data collected is the relative rotation and the limit state examined is strand yielding, which can be directly correlated to relative rotation. Since

the process of ground motion generation is currently under development, the numerical results that are shown should be viewed *only* as examples of the kind of information that such a procedure can produce.

Figure 6 shows the CDF of the maximum relative rotation (θ_r) in the entire frame, which represents the *demand*. The CDF is plotted for the 3, 9, and 20 story frames. Figure 6 shows that the 9 and 20 story frames have a similar CDF distributions but the 3 story has a lower mean and a higher probability of having reached any given θ_r . Examination of the ground motion characteristics shows that the average S_a for the fundamental period of the 3 story frame is significantly lower than the design S_a , which can lead to such results. The 9 and 20 story S_a is more consistent with that used in design.

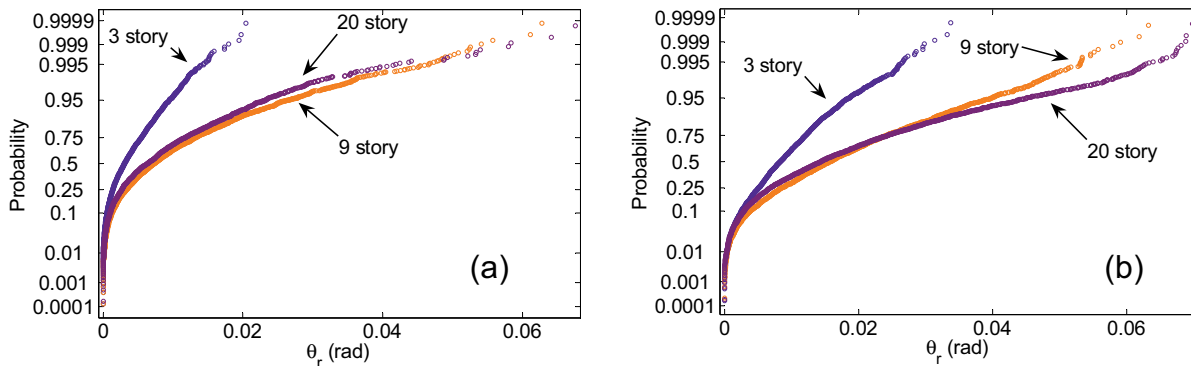


Figure 6: Probability Plot of relative rotation demand for (a) DBE and (b) MCE

Using a closed-form solution for the θ_r at which strands will yield (Garlock et al. 2007), a capacity CDF of the probability of strand yielding, given θ_r , is generated. This CDF, shown in Figure 7, is based on uncertainty in the strand yield stress (material uncertainty) and uncertainty in the initial post-tensioning force (construction uncertainty). By convolving the distributions of the capacity and demands we arrive at the probability that the limit state capacity is less than the demand:

$$P_{LS} = P[D > C] = \sum_{all_d} P[D > C | D = d] \cdot P[D = d]$$

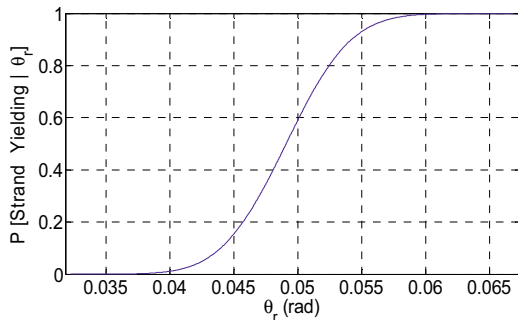


Figure 7: Capacity CDF of strand yielding in terms of relative rotation at level 2 in the 9 story prototype.

Applying this procedure to every floor, we arrive at Table 2 which indicates the probability of strand yielding. It is seen in this example that the probability for strand yielding in the 3-story frame is zero throughout, while in the other frames the probability of strand yielding varies. The 20 story frame shows a larger probability of yielding in the lower floors, a trend that is also seen in the 9 story frame.

This example of the proposed approach shows how one can evaluate the effectiveness of the design procedure for strands, where the design criteria does not permit strand yielding. By making such observations, one can adjust a particular design or design procedure not only for strands, but for other connection details as well.

Table 2. Probability of strand yielding at each floor for the MCE ground motions (%)

	1	2	3	4	5	6	7	8	9
3 story	0.00	0.00	0.00						
9 story	1.49	1.33	0.17	0.43	0.11	0.00	0.00	0.00	0.00
20 story*	87.2	14.2	21.2	11.4	10.7	10.1	9.40	9.18	10.4

* only shown for the first 9 floors

SUMMARY AND CONCLUSIONS

This paper has defined three new prototype self-centering moment-resisting frames (SC-MRFs) – 3, 9, and 20 stories – that have been designed based on a previous study of a 6 story frame that was subject to six ground motions. This study examined the applicability of this existing design procedure on the three new frames based on their response to six “code-scaled” ground motions and based on Monte Carlo simulations of thousands of realistic synthetically generated ground motions. The latter is now possible due to significant advances in computing systems.

The results show that a small sample of ground motions produces significant variability in the results depending on the ground motion characteristics and how that relates to the dynamic characteristics of the frame (as observed by the different responses of the 3, 9, and 20 story frames). The existing design procedure should be re-examined based on a large sample of ground motions. This ground motion selection and generation should be given serious consideration so that realistic frame responses can be studied.

This paper also defined a reliability-based approach for developing recommended design procedures of frames and connections. This methodology is a useful way of quantifying probabilities of reaching certain limit states and it is an appropriate tool for doing sensitivity analyses of connection details that can lead to design recommendations and improved design procedures for SC-MRFs that consider building height characteristics, for example. In the near future the authors will investigate other frame responses, such as drift and beam and column yielding, as well as perform sensitivity analyses of connection details. Also, the methodology for synthetic ground motion generation is being evaluated to realistically represent the attenuation relationship, and the spectral shape based on the dynamic characteristics of the frame.

ACKNOWLEDGEMENTS

This material is based upon work supported by American Institute of Steel Construction

(AISC) and the National Science Foundation (NSF) under Grant No. 0420974. Any opinions, findings, and conclusions expressed in this material are those of the authors and do not necessarily reflect the views of the sponsors. The authors would also like to thank Jie Li, and Mark Dobossy, for their contributions.

REFERENCES

- Bazzurro, P., Cornell, C. (1999). "Disaggregation of Seismic Hazard", *Bulletin of the Seismological Society of America*, Vol. 89, No. 2, 501-520.
- Building Seismic Safety Council. (1997). "NEHRP Recommended Provisions for Seismic Regulations for New Buildings and Other Structures. Part 1 – Provisions." *Rep. No. FEMA-302*, for the Federal Emergency Mgmt Agency, Washington, D.C.
- C.C. Chou, J.H. Chen, Y.C. Chen and K.C. Tsai, Evaluating performance of post-tensioned steel connections with high-strength strands, *Earthquake Engineering and Structural Dynamics* 35 (9) (2006), pp. 1167–1185.
- Christopoulos, C., Filiatrault, A., Uang, C.-M., Folz, B. (2002). "Posttensioned Energy Dissipating Connections for Moment-Resisting Steel Frames", *Journal of Structural Engineering*, ASCE, Vol. 128(9), 1111-1120.
- Dobossy, M, Garlock, M., and VanMarke, E. (2006). "Comparison of two self-centering steel moment frame modeling techniques: explicit gap models, and non-linear rotational spring models", *Proceedings of the 4th International Conference on Earthquake Engineering*, Taipei, Taiwan, October 12-13.
- Garlock, M, Ricles, J., and Sause, R. (2003). "Cyclic Load Tests and Analysis of Bolted Top-and-Seat Angle Connections," *Journal of Structural Engineering*, ASCE 129(12).
- Garlock, M, Ricles, J., and Sause, R. (2005) "Experimental Studies on Full-Scale Post-Tensioned Steel Connections", *Journal of Structural Engineering*, ASCE, 131(3).
- Garlock, M, Sause, R., and Ricles, J. (2007). "Behavior and Design of Post-Tensioned Steel Frames", *Journal of Structural Engineering*, ASCE, Vol. 133(3), 389-399.
- Garlock, M, Ricles, J., and Sause, R. (2008) "Influence of Design Parameters on Seismic Response of Post-Tensioned Steel MRF Systems, *Engineering Structures*, Elsevier, 30(4), p. 1037-1047
- Garlock, M, and Li, J. (2008). "Steel Self-Centering Moment Frames with Collector Beam Floor Diaphragms" (accepted for publication in *Journal of Constructional Steel Research*; available online at <http://dx.doi.org/10.1016/j.jcsr.2007.10.006>)
- International Building Code*. (2000). International Code Council, Falls Church, Virginia.
- McKenna, F., & Fenves, G. L. (2006). Opensees 1.7.0. Computer Software. UC Berkeley, Berkeley, CA.
- Ricles, J., Sause, R., Garlock, M., and Zhao, C. (2001). "Post-Tensioned Seismic Resistant Connections for Steel Frames," *Journal of Structural Engineering*, ASCE, Vol. 127, No 2
- Rojas, P., Ricles, J.M., and R. Sause (2005). "Seismic Performance of Post-Tensioned Steel MRFs With Friction Devices", *Journal of Structural Engineering*, ASCE, Vol. 131(4), 529-540.
- Sebetta, F., Pugliese, A., (1996). "Estimation of Response Spectra and Simulation of Nonstationary Earthquake Ground Motions", *Seismological Society of America*, Vol. 86, No. 2, 337-352.
- SAC Joint Venture. (2000). "Recommended Design Criteria for New Steel Moment Frame Structures", *Rep. No. FEMA-350*, for the Federal Emergency Management Agency, Washington, D.C.

M-N INTERACTION IN CONNECTIONS WITH THERMAL SEPARATION

František Wald, Zuzana Šulcová, Zdeněk Sokol,
Czech Technical University, Prague, Czech Republic
wald@fsv.cvut.cz

Roman Rabenseifer
Slovak University of Technology, Bratislava, Slovakia
rabens@svf.stuba.sk

ABSTRACT

The connections between inner and outer structures still seems to be in the steel structures one challenging question at the time of low-energy buildings and high claims of heat engineering standards. The construction of a bolted end-plate connection with a thermal-insulating layer, which has not only the function of thermal insulation, but also the bearing function in respect to its compression and shear resistance is under progress. As a suitable material, elastomer could be used. The research is focused on the new materials appearing in the market as well to study their suitability for this type of connections. The prediction of the connection mechanical behaviour is based on the component method. The component methods consist of decomposition of the joint into component, the description of the component behaviour and assembling into connection behaviour. The design model is developed and will be checked by experiments and FE simulation.

INTRODUCTION

The latest trend of heat-engineering, economical, technical and structural claims leads to a construction of new types of steel connections which should be heat-insulating and cost-effective as well as statically efficient. The steel connections with thermal barrier could be widely used in practical design such as connections of balconies, loggias, ramps, canopies, cold entry rooms, garages etc, see (Nasdala et al., 2007). This work is focused on the bolting end-plate connection of two beams where the intermediate thermal-insulating layer is used as shown in Fig. 1. The end-plate connection is under the effect of the combination of bending moment and normal force due to the application of the pre-stressed bolts and external forces. The possible shear force is not concerned in this work. It can be easily transferred by using a shear bracket, or the smaller shear force by the bolts themselves and the bigger shear force by the friction in the joint produced by the pre-stressed bolts. The component method is used to predict the behaviour of the joint and a couple of experiments are necessary to be made to check the propriety of this method. Furthermore the component method could be implemented to the standardized calculation process for this type of joints with thermal barrier.

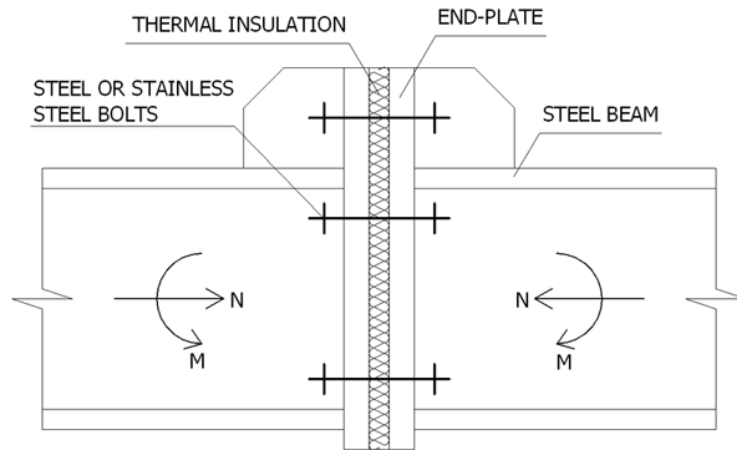


Fig. 1. Model of the bolted end-plate connection with thermal separation

APPLICATION OF COMPONENT METHOD

The goal of this paper is to check the serviceability of the component method for a thermal-insulating steel joint. The component method is the analytical method describing the behaviour of the joint as the moment-rotation relation. Firstly the connection is disintegrated into separate parts and the characteristics of these so-called components are being investigated. The most important characteristics are the resistance and the stiffness of the component. Then the components are assembled with respect to their position in the structure and the general characteristics of the joint are calculated from the partial values.

First of all the thermal-insulating connection is disintegrated into components shown in Fig. 2.

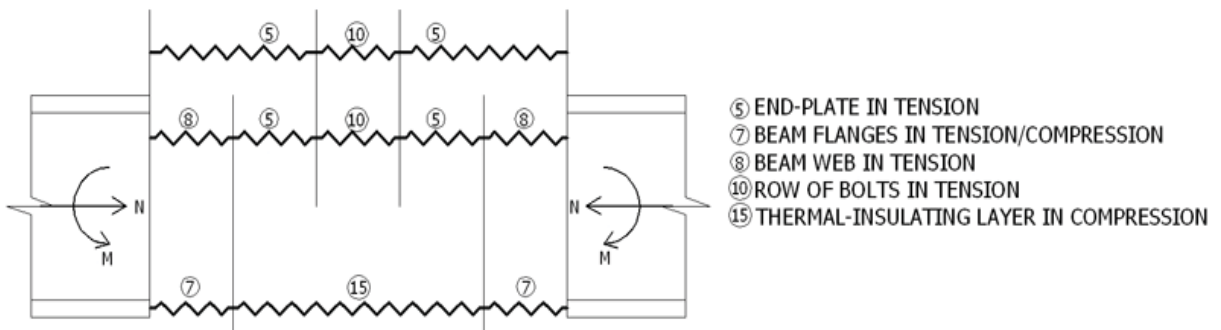


Fig. 2. Components of the thermal-insulating joint

Part in tension

The resistance of the tension part of the connection is the lowest value among the bearing resistances of the following components: ⑩ row of bolts in tension, ⑤ end-plate in tension, ⑧ beam web in tension.

The bearing resistances of the end-plate and the row of bolts in tension are both calculated by using the T-stub model. The failure of the component is caused by one of these three reasons:

a) the failure of the end-plate
$$F_{t,Rd1} = \frac{4M_{pl,1,Rd}}{m} \quad (1)$$

b) the failure of the end-plate and the bolts
$$F_{t,Rd2} = \frac{2M_{pl,2,Rd} + 2nB_{t,Rd}}{m + n} \quad (2)$$

c) the failure of the bolts
$$F_{t,Rd3} = 2B_{t,Rd} \quad (3)$$

where

$$M_{pl,Rd} = 0,25L_{eff}t_p^2f_y/\gamma_{M0} \quad (4)$$

$$B_{t,Rd} = \min \{0,9A_s f_{ub} / \gamma_{Mb} ; 0,6\pi d_m t_p f_u / \gamma_{Mb} \} \quad (5)$$

The bearing resistance of the beam web in tension in a bolted end-plate connection is given

$$F_{8,t,Rd} = \frac{L_{eff,t} t_w f_y}{\gamma_{M0}} \quad (6)$$

The stiffness of the end-plate in tension is calculated from

$$k_5 = 0,85 \frac{L_{eff} t_p^3}{m^3} \quad (7)$$

The stiffness of the bolts in tension is determined as

$$k_{10} = 1,6 \frac{A_s}{L_b} \quad (8)$$

The stiffness of the beam web in tension is supposed to be indefinite. The rotational stiffness of the tension part is then derived from

$$\frac{1}{k_t} = \frac{1}{k_5} + \frac{1}{k_{10}} \quad (9)$$

Part in compression

There are only two components in the part of the connection in compression - ⑦ the beam flanges and (15) the thermal-insulating layer which is the crucial component of the joint.

The bearing resistance of the beam flanges in tension/compression is determined as

$$F_{7,c,Rd} = \frac{W_{pl} f_y}{(h - t_f) \gamma_{M0}} \quad (10)$$

The bearing resistance of the thermal-insulating layer is predicted to be given by a relation known from column-bases:

$$F_{15,c,Rd} = \frac{A_{eff} f_{e,max}}{\gamma_{Me}} \quad (11)$$

where A_{eff} is the compression area in the distance c from the beam flange under compression, see Fig. 3, $f_{e,max}$ is the resistance of the thermal insulation and γ_{Me} is the safety factor of the thermal-insulation material.

As the beam flanges are supposed to have an indefinite bending stiffness, the stiffness of the thermal-insulating layer is also the stiffness of the whole compression part and is supposed to be calculated from

$$k_c = k_{15} = \frac{A_{eff}}{t_e} \quad (12)$$

where t_e is the thickness of the intermediate layer.

M-N INTERACTION

The simplified prediction model for the bending resistance and the rotational stiffness may take into account only the effective area at beam flanges and the effective area at the beam web is neglected, as shown in Fig. 3. It is assumed the compression force acts at the centre of the flange in compression also in cases of limited size of outstand of the plate. The tension force is located in the bolt row in tension. In case of two or more bolt rows in tension part, the resistance of the part in tension is obtained as the resulting force of the active bolt rows.

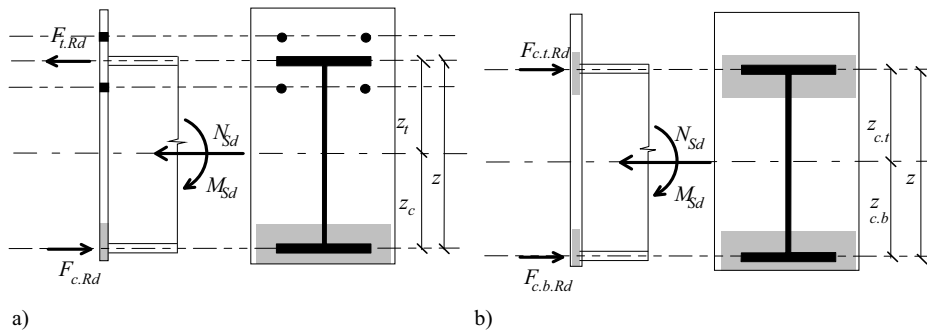


Fig. 3. Model with the effective area at the flanges only; a) one bolt row in tension; b) no bolts in tension.

Component method applied on the M-N interaction

The forces represent resistances of the components in tension $F_{t,Rd}$, and in compression $F_{c,t,Rd}$, $F_{c,b,Rd}$. For simplicity, the model will be derived for proportional loading only:

$$e = \frac{M_{Sd}}{N_{Sd}} = \frac{M_{Rd}}{N_{Rd}} = \text{const} \quad (13)$$

When the eccentricity $e = \frac{M_{Sd}}{N_{Sd}} \leq -z_c$, see Fig. 3a, there is tension force in the bolt row, and compression force in the lower flange. The bending resistance of the joint is derived as

$$M_{Rd} = \min \left\{ \frac{F_t z}{\frac{z_c}{e} + 1}; \frac{F_c z}{\frac{z_t}{e} - 1} \right\} \quad (14)$$

When the eccentricity $e = \frac{M_{Sd}}{N_{Sd}} \geq -z_c$, see Fig. 3b, there is no tension force in the bolt row, but both parts of the connection are loaded in compression. In this case

$$M_{Rd} = \min \left\{ \frac{F_{c,t} z}{\frac{z_{c,b}}{e} + 1}; \frac{-F_{c,b} z}{1 - \frac{z_{c,t}}{e}} \right\} \quad (15)$$

The joint rotation is calculated using the elastic deformation of the components in tension and compression parts (E is the elastic modulus of steel and E_e of the separating layer)

$$\phi = \frac{\delta_t + \delta_c}{z} = \frac{1}{z^2} \left(\frac{M_{Sd} + N_{Sd} z_c}{E k_t} + \frac{M_{Sd} - N_{Sd} z_t}{E_e k_c} \right) \quad (16)$$

The rotational stiffness of the joint depends on the bending moment which is induced by the normal force applied with constant eccentricity e is derived as

$$S_{j,ini} = \frac{M_{Sd}}{M_{Sd} + N_{Sd} e_0} \frac{z^2}{\left(\frac{1}{E_e k_c} + \frac{1}{E k_t} \right)} = \frac{e}{e + e_0} \frac{z^2}{\sum \frac{1}{E k}} \quad (17)$$

where the eccentricity e_0 is defined as follows

$$e_0 = \frac{z_c k_c E_e - z_t k_t E}{k_c E_e + k_t E} \quad \text{resp.} \quad e_0 = \frac{z_{c,b} k_{c,b} E_e - z_{c,t} k_{c,t} E_e}{k_{c,b} E_e + k_{c,t} E_e} = \frac{z_{c,b} k_{c,b} - z_{c,t} k_{c,t}}{k_{c,b} + k_{c,t}} \quad (18)$$

The non-linear part of the moment-rotation curve of the joint, which is loaded by proportional loading, may be modelled by introducing the shape factor μ which depends on ratio γ of the acting forces and their capacities:

$$\mu = (1,5 \gamma)^{2,7} \geq 1 \quad (19)$$

where

$$\gamma = \frac{e + \frac{h}{2}}{\left(\frac{M_{Rd}}{M_{Sd}} \right) e + \frac{h}{2}} \quad (20)$$

$$S_j = \frac{e}{e + e_0} \frac{z^2}{\mu \sum \frac{1}{E k}} \quad (21)$$

For detailed information see (Sokol et al., 2006) and (Sokol et al., 2002).

The relation between the eccentricity e and the initial stiffness $S_{j,ini}$ of the joint was calculated using the component method for different thicknesses of the separating intermediate layer $t_e = 8$ mm, 16 mm and 24 mm. The Figure 4 shows the shape of the relation as well as the influence of the thickness of the separating layer. Using the thicker intermediate layer leads to noticeable decrease of the initial stiffness of the joint.

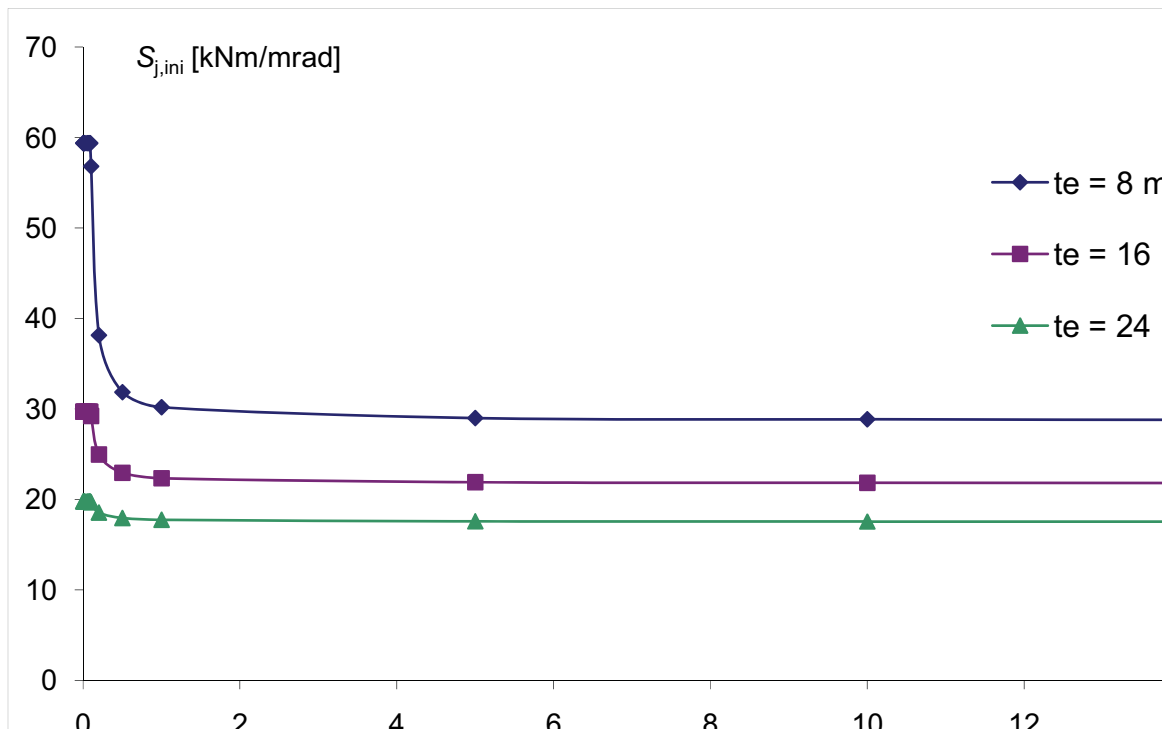


Fig. 4. The relation between the initial stiffness of the joint and the eccentricity of the normal force

The moment - normal force interaction diagram was created for the model of the thermal insulating joint with a thermal insulating layer of thickness 8 mm, see Fig. 5. The compression capacity of the joint (point C) is given by the compression capacity of the insulating layer in the compression areas between the both flanges of the connected beams. The maximum tension capacity of the joint (point A) is given by the capacity of the bolts and it is shifted to the positive moment quadrant because of the non-symmetry of the joint (2 rows of upper bolts vs. only 1 row of lower bolts). It is also shown, that the compressive normal force also helps to increase the moment capacity of the joint because it reduces the tension in the bolts produced by the bending moment (points B and D). In case of use the pre-stressed bolts, the horizontal axis of the interaction diagram would be simply shifted up to the value of the overstrain.

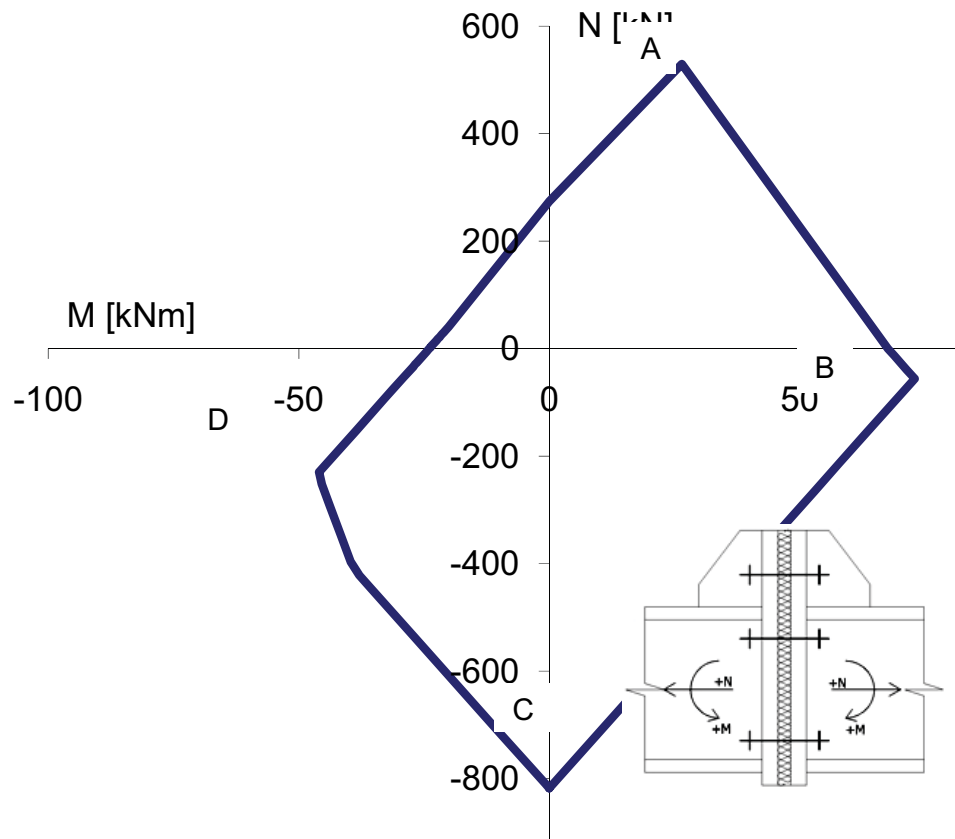


Fig. 5. M-N interaction diagram for the model of the thermal insulating joint

Experiments

To verify the above presented predictions a couple of experiments are ready to be undertaken with a specific thermal-insulating material and its real behaviour in the connection. The influences of the geometry as well as the creep behaviour of the material have to be taken into account and included into the calculation, see (Šulcová et al., 2007). Then the relations can be put more exactly and forward-looking they could be used for practical standardized design. The model and the experimental results are also going to be modelled using FE simulation.

HEAT ENGINEERING

The new heat-engineering standard provides the obligatory values for heat conductivity of the structures as well as values for energy intensity of the building. The most efficient way to decrease the loss of energy is to prevent the thermal bridges in the external cladding of the building, see (Šulcová et al., 2008).

The Figure 6 shows a simple 2D simulation of heat conduction in a steel structure between inner and outer environment. There is a comparison between the joint without thermal separation and the joint with thermal separation of thickness 5, 10 and 20 mm. It is clearly shown how visible is the insulation effect of the intermediate layer in the joint.

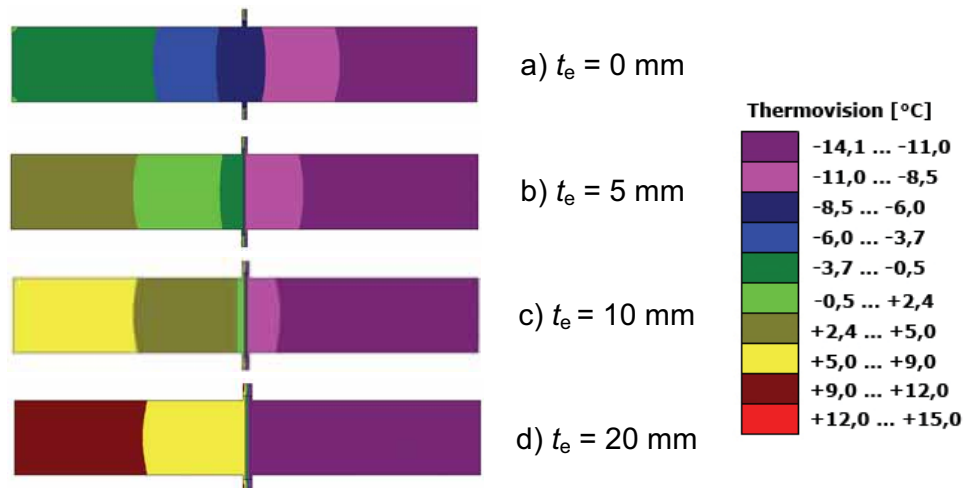


Fig. 6 Thermal simulation of the influence of the intermediate layer in the steel joint

The Figure 7 and 8 shows a 3D simulation of heat conduction in a real steel structure between inner and outer environment. The pictures were generated by the software TRISCO. There is a comparison between the thermal-insulating joint surrounded with thermal-insulation of thickness 100 and 200 mm. The joint is placed near the outer border of the surrounding thermal-insulation, closer to the exterior which is correct from the building and heat-engineering view. The thermal conductivity of the intermediate layer was chosen as 0,25 W/(mK), the thermal-insulation as 0,04 W/(mK) and steel as 50 W/(mK) to define the effective thermal-insulating joint. In case of 10 cm of surrounding thermal-insulation the increase of the thermal bridging portion on the whole flow of heat is 41% and with 200 mm of thermal-insulation 74% against the reference case with no steel beam. However, if no intermediate layer would have been used the thermal bridging effect would be 90% and 145% respectively, as shown in Fig. 9. The bolts which were not modeled would slightly increase the thermal bridge.

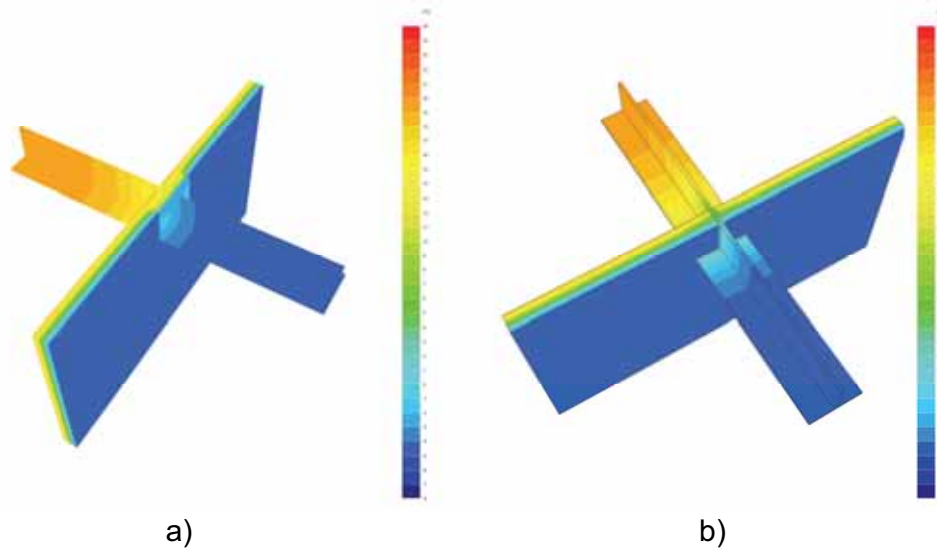


Fig. 7. 3D thermal simulation of the steel joint with 100 mm of surrounding thermal insulation

- a) Joint with intermediate layer, thermal bridge ratio 41%
- b) Joint without intermediate layer, thermal bridge ratio 90%

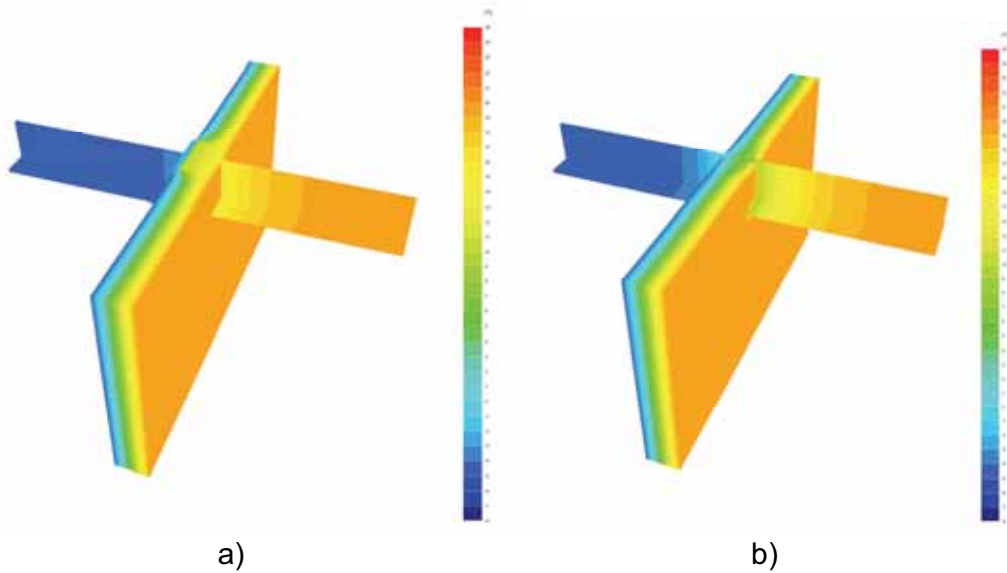


Fig. 8. 3D thermal simulation of the steel joint with 200 mm of surrounding thermal insulation
 a) Joint with intermediate layer (thermal bridge ratio 74%)
 b) Joint without intermediate layer (thermal bridge ratio 145%)

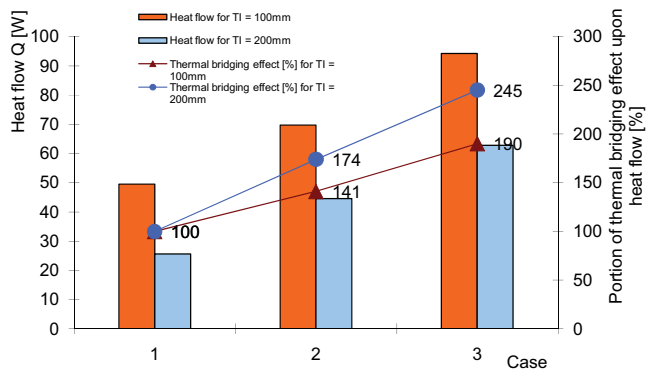


Fig. 9. Simulation of the thermal-insulating steel joint with surrounding thermal insulation
 Case 1 = Reference case (no beam, just thermal insulation)
 Case 2 = Beam with intermediate layer in the joint
 Case 3 = Beam without intermediate layer in the joint

SUMMARY

The research is trying to develop standardized design rules for thermal-insulating joints and introduce this new type of connections into a common use. The tendency is to give opportunity for steel structures and show the way how to construct buildings with low energy intensity and minimized heat costs. The bolted end-plate connection with intermediate thermal-insulating layer could be easily designed using the component method which determines the bearing resistance as well as the rotational stiffness of the joint. The predicted method needs to be verified by a couple of experiments. The presented type of joint is suitable for steel connections between inner and outer structures because it significantly contributes to the reduction of the thermal bridging effect in the external cladding.

ACKNOWLEDGEMENT

This paper describes of work on MSM 6840770001 Reliability, optimization and durability of building materials and constructions. The preparation of the paper was supported by grant GA ČR 103/08/H066. This support is gratefully appreciated.

REFERENCES

Nasdala L., Hohn B. and Rühl R. (2007), "Design of end-plate connections with elastomeric intermediate layer", *Journal of Constructional Steel Research*, Vol. 63, No. 4 (pp. 494-504), Oxford: Elsevier Ltd.

Sokol Z., Wald F. and Chlouba J. (2006), "Prediction of End Plate Joints Subject to Moment and Normal Forces", *Proceedings of the International Conference in Metal Structures*, Vol. 1 (pp. 235-240), London: Taylor & Francis.

Sokol Z., Wald F., Delabre V., Muzeau J. and Švarc M. (2002), "Design of End Plate Joints Subject to Moment and Normal force", *Eurosteel 2002*, Vol. 2 (pp. 1219-1228), Coimbra: Universidade de Coimbra.

Šulcová Z., Sokol Z. and Wald F. (2007), "Steel end-plate connection with thermal insulating layer", *Sustainability of Constructions – Integrated Approach to Life-time Structural Engineering* (pp. 3.109-3.114), Lisbon: Multicomp Lda.

Šulcová Z., Sokol Z. and Wald F. (2007), "Structural connections with thermal separation", *Proceedings of CESB 07 Prague International Conference*, Vol. 2 (pp. 672-677), Prague: Czech Sustainable Building Society and CBS Servis.

Šulcová Z., Sokol Z., Wald F. and Rabenseifer R. (2008), "Component method for connections with thermal separation", *Eurosteel 2008*, Graz (p. 6), accepted for publication.

HISTORIC SHEAR CONNECTIONS: RIVET AND MOMENT CAPACITY DATA

Scott Civjan
University of Massachusetts, Amherst, MA 01003, USA
civjan@ecs.umass.edu

Gershon Larsen
Weidlinger Associates, Inc. Cambridge, MA 02139, USA
glarsen@ma.wai.com

Eric Hines
LeMessurier Consultants, Inc. Cambridge, MA 02139, USA
ehines@lemessurier.com

ABSTRACT

Shear connections were obtained from two historic structures in the Boston area. Testing included the evaluation of individual rivets to determine effective test methods, tensile and shear strength, and relationship to Rockwell Hardness testing. Tests verified previously reported strength values, and determined that data from Rockwell Hardness testing was reasonably accurate and easiest to obtain. Four shear connections were cyclically tested, two beam to column and two beam to girder. Two connections were re-tested with concrete encasement. Results showed that the encased sections could reach moment capacities exceeding 25% of M_y even in the absence of top flange connection. Push over analysis of a three bay, five story structure was conducted to compare capacities of a traditional strengthened design analysis with the inherent capacities indicated by the test program. Partially restrained, encased connections increased the strengthened lateral capacities and may provide sufficient seismic resistance in the existing condition for some structures.

INTRODUCTION

Samples of historic connections were obtained during the renovation of two buildings in the Boston area. Referred to as Building 1 (1927 construction) and Building 2 (1940 construction), the structures consisted of steel frames with riveted connections and concrete encasement of members and connections for fireproofing. All encasement was plain concrete with no reinforcement. Original encasement remained on only one specimen, with encasement on another specimen placed by the research team. Renovations to each of these buildings did not trigger a formal seismic upgrade per the local Building Codes in place at the time of renovation. At the time, such an upgrade would have been required if the renovation included more than a ten percent alteration

of building mass or a renovation cost greater than fifty percent of the building value. Historic structure renovations are often limited to avoid upgrade requirements.

The goals of this project were to determine rivet material properties, experimentally obtain hysteretic behavior of “pinned” connections, and evaluate the lateral capacity of structures that include these connections. For design, these historic connections are typically assumed to act as pure “pinned” connections. Therefore seismic upgrade designs would depend entirely on a new lateral resisting system, which can be quite costly. Project results can be used to evaluate the inherent lateral resistance of existing structures, perhaps mitigating the need for extensive strengthening procedures and allowing cost effective renovations of a larger number of historic structures.

RIVET TESTING

The strength of individual rivets was evaluated through four methods. The goals were to evaluate test methods in addition to obtaining material properties. Rivets were tested in tension and in shear (in-situ condition), tested in tension after machining rivets into standard coupon dimensions, and tested for Rockwell Hardness data. Test samples are shown in Figure 1. In order to obtain tension test data on in-situ rivets, sections of the connection around the rivet were removed with the rivet intact, the rivet head ground smooth, and #7 reinforcing bars welded to the prepared head of the rivet (Figure 1a, five specimens). It was realized that grinding and welding operations in the vicinity of the rivet body might alter the material properties. However, failures occurred within the shank of the rivet, indicating minimal influence. Tension coupons were machined from the center material of rivets (Figure 1b, three specimens). The diameter was reduced to 0.250 ± 0.0005 inch and length of 1.000 ± 0.005 inch. These were then welded to prepared threaded ends. In-situ shear specimens were obtained by cutting sections around the rivets which extended through two steel sections, placing the rivet in single shear (Figure 1c, three specimens). Extension plates were welded to the existing plates to allow testing. These plates were welded such that the specimen would have minimal eccentricity. Finally, individual rivets were removed from the section and cut with a band saw longitudinally down the center of the rivet (Figure 1d, 21 specimens). These were used for Rockwell Hardness Testing (in accordance with ASTM A370.17). For each sample, 25 Rockwell B Scale values were recorded at a distribution of locations across the rivet area and averaged. Of these methods, tension coupons were the most time intensive to produce, while the other three specimens were relatively quick to obtain and evaluate. Only the tension coupons and Rockwell samples could realistically be removed with minimal damage to other connection materials.

Results were compared to Brokenbrough (2003), which recommends design values of $F_y=25-28$ ksi and $F_u=45-56$ ksi for rivets from 1924 to 1931 and $F_y=28-31$ ksi and $F_u=52-62$ ksi for 1939 to 1948. Design practice often notes shear capacities of approximately 0.6 times tensile strengths, though AISC has noted that values in rivets are often closer to 0.85 of tensile strengths. Rockwell Hardness values can be related to tensile strength

per ASTM A370. For values below the limits in this reference, the Mississippi Welder's Source (2005) provided guidance on the hardness and tensile strength relationship.

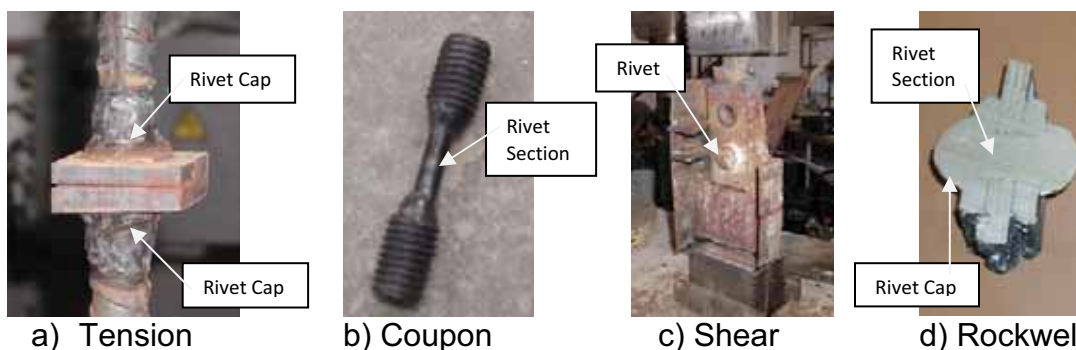


Figure 1: Rivet Test Specimens

For tests on in-situ rivets there are two cross sectional areas which could be considered, using either the nominal rivet diameter or the in-place rivet diameter (as it fills the hole). For this paper stresses are referenced to the larger in-place diameter to calculate stresses. All results are for rivets from Building 1 unless noted otherwise. Direct Tension on in-situ bolts provided F_u of 60.2 ksi, while direct tension coupon tests indicated $F_u=54.9$ ksi and also provided $F_y=35.0$ ksi and $E=30,800$ ksi. Direct shear tests resulted in $F_v=51.2$ ksi, in excess of 85 percent of the tensile stress of the rivets. Rockwell hardness test results were $F_u=58.4$ ksi for Building 1 and $F_u=59.2$ ksi for Building 2.

In general, rivet strengths are one potential failure mode in connections, but rarely control for the “pinned” connections evaluated in this study (typically controlled by flexibility of seat angles). The general tensile capacities obtained from Brokenbrough (2003) are conservative and sufficient for design. Shear capacities of rivets can conservatively be assumed to be 85 percent of the tensile capacity. Should testing be required to evaluate rivet properties, all 4 test methods provide a reasonable degree of accuracy. Rockwell Hardness values had a wider variation in results, but a sufficient sample size can be obtained relatively quickly through averaging numerous readings on a single rivet and quickly preparing a large number of rivets. Tension coupons, while requiring the most effort, reported lower tensile strengths and provide additional information (F_y and E). It is noted that all rivet materials were able to be welded and machined. Direct test methods are dependent on the in-situ rivet diameter, which can vary within a structure.

CONNECTION TESTING

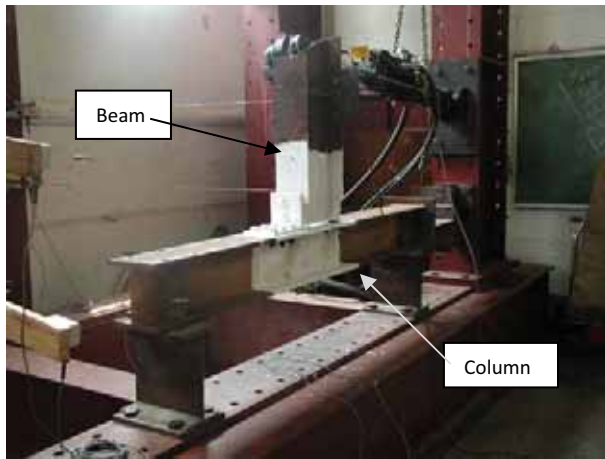
Four different “pinned” connections were obtained and evaluated to determine whether they could reliably be considered to provide partially restrained connection behavior. Connections included two beam to column connections: one seated beam connection with top stabilizing angle from Building 1 (Specimen 1CM1, Figure 2a) and one seated

beam connection with web stabilizing angle from Building 2 (Specimen 2CM1, Figure 3). Two beam to girder connections were also obtained, both double angle shear connections from Building 2 (Specimens 2CM2 and 2CM3, Figure 2b). Since the purpose of the research was to evaluate beam to column connections, a ¼ inch stiffener was welded to the 24WF94 girders opposite the beam connection in order to restrain girder web distortions. Specimen details are provided in Table 1. The contractor removed all Building 2 beam sections close to the connections and therefore specimens required the addition of extension beams for testing. These extensions consisted of a W8x40 connected through an end plate welded to each section and extensions varied in length from three to five feet. Typical tests are shown in Figure 2, with tests following the load sequence of Table 2. Test setup for specimen 2CM1 differed from 1CM1 in several ways. The connection attached to the top of an existing column, an extension beam was required, and the longitudinal movement of the column was rigidly restrained at the connection. Test setup for specimen 2CM2 differed from 2CM3 in that a longer extension beam was used. Details of test setups can be found in Larsen (2006).

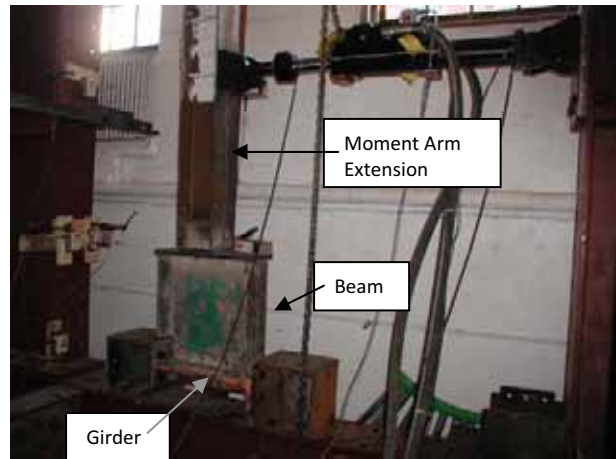
Two specimens were tested with and without concrete encasement. Specimen 2CM1 had the original concrete encasement (actual strength not determined) included at the connection location. The specimen was initially tested with this encasement intact. The encasement was then removed and the connection tested as a bare steel specimen. Specimen 2CM3 was originally tested as a bare steel specimen. Then the specimen was encased with plain concrete which was flush with the top flange and extended 3 inches below the bottom flange. Concrete compressive strength at the date of testing was 5.68 ksi. Encasement can be seen in Figure 4.

Table 1: Specimen Details

Specimen	Components		Connecting Angles (length) ¹	Beam Connectors	Column Connectors
	Beam	Supporting Member			
1CM1	12WF28	W8x40 (new) column flange	Top: L 6 x3.5x5/16 (6 in.)	2 rivets 3/4 in. dia.	2 bolts 7/8 in. dia.
			Bottom: L8x 6 x1/2 (6 in.)	2 rivets 3/4 in. dia.	6 bolts 7/8 in. dia.
2CM1	14WF34	10WF54 column web double sided	Web 4 x3x3/8 (6 in.)	2 rivets 7/8 in. dia.	2 rivets 7/8 in. dia.
			Bottom: L6x 4 x1/2 (6 in.)	2 rivets 7/8 in. dia.	4 rivets 7/8 in. dia.
2CM2	21WF68	24WF94 stiffened girder web	Web L 4 x 3 x3/8 (14-5/8 in.)	5 rivets 7/8 in. dia.	5 rivets 7/8 in. dia.
2CM3	21WF68	24WF94 stiffened girder web	Web L 4 x 3 x3/8 (14-5/8 in.)	5 rivets 7/8 in. dia.	5 rivets 7/8 in. dia.
Note 1: Bold leg is attached to beam					



a) 1CM1



b) 2CM3

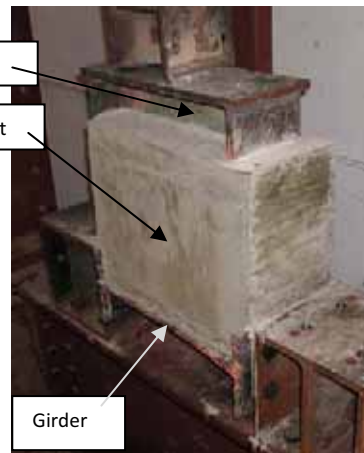
Figure 2) Specimen Setup



Figure 3) 2CM1 Connection



a) 2CM1

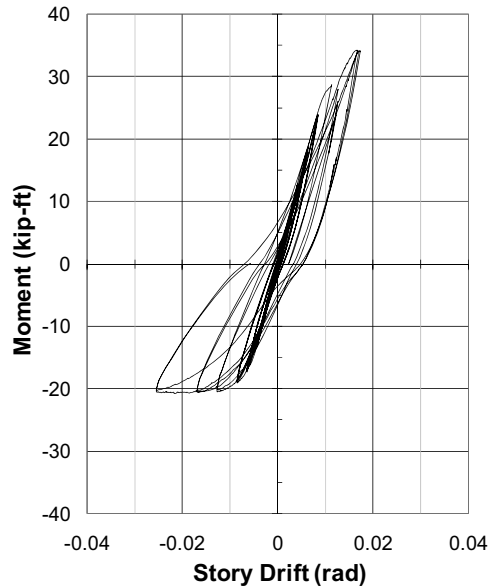


b) 2CM3

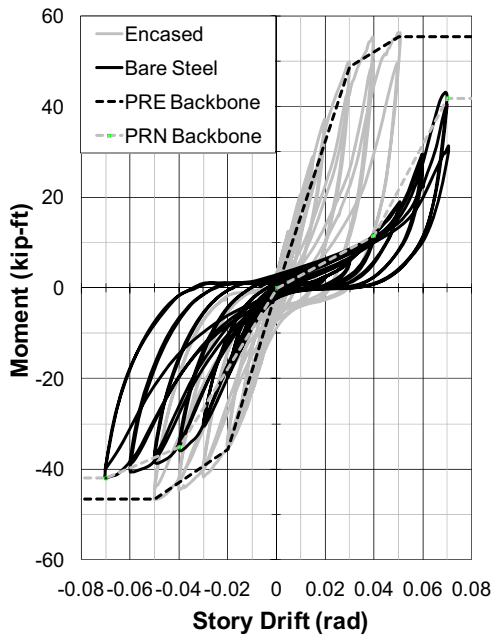
Figure 4: Encasement of Connections

Table 2: Test Sequence

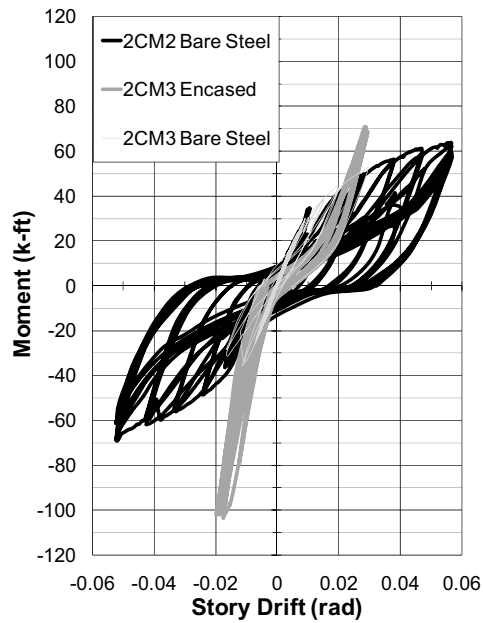
Drift (Radians)	Cycles
0.00375	6
0.005	6
0.0075	6
0.01	4
0.015	2
0.02	2
0.03	2
Subsequent 0.01	2 each



a) Specimen 1CM1



b) Specimen 2CM1



c) Specimens 2CM2 and 2CM3

Figure 5: Moment vs. Story Drift

Results of moment versus story drift for specimens are shown in Figure 5. Moment is evaluated at the face of the connection support, while drift is measured to the connection centerline in these plots. Drift differs slightly from Table 2 as load procedures referenced values to the connection face as well.

For 1CM1 (Figure 5a), it is noted that the capacity is significantly lower in negative bending (top flange in tension) and was limited by the yielding and “opening up” of the smaller top flange angle. In positive bending (top flange in compression) the specimen ultimately exhibited some local flange buckling and specimen twist. Twist was predominantly due to non-symmetric locations of the rivets, which were offset from the angle and beam centerlines.

Results for 2CM1 with and without encasement are shown in Figure 5b. The encased specimen exhibited similar stiffness in both positive and negative load directions, and resulted in positive moment capacity which was even larger than the negative moment capacity. This is due to the concrete being effective in compression, but pulling away from the top of the specimen when in tension. Negative moment capacity was improved over the bare steel test, but not significantly since there was no positive connection to the top flange of the beam. Testing was concluded once softening was observed to avoid damaging the connection prior to the bare steel testing. It is noted that bare steel connections had very little initial stiffness, especially in positive moment, with lack of top flange attachment and angle deformations controlling behavior. The very low stiffness in positive bending may be due to damage sustained when initially testing the encased connection.

Specimens 2CM2 and 2CM3 had very similar behavior in the bare steel condition, though only 2CM2 was tested through the non-linear range. Testing of 2CM3 was stopped to avoid specimen damage once non-linear response was observed. When concrete encasement was provided the initial connection stiffness was not significantly changed, but the connection did not exhibit any softening due to connector yielding as was observed in the bare steel tests. It was noted that the concrete encasement in 2CM3 cracked fairly early at the corners, as shown in Figure 6. Subsequent to this the encasement rotated as a solid block around the beam. However, this did not limit the connection capacity, as high moments were attained in both positive and negative moments. Encased capacity remained elastic well beyond the point where bare steel specimens exhibited damage and non-linear behavior. Testing was stopped due to limitations of the actuator.

MODELING

A 3 bay, five story structure was modeled in SAP2000. Overall sizes and dimensions were loosely based on Building 2, with column spacing of 18'-6", story height of 14'-8", W14x34 beams and W12x120 columns oriented with their strong axis in the plane of bending. Four conditions of beam to column connectivity were included. For the strengthened condition one bay was considered to include full moment connections, while all other connections were assumed to be pinned, partially restrained, or partially restrained with encasement (MP, MPRN and MPRE respectively). Of these conditions, MP would relate to a seismic upgrade design condition, MPRE would be the actual upgrade condition. The existing condition was modeled as entirely partially restrained with encasement (APRE). Partially restrained connection behavior was based on the

test results from 2CM1 (Figure 5b), which is a relatively weak connection with respect to moment capacity as it did not include any top flange connection. Hinge behavior was included as a kinematic link property with tri-linear behavior based on the backbone curve of test data. No degradation in experimental capacity was observed through 0.05 radian of story drift (Figure 5b), and no subsequent degradation was included in the analysis. It is important to note that MP and MPRE conditions would typically apply to 2 perimeter frames in the structure, while APRE would apply to all frames in the structure. Analysis only considered one frame of a structure, arbitrarily chosen as three bays. Pushover analysis was used as a basis for comparison.

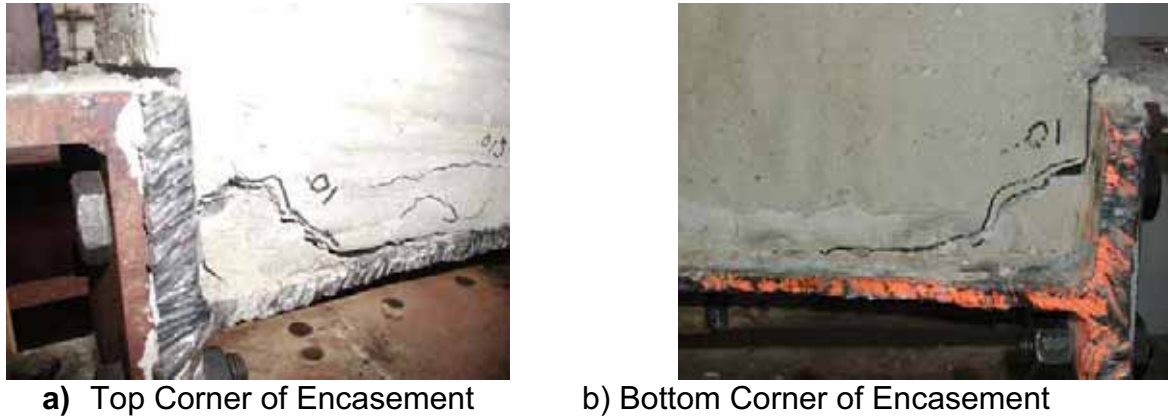


Figure 6: Concrete Encasement Cracking

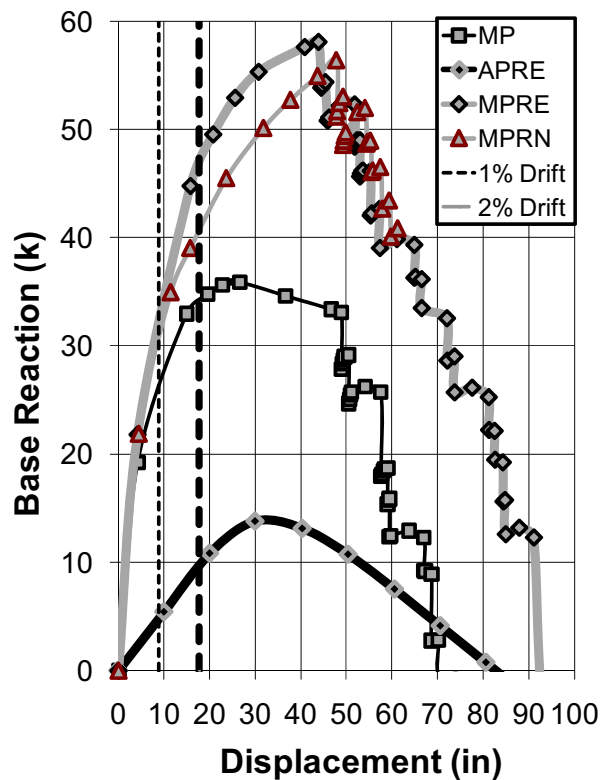


Figure 7: Pushover Analysis

Table 3: Pushover Analysis Results

Analysis	Base Reaction Kips (Percent MP Condition)		
	Maximum	1% Drift	2% Drift
MP	35.9 (100)	25.1 (100)	34.0 (100)
MPRN	56.4 (157)	30.0 (116)	40.6 (119)
MPRE	58.2 (162)	30.9 (123)	46.6 (137)
APRE	13.8 (38)	4.8 (19)	9.6 (28)

Results of the analysis can be seen in Figure 7 and Table 3. Incorporating the existing connection strength into a strengthening analysis resulted in a significantly higher peak base reaction (increased by 62 percent, though at a much higher drift ratio). At a constant average story drift of 2 percent (roof displacement divided by building height) base reactions were increased by 37 percent. While at 2 percent drift the APRE case only accounted for 28 percent of the MP case base reaction, but this is not insignificant. This indicates that an assumed strengthened condition (MP) where $\frac{1}{4}$ of the frames in a structure are strengthened would have similar behavior to the originally existing structure with encased shear connections. This analysis included the tested connection that had no top flange connection and conservatively assumed that a structure only included three bays

The fundamental period of the structure was significantly altered through strengthening, approximately 0.3 seconds for MP, and exceeding 2.0 seconds for APRE. This would significantly affect the demand on the system for a given earthquake or design spectrum.

CONCLUSIONS

Extensive renovation of older buildings often requires strengthening to resist seismic forces not accounted for in the original design. Strengthening of the lateral resisting system involves significant effort and cost, even in areas of low to moderate seismic activity such as Boston. Conservative estimates for the capacity of existing lateral resisting systems and connections are common due to lack of data on their seismic performance. In the case of older riveted structures, “pinned” connections are commonly assumed throughout a structure, but actual details provide for some moment transfer, especially in structures where concrete encasement was used as a method of fireproofing. The purpose of this research was to investigate the moment capacity of “pinned” riveted connections and include these effects in the evaluation of older building lateral load performance. The project was intended to provide a conceptual basis for design and testing by selecting a few representative connections of this era, rather than providing an inclusive study of the wide variety of existing connection details.

To this end, riveted connections were obtained from 2 East Coast buildings undergoing renovations. Experimental testing included tests on individual rivets as well as bare steel and concrete encased comparisons of riveted “pinned” shear connections. Using the results from the experimental testing, sample building frame performance was evaluated through push over analysis.

Rivet ultimate tensile capacities were in the range of 55 to 60 ksi and ultimate shear capacities exceeded 85 percent of tensile values. Rockwell hardness tests were easiest to obtain and provided relatively accurate results. Tests of “pinned” connections showed that bare steel connection capacities were limited by angle yielding and slippage. However, when these sections were encased with concrete capacities approached 30 percent of M_y . Frame analysis compared pinned connection assumptions typically used

in design to actual test results. These indicated that existing connections can contribute significantly to the overall lateral resistance of a structure. By accounting for actual connection behavior, it is possible that seismic upgrades could be minimized or even avoided in older buildings located in regions of low to moderate seismic activity.

ACKNOWLEDGEMENT

This research was made possible through the Brack Structural Engineering Graduate Student Fellowship at UMass, Amherst. This contribution is greatly appreciated.

REFERENCES

"A 370-97a: Standard Test Methods and Definitions for Mechanical Testing of Steel Projects." *Selected ASTM STANDARDS for Structural Steel Fabrication*. West Conshohocken, PA: ASTM, 2001.

Applied Technology Council. *NEHRP Guidelines for the Seismic Rehabilitation for Buildings*, FEMA Publication 273. Washington, DC: October, 1997.

Bethlehem Steel Company. *Bethlehem Sections Catalogue S-40*. Bethlehem, PA: BS Company, 1931.

Brokenbrough, R. L. (2003). *STEEL DESIGN GUIDE SERIES 15: AISC Rehabilitation and Retrofit Guide*. Chicago, IL: AISC.

Forciera, G.P., Leon, Roberto T., Severson, B.E. and Roeder, Charles W. (2002) "Seismic Performance of Riveted Connections." *Journal of Constructional Steel Research*. 58: 779-799.

Kulak, G.L., Fisher, J.W. and Struik, J.H.A. (2001). *Guide to Design Criteria for Bolted and Riveted Joints*. Second Edition. Chicago, IL: AISC, 2001.

Larsen, G. (2006). *Capacities of Historic Riveted Steel Connections*. M.S. Thesis. The University of Massachusetts. Department of Civil and Environmental Engineering.

Roeder, C. W., Knechtel, B., Thomas, E., Vaneaton, A., Leon, R. T. and Preece, F. R. (1996) "Seismic Behavior of Older Steel Structures." *Journal of Structural Engineering*. April 1996: 365-373.

Sarraf, M. and Bruneau, M. (1996) "Cyclical Testing of Existing and Retrofitted Riveted Stiffened Seat Angle Connections." *Journal of Structural Engineering*. 762-775.

Mississippi Welder's Supply. (1999). "Tensile Strength to Hardness Conversion Chart." Hobart Filler Metals. <<http://www.mwsco.com/kb/articles/19990630e.htm>> Accessed April 2005.

PERFORMANCE OF A HIGH-STRENGTH FRICTION GRIP CONNECTION WITH OPEN SLOTTED HOLE

Wylliam Husson,

Luleå University of Technology, Luleå, Sweden
Wylliam.Husson@ltu.se

Milan Veljkovic

Luleå University of Technology, Luleå, Sweden
Milan.Veljkovic@ltu.se

ABSTRACT

With constantly increasing demand for higher towers supporting multi-Megawatt wind turbines, driven by the need to use renewable energy sources, cost optimization of the steel tower becomes important and commercially justified. Towers for wind turbines are commonly made of tubular sections assembled by ring-flanges placed on the inner side of tube tower. Design of the tower is governed by rather low fatigue resistance of the connection, ranked in load category of 50 according to Eurocode, EN1993-1-9. This connection imposes limit on stresses in the tube and impairs the efficiency of the whole structure. High-Strength Friction Grip connection with long open slotted hole is expected to have better fatigue performance and thus improve competitiveness of the towers.

This paper presents a part of an ongoing research project and result of static tests on a segment of the tower connection. A total of 25 experiments were performed on hot rolled steel plates and weathering steel plates, and are shown here. Tension controlled bolts (TCB) grade S10T, which is equivalent to 10.9 grade (Cosgrove, 2004), were used. Bolts M20 and plate thickness 8mm were used in nine preliminary tests. Bolts M30 and 25mm-thick plates were used in 16 experiments to investigate behaviour of the “real tower” connections. Experimental results are compared to the prediction according to EN 1993-1-8

INTRODUCTION

Results presented here are part of the on-going RFCS (Research Fund for Coal and Steel), HISTWIN, where partners from 5 countries working on various topics. The partners are:

- Luleå University of Technology, Division of Steel Structures, Sweden (LTU)
- Rheinisch Westfälische Technische Hochschule Aachen (RWTH), Lehrstuhl für Stahlbau, Germany (RWTH)
- Germanischer Lloyd Industrial Services GmbH, Germany (GL-WIND)
- Aristotle University of Thessaloniki - Institute of Steel Structures, Greece (AUTH)
- Repower Portugal Equipamentos Eólicos SA, Portugal (REPOWER)

- University of Coimbra, Faculty of Science and Technology, Department of Civil Engineering, Portugal (FCTUC)
- Rautaruukki Oyj, Finland (RUUKKI)

Results and analysis on non-standardized High Strength Friction Grip connection presented here is a part of the authors' contribution to the project.

The steel tower costs is about 160.000€ per installed MW (Megawatt) for wind turbines with nominal outputs between 1MW and 2MW. Having in mind a huge expansion of use of wind power as the energy source the optimization of the tower design offers possibilities for substantial savings.

The steel towers for wind turbine are most often made of tubular section sections. The sections are transported in section 20-30m long and assembled using flanges commonly welded only at the inner side of the tube. The connection is bolted with high strength bolts, see Fig. 1. Prying effects have been shown to introduce disadvantageous nonlinear relations between external loads and bolt forces (Seidel, 2001). It is well known that threaded fasteners have low fatigue strength and are consequently ranked in load category of 50 (EN1993-1-9). Therefore the design of the towers is intrinsically governed by fatigue resistance.

High Strength Friction Grip connections were shown to have fatigue strength similar or better than that of good but welds (Cullimore, 1982). These joints also have higher stiffness and good energy dissipation properties. Their implementation in towers may shift the design limitations to shell resistance and thus improve the structural efficiency.

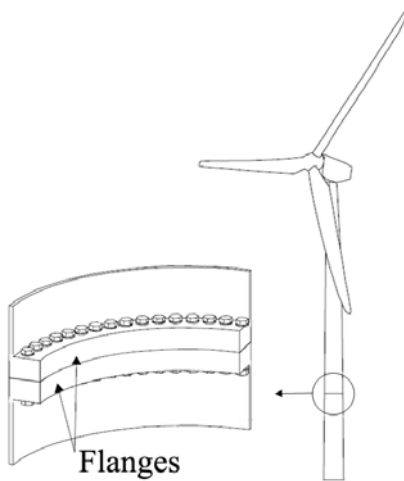


Fig. 1. Flange type connection

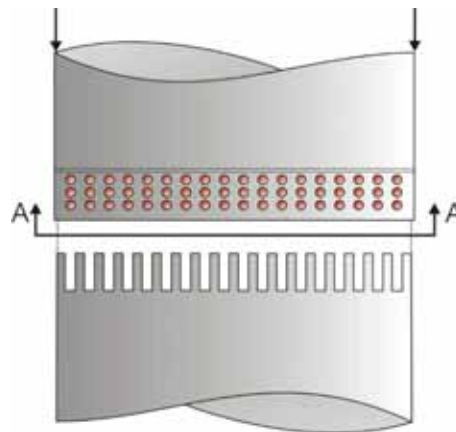


Fig. 2. Concept of a new friction type connection

TESTING PROGRAMME

The purpose of the segment test, shown in Fig. 3 and Fig.10-12, is to get an insight in the behaviour of the new connection type as well as to obtain characteristic as input for the Finite Element Analysis of the tower in the later stage of the project.

Specimens for preliminary segment tests

The clamping force was provided by a row of three M20 tension controlled bolts connecting two 8mm thick plates. The bolts were mounted in normal clearance holes 22mm diameter on the side of the bolt head and in the long and open slotted holes in the load direction on the nut side. According to the producer's installation instruction, no washer was necessary under the head. A single cover plate replaced the usual washers under the nuts in order to have a more uniformly distributed contact. Since the friction between nut and washer has a significant influence on the tightening torque, the cover plate material was chosen so it provides similar contact properties. Hardened steel Raex400 produced by Ruukki has hardness of HBW 360-420, equivalent to that of the standard washers, H_RC 35-45. Diameter of the holes was 21mm.

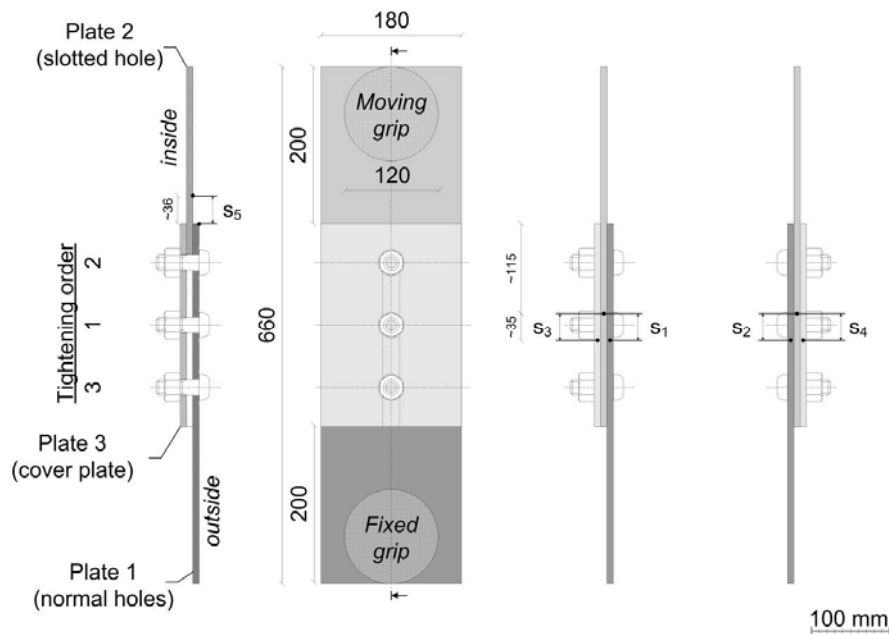


Fig.3 Segment specimen layout in the preliminary tests

Faying surfaces

Surface of plates made of weathering steel COR-TEN B of grade S355 are shown in Fig. 4. To achieve a surface quality of class A according to EN1090 [3], the plates were grit-blasted with steel grit of size G70 to a quality Sa2.5 (according to Swedish Visual Standard) i.e. near white metal. All dust was removed and the plates cleaned with acetone. The plates were assembled shortly afterwards therefore no rust was present. The surfaces were very rough to the touch.



Fig. 4. visual aspect of rust free COR-TEN B



Fig. 5. Ethyl silicate zinc coating appearance

The plates made of S355 steel were coated by Ethyl silicate zinc. They were first grit-blasted with steel grit of size G70 to a quality Sa2.5 and then coated with a two component ethyl silicate zinc rich paint with *TEMASIL 90* from *Tikkurila Coatings*. According to the producer, the coating can be used as single coat or as primer. The zinc content is between 70% and 90%. A coat thickness of 50 μm to 80 μm was required.

The coating presented a greenish grey appearance and seemed to be made of two layers; a pigmented outer layer and a layer of zinc adhering to the steel (see Fig).

Observations from preliminary tests

The central bolt was tightened first and then the bottom and top bolt, Fig.3. In the contrary to recommendations, the fasteners were not snug tightened first but fully preloaded at once. This leads to non-homogeneously distributed bolt forces. When a new bolt is tightened the additional clamping force slightly reduces the reaction of the plates on the already tightened bolts thus reducing their pretension. The phenomenon is greatest at the central bolt which pretension decreases in average by about 4,4%.

After pre-tensioning, the specimens were left overnight before testing to allow approximately 12 hours for relaxation of the bolts.

The pretension loss between 10s and 12hrs after tightening is less than 9% for the central bolts and 4% for the outer bolts, and all had a pretension higher than required by EN1993-1-8. Taking only the outer bolts into consideration the design force according to (ISO 2394, 1998) becomes 178kN which is more than 3% higher than the design force of EN1993-1-8.

Measurements

The applied tensile load was monitored by the testing machine load cell and a displacement of the hydraulic pistons was recorded as a measure of the total elongation.

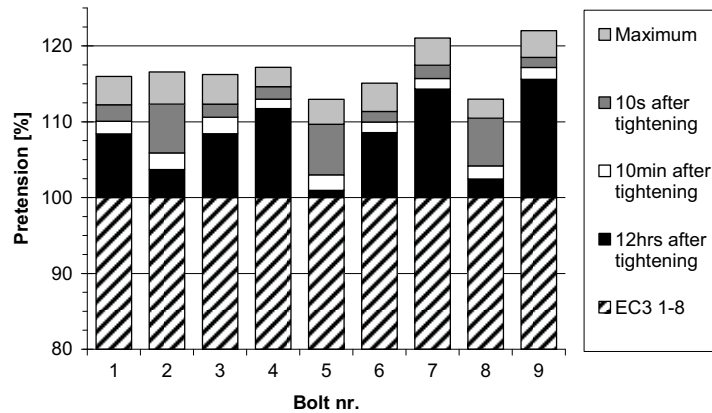


Fig. 6. Pretension of bolts connecting 8mm thick plate

The bolt forces were continuously measured after the tightening and throughout testing in order to have complete control of the actual level of pretension and distribution of the clamping forces during traction of the specimens.

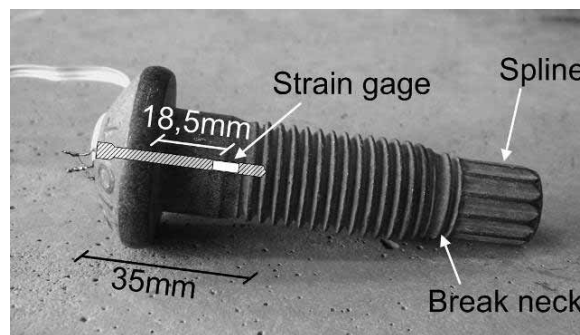


Fig. 7. Strain gages glued into Tension Control Bolt (TCB)

Relative displacements were measured with linear transducers to monitor the slip, at five different locations, Fig.3. The transducers were calibrated for strokes up to 4mm with an accuracy of 50 μ m.

The specimens were maintained by the hydraulic grips of the tensile test machine and pulled with stroke control at the constant rate of 5 μ m/s. The measurement frequency was 5Hz.

Experimental results of the preliminary tests

Results from one specimen, which is representative to all performed tests, are discussed in the paper, as shown in Fig.8 and Fig.9,.

At the beginning the behaviour is supposed to be linear. However, the load displacement curve shows some nonlinearity before the slip load (1) is reached. The linear relative slip is very small (microslip) due to local deformations of the plates at location where the contact pressure is low. The tensile load is still transferred by friction between the plates up to the ultimate load (2) where friction is overcome and

the two plates show the relative slip (macroslip). The drop in the transferred load can be explained by a lower cinematic friction coefficient and a small lost of the clamping force due to the abrupt introduction of bending in the bolts. The cover plate (Plate 3) is attached to the Plate 2 which indicates that the friction under the nuts is lower than that with the underlying plate. This is reasonable since the nuts were greased prior to tightening. Macroslip then proceeds until the clearance between holes in the cover plate and bolt shafts is closed and accordingly the bearing occurs (3) which leads to an increase in the tensile load since the Plate 1 additionally has to overcome the friction with the cover plate that is now maintained by the bolts which head "stick" on the fixed plate. The consequent increase in bolt bending leads to a faster decrease of the axial force of the outer bolts. The load then drops slightly when the static friction under the bolts heads is overcome. Now the bolt heads slip relatively to the fixed plate until the shafts are fully bearing (5).

The test is designed so the failure mode of the connection was ductile, Fig.8. The friction between the bolt heads and nuts is low enough so that the transmitted shear force becomes too small to produce bearing or shear failure. The maximum load drop of about 20% may be principally due to change from static to cinematic friction already noticeable at low velocity (Booser, 1984).

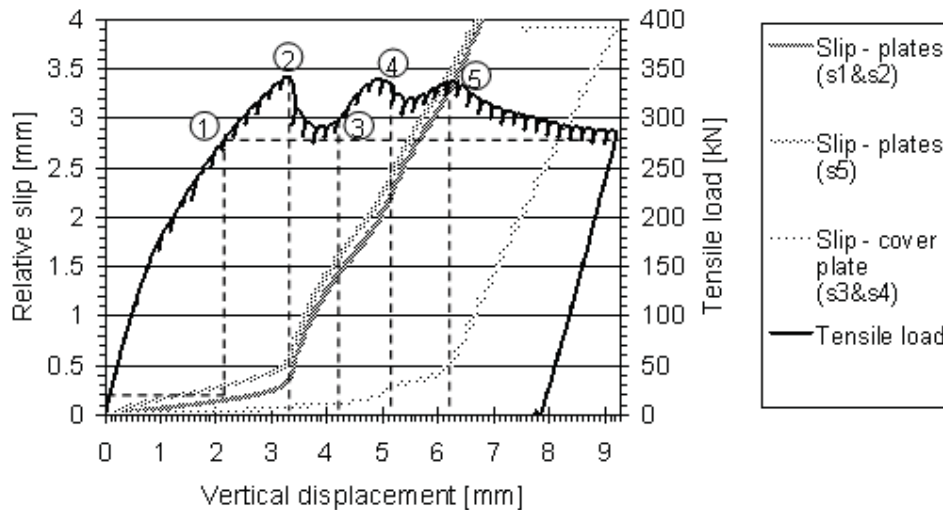


Fig. 8. Slip behavior

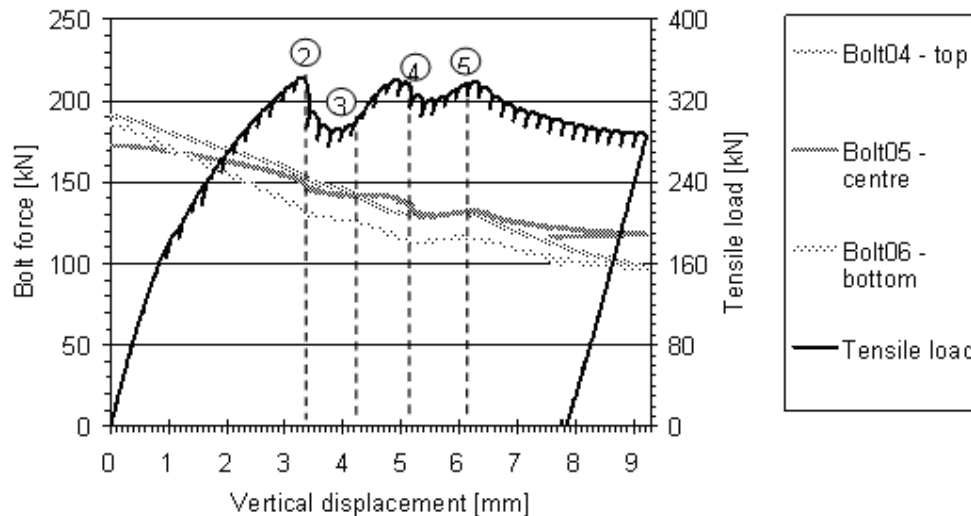


Fig. 9. Bolt Forces behavior in the preliminary series

SEGMENT TESTS FOR A REAL TOWER APPLICATION

Specimens

The bolts M30 grade S10T and 25 mm thick plates were used for specimens shown in Figures 10-12. *Greenkote*[®] is used for their coating. The bolts are tightened from the stiffest part of the connection outwards, i.e. from the lowest to the highest bolt number. TCBs are delivered as packages including nuts and washer and should be assembled as such to ensure the right amount of pretension. Moreover the installation process of the strain gages involves use of lubricants and solvents, and curing of the glue is done at high temperatures. This is thought to affect the coating and its frictional properties. Therefore it was not considered relevant to test the tightening performances of TCBs. Instead the fasteners were pre-tensioned with the shear wrench while reading the strain gage response. A target of 400kN, equivalent to the nominal value of EN1993-1-8, was fixed.

The specimens were pulled in load control mode at a rate of about $5\mu\text{m}\cdot\text{s}^{-1}$. Specimens 1x3-zinc were tested at LTU's machine with hydraulic grips. The other specimens with higher resistances were tested in a machine at Ruukki with self-tightening grips. In both cases care was taken so no bending was introduced because of the specimen eccentricity. However, the two machines having different lateral rigidities may have slightly different boundary conditions and load introductions. A small in-plane eccentricity was observed for the test with the Ruukki's machine. This was noticeable by a slight tilting of the plates.

The bolts were continuously monitored with help of BTM-6C strain gages installed in the shank and previously calibrated by tensile tests. The relative slip of the plates (s_x) was measured at 5 different locations with crack opening devices installed between steel edges spot welded on the plates.

Experimental results

The overall behavior of the specimens was similar as in case of preliminary tests. The relative magnitude of the bolt force drop was relatively constant for the specimens with 3 bolts. With 6 bolts the drop was less but the variation more important. The values also differed between 1x3-zinc and 1x3-ws with averages of about 25% and 40% respectively.

Most of the clamping loss is not recovered when the load is removed. The bolt where the slotted hole is open generally experienced a slightly greater decrease, except for specimens 1x3-ws where it is the opposite. These specimens had also the greatest tensile stresses and consequently the greatest clamping losses. In the long specimens 1x6-zinc, no difference was noticeable in the behavior of the central bolts (B2 to B5).

Typical measurements of relative displacements at the side edges are showed on Fig. 13. In the long specimens, at the joint centre, the initial slope was smaller indicating that lower shear stresses were transferred. This indicates that the proportion of load transferred by the leading bolts is maximal and decreases towards the joint centre.

The measurements at the edges perpendicular to load transfer incorporated a component of the material elongation much higher than that expected from micro slip. Therefore, it was not possible to interpret this data with regard to the latter.

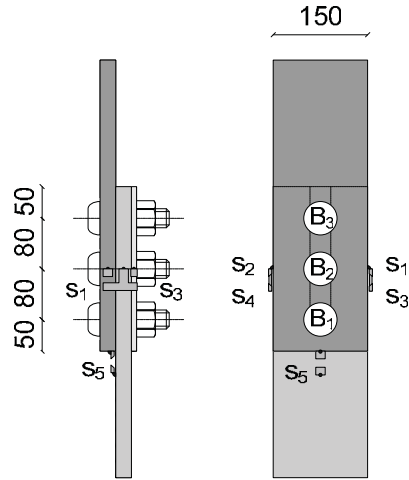


Fig. 10. Segment test specimen (1x3-zinc and 1x3-ws)

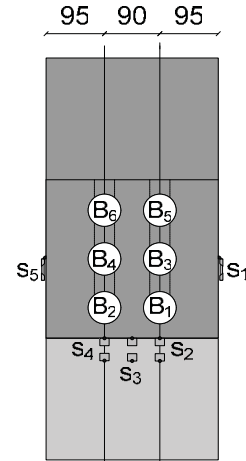


Fig. 11. Group test specimen (2x3-zinc)

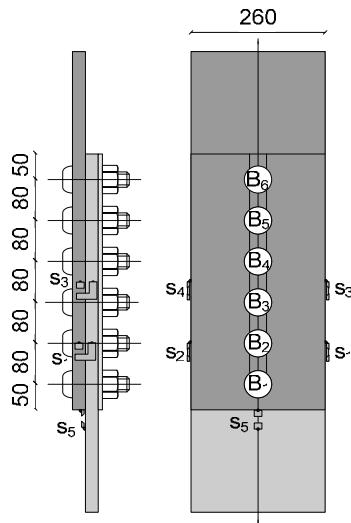


Fig. 12. Segment test specimen (1x6-zinc)



Fig. 13. Slip measurement device

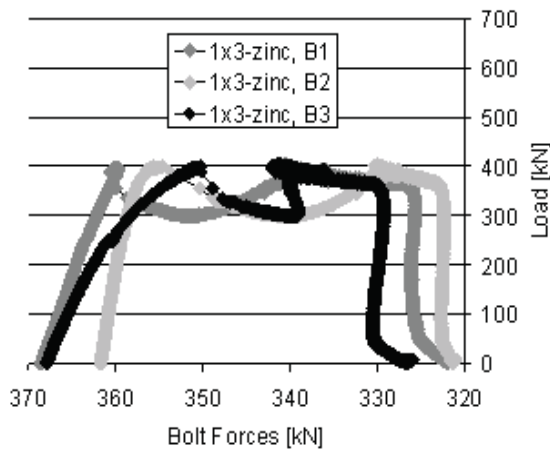


Fig. 14. Reduction of pre-tension force

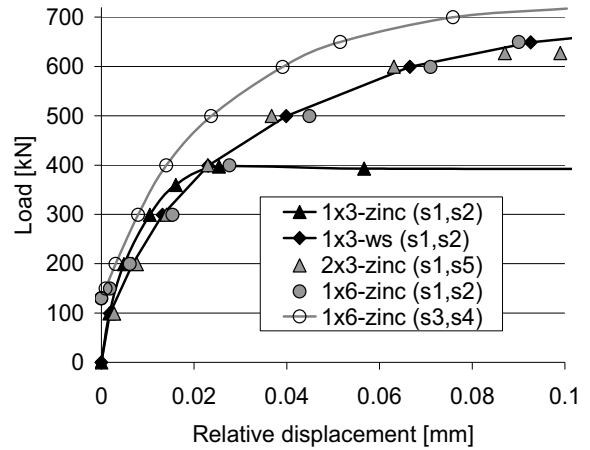


Fig. 15. Typical displacements at side edges

Resistance compared to EN1993-1-8

The design resistance of EN1993-1-8 for High Strength Friction Grip connections with a single friction surface is given in Eq. (1).

$$F_{S,Rd} = \frac{k_S}{\gamma_{M3}} \mu \sum_{\text{bolts}} F_{P,C} \quad (1)$$

where k_S , correction factor for oversized or slotted holes
 γ_{M3} partial factor, 1.25
 μ friction coefficient
 $F_{P,C}$ bolt pretension

This resistance model was assessed using the statistical method proposed in Annex D of EN1990 and the corresponding value of k_S was derived.

The experimental resistance (R_e) taken as the ultimate load is compared to the theoretical resistance (R_t) calculated with characteristic values. As it was not possible to determine it for each specimen an average value was taken for the friction coefficient.

As can be seen on Fig. 16 the specimens with 3 bolts have a similar R_e/R_t ratio whereas the specimens with 6 bolts have a lower value. The discrepancy is most noticeable for the specimens with 2 rows This tends to indicate a group effect which would require another resistance model for more accuracy. However, for the sake of simplicity, a single resistance model was preferred and all specimens were therefore considered.

The “Least Squares” best-fit to the R_e - R_t slope, $b=0,743$, is illustrated by the solid line in Fig. 17. The coefficient of variation is taken as 15% for the friction coefficient. It is about 4% for the total clamping force which is that of a group of 3 bolts, (Cosgrove, 2004). With these conservative values the maximal correction factor is $k_S=0.65$ which is very close from the actual value of 0.63 recommended in EN1993-1-8.

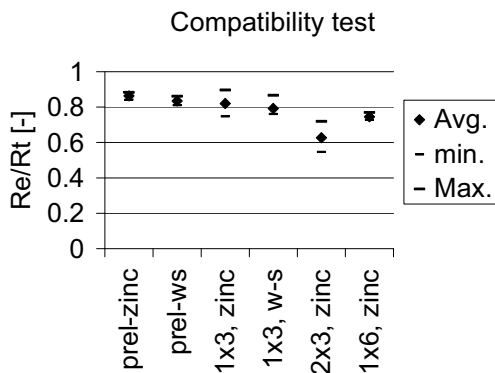


Fig. 16. Compatibility test

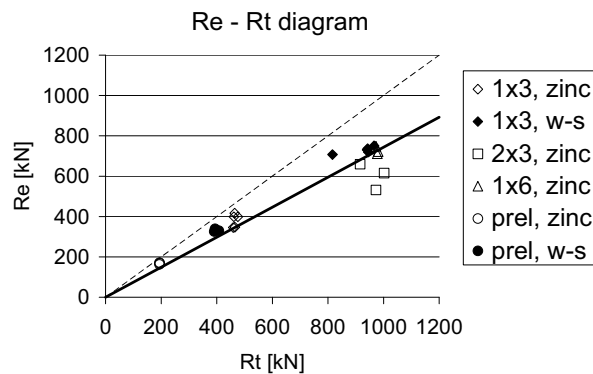


Fig. 17. Re – Rt diagram

CONCLUSION AND FURTHER WORK

Based on totally 25 segment tests following conclusions may be obtained:

- Resistance of connections with 3 and 6 bolts in a single long slotted hole is rather consistent with EN 1993-1-8.
- A group effect expressed in lower R_e/R_t ratio, up to 20%, exists in the segment tests performed on double row specimens with totally 6 bolts. The design resistance should be consequently reduced for multi row connections. This issue will be of major concern in further numerical study.
- For ethyl zinc silicate coating the average friction coefficient was $\mu=0,42$ with a variation of about 11%. For rusty weathering steel the average friction coefficient was $\mu=0,79$ with a variation of about 5%

ACKNOWLEDGEMENTS

Experimental results were obtained within the on-going project: HISTWIN, High-Strength Steel Tower for Wind Turbine, 2006-2009. The financial support obtained from the Research Programme of the Research Fund for Coal and Steel and the co-operation with our partners: RWTH Aachen, Germany; GL-WIND, Germany, AUTH, Thessaloniki, Greece; REPOWER, Portugal; FCTUC, Coimbra Portugal; and RUUKKI, Finland is gratefully acknowledged.

Financial support received from Energimyndigheten, Dnr. 2008-000225 is acknowledged.

REFERENCES

- Booser, E. R. (1984): CRC Handbook of Lubrication, Volume II - Theory and Design. *CRC Press, Inc.*
- Cosgrove, T.C. (2004), Tension Control Bolts, Grade S10T, in Friction Grip Connections, *The Steel Construction Institute*, SCI 234,
- Cullimore, M. (1982), Fatigue of HSFG Bolted Joints, *IABSE reports*, Vol.37, (pp.715-723).
- EN 1993 - Part 1-8: (2005), Eurocode 3, Design of joints,
- EN1993-1-9 (2005), Eurocode3: Design of steel structures, Part 1.9: Fatigue, European Committee for Standardisation
- ISO 2394: General principles on reliability for structures, 1998
- prEN 1090-2-Part 2,(2007), Technical requirements for the execution of steel structures - Stage 49,
- Seidel, M. (2001), Zur Bemessung geschraubter Ringflanschverbindungen von Windenergieanlagen, Universität Hannover.

CONNECTION RESEARCH NEEDS

Reidar Bjorhovde

The Bjorhovde Group, Tucson, AZ, USA

rbj@bjorhovde.com

ABSTRACT

The paper summarizes the research needs that have been identified by the workshop authors. The subjects include the items that have been discussed in the various technical sessions, as follows: (1) Bolts, welds and related fastening issues; (2) Connections for braced frames, including seismic performance concerns; (3) Seismic considerations for moment and other types of connections and frames; (4) Connections with tubular (HSS) elements; (5) Connections utilizing high strength steel elements; (6) Methods of analysis for connections and structures, including semi-rigid concepts for steel and composite construction; (7) Robustness and structural integrity of connections and structures, including fire resistance; (8) Design code criteria for steel connections; and (9) Special connection types and performance considerations.

INTRODUCTION

The Sixth International Workshop on Connections in Steel Structures has presented a range of subjects that address the state-of-the-art. Based on advanced analytical and experimental studies, the subjects incorporate a variety of issues. Specifically, the topics are related to serviceability and ultimate limit states, deformation demands and capacities and suitable design code requirements. The material that is presented in the following sections is by necessity only brief descriptions of each subject, given in the form of bullet points, and identifying the sources (*authors or other contributors*) of the recommendations.

BOLTS, WELDS AND RELATED FASTENING ISSUES

- Ductility and limit states of bolt assemblies during tightening, using various forms of bolt preloading (*Ryan*)
- Resistance factors for high strength bolts in combined tension and shear (*Moore, Rassati and Swanson*)
- Strength and ductility of bolted connections in high strength steel, especially with a large number of bolts in a row (*Ungermann and Schneider; Može and Beg*)
- End-Plate connections with large numbers of bolts in a single row (*Weynand, Klinkhammer, Ungermann, Schneider, Oberegge, Hockelmann and Ritterbusch*)
- Bolt tear-out and block shear limit states and suitable reliability indices for a variety of failure paths in connections (*Cai and Driver*)

- Redistribution of bolt forces in short and long shear connections, including imperfection effects (*Henriques, Jaspart and da Silva*)
- Reliability indices, resistance factors and improved limit state design of slip-resistant connections (*AISC research department*)
- Performance and design criteria for slip-resistant connections with open slotted holes (*Husson and Veljkovic*)
- Strength of bolt groups in single plate shear connections (*Baldwin-Metzger and Murray*)
- Modeling, strength assessment and design approaches for weld groups with differing geometries and orientations (*Muir*)
- Strength and behavior of connections with welds oriented in different directions (*Callele, Grondin and Driver*)
- Strength and behavior of spliced columns using bolted end plates (*Hoenderkamp and Snijder*)

SHEAR AND BRACING CONNECTIONS

- Effects of frame-induced distortional forces on gusset plates and other elements of braced frames (*Thornton and Muir*)
- Behavior and performance of connections for buckling-restrained braces (BRBs) in braced frames (*Fahnestock and Wigle*)
- Ultimate limit states for end connections in buckling-restrained braced frames (*Fahnestock and Wigle*)
- Inelastic response of concentrically braced frames, including post-buckling deformations (*Roeder and Lehman*)
- Stiffness and strength considerations for gusset plates in combination with framing members (*Roeder and Lehman*)
- Use of structural fuses in braced frames to achieve improved performance and construction economy (*Vincent*)
- Ductile behavior and limit states of plates in single plate shear connections (*Baldwin-Metzger and Murray*)
- Evaluations of connections used in historical structures, including fasteners such as rivets (*Civjan, Larsen and Hines*)

PORTAL FRAME CONNECTIONS

- Stiffness, rotation capacity and ultimate limit states for portal frame connections with slender elements (*Cristutiu, Grecea and Dubina*)
- Elastic and inelastic dynamic response characteristics of portal frames with semi-rigid connections (*Lopes, da Silva, Vellasco, de Lima and de Andrade*)

CONNECTIONS IN HIGH STRENGTH STEEL

- Use of very high strength steel in traditional and non-traditional shear connections (*Girão Coelho, Bijlaard and Kolstein*)
- Ductility and deformation capacity of very high strength steel connections (*Girão Coelho, Bijlaard and Kolstein*)
- Response characteristics of moment connections with elements of different steel grades (Dual-Steel Building Frames) (*Dubina, Stratan, Muntean and Grecea*)
- Behavior characteristics of two-sided beam-to-column connections in high strength steel with beams of unequal heights (*Jordão, da Silva and Simões*)
- Broad assessment of moment connection performance in steels with yield stress up to 460 MPa (65 ksi) (*Dubina, Stratan, Muntean and Dinu*)

CONNECTIONS AND FRAMES FOR SEISMIC RESISTANCE AND PERFORMANCE

- Strength, ductility and energy absorption capacity of various types of end-plate connections with pre-tensioned bolts (*Shi, Xiong, Shi and Wang*)
- Strength and deformation capacity of connections in special bolted moment frames with cold-formed beam members (*Sato and Uang*)
- Behavior, ultimate limit states and detailing of moment end-plate and other types of connections with attached concrete slabs (*Seek and Murray*)
- Further developments of prequalified T-stub connections for use in moment resisting frames (*Hantouche, Rassati, Swanson and Leon*)
- Enhanced behavior and ultimate limit states for link-to-column connections in eccentrically braced frames (*Okazaki, Engelhardt, Drolias, Schell, Hong and Uang*)
- Fracture considerations for welded connections in seismically resistant moment frames (*Okazaki, Engelhardt, Drolias, Schell, Hong and Uang*)
- Modeling and detailing of moment connections to recognize and modify the influence of flange shear forces (*Fleischman, Pan and Federico*)
- Response characteristics of post-tensioned moment connections (*Ricles, Seo, Lin and Sause*)
- Reliability analysis for evaluation of connections for self-centering framing systems (*Garlock and Herning*)
- Framing systems with focused areas of deformation and energy absorption for improved response, limited damage and enhanced repair procedures (*Ricles, Seo, Lin and Sause*)
- Framing systems with dedicated fuses for energy absorption and high-strength steel rods for restoration of frame after earthquake (*Eatherton, Hajjar, Deierlein, Krawinkler, Billington, Ma*).
- Framing systems with replaceable fuses for energy absorption (*Eatherton, Hajjar, Deierlein, Krawinkler, Billington, Ma*).
- Behavior, strength and detailing of hybrid framing systems for improved seismic characteristics (*Charney and Atlayan*)

- Use of post-tensioned column bases for improved response under seismic loads (*Chi and Liu*)
- Use of shape memory alloys for semi-rigid connections to reduce building damage and facilitate repair after an earthquake (*Leon and Hu*)
- Use of full-scale testing and advanced nonlinear analysis to assess seismic performance of connections (*Malley, Sinclair, Graf, Blaney, Fraynt, Uang, Newell and Ahmed*)
- Strength, seismic performance criteria and code requirements for rack structures (*Aguirre*)

ROBUSTNESS OF CONNECTIONS AND STRUCTURES

- Implications for design codes of the concepts of structural integrity, robustness and resistance to disproportionate collapse for connections and frames (*Gustafson, Duncan and Schlafly*)
- Assessment of structural robustness using the column removal scenario (*Sadek, Lew, Main and Gross*)
- Principles and applications of robustness of connections to avoid progressive collapse (*Davison and Tyas*)
- Strain-based modeling and analysis to assess the resistance to progressive welded connection fracture (*Marshall and Qian*)
- Behavior of composite connections under progressive collapse conditions (*Demonceau and Jaspert*)
- Design of bolted beam-to-column connections subjected to building fires (*Santiago, da Silva and Real*)
- Development of header plate connections with improved fire resistance (*Wald, Chloubá, Sokol and Kallerová*)
- Moment connections with thermal separation details for improved fire resistance (*Wald, Šulcova, Sokol and Rabenseifer*)

METHODS OF ANALYSIS OF CONNECTIONS AND FRAMES

- Component-based modeling approaches for connections for use with global analysis and frame stability assessment, including inelastic effects (*Bayo and Gracia*)
- Instantaneous center of rotation concepts applied to high-deformation seismic moment connections (*Sato and Uang*)
- Strain-based modeling and analysis to assess the resistance to progressive welded connection fracture (*Marshall and Qian*)
- Analysis of frames with inelastic, nonlinear geometric member behavior and semi-rigid connections (*Liu and Xu*)
- Analysis, design and performance assessment of semi-rigid frames using the AISC Direct Analysis Method (*White and Goverdhan*)

- Analysis of hybrid framing systems, utilizing a mix of members and connection details that are used in traditional framing systems (*Charney and Atlayan*)

CONNECTIONS WITH HOLLOW STRUCTURAL SECTIONS (HSS)

- Stiffening of connections with plates attached to circular hollow sections (CHS) (*Voth and Packer*)
- Structural response of tubular connections to static and dynamic loads (*de Lima, Vellasco, de Andrade, da Silva, Neves and Bittencourt*)
- Rotation capacity and ductility of various types of connections with rectangular hollow sections (RHS) (*Szlendak*)

COMPOSITE CONNECTIONS AND FRAMES

- Continuing development of performance and code criteria for composite connections (*Anderson*)
- Influence of concrete slab reinforcement ductility on connection rotation capacity (*Anderson*)
- Connections to beams in negative bending with partial shear connections (*Anderson*)
- Behavior, strength and design criteria for composite semi-rigid connections with various types of concrete slabs (*Lam*)
- Behavior of composite connections under progressive collapse conditions (*Demonceau and Jaspart*)

CONCLUSIONS AND ACKNOWLEDGEMENTS

A very large number of potential studies of connections and structural systems have been identified. Sincere appreciation is extended to the participants in the workshop for their work in preparing the written contributions and their active participation in all technical discussions.

Particular appreciation and thanks are extended to the American Institute of Steel Construction (AISC) and the European Convention for Constructional Steelwork (ECCS) for hosting the Sixth International Workshop on Connections in Steel Structures. Special thanks are due Nucor-Yamato Steel Company, Steel Dynamics and Gerdau-Ameristeel for their financial support. Last, but not least, the AISC staff was highly efficient and accurate, and the extensive labor of assembling the proceedings was handled expertly by Janet Cummins and Areti Gertos.

CONNECTION DESIGN AND CODE NEEDS

Charles J. Carter

American Institute of Steel Construction, Chicago, IL, USA
carter@aisc.org

ABSTRACT

This paper summarizes the topics presented at the Sixth International Workshop on Connection in Steel Structures, with special attention to design practices and code provisions. The summary is organized according to the following categories: (1) Bolted Joints; (2) Welded Joints; (3) Shear and Bracing Connections; (4) Moment Connections; (5) Tubular Connections; (6) Composite Connections; (7) Seismic Design; (8) Structural Integrity, Redundancy and Robustness; (9) Analysis and Modeling Techniques; (10) High-Strength Steels; and, (11) Other Innovative Concepts and Topics.

INTRODUCTION

A wide range of subjects were discussed at the Sixth International Workshop on Connections in Steel Structures. The following summary is a general distillation of the topics presented, with special attention to the potential for impact on design practices and code requirements. For convenience, the topics have been grouped in several general categories; some papers appear in multiple categories. The authors are shown with each topic so that the full text of each paper can be found by the interested reader.

BOLTED JOINTS

- Consideration of higher effective shear stress and alternative block mechanisms in prediction of block shear rupture strength (*Cai and Driver*).
- Consideration of actual force distribution in fasteners in shear connections (*Henriques, Jaspart and da Silva*).
- Use of slip-resistant joints with open slotted holes (*Husson and Veljkovic*).
- Improvements in resistance factors for high-strength bolts in tension and shear (*Moore, Rassati and Swanson*).
- Differences between European and North American provisions for bolts and bolted connections (*Ryan*).
- Bolted seismic moment connections in cold-formed steel applications using an instantaneous-center-of-rotation approach (*Sato and Uang*)

- Consideration of the impact of reduced ductility in high-strength steels on redistribution capability of connections in bearing (*Ungermann and Schneider*).

WELDED JOINTS

- Generalized provisions for the design of concentrically loaded fillet weld groups with welds oriented at different angles to the load (*Callele, Grondin and Driver*).
- Effects of load-deformation compatibility on strength of eccentrically loaded fillet weld groups (*Muir*).
- Connection strength prediction using CTOD-based finite element methods (*Marshall and Qian*).

SHEAR AND BRACING CONNECTIONS

- Verification and improvement of single-plate connection design methods (*Baldwin-Metzger and Murray*).
- Modeling of existing connections (as-built and with modifications) to account for contributions to lateral resistance in seismic upgrading of existing buildings (*Civjan, Larsen and Hines*).
- Consideration of impact of frame action on performance and design requirements for seismic braced frames with buckling-restrained braces (*Fahnestock and Wigle*).
- Design and detailing of eccentrically braced frames in the link-to-column configuration (*Okazaki, Engelhardt, Drolias, Schell, Hong and Uang*).
- Improvements in design and detailing of gusset plates in seismic braced frames (*Roeder and Lehman*).
- Effects of distortional forces on design and behavior of bracing connections in seismic applications (*Thornton and Muir*).
- Reduced brace section concept in bracing members to reduce tension demand in seismic applications (*Vincent*).

MOMENT CONNECTIONS

- Practical improvement and generalization of provisions for the design of composite beam-to-column moment connections (*Anderson*).
- Use of post-tensioned self-centering column-base moment connections with buckling-restrained elements to improve seismic performance (*Chi and Liu*).
- Proper accounting for lateral-torsional buckling instability of tapered girders in metal building frames due to compressive forces (*Cristutiu, Grecea and Dubina*).

- Use of composite beam-to-column moment connections to meet structural integrity requirements (*Demonceau and Jaspert*).
- Use of welded tee stubs with mixed steel grades for beam-to-column moment connections (*Dubina, Stratan, Muntean and Grecea*).
- Prediction and impact on design and connection detailing of shear in flanges of seismic beam-to-column moment connections (*Fleischman, Pan and Federico*).
- Use of post-tensioned self-centering moment frame concept and techniques for generation of a synthetic suite of ground motions for design, including based upon Monte Carlo simulation (*Garlock and Herning*).
- Design and prequalification of tee-stub moment connections for seismic applications (*Hantouche, Rassati and Swanson*).
- Design of composite beam-to-column moment connections with precast hollow-core slabs (*Lam*).
- Use of shape-memory alloys in composite beam-to-column moment connections (*Leon and Hu*).
- Use of post-tensioned self-centering beam-to-column moment connections with frictional dissipating devices to improve seismic performance (*Ricles, Seo, Lin and Sause*).
- Performance characteristics and modeling of seismic moment connections for monotonic loading in structural integrity applications (*Sadek, Lew, Main and Gross*).
- Design and detailing of end-plate moment connections for seismic applications when a slab is present (*Seek and Murray*).
- Performance of various end-plate moment connection configurations (*Shi, Xiong, Shi and Wang*).
- Design and analysis of partially restrained moment frames using the AISC direct analysis method (*White and Goverdhan*).

TUBULAR CONNECTIONS

- Use of deformation limits rather than plastification in assessing strength of T and K tubular joints (*de Lima, Vellasco, Andrade, da Silva, Neves and Bittencourt*).
- Connection strength prediction using CTOD-based finite element methods (*Marshall and Qian*).
- Connection strength prediction using CTOD-based finite element methods (*Marshall and Qian*).
- Rotation capacity and ductility in T and X tubular connections with rectangular hollow structural sections (*Szlendak*).
- Advancements in understanding and design provisions for T and X tubular joints with round hollow structural sections (*Voth and Packer*).

COMPOSITE CONNECTIONS

- Practical improvement and generalization of provisions for the design of composite beam-to-column moment connections (*Anderson*).
- Modeling of existing connections (as-built and with modifications) to account for contributions to lateral resistance in seismic upgrading of existing buildings (*Civjan, Larsen and Hines*).
- Design of composite beam-to-column moment connections with precast hollow-core slabs (*Lam*).

SEISMIC DESIGN

- Refinement of provisions for the seismic design of rack structures (*Aguirre*).
- Use of the hybrid design and detailing approach with defined hinge sequencing to improve seismic performance (*Charney and Atlayan*).
- Use of post-tensioned self-centering column-base moment connections with buckling-restrained elements to improve seismic performance (*Chi and Liu*).
- Modeling of existing connections (as-built and with modifications) to account for contributions to lateral resistance in seismic upgrading of existing buildings (*Civjan, Larsen and Hines*).
- Use of high-strength steel grades in non-dissipative structural framing to improve seismic performance (*Dubina, Stratan, Muntean and Dinu*).
- Consideration of impact of frame action on performance and design requirements for seismic braced frames with buckling-restrained braces (*Fahnestock and Wigle*).
- Prediction and impact on design and connection detailing of shear in flanges of seismic beam-to-column moment connections (*Fleischman, Pan and Federico*).
- Use of post-tensioned self-centering moment frame concept and techniques for generation of a synthetic suite of ground motions for design, including based upon Monte Carlo simulation (*Garlock and Herning*).
- Design of composite beam-to-column moment connections with precast hollow-core slabs (*Lam*).
- Use of shape-memory alloys in composite beam-to-column moment connections (*Leon and Hu*).
- Use of post-tensioned self-centering beam-to-column moment connections with frictional dissipating devices to improve seismic performance (*Ricles, Seo, Lin and Sause*).
- Bolted seismic moment connections in cold-formed steel applications using an instantaneous-center-of-rotation approach (*Sato and Uang*).

- Design and detailing of end-plate moment connections for seismic applications when a slab is present (*Seek and Murray*).
- Modeling and design of four-bolt-wide flush end-plate moment connections (*Weynand, Klinkhammer, Ungermann, Schneider, Oberegge, Hockelmann and Ritterbusch*).
- Reduced brace section concept in bracing members to reduce tension demand in seismic applications (*Vincent*).

STRUCTURAL INTEGRITY, REDUNDANCY AND ROBUSTNESS

- Transition in structural integrity requirements from prescriptive tie-force requirements to performance-based options (*Davison and Tyas*).
- Use of composite beam-to-column moment connections to meet structural integrity requirements (*Demonceau and Jaspert*).
- Risk assessment and minimum requirements for connections to provide structural integrity (*Gustafson, Duncan and Schlafly*).
- Design of composite beam-to-column moment connections with precast hollow-core slabs (*Lam*).
- Performance characteristics and modeling of seismic moment connections for monotonic loading in structural integrity applications (*Sadek, Lew, Main and Gross*).
- Robustness and performance design of steel connection details when exposed to fire effects (*Santiago, da Silva and Real*).
- Prediction of joint temperatures in connections subject to fire effects (*Wald, Chlouba, Sokol and Kallerová*).

ANALYSIS AND MODELING TECHNIQUES

- Refinement of provisions for the seismic design of rack structures (*Aguirre*).
- Advancement in analysis techniques to include direct modeling of connection behavior in evaluation of frame strength, stiffness and stability (*Bayo and Gracia*).
- Modeling of existing connections (as-built and with modifications) to account for contributions to lateral resistance in seismic upgrading of existing buildings (*Civjan, Larsen and Hines*).
- Prediction and impact on design and connection detailing of shear in flanges of seismic beam-to-column moment connections (*Fleischman, Pan and Federico*).
- Treatment of effective flexural demand in design of column splices in axially loaded columns (*Hoenderkamp and Snijder*).
- Analysis of frames considering inelasticity, geometric nonlinearity, and semi-rigid behavior (*Liu and Xu*).

- Use of non-linear dynamic analysis in practical design (*Lopes, da Silva, Vellasco, de Lima, de Andrade*).
- Seismic evaluation and upgrading using advanced modeling of existing and modified connections to achieve performance objectives (*Malley, Sinclair, Graf, Blaney, Fraynt, Uang, Newell and Ahmed*).
- Connection strength prediction using CTOD-based finite element methods (*Marshall and Qian*).

HIGH-STRENGTH STEELS

- Use of welded tee stubs with mixed steel grades for beam-to-column moment connections (*Dubina, Stratan, Muntean and Grecea*).
- Use of high-strength steel grades in non-dissipative structural framing to improve seismic performance (*Dubina, Stratan, Muntean and Dinu*).
- Liberalization of restrictions on use of high-strength steels in panel zones (*Girão Coelho, Bijlaard and Kolstein*).
- Consideration of actual force distribution in fasteners in shear connections (*Henriques, Jaspart and da Silva*).
- Design of column panel-zones with high-strength steel (*Jordão, da Silva and Simões*).
- Consideration of the impact of reduced ductility in high-strength steels on redistribution capability of connections in bearing (*Može and Beg*).
- Consideration of the impact of reduced ductility in high-strength steels on redistribution capability of connections in bearing (*Ungermann and Schneider*).

OTHER INNOVATIVE CONCEPTS AND TOPICS

- Use of post-tensioned self-centering column-base moment connections with buckling-restrained elements to improve seismic performance (*Chi and Liu*).
- Lateral-torsional buckling instability of tapered girders in metal building frames due to compressive forces (*Cristutiu, Grecea and Dubina*).
- Use of post-tensioned self-centering moment frame concept and techniques for generation of a synthetic suite of ground motions for design, including based upon Monte Carlo simulation (*Garlock and Hering*).
- Use of slip-resistant joints with open slotted holes (*Husson and Veljkovic*).
- Design of composite beam-to-column moment connections with precast hollow-core slabs (*Lam*).
- Use of shape-memory alloys in composite beam-to-column moment connections (*Leon and Hu*).

- Use of post-tensioned self-centering beam-to-column moment connections with frictional dissipating devices to improve seismic performance (*Ricles, Seo, Lin and Sause*).
- Use of thermal break material in connections between façade elements and structure (*Wald, Šulcová, Sokol and Rabenseifer*).

CONCLUSIONS

This paper provided a general distillation of the topics presented, with special attention to the potential for impact on design practices and code requirements. As with the five workshops that preceded this Sixth International Workshop on Connections in Steel Structures, the information generated is significant and useful. The sharing of knowledge and ideas across geographic borders continues to be as fruitful as it is enjoyable. Thanks to all the participants for making the Sixth Workshop a success.

PARTICIPANTS – CONNECTIONS VI WORKSHOP

Bjoern Aasen	Norconsult AS, Norway
Carlos Aguirre	Technical University Federico Santa Maria, Chile
David Anderson.....	University of Warwick, England
Eduardo Bayo	University of Navarra, Spain
Darko Beg.....	University of Ljubljana, Slovenia
Frans Bijlaard	Delft University of Technology, The Netherlands
Reidar Bjorhovde	The Bjorhovde Group, USA
Mary Brettle	The Steel Construction Institute, England
Charles J. Carter	American Institute of Steel Construction, USA
Finley Charney	Virginia Polytechnic Institute, USA
Scott Civjan	University of Massachusetts, USA
John Davison	University of Sheffield, England
Jean-François Démonceau.....	University of Liège, Belgium
Bo Dowswell	American Institute of Steel Construction, USA
Robert Driver.....	University of Alberta, Canada
Dan Dubina.....	University of Timisoara, Romania
Cynthia J. Duncan	American Institute of Steel Construction, USA
Michael Engestrom.....	Nucor-Yamato Steel Company, USA
Larry Fahnestock.....	University of Illinois at Urbana-Champaign, USA
Marshall Ferrell	Ferrell Engineering, Inc., USA
Robert Fleischman.....	University of Arizona, USA
Maria Garlock.....	Princeton University, USA
Louis F. Geschwindner.....	American Institute of Steel Construction, USA
Ana Girão Coelho.....	Polytechnic Institute of Coimbra, Portugal
Arvind Goverdhan	Stanley D. Lindsey & Associates, USA
A.M. (Nol) Gresnigt	Delft University of Technology, The Netherlands
Gilbert Grondin	University of Alberta, Canada
John Gross	National Institute of Standards & Technology, USA
Kurt Gustafson	American Institute of Steel Construction, USA
Jerome Hajjar	University of Illinois at Urbana-Champaign, USA
J.C.D. Hoenderkamp	Eindhoven University of Technology, The Netherlands
Gorka Iglesias.....	Parque Tecnológico, Spain
Sandra Jordão	University of Coimbra, Portugal
Dennis Lam	University of Leeds, England
Roberto Leon.....	Georgia Institute of Technology, USA
Luciano Lima	State University of Rio de Janeiro, Brazil
Judy Liu.....	Purdue University, USA
Abdul Malik	The Steel Construction Institute, England
James Malley	Degenkolb Engineers, USA
Peter Marshall.....	National University of Singapore, Singapore

David Moore..... British Constructional Steel Association, England
 Primož Može University of Ljubljana, Slovenia
 Larry Muir Cives Engineering Corporation, USA
 Thomas Murray Virginia Polytechnic Institute, USA
 Taichiro Okazaki University of Minnesota, USA
 Jeffrey Packer University of Toronto, Canada
 Gian Rassati..... University of Cincinnati, USA
 James Ricles Lehigh University, USA
 Charles Roeder University of Washington, USA
 Fahim Sadek National Institute of Standards & Technology, USA
 Aldina Santiago University of Coimbra, Portugal
 Atsushi Sato..... Kyoto University, Japan
 Thomas J. Schlafly American Institute of Steel Construction, USA
 Stephan Schneider University of Dortmund, Germany
 Gang Shi Tsinghua University, China
 Luis Simões da Silva University of Coimbra, Portugal
 Aurel Stratan..... University of Timisoara, Romania
 Andrea Surovek..... South Dakota School of Mines & Technology, USA
 James Swanson..... University of Cincinnati, USA
 Jerzy K. Szlendak Bialystok Technical University, Poland
 William Thornton Cives Engineering Corporation, USA
 Amit Varma Purdue University, USA
 Milan Veljkovic..... Luleå University of Technology, Sweden
 Pedro Vellasco..... State University of Rio de Janeiro, Brazil
 Richard Vincent..... Canam Group, Canada
 Andrew Voth University of Toronto, Canada
 František Wald Czech Technical University, Czech Republic
 Klaus Weynand Feldmann + Weynand GmbH, Germany
 Donald White Georgia Institute of Technology, USA
 Alfred Wong Canadian Institute of Steel Construction, Canada
 Lei Xu..... University of Waterloo, Canada

AUTHOR INDEX

- Aguirre, C. 545
Ahmed, T. 535
Anderson, D. 491
Andrade, S. 197 401
Atlayan, O. 331
- Baldwin-Metzger, K. 143
Bayo, E. 219
Beg, D. 65
Bijlaard, F. S. K. 7 155
Bittencourt, M. C. 401
Bjorhovde, R. 597
Blaney, C. 535
Brekelmans, J. W. P. M. 7
- Cai, Q. 41
Callele, L. J. 525
Carter, C. J. 603
Charney, F. A. 331
Chi, H. 367
Chlouba, J. 209
Civjan, S. 575
Cristutiu, I. M. 165
- Davison, J. B. 455
Demonceau, J. F. 567
Dinu, F. 355
Driver, R. G. 41 525
Drolias, A. 297
Dubina, D. 165 185 355
Duncan, C. J. 431
- Engelhardt, M. D. 297
- Fahnestock L. A. 105
Fraynt, M. 535
- Garlock, M. E. 555
Geschwindner, L. F. 1
Girão Coelho, A. M. 155
Goverdhan, A. V. 255
Gracia, J. 219
Graf, T. 535
Grecea, D. 165 185
- Gresnigt, A. M. 75
Grondin, G. Y. 525
Gross, J. L. 443
Gustafson, K. 431
- Hantouche, E. G. 287
Henriques, J. 51
Herning, G. 555
Hines, E. 575
Hockelmann, H. P. 501
Hoenderkamp, J. C. D. 421
Hong, J. K. 297
Hu, J. W. 513
Husson, W. 585
- Jaspart, J. P. 51 567
Jordão, S. 343
- Kallerová, P. 209
Klinkhammer, R. 501
Kolstein, M. H. 155
- Lam, D. 265
Larsen, G. 575
Lehman, D. E. 117
Leon, R. T. 287 513
Lew, H. S. 443
Lima, L. 197 401
Lin, Y. C. 319
Liu, J. 367
Liu, Y. 243
Lopes, F. 197
- Main, J. A. 443
Malley, J. O. 535
Marshall, P. W. 389
Moore, A. M. 19
Može, P. 65
Muir, L. S. 93 309
Muntean, N. 185 355
Murray, T. M. 143 277
- Neves, L. 401

Oberegge, O. 501
Okazaki, T. 297

Packer, J. A. 377

Rabenseifer, R. 565
Rassati, G. A. 19 287
Real, P. 479
Ricles, J. M. 319
Ritterbusch, N. 501
Roeder, C. W. 117

Sadek, F. 443
Santiago, A. 479
Sato, A. 231
Sause, R. 319
Schell, E. 297
Schlafly, T. 431
Schneider, S. 31 501
Seek, M. W. 277
Seo, C. Y. 319
Shi, G. 175
Shi, Y. 175
Silva, J. 197 401
Simões da Silva, L. 51 343 479
Simões, R. D. 343
Sinclair, M. 535
Snijder, H. H. 421
Sokol, Z. 209 565
Stratan, A. 185 355
Šulcová, Z. 565
Swanson, J. A. 19 287
Szlendak, J. K. 411

Thornton, W. A. 93
Tyas, A. 455

Uang, C. M. 231 297 535
Ungermann, D. 31 501

VanMarcke, E. 555
Veljkovic, M. 585
Vellasco, P. 197 401
Vincent, R. B. 127
Voth, A. P. 377

Wald, F. 209 565
Wang, Y. 175
Weynand, K. 501
White, D. W. 255
Wigle, V. A. 105

Xiong, J. 175
Xu, L. 243
Xudong, Q. 389